

The effect of particle geometry and surface asperities on the result of Discrete
Element Simulations

Siyang Zhang

A Thesis
in
The Department
of
Building, Civil and Environmental Engineering

Presented in Partial Fulfillment of the Requirements
For the Degree of
Master of Science (Building, Civil and Environmental Engineering) at
Concordia University
Montreal, Quebec, Canada

July 2017

© Siyang Zhang, 2017

CONCORDIA UNIVERSITY

School of Graduate Studies

This is to certify that the thesis is prepared

By: Siyang Zhang

Entitled: The effect of particle geometry and surface asperities on the
result of Discrete Element Simulations

and submitted in partial fulfillment of the requirements of the degree of

Master of Science (Building, Civil and Environmental Engineering)

complies with the regulations of the University and meets the accepted standards with respect
to originality and quality.

Signed by the final Examining Committee:

_____ Chair
Chair's name

_____ Examiner
Examiner's name

_____ Examiner
Examiner's name

_____ Supervisor
Supervisor's name

Approved by _____

Chair of Department or Graduate Program Director

_____ 2017 _____

Dean of Faculty

Abstract

The effect of particle geometry and surface asperities on the result of Discrete Element Simulations

Siyang Zhang

In recent years, analysis of the behavior of brittle materials, such as concrete, rocks or granular materials, is receiving more attention. These brittle materials share common characteristics, which are their high complexity and heterogeneity, especially when they fragment from their original shape into smaller particles. Traditionally, it was common to use continuum methods (like the finite element method) to reproduce the behavior of these materials, even though these methods require complex constitutive models, which contain a lot of parameters and variables. The *Discrete Element Method (DEM)*, originally developed by Cundall and Strack (1979), in contrast to continuum methods, has been proven to be an irreplaceable and powerful tool for conducting analysis and modelling the behavior of granular (spherical) and polyhedral (non-spherical) particle systems, which also focus on micromechanics of soil particle interactions and displacements. Meanwhile, the DEM has been proven to be suitable for analysis of continuum materials and models as well. In addition, there is another method named *The Combined Finite-Discrete Element Method (FEM/DEM)* (Munjiza, 2004), which is a numerical solution that focuses on the analysis of problems for solids that are considered as both continua and discontinua.

This research will present the basic numerical principles of DEM and FEM/DEM, then by using these methods, the analysis of the influence of the changes of the geometry or asperities of polyhedral granular particles will be investigated. Both the influence on solution time and solution accuracy will be critically reviewed and recommendations will be given for practical use in simulations.

Acknowledgement

First and foremost, I would like to express my deepest gratitude to my research supervisor, Dr. Attila Zsaki, for his invaluable help, guidance and support throughout the research in all aspects over the years. It was him who provided the opportunity for me to conduct the research and introduced me into the field of geotechnical engineering.

I would also like to extend my highest appreciations and gratitude to my family. Without their support and encouragement, I would not have the chance to be a student at Concordia University.

Authorization

I hereby declare that I am the sole author of the thesis.

I authorize The Concordia University of Civil Engineering Department to lend this thesis to other institutions or individuals for the purpose of scholarly research.

I also authorize The Concordia University of Civil Engineering Department to reproduce this thesis by photocopying or by other means, in total or in part, at the request of other institutions or individuals for the purpose of scholarly research.

A handwritten signature in black ink, appearing to read '张斯阳' (Zhang Siyang), written in a cursive style.

Siyang Zhang

May 20

Table of Contents

Abstract	iii
Acknowledgement	iv
Authorization	v
List of Symbols	vi
List of Figures	ix
1 Introduction of the Thesis	1
2 Introduction to Discrete Element Methods	3
2.1 Introduction to Discrete Element Methods	3
2.2 Principles of DEM	4
2.3 Numerical simulation by DEM	5
3 Basic Physical and Mathematical Background of DEM	7
3.1 Particle motion and numerical solutions	7
3.1.1 Introduction	7
3.1.2 Updating particle positions	9
3.1.3 Determination of computational time step	12
3.1.4 Damping	13
3.2 Force-Displacement Laws	16
3.2.1 Introduction and a brief overview of contact mechanics	16
3.2.2 Contact response based on linear elasticity	17
3.2.3 Normal force-displacement models in DEM	21
3.2.4 Tangential force-displacement models in DEM	25
3.3 The Combined FEM/DEM method	31
3.3.1 Introduction	31
3.3.2 General considerations of Combined FEM/DEM	32
3.3.3 Contact force evaluation	33
4 Simulation of Particle Contacts Using the Combined FEM/DEM	39
4.1 Obtaining 3D particle geometry using 3D scanning	39
4.2 Pre-simulation Process – model generation	41
4.2.1 The Virtual Geoscience Workbench (VGW)	41
4.2.2 Supplementary programs for simulation	44
4.2.3 Particle description	48

4.3	Post-simulation process	51
4.4	Discussion of simulation results	52
4.4.1	Phase 1. - Particle collision with a solid block	52
4.4.2	Phase 2 – Simulation of multi-particle collisions inside a container	88
5	Conclusion and Recommendations for Future Work	98
5.1	Conclusion	98
5.2	Future work	99
6	Bibliography	102
	Appendix	106

List of Symbols

M	inertia matrix
C	damping matrix
$\Delta \mathbf{u}$	incremental displacement vector
$\Delta \mathbf{F}$	incremental force vector
K	global stiffness matrix
$\dot{\mathbf{u}}$	velocity vector
$\ddot{\mathbf{u}}$	acceleration vector
\mathbf{u}	combined incremental displacement
u_x^p, u_y^p, u_z^p	three dimensional incremental translational displacements
p	particular particle
N_p	total number of particles
F_{pc}^{con}	contact forces between a particle and a contactor
$F_{pj}^{non-con}$	non-contact forces
F_p^f	fluid interaction forces
F_p^g	gravitational forces
F_p^{app}	special applied forces
I_p	moment of inertia
ω_p	vector of angular velocity
M_{pj}	moment resulting from the j th moment-transmitting contact forces
N_{mom}	total number of moment-transmitting forces
a	acceleration vector
m	mass matrix
V	velocity vector

List of Symbols

\mathbf{X}	position vector
Δt	incremental time
ω	angular velocity
r	radius
ρ	density
k_{max}	maximum contact stiffness
\mathbf{C}	damping matrix
f_n	normal traction
F_n	normal force
f_t	tangential traction
F_t	tangential force
R^*	effective particle radius
E^*	effective Young's modulus
δ	normal deformation
K_n	normal directional contact stiffness
δ_n	normal overlap depth
R	radius of spherical particle
ν	Poisson's ratio
G	elastic shear modulus
e	restitution coefficient
δ_t	cumulative relative deformation
$\dot{\delta}_t$	relative velocity at contact point
x	position of centroids
$K_{s,t}$	tangential stiffness at time t

List of Symbols

φ_t	force potential on target
φ_c	force potential on contactor
$\varphi(P_G)$	potential of Gauss point
E_p	penalty parameter
E	modulus of elasticity
d	allowed penetration
u	displacement field
S	overlapping area
V	overlapping volume

List of Figures

- Figure 2.1 Schematic diagram of sequence of calculations in a DEM simulation (O'Sullivan, 2011)
- Figure 3.1 Walton-Braun linear contact model illustration (O'Sullivan, 2011)
- Figure 3.2 Thornton and Yin (1991) model of the tangential force, which has oblique contact and no adhesion (O'Sullivan, 2011)
- Figure 3.3 The FEM/DEM problem containing two discrete elements, which are discretized into finite elements (Munjiza, 2004)
- Figure 3.4 An illustration of infinitesimal overlap about points P_c and P_t , and the resultant contact force (Munjiza, 2004)
- Figure 3.5 The potential at any point P on a triangular finite element (Munjiza, 2004)
- Figure 3.6 Potential definition over domain of a single tetrahedron (Munjiza, 2004)
- Figure 4.1 Screenshot of the virtual shape library and one rock particle is visualized
- Figure 4.2 Procedure to generate a required input file for the Y3D FEM/DEM solver (Xiang et al., 2008)
- Figure 4.3 Illustration of expected order of element's nodes defined by GiD manual for quadratic tetrahedron (Coll et al. 2016)
- Figure 4.4 Illustration of one element order plotted by the GiD for one of the 10-node tetrahedral mesh generated by the TET_MESH_L2Q
- Figure 4.5 Plot of resultant forces during collision event for Particle 3
- Figure 4.6 Plot of resultant forces during collision event for Particle 4
- Figure 4.7 Plot of resultant forces during collision event for Particle 1
- Figure 4.8 Illustration of Particle 1 with 4 different element numbers
- Figure 4.9 Screen shot of the initial place for Particle 1 with 100 elements and the solid block from the GiD program

List of Figures

- Figure 4.10 The initial position of Particle 1 with 100 elements relating to the solid block
- Figure 4.11 Comparison of the initial place for particle 1 with 100 elements (blue) and particle 1 with 250 elements (red), presented by Paraview
- Figure 4.12 Plot of resultant forces during collision event for Particle 11
- Figure 4.13 Plot of resultant forces during collision event for Particle 13
- Figure 4.14 Plot of resultant forces during collision event for Particle 15
- Figure 4.15 Plot of resultant forces during collision event for Particle 17
- Figure 4.16 Plot of resultant forces during collision event for Particle 24
- Figure 4.17 Plot of resultant forces during collision event for Particle 28
- Figure 4.18 Plot of resultant forces during collision event for Particle 44
- Figure 4.19 Plot of resultant forces during collision event for Particle 6
- Figure 4.20 Peak collision for the four particle geometry resolutions for Particle 6
- Figure 4.21 Comparison animation for Particle 6 with 500 elements (white) and Particle 6 with 1000 elements (blue)
- Figure 4.22 Final position comparison for Particle 6 with 500 elements (white) and Particle 6 with 1000 elements (blue)
- Figure 4.23 Animation of the initial position for Particle 6 with 100 elements (white) and Particle 6 with 500 elements (blue)
- Figure 4.24 Plot of resultant forces during collision event for Particle 7
- Figure 4.25 Top view (X-Z) plane of initial position comparison for Particle 7 with 100 elements (blue), 250 elements (blue outlines only), 500 elements (red) and 1000 elements (red with outlines)
- Figure 4.26 Side view (X-Y) plane of initial position comparison for Particle 7 with 100 elements (blue), 250 elements (blue outlines only), 500 elements (red) and 1000 elements (red with outlines)
- Figure 4.27 Comparison of position when full contact occurs for particle 7

List of Figures

- with different element numbers (Particle 7 with 100 in the left most and 250 been placed on the right next to 100, and so on)
- Figure 4.28 Plot of resultant forces during collision event for Particle 8
- Figure 4.29 Plot of resultant forces during collision event for Particle 9
- Figure 4.30 Plot of resultant forces during collision event for Particle 19
- Figure 4.31 Plot of resultant forces during collision event for Particle 22
- Figure 4.32 Screenshot of the initial position for particle 22 with 100 elements and the solid block, viewed from X-Y plane
- Figure 4.33 Screenshot of the initial position for particle 22 with 100 elements and the solid block, viewed from X-Z plane
- Figure 4.34 Screenshot of the initial contacting moment for Particle 22 with 100 elements and the solid block, viewed from X-Z plane
- Figure 4.35 Screenshot of the initial contacting moment in time for Particle 22 with 100 elements and the solid block, viewed from X-Z plane
- Figure 4.36 Screenshot of the contacting moment in time when Particle 22 having the largest deformation, viewed from X-Z plane
- Figure 4.37 Screenshot of the contacting moment in time when Particle 22 having the largest deformation, viewed from X-Z plane
- Figure 4.38 Plot of resultant forces during collision event for Particle 23
- Figure 4.39 Plot of resultant forces during collision event for Particle 30
- Figure 4.40 Plot of resultant forces during collision event for Particle 34
- Figure 4.41 Plot of resultant forces during collision event for Particle 32
- Figure 4.42 Screenshot of initial position for Particle 32 with 100 elements (blue) and Particle 32 with 1000 elements (red)
- Figure 4.43 Plot of resultant forces during collision event for Particle 33
- Figure 4.44 Illustration of initial position for Particle 33 with 100 elements (blue) and 1000 elements (red)
- Figure 4.45 Plot of resultant forces during collision event for Particle 38
- Figure 4.46 CPU time vs. model geometry resolution for Particle 22

List of Figures

- Figure 4.47 Illustration of the original locations after imported from VGW to GiD for particle samples with 100 elements along with the container
- Figure 4.48 Illustration of particles' initial pre-contact position for particle with 100 elements, viewing from X-Y plane
- Figure 4.49 Illustration of particles' initial pre-contact position for particles with 100 elements, viewing from X-Z plane
- Figure 4.50 Total resultant forces acted on the container (all forces acted on both bottom and sides) comparison during different collision events
- Figure 4.51 Resultant forces comparison for Particle 1 during different collision events
- Figure 4.52 Resultant forces comparison for Particle 2 during different collision
- Figure 4.53 Resultant forces comparison for Particle 3 during different collision events
- Figure 4.54 Resultant forces comparison for Particle 4 during different collision events
- Figure 4.55 Resultant forces comparison for Particle 6 during different collision events
- Figure 4.56 Resultant forces comparison for Particle 6 during different collision events
- Figure 4.57 Resultant forces comparison for Particle 7 during different collision events
- Figure 4.58 Resultant forces comparison for Particle 8 during different collision events
- Figure 4.59 Resultant forces comparison for Particle 9 during different collision events
- Figure 4.60 Resultant forces comparison for Particle 10 during different

List of Figures

collision events

1 Introduction of the Thesis

This thesis is focused on the analysis of simulations of particle behaviour during collision events from the perspective of Discrete Element Method (DEM) (Cundall and Strack, 1979), and the application of the Combined Finite and Discrete Element Method (FEM/DEM) (Munjiza et al., 1995) during the simulation process. The main focus of the thesis is the issue that if the increase of particle's geometrical detail will influence the simulation duration; or whether with the increase of particle's number of elements comprising its mesh, the simulation time will be increased correspondingly.

This thesis will begin with a brief introduction of DEM, then continues with a comprehensive chapter about the physical and mathematical background of both DEM and FEM/DEM for readers to have a general idea about what type of physical laws have been applied and considered in this research. After these follows the most important chapter, which is the simulation process and the discussion of results, which is the main contribution of this research. Then, the thesis concludes with a summary of findings and recommendations.

The simulation process is divided into two phases, one is about having individual particles, discretized into different number of elements, collide with a solid block. While the second phase simulates the collision of multiple particles inside a container. The results of simulations show that with the increase of particle's discretization resolution, the simulation duration and CPU time will increase as well; especially when particle's number of mesh elements increased to 1000, both the simulation duration and CPU time will have a dramatic increase. Since the time consumption becomes non-affordable with the increase of element numbers over 1000 elements, and the accuracy of simulation results (comparison of the mean value and standard deviation of forces and impulses) are showing that there are not many changes between particles with the lowest resolution to higher resolutions, which underlines that it is not necessary to conduct more simulations with increasing particle discretization beyond 1000 elements.

The importance of this thesis is in evaluating the use of the FEM/DEM method to analyse

the collision of particles with different discretizations, Thus the findings contained within the thesis can serve as a reference for future research concerning simulation of soil, rock or general granular particle collisions to determine the sufficient geometric detail of particles that still leads to an affordable simulation time, yet without losing the accuracy of simulation due to oversimplification of geometry.

2 Introduction to Discrete Element Methods

2.1 Introduction to Discrete Element Methods

The term DEM could be referred to the abbreviation of two forms; the *discrete element method* (Cundall and Strack, 1979) or the *distinct element method* (O'Sullivan, 2011). DEM is a numerical method which could be used for simulating the behavior of soil or granular materials. Using Cundall's words: "A discrete element method is a simulation method where the finite displacements and rotations of discrete bodies are simulated" (Dickinson, 2013). After the establishment of formulations by Cundall, these fundamental formulations were adopted to develop the commercial DEM codes such as "Particle Flow Codes" *PFC2D and PFC3D* (Itasca Consulting Group, 2004, 2008).

The major difference of DEM, with respect to continuum methods (such as the finite element method), is that it explicitly focuses on the level of individual particles in order to conduct discrete analyses of interactions or displacements. For spherical or polyhedral granular particles, there is a microscopic scale (molecular forces), a mesoscopic scale (single particles), and a macroscopic scale (distances inside the material over many particle diameters) (Matuttis and Chen, 2014). Given that continuum methods focus on a macroscopic scale, which assumes that the analyzed model is behaving as continuum material, and ignores the interior movements and rotations of particles (e.g. soil solids). In contrast, DEM not only serves as an ideal method for analyzing mesoscopic scale problems, which the continuum methods ignore or can hardly cope with, it also can be used for solving continuum problems in the first place and providing more comprehensive and detailed analysis. Given these properties of DEM, more precise constitutive models are then needed for conducting such an analysis in order to represent the complexity of the nature of a material.

2.2 Principles of DEM

In DEM, it is common to use simplified shapes of particles (e.g. using spheres in 3D or disks in 2D) to simulate inter-particle contacts for reducing the computational cost or time. If there are additional details that should be modeled, such as the asperity details, then it is also convenient to modify the detail on the basis of a pre-estimated simple model than a complex model (which may bring chaos during the simulation). Even though the application of basic numerical models is using ideal particle geometries, those most outstanding soil mechanical responses can still be characterized by DEM (O'Sullivan, 2011).

DEM is a method based on precise time-stepping calculations focused on applying Newton's Second Law for particles and the force-displacement law for contacts, where Newton's Second Law is aimed at the determination of particle movement due to contacts or external forces, and the force-displacement law is applied for the update of contact forces due to contacts resulting from movements and collision of particles. In particular, Figure 1.1 can concisely illustrate the simulation cycle of DEM, which begins with the input of initial geometry characteristics of the system, and the input of material properties, expressed by the specification of contact model parameters. After this, a continuously repeating calculation cycle includes the identification of particle movements and collisions, contact forces, resultant forces, velocities and accelerations in order to update particle position which will be used as the new particle arrangement for the next calculation cycle, which is increased by a small time step. The calculation ends when all the particles to be analyzed are all at rest, in a steady-state deformation without collisions, or have reached a user-specified time.

What should be noticed is the choice of time step should be as small as possible in order to eliminate the propagation of disturbances of any particle during a single time step, and the particles should have independent movements between each other. These are essential for defining each particle to be analyzed exclusively by interactions when particles are in contacts. This is the vital factor for conducting a non-linear analysis for a large number of particles with no need of an excessive computer memory requirement.

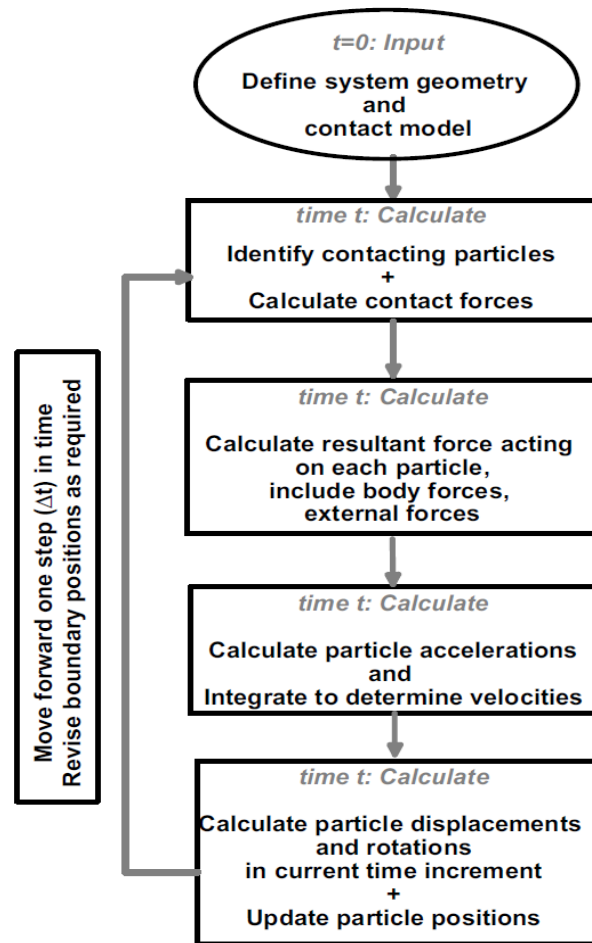


Figure 2.1: Schematic diagram of sequence of calculations in a DEM simulation (O'Sullivan, 2011)

It is advantageous to use DEM for the reason that the objective will be reached at the steady state, consuming the minimum computer effort.

2.3 Numerical simulation by DEM

As stated by Cundall and Hart (1993), the features of numerical simulation of discrete element method that are different from the continuum methods can be as: (1) objects or bodies can have large rotation and large displacement relative to one another; (2) the alteration of relative particle geometrical configurations is the main reason for triggering the interaction forces between particles; (3) the solution scheme is explicit in time (Hart, 1988). All these three features make the DEM well-suited for the analysis of mechanical behavior of

spherical or polyhedral granular particles.

Even for systems which exhibit instability features, the DEM can also be applied without much numerical difficulties. By explicitly choosing each time step for calculation, and when the object is subjected to unbalanced external force, the object will accelerate and move to a new point. If all the forces related to the object are balanced, the object may either move with constant velocity or stay at rest.

In a DEM simulation, one important process is called *contact detection*, which focuses on the detection and categorization of contacts between particles close to each other in order to determine the interaction. This is a relatively time-consuming process given that there may be a large number of particles, and it could be very computationally expensive. Thus, it is crucial to eliminate those pairs of discrete elements that are not in contact (Munjiza, 2004). In other words, this process is aimed at decreasing CPU requirements and eliminating calculation times by avoiding the computer to process those pairs of particles that cannot be in contact. In general, the process of *contact detection* can be divided into two phrases, which are the neighbor searching and geometric solution. Starting with a target particle, the neighbor searching focuses on the detection and identification of objects that are possibly located within a certain distance or in a certain zone around the target particle. Then, by having a neighbor list of these objects, the geometric resolution can be used in order to compare the target particle geometry with those objects on the neighbor list.

Moreover, in order to successfully conduct the simulation by using DEM for granular analysis problems, the problem itself must have the following features. First, it should be specified as a problem related to an assembly of particles, which contain the size distribution and location of particles; second, a clearly specified contact behavior and properties of the material to be analysed; and third, well-defined boundary and initial conditions. After these pre-defined conditions are met, can the set of calculations for detecting the movements of individual particles, the initial equilibrium of displacements and contact forces be found

3 Basic Physical and Mathematical Background of DEM

3.1 Particle motion and numerical solutions

3.1.1 Introduction

Generally, in a DEM analysis, particles are analyzed dynamically or transiently with focus on the dynamic interaction for all contacting particles in the system. During the simulation, particles are created as ideal rigid models, and the connection is simulated as rigid springs for the simulation of interactions. Due to the reason that particles are continuously moving away from each other with the breaking of the connections, then they will be connected with other particles in the same time, which creates a new connection or starts a sliding motion. All these will bring along a change in stiffness and make the analysis non-linear.

Given that the fundamental principles of DEM are directly considering the dynamic equilibrium of each particle in the system, and comparing with those methods covered in the analysis of structural and finite element methods, our discrete elements can be approximately analogous to the degree of freedom as end points of elements in structural analysis, or analogous to nodes used in the finite element method. Then, the general governing equation for the whole system, which, expressing the dynamic equilibrium, can be written in the form as

$$\mathbf{M}\ddot{\mathbf{u}} + \mathbf{C}\dot{\mathbf{u}} + \mathbf{K}(\Delta\mathbf{u}) = \Delta\mathbf{F} \quad (3.1)$$

where \mathbf{M} stands for the inertia matrix, which contains mass and rotational inertia, \mathbf{C} stands for the damping matrix, $\Delta\mathbf{u}$ stands for the incremental displacement vector, which contains translational and rotational displacement, $\Delta\mathbf{F}$ stands for the incremental force vector, \mathbf{K} is referred to as the global stiffness matrix, which mainly depends on the geometry of the

system, and $\dot{\mathbf{u}}$, $\ddot{\mathbf{u}}$ stand for the velocity and acceleration vectors, respectively. For solving this dynamic equilibrium, there are two approaches that could be used; *implicit* and *explicit* approaches.

The *implicit* approach, the most outstanding feature is similar to what is used in a finite element method, which is by creating a single vector \mathbf{u} in order to represent the combined incremental displacements for all the centroids of particles in the system, i.e.

$$\mathbf{u} = \begin{pmatrix} u_x^1 \\ u_y^1 \\ u_z^1 \\ u_x^p \\ u_y^p \\ u_z^p \\ u_x^{N_p} \\ u_y^{N_p} \\ u_z^{N_p} \end{pmatrix} \quad (3.2)$$

where u_x^p , u_y^p , u_z^p are used for indicating, in the three dimension, the incremental translational displacements for one particular particle p in the system of total N_p particles. And in a similar way, the expression for the force vector $\Delta\mathbf{F}$ is constructed, for the whole set of N_p particles. However, the shortcoming of using the implicit method is that during the formulation of stiffness matrix for the whole system, a large amount of resultant equations will be generated because of numerous particles considered, which creates excessive calculation efforts and computational costs for the simulation. It is more popular to use an *explicit* method (Cundal and Strack, 1979) to solve the dynamic equilibrium, which, particularly considering the individual particle's dynamic equilibrium rather than for the global system, thus eliminates the necessity for storing the global stiffness matrix (Potyondy, 2004). According to Zhu et al. (2007), the most general equation describing the translational dynamic equilibrium for a single particle p , having mass m_p can be:

$$m_p \ddot{\mathbf{u}}_p = \sum_{c=1}^{N_{c,p}} \mathbf{F}_{pc}^{\text{con}} + \sum_{j=1}^{N_{nc,p}} \mathbf{F}_{pj}^{\text{non-con}} + \mathbf{F}_p^f + \mathbf{F}_p^g + \mathbf{F}_p^{\text{app}} \quad (3.3)$$

where $\ddot{\mathbf{u}}_p$ represents the acceleration vector of particle p ; $\mathbf{F}_{pc}^{\text{con}}$ represents the contact forces owing to contact c at the time that there are $N_{c,p}$ contacts between particle p and the other particles or the boundaries; similarly, $\mathbf{F}_{pj}^{\text{non-con}}$ represents non-contact forces, the existence of this force can be exemplified by the capillary force in unsaturated soils; \mathbf{F}_p^f , \mathbf{F}_p^g and $\mathbf{F}_p^{\text{app}}$ are fluid interaction forces, gravitational forces and specified applied forces on particle p , respectively.

Besides, the resulting torque for every contact point can be calculated simply by taking a cross-product between the contact force and the vector connecting the contact point to the center of a particle. Also, the dynamic rotational equilibrium will be calculated as:

$$I_p \frac{d\omega_p}{dt} = \sum_{j=1}^{N_{\text{mom}}} M_{pj} \quad (3.4)$$

where I_p is the moment of inertia for particle p , ω_p is the vector of angular velocity, M_{pj} is the moment resulting from the j th moment-transmitting contact forces, which contains the transmitting force from particle p , and N_{mom} is the total number of moment transmitting forces.

3.1.2 Updating particle positions

As stated in Section 1.2, during a DEM simulation, the granular material's deformation keeps changing and results in a continuous alteration of particle position and resultant forces,

then it is necessary to trace the particle position in order to update the contact forces based on the latest particle position. This indicates a most general assumption that the applied forces and torques in Eq. (3.3) and (3.4) are assumed to be known and calculated by applying the translational and rotational accelerations ($\dot{\omega}_p$ and $\ddot{\mathbf{u}}_p$).

Then, after manipulating the forces acting on a particle, the acceleration can be calculated based on dynamic equilibrium by assuming that the translational motion for particle p is isolated, which is given by (O'Sullivan, 2011):

$$\mathbf{m}_p \mathbf{a}_p^t = \mathbf{F}_p^t \quad (3.5)$$

where \mathbf{m}_p is the mass matrix, which will be a 2×2 matrix in two dimensions (as shown below in Eq. 3.6); \mathbf{a}_p^t which also equals to $\ddot{\mathbf{u}}_p^t$ is indicating the acceleration vector at time t , which only takes into consideration the translational degree of freedom that contains two components in two dimensions and three components in three dimensions; and \mathbf{F}_p^t is simply the resultant force vector which also contains two components in two dimensions and three components in three dimensions (O'Sullivan, 2011).

$$\mathbf{m}_p = \begin{pmatrix} m_p & 0 \\ 0 & m_p \end{pmatrix} \quad (3.6)$$

By calculating the values of acceleration, a corresponding incremental displacement can be computed, and then used for updating the particle position by using the first and second derivatives with respect to time, which is known as the *time integration methods*. This method is applied by taking into consideration of a time increment Δt and use it in the calculation between acceleration and velocity vectors for particle p as:

$$\mathbf{a}_p^t = \frac{1}{\Delta t} \left(\mathbf{V}_p^{t+\Delta t/2} - \mathbf{V}_p^{t-\Delta t/2} \right) \quad (3.7)$$

where the $\mathbf{V}_p^{t+\Delta t/2}$ and $\mathbf{V}_p^{t-\Delta t/2}$ are the corresponding velocity vectors at incremental time $t + \Delta t/2$ and $t - \Delta t/2$. By applying Eq. (3.5), the calculation of velocity in three

dimensions at time $t + \Delta t/2$ can be expressed as:

$$\mathbf{V}_p^{t+\Delta t/2} = \mathbf{V}_p^{t-\Delta t/2} + \Delta t \mathbf{m}_p^{-1}(\mathbf{F}_p^t) \quad (3.8)$$

which will be treated as the average velocity over the incremental time interval from t to $t + \Delta t$. Then, the updated position vector $\mathbf{X}_p^{t+\Delta t}$ for particle p can be calculated as:

$$\mathbf{X}_p^{t+\Delta t} = \mathbf{X}_p^t + \Delta t \times \mathbf{V}_p^{t+\Delta t/2} \quad (3.9)$$

which can provide the particle's Cartesian coordinates with three-dimensional rotation about the principal axis.

For two dimensional simulations, the particle's rotational velocities can be computed by taking the dynamic rotational equilibrium equation as:

$$I_{p,z} \dot{\omega}_{p,z} = M_{p,z} \quad (3.10)$$

where $\omega_{p,z}$ is the angular velocity about one specific axis that goes through the center of a particle, and normal to the plane to be analyzed; $I_{p,z}$ stands for the moment of inertia, which is equal to $\frac{\rho \pi r_p^4}{2}$ for a circular or spherical particle p with radius of r and density ρ . Again, by applying the *time integration method*, the incremental solution for the angular velocity over the time interval from $t + \Delta t/2$ to $t - \Delta t/2$ can be calculated as:

$$\omega_{p,z}^{t+\Delta t/2} = \omega_{p,z}^{t-\Delta t/2} + \Delta t \frac{M_{p,z}^t}{I_{p,z}} \quad (3.11)$$

which can be used for the calculation of the tangential forces, as will be seen in further discussions.

3.1.3 Determination of computational time step

Based on the preceding discussion, it can be noted that the estimation of a value for the time step Δt is very important. It will pose significant influence on the calculation for all physical components calculated above. Ideally, the time increment that is chosen should be small enough to control the incremental influences of motion during the simulation for a single particle to its neighboring particles in a certain time step, and in order to maintain the non-linearity property for the whole system. As stated by Cundall and Strack (1978), the basic principle for DEM simulation is that the chosen time step should be small enough such that the propagation of disturbance from a disk (or sphere) will not reach its nearest neighbors.

In the simulation codes, such as the Particle Flow Code (PFC2D and PFC3D), the time step Δt is chosen to be smaller than one of the critical time steps. According to the Particle Flow Code (PFC3D) by Itasca (2003), the general equation for the calculation of critical time step (T_c) will be:

$$T_c = \sqrt{\frac{m_p}{k_{max}}} \quad (3.12)$$

where m_p is the mass of particle p and k_{max} is the maximum contact stiffness for the assembly of granular materials.

During the DEM simulation, it is more conservative to choose a critical time step by taking into consideration a factor of safety. According to the study by O'Sullivan and Bray (2004), the critical time step should be determined as a function of assembly configuration and the total number of contacts for each particle. It is suggested by them that the critical time step for a three-dimensional assembly of granular particles, considering the influence of rotation, should be smaller than $0.221\sqrt{m/k_{max}}$.

After the determination of critical time step, the time step can be simply calculated by multiplying by a user defined coefficient α , which is in essence: $\Delta t = \alpha \cdot T_c$. According to

the default value specified in PFC2D, $\alpha = 0.8$ while for different contact models, the value of α should be carefully chosen.

3.1.4 Damping

Every mechanical system possesses a property that the mechanical energy will gradually dissipate during vibration, and end up with the damping out of the vibration for a vibrating system. This kind of dissipation always occurs due to two causes: by friction and damping.

Generally, for discrete element models, we define friction as either solid friction, dry friction or Coulomb friction that occurs at the contacts in mesoscopic scale between particles (Matuttis and Chen, 2014). Friction takes place during sliding whenever the shear force's absolute value between contacts exceeds the limit point beyond which the relative movements will be encountered. For damping, or lack of which, there will be no yield during the separation of particles and sliding, and the simulation of DEM particles will vibrate constantly, which will result in a highly complex system that all particles are connected by elastic springs. Then it is necessary to introduce an artificial damping during the simulation in order to avoid this non-physical phenomenon, reducing the energy of vibration between particles in a system that is physically stable, and making the assemblies reach faster the state of equilibrium.

3.1.4.1 Mass damping

Based on the proposal of establishing a global damping which “can be envisioned as the effect of dashpots connecting each particle to the ground” by Cundall and Strack (1979a), which means that this damping enables each particle's response to be proportional to their relative mass. During the simulation, this concept is implemented as the following equation (Bardet, 1998):

$$\mathbf{M}\mathbf{a}^t + \mathbf{C}\mathbf{v}^t = \mathbf{F}^t \quad (3.13)$$

where \mathbf{M} and \mathbf{C} represent the mass matrix and damping matrix, respectively; \mathbf{a}^t , \mathbf{v}^t and \mathbf{F}^t are the acceleration vector, velocity vector and the force vector at time t , respectively. And then, by utilizing the Verlet time integration approach, over an incremental time Δt we obtain:

$$\begin{aligned} \mathbf{a}^t &= \frac{1}{\Delta t} (\mathbf{v}^{t+\Delta t/2} - \mathbf{v}^{t-\Delta t/2}) \\ \mathbf{v}^{t+\Delta t/2} &= \frac{1}{\Delta t} (\mathbf{x}^t - \mathbf{x}^{t-\Delta t}) \\ \mathbf{v}^t &= \frac{1}{2} (\mathbf{v}^{t+\Delta t/2} + \mathbf{v}^{t-\Delta t/2}) \end{aligned} \quad (3.14)$$

where \mathbf{x}^t is the displacement vector at time t .

Then, combining Eq. 3.13 and Eq. 3.14, with the assumption that the damping matrix is proportional to the mass matrix with an optimum proportionality constant α , the following general equation, which is equivalent to the dynamic relaxation equation, can be computed (Bardet, 1998):

$$\mathbf{v}^{t+\Delta t/2} = \mathbf{v}^{t-\Delta t/2} \left(\frac{1 - \alpha\Delta t/2}{1 + \alpha\Delta t/2} \right) + \left(\frac{\Delta t}{1 + \alpha\Delta t/2} \right) \mathbf{M}^{-1}(\mathbf{F}^t) \quad (3.15)$$

While, Cundall (1987) stated some limitations about the assumption relating to mass proportional damping such as the optimum proportionality constant α , which largely relates the eigenvalues of the stiffness matrix; and equally applicable for all nodes, which is in fact not true in reality.

3.1.4.2 Local non-viscous damping

Based on the limitations as stated above, an alternative system of damping was proposed by Cundall (1987), which was aimed at making the damping force proportional to the magnitude of the “out-of-balance” force at each node, due to which was the cause of acceleration for each particle. Then, provided by the PFC2D/PFC3D by Itasca (2004, 2008) for achieving the steady-state within a reasonable calculation cycles about this type of damping, the general expression of motion was written as following equation with an addition of damping-force for particle p (F_d^p):

$$F_i^p + F_{d_i}^p = M_i^p a_i^p, \quad i = 1,2,3 \quad (3.16)$$

$$M_i^p a_i^p = \begin{cases} m\ddot{x}_i & i = 1,2 \\ I\dot{\omega}_i & i = 3 \end{cases} \quad (3.17)$$

where i is the indication of dimension; $F_{d_i}^p$ is the damping force, M_i^p and a_i^p are the components of generalized mass and acceleration respectively; and the F_i^p is the resultant or “out-of-balance” force. The following equation will be the specific expression for the damping force of particle p :

$$F_{d_i}^p = -\alpha |F_i^p| \text{sign}(v_i^p), \quad i = 1,2,3 \quad (3.18)$$

where α is the damping constant, which was set to be 0.7 by default (O'Sullivan, 2011), and v_i^p is the velocity vector for particle p that:

$$v_i^p = \begin{cases} \dot{x}_i^p & i = 1,2 \\ \omega_i^p & i = 3 \end{cases} \quad (3.19)$$

and the direction of $F_{d_i}^p$ is opposite to the direction of v_i^p .

The advantage of using this form of damping can be concluded as: 1) only damps the

motion of acceleration, which eliminates the erroneous damping forces during the motion of steady-state; 2) the proportionality constant α for the damping is non-dimensional; 3) the damping will be different among each pair of points in the system, which is more suitable to reality that the system may have variety of behavior for different parts. And thus, applying this type of damping will be much more convenient for simulation and analysis of the steady-state.

3.2 Force-Displacement Laws

3.2.1 Introduction and a brief overview of contact mechanics

During a DEM simulation, particles are interacting with each other, which requires the interaction analysis for those pairs that are in contact and those bodies that are potentially will get in contact. Then, it will be necessary to identify which particles are in contact and so the resulting forces can be determined. These two phases are defined as the *contact detection* and *contact resolution* phases during the simulation (Hogue, 1998). The difficult part is to develop an algorithm for the contact detection stage, which is related to the difficulties on how to keep track those particles that are in contact and identify those particles will potentially get in contact. For a more detailed background and an overview of contact detection codes that are used in DEM simulation, the reader can be referred to the work by Munjiza (2004).

For the contact resolution stage, the contact geometry and kinematics are required to be accurately determined, which will be aided by the implementation of a constitutive model and simplified overlap assumptions.

For the specific calculation of contact forces, which represent the integral of stresses along contact surface, that are being considered into two orthogonal parts, normal and tangential directions with respect to the point of contact. These two forces always are represented by rheological models which comprise of springs, sliders and dashpots, and these rheological models are usually called as *contact constitutive models* (O'Sullivan, 2011).

In the following section, different contact constitutive models will be introduced, which are commonly used during a DEM simulation. While, before the detailed discussion of these models, it is quite necessary to introduce the contact mechanics in reference to the work of Johnson (1985). It was Johnson who has raised the discussions of contact responses between solid bodies, and clearly distinguished contact categories into *conforming* and *non-conforming*. For DEM simulations, it is common to simulate contacts as non-conforming and point contact assumption, due to the widely-used DEM models that employ a simplification of geometry such as spheres or disks. While in reality, the contacting situation is more likely to be a non-conforming contact initially, and will transform into a conforming contact with the yielding of asperities.

Another important phenomenon during contact should be clarified, which is called as *traction* that describes the surface pressure exerted along the contact surface as a result of contact forces. Symbols f_n and f_t are used to express the normal and tangential tractions independently, and the numerical resolution of contact forces in normal and tangential directions can be expressed by integration of these tractions over the contact area A_c as such (Matuttis and Chen, 2014):

$$\begin{aligned} F_n &= \int_{A_c} f_n dA \\ F_t &= \int_{A_c} f_t dA \end{aligned} \tag{3.20}$$

3.2.2 Contact response based on linear elasticity

3.2.2.1 Elastic normal contact response

It is pedagogically common to conduct a linear elastic response assumption for real soils interpreting the real stress distributions, combined with the usage of continuum elasticity analysis for explaining the responses between soil particles. And by applying the elastic theory for two contacting particles, the stress distribution and deformation can be expressed

in algorithms. One of the most outstanding mechanical theories can be attributed to Hertz, who clearly expressed the form for the load-deformation responses for contacting particles by using the assumption that solid bodies are initially contacting at a single point followed by the growth of the contacting area, the subsequent changing of traction forces over the surface, and finally, the constant deformation of surface and the variation of stresses within the particles (O'Sullivan, 2011). By applying this contact mechanics theory, the following assumptions should be obtained in order to fit Hertz's theory:

- The surface of contact should be assumed perfectly smooth, by neglecting the asperities of the surface with frictionless property;
- The area of contact and the strains induced should be assumed to be small enough to maintain the property of elasticity;
- The interaction outside the area that is loaded is assumed to be absent;
- And the friction should not be taken into consideration if the two contacting particles have the same stiffness.

The specific expression of the circular contact response by applying the Hertzian theory for two interacting particles A and B contains the effective particle radius, R^* and the effective Young's modulus, E^* . The expression of these two parameters are provided as:

$$\frac{1}{R^*} = \frac{1}{R_A} + \frac{1}{R_B} \quad (3.21)$$

and

$$\frac{1}{E^*} = \frac{1 - \nu_A^2}{E_A} + \frac{1 - \nu_B^2}{E_B} \quad (3.22)$$

where R_A and R_B are simply the radii, the E_A and E_B are the Young's moduli, and ν_A , ν_B are the Poisson's ratio of particle A and B , respectively.

Furthermore, according to Hertzian's theory, the radius a which represents the contact circle is defined as:

$$a = \left(\frac{3F_n R^*}{4E^*} \right)^{1/3} \quad (3.23)$$

The maximum contact traction (pressure) is defined as:

$$f_n^{max} = \left(\frac{6F_n E^{*2}}{\pi^3 R^{*2}} \right)^{1/3} \quad (3.24)$$

With the definition of normal deformation (δ) at the contact point as:

$$\delta = \left(\frac{9F_n^2}{16R^* E^{*2}} \right)^{1/3} \quad (3.25)$$

3.2.2.2 Elastic tangential contact response

With respect to the tangential contact response, some of the most fundamental and essential models used in DEM simulations can be attributed to Mindlin (1949) and Mindlin and Deresiewicz (1953). The most essential assumption for these models is that the tangential traction is assumed to pose no influence on the normal traction distribution, which will be valid as long as the two contacting spheres have the same elastic properties. Mindlin (1949) also stated that if during the contact the normal force is not changing, and with the application of tangential force, two different result areas can be observed. One is named as the “slip” region over some portion of the contact area, and the remaining area can be named as the “stick” region, over which there will be no relative movement.

According to the friction laws proposed by Amontons and Coulomb (O'Sullivan, 2011), the normal and tangential tractions are sharing the following relationship over the slip region, as:

$$f_t(r) = \mu f_n(r) \quad (3.26)$$

where, r stands as the distance from the center of the contacting circular area to the contact surface, as long as the normal contact condition fits within the Hertzian contact laws; and f_t , f_n are the tangential and normal tractions, respectively.

3.2.2.3 Initial tangential loading

In the initial stage, the tangential force at the contact is assumed to experience an increase of force from 0 to F_t , subjected to the constant normal force F_n . The following equations are given for defining the tangential traction at a point having distance r to the center of the contact area:

$$\begin{aligned} f_t(r) &= \frac{3\mu F_n}{2\pi a^3} \sqrt{a^2 - r^2}, & b \leq r \leq a \\ f_t(r) &= \frac{3\mu F_n}{2\pi a^3} (\sqrt{a^2 - r^2} - \sqrt{b^2 - r^2}), & 0 \leq r \leq b \end{aligned} \quad (3.27)$$

where, b stands for the radius of the stick region, a stands for the radius of the contact area. According to Mindlin (1949), the tangential displacement between two contacting particles (A and B) can be described as:

$$\delta_t = \frac{3\mu F_n}{16G^* a} \left(1 - \frac{b^2}{a^2}\right) \quad (3.28)$$

where

$$\frac{1}{G^*} = \frac{2 - \nu_A}{G_A} + \frac{2 - \nu_B}{G_B} \quad (3.29)$$

in which the G_A and G_B stand for the shear moduli of the contacting particles A and B , respectively. And thus, the resulting tangential force can be calculated as:

$$F_t = 2\pi \int_0^a f_t(r) r dr = \mu F_n \left(1 - \frac{b^3}{a^3}\right) \quad (3.30)$$

3.2.2.4 Unloading (reversal of tangential force)

Given that the property of the slip process is dissipative, then if the loading condition is reversed, the slip region ends up with three different areas: one without slip, one with slip and another one remaining in counter slip condition. Then, according to Thornton (1999), the tangential traction force distribution over the contact surface can be defined as:

$$\begin{aligned}
 f_t(r) &= -\frac{3\mu F_n}{2\pi a^3} \sqrt{a^2 - r^2}, & c \leq r \leq a \\
 f_t(r) &= -\frac{3\mu F_n}{2\pi a^3} \left(\sqrt{a^2 - r^2} - \sqrt{c^2 - r^2} \right), & b \leq r \leq c \\
 f_t(r) &= -\frac{3\mu F_n}{2\pi a^3} \left(\sqrt{a^2 - r^2} - 2\sqrt{c^2 - r^2} + \sqrt{b^2 - r^2} \right), & 0 \leq r \leq b
 \end{aligned} \tag{3.31}$$

and the corresponding tangential force can then be calculated as the integral of Eq. 2.31, as:

$$F_t = \mu F_n \left[1 - \left(\frac{b}{a} \right)^3 \right] - 2\mu F_n \left(\frac{c}{a} \right)^3 \tag{3.32}$$

3.2.3 Normal force-displacement models in DEM

3.2.3.1 Linear elastic contact springs

The simplest model for simulating the normal direction force-displacement response in DEM is the linear elastic spring, which, using a normal force F_n can be calculated as:

$$F_n = K_n \delta_n \tag{3.33}$$

where K_n stands for the normal directional contact stiffness (e.g. N/mm), δ_n stands for the normal overlap depth for the two contacting particles (mm). And the spring stiffness can be separately expressed for two contacting particles A and B as k_n^A, k_n^B and k_t^A, k_t^B in normal and tangential directions, respectively. Then the effective normal stiffness in normal

and tangential directions at the contact point can be expressed as:

$$\begin{aligned}
 K_n^{\text{contact}} &= \frac{k_n^A k_n^B}{k_n^A + k_n^B} \\
 K_t^{\text{contact}} &= \frac{k_t^A k_t^B}{k_t^A + k_t^B}
 \end{aligned}
 \tag{3.34}$$

What should be noticed for using this simple linear elastic model is that it cannot fully describe the complexity of the properties for the contacting materials, and thus the spring should be treated as “penalty springs” which will be used for the minimizing of overlap at the contact point (O'Sullivan, 2011).

3.2.3.2 Simplified Hertzian contact model

In order to compensate the non-physical character of the stiffness in the linear elastic model, some other models were developed by applying the Hertzian theory, which were aimed at connecting the material properties of particles to the parameter of the spring that is defined in a model. And then the stiffness in the normal contact direction can be defined combining the Hertzian contact model as:

$$K_n = \left(\frac{2\langle G \rangle \sqrt{2\tilde{R}}}{3(1 - \langle \nu \rangle)} \right) \sqrt{\delta_n}
 \tag{3.35}$$

The contact force in the normal direction is the same as Eq.3.33. And for sphere *A* contacting with sphere *B* condition, the \tilde{R} , $\langle G \rangle$ and $\langle \nu \rangle$ can be expressed as:

$$\begin{aligned}
 \tilde{R} &= \frac{2R_A R_B}{R_A + R_B} \\
 \langle G \rangle &= \frac{1}{2} (G_A + G_B)
 \end{aligned}
 \tag{3.36}$$

$$\langle \nu \rangle = \frac{1}{2} (\nu_A + \nu_B)$$

where R is the radius of the spherical particle, ν is the Poisson's ratio and G is the elastic shear modulus. If the contact condition is a sphere contacting with a boundary, then:

$$\begin{aligned} \tilde{R} &= R_{sphere} \\ \langle G \rangle &= G_{sphere} \\ \langle \nu \rangle &= \nu_{sphere} \end{aligned} \tag{3.37}$$

3.2.3.3 Yield inclusive normal contact models

3.2.3.3.1 Walton-Braun linear model

Instead of considering that the conservative characteristic, i.e. energy stored during the loading process, will equal to the energy released during unloading, as held by applying the elastic contact model, Walton and Braun (1986) proposed an energy dissipative linear contact model which was assumed that it is non-conservative for particle interactions. The normal force during the first loading is therefore can be defined as:

$$F_n = K_{1,n} \delta_n \tag{3.38}$$

and the normal force over the process of unloading will be:

$$F_n = K_{2,n} (\delta_n - \delta_{n,p}) \tag{3.39}$$

where δ_n is the normal directional overlap relative to the contact point, $\delta_{n,p}$ is defined as the plastic deformation which can be described as a function of the maximum historical

normal force, $F_{n,max}$. For the stiffness over the unloading process, $K_{2,n}$ will be larger than the stiffness at the first loading stage, and the value should be carefully evaluated which will be either user-defined or calculated as a function of the maximum historical normal force. The graphical illustration of the Walton-Braun linear model can be referred to the following figure as used in the PFC codes:

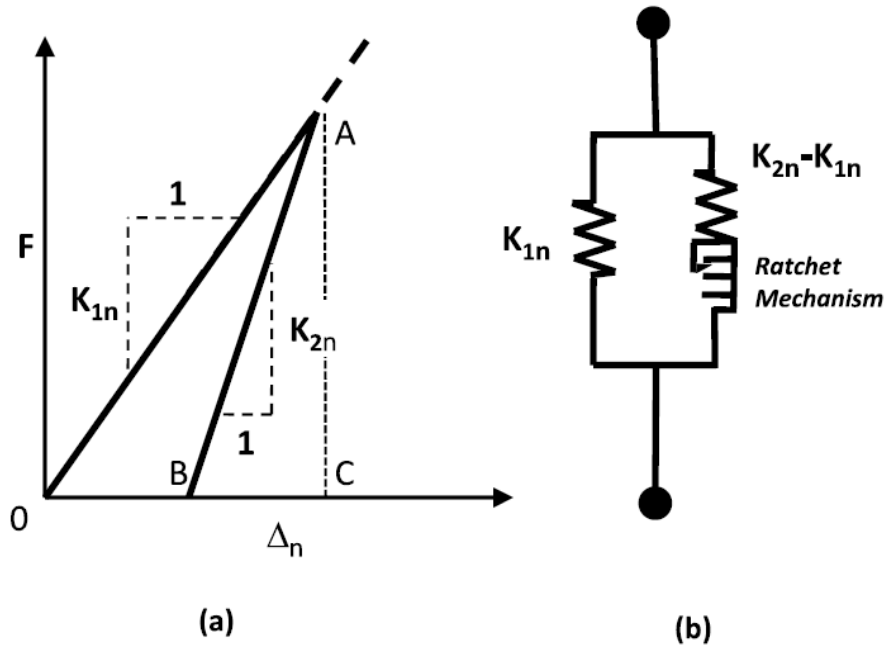


Figure 3.1. Walton-Braun linear contact model illustration (O'Sullivan, 2011)

Another specification that needs to be mentioned is the coefficient of *restitution*, e , which can be used for the quantification of the loss of energy during collision between two particles, and will be calculated by using the relative velocities of these two particles before and after collision. To be specific, the following equation is the expression for restitution coefficient, e , by considering two particles A and B :

$$e = \frac{v_n'^B - v_n'^A}{v_n^B - v_n^A} \quad (23.40)$$

where v_n^A and v_n^B are the normal directional velocities before collision, and $v_n'^A$, $v_n'^B$ are the velocities after collision for particle A and B , respectively.

3.2.3.3.2 Spring-dashpot model

The main characteristic of using a spring-dashpot model is the implementation of a dissipative viscous dashpot at the point of contact in order to simulate the dissipation of energy caused by the plastic deformation (O'Sullivan, 2011). The force-deformation relationship is similar to the Kelvin rheological model, and the formulation can be stated as:

$$F_n = K_n \delta_n + C_n \dot{\delta}_n \quad (3.41)$$

where C_n is the dissipative term, the other parameters are the same as already defined in previous sections.

While, Delaney et al. (2007) raised another argument that the dissipation of energy should be dependent on the velocity, and they proposed an alternative formula that implemented the Hertzian-type non-linear spring in the simulation; and thus the expression of the contact force will be:

$$F_n = K_n \delta_n^{3/2} + C_n^* \dot{\delta}_n \delta_n^{3/2} \quad (3.42)$$

where C_n^* stands for the modified term of dissipation.

3.2.4 Tangential force-displacement models in DEM

3.2.4.1 Introduction

Physically, the term “tangential force” is used for indicating the component of force that is exerted along the contact surface, which will usually be orthogonal to the normal direction of

contact. Then, it is required to develop tangential contact models which are available to simulate the particle responses before gross sliding takes place, also simulating the responses when sliding occurs. By assuming the yielding is in the model of Coulomb friction, the coefficient of friction, μ ($0 \leq \mu \leq 1$), is then used to represent the relationship between a normal force F_n and tangential force F_t . When $|F_t| < \mu F_n$, the contact condition is named as “stuck”, which means that there will be no relative movement observed between the two contacting particles, and when $|F_t| = \mu F_n$, relative sliding can be observed and the tangential force will be acting in the opposite direction to the slipping direction.

During the simulation, the cumulative tangential contact displacement is assumed to be zero at the moment that the contact is detected. And during the “stuck” stage of the contact, the contact force will be calculated as the product of the tangential spring stiffness and the tangent directional cumulative displacement (total of the relative incremental displacements for the interacting particles). For an ideal contact model that is cohesionless, the tangential force will be calculated as:

$$F_t = -\min\left(|\mu F_n|, F_t(\delta_t, \dot{\delta}_t)\right) \frac{\dot{\delta}_t}{|\dot{\delta}_t|} \quad (3.43)$$

where $F_t(\delta_t, \dot{\delta}_t)$ represents the shear force prior to sliding, and is calculated by computing the contact constitutive model; δ_t represents the cumulative relative deformations, and $\dot{\delta}_t$ is the relative velocity at the contact point.

Due to the complexity of the nature of contact, it is difficult to precisely estimate the coefficient of friction, and to fully understand the response of a contact in the tangential direction. The commonly used model for the simulation is to make the assumption that the tangential contact forces and the cumulative tangential displacement have linear relationship prior to sliding occurring. Thus, the pre-sliding shear force can be calculated as:

$$F_t(\delta_t, \dot{\delta}_t) = K_t \int_{t_c^0}^t \dot{\delta}_t dt \approx K_t \sum_{t_c^0}^t \dot{\delta}_t \Delta t \quad (3.44)$$

where K_t is the stiffness of the linear spring representing the linear relationship as mentioned, t_c^0 is the point in time that the contact of two particles are initially detected, and the integration of the relative velocities $\dot{\delta}_t$ is for calculating the cumulative displacements. And when sliding occurs, the following formula can be used to calculate the tangential force:

$$F_t = |\mu F_n| \frac{F'_t}{|F'_t|} \quad (3.45)$$

where F'_t is the component that is calculated by using Eq. 2.44.

3.2.4.1.1 Calculation of tangential velocities, $\dot{\delta}_t$

The calculation of the tangential relative velocity can be referred to Itasca (2004) in two-dimensional analysis, which is defined as (for particle a relative to particle b):

$$\dot{\delta}_t = (v_i^B - v_i^A)t_i - \omega_z^B |x_i^C - x_i^A| - \omega_z^A |x_i^C - x_i^B| \quad (3.46)$$

where t_i stands for the unit vector which indicates the unit vector tangential to the contact, v_i^A and v_i^B are indicating the translational velocities for particle A and B , x_i^A and x_i^B are the positions of the centroids of particle A and B , x_i^C is standing for the contact coordinates, and ω_z^A , ω_z^B are the rotational velocities about the axes through the centroids.

For three-dimensional case, first the relative velocity at the contact point should be evaluated as (Itasca, 2008):

$$\dot{\delta}_i = [v_i^B + e_{ijk}\omega_j^B(x_k^C - x_k^B)] - [v_i^A + e_{ijk}\omega_j^A(x_k^C - x_k^A)] \quad (3.47)$$

where e_{ijk} is the alternating tensor, and then, by subtracting the component of relative velocity in normal direction, the tangential relative velocity can be calculated as:

$$\begin{aligned}\delta_i^t &= \dot{\delta}_i - \delta_i^n \\ \delta_i^t &= \dot{\delta}_i - \dot{\delta}_j n_j n_i\end{aligned}\tag{3.48}$$

3.2.4.2 Mindlin-Deresiewicz tangential models

As developed by Mindlin and Deresiewicz (1953), the specification of the stiffness of a tangential contact spring, the following factors should be considered, as: the current load in tangential direction, the current load in normal direction, the load history and the loading condition of the tangential load (whether it is increasing or decreasing). The following two models are proposed by Vu-Quoc et al. (2000) and Thornton and Yin (1991) by using constitutive models during contact, also taking the load history influences into the consideration to retain the tangential load response.

3.2.4.2.1 Vu-Quoc model

According to Vu-Quoc et al. (2000), the tangential force can be calculated by using their model, which is a simplified expression of the Mindlin-Deresiewicz model, as:

$$F_s^{t+dt} = F_s^t + K_{s,t} \delta_s\tag{3.49}$$

where the tangential force is calculated at time $t + dt$ as F_s^{t+dt} , and $K_{s,t}$ stands for the tangential stiffness at time t , which is calculated as:

$$K_{s,t} = \begin{cases} K_{s,0} \left(1 - \frac{F_s^t - F_s^*}{\mu F_n^t - F_s^*} \right)^{1/3} & F_s \text{ increase} \\ K_{s,0} \left(1 - \frac{F_s^* - F_s^t}{\mu F_n^t + F_s^*} \right)^{1/3} & F_s \text{ decrease} \end{cases} \quad (3.50)$$

where $K_{s,0}$ stands for the initial tangential stiffness, and μ is the friction coefficient. And, at the last turning point, the tangential force is presented by F_s^* , which means that when the magnitude of the tangential force changes from increasing to decreasing, or in the opposite way, the value of F_s^* is subsequently set to the value of the tangential force. For a virgin loading, the magnitude of F_s^* is set to be zero (Vu-Quoc et al., 2007).

3.2.4.2.2 Thornton and Yin model

Another model that focuses on the oblique contact and simulates the interaction was proposed by Thornton and Yin (1991), which was developed based on the previous experimental work by Mindlin and Deresiewicz (1953). The model also contains the analysis of the impact of particle adhesion, while we only focus on the implementation without adhesion here and the normal force will be calculated by using Hertzian's theory during the modelling. The relationship of the tangential force (F_t) and displacement (δ_t) can be illustrated in the following figure for a normal force pattern as load-unload-reload cycle:

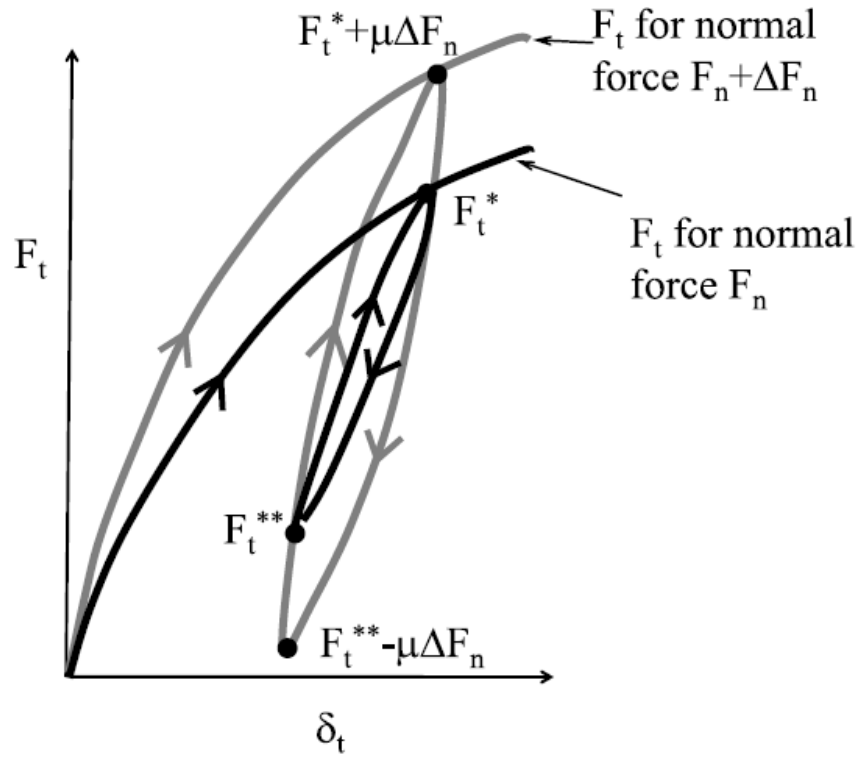


Figure 3.2. Thornton and Yin (1991) model of the tangential force, which has oblique contact and with no adhesion (O'Sullivan, 2011)

The tangential stiffness is defined as:

$$K_t = 8G^* \theta \delta_n \pm \mu(1 - \theta) \frac{\Delta F_n}{\Delta \delta_t} \quad (3.51)$$

where during an unloading process, the negative sign is to be used. And for a two particle contact (e.g. particle *A* and *B*), G^* which is the Young's modulus is the same as Eq. 3.29 in Section 3.2.2.2. Also, δ_n is the displacement in normal direction and the parameter θ is calculated as:

$$\theta^3 = 1 - \frac{F_t + \mu \Delta F_n}{\mu \Delta F_n} \quad (\text{loading process}) \quad (3.52)$$

$$\theta^3 = 1 - \frac{F_t^* - F_t + 2\mu\Delta F_n}{2\mu\Delta F_n} \quad (\text{unloading process})$$

$$\theta^3 = 1 - \frac{F_t - F_t^{**} + 2\mu\Delta F_n}{2\mu\Delta F_n} \quad (\text{reloading process})$$

where F_t^* and F_t^{**} are indicating the reversal point of loading as illustrated in Fig. 3.2.

3.3 The Combined FEM/DEM method

3.3.1 Introduction

In the previous sections, the discrete element method (DEM) has been introduced, with the emphasis focused on discontinuous problems, as pioneered by Cundall and Strack (1979). While in the following discussions, an alternative, or a complementary method will be introduced, the so-called *combined finite-discrete element method* (FEM/DEM), which was pioneered by Munjiza et al.(1995).

The necessity of using the FEM/DEM method in a simulation can be comprehensively interpreted by the problem that is called the *flexible container problem* (Munjiza, 2004). As discussed by Munjiza (2004), the different performance for variable mixture types of particle distributions in a container, the results are concluding that the deformability (elastic properties) of the container and each individual particles are posing considerable influences on the performance of particles' movements and arrangements inside a container. Considering that the changes of the shape and size for each particle will be a problem of finite strain elasticity, then the deformability of each particle is then represented by a continuum-based model. While the interaction among particles and the interaction between the container and particles is well represented by discontinuum-based model. Thus, the *flexible container problem* provides us with a good illustration of the advantages of using both the finite element method for modelling the continuum-based phenomena and the discrete element method for modelling the discontinuum-based phenomena, which is termed as *the combined*

finite-discrete element method (FEM/DEM) (Munjiza, 2004).

The major difference between the FEM/DEM and the DEM is the application of finite element discretization, which discretizes the interior of domains that are in contact, and thus the contact solutions are implemented for contact detection and interaction (Munjiza et al., 1997). Specifically, the discretization enables the individual particles to be represented by single discrete elements that interact with each other when in close proximity. Meanwhile, each discrete element will be discretized into finite elements, and possess their own finite element mesh, which can be shown on Fig. 3.3. The sum of the employed finite element meshes is equal to the sum of the discrete elements, and each mesh employed possesses the deformability of a single discrete element (Munjiza, 2004). In addition, the contact force and inter-penetration between particles are well controlled by utilizing a penalty function.

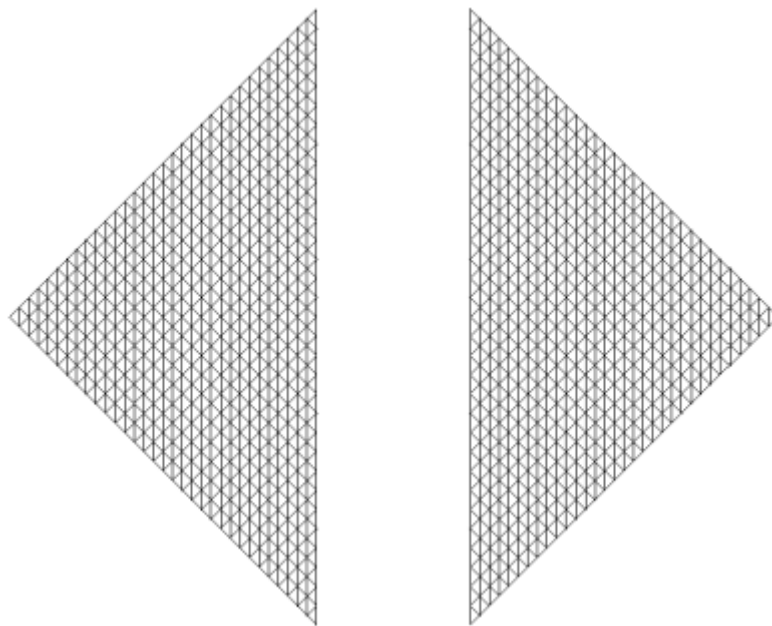


Figure 3.3. The FEM/DEM problem containing two discrete elements, which are discretized into finite elements (Munjiza, 2004).

3.3.2 General considerations of Combined FEM/DEM

The FEM/DEM (Munjiza, 2004), which is the abbreviation of the combined finite-discrete element method, is an advanced and novel numerical method that aims at those problems that

take the combination of both continuum and discontinuum properties for solids into consideration, and for those problems that contain transient dynamics of systems which are comprised by numerous deformable bodies.

In the simulation that uses this method, deformability is represented by using continuum formulation (FEM) for particles, while discontinuum format (DEM) will be applied for the motion and interaction among particles. As discussed in previous sections, the motion and interaction between particles in the DEM simulation is governed by the Newton's Second Law, while the FEM is implemented for stress and deformation analysis of each discrete element.

In the following section, the evaluation of the contact force for the FEM/DEM will be discussed. By considering the gradients of the corresponding potential functions of a quantity for two interacting discrete elements (corresponding potentials over the overlapping area), and combining with the application of FEM, the contact forces will be evaluated for 2D and 3D.

3.3.3 Contact force evaluation

As discussed by Munjiza (2004), who developed the contact force evaluation process, that it is based on a contacting model composed of two discrete elements, and expressed the distribution of contact force. During the contact stage, one element is denoted as the *contactor* and the other element is denoted as the *target* (Munjiza, 2004). During a contact, the overlapping area between the contactor and target is denoted as S , which is bounded by a boundary Γ . The detailed illustration can be referred to the following figure as:

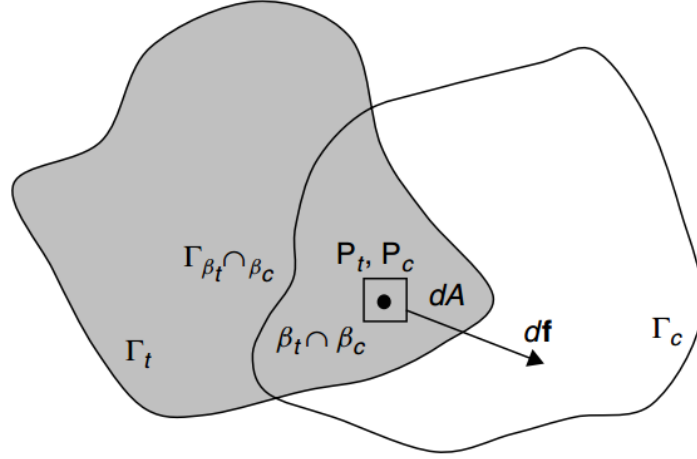


Figure 3.4. An illustration of infinitesimal overlap about points P_c and P_t , and the resultant contact force (Munjiza, 2004).

In 2D, it is assumed that the contact force that is resulting from the penetration of any elemental area dA of the contactor into the target will be calculated as:

$$df_t = -grad\varphi_t(P_t)dA \quad (3.53a)$$

and, similarly, the resulted infinitesimal contact force from the target penetrating the contactor will be:

$$df_c = grad\varphi_c(P_c)dA \quad (3.53b)$$

where the P_t , P_c are points belong to target and contactor, respectively (as shown in Figure. 3.4), $grad$ indicates the gradient of corresponding potential functions, and φ_t , φ_c stand for force potentials on the target and contactor element, respectively.

According to Munjiza (2004), it is recommended to multiply the previous two infinitesimal forces (Eq. (3.53a) and Eq. (3.53b)) by a penalty parameter, E_p which also equals to p , as defined by Munjiza. The penalty parameter is used for controlling and limiting the penetration between elements. It can be selected based on a function that is proportional to the modulus of elasticity, E , as:

$$p = \alpha E \quad (3.54)$$

where α stands for a user defined coefficient. Then, the contribution of the allowed

penetration d to the displacement field u can be calculated as:

$$d = \frac{u}{\alpha} \quad (3.55)$$

In this way, the error in the displacements can be easily controlled by setting reasonable penalty p (Munjiza, 2004).

Thus, the total of infinitesimal contact force can be described as:

$$df = E_p [grad\varphi_c(P_c) - grad\varphi_t(P_t)]dA \quad (3.56)$$

If we take the integral of Eq. (3.4) over the overlapping area S between the contactor and target element, then the total of contact force yields:

$$f = E_p \int_{S=\beta_t \cap \beta_c} [grad\varphi_c - grad\varphi_t] dA \quad (3.57)$$

which also equals to the integration over the boundary of the overlapping area Γ

$$f = E_p \oint_{\Gamma_{\beta_t \cap \beta_c}} n \Gamma(\varphi_c - \varphi_t) dA \quad (3.58)$$

where n is the outward unit normal perpendicular to the boundary of the overlapping area, $\beta_t \cap \beta_c$ equals to the overlapping area S , as can be seen in Figure. 3.54, and other parameters are the same as defined previously.

As for the force potential φ in 2D calculation over the contactor triangle for linear triangular element, there are many different methods can be used, as mentioned by Munjiza et al. (2011). For any discrete element, the potential should be constant on the boundary, and this constraint is satisfied if the following requirement is met: the potential should be constant on the boundaries of the finite element (Munjiza, 2004). Based on the requirement, the following equation can be used for calculating the potential φ at point P inside the triangular element, as:

$$\varphi(P) = \min\{3A_1/A, 3A_2/A, 3A_3/A\} \quad (3.59)$$

where $A_i (i = 1,2,3)$ stands for the corresponding sub-triangles, as shown in Figure 3.5.

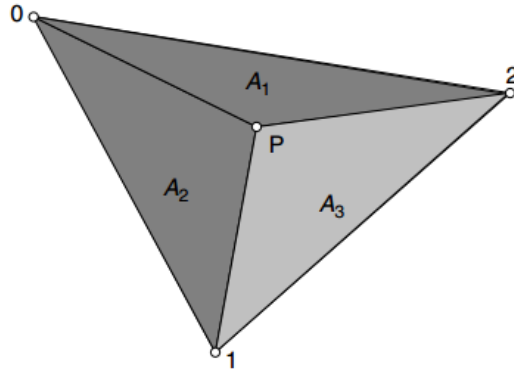


Figure 3.5. The potential at any point P on a triangular finite element (Munjiza, 2004)

Besides, in the FEM/DEM programming, Munjiza et al. (2011) defined that the contact force can be calculated in the FEM/DEM code as:

$$f = E_p \varphi(P_G) S \quad (3.60)$$

where $\varphi(P_G)$ stands for the potential of Gauss point, which is the same as expressed in Eq. (3.59); and S is the same as defined previously.

In 3D, instead of considering the overlapping area S , the total contact force is calculated based on the overlapping volume V , as:

$$f = E_p \int_V [grad\varphi_c - grad\varphi_t] dV \quad (3.61)$$

and the potential is expressed over the tetrahedron, which can be illustrated in Figure 3.6:

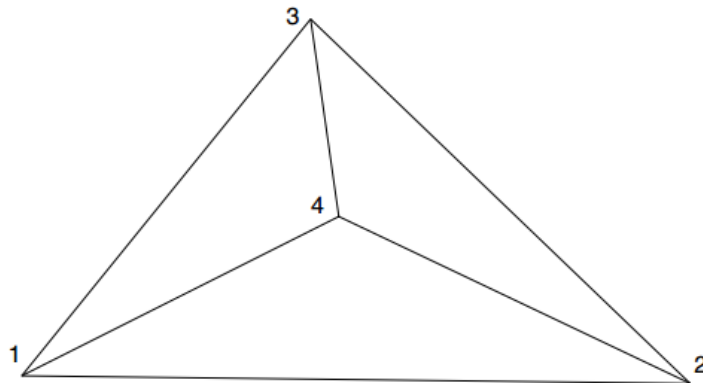


Figure 3.6. Potential definition over domain of a single tetrahedron (Munjiza, 2004)

By using the tetrahedron model, the coordinates of the centroid of the tetrahedron can be calculated, which can provide us four sub-tetrahedra. For any point \mathbf{p} in the sub-tetrahedra ($i - j - k - l$), the potential φ is defined as:

$$\varphi(\mathbf{p}) = k \left(\frac{V_{i-j-k-p}}{4V_{i-j-k-l}} \right) \quad (3.62)$$

where k stands for the penalty parameter, $V_{i-j-k-l}$ is the volume of the tetrahedron $i - j - k - l$, while $V_{i-j-k-p}$ stands for the volume of the sub-tetrahedron $i - j - k - p$. For more detailed analysis about how to calculate the coordinates of the centroid of the tetrahedron, the reader can be referred to the work by Munjiza (2004).

4 Simulation of Particle Contacts Using the Combined FEM/DEM

This chapter, the simulation process will be introduced by using a program that implements the Combined Finite Element Method and the Discrete Element Method (FEM/DEM) (Munjiza, 2004), together with several additional programs that help the pre-simulation and post-simulation process.

The simulation process is divided into two phases; first phase is the simulation of particle samples (discretized into different number of elements) colliding with a solid block; and the second phase is the simulation of 10 particles colliding with each other and a container. After the discussion of simulation process, simulation results will be discussed and concluded.

During the two simulation phases, all particles and simulation targets for particles (the solid block for phase 1 and the container for phase 2) have been set with the property of concrete. These properties includes: 1) Density: 2340 kg/m^3 ; 2) Young's modulus: 17 Gpa; 3) Poisson's ratio: 0.20.

4.1 Obtaining 3D particle geometry using 3D scanning

The simulation has used fifty rock samples in total for contact analysis (contact between each individual rock sample and a solid block), and the reason for using fifty rock samples is by taking into consideration a reasonable statistical representation of particle size and shape distributions. All particle samples have been scanned into 3D models and saved as triangulated geometry (.obj file format). The scanning equipment that has been used was a NextEngine 3D Laser Scanner (NextEngine Inc., 2014), with the 3D Scanner Ultra HD software. This product has a relatively high quality of scanning resolution, and the scanned sample detail that's been captured can be up to 100 micron precision (NextEngine Inc., 2014).

The detailed specification of the scanner is provided by NextEngine and it is listed in the tables below (NextEngine Inc., 2014):

ARCHITECTURE	
Measurement System	NextEngine Patented MultiStripe Laser Triangulation (MLT) technology.
Source	Twin arrays of four, Class 1M, 10 mW solid-state lasers with custom optics, 650 nm wavelength.
Sensor	Twin 5.0 Megapixel CMOS image sensors.
Photo Surface	Optically synchronous 7-color surface capture for precision-locked geometry correlation.
Photo Lighting	Built-in spatially diverse LED white-light texture illuminators with wide color gamut.
AutoDrive™	High-precision rotary servo positioner, auto-incremented under scanner control. 20lb capacity.
PartGripper™	Universal part holder to adjust height, angle, and orientation of capture. 10 lb capacity.

Table 4.1. Architectural features of the NextEngine 3D Scanner (NextEngine Inc., 2014)

SOFTWARE	
ScanStudio™	Software to scan, Align, Polish, and Fuse 3D models. High-performance OpenGL 3D viewer.
Format Options	Scan data can be output as mesh file formats: STL, OBJ, VRML, XYZ, and PLY files.
File Size	200MB for typical model, based on 10-facet scans.
Modeling Tools	Assemble views into a model conveniently with built-in Smart Alignment and trim tools.
ScanStudio™	Points-to-Mesh solution. Drives scanner and builds 3D mesh models.

Table 4.2. General software features of NextEngine 3D Scanner (NextEngine Inc., 2014)

PERFORMANCE	
Object Size	No preset limit. Object larger than field can be composed-captured with supplied software.
Field Size	5.1" × 3.8" (Macro) and 13.5" × 10.1" (Wide). ("Soda can" and "shoebox" sizes, respectively.)
Capture Density	Capture density on target surface is up to 268K points/in ² (Macro) and 29K points/in ² (Wide).
Texture Density	500DPI on target surface in Macro Mode and 200DPI in Wide Mode.
Dimensional Accuracy	±100 micron in Macro Mode and ±300 micron in Wide Mode.
Acquisition Speed	50,000 processed points/sec throughput. Typically, 2 minutes per scan of each facet.
Typical Datasets	Typical small models are a quarter-million points, after oversampling and optimization.
Environmental	Desktop use under ordinary office lighting. No darkroom or special backgrounds required.

Table 4.3. Performance features of the NextEngine 3D Scanner (NextEngine Inc., 2014)

For more detail information for the scanner that is used for scanning particle samples, the reader can be referred to the official website <http://www.nextengine.com/>. (NextEngine Inc., 2014)

4.2 Pre-simulation Process – model generation

4.2.1 The Virtual Geoscience Workbench (VGW)

The experimental and simulation procedure is mainly based on the use of the Virtual Geoscience Workbench (VGW), which is a suite of Open Source Tools workbench for discontinuous modelling based on the combined Finite-Discrete Element Method

(FEM/DEM) (Xiang et al., 2008). The VGW is especially suitable for simulating discontinuous systems like granular, blocky or particulate systems, which is exactly what this thesis is about (the simulation of collision between rock samples and a solid block by using the combined FEM/DEM method).

The VGW is built from several parts, in which there are four main parts that are used in this thesis, together with some other software and programs for data visualization, pre-processing and post-processing.

- 1) The first part of the VGW that's been used is the P3D Virtual Shape Library (Xiang et al., 2008) for loading, saving and extracting particle's digital data that's been pre-scanned, as seen on Fig. 4.1. Once the mesh data is stored in the Virtual Shape Library, the pair of meshes that are going to be simulated can be selected and exported into a .gid file and will be read by the GiD program, which will be introduced later. The detailed information about how to load mesh samples into the Virtual Shape Library, the reader shall download the whole pack of files from the VGW website, and look for the folder "P3D" and find the "note" file inside the folder, then follow the instruction about how to load meshes. Due to the current version of the Virtual Shape Library ability to only record those .mesh files or mesh formats in .gid volumetric meshes, which is specifically required as 10-node tetrahedral (tetrahedral linear/non-linear format), and those particles that's been scanned and stored for this thesis are in triangulated format (3-node triangular mesh), thus, a conversion from 3-node triangular mesh to 10-node quadratic tetrahedral was required. Detailed information for the conversion will be introduced later.

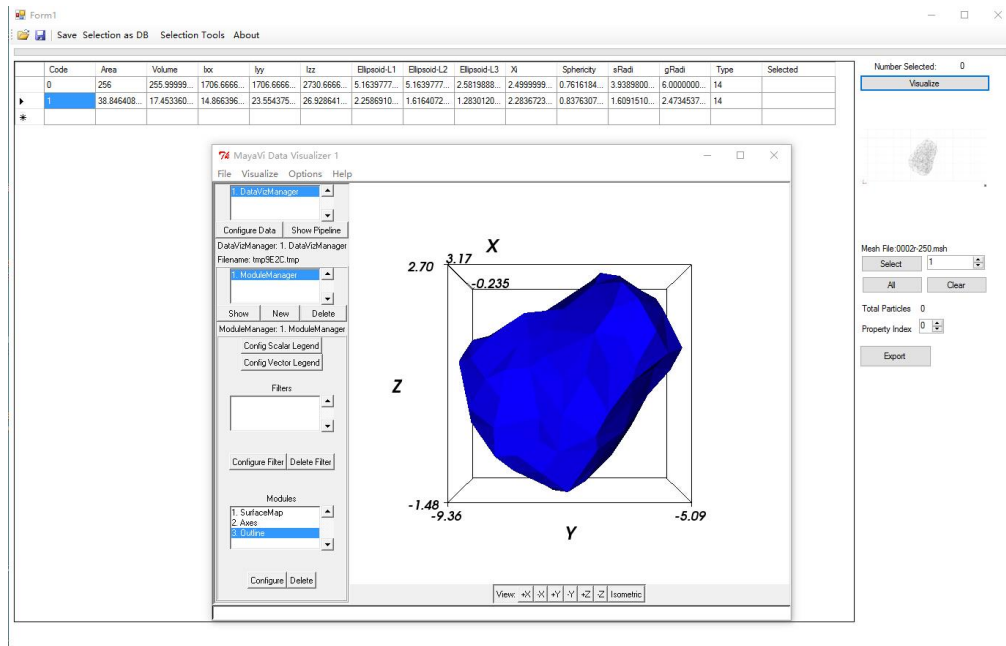


Figure 4.1. Screenshot of the virtual shape library and one rock particle is visualized (by the MayaVi visualizer)

2) The second part that is used for the simulation is the B3D library of boundary conditions (Xiang et al., 2008), which is a folder that contains various tools that are designed to enable the implementation of different boundary condition settings. As recommended by the VGW group, the program GiD is used for customized simulation settings, like the primitive boundary conditions. As instructed by the VGW group, the problem type FEM/DEM should be added into the GiD program, for further instructions, the reader shall be referred to the VGW website for detailed information about the adding process.

Once the problem type has been added to GiD, the mesh pairs (GiD .msh file) that's been exported as introduced in the previous step can be loaded by the GiD program, and the simulation setting process can be further conducted. When the simulation is done, a .B3D file will be generated for each simulation, and for each .B3D file, which contains all the simulation information, will be transmitted through a purposed-built translator GID_B3D to build up all the final input information to the final solver Y3D for the FEM/DEM analysis. A flowchart of this process is shown on Fig. 4.2.

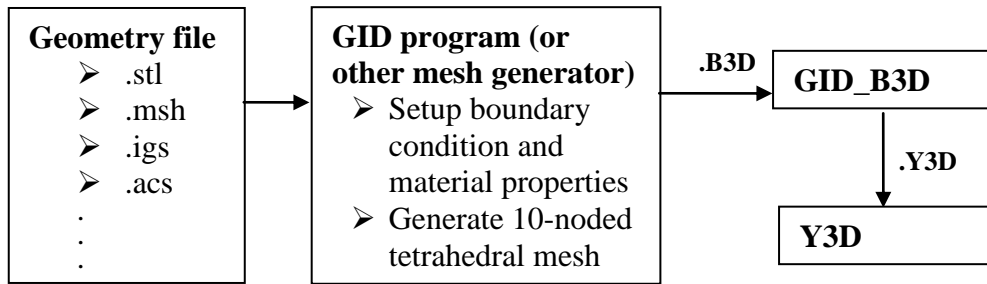


Figure 4.2. Procedure to generate a required input file for the Y3D FEM/DEM solver (Xiang et al., 2008)

- 3) The third main part, which is also the relatively most important part of the VGW is the Y3D FEM/DEM solver. By definition, the Y3D is a C language based, three-dimensional computer program combining the finite-discrete element method developed by Munjiza and Xiang. Y3D is also a solver that can simulate different physical processes (e.g. two-particle collisions and/or multi-body collisions) by using the B3D library of boundary as introduced above (Xiang et al., 2008).

For detailed information about how the Y3D computer program works, and what kind of input file requirements should be satisfied as required to run the Y3D program, the reader should be referred to the manual for the Y3D program written by Xiang et al. (2008).

4.2.2 Supplementary programs for simulation

There are several programs needed as supplementary tools for completing the simulation by supporting the VGW. For pre-simulation, as required by the VGW, the GiD program was used; for mesh resizing and particle statistics collecting purposes, the MeshLab (Cignoni et al., 2008) program was used. Mesh type conversion (from 3-node triangles to 10-node tetrahedra) was done by using both the GiD and the TET_MESH_L2Q (Burkardt, 2009) program.

1. **GiD** is a program, which interacts with the VGW as a graphical user interface for generating the .Y3D files through the GiD_B3D purpose-built translator. For how

to generate mesh file in .msh format that can be loaded by GiD, and for how to assign conditions and running the simulation, user should be referred to the folder named *Moves* in the VGW code files after downloaded. User should follow the instruction during the condition setting process in order to have the simulation run successfully.

2. **MeshLab.** The original 50 meshes of scanned rock pieces that were saved as .obj files, and were stored with all the geometric data, lack real-world dimensions, as shown in MeshLab. For this thesis, the simulation will have each particle to collide with a solid block, which is the size of 8m×8m×4m. Thus a re-sizing process was required to have all the particle sizes correspond to the size of the block, which was done using MeshLab (Filters → Normals, Curvatures and Orientation → Transform: Scale). For this simulation, all particles were scaled by 0.09 relative to their original size. Another reason for applying the re-scaling process is due to the fact that the Y3D program is a high CPU utilizing program (larger the size of a particle, the longer the simulation time will be required).
3. **TET_MESH_L2Q.** As introduced previously, the original mesh files were stored as .obj files with 3-node triangulated surface, while the Virtual Shape Library, that has been used for loading mesh files and exporting meshes into .msh files for simulation usage can only read 10-node tetrahedron files. Then a conversion from 3-node triangulated surface mesh to 10-node tetrahedral mesh was required. For this process, various programs have been tested, such as gmesh and SALOME; or programs based on C language such as Distmesh. However, none of these programs can generate a desired 10-node quadratic tetrahedral mesh directly from the 3-node triangular mesh, because the file formats are different from what is required by the Virtual Shape Library. Thus, another method was chosen by converting those 3-node triangular meshes into 4-node tetrahedra first, and then converting 4-node tetrahedral meshes into 10-node tetrahedral meshes.

Converting 3-node triangular mesh to 4-node tetrahedral mesh can be simply done in the GiD program by applying a GiD code in the command line as “Mescape Meshing MeshFromboundary” and select the closed region formed by

triangles to create tetrahedron inside.

After the creation of 4-node tetrahedral mesh, another program, named as TET_MESH_L2Q, was used for converting the 4-node tetrahedral mesh to 10-node tetrahedral mesh, and it has three versions available in C++, FORTRAN90 and MATLAB under the license of GNU LGPL. For this thesis, a MATLAB version was used.

The TET_MESH_L2Q reads the 3D points' information and 4-node tetrahedral mesh of those points, then creates a quadratic tetrahedral mesh that has the equal number of tetrahedrons as the 4-node tetrahedron. The refinement process is straightforward as each pair of nodes are used for generating a new node located on the average coordinates of the original two nodes that are used. It also takes consideration of the situations such as how to generate a new node exactly once because many tetrahedra might share the same edge, and if the node that is going to be generated has already been created (Burkardt, 2009).

For detailed coding information, reader should be referred to the MATLAB source code which is available for download via the website as shown in the reference (Burkardt, 2009). Reader should follow the examples and tests shown on the website as well to run the program successfully, and generates desired files.

Once the new 10-node quadratic tetrahedrons were generated, they could then be loaded by the Virtual Shape Library, and be extracted as a .msh file that is going to be used by the GiD program for simulation. While, what should be noticed before generating a new tetrahedron is that the order of new nodes created by the TET_MESH_L2Q is different from the required order for quadratic tetrahedron as shown in the manual of GiD (as shown in the following Figure 4.3). If not rearranged, a distorted element will be created, as seen on Figure 4.4.

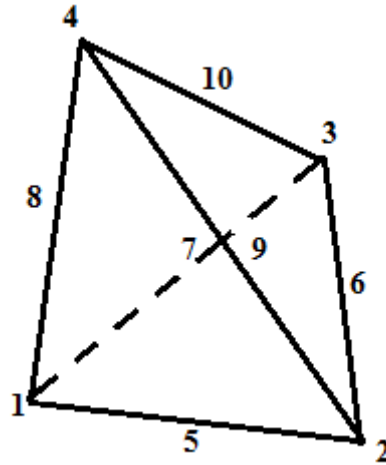


Figure 4.3. Illustration of expected order of element's nodes defined by GiD manual for quadratic tetrahedron (Coll et al. 2016)

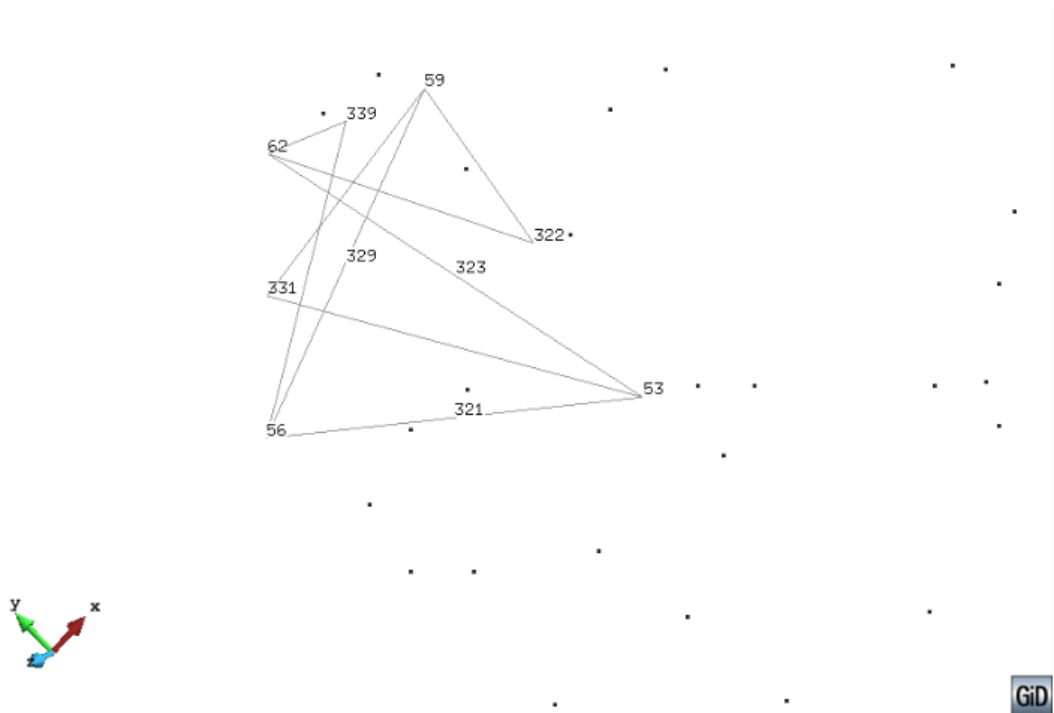


Figure 4.4 Illustration of one element order plotted by the GiD for one of the 10-node tetrahedral mesh generated by the TET_MESH_L2Q.

4.2.3 Particle description

In describing the particle statistics several aspects will be discussed; since the thesis is focused on the effect of variation of particle geometry/surface asperities on the simulation result, it follows that all particles' surface geometry will be changed from full surface detail to almost complete absence of detail. Thus, for the fifty scanned particles, their geometry was simplified (e.g. the number of faces/nodes was reduced) by different amount, and been classified into different groups such as with 100, 250, 500 and 1000 number of faces (or elements). Then several classes of approximate visual judgements and physical measurements were made for presenting particle statistics by the program MeshLab and another supplementary program that's written by my supervisor, Prof. Zsaki.

The geometry simplification process can be achieved by using MeshLab, by loading the mesh and selecting Filters → Remeshing, Simplification and Reconstruction → Quadric Edge Collapse Decimation. Then in the dialog box by entering the desired face number in the 'Target number of faces' input box for completing the simplification process.

The rest of the quantities, as referring to the document (Garcia, 2009) presented by the VGW (Manual-P3D), were also calculated as:

1. Inertia tensor

The Inertia tensor for each particle can be obtained by loading particle mesh in MeshLab then apply the following steps: Filter → Quality Measure and Computations → Compute Geometric Measure.

2. Principal axes of inertia

Can be obtained from the data presented in step 1.

3. Moments of inertia about principal axes I_1 , I_2 and I_3

Can be obtained from the data presented in step 1 (shown as "axes momenta").

4. Aspect Ratio α and particle lengths L , I , S

According to the B3D manual (Garcia, 2009), the extents of particle mesh are computed along the principal axes. Given that $I_1 > I_2 > I_3$ (obtained from step 3), then the three semi-axes of the ellipsoid can be calculated as:

$$\begin{aligned}
 a &= \sqrt{\frac{5}{m}(I_2 + I_3 - I_1)} \\
 b &= \sqrt{\frac{5}{m}(I_1 + I_3 - I_2)} \\
 c &= \sqrt{\frac{5}{m}(I_1 + I_2 - I_3)}
 \end{aligned} \tag{4.1}$$

where m is the mass of the particle, which will be shown in the appendix for obtaining all particle mass information. Then the smallest semi-axes S can be obtained as $S = \min(a, b, c)$, and the greatest one, L can be obtained as $L = \max(a, b, c)$. Then length I will be the intermediate value. Thus, the aspect ratio is calculated as:

$$\alpha = L/S \tag{4.2}$$

5. Gyration Ratio R_g

According to the B3D manual (Garcia, 2009), the gyration ratio R_g is calculated as the greatest distance from the center of mass of the mesh to the surface vertices of the particle. A program *meshgyrratio* (Zsaki, 2015) was used for this purpose, which can compute the R_g value once the center of gravity (required as cg_x , cg_y and cg_z in the program) is provided.

6. Volume V

Can be obtained from the data presented in step 1.

7. Surface Area

Can be obtained from the data presented in step 1.

8. Sphericity ψ

The sphericity ψ can be computed as:

$$\psi = \frac{\sqrt[3]{(36\pi V^2)}}{S} \tag{4.3}$$

where S is referring to surface area from step 7.

9. Equivalent volume sphere radius R_v

The equivalent volume sphere radius is defined as the radius of the sphere that has the equal volume as the mesh, which can be calculated as:

$$R_v = \sqrt[3]{\frac{3V}{4\pi}} \quad (4.4)$$

Once all the quantities are obtained as shown above, a table that contains all these quantities can be presented for each particle. One example is shown below:

Particle statistics (part 1)								
Particle ID	# vertices	# elements	Mass (g)	Moments of Inertia			Volume (cm ³)	Sfc. Area (cm ²)
				I1	I2	I3		
				(gcm ²)	(gcm ²)	(gcm ²)		
1 (100 elements)	52	100	104.371	1439523.1	1302885.7	396195	37.37396	71.32307
1 (250 elements)	127	250	104.371	1554749	1410144.9	419641.65	38.82754	72.71371
1 (500 elements)	252	500	104.371	1574833.9	1428910.6	424177.9	39.06975	73.52756
1 (1000 elements)	502	1000	104.371	1584457.5	1437565.5	425222.65	39.14609	74.00485

Table 4.4 Particle statistics for Particle 1– part 1

Particle Statistics (part 2)							
Particle ID	α	R_g (cm)	ψ	R_v (cm)	L (cm)	I (cm)	S (cm)
1 (100 elements)	3.00654	4.00290	0.75794	2.07409	335.25779	159.76822	111.50952
1 (250 elements)	3.04207	4.01520	0.76260	2.10063	349.18895	164.41038	114.78657
1 (500 elements)	3.04475	4.01709	0.75729	2.10499	351.53490	165.26126	115.45593
1 (1000 elements)	3.05449	4.01359	0.75338	2.10636	352.70723	165.55283	115.47171

Table 4.5 Particle statistics for Particle 1– part 2

4.3 Post-simulation process

For the post-simulation process, there were several programs used for presenting the simulation animation and collecting the simulation data. As necessitated by the VGW group, the visualization program MayaVi (Ramachandran, 2007) has been used as a default visualizer. Since the simulation that can only generate *.vtu* files after simulation was complete, while the current version of GiD does not have the capability of processing *.vtu* files, then the program Paraview (Ahrens et al., 2005) was chosen for post-processing the data contained inside those *.vtu* files.

For extracting simulation data contained inside the *.vtu* files, which were generated by the Y3D program, can be simply done in the Paraview (Ahrens et al., 2005). Each simulation will result in a group of *.vtu* files, and the simulation data contained inside these files can be

obtained by loading all the *.vtu* files for one simulation, then click the Save Data option and in the Configure Writer dialogue box, then selecting the Write All Time Steps option. Using this step, the whole data that contained inside the *.vtu* files can be obtained into *.csv* format, which is an editable table that allows the user to make further calculations. For this thesis, which is mainly focusing on the change of contact forces, then after loading the *.vtu* files, the Velocity Vectors and Stress options were unselected, since not needed.

4.4 Discussion of simulation results

4.4.1 Phase 1. - Particle collision with a solid block

The first simulation phase that was conducted focused on a single particle mesh colliding with a solid block with a given preliminary velocity and under the influence of gravity. Although each simulation uses a single, but different, particle, there were a total 200 simulations performed (one for each of the 50 particles at a given mesh resolution, and 4 different resolutions per particle), the results of which will be discussed.

For each simulation, several aspects of the collision results have been collected as a function of the change of the number of mesh elements (particles with 100 mesh elements, particles with 250 mesh elements, particles with 500 mesh elements and particles with 1000 mesh elements), which are: 1) resultant forces during collision for each particle; 2) comparison of impulses for different simulation results; 3) comparison of peak force for different simulation results; 4) comparison of CPU usage.

Ideally, each resultant force versus time curve should overlap each other. However, due to the differing geometric detail affecting collision times, for some particles the collision and force behaviour will be different. Among the four aspects for each particle's simulation results, the first aspect is the main focus of the discussion of simulation Phase 1, and all reasons for non-overlapping resultant force curves will be explained; such as the dispersion of certain curves in resultant force plot are different from other curves; certain curves in the resultant force plot are having "tail" and certain curves are having asymmetry characteristics. All these points will be grouped and discussed below.

Before the discussion about those particles having non-overlapping resultant force curves, the following figures (Figure 4.5 and Figure 4.6) are showing two particles, which have the resultant force result perfectly overlapped, and based on these examples, discussions will be developed thereafter.

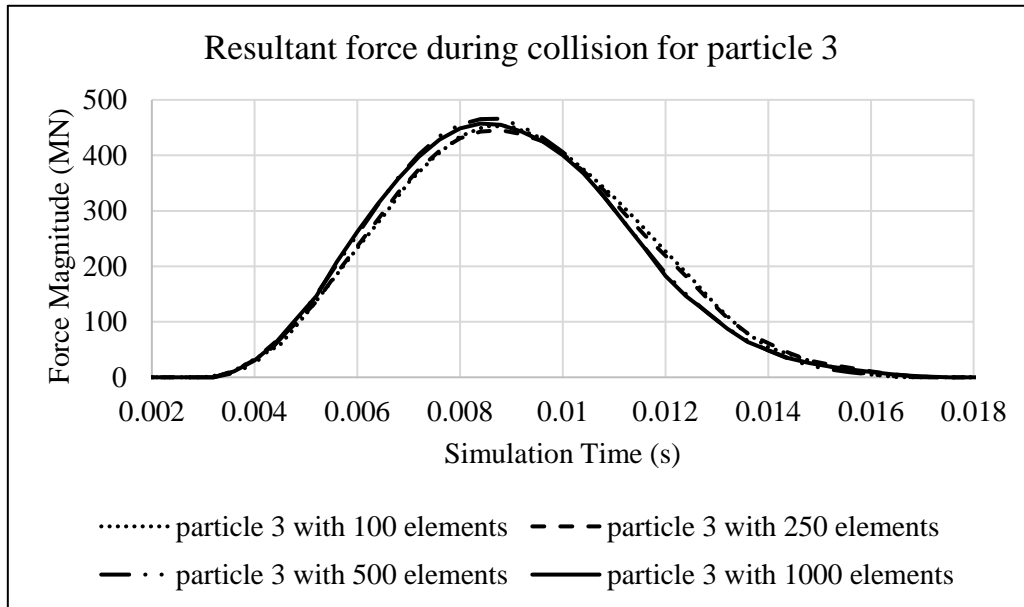


Figure 4.5 Plot of resultant forces during collision event for Particle 3.

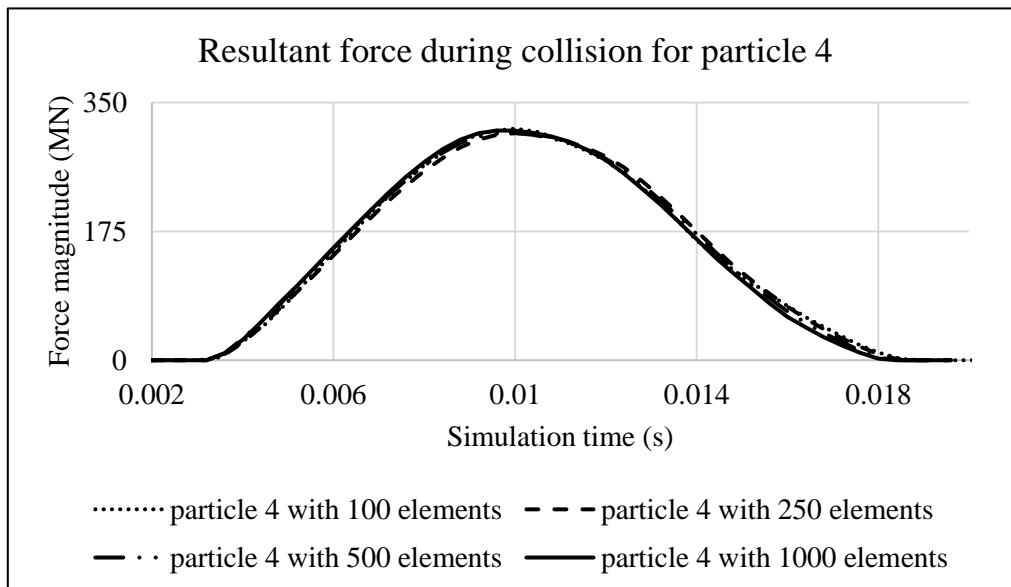


Figure 4.6 Plot of resultant forces during collision event for Particle 4.

4.4.1.1 Differences in resultant force curves

Among all the simulation results, some particles show differences in the resultant force plots, and the total resultant forces are calculated as the summation of resultant forces in x, y and z directions as:

$$F_{total} = \sqrt{F_x^2 + F_y^2 + F_z^2} \quad (4.5)$$

As noted earlier, due to the differing geometric detail affecting collision times, for some particles the collision and force behaviour is different. There are 8 particles in total of out 50 exhibiting this, which are: Particle 1 (with 100 elements); Particle 6 (with 500 and 1000 elements); Particle 11 (with 100 elements); Particle 13 (with 100 elements); Particle 15 (with 100 elements); Particle 17 (with 250 elements); Particle 24 (with 250 elements); Particle 28 (with 100 elements); Particle 44 (with 100 elements).

For Particle 1 with 100 elements, the simulation result of the resultant force plot is shown below:

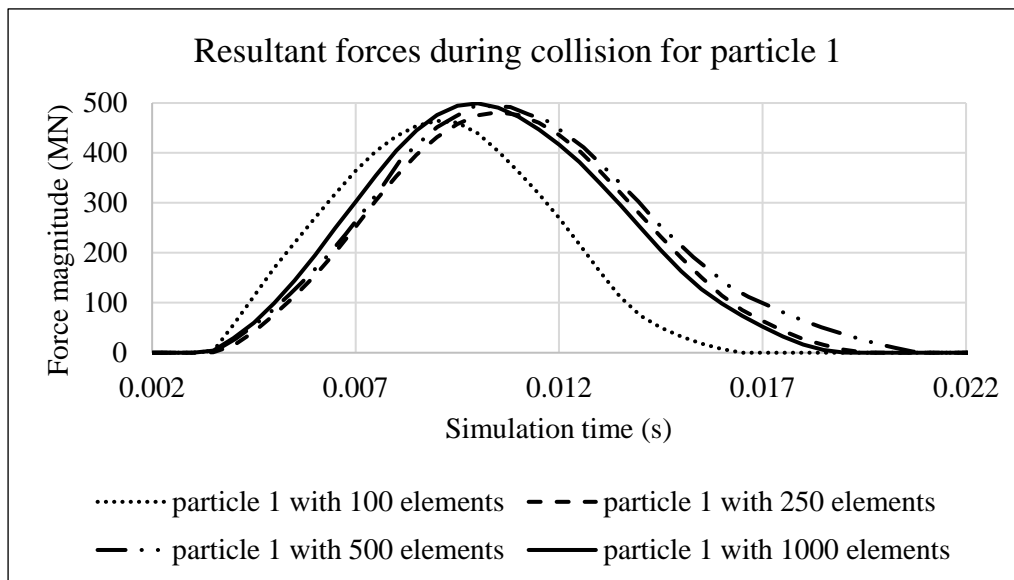


Figure 4.7 Plot of resultant forces during collision event for Particle 1.

As shown in the plot, the curve that represents Particle 1 with 100 elements is exhibiting a different pattern from other curves for the same collision, but with larger number of elements

used in the discretization for this particle. The reason for this might may come from several aspects. First is the simplification process, which has changed the geometry, asperities and physical properties of the particle that can lead to the difference of simulation result. By comparing the particle statistics, the change of volume is readily noticeable:

Particle 1	Volume (cm ³)
100 elements	37.37396
250 elements	38.82754
500 elements	39.06975
1000 elements	39.14609

Table 4.6 Change of volume corresponding to different element number for Particle 1.

which shows that Particle 1 with 100 elements has relatively smaller volume than Particle 1 with other number of elements. This was caused by the simplification process which makes the particle surface geometry over-simplified as compared to a particle with higher resolution by successively removing geometric detail. By taking a look at their corresponding shapes after simplification, the asperity changes can be easily observed as shown on Figure 4.8. It is obvious that with the increase in the number of elements, Particle 1 with 1000 elements has a better representation of the original particle's geometry and asperity details than Particle 1 with 100 elements. And this difference is leading to the second reason that might have caused the different results in the resultant forces plot. In addition, since the nodal contact detection process during the simulation is the algorithm that's been used by the combined FEM/DEM, then the difference of particle resolution may have influence on the detection process. In other words, the simplification process applied on particle surface may have changed the continuity property, and for particle with 100 elements has fewer contacting nodes that can be detected by the algorithm, while the particle with higher resolution (more elements) provides more contacting couples of nodes for the detection process. This difference ended up with a longer contact duration for particle with higher resolutions, which makes them more likely to

have a deeper penetration into the solid block, and this pattern can be observed in Figure 4.7.

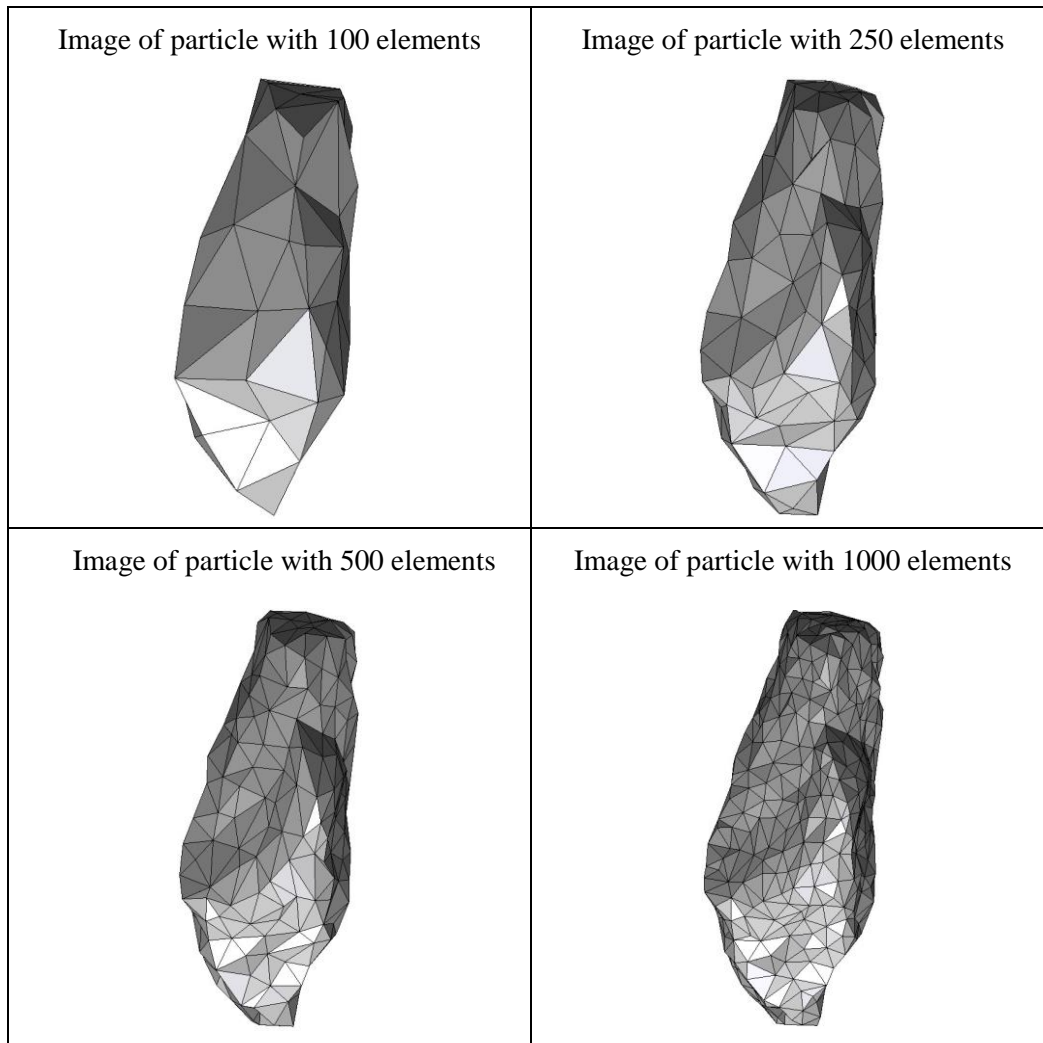


Figure 4.8 Illustration of Particle 1 with 4 different resolution.

The second reason that can explain the difference is on the perspective of the contact mechanism that is used by the FEM/DEM system. As introduced in Chapter 3, section 3.2.2, the contact force is obtained by counting the equivalent nodal forces resulting from the contact process between contactor triangles into target triangles. Since the first phase of simulation is focusing on particle collision with a solid block, then the contact force will always be considered as a contact of contactor triangles with the edge of target triangles. According to this, and the algorithm that is used for the FEM/DEM system (Andrews, 2000), and comparing the post-simplification pictures as shown in Figure 4.8, the difference of the curve for Particle 1 with 100 elements to other curves may be caused by the fact that there are

relatively fewer contactor triangles during the contact process, as compared to Particle 1 with other element numbers. From pictures shown in Figure 4.8, it is obvious that Particle 1 with 100 elements has a relatively less geometry and asperity details than those with higher resolutions.

The third reason for explaining the difference is connected to the second reason, which is the potential influence of particle's initial position. Due to the reason that the VGW requires exporting simulation particle and the solid block (a .msh file containing both the particle and solid block) from the Virtual Shape Library into the GiD program, while by importing the exported .msh file into the GiD, the position of the particle is not on the desired place as required for simulation purpose (as shown below).

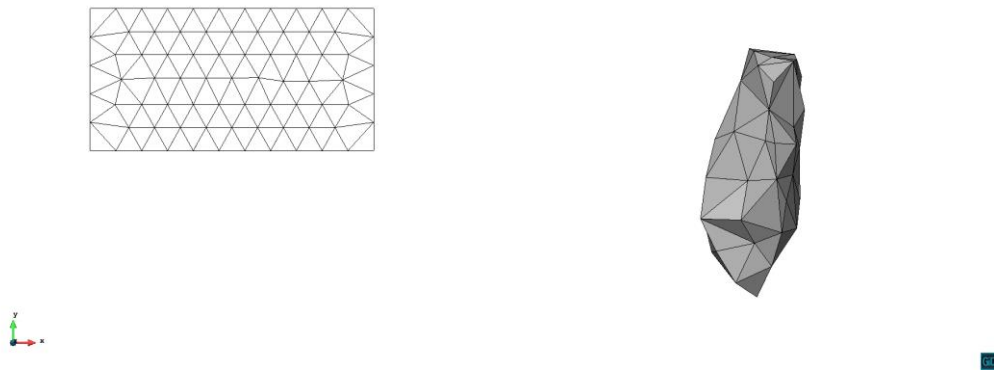


Figure 4.9 Screen shot of the initial place for Particle 1 with 100 elements and the solid block from the GiD program.

Then the particle needs to be moved and rotated to a desired position in order to make the particle and the solid block have more initial contact points rather than one single contact point. The particle's position after rotation and moving process is shown in the following figure.

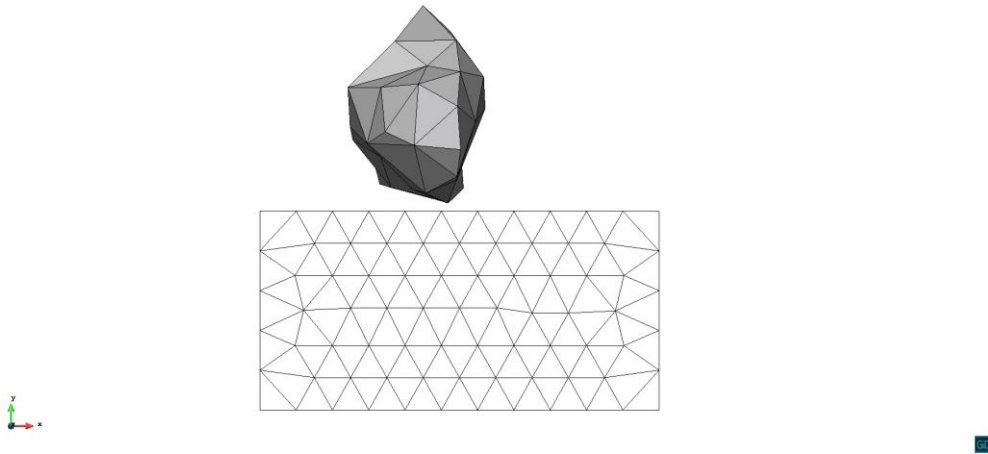


Figure 4.10 The initial position of Particle 1 with 100 elements relating to the solid block. Ideally, particle with different element numbers should be put in the same position (e.g. same location of its center of gravity), to minimize the influence on simulation process arises from the difference of initial position. However, during the rotation and moving process, in the GiD program, these two process is conducted by the choosing of two nodal points manually. While, because of the difference of element number, nodal points' position will be changed with the change of geometry resolution as shown in Figure 4.8, then it becomes almost impossible to choose the same nodal points for particle with different element numbers, and it is difficult to have all those particles with different element numbers have the same rotation and movement. According to the algorithm that's been used for calculating the total contact force exerted from target triangle onto the edge of contactor triangle, which is governed by the area of potential that is calculate by the interpolation between the edge node and the central node corresponding to contacting triangles (Andrews, 2000). Thus, the difference of rotation and initial position may pose potential influences on the accuracy of contact force calculation algorithm, which resulted in the difference of curve as shown in Figure 4.7 for Particle 1 with 100 elements to other curves.

By placing the initial position of Particle 1 with 100 and 250 elements together in the Paraview, the following Figure can provide a direct view of the difference of initial position, where a small angle can be observed between these two particles.

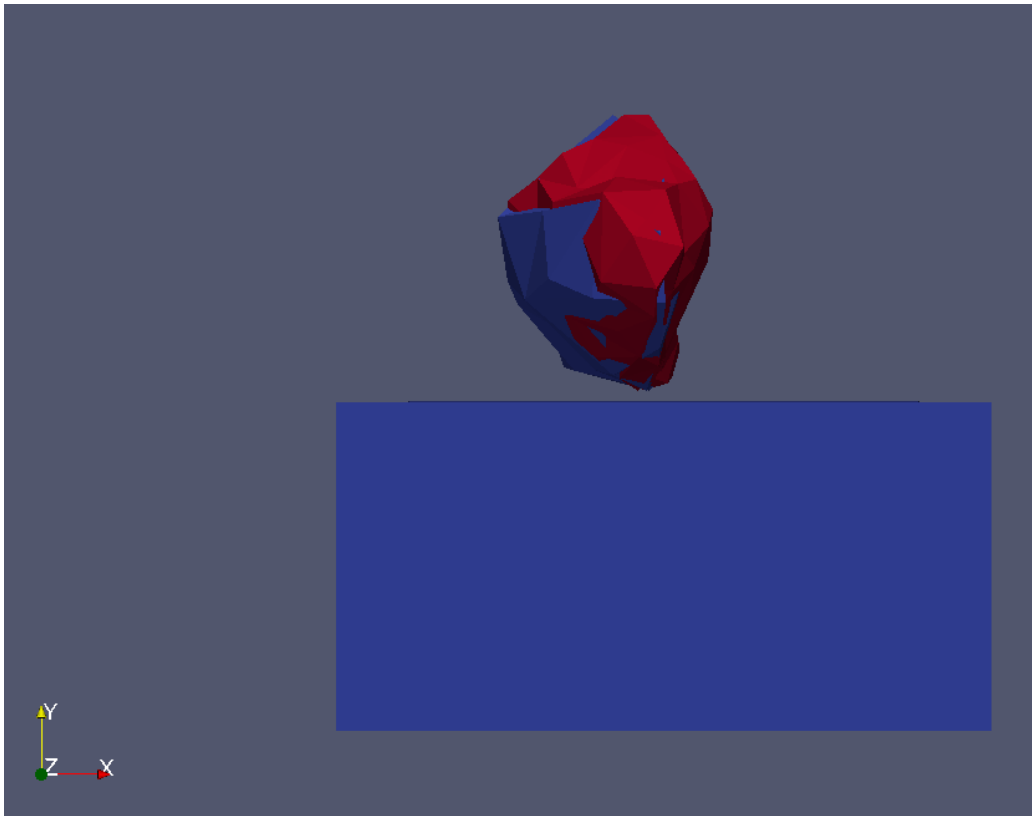


Figure 4.11 Comparison of the initial place for Particle 1 with 100 elements (blue) and Particle 1 with 250 elements (red), presented by Paraview.

The explanation applying on the plot difference between Particle 1 with 100 elements with other element numbers in the Resultant Force diagram should also be applied to the following samples, which is showing similar situations that their plots' patterns are different with others:

- a. Particle 11 with 100 elements, of which the Resultant Force diagram is shown below:

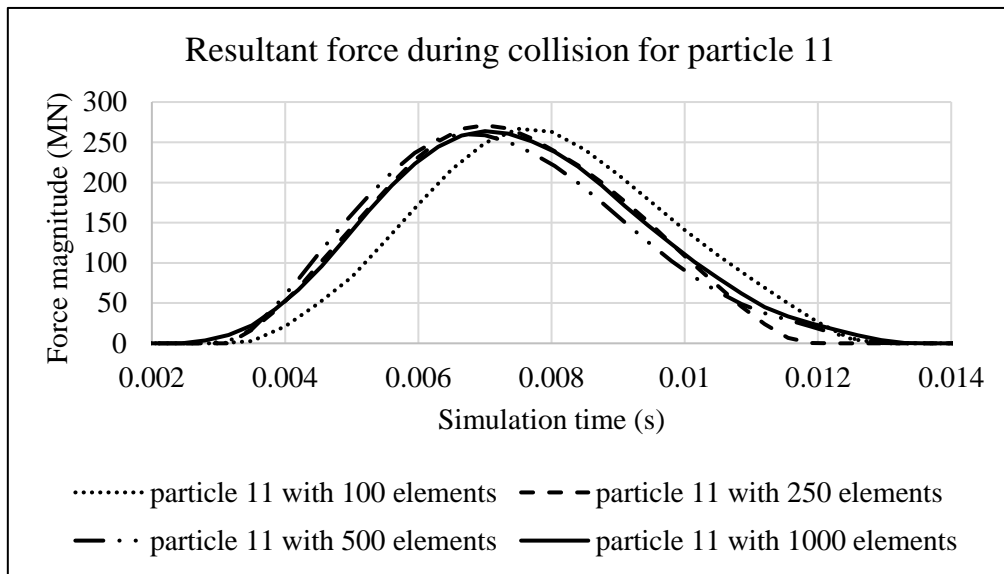


Figure 4.12 Plot of resultant forces during collision event for Particle 11.

b. Particle 13 with 100 elements, of which the “Resultant Force” diagram is shown below:

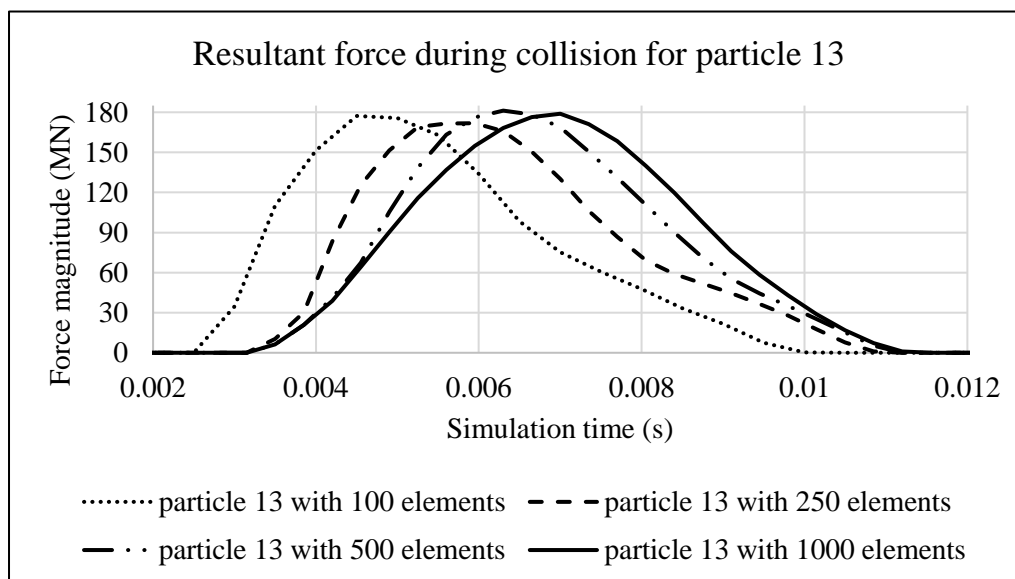


Figure 4.13

Plot of resultant forces during collision event for Particle 13.

By checking the animation of simulation for Particle 13 with all different element numbers, the difference from the curve of Particle 13 with 100 elements to other curves was mainly caused by the difference of initial positioning. In the animation, it is shown that the lowest point of Particle 13 with 100 is relatively closer comparing to other samples; also, after the simplification process, particle samples with different number of elements resulted in

different extent of geometry, which means that those with lower resolutions have relatively further protrusions than those with higher resolutions, and this resulted in an earlier contact with the solid block. These two aspects combined should be the main reason to explain that why the simulation started at an earlier time than other samples.

c. Particle 15 with 100 elements, of which the Resultant Force diagram is shown below:

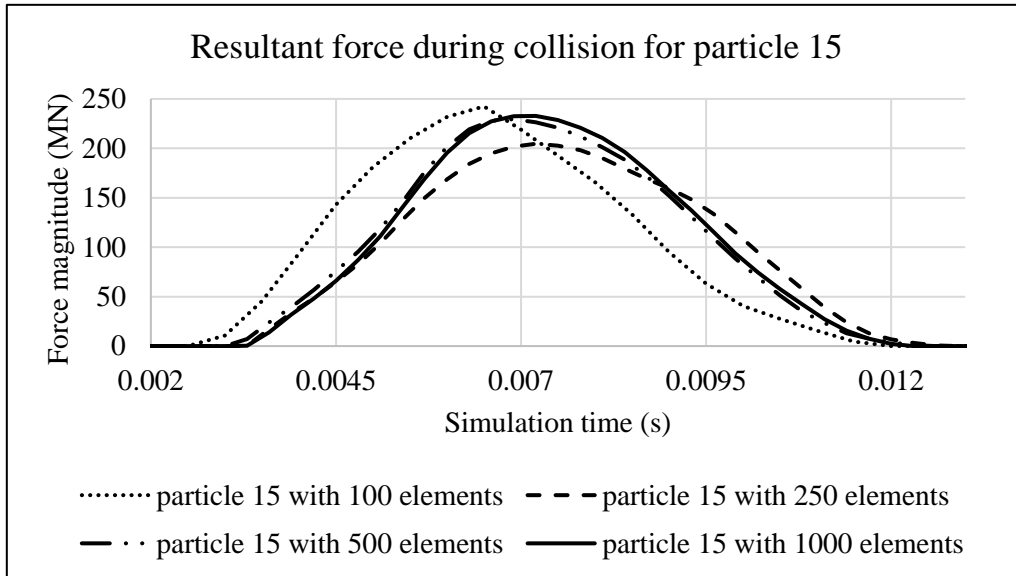


Figure 4.14 Plot of resultant forces during collision event for Particle 15.

d. Particle 17 with 250 elements, of which the Resultant Force diagram is shown below:

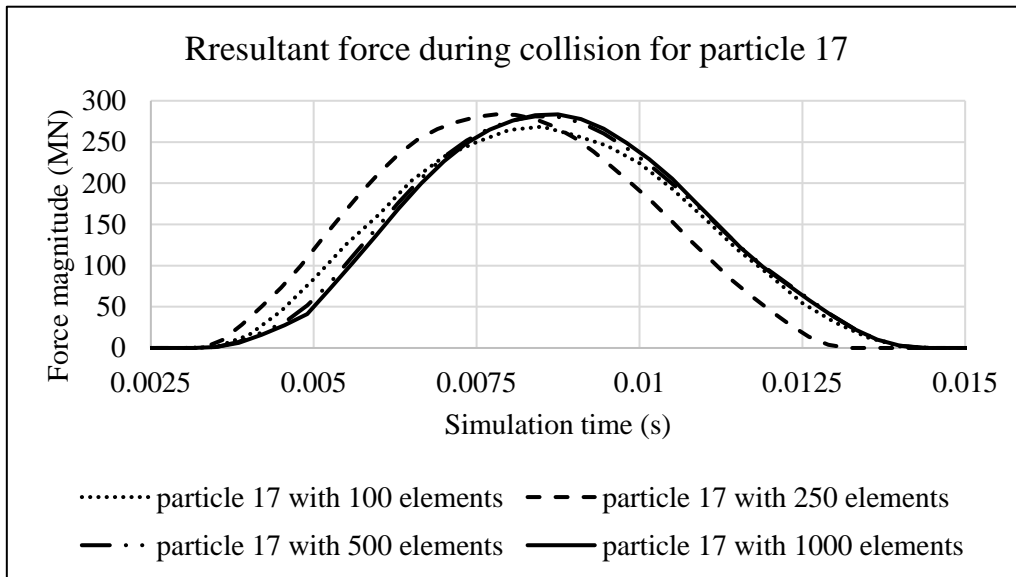


Figure 4.15 Plot of resultant forces during collision event for Particle 17.

e. Particle 24 with 250 elements, of which the Resultant Force diagram is shown below:

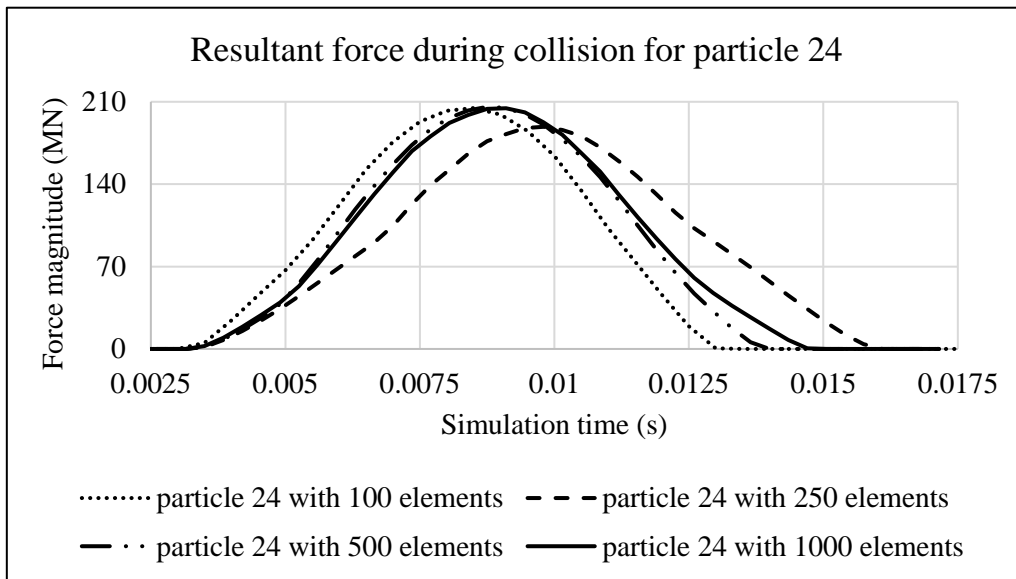


Figure 4.16 Plot of resultant forces during collision event for Particle 24.

f. Particle 28 with 100 elements, of which the Resultant Force diagram is shown below:

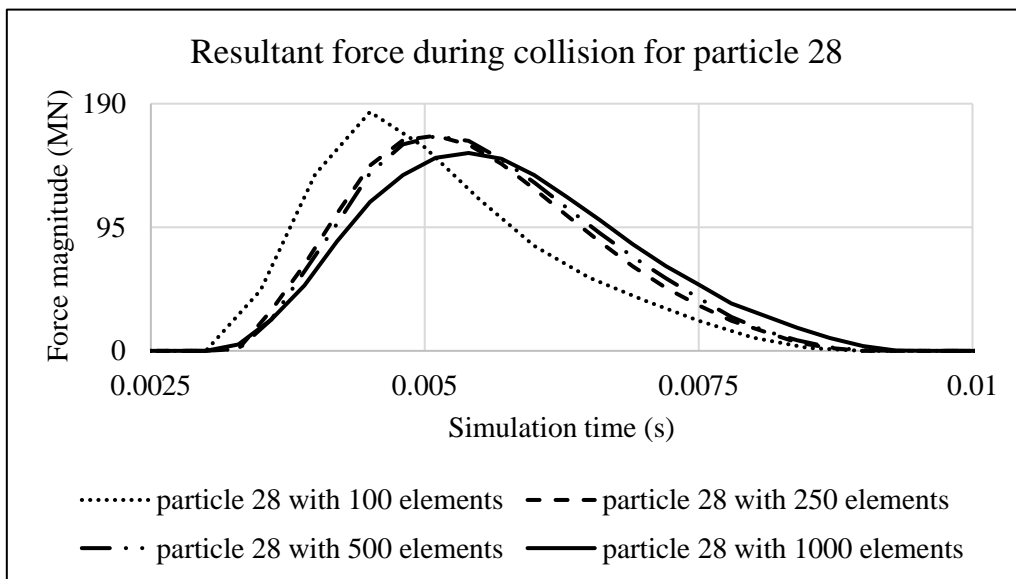


Figure 4.17 Plot of resultant forces during collision event for Particle 28.

g. Particle 44 with 100 elements, of which the Resultant Force diagram is shown below:

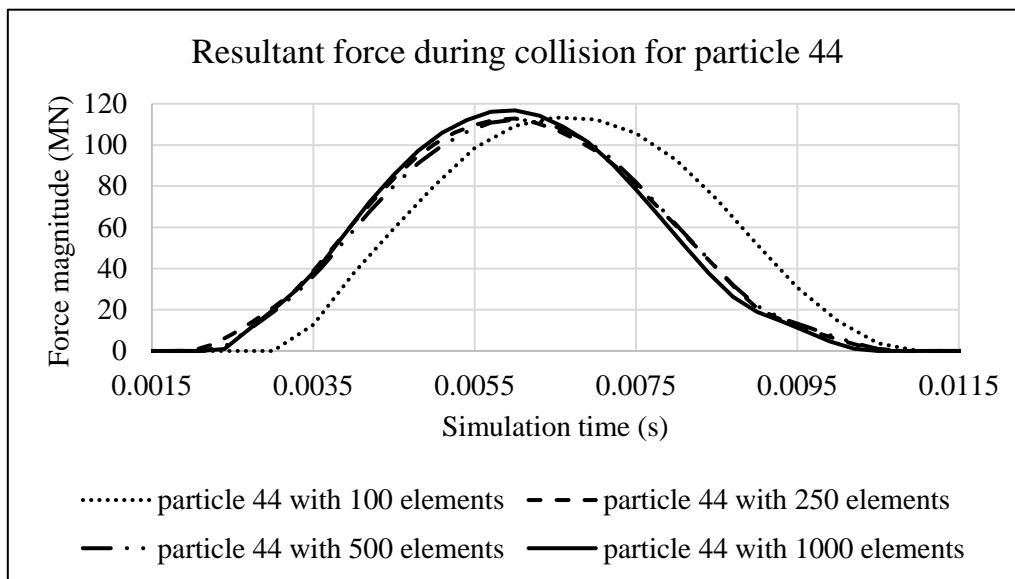


Figure 4.18 Plot of resultant forces during collision event for Particle 44.

h. For particle 6 with 500 and 1000 elements, the simulation result of the Resultant force plot is showing below:

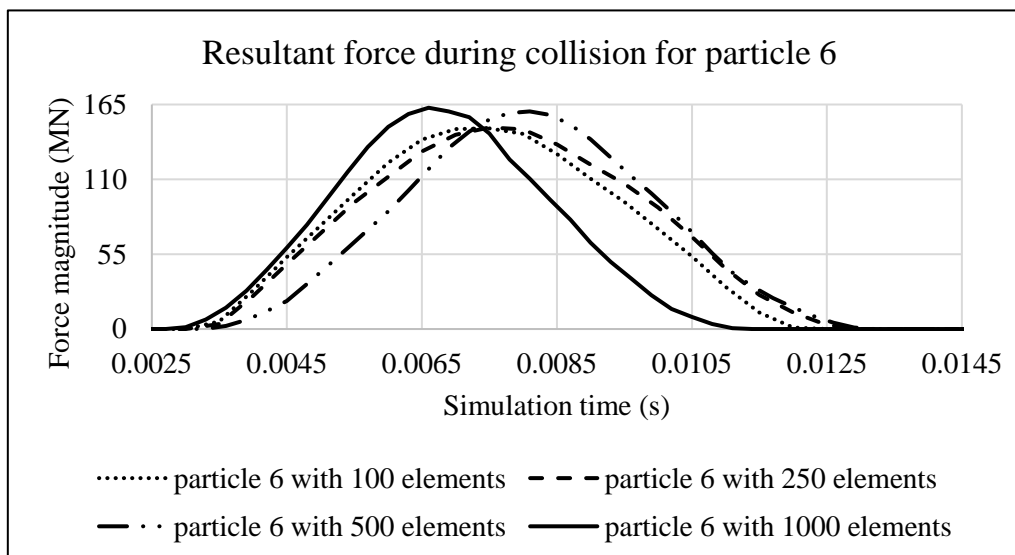


Figure 4.19 Plot of resultant forces during collision event for Particle 6.

The Resultant Force plot shown in Figure 4.19 for Particle 6 is presenting a different pattern as shown in the previous case for Particle 1. For this case, the resultant force plots can be divided into two groups, one is for Particle with 100 and 250 element numbers, and the

other group is for Particle 6 with 500 and 1000 element numbers.

Although the curves for Particle 6 with 500 elements and Particle 6 with 1000 elements are not fully overlapping each other in the figure, their plots are still showing a same pattern and provided almost the same peak force after simulation, as shown in the following figure:

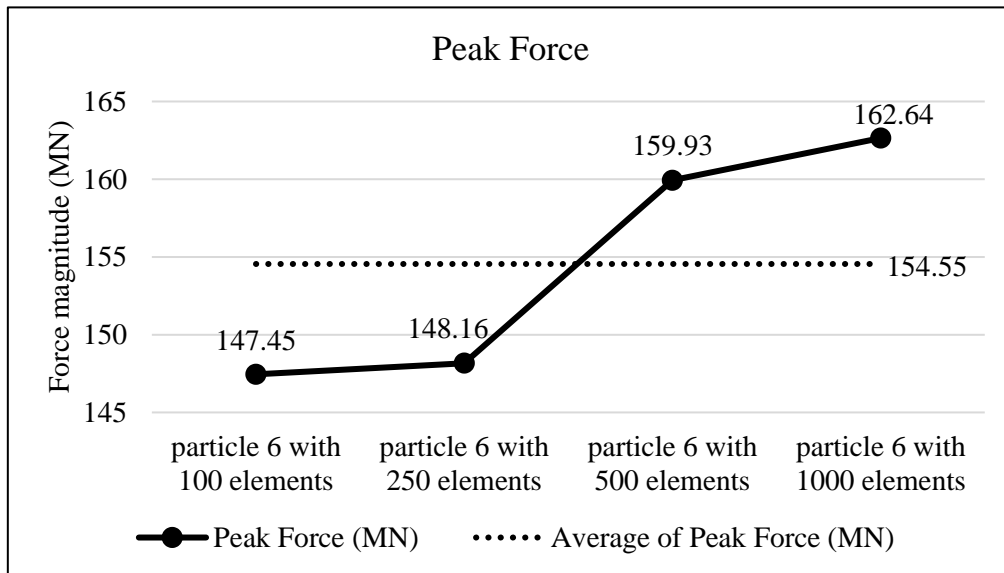


Figure 4.20 Peak collision for the four particle geometry resolutions for Particle 6.

By analysing the animation from the Paraview program for the simulation results of both Particle 6 with 500 and 1000 elements frame by frame, the reason of the non-overlapping may be connected to the difference of initial place of particle's position, also influenced by the extend of geometry, which has been discussed in previous example (for Particle 13). Same as the reason explained in previous case, with the change of particle's resolution, nodal position will be altered, which makes particle with different resolutions can hardly locate at the same initial position during the moving and rotating procedure. And for Particle 6 with 500 and 1000 elements, from the comparison animation (Figure 4.16), it is clear that these two samples have more overlapping area at the bottom part (-z direction), while they have relatively less overlapping area at the top part (+z direction) referring to the figure shown below:

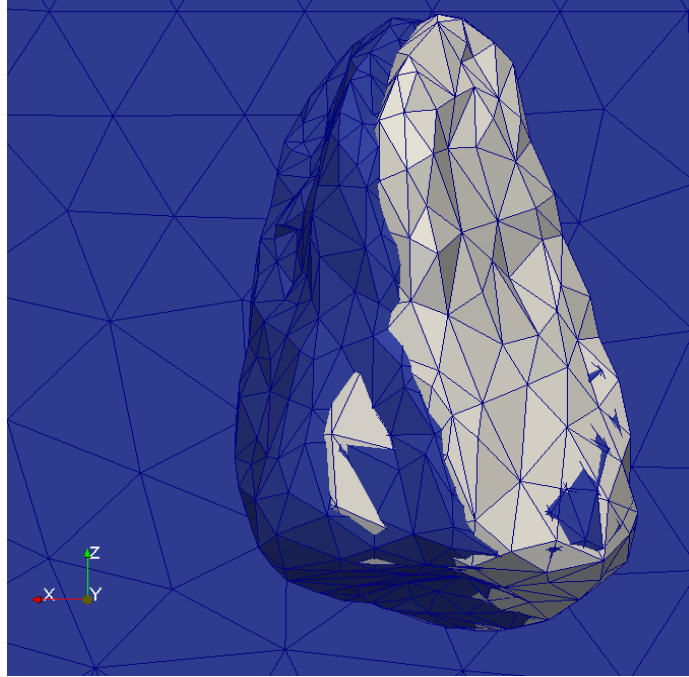


Figure 4.21 Comparison animation for Particle 6 with 500 elements (white) and Particle 6 with 1000 elements (blue).

Also, the whole animation for their simulation is providing a proof for this explanation as Particle 6 with 1000 elements in the animation process has relatively more rotation about y axis, while Particle 6 with 500 is experiencing less rotation after the contact. Their final position is shown in the following figure:

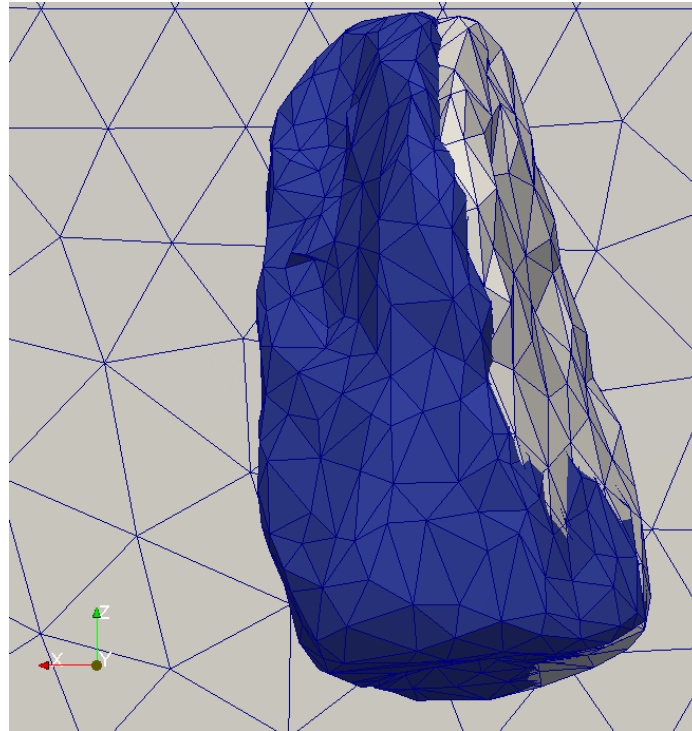


Figure 4.22 Final position comparison for Particle 6 with 500 elements (white) and Particle 6 with 1000 elements (blue).

From the above figure, Particle 6 with 1000 elements has rotated more about the y axis (clockwise) as compared to Particle 6 with 500 elements. This difference may have resulted in the difference of contact duration for these two particles, even though they have almost the same contact time with the solid block as shown in the Figure 4.19. As for the difference between Particle 6 with 100 and 250 elements and Particle 6 with 500 and 1000 elements, by comparing them as two groups, the difference could be caused by the same reason as for Particle 1 with 100 elements, which is the difference of initial position. In the Paraview animation, it is shown that Particle 6 with 100 and 250 elements has almost the same initial position and have turned into a position that is relatively more “parallel” to the solid block comparing to Particle 6 with 500 and 1000 elements, which is shown in Figure 4.19.

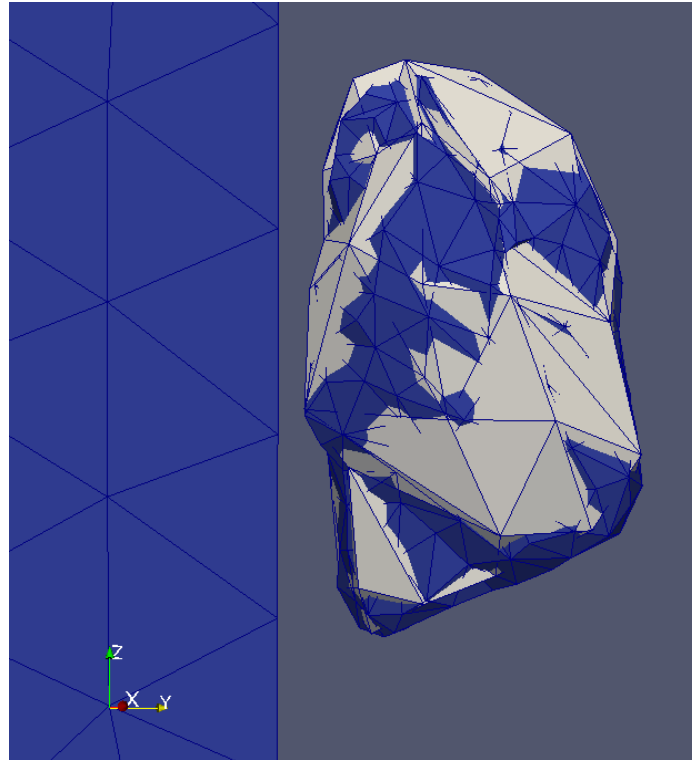


Figure 4.23 Animation of the initial position for Particle 6 with 100 elements (white) and Particle 6 with 500 elements (blue).

Since Particle 6 with 500 and 1000 elements are almost in the same initial position, then Figure 4.23 only compares two samples as a group. As shown in Figure 4.23, the initial position for Particle 6 with 100 (same for 250 elements) is relatively more rotated over at upper part (+z direction) towards -y direction, which resulted in a faster development of full contact with the solid block during the collision event. While Particle 6 with 500/1000 elements experienced a longer duration of the contact event with the solid block, starting with a smaller area contact and then followed with full contact, in comparison with Particle 6 with 100 and 250 elements. This small difference may have posed an influence on the FEM/DEM algorithm for calculating these two groups' contact forces since they have slightly different nodal contact process, which resulted in the difference in the Resultant Force plots.

4.4.1.2 Discussion of results that have relatively large differences in force magnitude and duration

In all Resultant Force plots, there are only three results of particle-block collisions that have ‘anomalies’ in the resultant force magnitude and contact duration (Particles 7, 8 and 9). For example, Particle 7, the simulation result for Resultant Force plot is shown below:

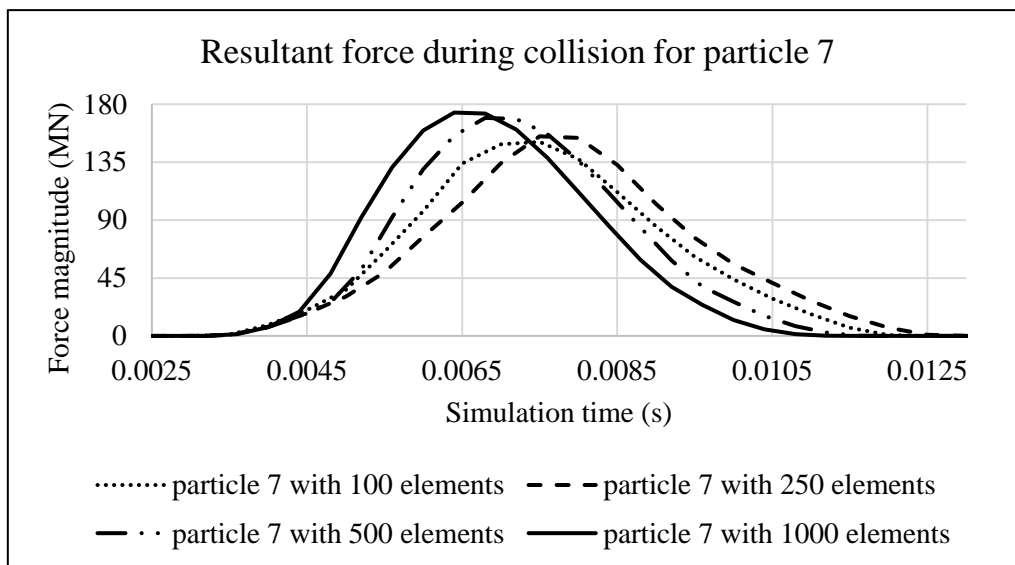


Figure 4.24 Plot of resultant forces during collision event for Particle 7.

From Figure 4.24, it is evident that the magnitude of resultant force plots is gradually increasing with the increasing discretization, which might be caused by the following reasons:

First, same the reason that has been explained for Particle 1, which is the simplification process that has changed the geometry, asperity and physical properties of the particle that may influence the simulation results. By comparing the particle statistics, the change of volume for Particle 7 is shown below:

Particle 7	Volume (cm ³)
100 elements	4.95651
250 elements	5.00226
500 elements	5.03909
1000 elements	5.05476

Table 4.7 Change of volume corresponding to different element number for Particle 7.

from which is evident that the simplification process has resulted in an increase of volume for Particle 7 from 100 elements to 1000 elements. These volumetric differences should have influences during the collision events, since at the pre-simulation process, all particles are set with the same density. Accordingly, given that $m = \rho \times v$, those ones with larger volume will have relatively larger mass that influences the simulation results.

In addition, as introduced in Section 3.2.2, the contact force calculation for 3D models is based on the overlapping volume V , then for those samples with oversimplified face elements and smaller volumes than those with higher resolutions and larger volumes, the resultant force should be relatively smaller. While, this explanation should be combined with the following point which supersedes and dominates the simulation process and result expression.

Second and most important point is the initial position of particles with different number of elements, which could result in direct effects on the simulation process and influence the collision results. As explained in the previous section (4.4.1.1) for Particle 1, the rotation and moving process for particles with different element numbers was conducted by selecting two different nodal points in the GiD program. Again, after the simplification process, particle's geometric properties have large differences between four different samples. Then, with the change of geometric details it is impossible to select the same nodal points, these samples can only be rotated and moved to the same initial position as close as possible while comparing to each other. The following figure is showing the comparison of initial positions (top view and side view) for four individual particles in different number of elements as:

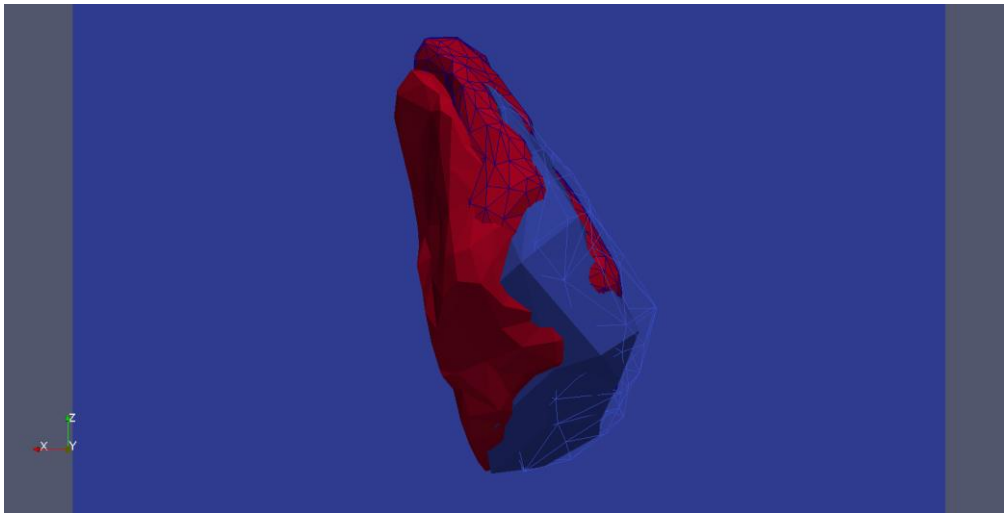


Figure 4.25. Top view (X-Z) plane of initial position comparison for Particle 7 with 100 elements (blue), 250 elements (blue outlines only), 500 elements (red) and 1000 elements (red with outlines), as shown via Paraview.

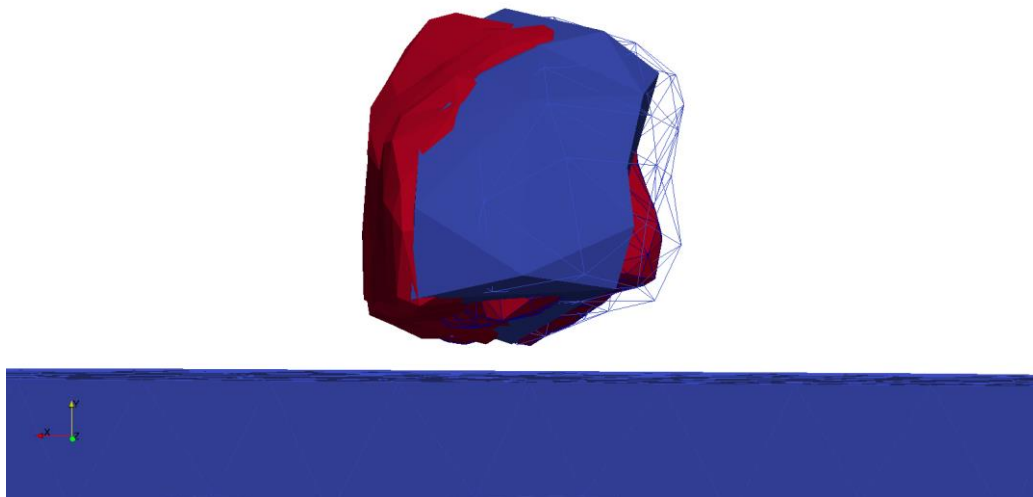


Figure 4.26. Side view (X-Y) plane of initial position comparison for Particle 7 with 100 elements (blue), 250 elements (blue outlines only), 500 elements (red) and 1000 elements (red with outlines), as shown via Paraview.

From these two figures presented above, particles with different number of elements are showing differences at their initial positions as compared to each other. This directly leads to initial contact discrepancies when colliding with the block, which results in relatively large differences in the contact behaviour during a contact. Also, after the simplification process, those samples with smaller number of elements will have relatively fewer contactor triangles that are used by the contact calculation process, as introduced in previous section (4.4.1.1), than those samples with higher resolutions. This could be interpreted as those samples with more face elements provide more contacting nodal points for the contact force calculation algorithm. And, combining with the point that, for those with lower resolutions, their geometrical and asperity details are over-simplified comparing to those with higher resolutions, which potentially affected their continuity characteristics, and directly posed influences on their behaviours during the contact event. This can be illustrated by the following comparison figure between four individual samples when they have full contact with the solid block, as:

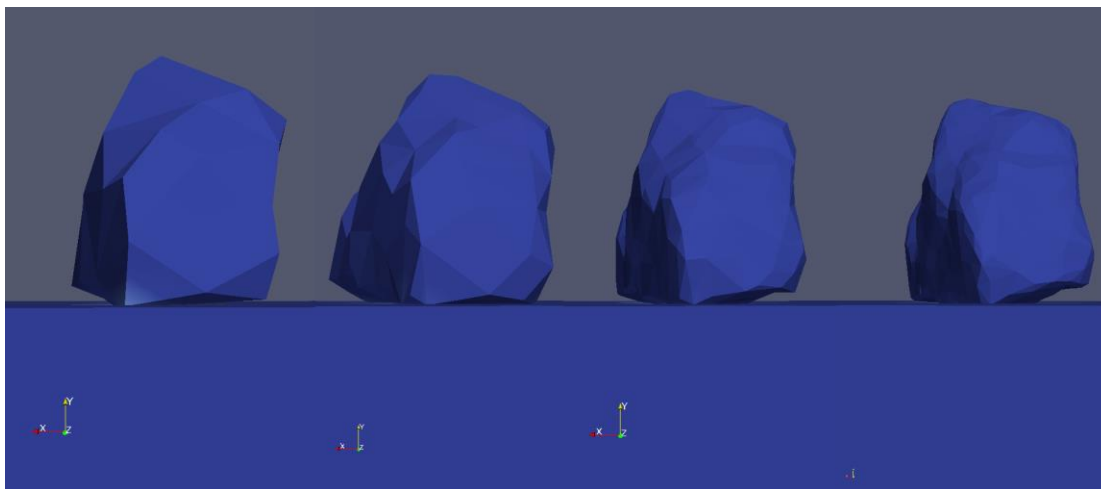


Figure 4.27. Comparison of position when full contact occurs for Particle 7 with different element numbers (Particle 7 with 100 in the left most and 250 is been placed on the right next to 100, and so on), shown via Paraview.

The figure displayed above is showing the moment in time when Particle 7 (discretized with different number of elements) achieves a full contact with the solid block, and the reason that these samples are having slight size differences is due to the manual zooming by using the Paraview program, which does not mean that they are in different sizes in reality (particle

samples are placed in four different windows in the Paraview program, and when the screenshot was printed out of the program, windows borders are deleted automatically).

These samples are all been viewed from X-Y plane, and at this moment in time, they are show different contact situations. By going through animations frame by frame of the contact events of four different samples with the solid block in Paraview, Particle 7 with 100 and 250 elements experienced relatively larger deformations than Particle 7 with 500 and 1000 elements, which ended up with what is showing in the figure that at the +Z and -X point, they have more contacting area. This should be linked with the reason presented above that with lower resolutions, their structural characteristics are over-simplified, which altered their continuity properties. And this contact difference has posed large influence on the resultant force calculation as the contacting area and contacting angle are different.

By combining all the reasons and explanations, the plot pattern for Particle 7 can be explained as, when the particle samples are having relatively large volumetric differences after the simplification process; initial positions are differing from each other which makes particle samples having different contact angles form the start of contact events; and during the contact, the particle samples are deforming differently, these all together may explain the resulting plot in the resultant force pattern as shown in Figure 4.24.

Similar explanations could be applied for Particle 8 and Particle 9, which have similar patterns of the resultant force plots, as shown below:

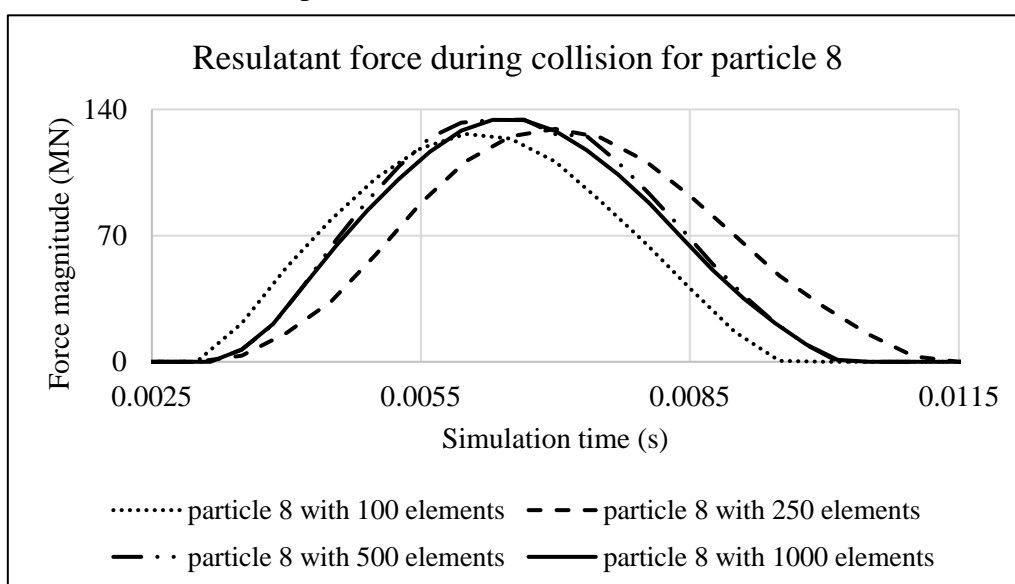


Figure 4.28 Plot of resultant forces during collision event for Particle 8.

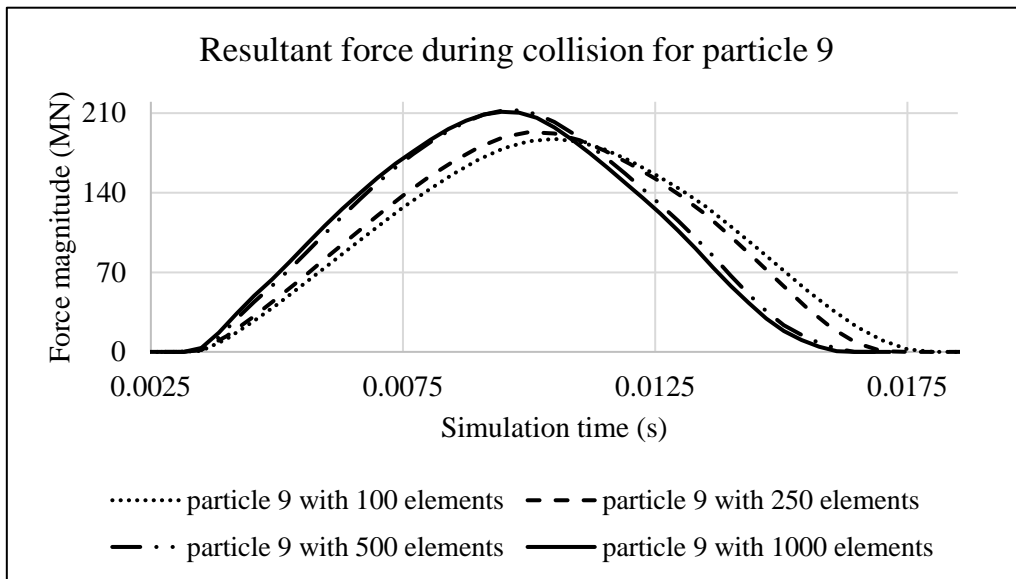


Figure 4.29 Plot of resultant forces during collision event for Particle 9.

4.4.1.3 Hump near the end of resultant force curve

In this section, the situation where there is a hump near the end of the resultant force curve will be discussed, and this situation only occurred for one particle, which was Particle 19. The simulation result of resultant force plot is shown below:

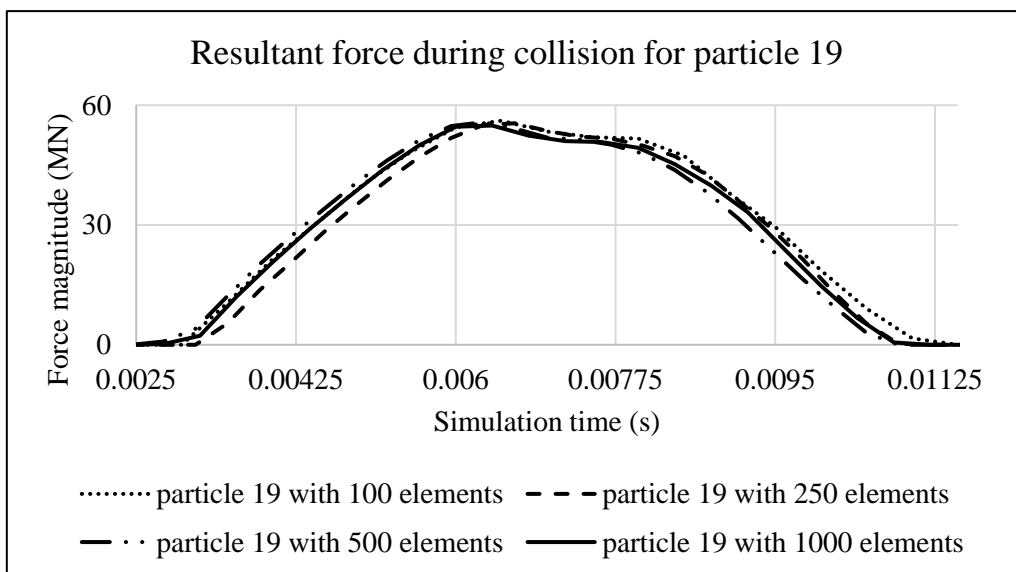


Figure 4.30 Plot of resultant forces during collision event for Particle 19.

As shown in Figure 4.30, the resultant force plots for Particle 19 with different number of elements are almost perfectly overlap, yet, after the first peak point (at the simulation time around 0.006s) there is another hump (at the simulation time around 0.00775s - 0.00785s). The explanation for this phenomenon is simply due to an inclined initial contact between the contactor (Particle 19) with the target (solid block), which leads to a small rotation after the first peak force point (also the first full contact). In more detail, the process was examined by going through the animation of the full simulation, where Particle 19 experienced a direct contact with the solid block, while after the first full contact occurred, because to there was a small angular difference between the two, Particle 19 showed a small rotation that resulted in another (secondary) contact between the other part of Particle 19 with the solid block, rather than directly bouncing back and detaching from the solid block.

4.4.1.4 Resultant force curves with tails

In this section, the particle simulations that produce resultant force curves having a “tail” will be discussed. This characteristic was observed for four particles (Particle 22, Particle 23, Particle 30 and Particle 34).

For example, the resultant force curve for Particle 22 is shown in the following figure, as:

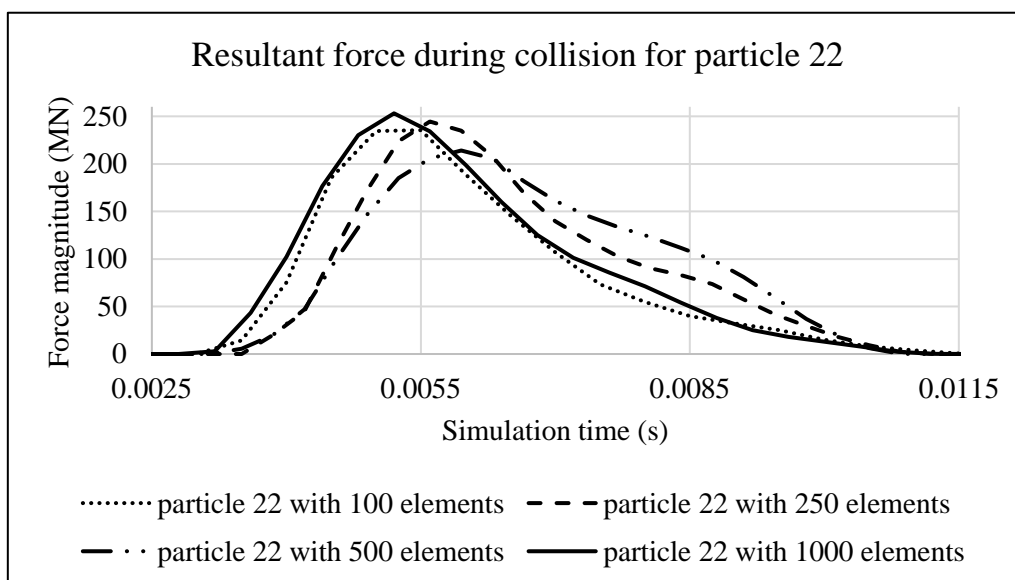


Figure 4.31 Plot of resultant forces during collision event for Particle 22.

As shown in the figure, the resultant force plots have a “tail”, which means that the collision events are not the same as those have been discussed above, they are neither having a simple “collide and detach” pattern, nor a “collide and re-contact with a small rotation”, like the one discussed in Section 4.4.1.3.

The reason to explain this situation is due to the large deformation of the particle with different number of elements. By going through the animation in Paraview, particle samples were having relatively larger contacting areas, as compared to other particle collision events, and a relatively larger deformation were observed. For the other particles, like those figures have been shown in previous sections, they had a multi-nodal-point contact pattern and the contacting surface for those particles to the solid block are along a sharp edge. While, for this group of particles, the collision event started with a large contact area, which can be illustrated by the following figures:

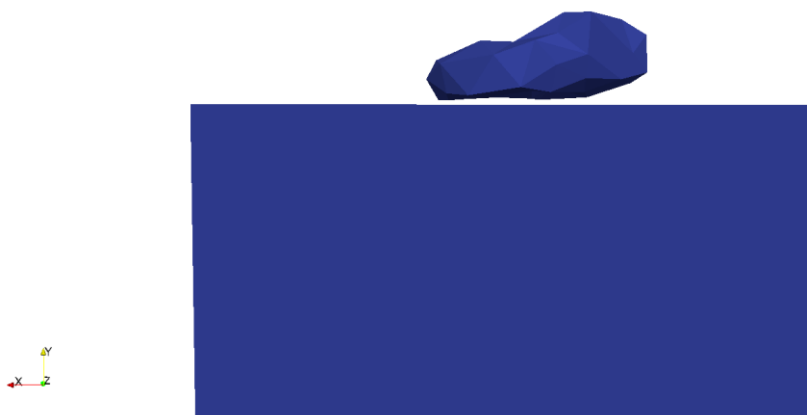


Figure 4.32 Screenshot of the initial position for Particle 22 with 100 elements and the solid block, viewed from X-Y plane.

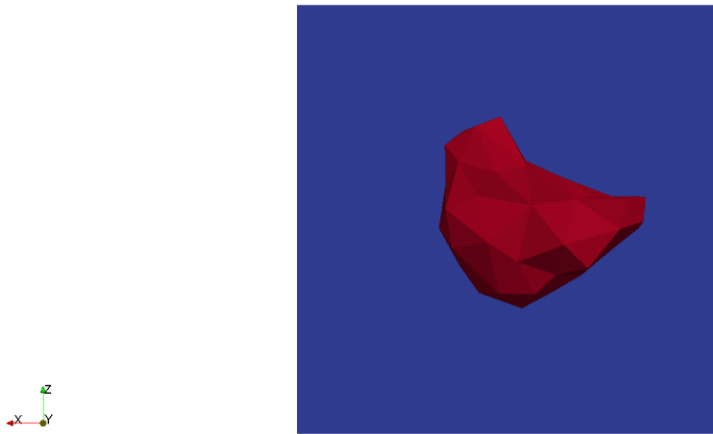


Figure 4.33 Screenshot of the initial position for Particle 22 with 100 elements and the solid block, viewed from X-Z plane.

As shown in Figure 4.32 and Figure 4.33, the contacting area is clearly larger than those particles having a sharp edge collision (point-like or needle-like) with the solid block. This directly influenced the collision process of the particle sample as there are more contacting nodal points, which resulted in a large deformation that can be illustrated by the following figures:

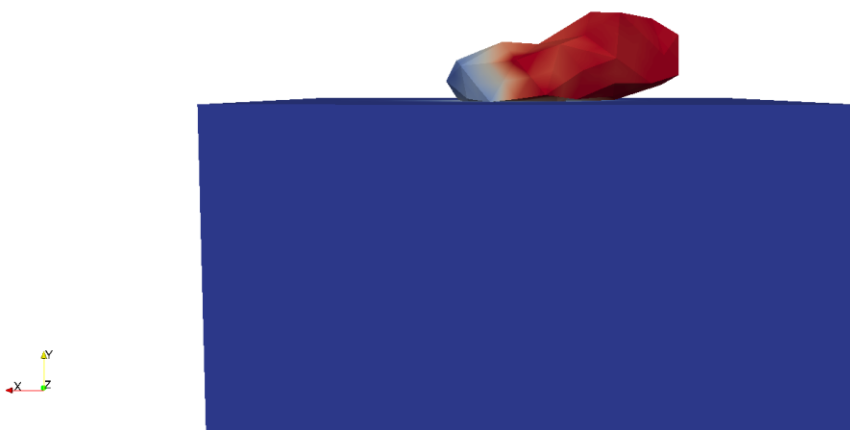


Figure 4.34 Screenshot of the initial contacting moment for Particle 22 with 100 elements and the solid block, viewed from X-Z plane.

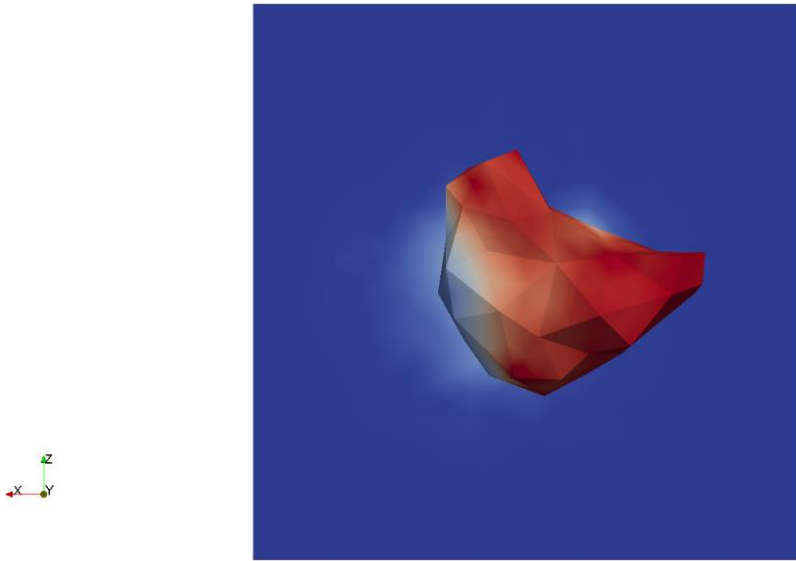


Figure 4.35 Screenshot of the initial contacting moment in time for Particle 22 with 100 elements and the solid block, viewed from X-Z plane.

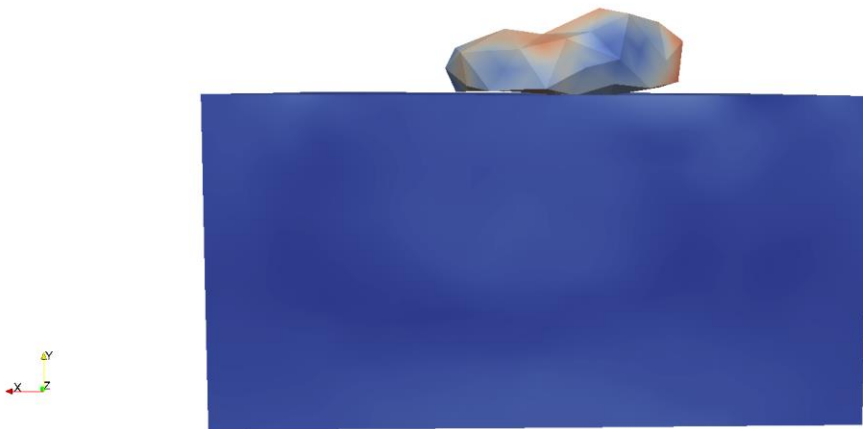


Figure 4.36 Screenshot of the contacting moment in time when Particle 22 having the largest deformation, viewed from X-Z plane.

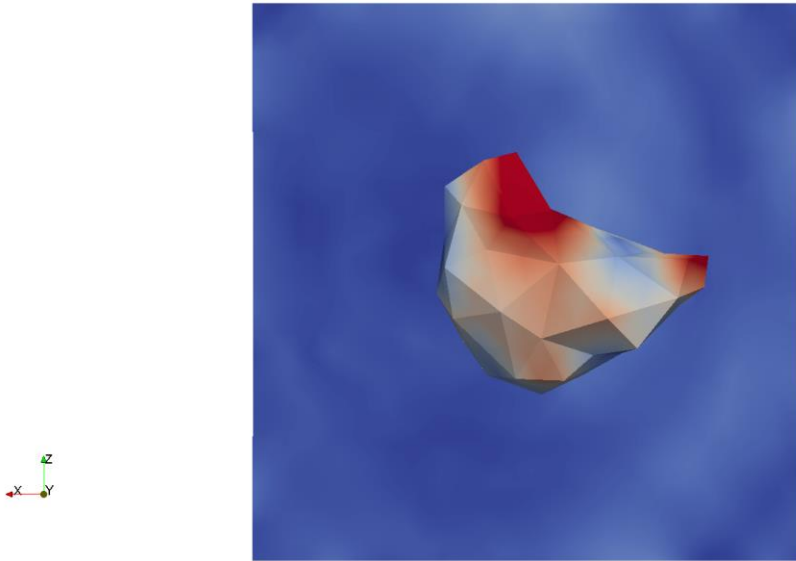


Figure 4.37 Screenshot of the contacting moment in time when Particle 22 having the largest deformation, viewed from X-Z plane.

As shown in Figure 4.34 and Figure 4.35, at the moment in time then Particle 22 (with 100 elements) has the initial contact with the solid block, it still maintained its shape, and from the top view (as shown in Figure 4.35, X-Z plane), where the color is light is indicating the contacting part. While, when particle sample is about to detach with the solid block, as shown in Figure 4.36 and Figure 4.37, which is the moment in time when the particle's deformation has the largest deformation to be observed. By comparing the shape, it's observable at the -X part of the particle experienced large deformation as that part is showing more contact area than it was in the state shown in Figure 4.34. Also, combining with a small rotation which is the same situation as been discussed in the previous Section (4.4.1.3), it follows that the collision process will be elongated comparing to those with sharp edge contact and quick detachment. These together are the explanations to interpret the shape of the curves shown in Figure 4.31 for the resultant force plots with a tail.

Same explanations could be applied to the other three particles with different number of elements that show the same pattern of resultant force curves, which are:

- a. Particle 23:

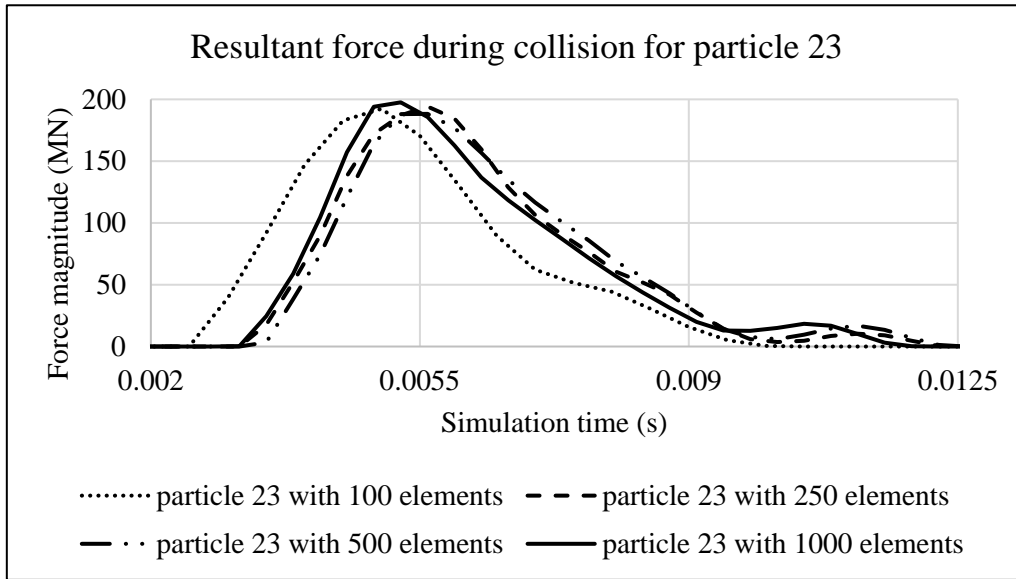


Figure 4.38 Plot of resultant forces during collision event for Particle 23.

For Particle 23 with 100 elements, which shows that it started the contact process with the solid block relatively earlier than the other samples, the explanation that has been discussed in previous section should be applied, as referring to Section 4.4.1.1 for Particle 13. Same analysis should be applied for the following case for Particle 30 with 100 elements and Particle 34 with 100 elements.

b. Particle 30:

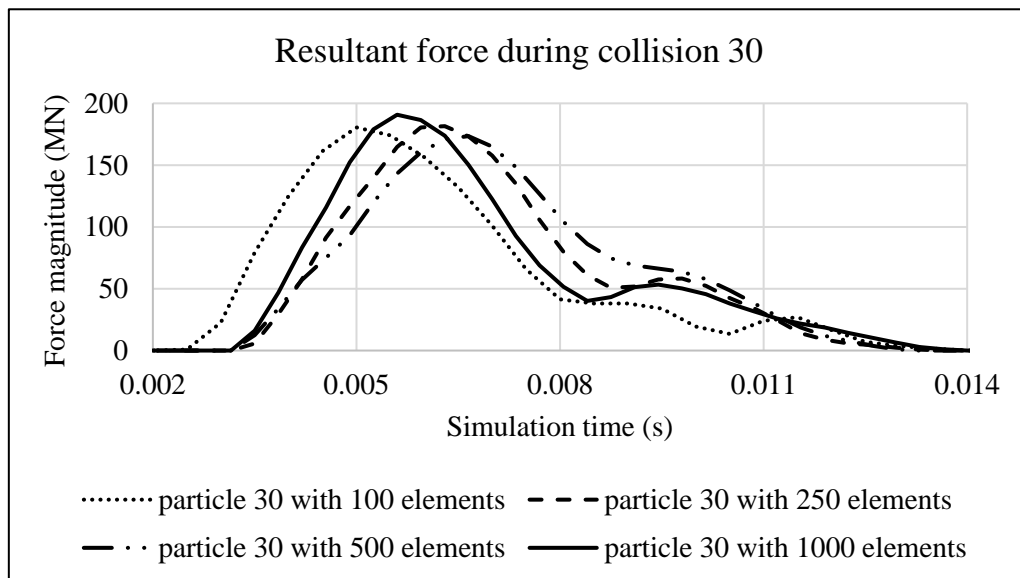


Figure 4.39 Plot of resultant forces during collision event for Particle 30.

c. Particle 34:

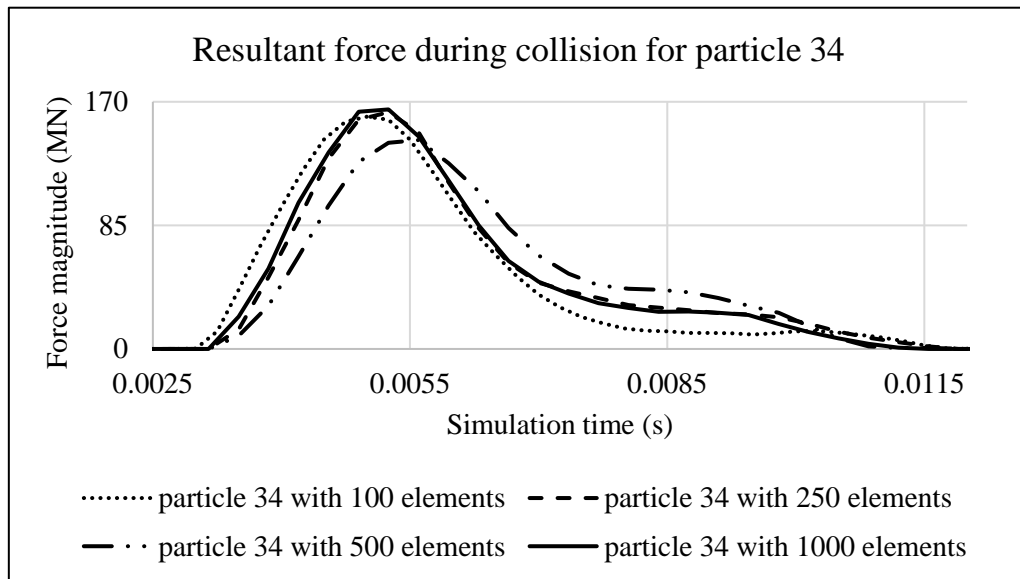


Figure 4.40 Plot of resultant forces during collision event for Particle 34.

4.4.1.5 Resultant force curves are dispersed in time

In this section, the situation is discussed when in the simulation results for the resultant force plots there are curves that have a dispersion in time, and this situation has been observed for three particles (Particle 32, Particle 33 and Particle 38)

For Particle 32, the simulation result of the resultant force plot is shown below:

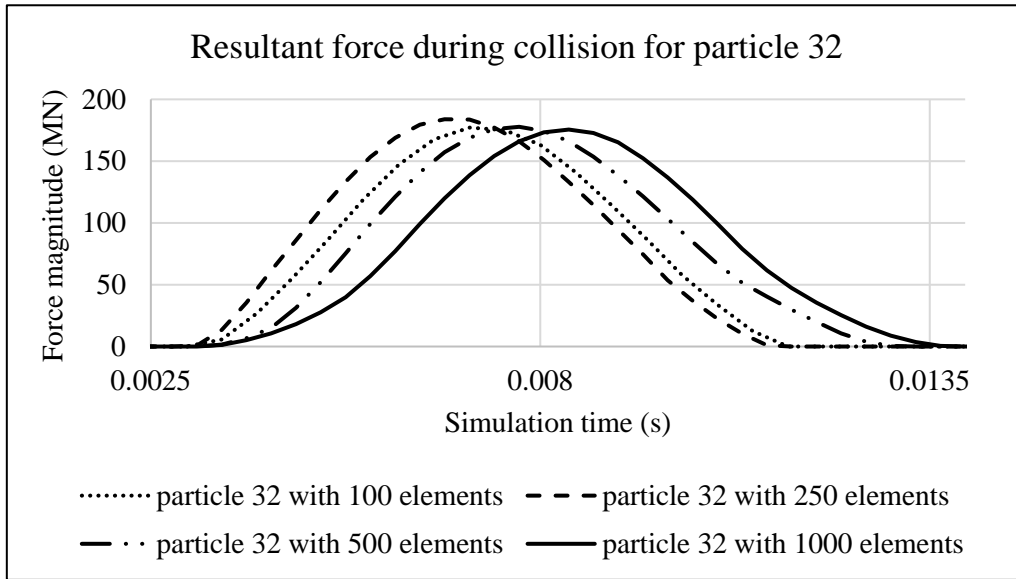


Figure 4.41 Plot of resultant forces during collision event for Particle 32.

As shown in Figure 4.41, Particle 32 with different number of elements is showing that the resultant force curves are dispersed from each other, which could be caused by the fact that their initial positions are different. This can be verified by the following figure as:

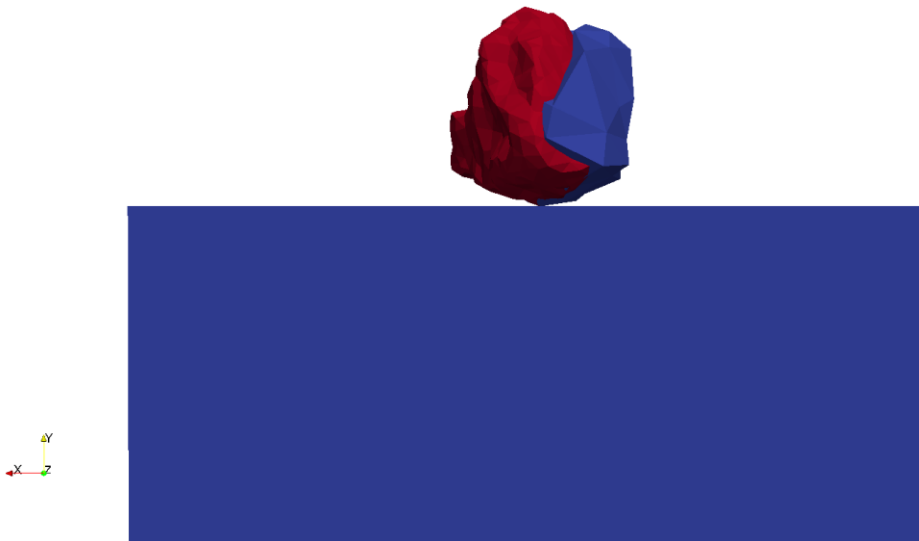


Figure 4.42 Screenshot of initial position for Particle 32 with 100 elements (blue) and Particle 32 with 1000 elements (red), visualized by Paraview.

Given the fact that Particle 32 with 100 elements and with 1000 elements are the two cases that represent the most dispersed curves in the resultant force plots and their initial position have relatively larger differences by comparing to the other samples, then, for the sake of

illustration, only Particle 32 with 100 and with 1000 elements will be discussed.

As shown in Figure 4.42, Particle 32 with 1000 elements is more parallel to the Y axis than Particle 32 with 100 elements, which means that they will experience a different angle of initial contact, which will influence the collision processes and results. This difference is caused by the inevitable error of the manual selection of nodal point and moving the particle sample to desired initial point process, which has been discussed in previous section (Section 4.4.1.1). Due to this major difference, it follows that the collision process will result in a different resultant force curves. By looking at the animation of the whole process of collision, those samples which are more parallel to Y axis represent a deeper penetration to the solid block and longer contacting time duration than those relatively inclined to $-X$ direction.

These together can explain the pattern of resultant force curves in Figure 4.41, and can be used for the other particles with different number of elements:

a. Particle 33:

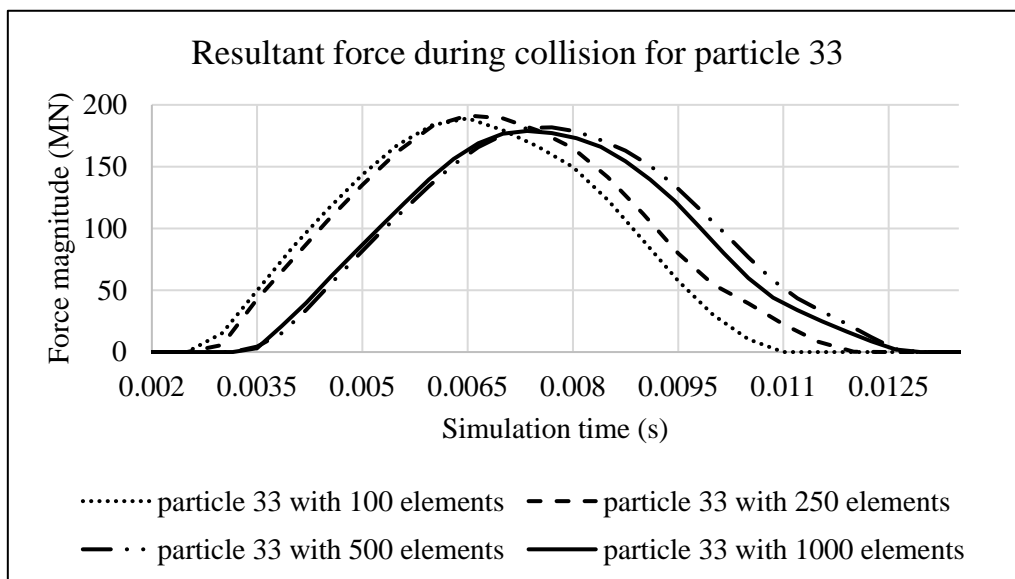


Figure 4.43 Plot of resultant forces during collision event for Particle 33.

For Particle 33 and the following case (Particle 38), the plots show that the simulation result of resultant forces have achieved almost the same force magnitude-time (impulse), and there is only a shift in time for certain curves, which is Particle 33 with 100 and 250 elements as compared to the rest of the curves; and Particle 38 with 500 elements as compared to other curves in their group, respectively.

The explanation for this situation should be connected to the change of particle's geometry after the simplification process, which has been explained in previous section (Section 4.4.1.1) that particle samples simplified into different number of elements is showing different extent of geometry, and those with lower resolutions have relatively farther protrusions than those with higher resolutions. Also, combining with the different initial contact positions resulted from inevitable errors during the moving and rotating process of particle samples, particles will correspondingly have different initial contact time, which manifested itself as the shift in time as shown in Figure 4.43 and Figure 4.45. The initial position for Particle 33 with 100 elements and 1000 elements are shown below:

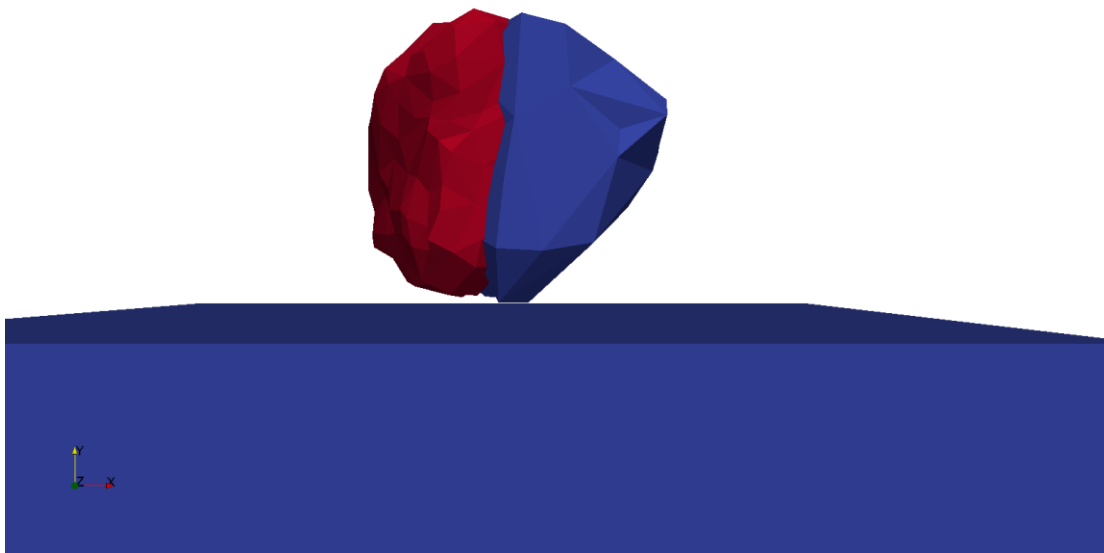


Figure 4.44 Illustration of initial position for Particle 33 with 100 elements (blue) and 1000 elements (red)

From the figure shown above, the initial position for Particle 33 with 100 elements is relatively closer to the target block, which is proving the explanation above.

b. Particle 38:

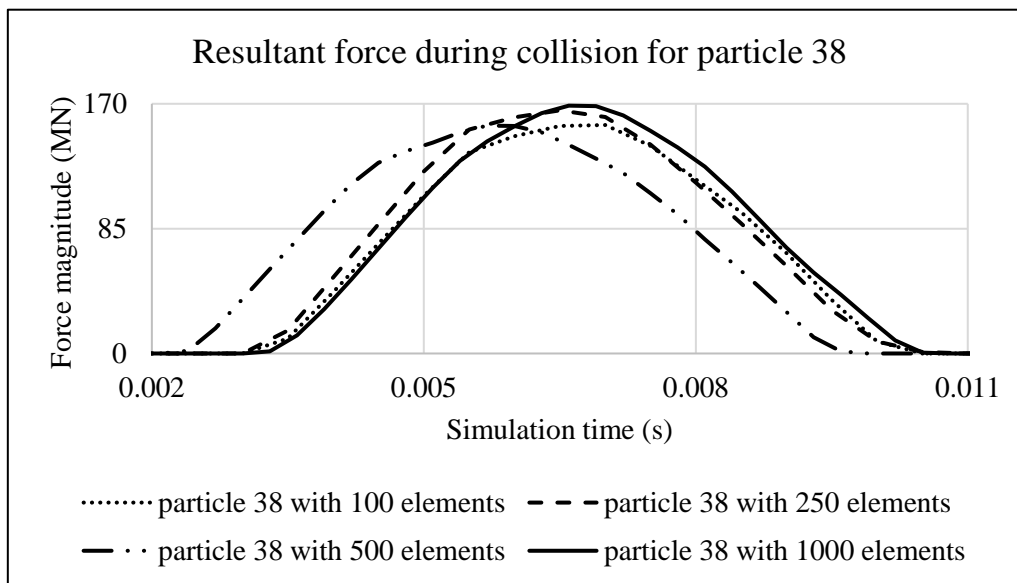


Figure 4.45 Plot of resultant forces during collision event for Particle 38.

4.4.1.6 Comparative summary of simulation data and conclusions

After the completion of simulation for phase one, all resulting data can be compared, including the impulse, peak force, start time, CPU time and simulation time (duration of the collision event). The comparison for each particle (with different element numbers) is presented as the difference of analysis results relative to the same particle ID with 100 elements. One example of the data comparison is shown below:

Percent difference analysis compared to Particle 1 with 100 elements for different group of data			
	particle 1 with 250 elements	particle 1 with 500 elements	particle 1 with 1000 elements
Impulse (MN*s)	19.73	30.35	23.04
Peak Force (MN)	3.73	6.35	7.53
Start Time (sec)	0.00	2.86	0.00
CPU Time (sec)	0.00	800.00	1250.00
Simulation Time (sec)	28.00	40.40	24.00

Table 4.8 Example of data comparison for Particle 1 with different elements comparing to Particle 1 with 100 elements.

From the data comparison for Particle 1, the percentage difference for impulse, peak force and start time of simulation for different elements is not showing much percentage changes when comparing to Particle 1 with 100 elements, and the simulation time is showing a relatively small increase, while the CPU time presented a dramatic increase with the increase of element numbers. The same was observed for the other particle simulations as well, and the extreme case for all simulations is that the CPU time increased 14200 percent for Particle 22 (with 1000 elements) as compared to Particle 22 (with 100 elements), this increase in CPU time can be illustrated on Figure 4.46 below:

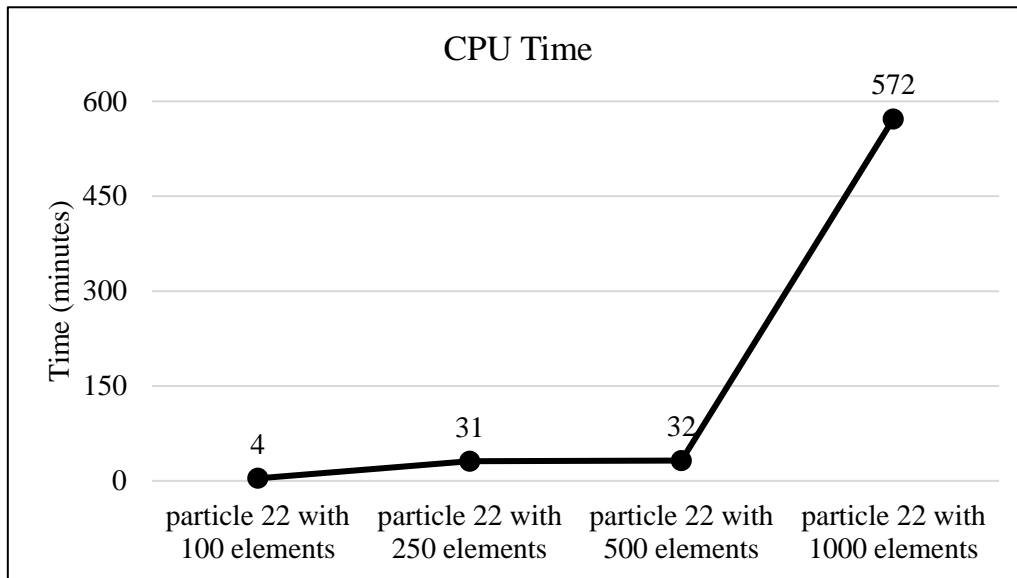


Figure 4.46 CPU time vs. model geometry resolution for Particle 22

With all simulation data collected for all particles, the mean and standard deviation were calculated for particle with different elements, comparing to the base particle with the same ID, but discretized with 100 elements, which is summarized in the following tables:

Discretization with 200 elements compare to 100 elements for 50 particles	Mean	Std. Dev.
Impulse	2.74	4.29
Peak Force	0.79	6.82
Start Time	0.27	14.44
CPU Time	458.61	312.74
Simulation Time	6.05	10.22

Table 4.9 Mean and Standard deviation calculation for all particles with 200 elements as compared to 100 elements

Discretization with 500 elements compare to 100 elements for 50 particles	Mean	Std. Dev.
Impulse	3.36	5.62
Peak Force	1.54	7.68
Start Time	-0.59	13.93
CPU Time	771.04	262.67
Simulation Time	7.05	11.21

Table 4.10 Mean value and Standard deviation calculation for all particles with 500 elements
compare to 100 elements

Discretization with 1000 elements compare to 100 elements for 50 particles	Mean	Std. Dev.
Impulse	2.82	5.88
Peak Force	3.16	8.33
Start Time	-0.48	11.98
CPU Time	2007.53	3012.19
Simulation Time	6.55	14.09

Table 4.11 Mean value and Standard deviation calculation for all particles with 1000 elements
compare to 100 elements

From the calculation of mean and standard deviation, it can be concluded that there is no really a need for increasing the discretization element numbers for all particles to run extra simulations, due to the fact that the CPU time increase dramatically with the increase of discretization elements, while the other data (impulse, peak force) are not presenting much increases. Also, from the manual of FEM/DEM that was introduced by Munjiza (2004), the total CPU time will be doubled only for the computational cost for contact detection if the size of problem doubles, and if taking consideration of the contact force calculation, the computational cost will be even larger with the increase of geometrical resolutions (Munjiza, 2004).

4.4.2 Phase 2 – Simulation of multi-particle collisions inside a container

In this section, which is the second phase of simulations, a model will be simulated in which ten particles were dropped into a container and both inter-particle and particle-container collisions were investigated. A comparison of the evolution of resultant force for each particle in different objects will be discussed as well.

Similar to phase one of the simulation, for a particle collision with a solid block, all particles were 3D scanned and their geometric details have been simplified to 100, 250, 500 and 1000 triangular elements. After the simplification process, all particles with different number of elements were separately placed into different groups. The simplification and particle generation process was the same as discussed in the previous section (Section 4.2). The following figure shows the original locations for particles with 100 elements that have been imported from the VGW into the GiD program.

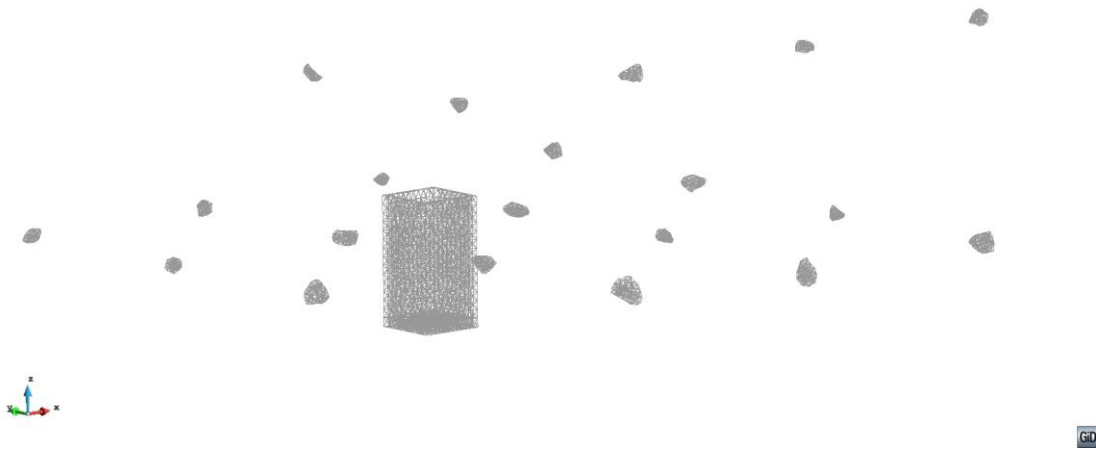


Figure 4.47 Illustration of the original locations after imported from VGW to GiD for particle samples with 100 elements along with the container.

As seen in Figure 4.47, initially the particles were randomly placed outside the container, which means that they need to be placed to their initial pre-contact positions inside the container. It is important that particles with different number of elements in subsequent simulations should maintain the same initial positions as much as possible with respect to the particles with 100 elements, to ensure a basis for comparison. What should be noticed is that all particles were placed as close as possible to each other at their initial pre-contact positions, yet there is no contact between each other. This should be done for all simulations, to minimize simulation time. The following figures show the initial pre-contact positions for all particles with 100 elements inside the container, since the opaque container will block the view of particles inside, thus the container was removed for clarity:

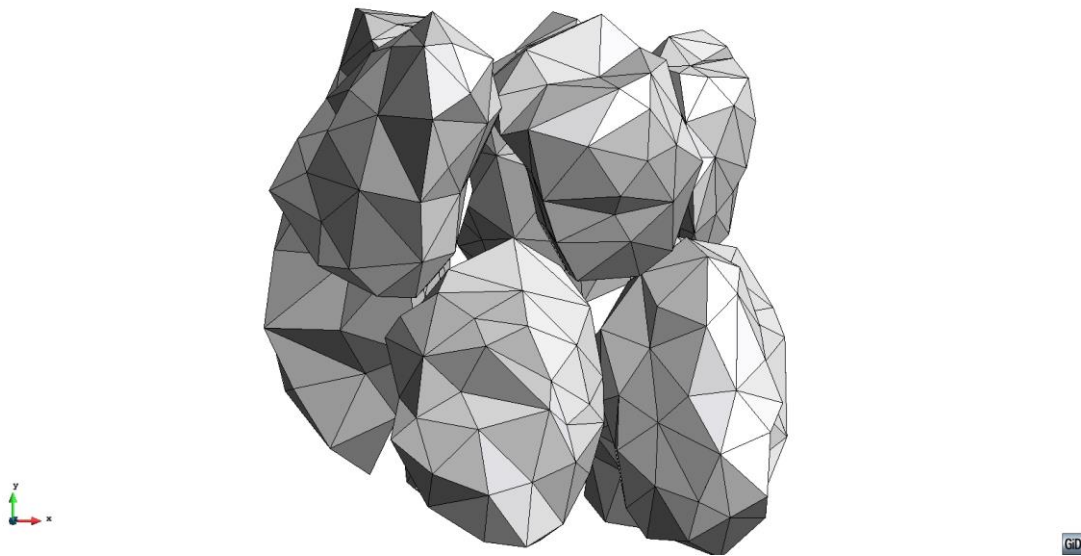


Figure 4.48 Illustration of particles initial pre-contact position for particles with 100 elements, viewing from X-Y plane

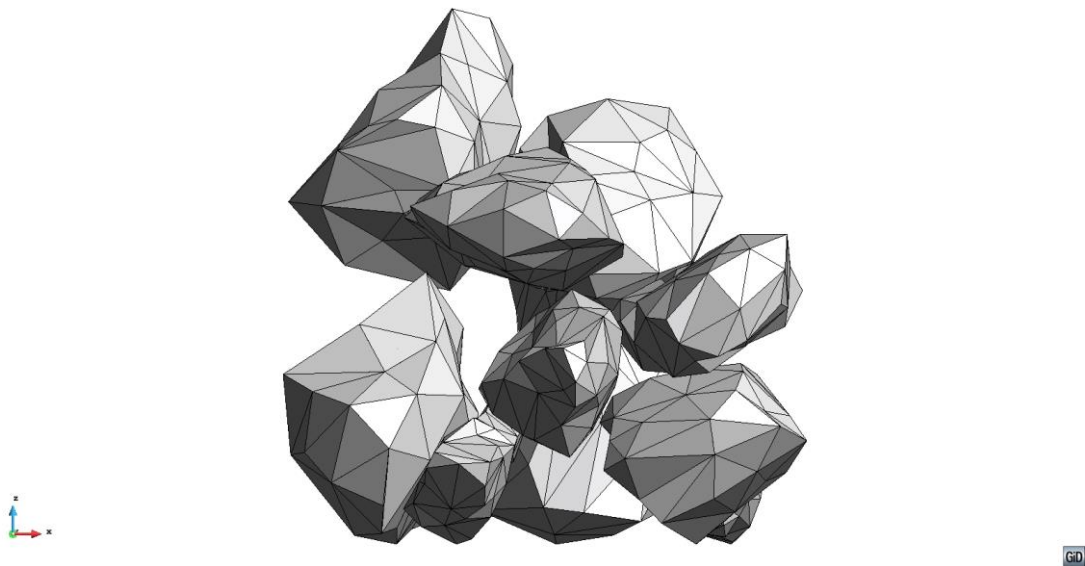


Figure 4.49 Illustration of particles initial pre-contact position for particles with 100 elements, viewing from X-Z plane

Similar to already discussed in a preceding section, for the particles with higher resolutions, the selected face nodal points on particles will always be different from lower resolutions due to the simplification process. This results in that particle samples with higher resolution can only be moved to positions as close as possible to particles with 100 elements, and followed with adjustment of positions in order to make them having the same initial pre-contact

positions as much as possible., by aligning their centers of gravity.

The pre-simulation settings, which include the initial velocity (40 m/s on $-Z$ direction) for all particle samples, except the container, and under the influence of gravity ($-9.81 \text{ m}\cdot\text{s}^{-2}$), simulation have been conducted after several trial runs. Since the simulation for higher resolutions involves large numbers of contacting couples, and taking consideration of computational cost, the simulation time range was tested for a few times in order to have an optimal selection; high enough resolution for particle geometry but a reasonable computation time (a few days). While, for particles with 1000 elements, the CPU time cost was prohibitive, which was estimated to be over a month to have the simulation complete and thus the simulation for particles with 1000 elements was abandoned.

The following figures show the simulation results of the resultant force comparison for each particle geometry discretization:

a. The forces on the container:

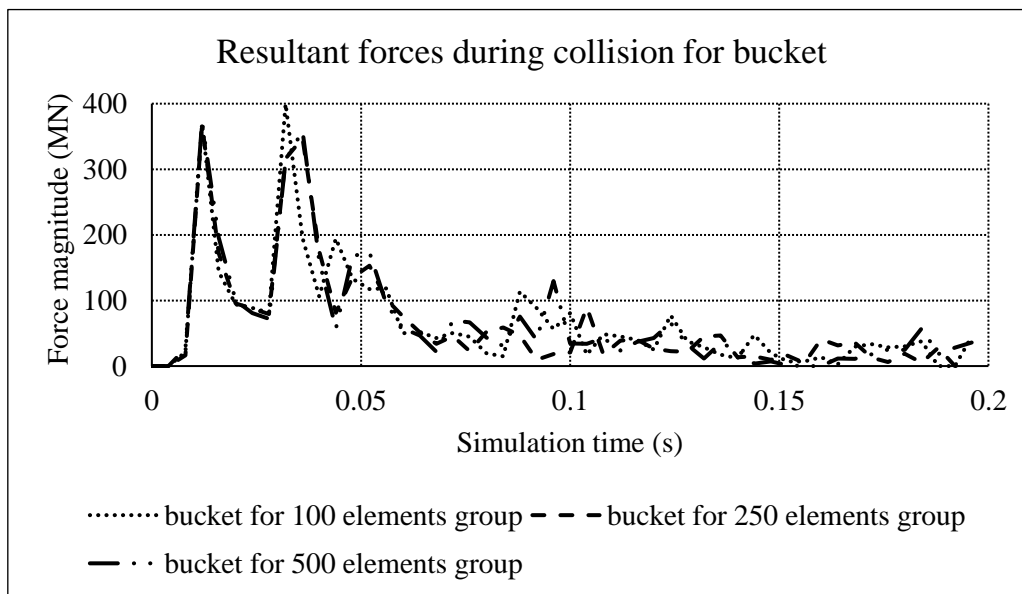


Figure 4.50 Total resultant forces acted on the container (all forces acted on both bottom and sides) comparison during different collision events.

From the resultant force comparison as shown above, the container experienced almost the same force-magnitude time (impulse) during the different collision events, and the curves shown in Figure 4.50 are almost overlapping with each other. It can be observed from the figure that the first two peaks (collisions) generally coincide, regardless of the element discretization used. Subsequent collisions show variation, but their average magnitude

remains the same. This verifies that the total resultant force acted on the container during different collision events are very similar in magnitude and exhibit the same pattern during the whole simulation process.

b. Resultant force plots are almost overlapping and showing very similar pattern:

For example, in this group, a number of selected particle simulation results will be presented, which is showing that their resultant force curves are relatively overlap with each other. Similar overlap was found for the rest of the particles used in the simulation. This select group includes Particles 1 through 6. Their resultant force plots are shown below:

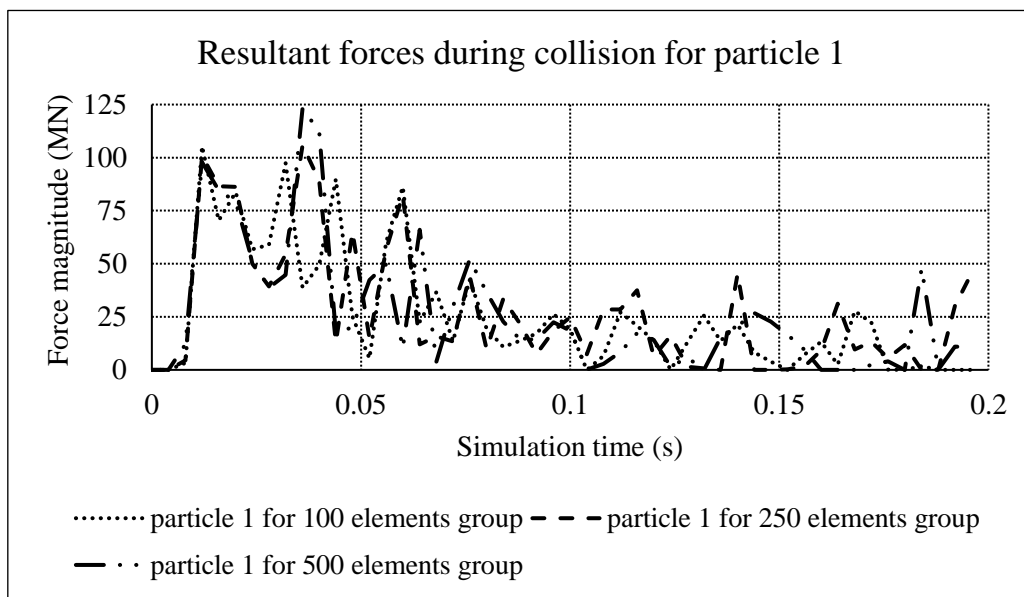


Figure 4.51 Resultant forces comparison for Particle 1 during different collision events

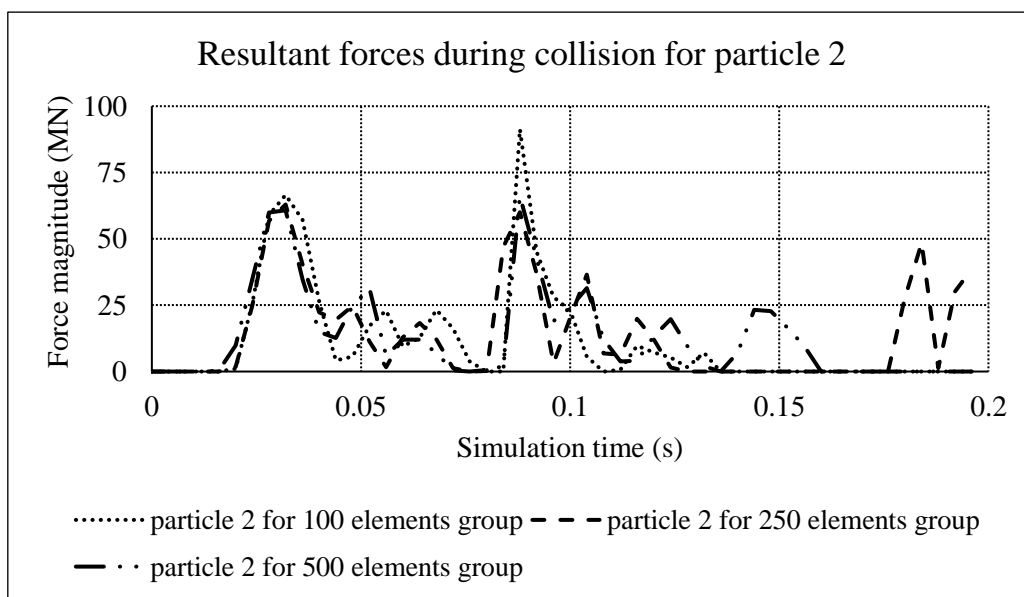


Figure 4.52 Resultant forces comparison for Particle 2 during different collision events

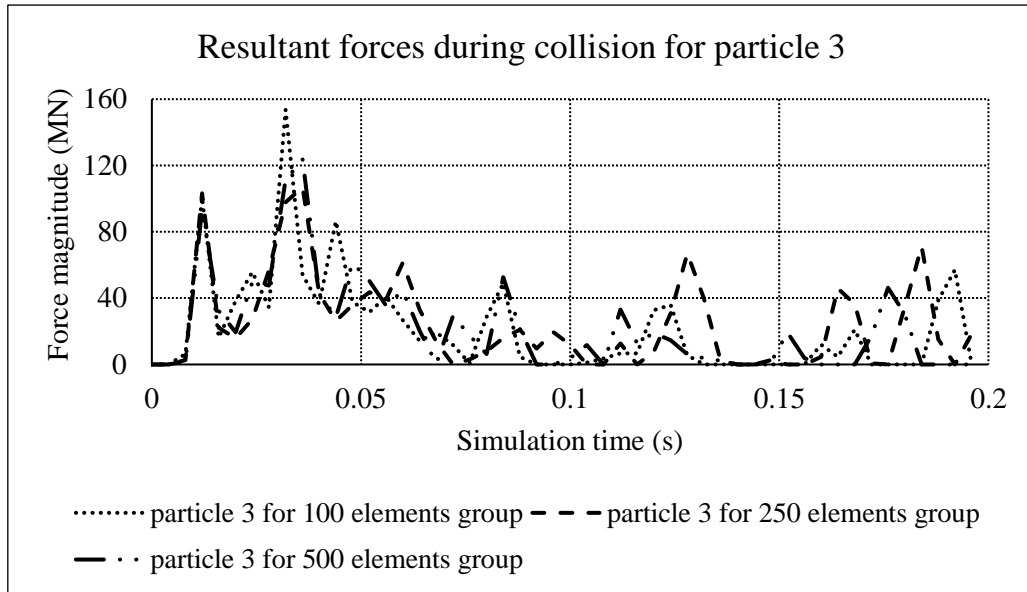


Figure 4.53 Resultant forces comparison for Particle 3 during different collision events

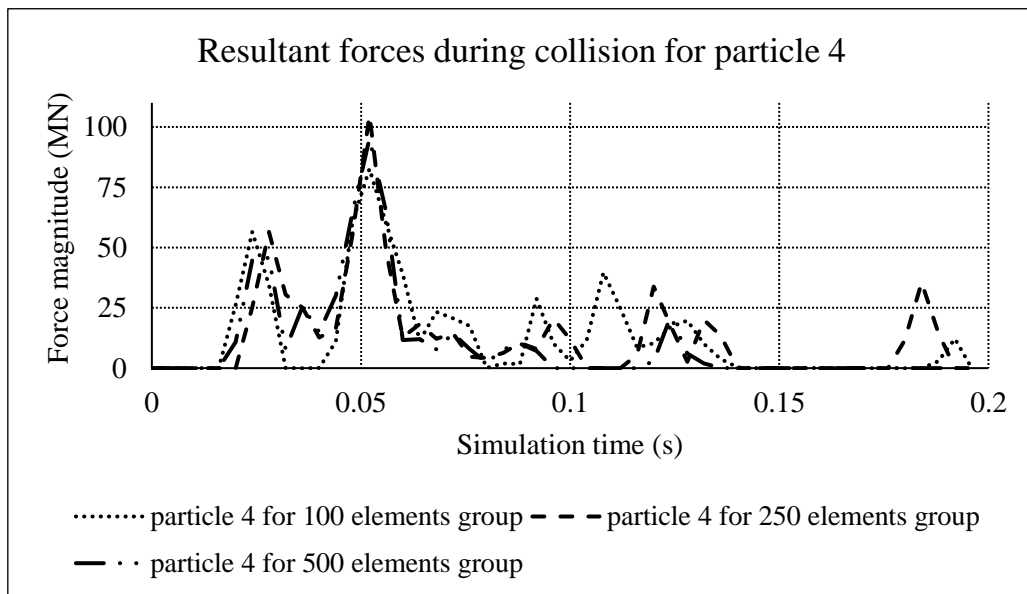


Figure 4.54 Resultant forces comparison for Particle 4 during different collision events

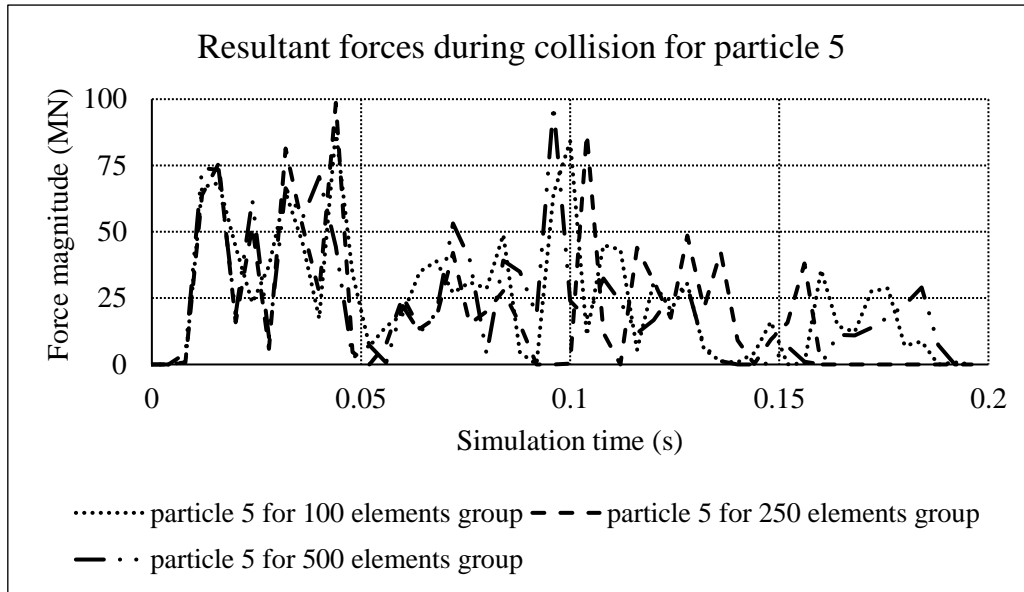


Figure 4.55 Resultant forces comparison for Particle 6 during different collision events

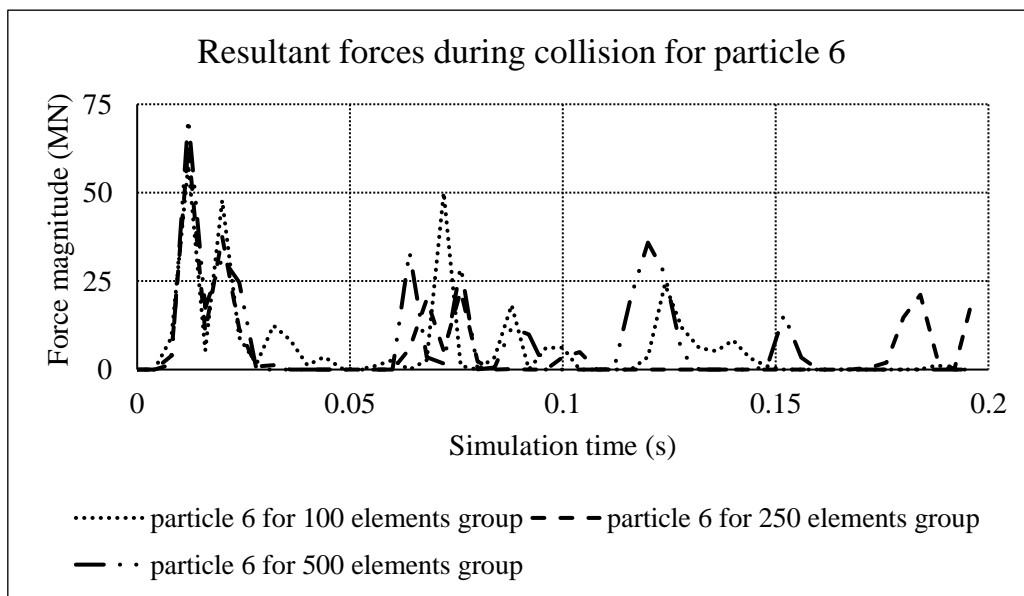


Figure 4.56 Resultant forces comparison for Particle 6 during different collision events

From the figures shown above, even though these curves of resultant forces for different particles during different collision events are not perfectly overlapping, it can be concluded that a similar pattern of resultant force during the whole simulation emerges. For those parts that are not overlapping with each other, it should be recalled that the difference of initial pre-contact positions and different geometric discretization does influence some particle's behavior in the process of simulation, and this resulted in those non-overlapping parts on

these curves presented above.

c. Resultant force plots showing relatively large differences

In this this group fall all the particles not included in the previous group; Particles 7 through 10. Their resultant force comparison figures are shown below:

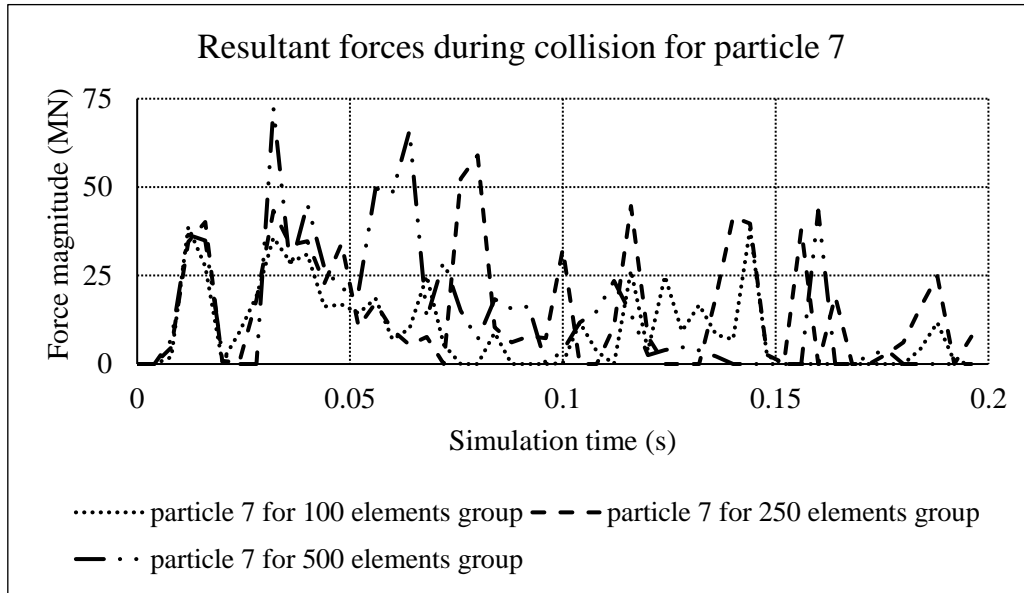


Figure 4.57 Resultant forces comparison for Particle 7 during different collision events

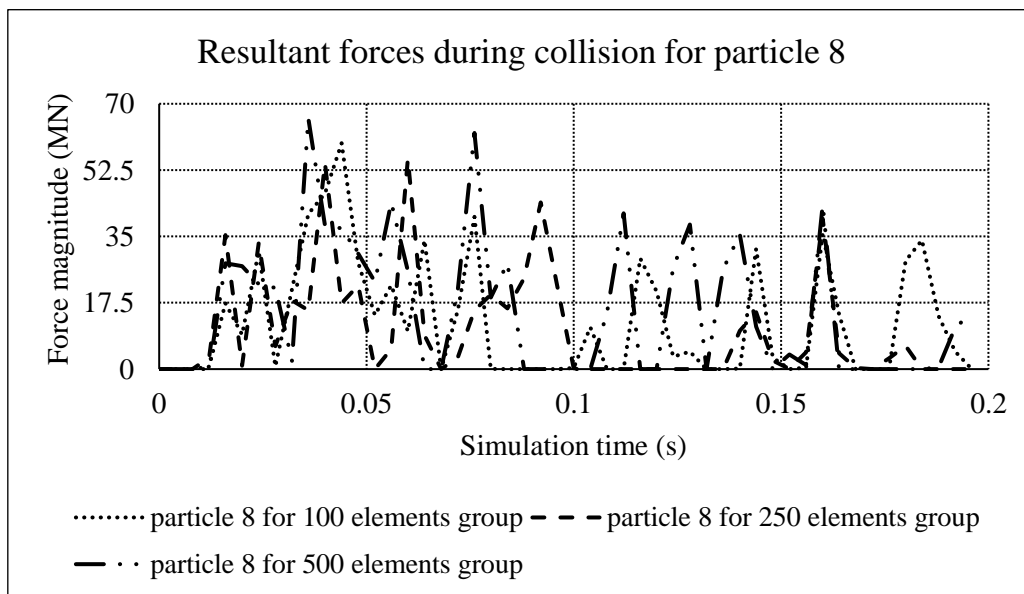


Figure 4.58 Resultant forces comparison for Particle 8 during different collision events

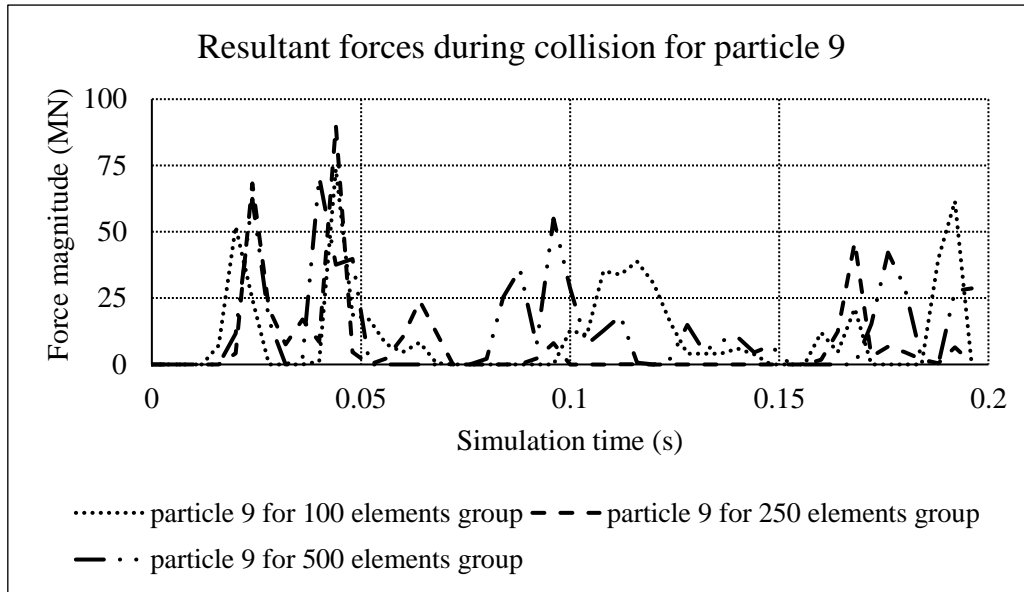


Figure 4.59 Resultant forces comparison for Particle 9 during different collision events

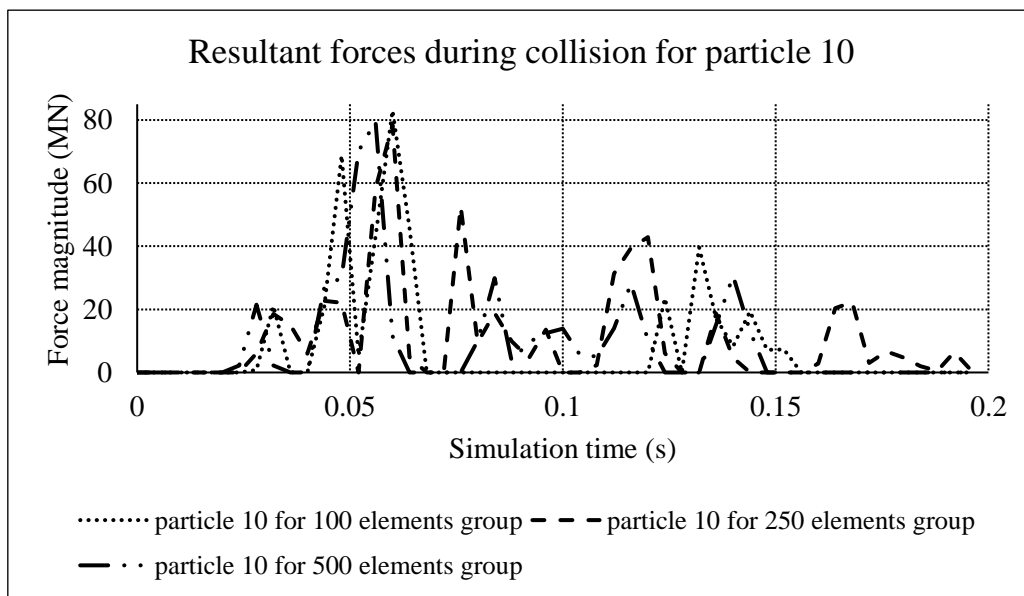


Figure 4.60 Resultant forces comparison for Particle 10 during different collision events

From the figures shown above, these particles' resultant force curves are showing a pattern that at the beginning, the curves are almost overlapping or close to each other. This means that the resultant forces or the initial contact for these particles are similar to each other; while, after the first peak occurs (which represents the first full contact for these particles with adjacent particle(s)), the resultant force curves are diverging from each other both in time and magnitude. This could be related to the initial pre-contact position and different

extent of geometry, which influenced the contacting process for these particles with other particles. Since the simulation is about multi-particles collision, the influence of initial position will be enlarged with the progression of collision events; and for those particles with higher resolutions, the nodal points that are used during the contact event will be much higher than those with lower resolutions, which also influenced the resultant force calculation during the whole simulation process. Also, with the change of geometric detail, the difference of the extent of geometry will influence the contact detection algorithm, which is assuming that all discrete elements have cubic bounding objects, and the edge of the bounding cube is determined by the largest discrete element. The algorithm for contact detection will assume that the contacting couples are in contact once the bounding objects are intersecting each other (Munjiza, 2004). Thus, with the change of resolution and extent of geometry, the contact detection algorithm will be different and provide different simulation results.

5 Conclusion and Recommendations for Future Work

This chapter will conclude the work that has been done in the thesis and summarize the results. In addition, recommendations of improvements for the FEM/DEM simulation of granular media will be given as well. The aims and targets that have been proposed in Section 4 have all been achieved. In this thesis, the collision behavior of a particle-block collision and a group of particles colliding with each other and a container were simulated using the FEM/DEM. The simulation results have all been collected, which include the resultant force, impulse and CPU time, and these results have all been compared to each other with respect to the particle that has the lowest resolution (discretized with 100 elements).

5.1 Conclusion

The aim of this thesis was focused on the study of the effect of geometrical details on the outcome of DEM simulation results by using the FEM/DEM. By comparing different numerical and experimental methods, the FEM/DEM was chosen as a suitable tool for the simulation purpose, as its advantages have been introduced in Section 3.3. From Section 4, the simulation process has been introduced in detail, and, as far as the author is aware of, this is the first time the influence on simulation results from the change of geometric and asperity details has been studied, and the process of converting 3D scanned particles into suitable formats of 10-node tetrahedrons as required by the FEM/DEM program should be carefully applied (the reader is referred to Section 3.2.2 for more details).

As covered in Section 3.4, the simulation results have all been presented and analyzed based on individual particle collisions with a solid block and groups of particles colliding inside a container.

For individual particles with different number of elements, colliding with a solid block under the influence of gravity respecting the same initial velocities for each particle, the results of resultant forces show that most of particles (with different number of elements) have similar results (overlapping resultant force plots). For those particles, which simulation

results present differences in the shape of resultant force plots, a variety of reasons have been discussed in Section 4.4.1. Including the inevitable operational errors and potential reasons connected to the computational algorithm that is used by the FEM/DEM.

For the simulation with a group of particles (10 particles with different number of elements) colliding inside a container under the influence initial velocity for all particles and gravity for both particles and the container, the simulation results show that the container did not experience a significant change in the forces applied as the geometrical detail of particles was changed. For individual particles (with different number of elements), some of the particles showed similar pattern of resultant force plots while some of them had relatively large differences in the shape of plots for resultant force curves. These differences also have been explained in Section 4.4.2, which is mainly connected to the influence of initial positions and potential influences connected to the contact detection algorithm affected by the change of geometrical details and extend of geometries.

By having all data compared for the two different simulation results, it is evident that the increase of CPU time with the increase of particles' resolutions is dramatic, and it becomes non-affordable with even higher resolutions, especially for simulations in phase two of this thesis, having multi-particles colliding inside a container, which has been detailed explained in Section 4.4.2. Then, as recommended by author, if the reader is performing simulations involving large quantities of particles with different number of elements, it appears that 500 elements for each particle should be adopted as an upper limit to have a reasonable computational time with the application of FEM/DEM while ensuring that simulation results are representative.

5.2 Future work

Even though the aims and objectives all have been achieved for this thesis, there are still some aspects that can be improved in the future, which includes the following issues:

1. High computational cost and CPU usage

Generally, the computational cost of FEM/DEM is too high, especially for simulation

of 3D model geometries with high resolution. It is pressing that a faster execution should be developed to decrease the computational cost and CPU usage in order to have simulations with higher resolutions. Perhaps a parallel, multi-core implementation or a GPU-based version should be developed.

2. Support of different particle geometry formats

Currently, as has been discussed in Section 4.4.2, the VGW only supports particle formats as constant strain tetrahedra in 3D. This is by taking consideration that they are the simplest type of elements, which can save the computational cost to some extent and the contact detection will be simpler. While the drawbacks are also outstanding as that there will be a greater number of elements that need to be generated as compared to if the use a higher-order element type is adopted. Hexahedral elements for example would be an alternative, since there will be five to six tetrahedra needed to generate a parallel hexahedron, and in this way the total number of elements will be decreased that can save more computational time.

3. Restart file and a unified pre/post-processing environment

Currently, the pre/post-processing for this thesis includes 3 different programs; GiD, VGW and Paraview, which is not convenient for user to collect simulation data and the whole process is intricate since there are a lot of files generated from different programs. Thus, a unified pre/post-processing environment should be developed for the convenience of simulation and data collection.

Another concern is that during the simulation process, there is no restart file in the current FEM/DEM program. If there are unexpected incidents happen during the running process of simulation, the execution of data will be lost before the completion of simulation, and the user will not be able to execute any data even some output files have already been generated (.ym files), and the user has to restart the whole simulation from the beginning. Thus, a restart file is needed to allow the user to continue the simulation from the break point, and this is helpful for simulations with high resolutions due to the fact that these simulations are about

to have long simulation time (days) and they have high risks of having unexpected incidents during the simulation process.

6 Bibliography

1. Ahrens, J., Geveci, B., Law, C.. (2005). *ParaView: An End-User Tool for Large Data Visualization*. Visualization Handbook, Elsevier, ISBN-13: 978-0123875822.
2. Andrews, A. M. (2000). Penalty function method for combined element systems comprising large number of separate bodies. *INTERNATIONAL JOURNAL FOR NUMERICAL METHODS IN ENGINEERING*, 49:1377-1396.
3. Bardet, J. (1998). Introduction to computational granular mechanics. *Behaviour of granular materials*, Number 385 in CISM Courses and Lectures. Springer-Verlag.
4. Burkardt, J. (2009, October 01). *TET_MESH_L2Q*. Retrieved from https://people.sc.fsu.edu/~jburkardt/m_src/tet_mesh_l2q/tet_mesh_l2q.html
5. Burkardt, J. (2009, October 01). *TET_MESH_L2Q*. Retrieved from http://people.sc.fsu.edu/~jburkardt/m_src/tet_mesh_l2q/tet_mesh_l2q.html
6. Coll, A. and Ribio, R. and Pasenau, M. and Escolano, E. and Perez, J.Suit. and Melendo, A. and Monros, and Giarate. A. (2016). *Reference Manual*. Retrieved from GiD The personal pre and post processor: <http://www.gidhome.com/documents/referencemanual/PREPROCESSING/Mesh%20Menu/Element%20type>
7. Cundal P.A., Strack O.D.L. (1979). A discrete element model for granular assemblies. *Geotechnique*, 29(1):47-65.
8. Cundall, P. (1987). Distinct element models of rock and soil structure. In E. Brown (Ed.), *Analytical and Computational Methods in Engineering Rock Mechanics*, Allen and Unwin.
9. Cundall, P.A. and Hart, R.D. (1993). Numerical modeling of discontinua. *Comprehensive Rock Engineering*, 35-39.
10. Cundall, P. and Strack, O. (1978). The distinct element methods as a tool for research in granular media, Part I. *Report to NSF*.

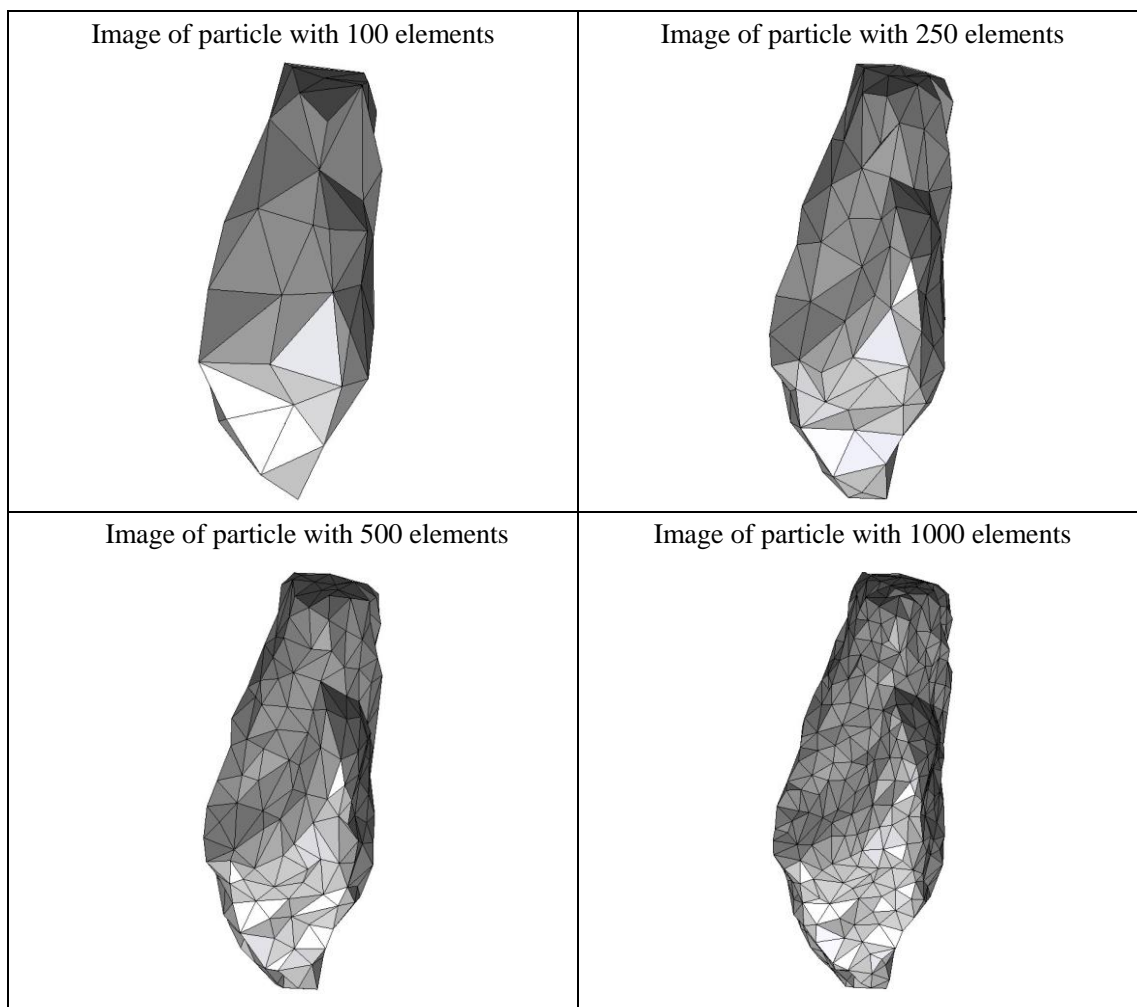
11. Cundall, P. and Strack., O. (1979a). A discrete numerical model for granular assemblies. *Geotechnique* 29 (1), 47-65.
12. Delaney, G., Inagaki, S., and Aste, T. (2007). Fine tuning DEM simulations to perform virtual experiments with three dimensional granular packings. In Y. Aste, T. Di Matteo, and Tordesillas A. (Eds.). *Granular and Complex Materials*, 141–168. World Scientific.
13. Dickinson, C. (October 2013). *Learning Game Physics with Bullet Physics and OpenGL*. Birmingham: Packt Publishing.
14. Garcia, X. (2009, 12). *Appendix A: Notes on the Shape Library*. Retrieved from Manual-P3D_XGarcia.pdf:
http://vgest.net/wp-content/uploads/2009/12/Manual-P3D_XGarcia.pdf
15. Hogue, C. (1998). Shape representation and contact detection for discrete element simulations of arbitrary geometries. *Engineering Computations* 15 (10), 374–389.
16. Itasca. (2003). *PFC 3D user manual*. Minneapolis.: Itasca consulting group Inc.
17. Itasca Consulting Group, I. (2004). *PFC2D 3.10 Particle Flow Code in Two Dimensions, Theory and Background volume (Third ed.)*. Minneapolis,Minnesota.
18. Itasca Consulting Group, I. (2008). *PFC3D 4.0 Particle Flow Code in Three Dimensions, Theory and Implementation Volume*. Minneapolis, Minnesota.
19. Xiang, J., Latham, J.-P., Munjiza, A. (2008). *Read me: Tour of the " Virtual Geoscience Workbench"*. London: Queen Mary University of London (QMUL) & Imperial College of Science, Technology and Medicine (ICSTM).
20. Xiang, J., Munjiza., A. (2008). *Manual For The "Y3D" FEM/DEM Computer Program*. London: Queen Mary University of London (QMUL) & Imperial College of Science, Technology and Medicine (ICSTM). .
21. Johnson, K. (1985). *Contact Mechanics*. Lundun: the Press Syndicate of the University of Cambridge.
22. Matuttis, H-G. and Chen, J. (2014). *Understanding the Discrete Element Method: Similation of Non-Spherical Particles for Granular and Multi-body Systems*. Singapore: John Wiley & Sons.
23. Mindlin, R. (1949). Compliance of elastic bodies in contact. *ASME Journal of Applied*

- Mechanics* 16, 259-269.
24. Mindlin, R. and Deresiewicz., H. (1953). Elastic spheres in contact under varying oblique forces. *ASME Journal of Applied Mechanics* 20, 327-344.
 25. Munjiza, A. (2004). *The Combined Finite-Discrete Element Method*. London: John Wiley & Sons, Ltd.
 26. Munjiza, A., Andrews, K.R.F., White, J.R. (1997). Discretized contact solution for combined finite–discrete method. *5th ACME Conference*, (pp. 96–100). London UK.
 27. Munjiza, A., Knight, E. and Rougier, E. (2011). *Computational Mechanics of Discontinua*. John Wiley and Sons.
 28. Munjiza, A., Owen, D.R.J., and Bicanic, N. (1995). A combined finite-discrete element method in transient dynamics of fracturing solids. *Engineering Computations*,12, 145-174.
 29. NextEngine Inc. (2014). *NextEngine 3D Laser Scanner*. Retrieved from NextEngine 3D Laser Scanner Web site: <http://www.nextengine.com/>
 30. O’Sullivan, C., Bray, J.D. (2004). Selecting a suitable time step for discrete element simulations that use the central difference time integration scheme. *Eng.Comput.* 21,, 347–358.
 31. O’Sullivan, C. (2011). *Particulate Discrete Element Modelling: A Geomechanics Perspective*. London and New York: Spon Press.
 32. P. Cignoni, Callieri, M., Corsini, M., Dellepiane, M., Ganovelli, Ranzuglia, G. (2008). MeshLab: an Open-Source Mesh Processing Tool . *Sixth Eurographics Italian Chapter Conference*, page 129-136.
 33. Potyondy, D.O. (2004). A bonded-particle model for rock. *International Journal of Rock Mechanics and Mining Sciences* 41(8), 1329-1364.
 34. Hart, P.A. (1988). part ii. mechanical calculations for motion and interaction of a system composed of many polyhedral blocks. In P. A. R. Hart, *Formulation of a three-dimensional distinct element model* (pp. 25(3):117-125). International journal of rock mechanics and mining sciences & geomechanics abstracts.
 35. Ramachandran, P. (2007). *Mayavi*. Retrieved from The MayaVi Data Visualizer: <http://mayavi.sourceforge.net/index.html>

36. Thornton, C. (1999). Interparticle relationships between forces and displacements. In *M. Oda and K. Iwashita (Eds.), Mechanics of Granular Materials* (pp. 207-217, Chapter 3.4). A.A. Balkema.
37. Thornton, C. and Yin, K. (1991). Impact of elastic spheres with and without adhesion. *Powder Technology* 65, 153-166.
38. Vu-Quoc, L., Lesburg, L., and Zhang, X. (1 July 2007). An accurate tangential force-displacement model for granular-flow simulations: Contacting spheres with plastic deformation, force-driven formulation. *Journal of Computational Physics*, Vol.225, No.1, pp.730-752.
39. Vu-Quoc, L., X. Zhang, and Walton, O. (2000). A 3-D discrete element method for dry granular flows of ellipsoidal particles. *Comput. Methods Appl. Mech. Engrg.* 187, 483-528.
40. Walton, O. and Braun, R. (1986). Viscosity, granular-temperature and stress calculations for shearing assemblies of inelastic, frictional disks. *Journal of Rheology* 30 (5), 949–980.
41. Zhu, H.Z. (2007). Discrete particle simulation of particulate systems: Theoretical developments. *Chemical Engineering Science* 62 (13), 3378–3396.
42. Zsaki, A. (2015). Computer program to calculate radius of gyration of polyhedral bodies. Concordia University.

Appendix

Summary of particle characteristics and collision simulation details for Particle 1 (of 50)



Particle statistics (part 1)								
Particle ID	# vertices	# elements	Mass (g)	Moments of Inertia			Volume (cm ³)	Sfc. Area (cm ²)
				I1	I2	I3		
				(gcm ²)	(gcm ²)	(gcm ²)		
1 (100 elements)	52	100	104.371	1439523.1	1302885.7	396195	37.37396	71.32307
1 (250 elements)	127	250	104.371	1554749	1410144.9	419641.65	38.82754	72.71371
1 (500 elements)	252	500	104.371	1574833.9	1428910.6	424177.9	39.06975	73.52756
1 (1000 elements)	502	1000	104.371	1584457.5	1437565.5	425222.65	39.14609	74.00485

Appendix

Particle Statistics (part 2)							
Particle ID	α	R_g (cm)	ψ	R_v (cm)	L (cm)	I (cm)	S (cm)
1 (100 elements)	3.00654	4.00290	0.75794	2.07409	335.25779	159.76822	111.50952
1 (250 elements)	3.04207	4.01520	0.76260	2.10063	349.18895	164.41038	114.78657
1 (500 elements)	3.04475	4.01709	0.75729	2.10499	351.53490	165.26126	115.45593
1 (1000 elements)	3.05449	4.01359	0.75338	2.10636	352.70723	165.55283	115.47171

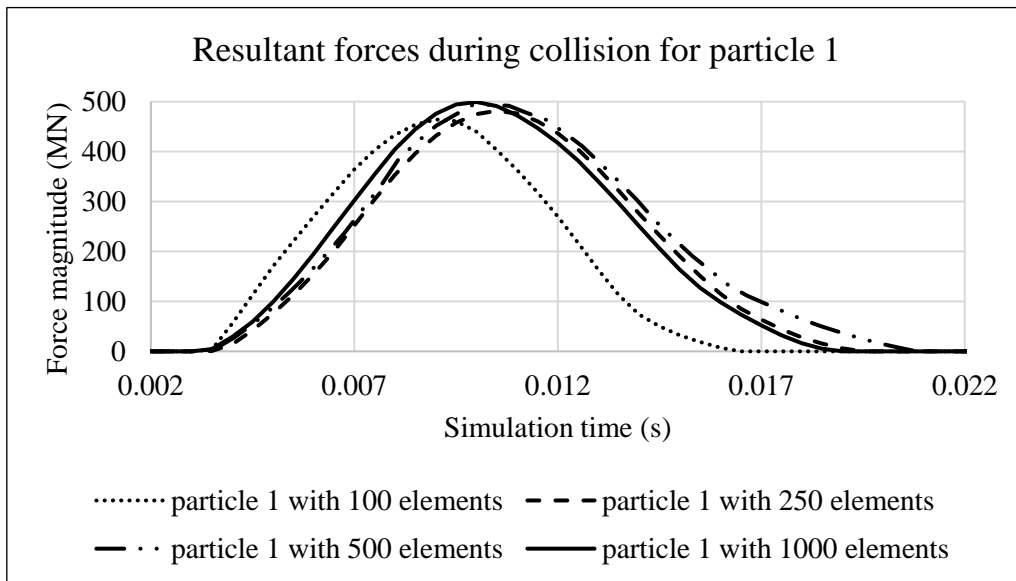


Figure A1.1 Plot of resultant forces during collision event for Particle 1.

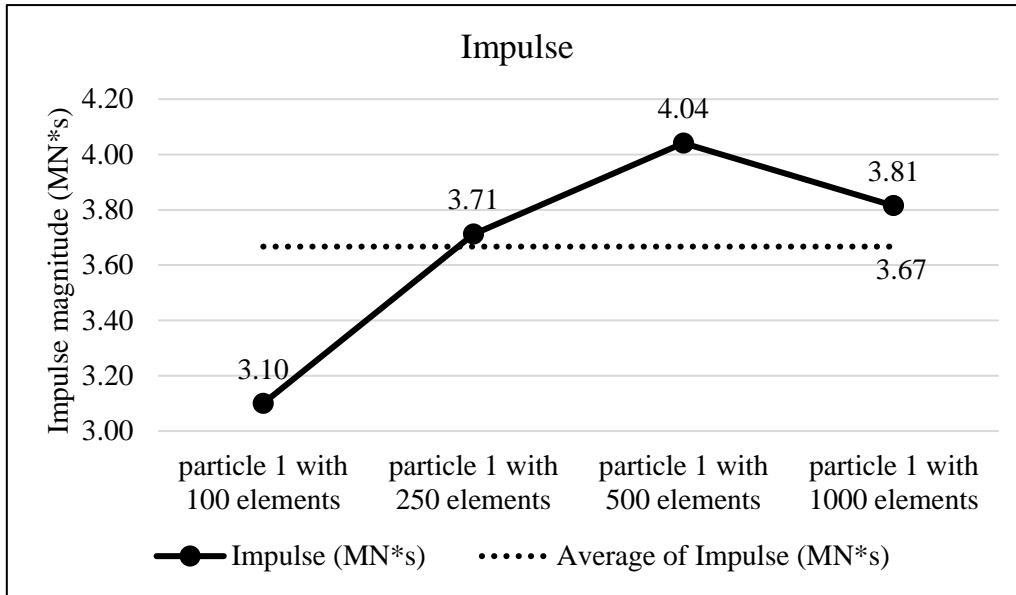


Figure A1.2 Plots of collision impulse for Particle 1.

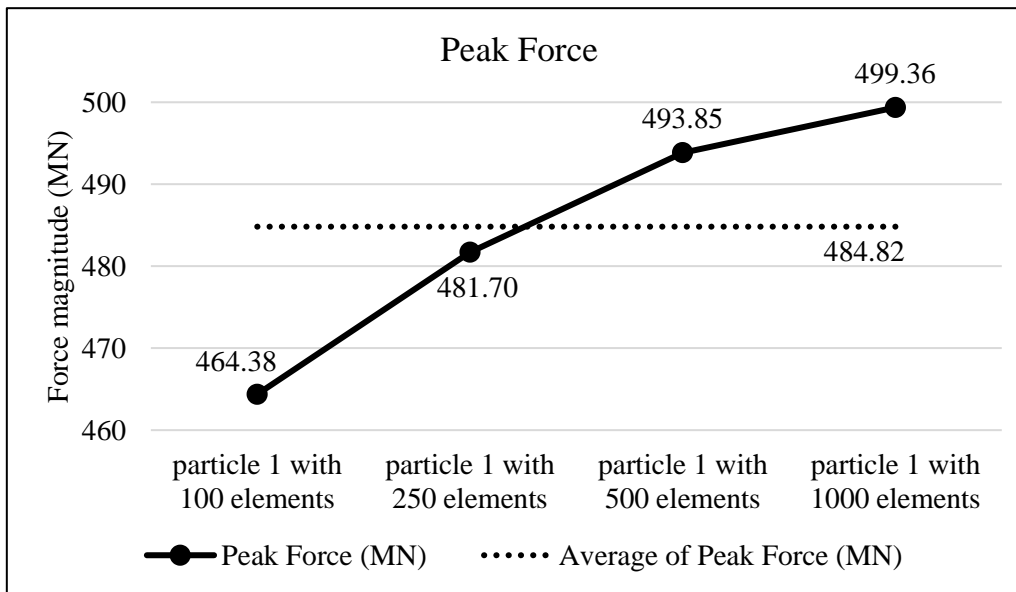


Figure A1.3 Peak collision for the four particle geometry resolutions for Particle 1.

Appendix

Collision results data analysis					
Model	particle 1 with 100 elements	particle 1 with 250 elements	particle 1 with 500 elements	particle 1 with 1000 elements	Average
Impulse (MN*s)	3.10	3.71	4.04	3.81	3.67
Percent difference from Avg. Impulse	-15.46	1.23	10.20	4.02	
Peak Force (MN)	464.38	481.70	493.85	499.36	484.82
Percent difference from Avg. Peak Force	-4.22	-0.64	1.86	3.00	

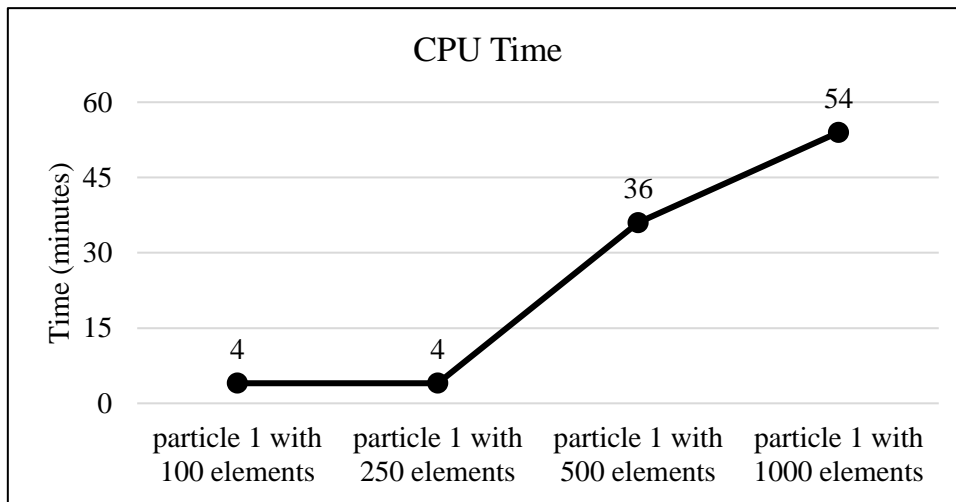
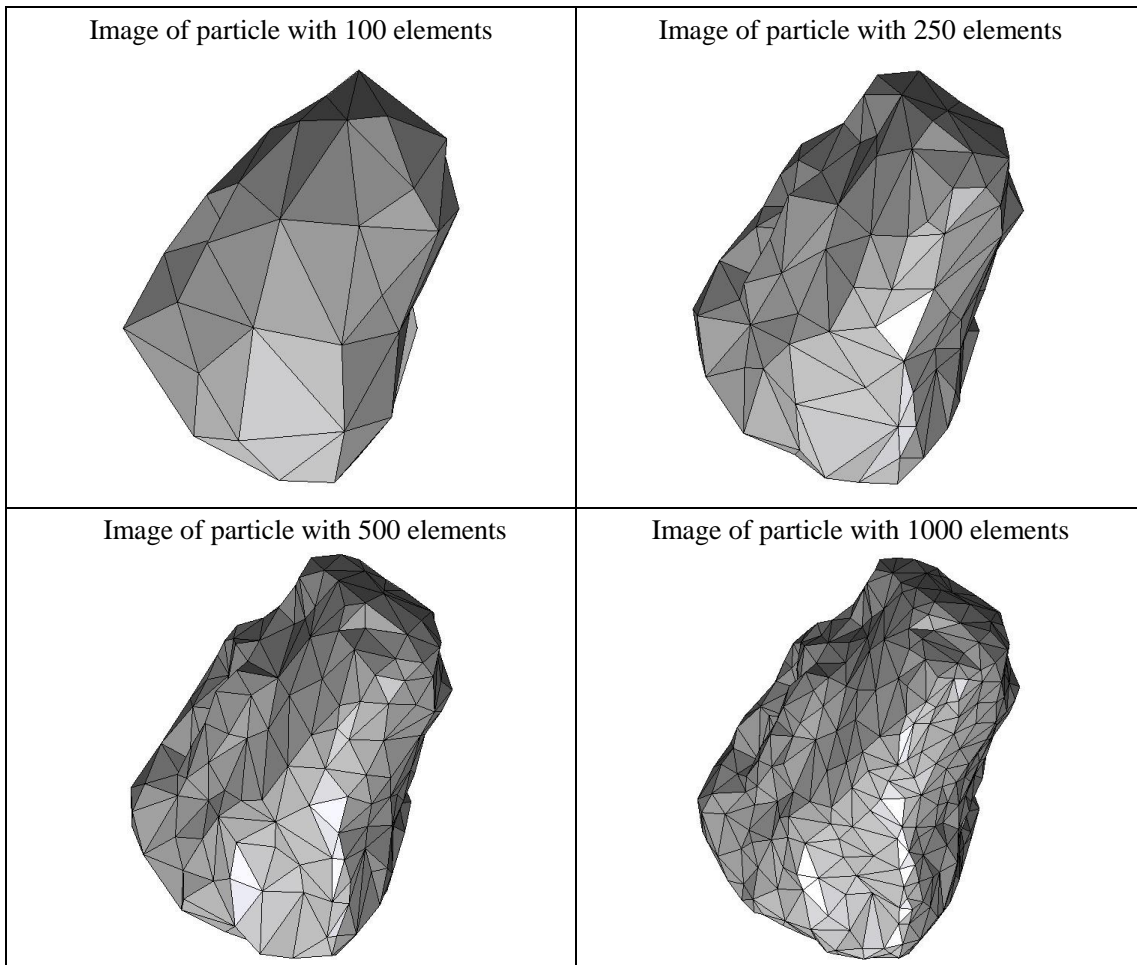


Figure A1.4 CPU computation time vs. model geometry resolution

Appendix

Percent difference analysis compare to particle 1 with 100 elements for different group of data			
	particle 1 with 250 elements	particle 1 with 500 elements	particle 1 with 1000 elements
Impulse	19.73	30.35	23.04
Peak Force	3.73	6.35	7.53
Start Time	0.00	2.86	0.00
CPU Time	0.00	800.00	1250.00
Simulation Time	28.00	40.40	24.00

Summary of particle characteristics and collision simulation details for Particle 2 (of 50)



Particle statistics (part 1)								
Particle ID	# vertices	# elements	Mass (g)	Moments of Inertia			Volume (cm ³)	Sfc. Area (cm ²)
				I1	I2	I3		
				(gcm ²)	(gcm ²)	(gcm ²)		
2 (100 elements)	52	100	59.744	437088.1	386249.05	243892.7	23.51913	47.18736
2 (250 elements)	127	250	59.744	456038.5	398895.125	251763.45	23.94151	47.95853
2 (500 elements)	252	500	59.744	459236.35	402343.575	253879.05	24.03775	48.11104
2 (1000 elements)	502	1000	59.744	461032.7	403917.625	254895.55	24.08770	48.15363

Appendix

Particle Statistics (part 2)							
Particle ID	α	R_g (cm)	ψ	R_v (cm)	L (cm)	I (cm)	S (cm)
2 (100 elements)	1.73247	2.79305	0.84128	1.77737	220.21341	157.05484	127.10916
2 (250 elements)	1.76046	2.74828	0.83763	1.78795	224.67657	160.78725	127.62380
2 (500 elements)	1.75641	2.76137	0.83721	1.79034	225.51882	161.27189	128.39728
2 (1000 elements)	1.75628	2.77351	0.83763	1.79158	225.95516	161.59300	128.65586

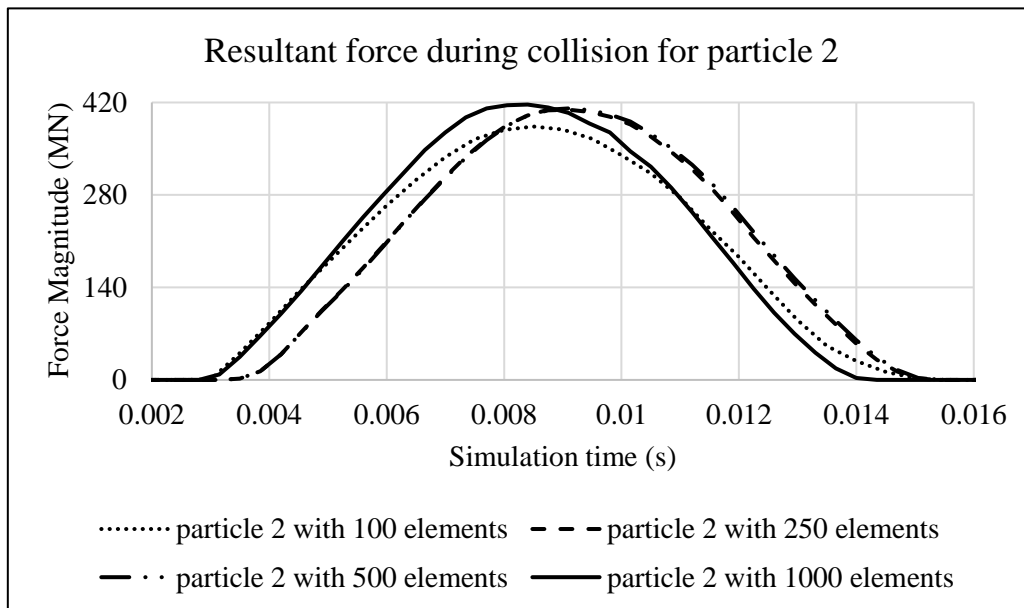


Figure A2.1 Plot of resultant forces during collision event for Particle 2.

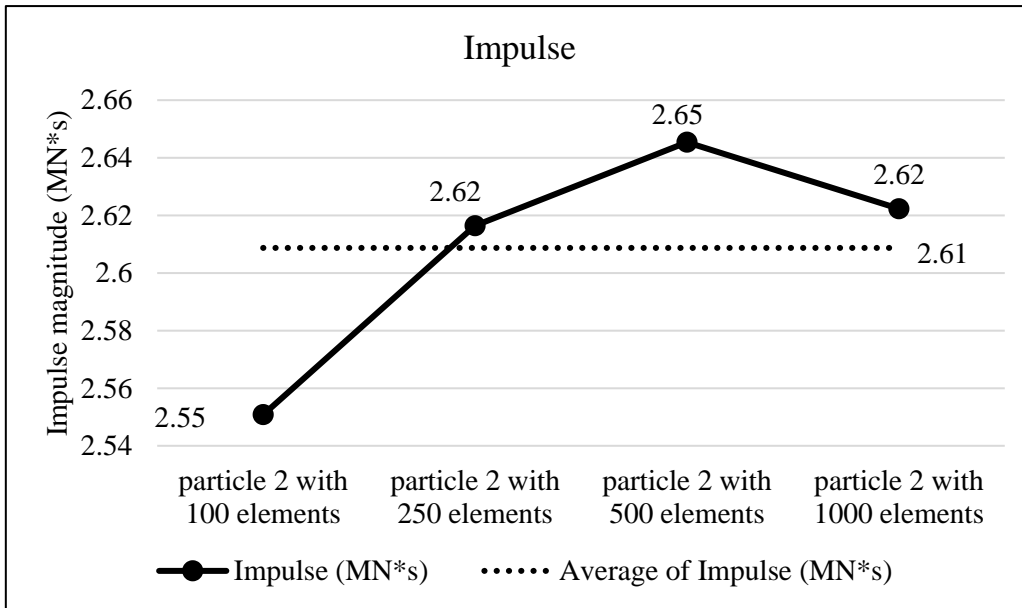


Figure 2.2 Plots of collision impulse for Particle 2.

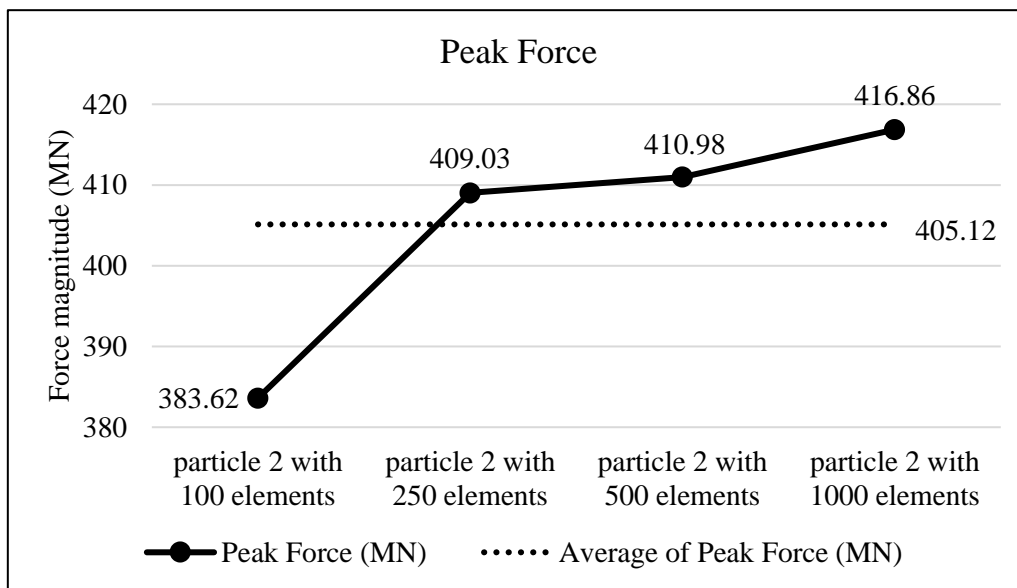


Figure A2.3 Peak collision for the four particle geometry resolutions for Particle 2.

Appendix

Collision results data analysis					
Model	particle 2 with 100 elements	particle 2 with 250 elements	particle 2 with 500 elements	particle 2 with 1000 elements	Average
Impulse (MN*s)	2.55	2.62	2.65	2.62	2.61
Percent difference from Avg. Impulse	-2.22	0.29	1.41	0.52	
Peak Force (MN)	383.62	409.03	410.98	416.86	405.12
Percent difference from Avg. Peak Force	-5.31	0.97	1.45	2.90	

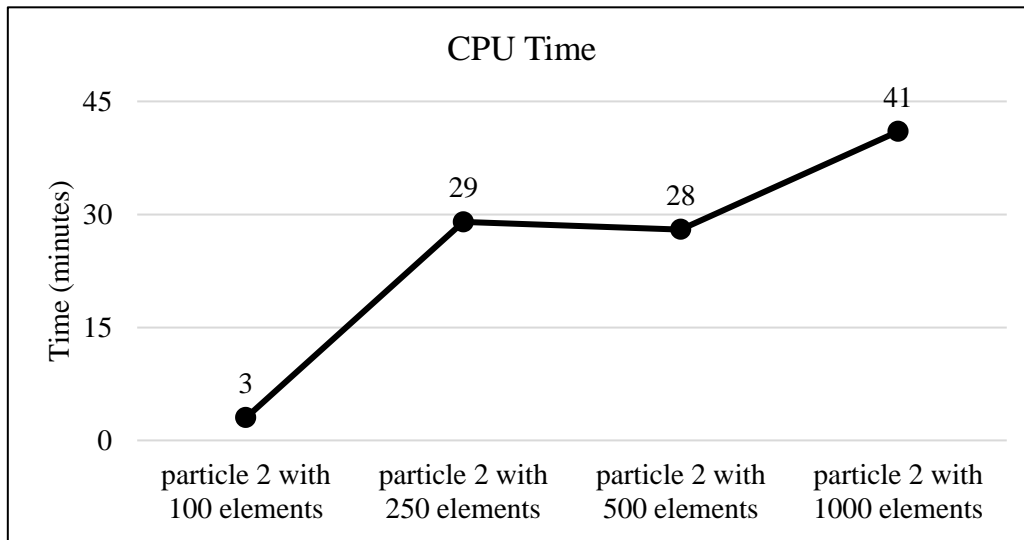
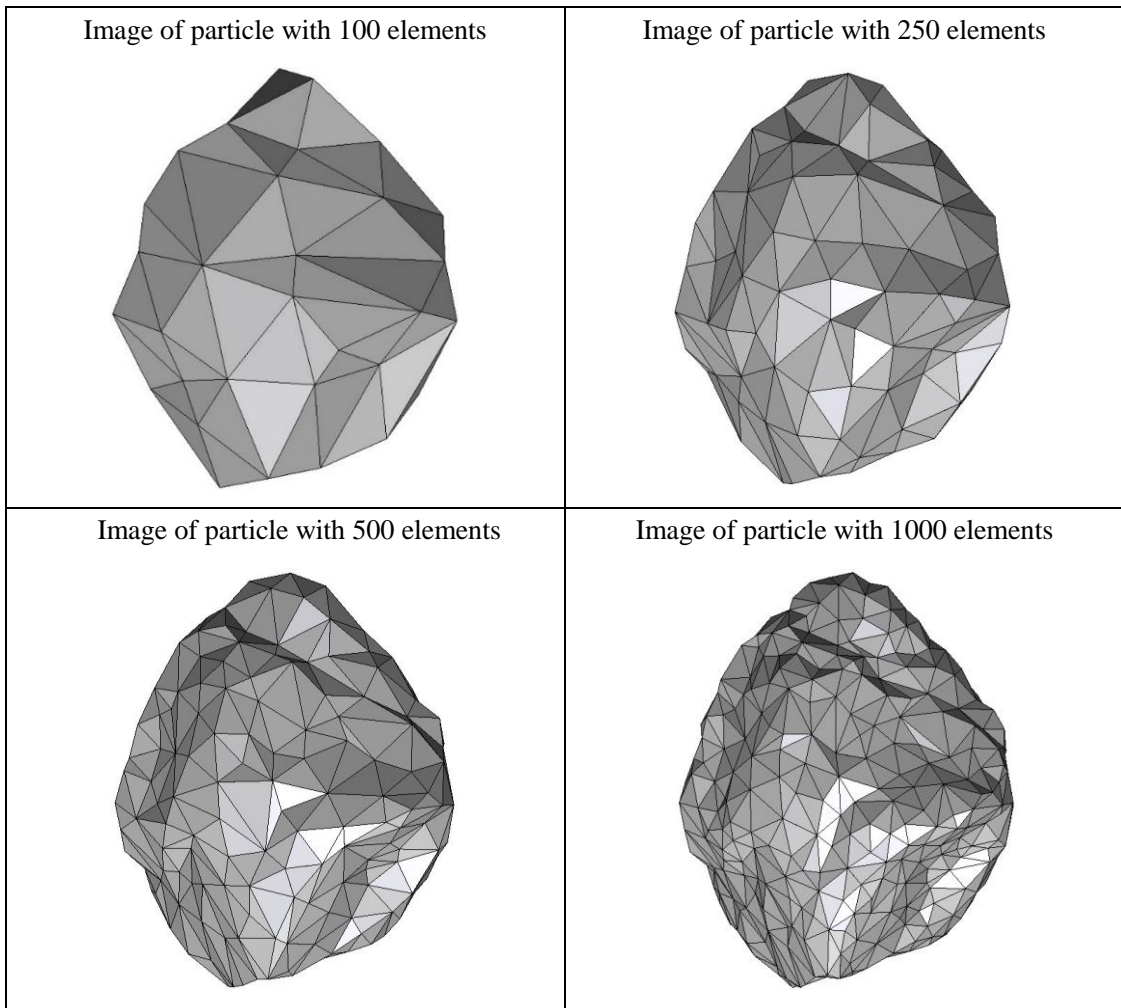


Figure A2.4 CPU computation time vs. model geometry resolution

Appendix

Percent difference analysis compare to particle 2 with 100 elements for different group of data			
	particle 2 with 250 elements	particle 2 with 500 elements	particle 2 with 1000 elements
Impulse	2.57	3.71	2.80
Peak Force	6.63	7.13	8.67
Start Time	16.67	16.67	5.00
CPU Time	866.67	833.33	1266.67
Simulation Time	-7.60	-4.80	-10.40

Summary of particle characteristics and collision simulation details for Particle 3 (of 50)



Particle statistics (part 1)								
Particle ID	# vertices	# elements	Mass (g)	Moments of Inertia			Volume (cm ³)	Sfc. Area (cm ²)
				I1	I2	I3		
				(gcm ²)	(gcm ²)	(gcm ²)		
3 (100 elements)	52	100	73.84	472234.6	410898.5	301908.85	26.14763	49.32647
3 (250 elements)	127	250	73.84	494375.9	431894.75	313737.25	26.83294	50.25493
3 (500 elements)	252	500	73.84	502225.6	437914.6	319115.47	27.07433	50.61944
3 (1000 elements)	502	1000	73.84	504477.4	439423.55	320533.475	27.13243	50.82574

Appendix

Particle Statistics (part 2)							
Particle ID	α	R_g (cm)	ψ	R_v (cm)	L (cm)	I (cm)	S (cm)
3 (100 elements)	1.55435	2.85866	0.86369	1.84126	198.38600	156.83354	127.63282
3 (250 elements)	1.56137	2.86913	0.86248	1.85721	203.65921	159.60966	130.43600
3 (500 elements)	1.56117	2.86612	0.86140	1.86276	205.06597	161.13141	131.35381
3 (1000 elements)	1.56205	2.88102	0.85913	1.86409	205.45240	161.58481	131.52772

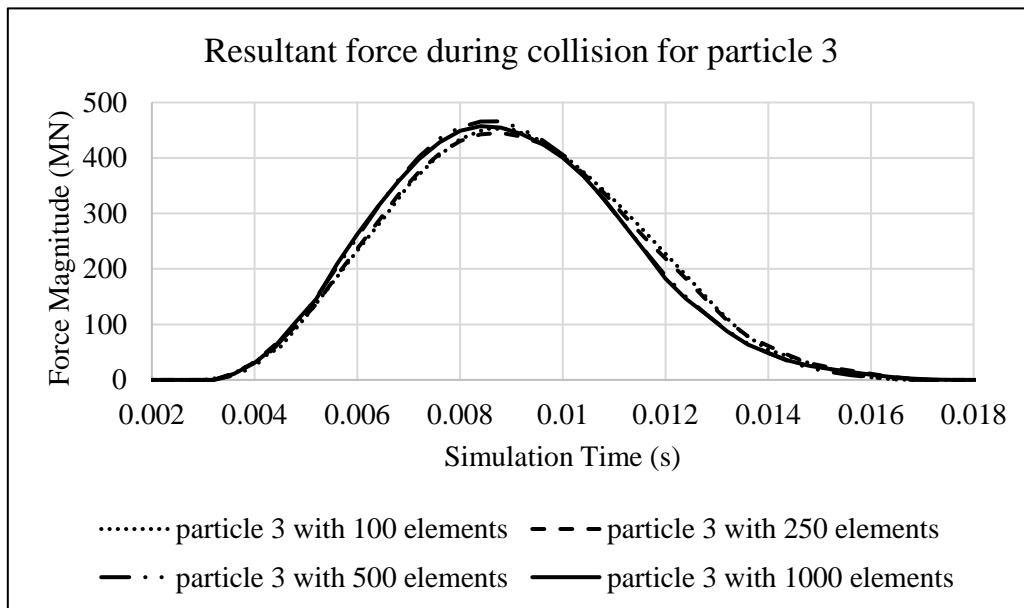


Figure A3.1 Plot of resultant forces during collision event for Particle 3.

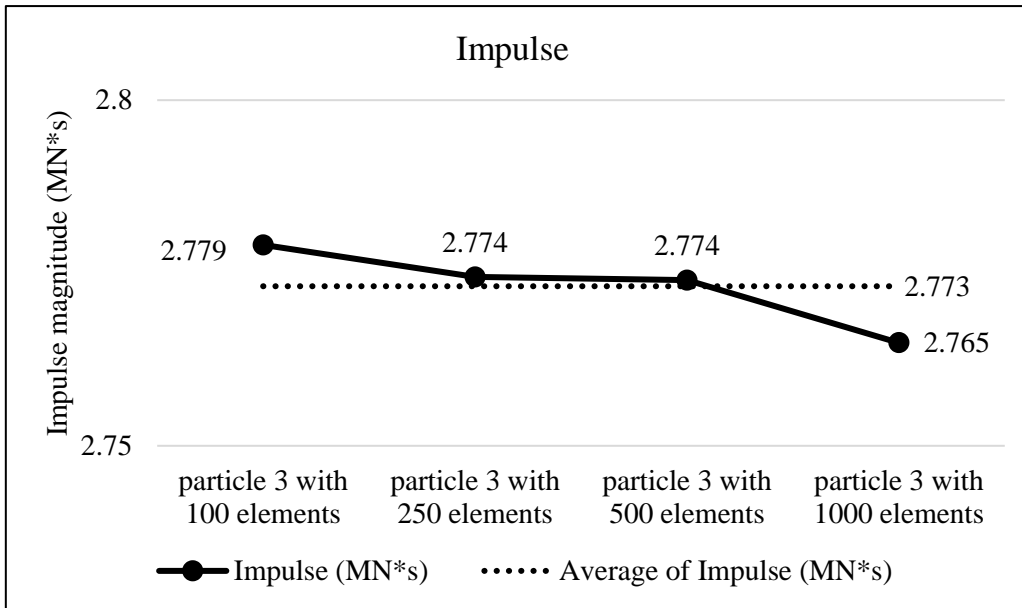


Figure A3.2 Plots of collision impulse for Particle 3.

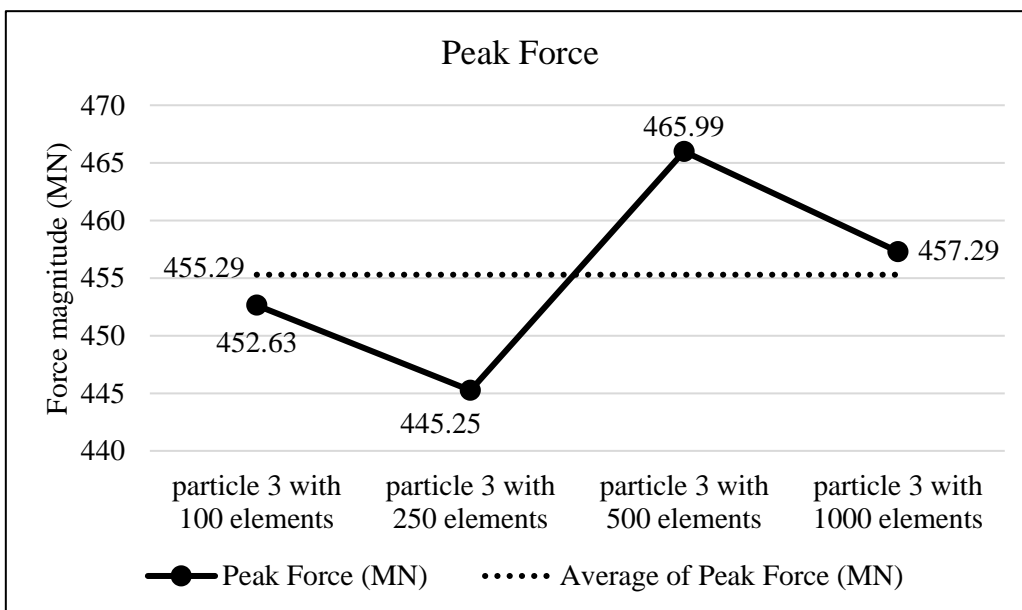


Figure A3.3 Peak collision for the four particle geometry resolutions for Particle 3.

Appendix

Collision results data analysis					
Model	particle 3 with 100 elements	particle 3 with 250 elements	particle 3 with 500 elements	particle 3 with 1000 elements	Average
Impulse (MN*s)	2.779	2.774	2.774	2.765	2.773
Percent difference from Avg. Impulse	0.22	0.05	0.03	-0.30	
Peak Force (MN)	452.63	445.25	465.99	457.29	455.29
Percent difference from Avg. Peak Force	-0.58	-2.21	2.35	0.44	

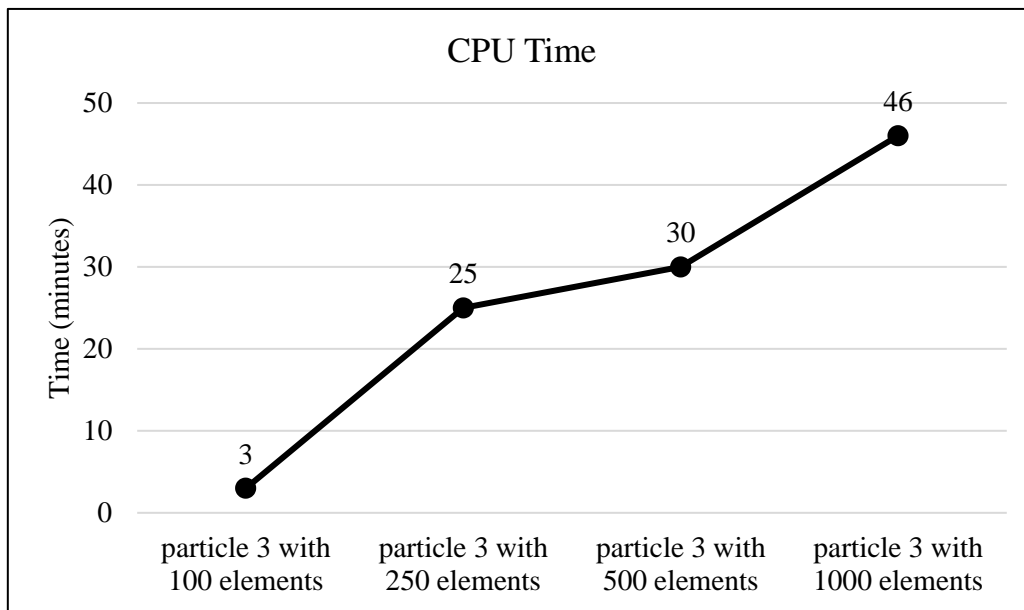
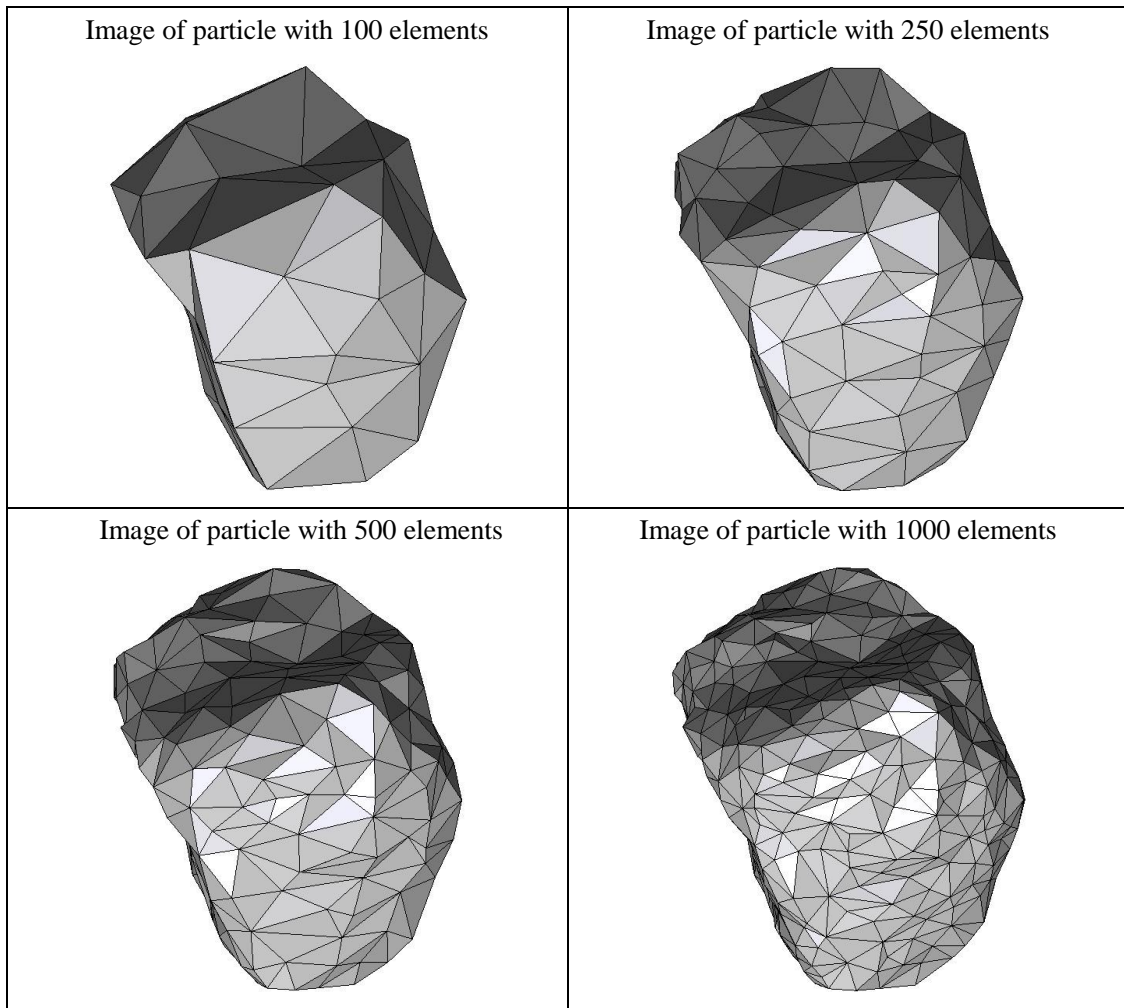


Figure A3.4 CPU computation time vs. model geometry resolution

Appendix

Percent difference analysis compare to particle 3 with 100 elements for different group of data			
	particle 3 with 250 elements	particle 3 with 500 elements	particle 3 with 1000 elements
Impulse	-0.17	-0.18	-0.51
Peak Force	-1.63	2.95	1.03
Start Time	3	3	3
CPU Time	733.33	900.00	1433.33
Simulation Time	4.62	1.54	7.69

Summary of particle characteristics and collision simulation details for Particle 4 (of 50)



Particle statistics (part 1)								
Particle ID	# vertices	# elements	Mass (g)	Moments of Inertia			Volume (cm ³)	Sfc. Area (cm ²)
				I1	I2	I3		
				(gcm ²)	(gcm ²)	(gcm ²)		
4 (100 elements)	52	100	65.051	396339.15	300490.725	286791.925	23.20415	45.97825
4 (250 elements)	127	250	65.051	405060.7	311425.8	295183.425	23.57324	46.66729
4 (500 elements)	252	500	65.051	408593.575	315061.775	297770.35	23.68872	47.08743
4 (1000 elements)	502	1000	65.051	410986.45	317349.925	299410.1	23.77337	47.17868

Appendix

Particle Statistics (part 2)							
Particle ID	α	R_g (cm)	ψ	R_v (cm)	L (cm)	I (cm)	S (cm)
4 (100 elements)	1.46541	2.50261	0.85567	1.76940	177.52930	171.49576	121.14638
4 (250 elements)	1.44580	2.48748	0.85196	1.77873	179.95144	172.87467	124.46517
4 (500 elements)	1.44403	2.46094	0.84711	1.78163	180.92733	173.42597	125.29302
4 (1000 elements)	1.44377	2.46295	0.84749	1.78375	181.57219	173.81212	125.76298

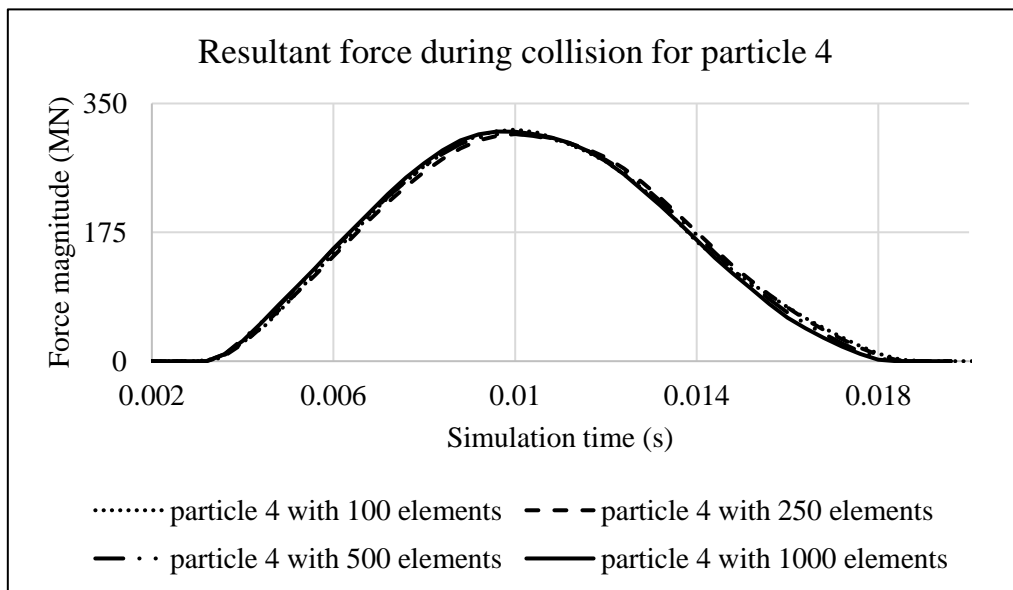


Figure A4.1 Plot of resultant forces during collision event for Particle 4.

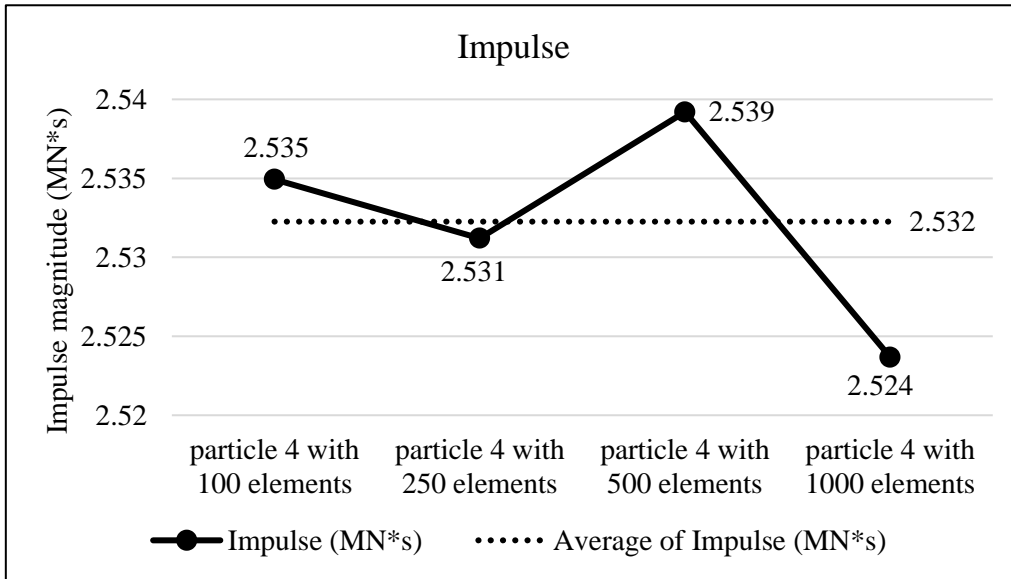


Figure 4.2 Plots of collision impulse for Particle 4.

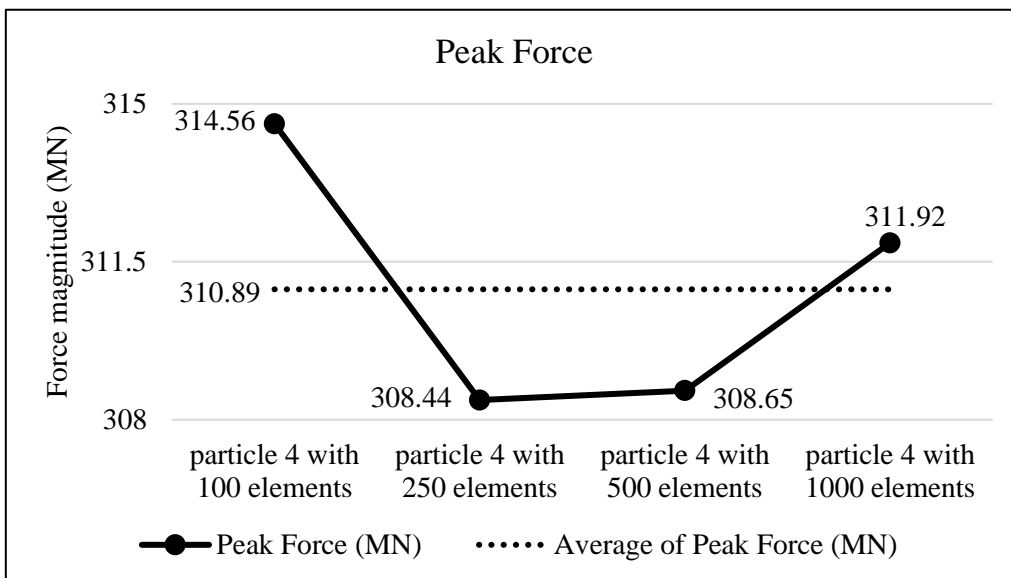


Figure A4.3 Peak collision for the four particle geometry resolutions for Particle 4.

Appendix

Collision results data analysis					
Model	particle 4 with 100 elements	particle 4 with 250 elements	particle 4 with 500 elements	particle 4 with 1000 elements	Average
Impulse (MN*s)	2.535	2.531	2.539	2.524	2.532
Percent difference from Avg. Impulse	0.11	-0.04	0.27	-0.34	
Peak Force (MN)	314.56	308.44	308.65	311.92	310.89
Percent difference from Avg. Peak Force	1.18	-0.79	-0.72	0.33	

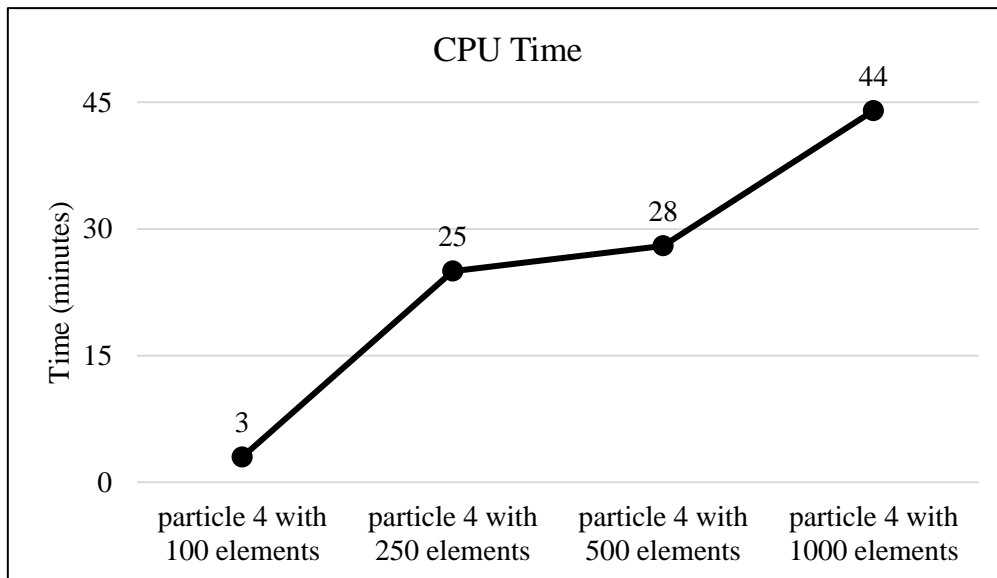
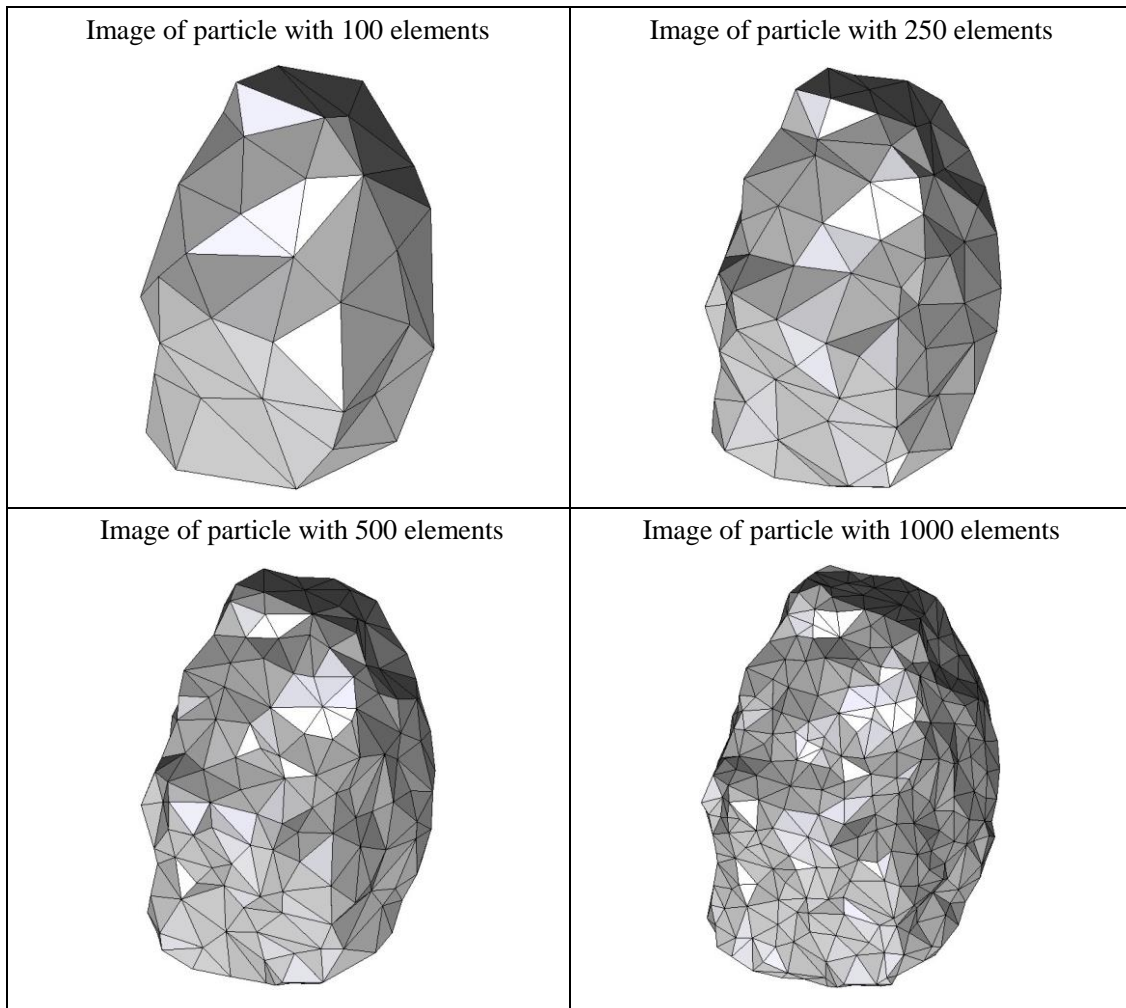


Figure A4.4 CPU computation time vs. model geometry resolution

Appendix

Percent difference analysis compare to particle 4 with 100 elements for different group of data			
	particle 4 with 250 elements	particle 4 with 500 elements	particle 4 with 1000 elements
Impulse	-0.15	0.17	-0.44
Peak Force	-1.95	-1.88	-0.84
Start Time	2.86	2.86	2.86
CPU Time	733.33	833.33	1366.67
Simulation Time	-1.33	-1.33	-4.00

Summary of particle characteristics and collision simulation details for Particle 5 (of 50)



Particle statistics (part 1)								
Particle ID	# vertices	# elements	Mass (g)	Moments of Inertia			Volume (cm ³)	Sfc. Area (cm ²)
				I1	I2	I3		
				(gcm ²)	(gcm ²)	(gcm ²)		
5 (100 elements)	52	100	52.607	305786.875	280801.375	145914.35	18.56999	40.46288
5 (250 elements)	127	250	52.607	314575.425	289024.525	149208.7625	18.82316	41.34569
5 (500 elements)	252	500	52.607	316135.225	290826.725	149824.3375	18.85281	41.70590
5 (1000 elements)	502	1000	52.607	317601	292019.25	150422.1375	18.89531	41.83157

Appendix

Particle Statistics (part 2)							
Particle ID	α	R_g (cm)	ψ	R_v (cm)	L (cm)	I (cm)	S (cm)
5 (100 elements)	1.90895	2.61485	0.83811	1.64276	204.65478	127.44831	107.20825
5 (250 elements)	1.91692	2.63069	0.82765	1.65019	207.81562	128.87950	108.41119
5 (500 elements)	1.91607	2.63103	0.82137	1.65106	208.44271	129.01703	108.78663
5 (1000 elements)	1.91788	2.64272	0.82013	1.65230	208.91195	129.33747	108.92832

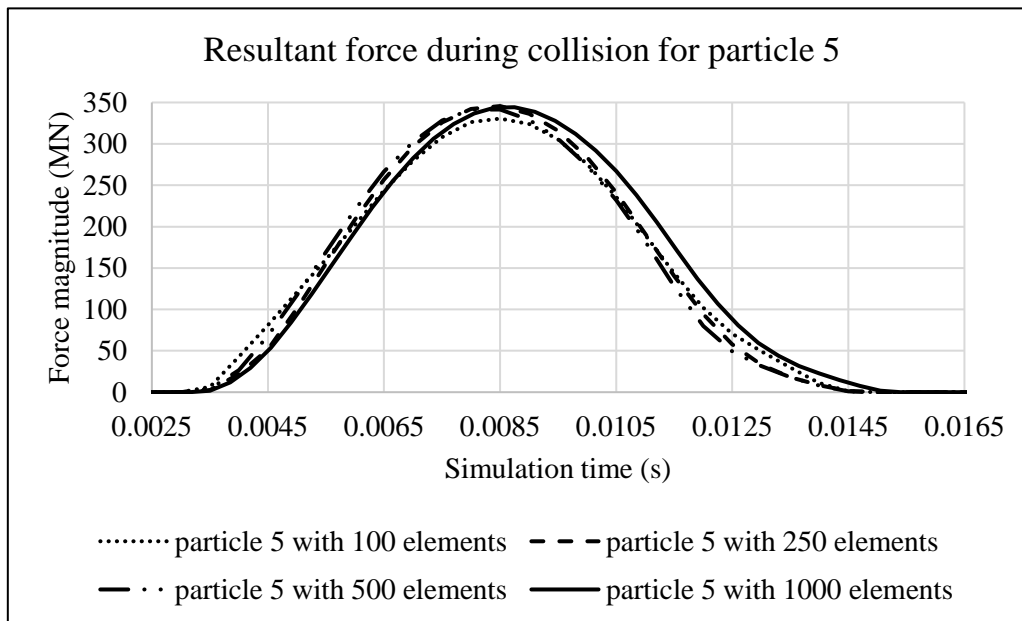


Figure A5.1 Plot of resultant forces during collision event for Particle 5.

Appendix

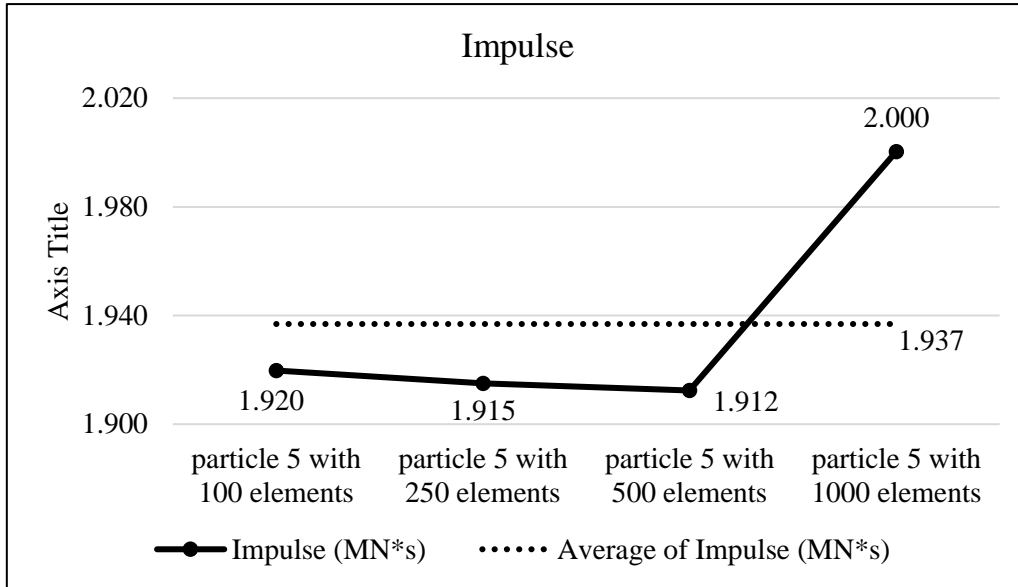


Figure A5.2 Plots of collision impulse for Particle 5.

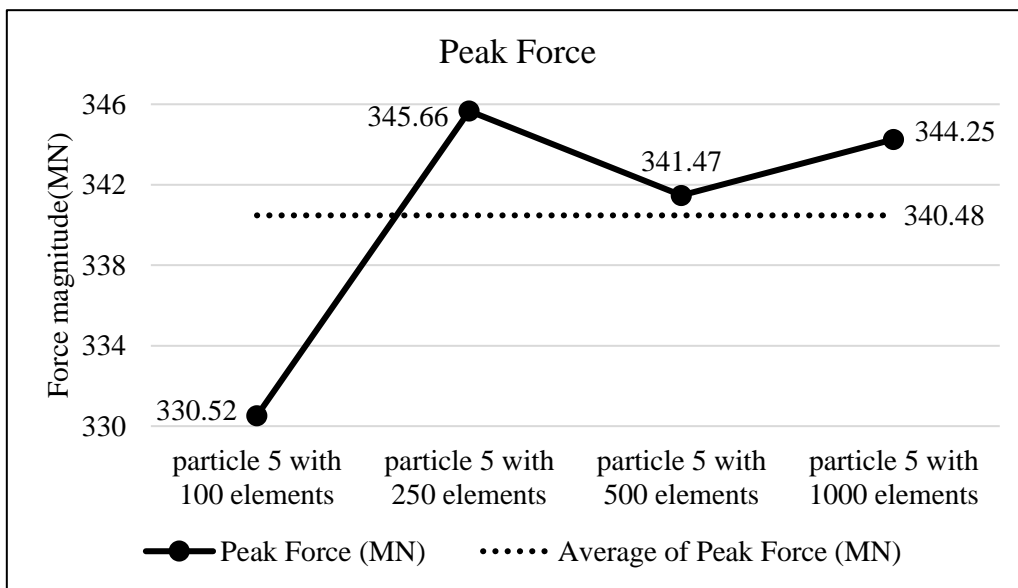


Figure A5.3 Peak collision for the four particle geometry resolutions for Particle 5.

Appendix

Collision results data analysis					
Model	particle 5 with 100 elements	particle 5 with 250 elements	particle 5 with 500 elements	particle 5 with 1000 elements	Average
Impulse (MN*s)	1.920	1.915	1.912	2.000	1.937
Percent difference from Avg. Impulse	-0.88	-1.13	-1.26	3.28	
Peak Force (MN)	330.52	345.66	341.47	344.25	340.48
Percent difference from Avg. Peak Force	-2.92	1.52	0.29	1.11	

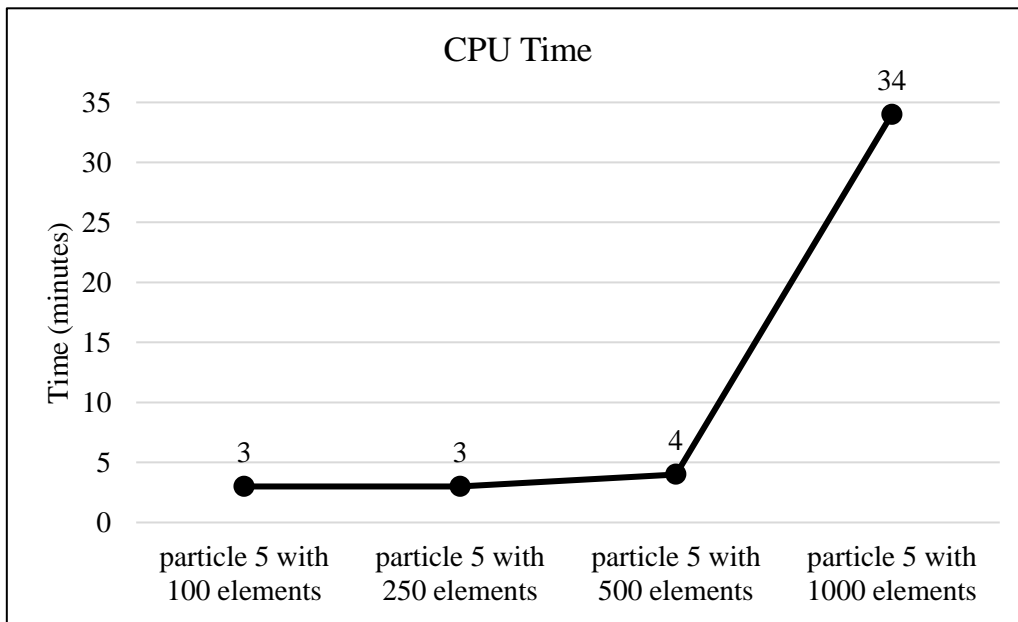
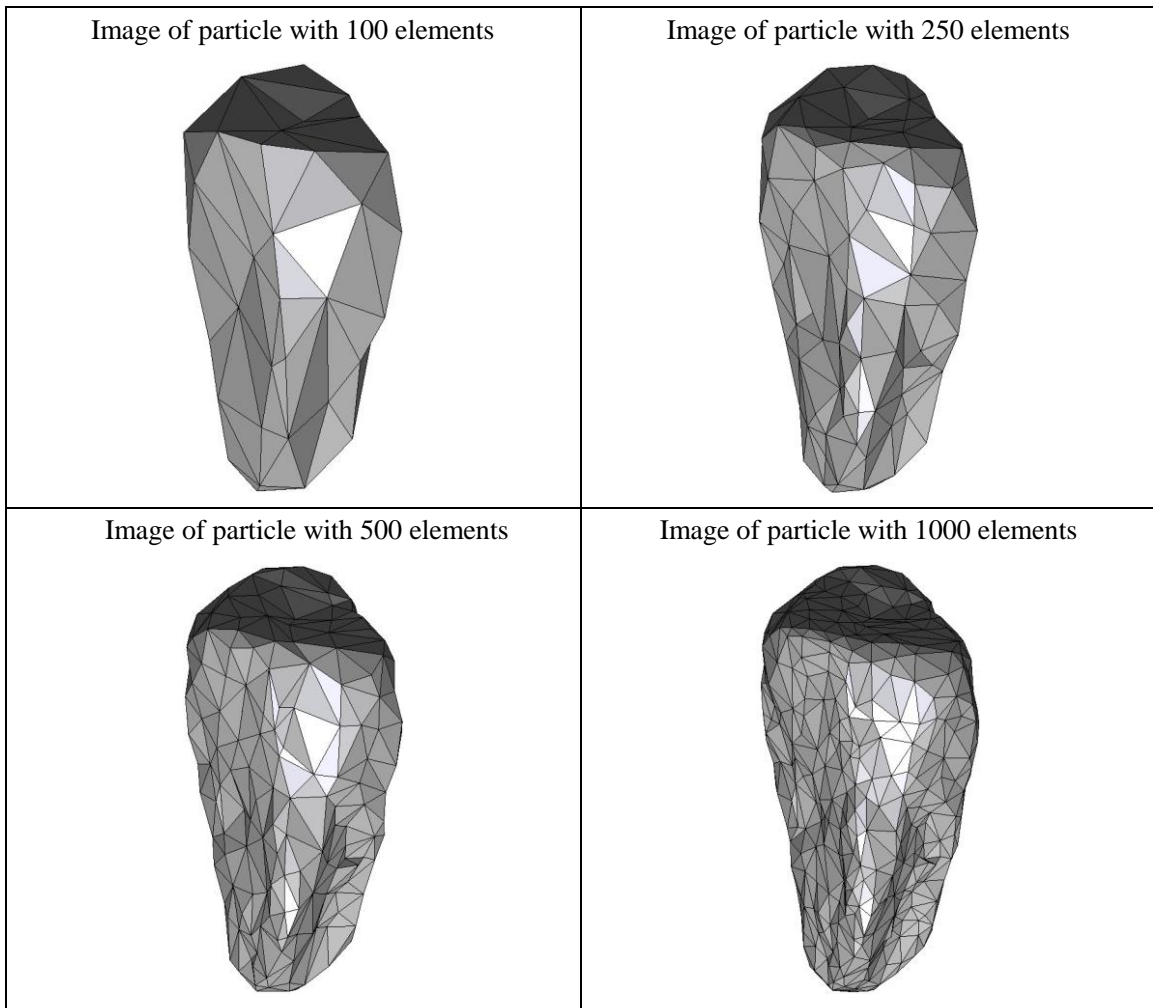


Figure A5.4 CPU computation time vs. model geometry resolution.

Appendix

Percent difference analysis compare to particle 5 with 100 elements for different group of data			
	particle 5 with 250 elements	particle 5 with 500 elements	particle 5 with 1000 elements
Impulse	-0.25	-0.38	4.20
Peak Force	4.58	3.31	4.15
Start Time	0.00	0.00	0.00
CPU Time	0.00	33.33	1033.33
Simulation Time	0.00	0.00	5.00

Summary of particle characteristics and collision simulation details for Particle 6 (of 50)



Particle statistics (part 1)								
Particle ID	# vertices	# elements	Mass (g)	Moments of Inertia			Volume (cm ³)	Sfc. Area (cm ²)
				I1	I2	I3		
				(gcm ²)	(gcm ²)	(gcm ²)		
6 (100 elements)	52	100	18.715	64855.6625	58671.71875	25174.15625	6.63176	21.10789
6 (250 elements)	127	250	18.715	66286.26875	60008.7	25617.73438	6.71323	21.27755
6 (500 elements)	252	500	18.715	66924.2375	60543.5125	25876.43906	6.74585	21.31944
6 (1000 elements)	502	1000	18.715	67299.0875	60872.78125	26040.74688	6.76680	21.31086

Appendix

Particle Statistics (part 2)							
Particle ID	α	R_g (cm)	ψ	R_v (cm)	L (cm)	I (cm)	S (cm)
6 (100 elements)	2.27578	2.85730	0.80871	1.16550	162.10051	91.53031	71.22870
6 (250 elements)	2.28158	2.15585	0.80882	1.17026	164.00449	92.31100	71.88200
6 (500 elements)	2.28275	2.15428	0.80984	1.17215	164.74732	92.83317	72.17049
6 (1000 elements)	2.28187	2.1556	0.81184	1.17336	165.18444	93.13470	72.38991

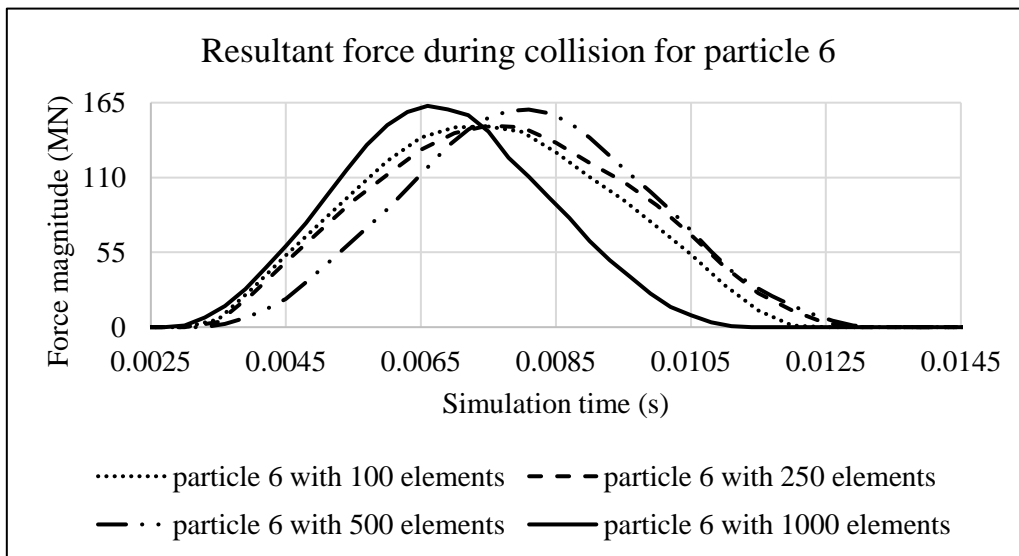


Figure A6.1 Plot of resultant forces during collision event for Particle 6.

Appendix

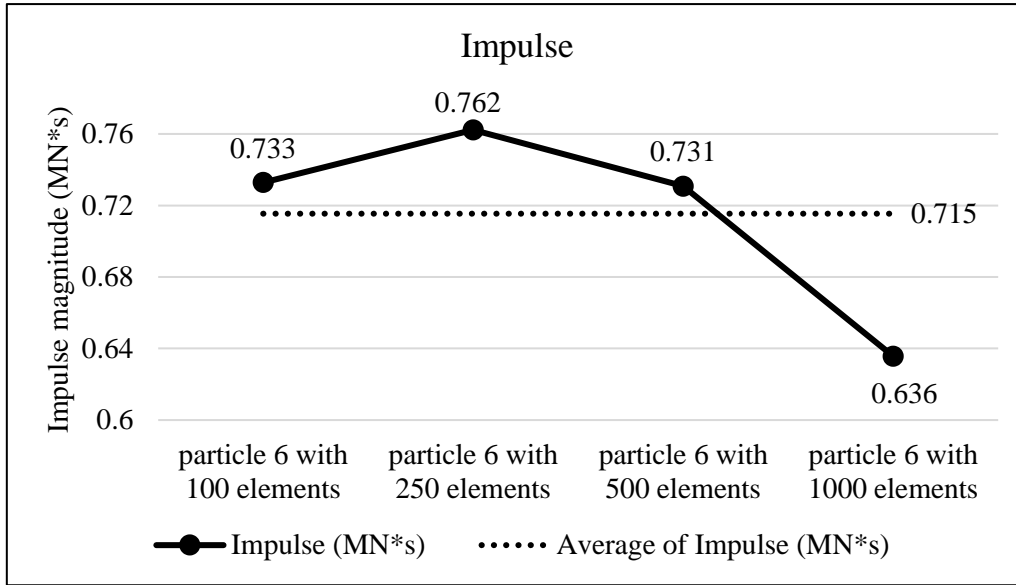


Figure A6.2 Plots of collision impulse for Particle 6.

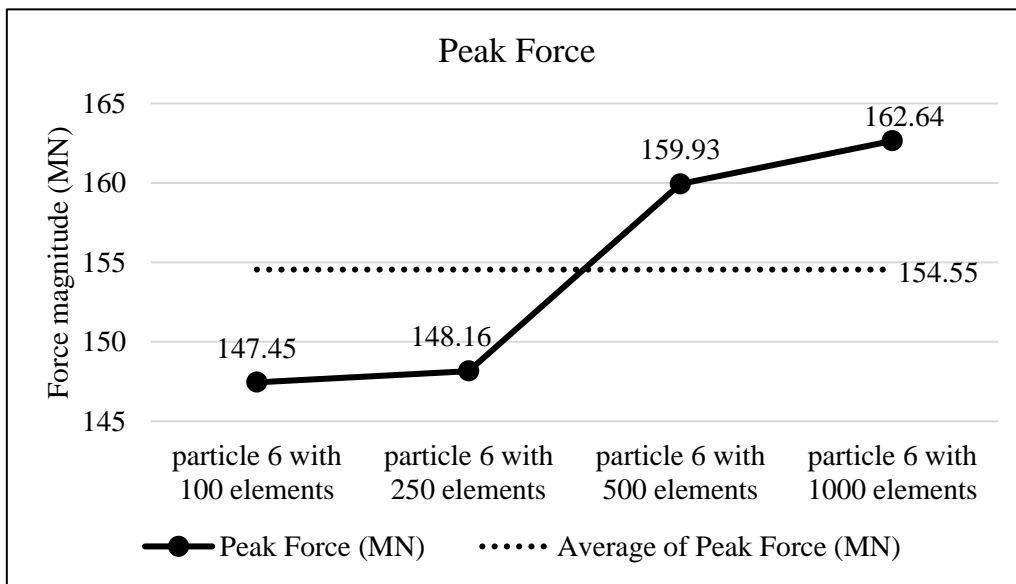


Figure A6.3 Peak collision for the four particle geometry resolutions for Particle 6.

Appendix

Collision results data analysis					
Model	particle 6 with 100 elements	particle 6 with 250 elements	particle 6 with 500 elements	particle 6 with 1000 elements	Average
Impulse (MN*s)	0.733	0.762	0.731	0.636	0.715
Percent difference from Avg. Impulse	2.44	6.55	2.15	-11.14	
Peak Force (MN)	147.45	148.16	159.93	162.64	154.55
Percent difference from Avg. Peak Force	-4.59	-4.13	3.48	5.24	

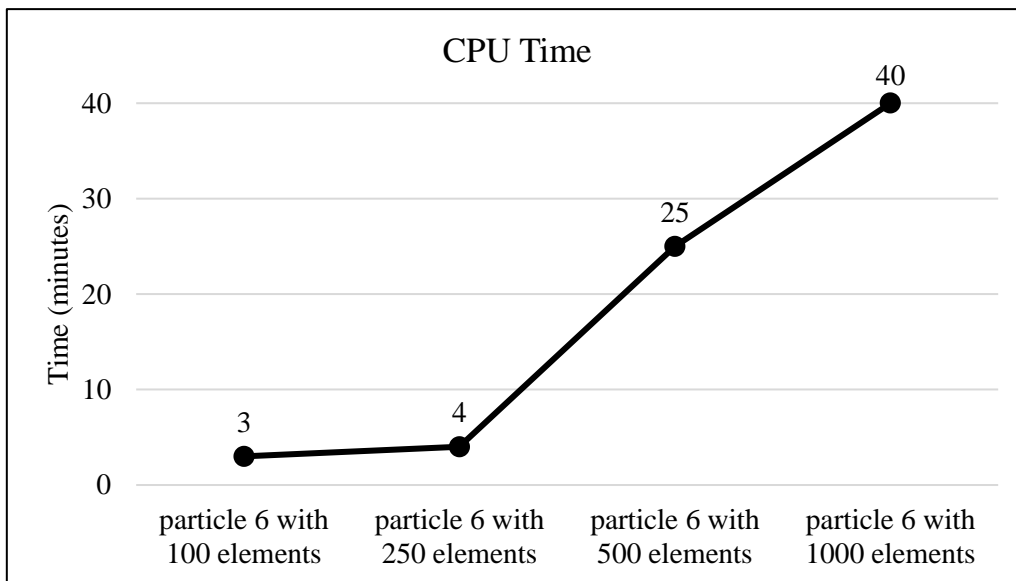


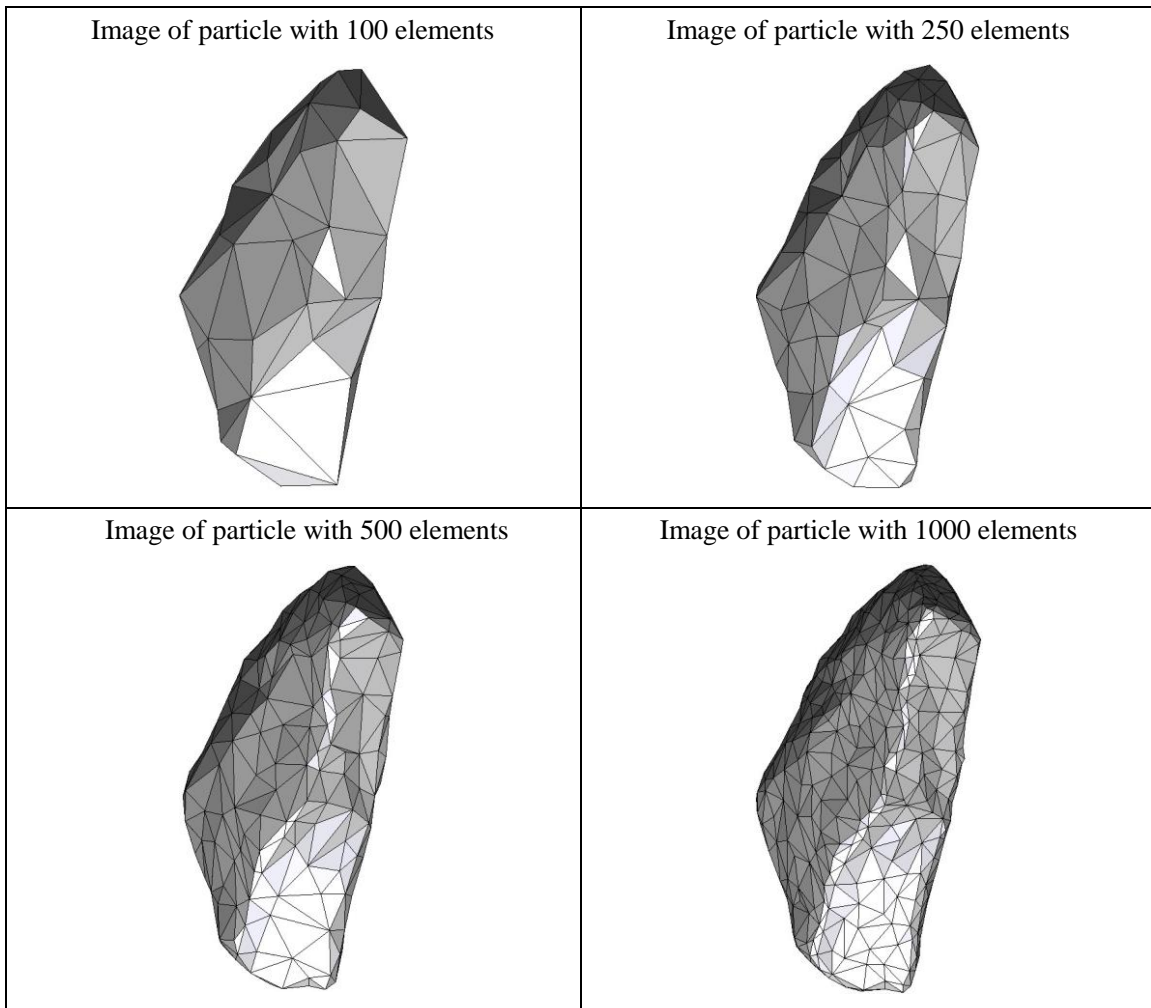
Figure A6.4 CPU computation time vs. model geometry resolution.

Appendix

Percent difference analysis compare to particle 6 with 100 elements for different group of data			
	particle 6 with 250 elements	particle 6 with 500 elements	particle 6 with 1000 elements
Impulse	4.02	-0.28	-13.25
Peak Force	0.48	8.47	10.30
Start Time	0.00	-5.71	-14.29
CPU Time	33.33	733.33	1233.33
Simulation Time	5.88	12.94	-4.71

Appendix

Summary of particle characteristics and collision simulation details for Particle 7 (of 50)



Particle statistics (part 1)

Particle ID	# vertices	# elements	Mass (g)	Moments of Inertia			Volume (cm ³)	Sfc. Area (cm ²)
				I1	I2	I3		
				(gcm ²)	(gcm ²)	(gcm ²)		
7 (100 elements)	52	100	12.039	48629.43125	40502.7875	16077.4875	4.95651	18.57455
7 (250 elements)	127	250	12.039	49629.62188	41460.34375	16338.40469	5.00226	18.52654
7 (500 elements)	252	500	12.039	49903.56563	41694.99063	16436.34688	5.03909	18.47445
7 (1000 elements)	502	1000	12.039	50188.1	41921.175	16534.8625	5.05476	18.45878

Appendix

Particle Statistics (part 2)							
Particle ID	α	R_g (cm)	ψ	R_v (cm)	L (cm)	I (cm)	S (cm)
7 (100 elements)	3.03122	2.07041	0.75686	1.05770	174.18629	100.26158	57.46407
7 (250 elements)	3.02498	2.03900	0.76349	1.06094	176.19758	100.88833	58.24754
7 (500 elements)	3.02245	2.04453	0.76939	1.06354	176.68088	101.17041	58.45625
7 (1000 elements)	3.02335	2.03025	0.77164	1.06464	177.16470	101.49188	58.59875

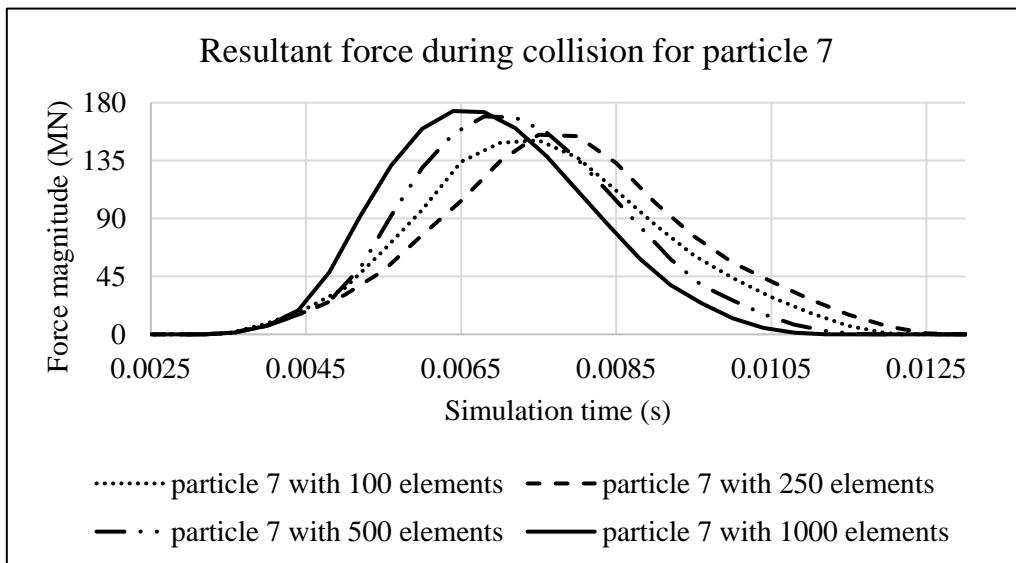


Figure A7.1 Plot of resultant forces during collision event for Particle 7.

Appendix

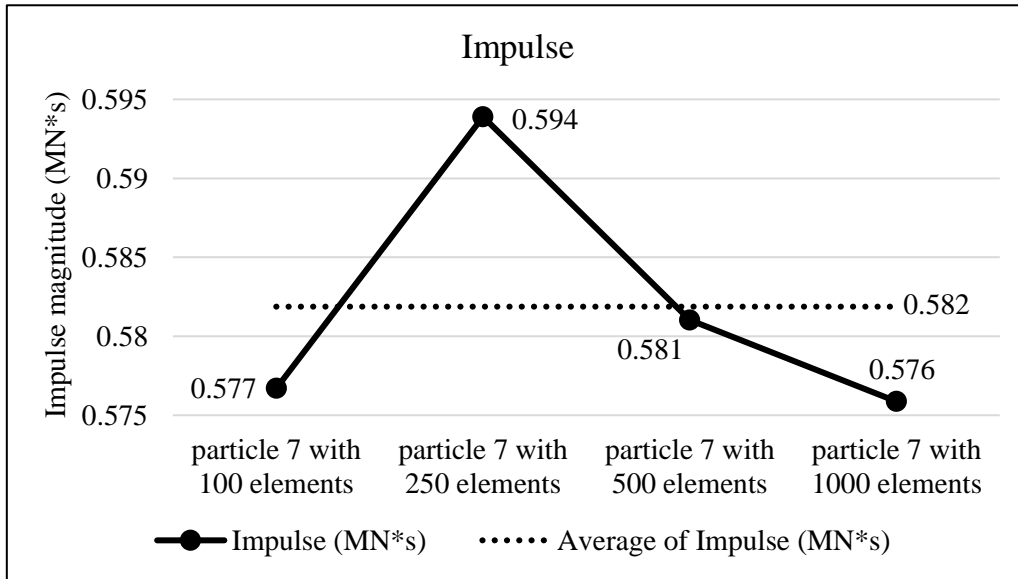


Figure 7.2 Plots of collision impulse for Particle 7.

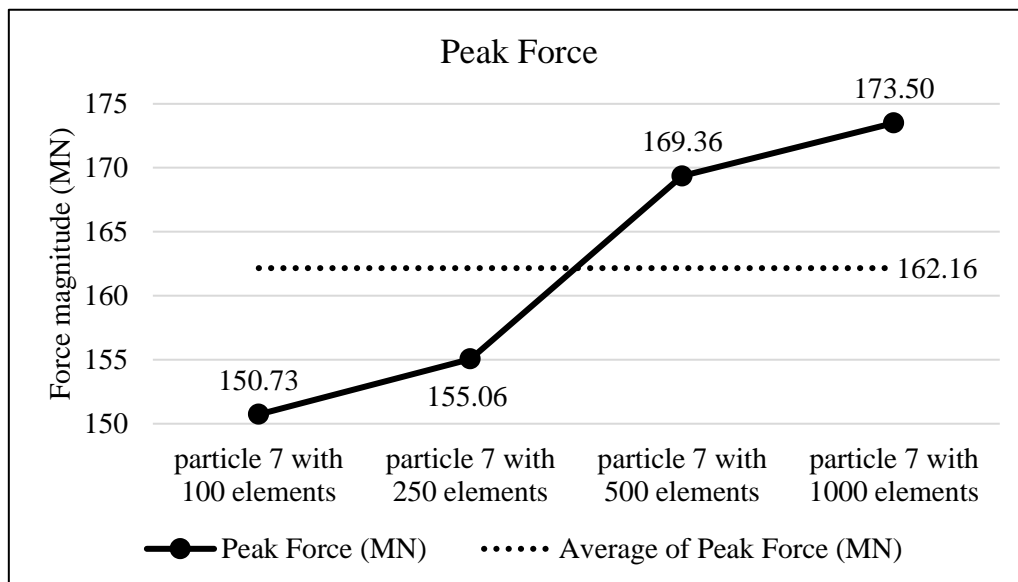


Figure A7.3 Peak collision for the four particle geometry resolutions for Particle 7.

Appendix

Collision results data analysis					
Model	particle 7 with 100 elements	particle 7 with 250 elements	particle 7 with 500 elements	particle 7 with 1000 elements	Average
Impulse (MN*s)	0.577	0.594	0.581	0.576	0.582
Percent difference from Avg. Impulse	-0.89	2.07	-0.15	-1.03	
Peak Force (MN)	150.73	155.06	169.36	173.50	162.16
Percent difference from Avg. Peak Force	-7.05	-4.38	4.44	6.99	

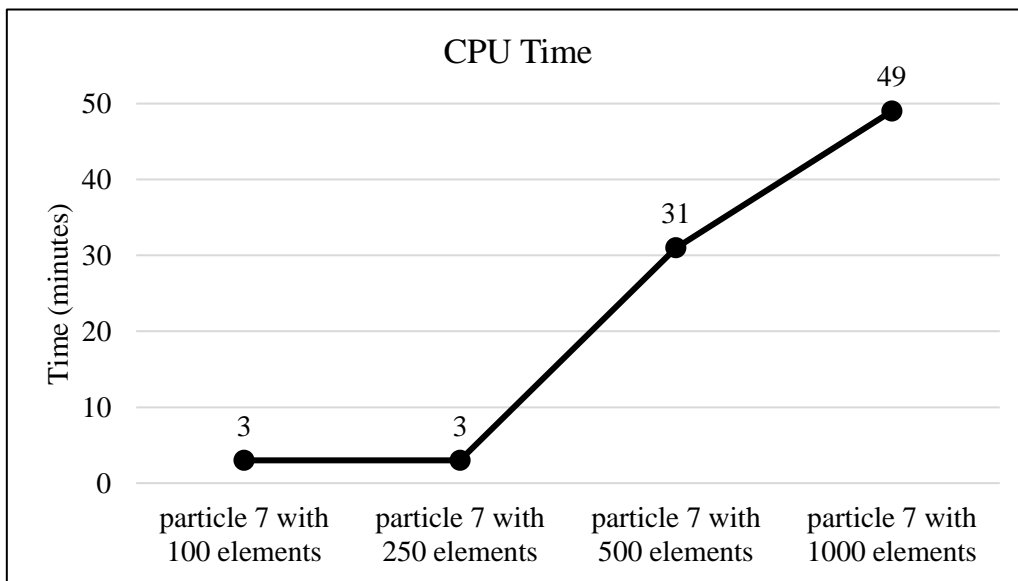


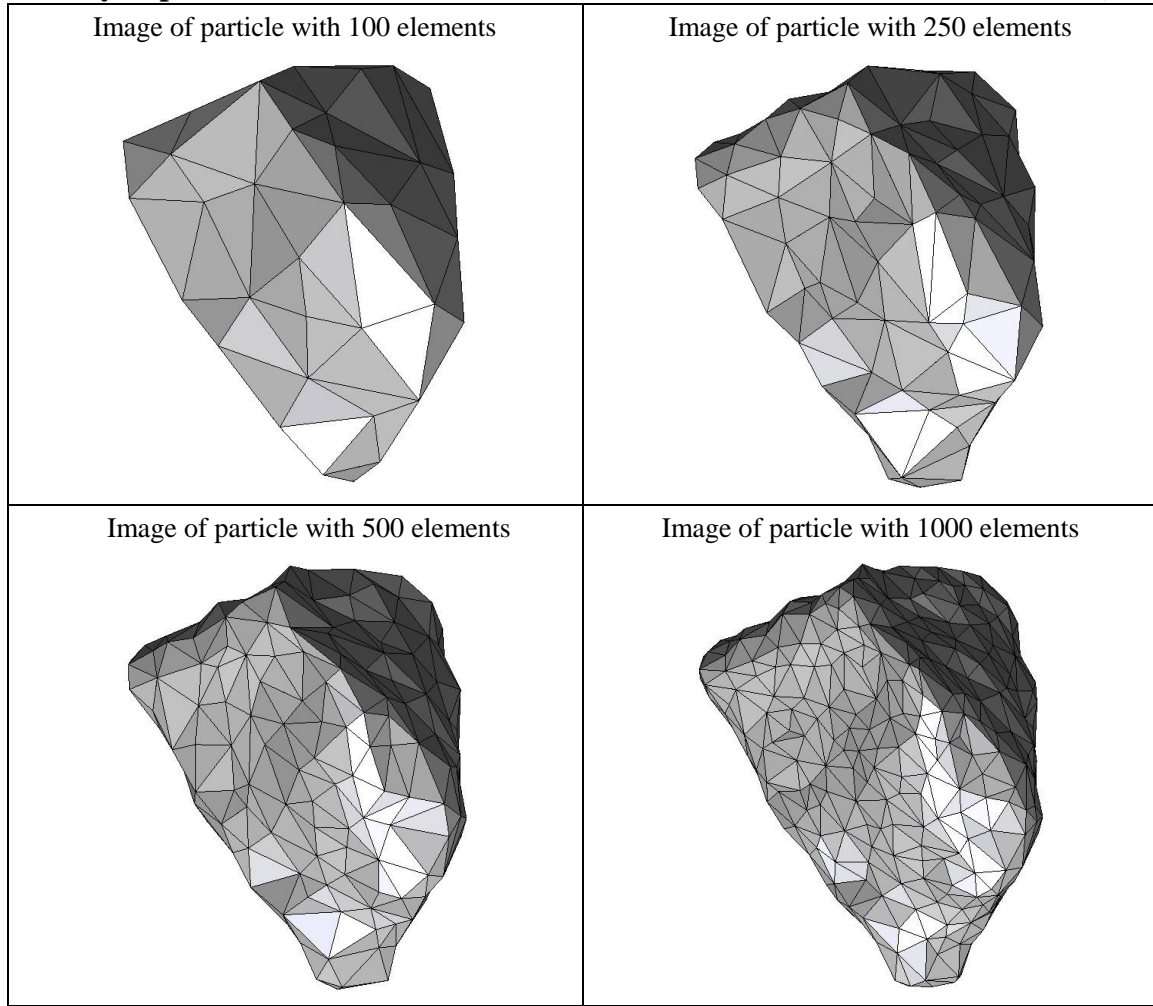
Figure A7.4 CPU computation time vs. model geometry resolution.

Appendix

Percent difference analysis compare to particle 7 with 100 elements for different group of data			
	particle 7 with 250 elements	particle 7 with 500 elements	particle 7 with 1000 elements
Impulse	2.98	0.75	-0.14
Peak Force	2.88	12.36	15.11
Start Time	0.00	2.86	2.86
CPU Time	0.00	933.33	1533.33
Simulation Time	5.88	3.53	-10.59

Appendix

Summary of particle characteristics and collision simulation details for Particle 8 (of 50)



Particle statistics (part 1)

Particle ID	# vertices	# elements	Mass (g)	Moments of Inertia			Volume (cm ³)	Sfc. Area (cm ²)
				I1	I2	I3		
				(gcm ²)	(gcm ²)	(gcm ²)		
8 (100 elements)	52	100	16.043	39749.225	33676.17188	27038.71563	5.90910	18.61565
8 (250 elements)	127	250	16.043	40210.06563	33913.75	27436.8125	5.93902	18.63368
8 (500 elements)	252	500	16.043	40482.1875	34153.68438	27660.625	5.96237	18.65242
8 (1000 elements)	502	1000	16.043	40658.49375	34307.75938	27773.63438	5.97626	18.61401

Particle Statistics (part 2)							
Particle ID	α	R_g (cm)	ψ	R_v (cm)	L (cm)	I (cm)	S (cm)
8 (100 elements)	1.48745	1.69816	0.84909	1.12153	120.23720	101.58589	80.83445
8 (250 elements)	1.48607	1.70126	0.85113	1.12342	120.62580	102.53462	81.17080
8 (500 elements)	1.48394	1.71886	0.85250	1.12489	120.99760	102.92295	81.53785
8 (1000 elements)	1.48422	1.71442	0.85559	1.12576	121.27722	103.12751	81.71115

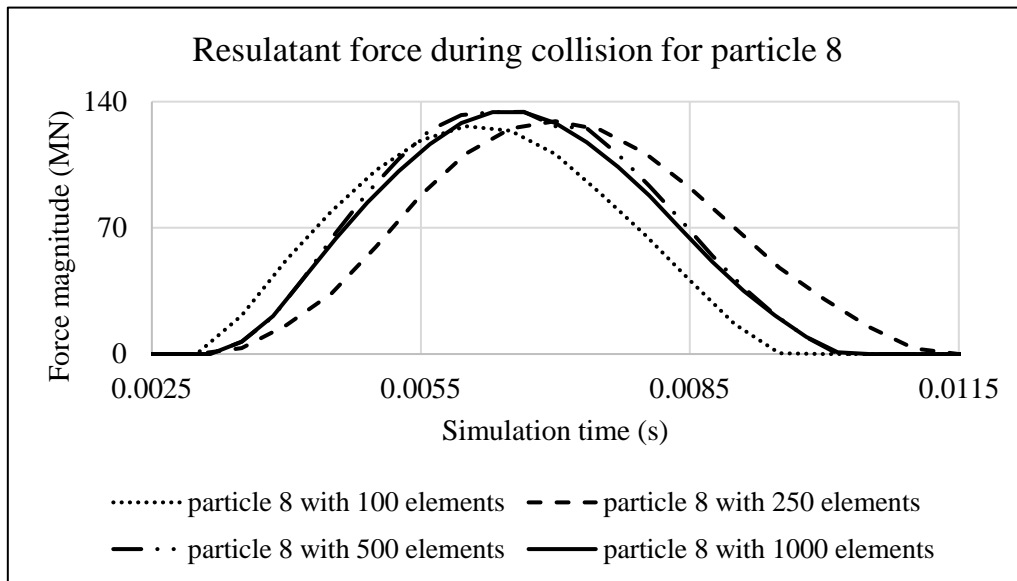


Figure A8.1 Plot of resultant forces during collision event for Particle 8.

Appendix

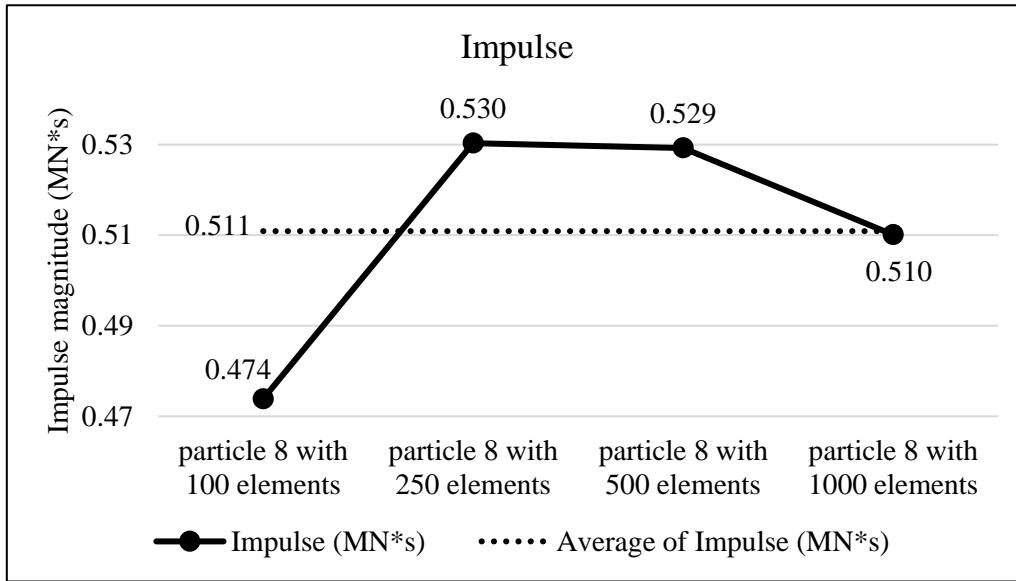


Figure A8.2 Plots of collision impulse for Particle 8.

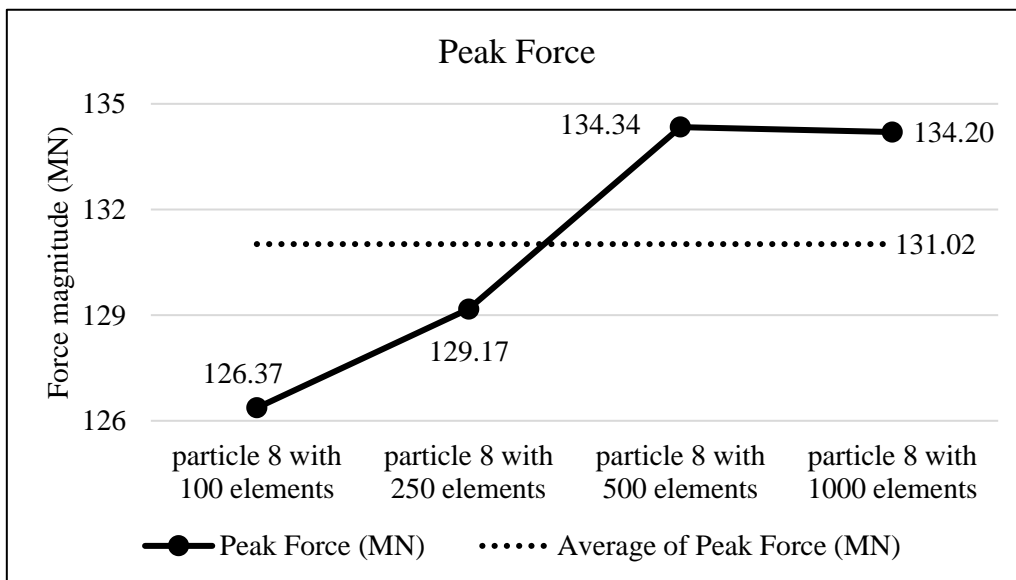


Figure A8.3 Peak collision for the four particle geometry resolutions for Particle 8.

Appendix

Collision results data analysis					
Model	particle 8 with 100 elements	particle 8 with 250 elements	particle 8 with 500 elements	particle 8 with 1000 elements	Average
Impulse (MN*s)	0.474	0.530	0.529	0.510	0.511
Percent difference from Avg. Impulse	-7.25	3.80	3.60	-0.15	
Peak Force (MN)	126.37	129.17	134.34	134.20	131.02
Percent difference from Avg. Peak Force	-3.55	-1.41	2.53	2.43	

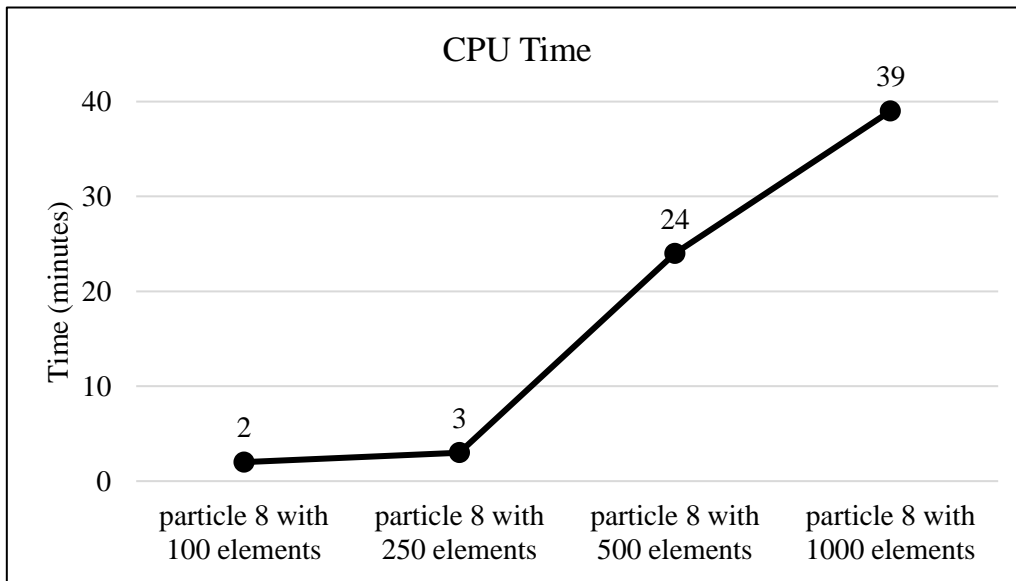


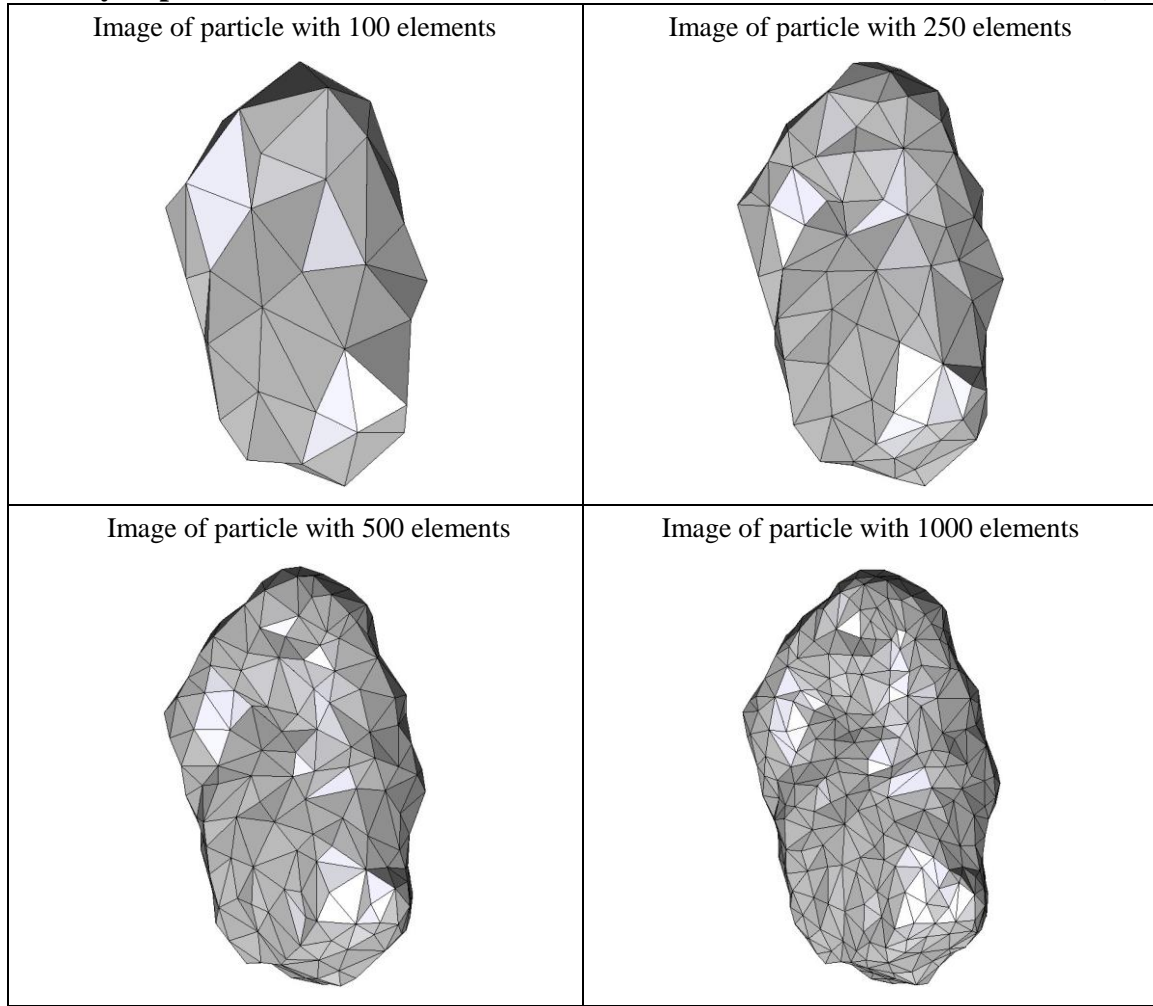
Figure A8.4 CPU computation time vs. model geometry resolution.

Appendix

Percent difference analysis compare to particle 8 with 100 elements for different group of data			
	particle 8 with 250 elements	particle 8 with 500 elements	particle 8 with 1000 elements
Impulse	11.91	11.69	7.65
Peak Force	2.22	6.31	6.20
Start Time	0.00	0.00	0.00
CPU Time	50.00	1100.00	1850.00
Simulation Time	25.00	10.83	10.83

Appendix

Summary of particle characteristics and collision simulation details for Particle 9 (of 50)



Particle statistics (part 1)

Particle ID	# vertices	# elements	Mass (g)	Moments of Inertia			Volume (cm ³)	Sfc. Area (cm ²)
				I1	I2	I3		
				(gcm ²)	(gcm ²)	(gcm ²)		
9 (100 elements)	52	100	39.563	277986.15	227419.725	88956.35625	14.01484	36.29209
9 (250 elements)	127	250	39.563	283444	232391.025	89938.14375	14.16276	36.54552
9 (500 elements)	252	500	39.563	286214.575	234888.5	90489.8125	14.22713	36.67860
9 (1000 elements)	502	1000	39.563	287606.15	235942.6	90948.4875	14.25819	36.65083

Appendix

Particle Statistics (part 2)							
Particle ID	α	R_g (cm)	ψ	R_v (cm)	L (cm)	I (cm)	S (cm)
9 (100 elements)	3.29361	2.87476	0.77458	1.49566	229.41488	132.78926	69.65448
9 (250 elements)	3.30948	2.81810	0.77461	1.50090	232.00248	133.48617	70.10232
9 (500 elements)	3.31590	2.81554	0.77413	1.50318	233.28354	133.87603	70.35297
9 (1000 elements)	3.31841	2.81604	0.77585	1.50427	233.82115	134.25130	70.46175

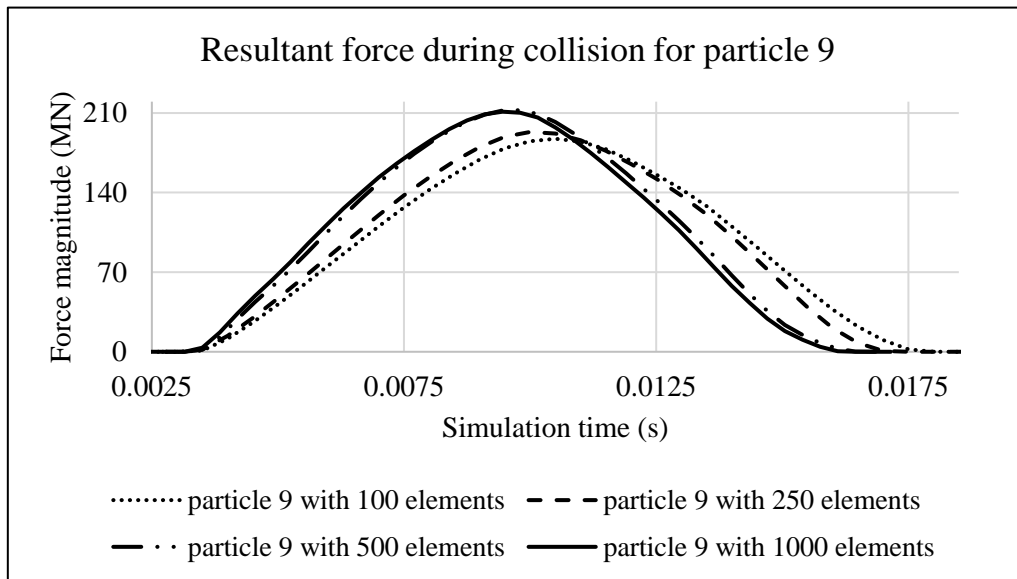


Figure A9.1 Plot of resultant forces during collision event for Particle 9.

Appendix

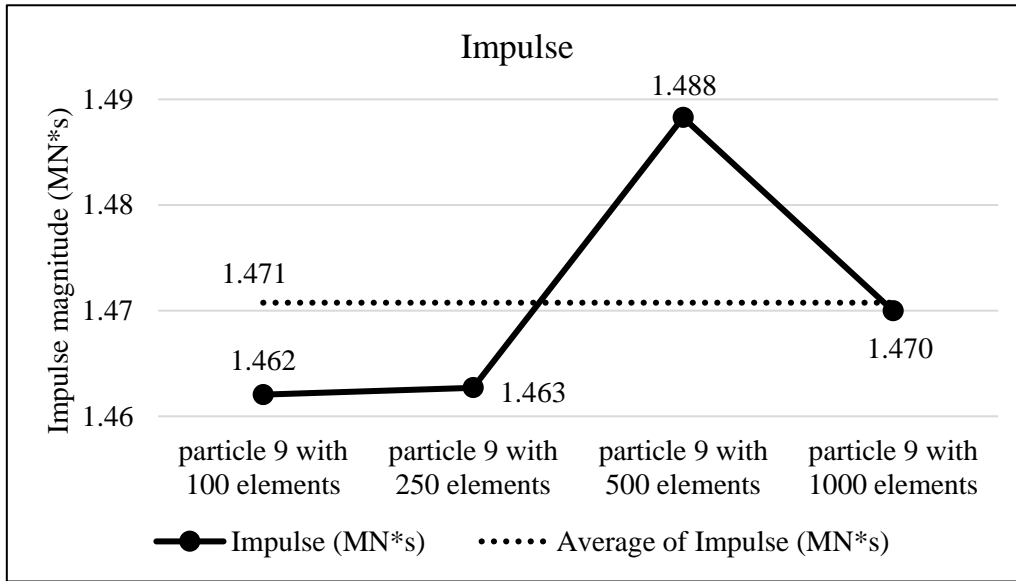


Figure A9.2 Plots of collision impulse for Particle 9.

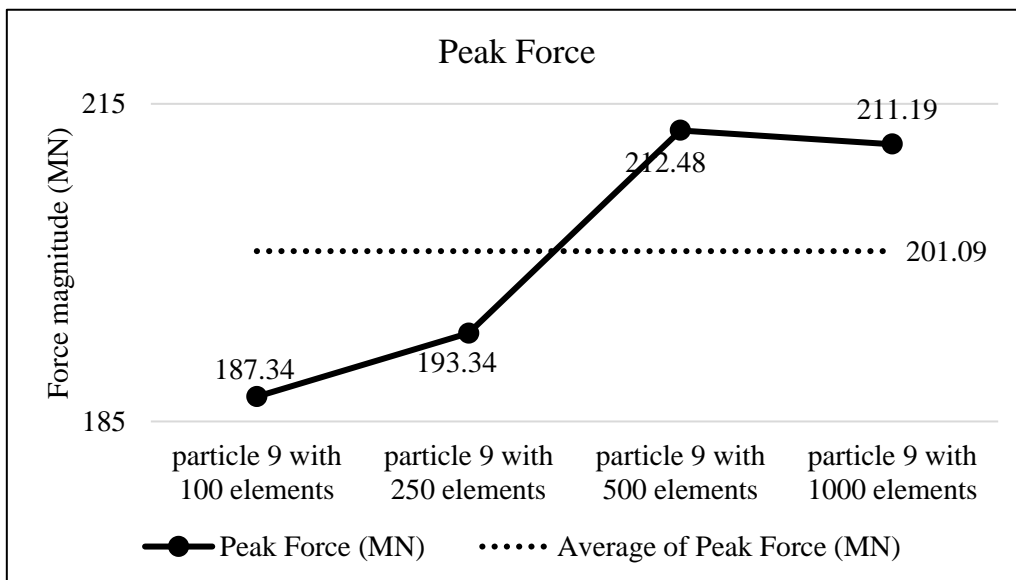


Figure A9.3 Peak collision for the four particle geometry resolutions for Particle 9.

Appendix

Collision results data analysis					
Model	particle 9 with 100 elements	particle 9 with 250 elements	particle 9 with 500 elements	particle 9 with 1000 elements	Average
Impulse (MN*s)	1.462	1.463	1.488	1.470	1.471
Percent difference from Avg. Impulse	-0.59	-0.55	1.19	-0.05	
Peak Force (MN)	187.34	193.34	212.48	211.19	201.09
Percent difference from Avg. Peak Force	-6.84	-3.85	5.67	5.02	

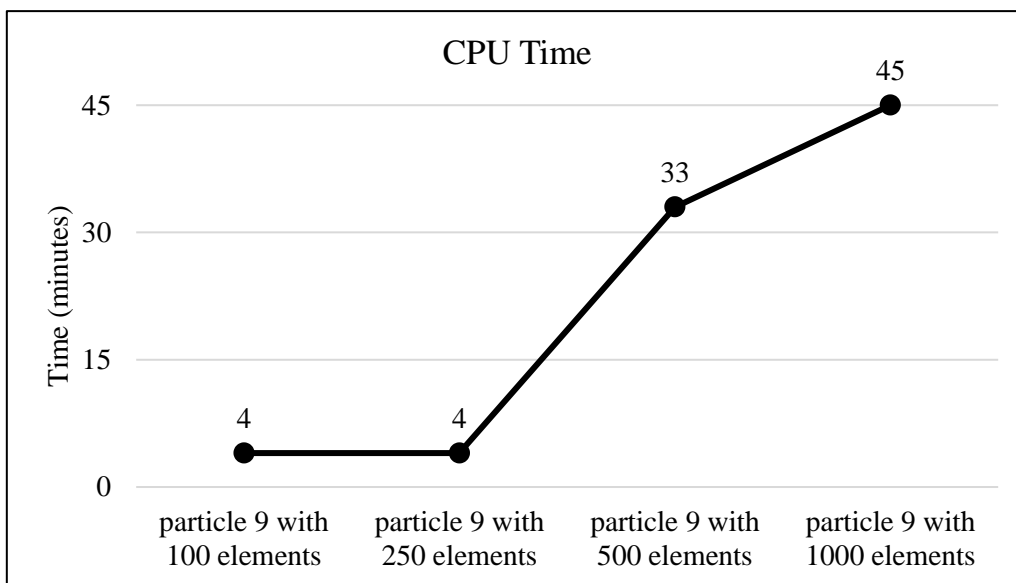
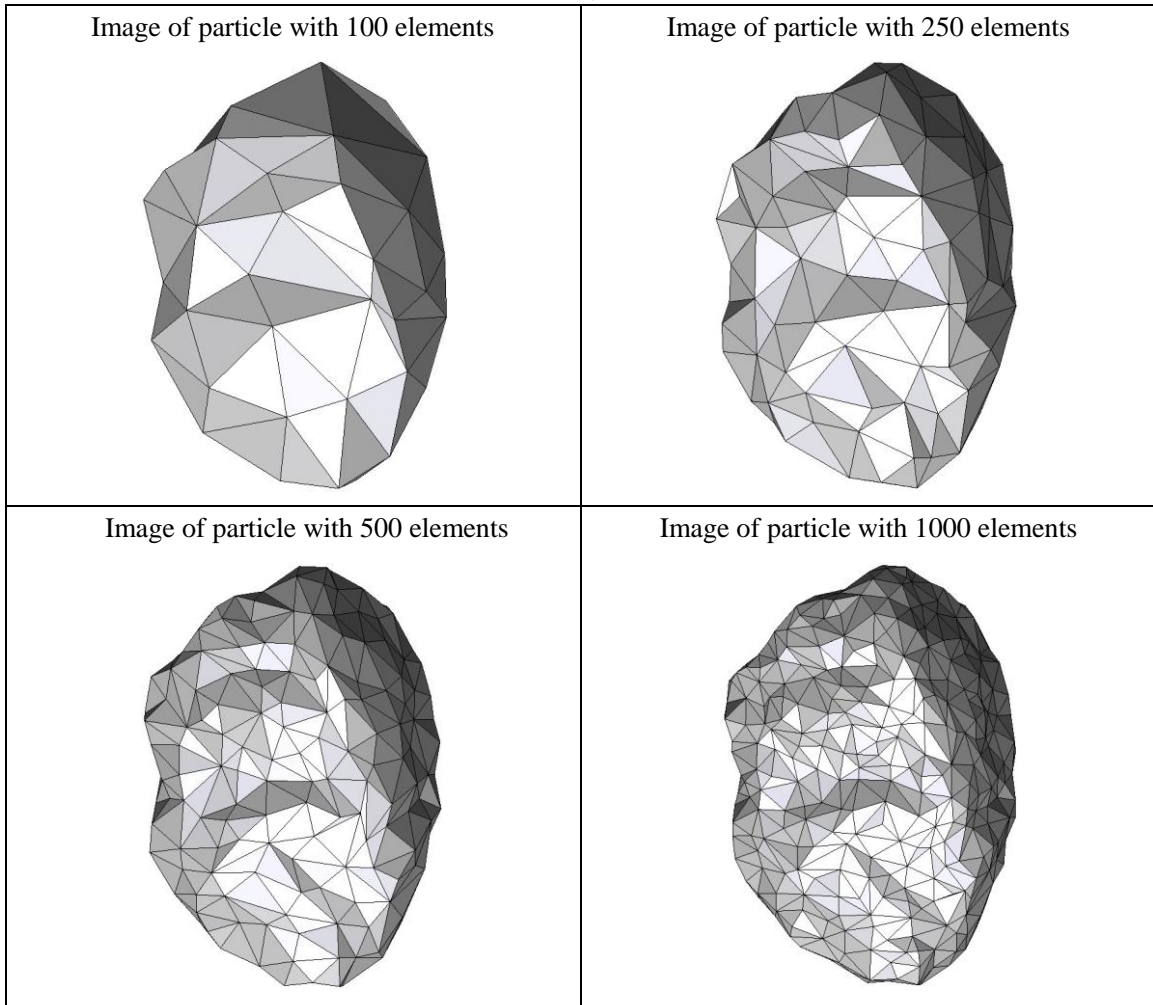


Figure A9.4 CPU computation time vs. model geometry resolution.

Appendix

Percent difference analysis compare to particle 9 with 100 elements for different group of data			
	particle 9 with 250 elements	particle 9 with 500 elements	particle 9 with 1000 elements
Impulse	0.04	1.79	0.54
Peak Force	3.20	13.42	12.73
Start Time	40.00	40.00	12.00
CPU Time	0.00	725.00	1025.00
Simulation Time	0.00	5.00	40.00

Summary of particle characteristics and collision simulation details for Particle 10 (of 50)



Particle statistics (part 1)

Particle ID	# vertices	# elements	Mass (g)	Moments of Inertia			Volume (cm ³)	Sfc. Area (cm ²)
				I1	I2	I3		
				(gcm ²)	(gcm ²)	(gcm ²)		
10 (100 elements)	52	100	45.098	275190.425	219005.9	117092.05	15.64067	38.14708
10 (250 elements)	127	250	45.098	290264.65	230685.15	123095.675	16.10373	38.69846
10 (500 elements)	252	500	45.098	294745.75	233835.325	125152.5	16.22982	38.95131
10 (1000 elements)	502	1000	45.098	295631.625	234667.175	125675.475	16.26773	38.98197

Particle Statistics (part 2)							
Particle ID	α	R_g (cm)	ψ	R_v (cm)	L (cm)	I (cm)	S (cm)
10 (100 elements)	2.48826	2.64461	0.79647	1.55139	204.47353	138.60417	82.17540
10 (250 elements)	2.50276	2.63420	0.79586	1.56656	210.02369	142.31351	83.91673
10 (500 elements)	2.50596	2.63452	0.79691	1.57063	211.48993	143.62706	84.39489
10 (1000 elements)	2.50055	2.63339	0.79285	1.57186	211.80286	143.84959	84.70236

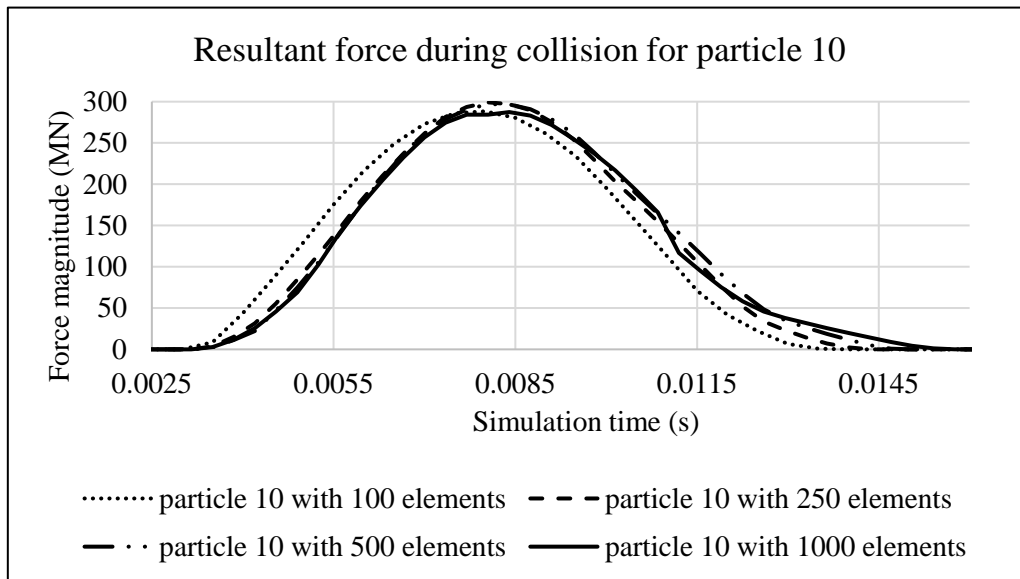


Figure A10.1 Plot of resultant forces during collision event for Particle 10.

Appendix

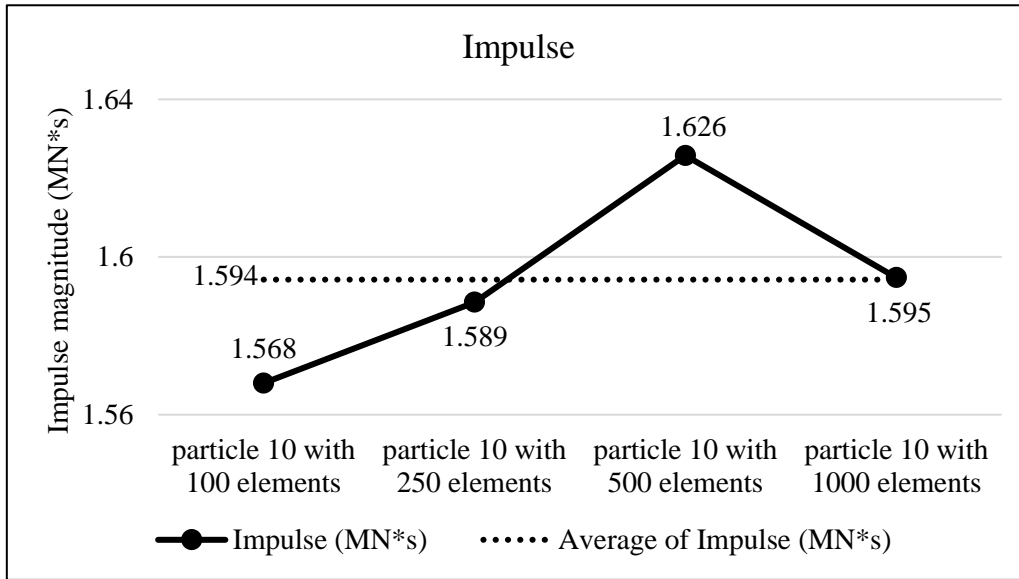


Figure A10.2 Plots of collision impulse for Particle 10.

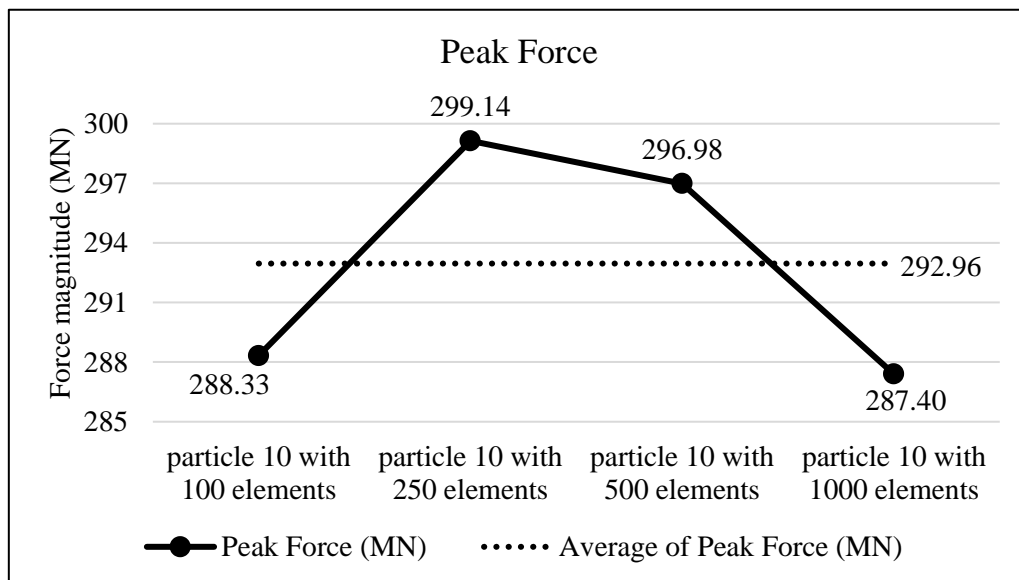


Figure A10.3 Peak collision for the four particle geometry resolutions for Particle 10.

Appendix

Collision results data analysis					
Model	particle 10 with 100 elements	particle 10 with 250 elements	particle 10 with 500 elements	particle 10 with 1000 elements	Average
Impulse (MN*s)	1.568	1.589	1.626	1.595	1.594
Percent difference from Avg. Impulse	-1.65	-0.36	1.98	0.03	
Peak Force (MN)	288.33	299.14	296.98	287.40	292.96
Percent difference from Avg. Peak Force	-1.58	2.11	1.37	-1.90	

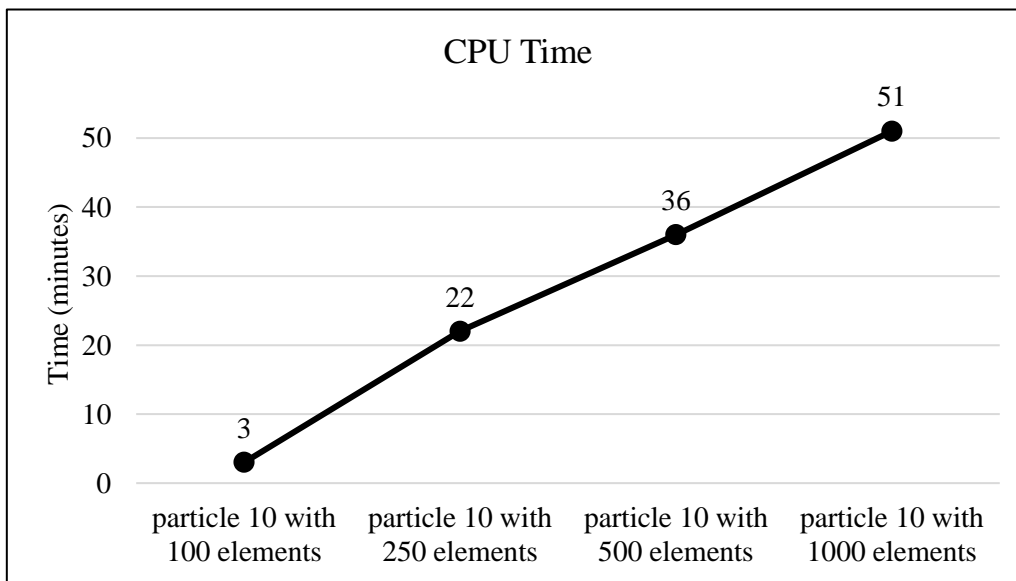


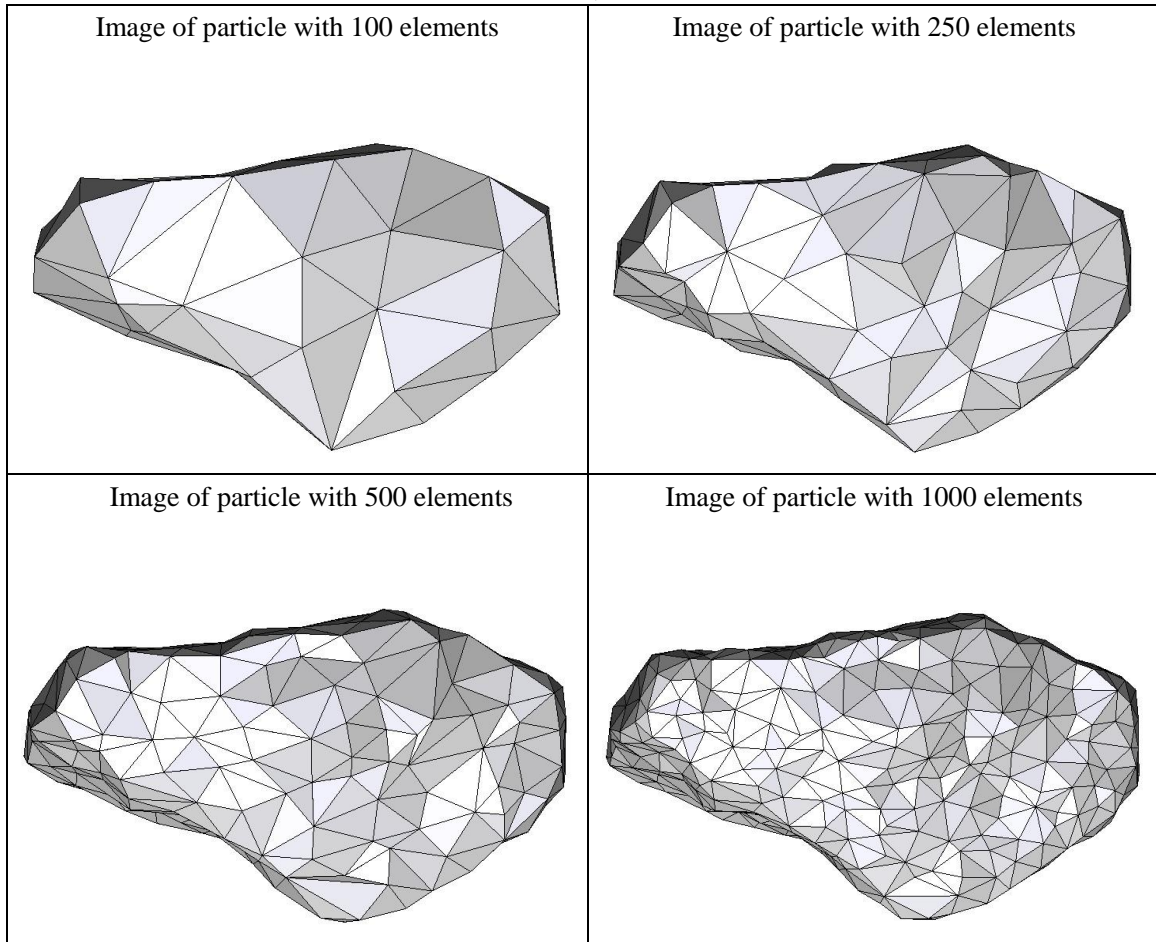
Figure A10.4 CPU computation time vs. model geometry resolution.

Appendix

Percent difference analysis compare to particle 10 with 100 elements for different group of data			
	particle 10 with 250 elements	particle 10 with 500 elements	particle 10 with 1000 elements
Impulse	1.31	3.68	1.71
Peak Force	3.75	3.00	-0.32
Start Time	0.00	0.00	0.00
CPU Time	633.33	1100.00	1600.00
Simulation Time	8.50	12.00	22.50

Appendix

Summary of particle characteristics and collision simulation details for Particle 11 (of 50)



Particle statistics (part 1)								
Particle ID	# vertices	# elements	Mass (g)	Moments of Inertia			Volume (cm ³)	Sfc. Area (cm ²)
				I1	I2	I3		
				(gcm ²)	(gcm ²)	(gcm ²)		
11 (100 elements)	52	100	31.543	177806.88	156352.41	55574.63	11.16326	30.61088
11 (250 elements)	127	250	31.543	182436.69	160384.95	57071.93	11.32059	30.92329
11 (500 elements)	252	500	31.543	183552.59	161284.03	57554.75	11.35805	31.02494
11 (1000 elements)	502	1000	31.543	184326.49	161995.29	57823.21	11.38927	31.04400

Appendix

Particle Statistics (part 2)							
Particle ID	α	R_g (cm)	ψ	R_v (cm)	L (cm)	I (cm)	S (cm)
11 (100 elements)	2.85741	2.53635	0.78911	1.38644	210.14163	110.49965	73.54262
11 (250 elements)	2.85650	2.54056	0.78846	1.39292	212.82684	111.99193	74.50626
11 (500 elements)	2.85333	2.54000	0.78761	1.39446	213.39666	112.48598	74.78868
11 (1000 elements)	2.85106	2.54345	0.78856	1.39573	213.84807	112.71902	75.00649

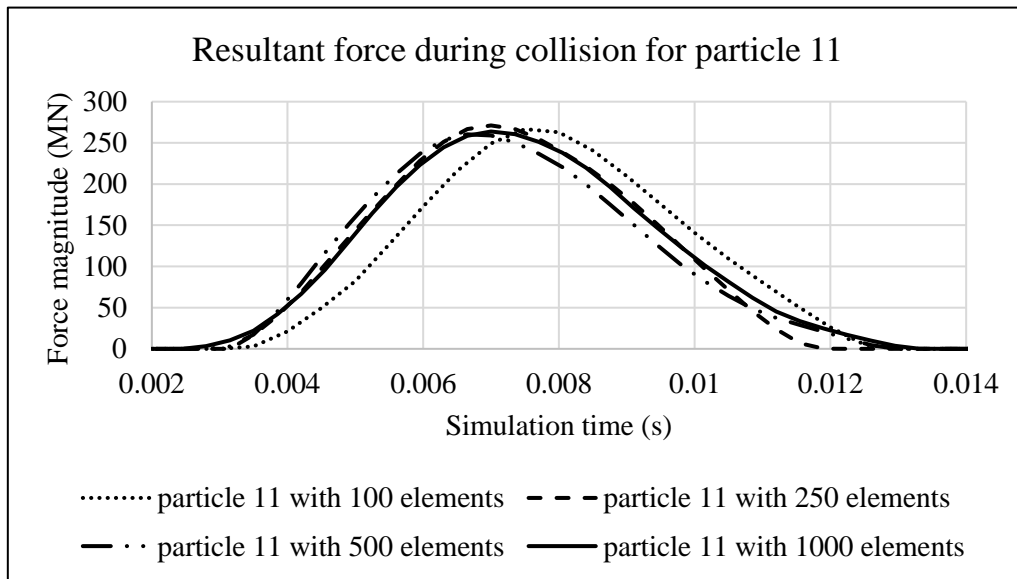


Figure A11.1 Plot of resultant forces during collision event for Particle 11.

Appendix

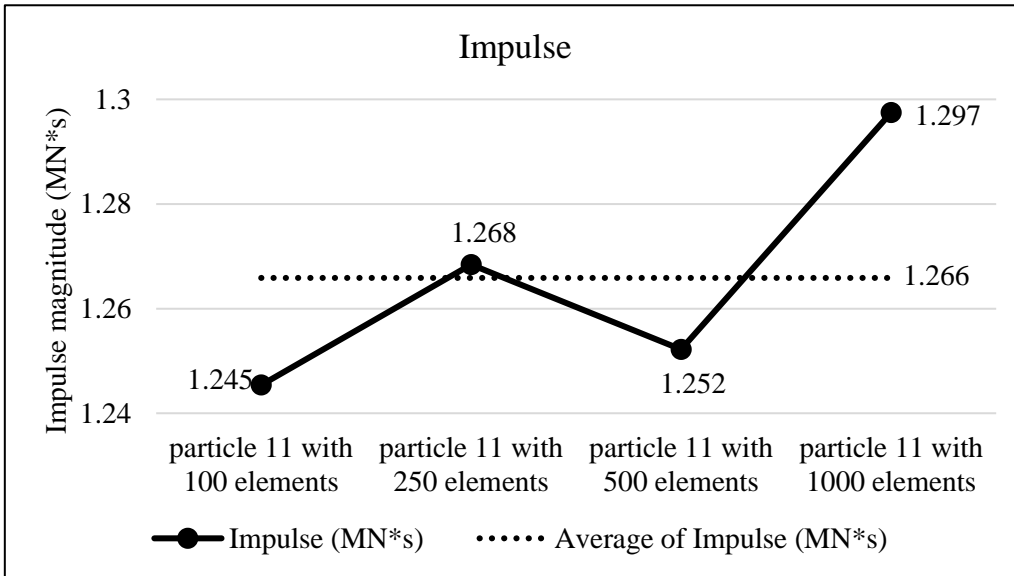


Figure A11.2 Plots of collision impulse for Particle 11.

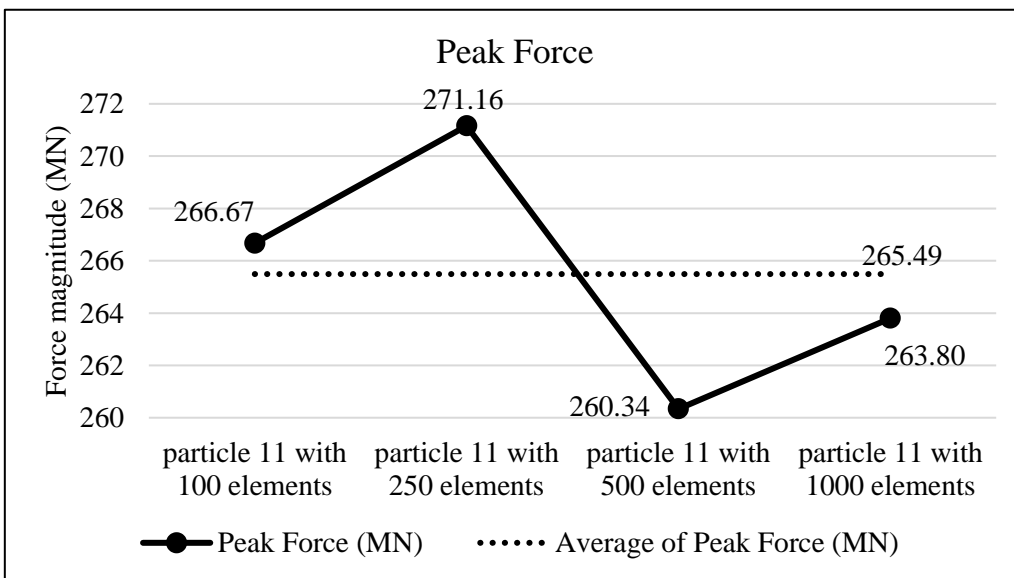


Figure A11.3 Peak collision for the four particle geometry resolutions for Particle 11.

Appendix

Collision results data analysis					
Model	particle 11 with 100 elements	particle 11 with 250 elements	particle 11 with 500 elements	particle 11 with 1000 elements	Average
Impulse (MN*s)	1.245	1.268	1.252	1.297	1.266
Percent difference from Avg. Impulse	-1.62	0.20	-1.08	2.50	
Peak Force (MN)	266.67	271.16	260.34	263.80	265.49
Percent difference from Avg. Peak Force	0.44	2.13	-1.94	-0.64	

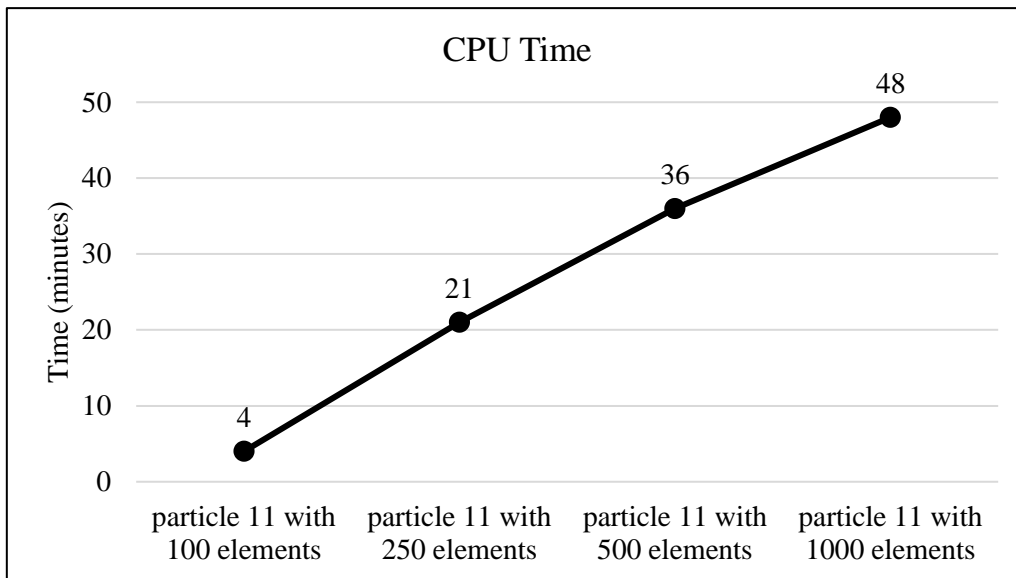
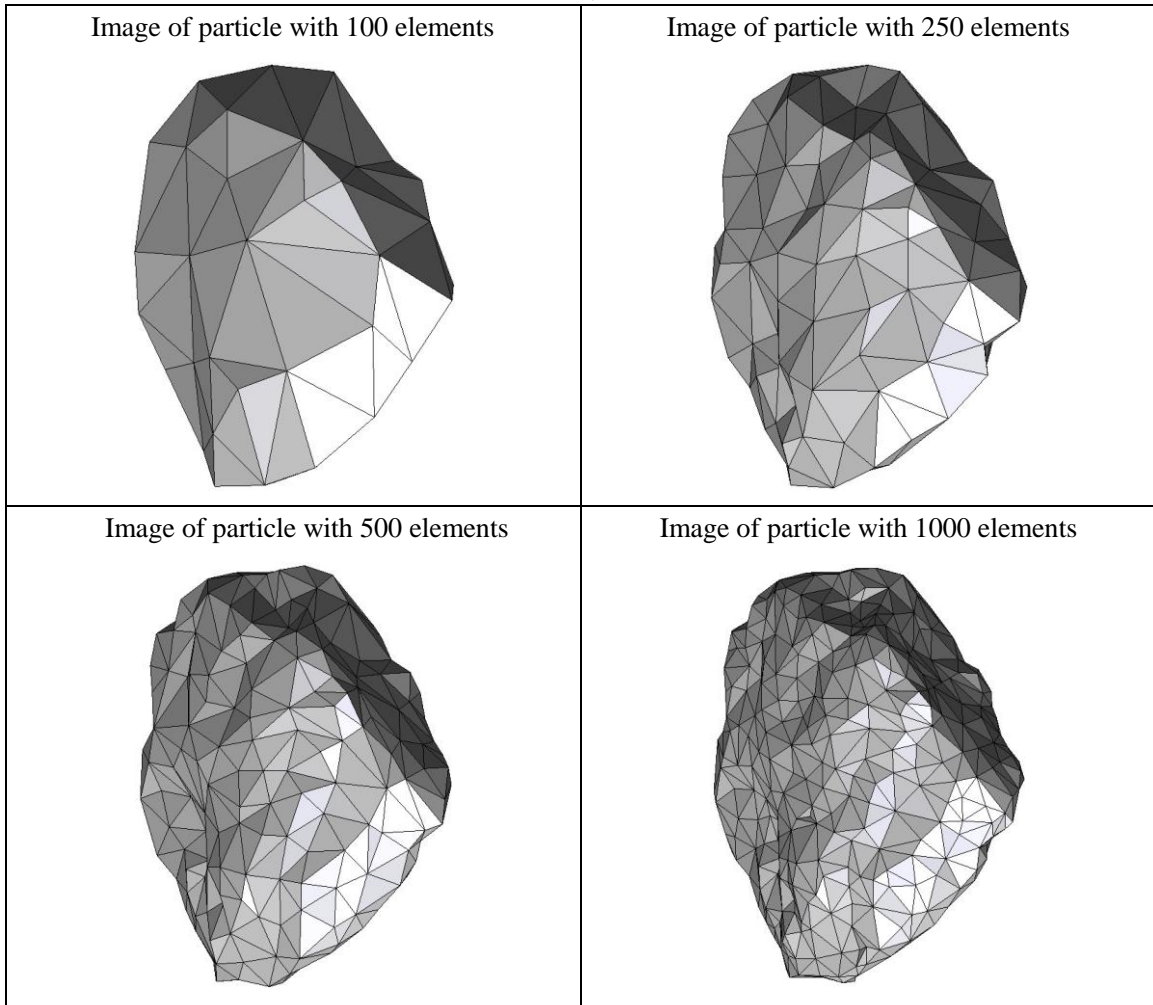


Figure A11.4 CPU computation time vs. model geometry resolution.

Appendix

Percent difference analysis compare to particle 11 with 100 elements for different group of data			
	particle 11 with 250 elements	particle 11 with 500 elements	particle 11 with 1000 elements
Impulse	1.85	0.55	4.18
Peak Force	1.68	-2.38	-1.08
Start Time	-10.00	-10.00	-20.00
CPU Time	425.00	800.00	1100.00
Simulation Time	-2.78	8.89	16.67

Summary of particle characteristics and collision simulation details for Particle 12 (of 50)



Particle statistics (part 1)								
Particle ID	# vertices	# elements	Mass (g)	Moments of Inertia			Volume (cm ³)	Sfc. Area (cm ²)
				I1	I2	I3		
				(gcm ²)	(gcm ²)	(gcm ²)		
12 (100 elements)	52	100	16.572	64963.2875	42998.01875	29843.29375	5.92413	22.25529
12 (250 elements)	127	250	16.572	67911.9375	44894.125	31060.11875	6.05032	22.53997
12 (500 elements)	252	500	16.572	69134.11875	45736.475	31541.525	6.10434	22.65887
12 (1000 elements)	502	1000	16.572	69537.3875	46011.31875	31671.37188	6.11665	22.69027

Appendix

Particle Statistics (part 2)							
Particle ID	α	R_g (cm)	ψ	R_v (cm)	L (cm)	I (cm)	S (cm)
12 (100 elements)	3.14896	2.00093	0.71143	1.12248	153.52289	125.02542	48.75355
12 (250 elements)	3.18818	1.99766	0.71239	1.13039	157.04736	127.73431	49.25926
12 (500 elements)	3.19877	1.98981	0.71286	1.13375	158.56079	128.74743	49.56935
12 (1000 elements)	3.20899	1.98568	0.71283	1.13451	159.08156	129.04970	49.57368

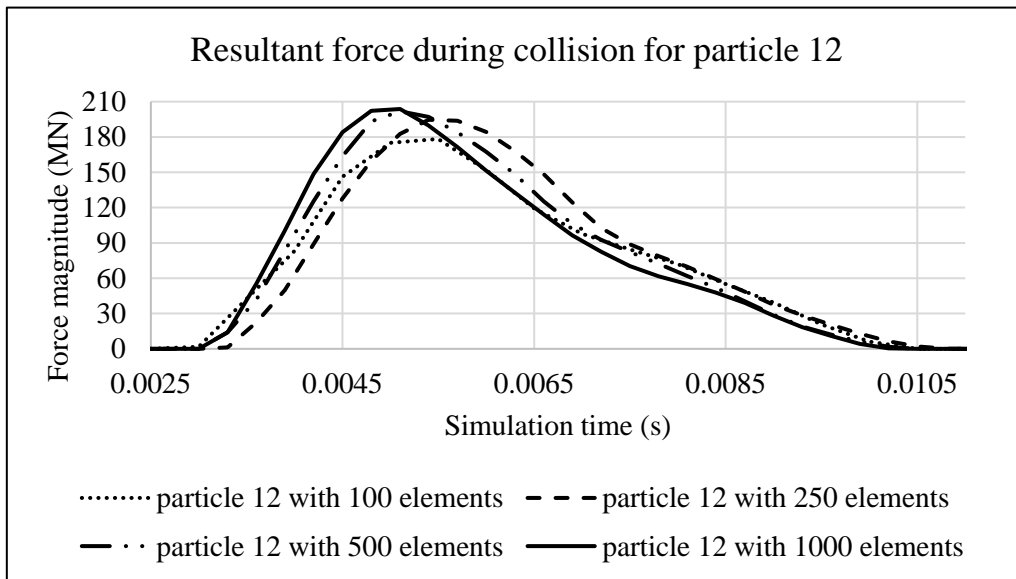


Figure A12.1 Plot of resultant forces during collision event for Particle 12.

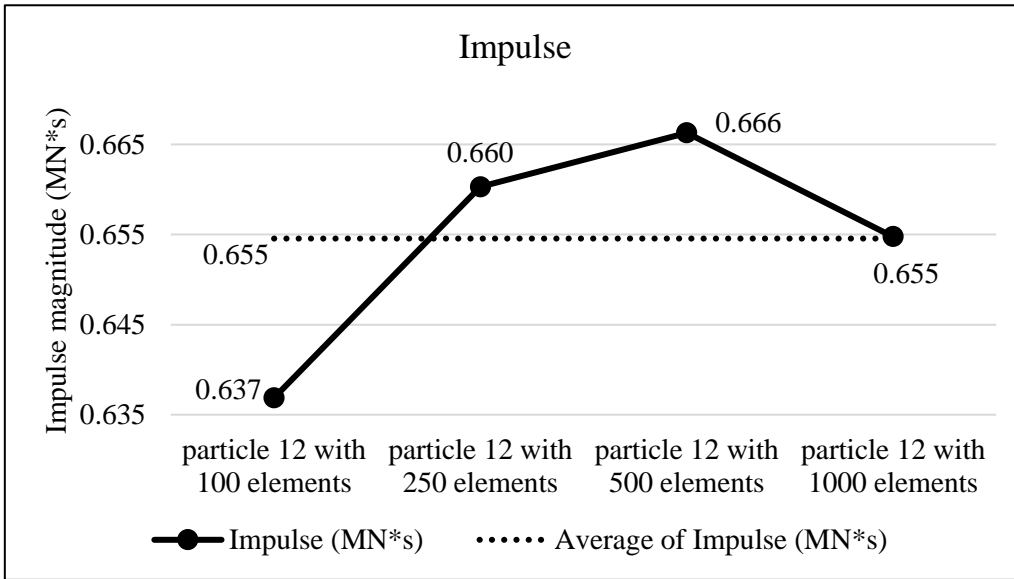


Figure A12.2 Plots of collision impulse for Particle 12.

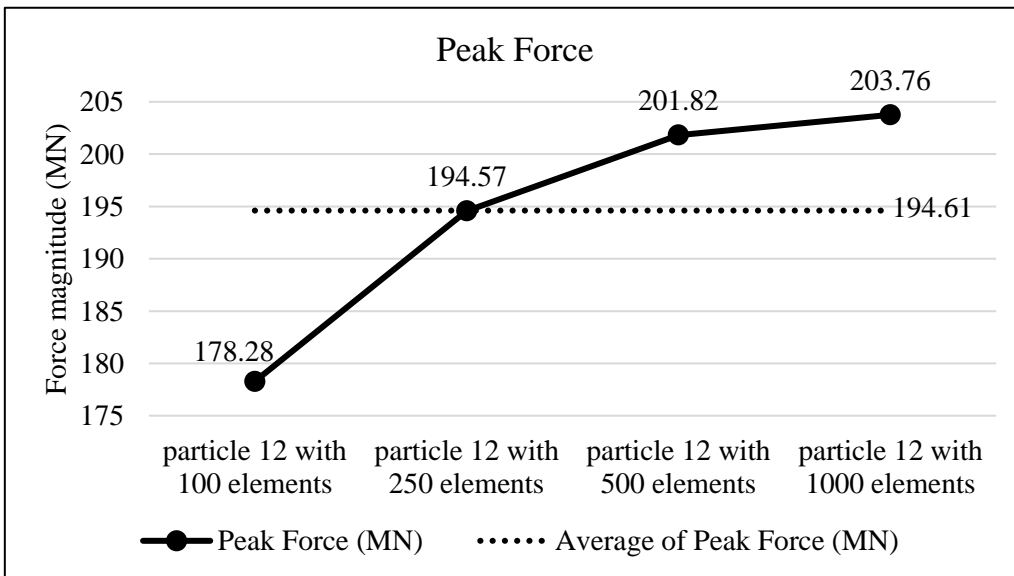


Figure A12.3 Peak collision for the four particle geometry resolutions for Particle 12.

Appendix

Collision results data analysis					
Model	particle 12 with 100 elements	particle 12 with 250 elements	particle 12 with 500 elements	particle 12 with 1000 elements	Average
Impulse (MN*s)	0.637	0.660	0.666	0.655	0.655
Percent difference from Avg. Impulse	-2.70	0.88	1.79	0.03	
Peak Force (MN)	178.28	194.57	201.82	203.76	194.61
Percent difference from Avg. Peak Force	-8.39	-0.02	3.71	4.70	

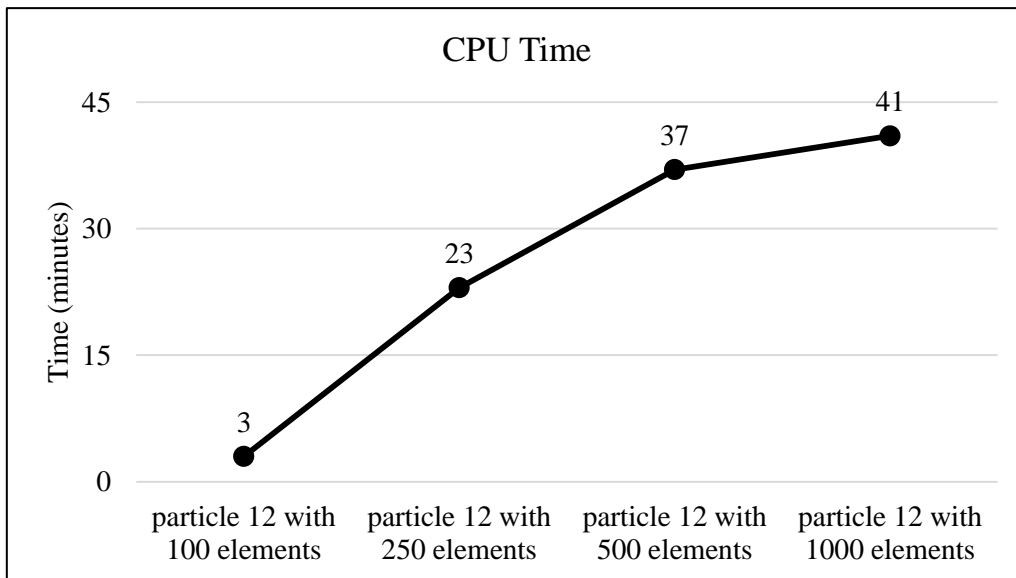


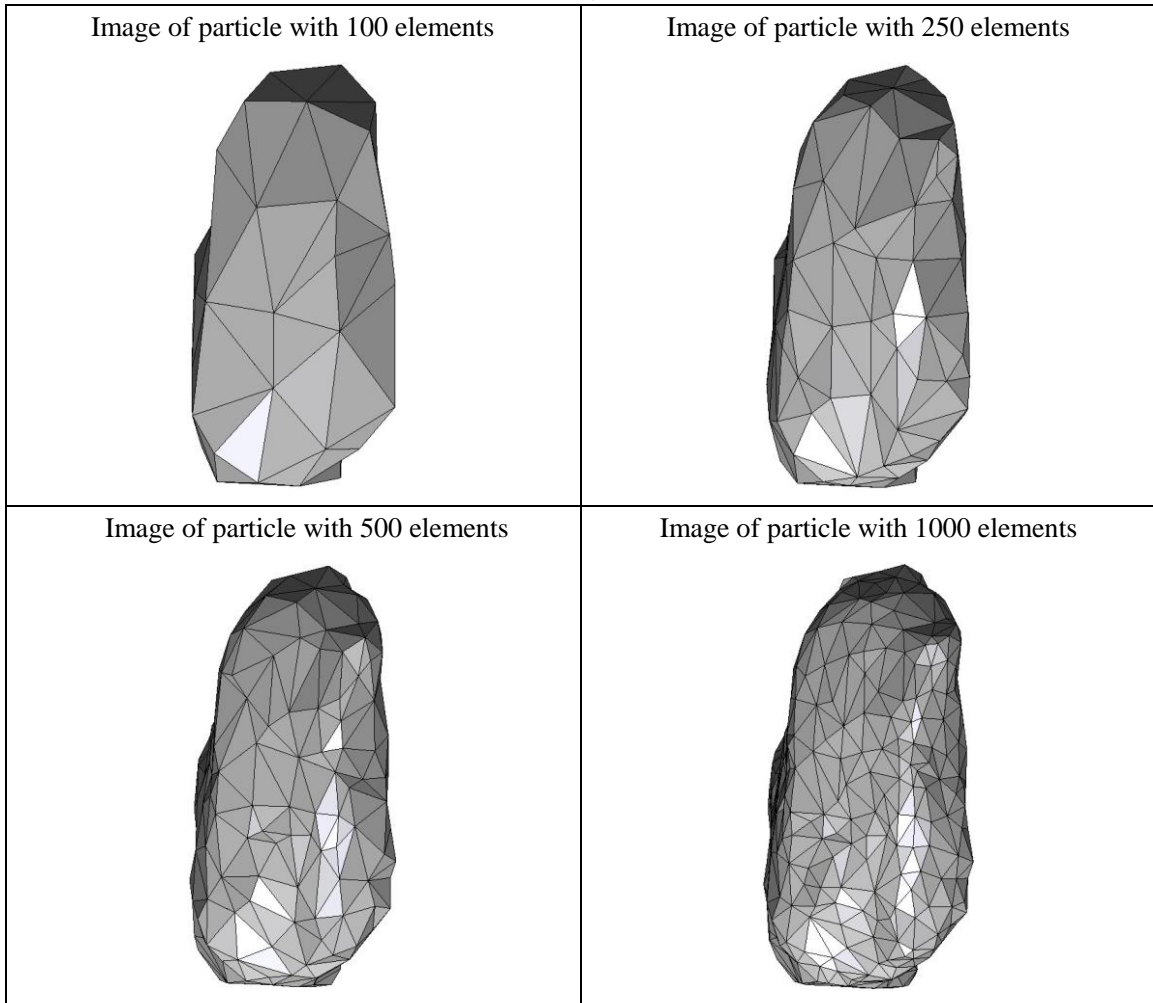
Figure A12.4 CPU computation time vs. model geometry resolution.

Appendix

Percent difference analysis compare to particle 12 with 100 elements for different group of data			
	particle 12 with 250 elements	particle 12 with 500 elements	particle 12 with 1000 elements
Impulse	3.68	4.62	2.81
Peak Force	9.14	13.21	14.29
Start Time	10.00	0.00	0.00
CPU Time	666.67	1133.33	1266.67
Simulation Time	7.14	7.14	2.86

Appendix

Summary of particle characteristics and collision simulation details for Particle 13 (of 50)



Particle statistics (part 1)								
Particle ID	# vertices	# elements	Mass (g)	Moments of Inertia			Volume (cm ³)	Sfc. Area (cm ²)
				I1	I2	I3		
				(gcm ²)	(gcm ²)	(gcm ²)		
13 (100 elements)	52	100	15.118	59234.1125	44104.92188	25550.19688	6.03021	20.51947
13 (250 elements)	127	250	15.118	61414.475	45618.375	26494.80938	6.14478	20.68477
13 (500 elements)	252	500	15.118	62041.875	46094.94688	26737.08438	6.18231	20.71637
13 (1000 elements)	502	1000	15.118	62341.9875	46306.32813	26881.6125	6.20062	20.67666

Appendix

Particle Statistics (part 2)							
Particle ID	α	R_g (cm)	ψ	R_v (cm)	L (cm)	I (cm)	S (cm)
13 (100 elements)	2.73215	1.85136	0.78080	1.12914	160.39709	115.99120	58.70737
13 (250 elements)	2.74369	1.85996	0.78434	1.13625	163.20684	118.26639	59.48446
13 (500 elements)	2.74661	1.85937	0.78633	1.13856	164.07761	118.81478	59.73814
13 (1000 elements)	2.74571	1.85845	0.78939	1.13968	164.44705	119.13898	59.89240

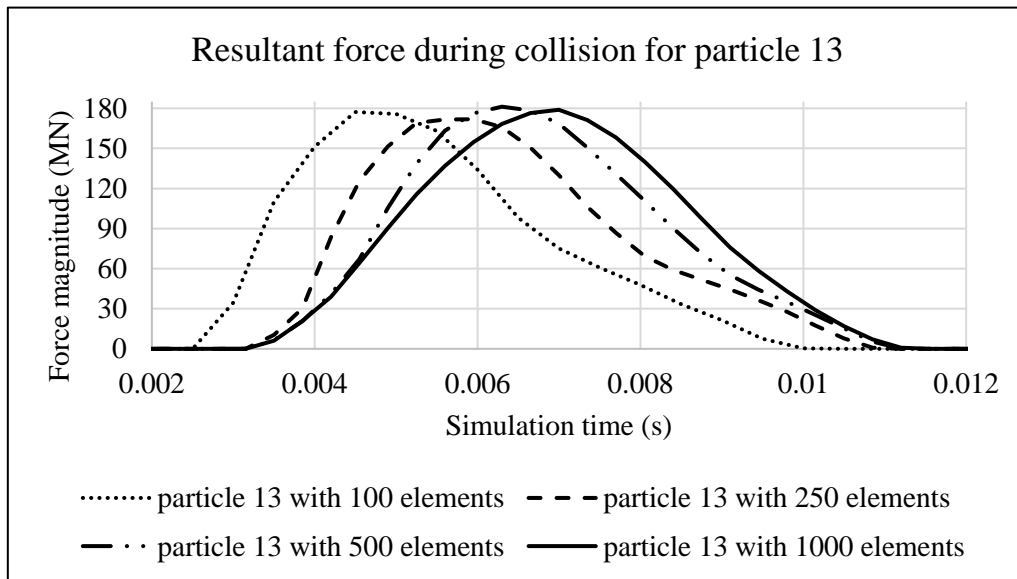


Figure A13.1 Plot of resultant forces during collision event for Particle 13.

Appendix

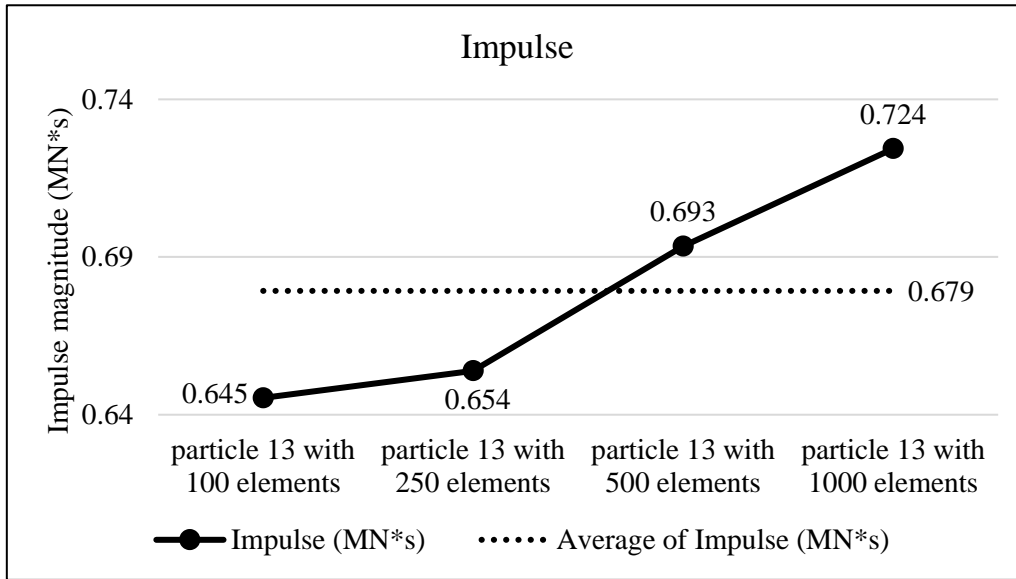


Figure A13.2 Plots of collision impulse for Particle 13.

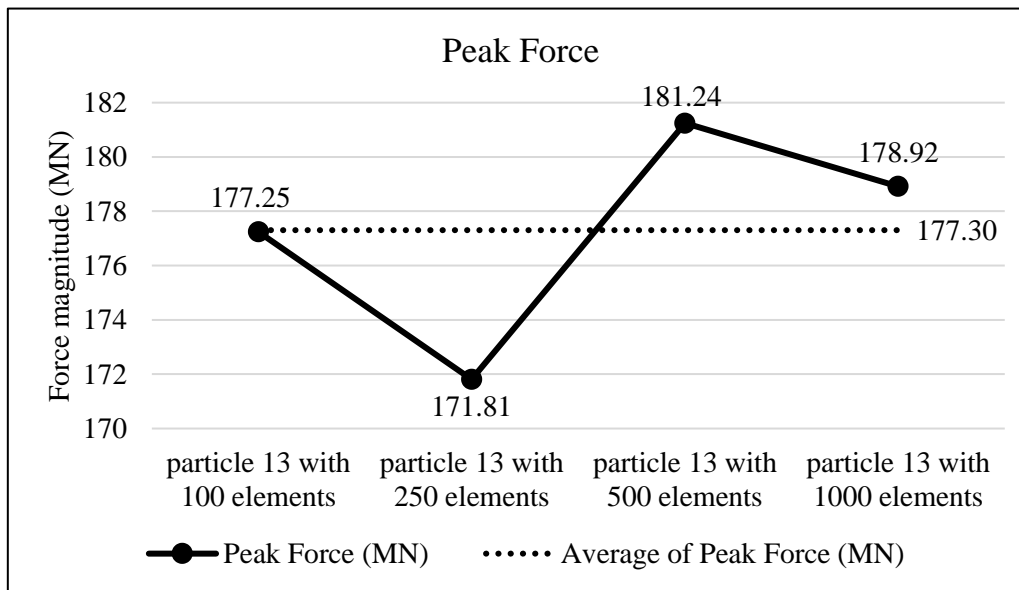


Figure A13.3 Peak collision for the four particle geometry resolutions for Particle 13.

Appendix

Collision results data analysis					
Model	particle 13 with 100 elements	particle 13 with 250 elements	particle 13 with 500 elements	particle 13 with 1000 elements	Average
Impulse (MN*s)	0.645	0.654	0.693	0.724	0.679
Percent difference from Avg. Impulse	-5.00	-3.73	2.08	6.64	
Peak Force (MN)	177.25	171.81	181.24	178.92	177.30
Percent difference from Avg. Peak Force	-0.03	-3.10	2.22	0.91	

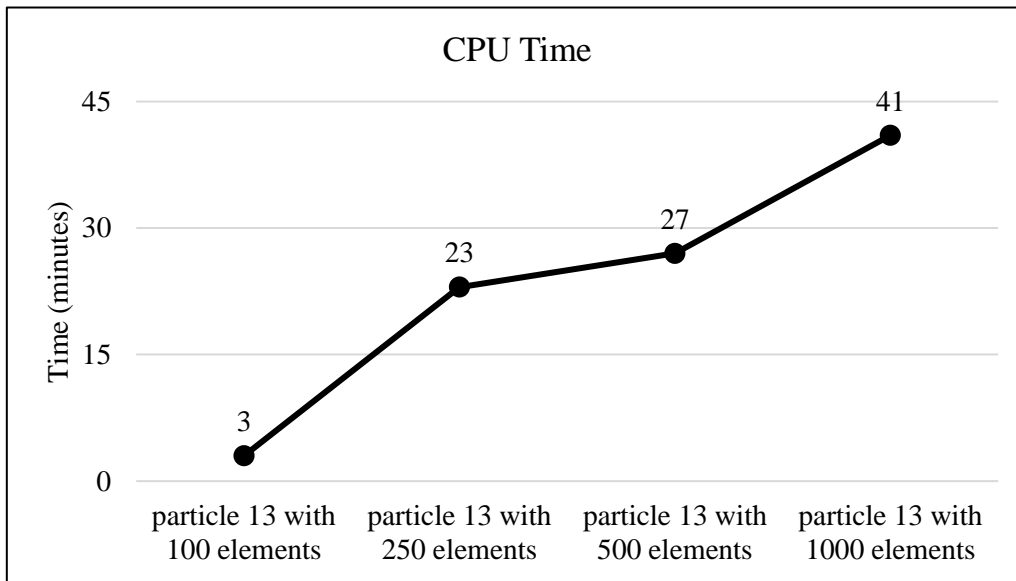
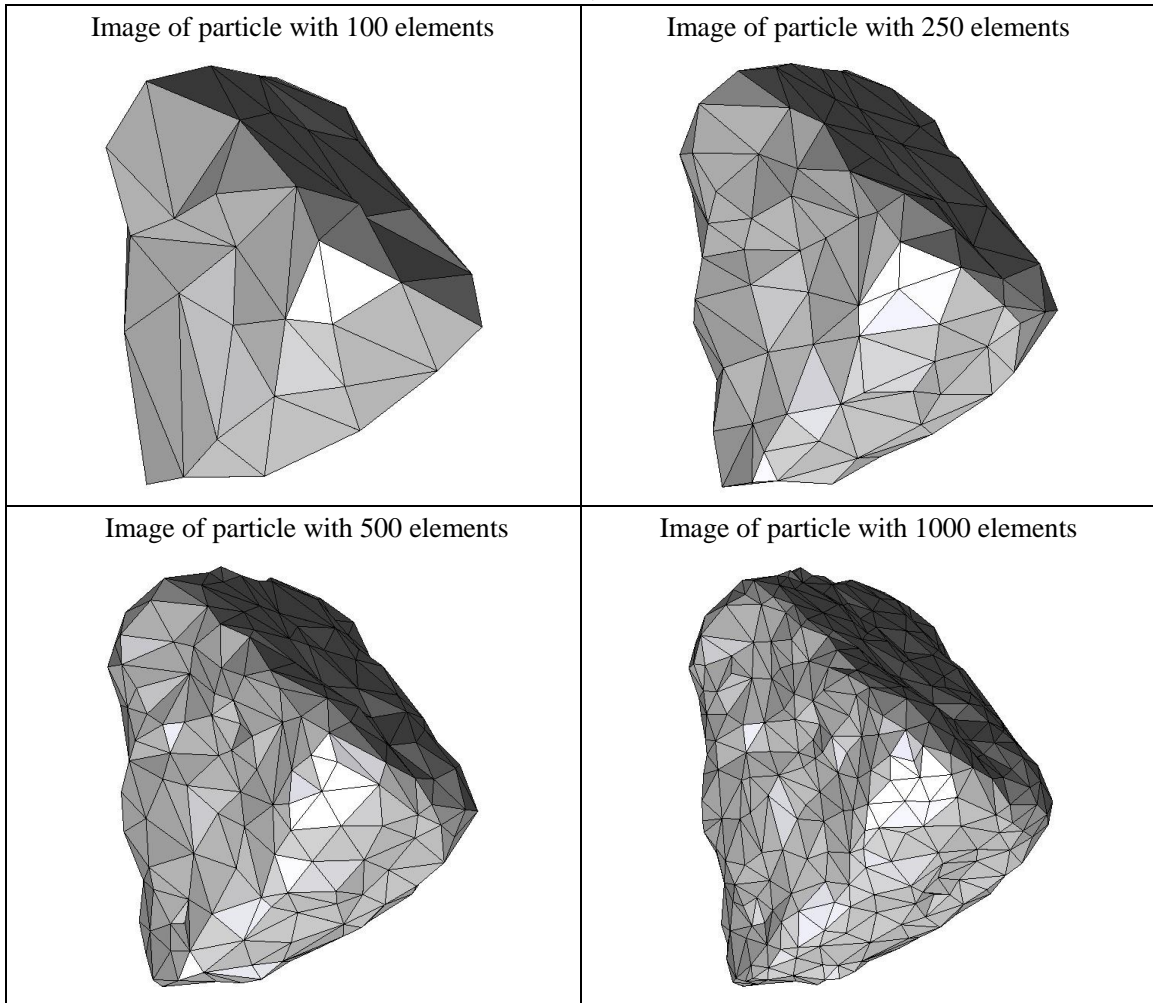


Figure A13.4 CPU computation time vs. model geometry resolution.

Appendix

Percent difference analysis compare to particle 13 with 100 elements for different group of data			
	particle 13 with 250 elements	particle 13 with 500 elements	particle 13 with 1000 elements
Impulse	1.34	7.45	12.24
Peak Force	-3.07	2.26	0.94
Start Time	16.67	16.67	16.67
CPU Time	666.67	800.00	1266.67
Simulation Time	5.00	10.00	10.00

Summary of particle characteristics and collision simulation details for Particle 14 (of 50)



Particle statistics (part 1)								
Particle ID	# vertices	# elements	Mass (g)	Moments of Inertia			Volume (cm ³)	Sfc. Area (cm ²)
				I1	I2	I3		
				(gcm ²)	(gcm ²)	(gcm ²)		
14 (100 elements)	52	100	15.118	59234.1125	44104.92188	25550.19688	6.03021	20.51947
14 (250 elements)	127	250	15.118	61414.475	45618.375	26494.80938	6.14478	20.68477
14 (500 elements)	252	500	15.118	62041.875	46094.94688	26737.08438	6.18231	20.71637
14 (1000 elements)	502	1000	12.348	25816.80938	22624.05469	18556.39531	4.54133	15.97491

Appendix

Particle Statistics (part 2)							
Particle ID	α	R_g (cm)	ψ	R_v (cm)	L (cm)	I (cm)	S (cm)
14 (100 elements)	2.73215	1.85136	0.82620	1.12914	160.39709	115.99120	58.70737
14 (250 elements)	2.74369	1.85996	0.82678	1.13625	163.20684	118.26639	59.48446
14 (500 elements)	2.74661	1.85937	0.82807	1.13856	164.07761	118.81478	59.73814
14 (1000 elements)	1.39468	1.65357	0.83017	1.02730	110.00425	93.84429	78.87398

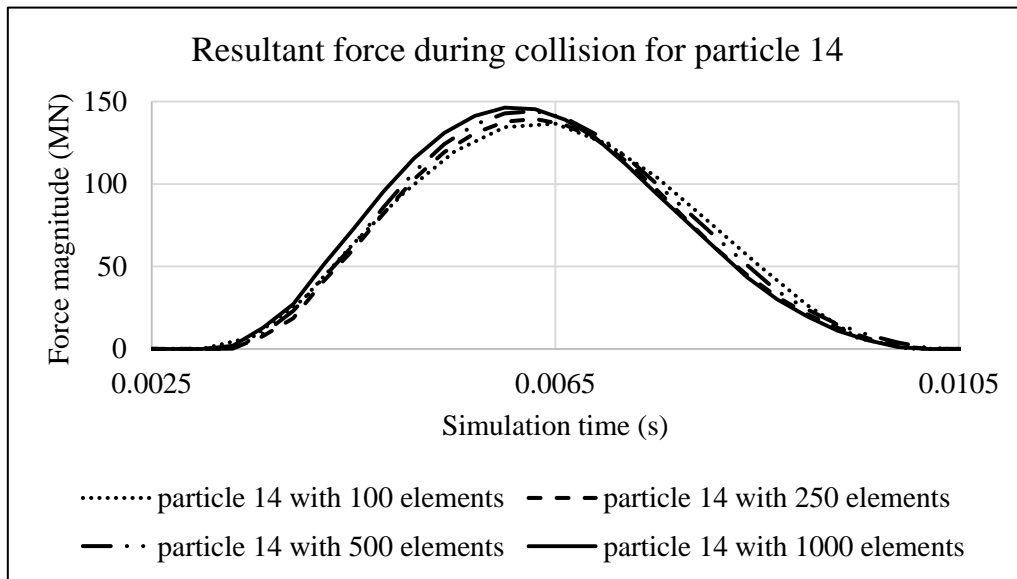


Figure A14.1 Plot of resultant forces during collision event for Particle 14.

Appendix

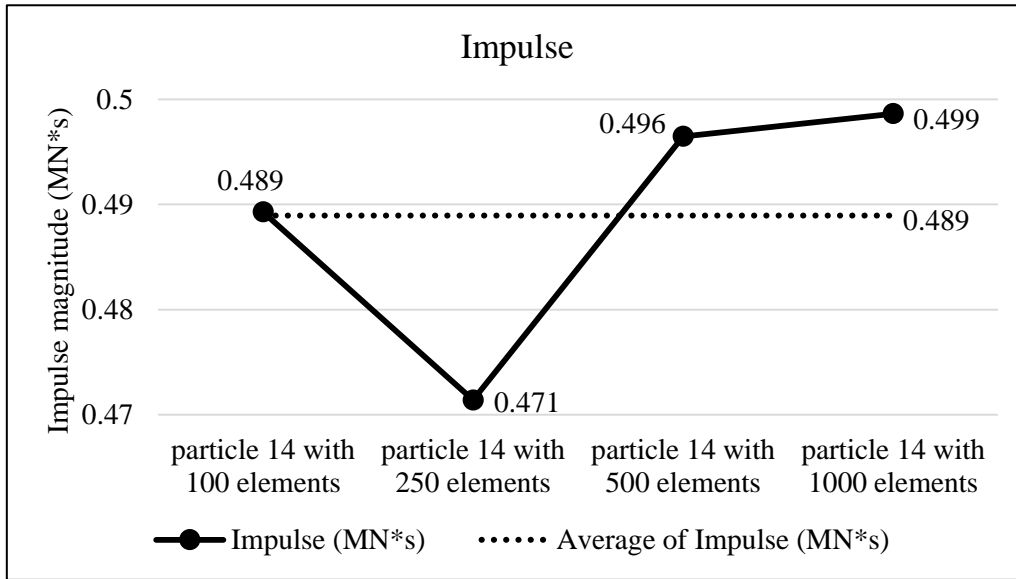


Figure A14.2 Plots of collision impulse for Particle 14.

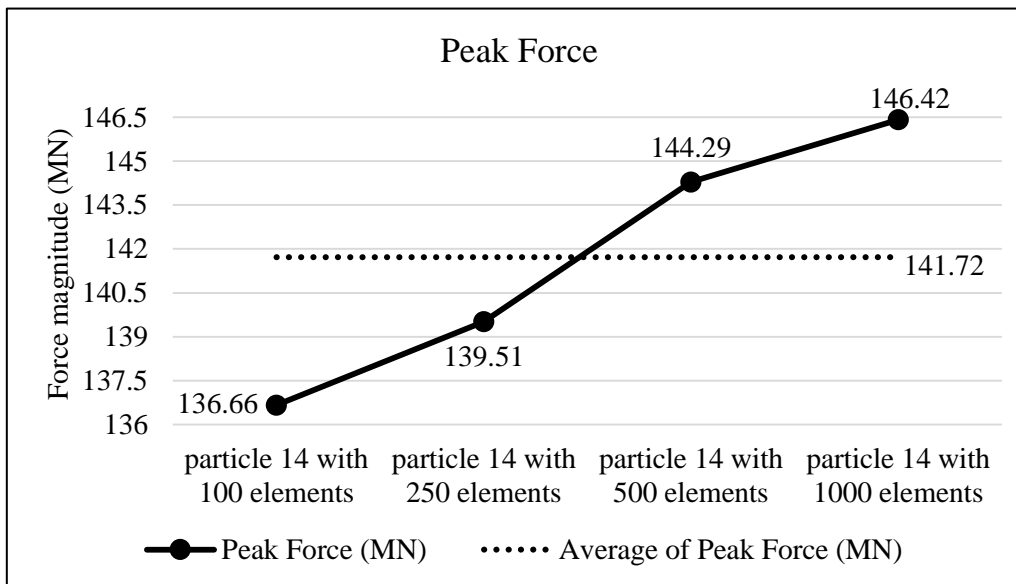


Figure A14.3 Peak collision for the four particle geometry resolutions for Particle 14.

Appendix

Collision results data analysis					
Model	particle 14 with 100 elements	particle 14 with 250 elements	particle 14 with 500 elements	particle 14 with 1000 elements	Average
Impulse (MN*s)	0.489	0.471	0.496	0.499	0.489
Percent difference from Avg. Impulse	0.07	-3.59	1.54	1.98	
Peak Force (MN)	136.66	139.51	144.29	146.42	141.72
Percent difference from Avg. Peak Force	-3.57	-1.56	1.81	3.31	

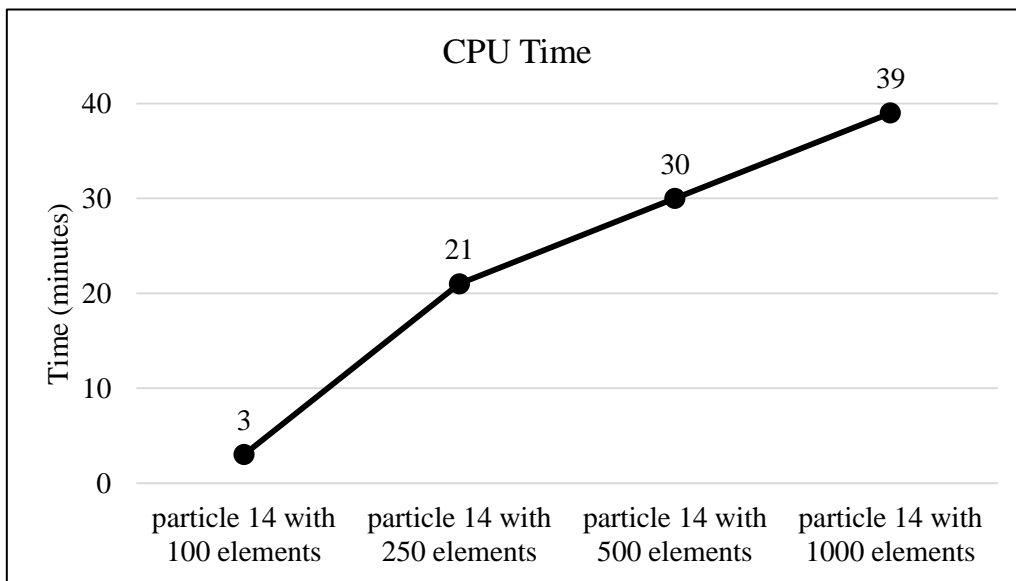
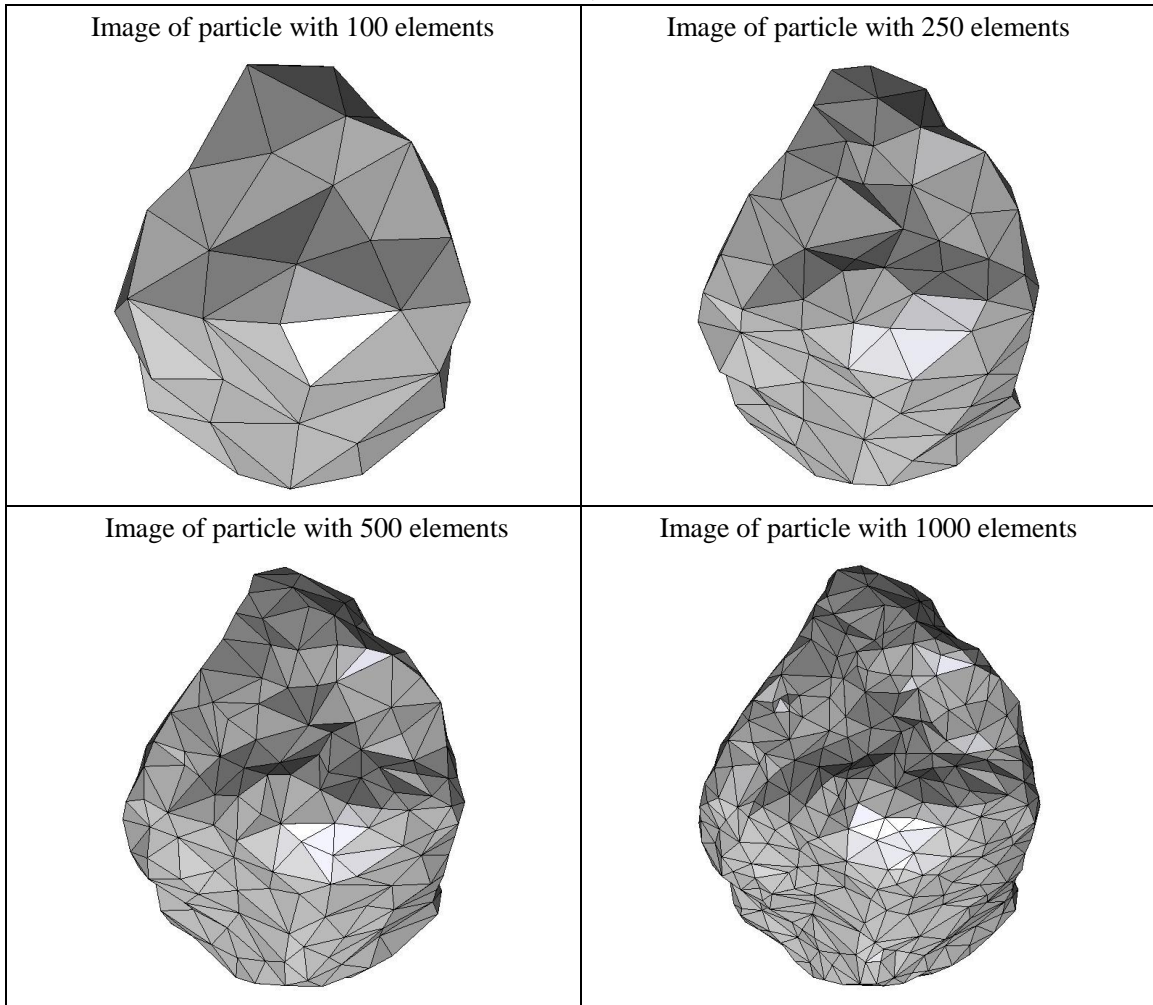


Figure A14.4 CPU computation time vs. model geometry resolution.

Appendix

Percent difference analysis compare to particle 14 with 100 elements for different group of data			
	particle 14 with 250 elements	particle 14 with 500 elements	particle 14 with 1000 elements
Impulse	-3.66	1.47	1.91
Peak Force	2.09	5.58	7.14
Start Time	-5.71	-5.71	-5.71
CPU Time	600.00	900.00	1200.00
Simulation Time	1.54	6.15	1.54

Summary of particle characteristics and collision simulation details for Particle 15 (of 50)



Particle statistics (part 1)								
Particle ID	# vertices	# elements	Mass (g)	Moments of Inertia			Volume (cm ³)	Sfc. Area (cm ²)
				I1	I2	I3		
				(gcm ²)	(gcm ²)	(gcm ²)		
15 (100 elements)	52	100	27.723	88110.7875	78874.79375	62025.75625	9.74536	25.90280
15 (250 elements)	127	250	27.723	90570.21875	80916.79375	63972.19375	9.90897	26.14172
15 (500 elements)	252	500	27.723	91321.375	81658.33125	64525.675	9.95298	26.31748
15 (1000 elements)	502	1000	27.723	91687.8	81979.91875	64780.0125	9.97037	26.31432

Appendix

Particle Statistics (part 2)							
Particle ID	α	R_g (cm)	ψ	R_v (cm)	L (cm)	I (cm)	S (cm)
15 (100 elements)	1.41006	1.93005	0.85180	1.32506	137.58670	113.36869	97.57527
15 (250 elements)	1.40689	1.98011	0.85343	1.33244	139.25123	115.23366	98.97827
15 (500 elements)	1.40600	2.00509	0.85024	1.33441	139.85814	115.67349	99.47254
15 (1000 elements)	1.40612	2.00494	0.85133	1.33518	140.13748	115.90649	99.66228

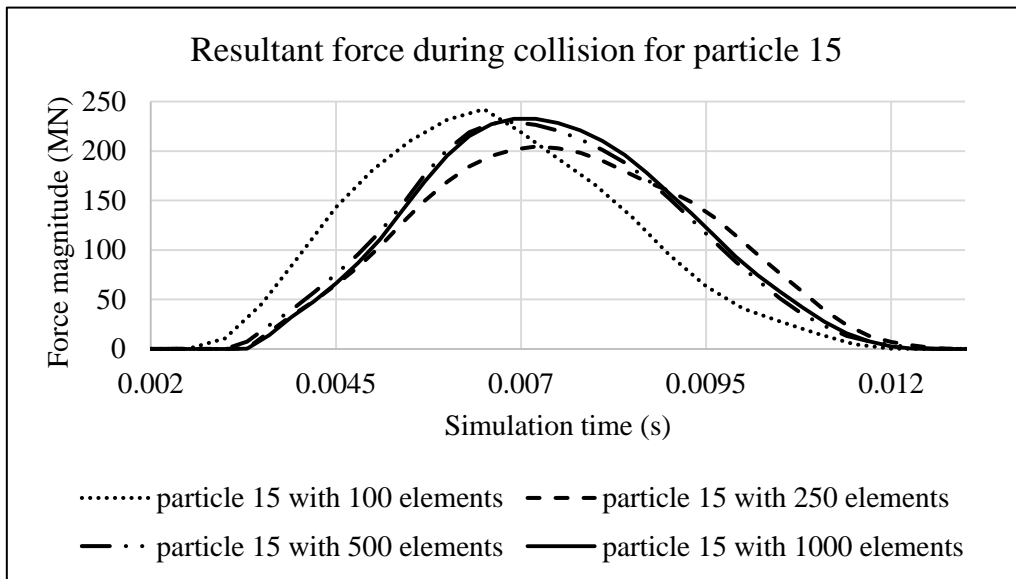


Figure A15.1 Plot of resultant forces during collision event for Particle 15.

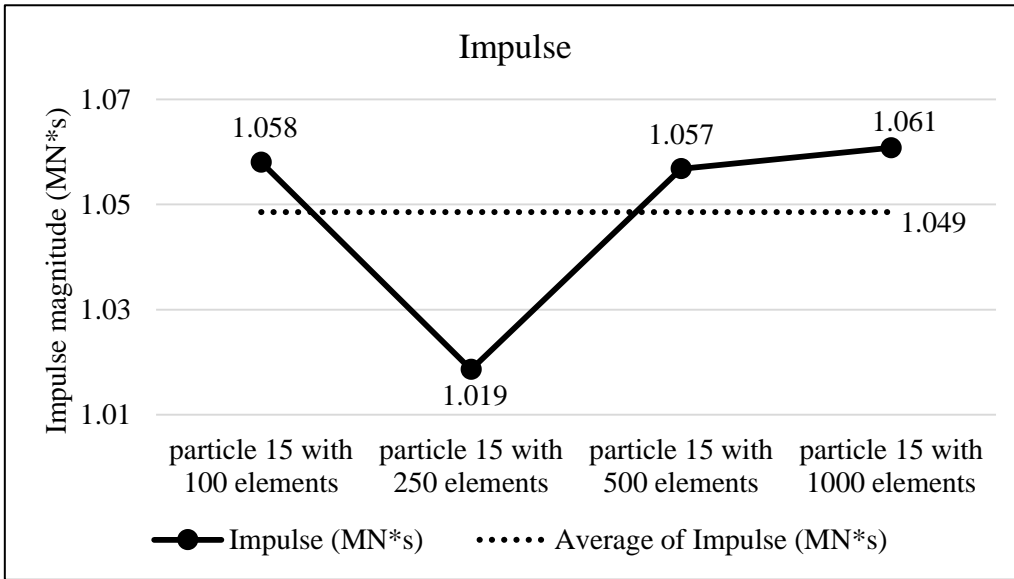


Figure A15.2 Plots of collision impulse for Particle 15.

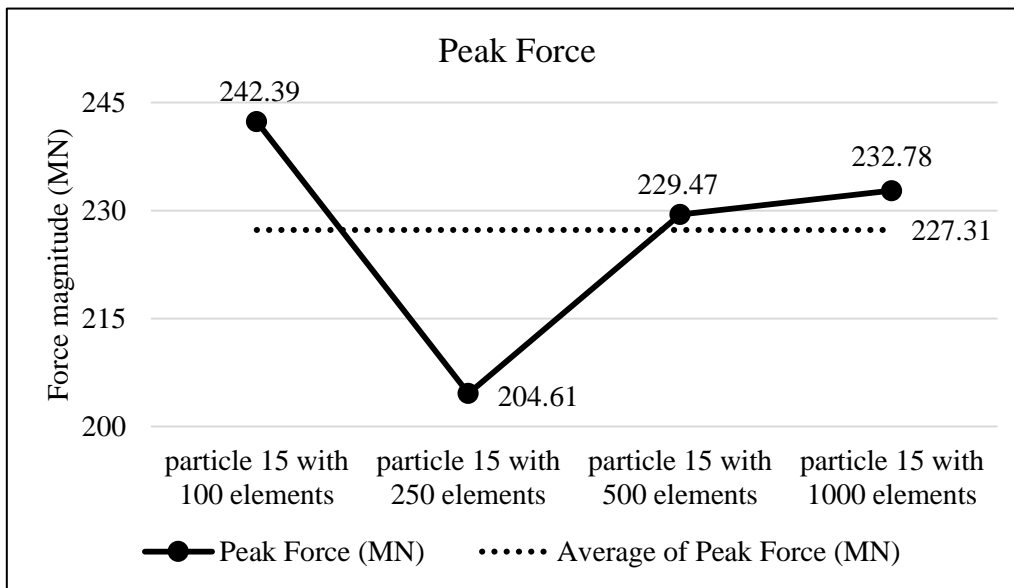


Figure A15.3 Peak collision for the four particle geometry resolutions for Particle 15.

Appendix

Collision results data analysis					
Model	particle 15 with 100 elements	particle 15 with 250 elements	particle 15 with 500 elements	particle 15 with 1000 elements	Average
Impulse (MN*s)	1.058	1.019	1.057	1.061	1.049
Percent difference from Avg. Impulse	0.91	-2.86	0.78	1.17	
Peak Force (MN)	242.39	204.61	229.47	232.78	227.31
Percent difference from Avg. Peak Force	6.63	-9.99	0.95	2.41	

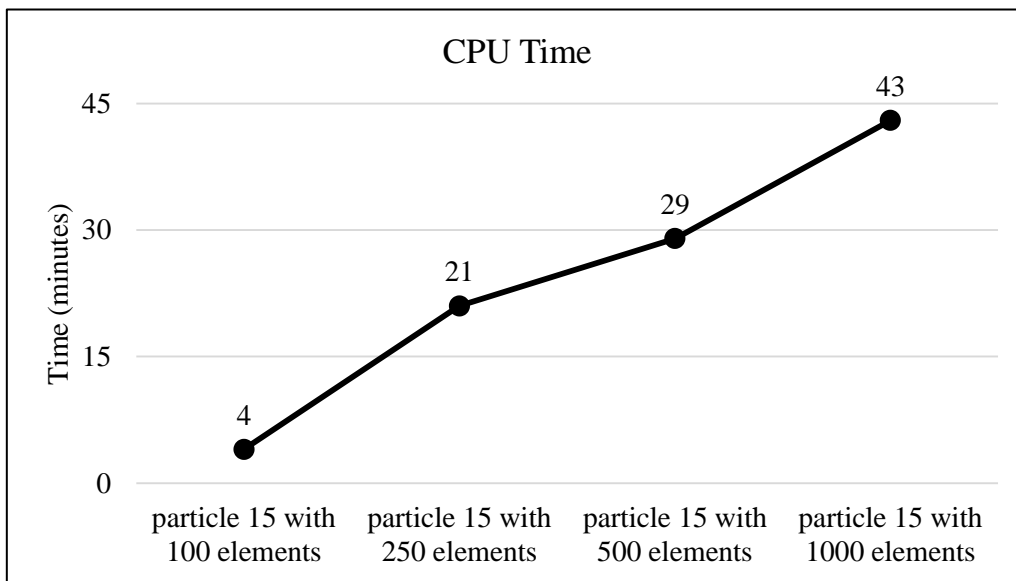
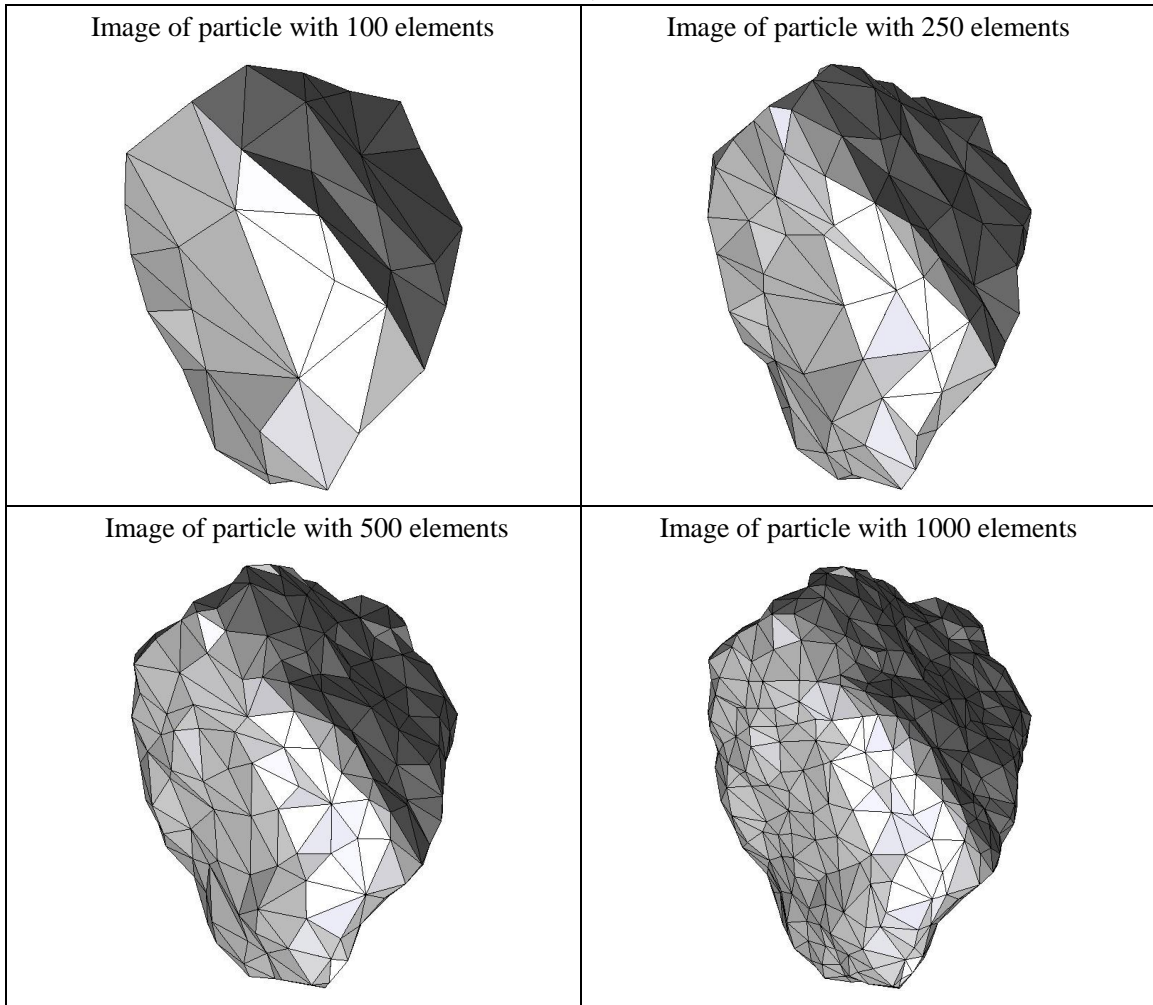


Figure 15.4 CPU computation time vs. model geometry resolution.

Appendix

Percent difference analysis compare to particle 15 with 100 elements for different group of data			
	particle 15 with 250 elements	particle 15 with 500 elements	particle 15 with 1000 elements
Impulse	-3.73	-0.12	0.26
Peak Force	-15.59	-5.33	-3.96
Start Time	10.00	0.00	10.00
CPU Time	425.00	625.00	975.00
Simulation Time	3.33	6.67	0.00

Summary of particle characteristics and collision simulation details for Particle 16 (of 50)



Particle statistics (part 1)								
Particle ID	# vertices	# elements	Mass (g)	Moments of Inertia			Volume (cm ³)	Sfc. Area (cm ²)
				I1	I2	I3		
				(gcm ²)	(gcm ²)	(gcm ²)		
16 (100 elements)	52	100	21.119	58609.31875	51294.99063	41848.05	7.41574	22.83439
16 (250 elements)	127	250	21.119	61083.025	53551.275	43457.00313	7.58115	22.88829
16 (500 elements)	252	500	21.119	61568.1875	54140.275	43853.70313	7.62501	22.89512
16 (1000 elements)	502	1000	21.119	61892.5	54416.4875	44034.36563	7.64173	22.87380

Appendix

Particle Statistics (part 2)							
Particle ID	α	R_g (cm)	ψ	R_v (cm)	L (cm)	I (cm)	S (cm)
16 (100 elements)	1.40382	1.86811	0.82024	1.20973	126.93529	107.88592	90.42115
16 (250 elements)	1.40757	1.87873	0.81828	1.21866	129.81326	109.87162	92.22491
16 (500 elements)	1.40450	1.83972	0.81538	1.22100	130.42958	110.18670	92.86516
16 (1000 elements)	1.40605	1.84522	0.80537	1.22190	130.81009	110.43219	93.03399

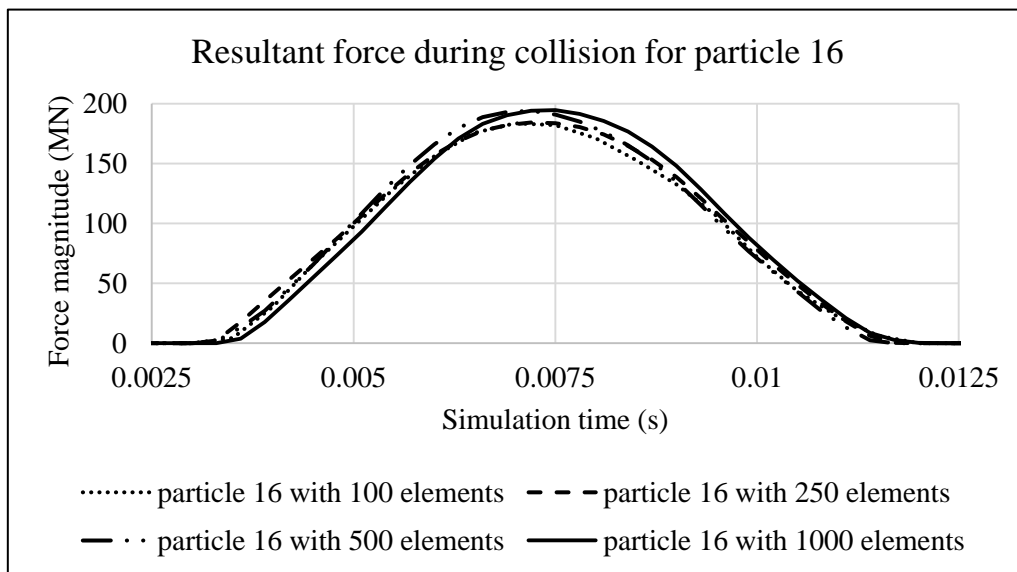


Figure A16.1 Plot of resultant forces during collision event for Particle 16.

Appendix

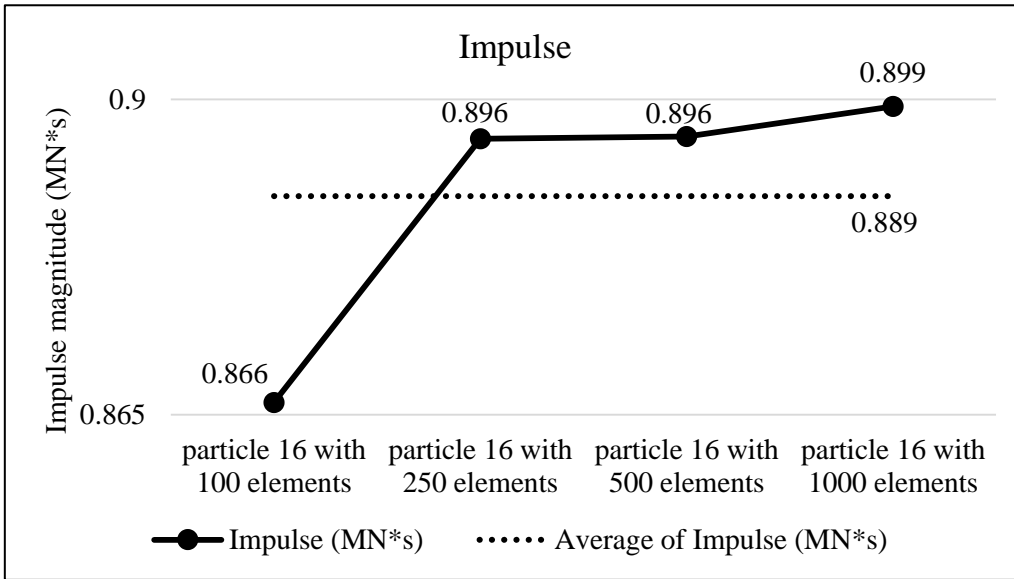


Figure A16.2 Plots of collision impulse for Particle 16.

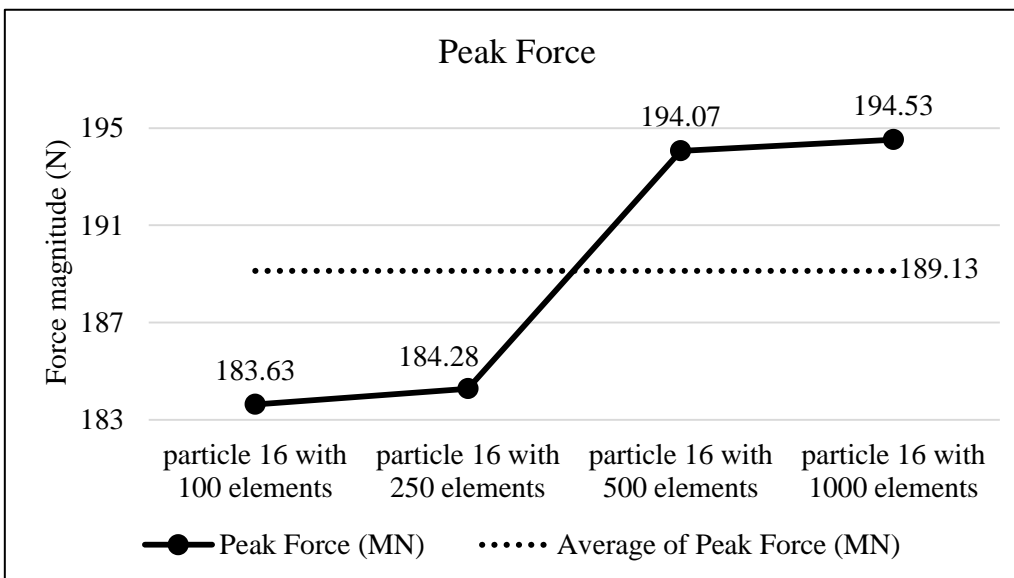


Figure A16.3 Peak collision for the four particle geometry resolutions for Particle 16.

Appendix

Collision results data analysis					
Model	particle 16 with 100 elements	particle 16 with 250 elements	particle 16 with 500 elements	particle 16 with 1000 elements	Average
Impulse (MN*s)	0.866	0.896	0.896	0.899	0.889
Percent difference from Avg. Impulse	-2.58	0.72	0.74	1.12	
Peak Force (MN)	183.63	184.28	194.07	194.53	189.13
Percent difference from Avg. Peak Force	-2.91	-2.56	2.61	2.86	

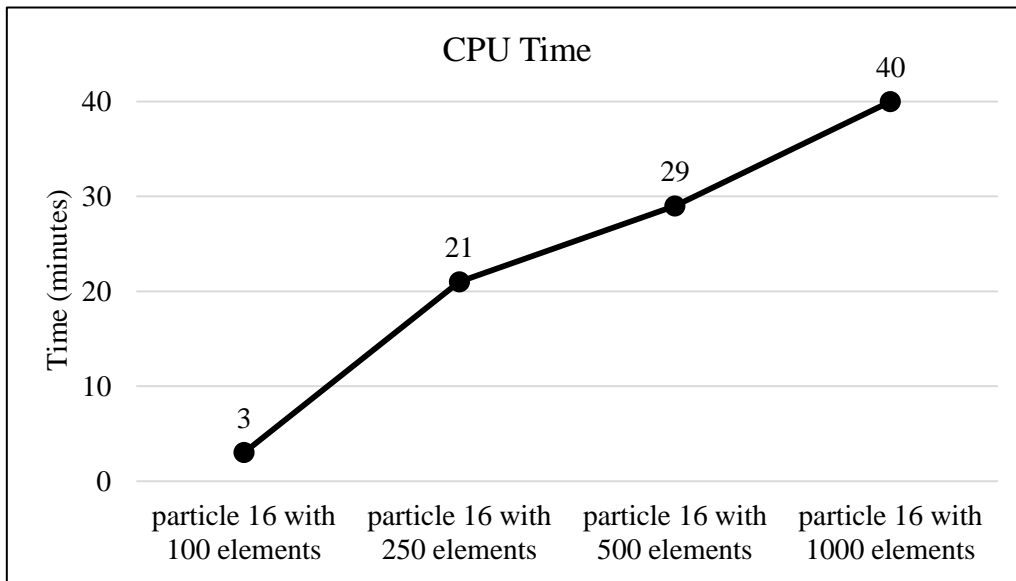
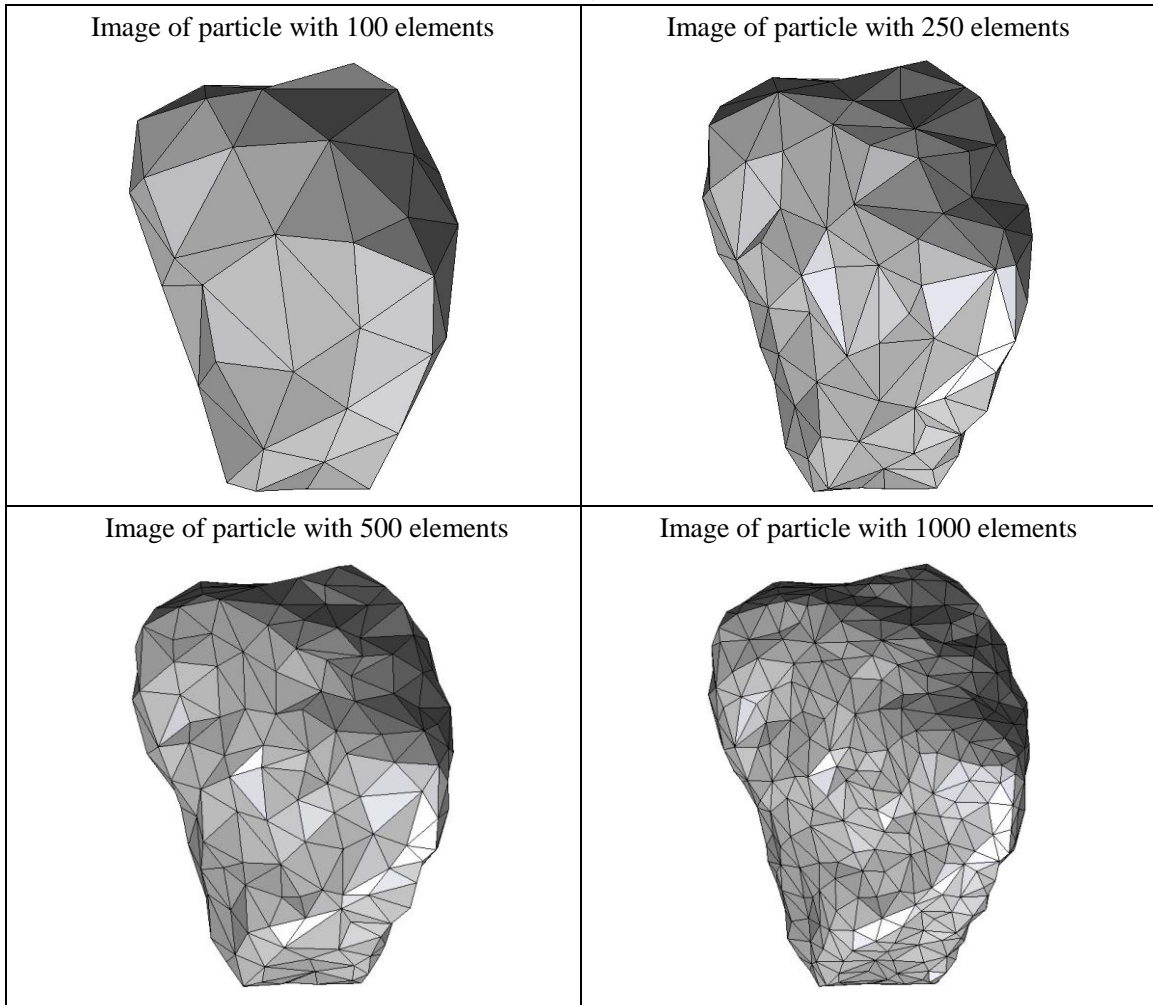


Figure A16.4 CPU computation time vs. model geometry resolution.

Appendix

Percent difference analysis compare to particle 16 with 100 elements for different group of data			
	particle 16 with 250 elements	particle 16 with 500 elements	particle 16 with 1000 elements
Impulse	3.38	3.41	3.79
Peak Force	0.35	5.68	5.93
Start Time	-5.71	-5.71	-5.71
CPU Time	600.00	866.67	1233.33
Simulation Time	-1.18	-4.71	2.35

Summary of particle characteristics and collision simulation details for Particle 17 (of 50)



Particle statistics (part 1)								
Particle ID	# vertices	# elements	Mass (g)	Moments of Inertia			Volume (cm ³)	Sfc. Area (cm ²)
				I1	I2	I3		
				(gcm ²)	(gcm ²)	(gcm ²)		
17 (100 elements)	52	100	37.343	193189.9375	160617.6125	91723.1	13.14927	33.75661
17 (250 elements)	127	250	37.343	198361.025	165913.75	94653.1	13.39009	33.89470
17 (500 elements)	252	500	37.343	200411.125	167664.75	95733.275	13.47670	33.92991
17 (1000 elements)	502	1000	37.343	201359.3	168515.7875	96188.99375	13.50899	33.99911

Appendix

Particle Statistics (part 2)							
Particle ID	α	R_g (cm)	ψ	R_v (cm)	L (cm)	I (cm)	S (cm)
17 (100 elements)	2.10494	2.29350	0.79810	1.46421	187.32728	129.00542	88.99398
17 (250 elements)	2.08191	2.34870	0.80453	1.47310	190.00184	130.45292	91.26325
17 (500 elements)	2.07937	2.33507	0.80716	1.47627	190.95815	131.15884	91.83443
17 (1000 elements)	2.07859	2.3325	0.80680	1.47745	191.42857	131.44073	92.09546

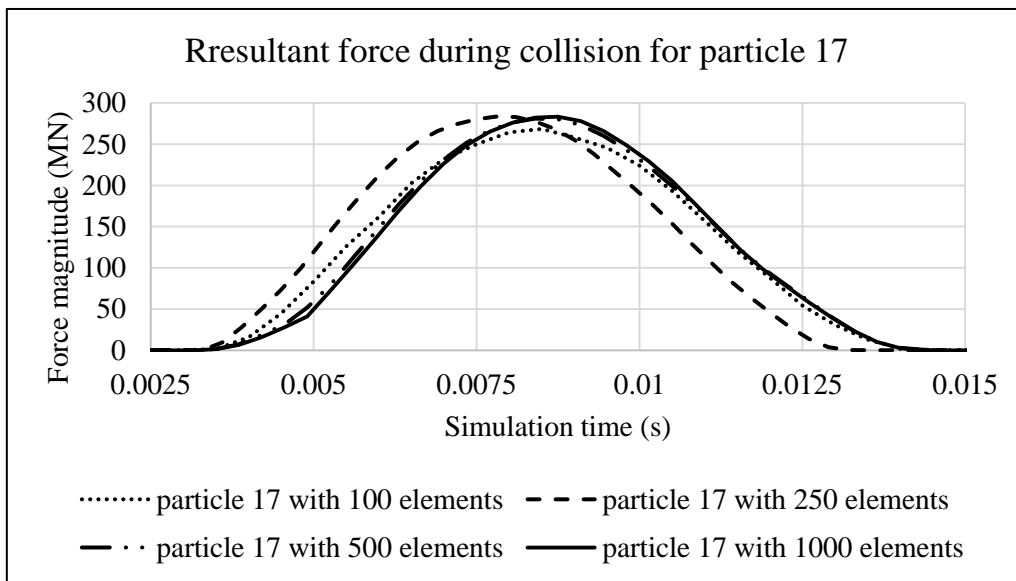


Figure A17.1 Plot of resultant forces during collision event for Particle 17.

Appendix

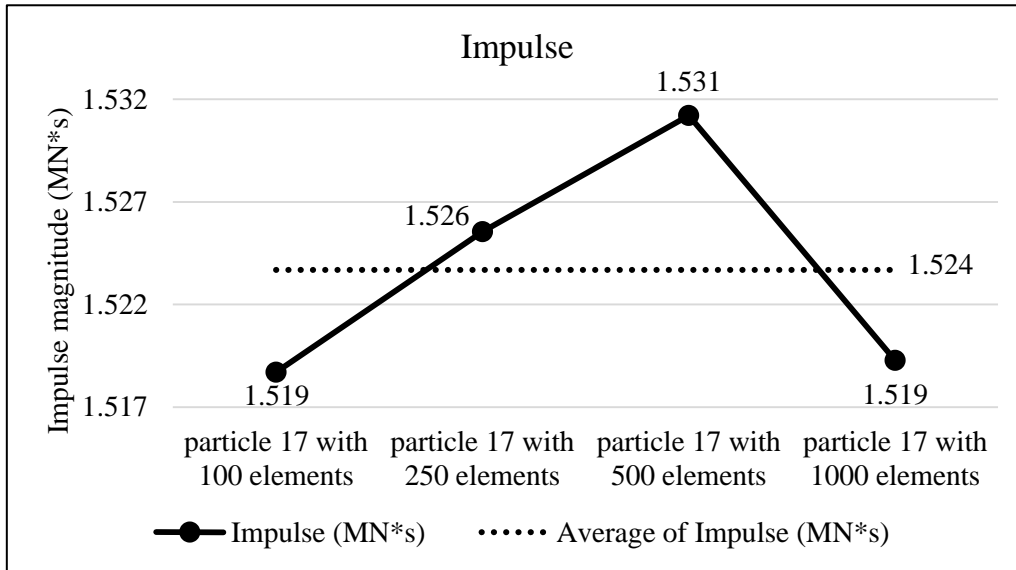


Figure A17.2 Plots of collision impulse for Particle 17.

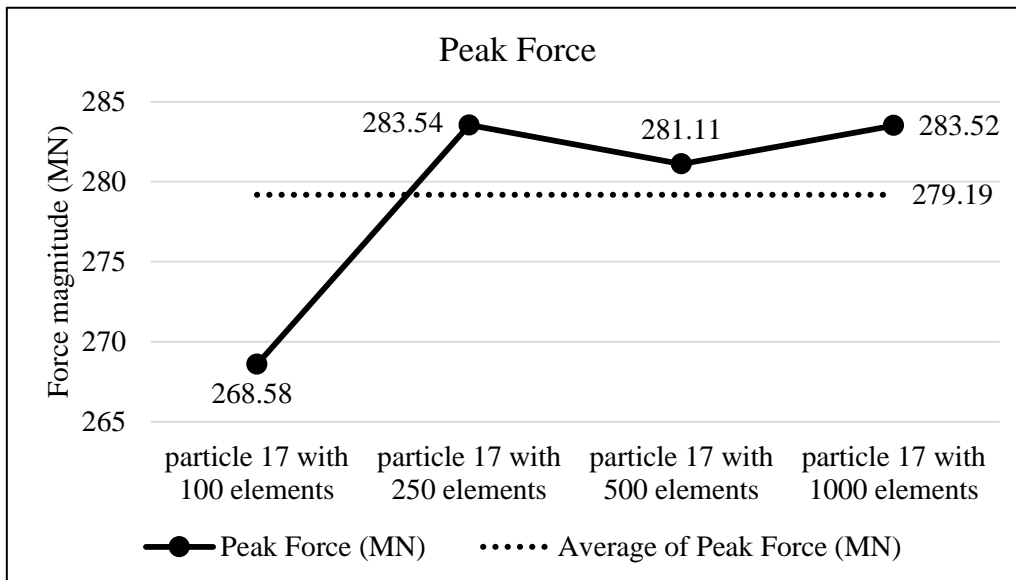


Figure A17.3 Peak collision for the four particle geometry resolutions for Particle 17.

Appendix

Collision results data analysis					
Model	particle 17 with 100 elements	particle 17 with 250 elements	particle 17 with 500 elements	particle 17 with 1000 elements	Average
Impulse (MN*s)	1.519	1.526	1.531	1.519	1.524
Percent difference from Avg. Impulse	-0.33	0.12	0.49	-0.29	
Peak Force (MN)	268.58	283.54	281.11	283.52	279.19
Percent difference from Avg. Peak Force	-3.80	1.56	0.69	1.55	

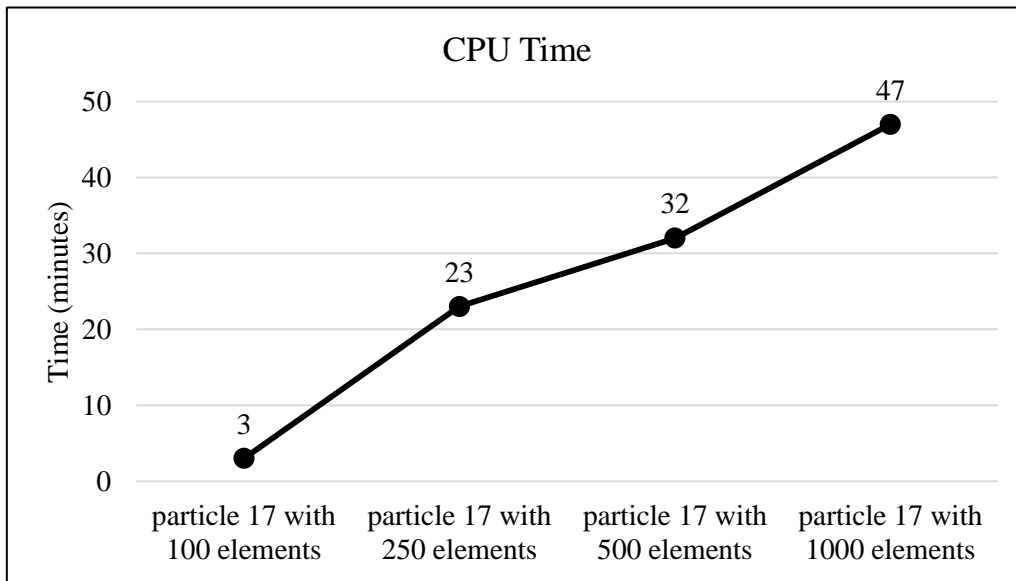


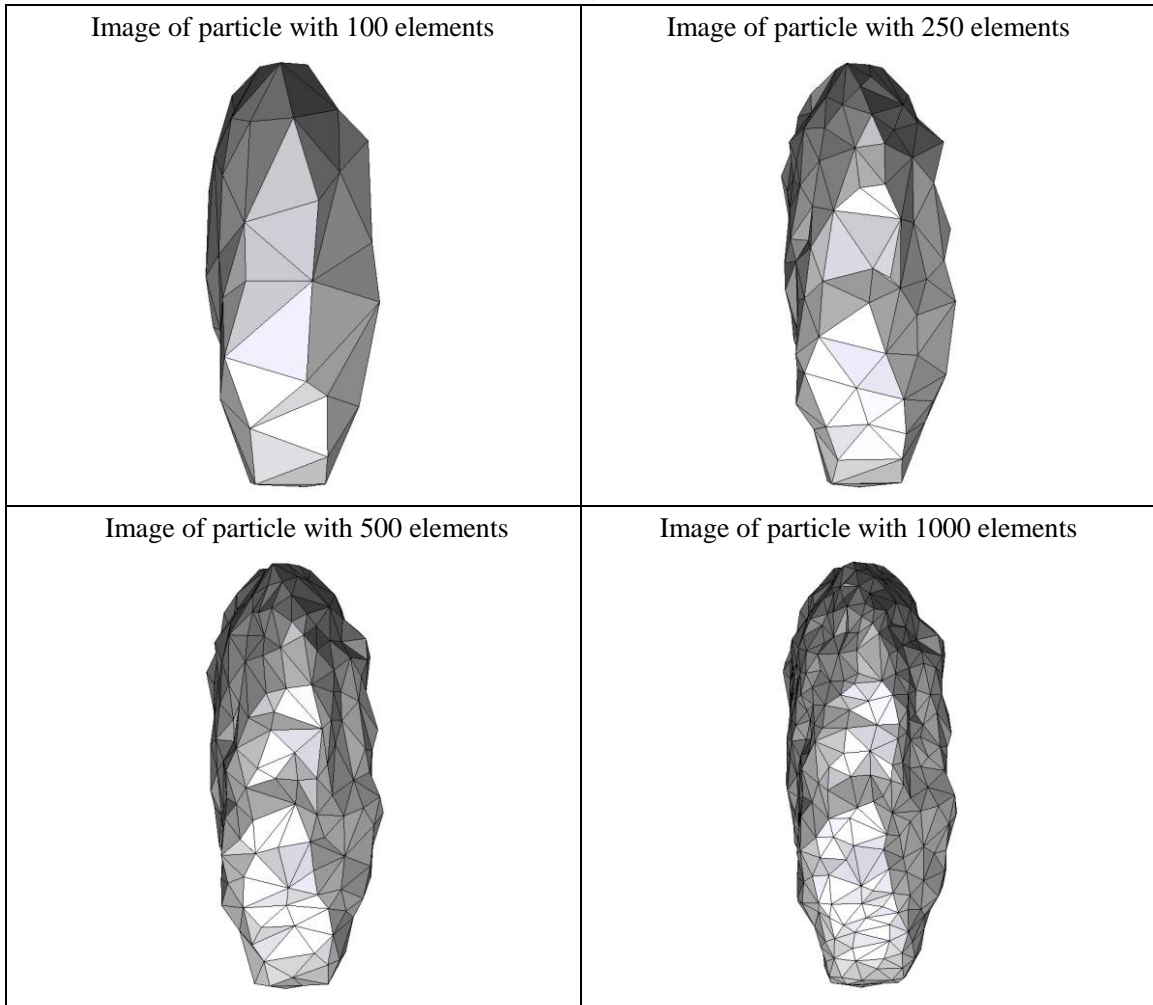
Figure A17.4 CPU computation time vs. model geometry resolution.

Appendix

Percent difference analysis compare to particle 17 with 100 elements for different group of data			
	particle 17 with 250 elements	particle 17 with 500 elements	particle 17 with 1000 elements
Impulse	0.45	0.82	0.04
Peak Force	5.57	4.66	5.56
Start Time	-5.71	0.00	0.00
CPU Time	666.67	966.67	1466.67
Simulation Time	-5.71	3.33	3.33

Appendix

Summary of particle characteristics and collision simulation details for Particle 18 (of 50)



Particle statistics (part 1)								
Particle ID	# vertices	# elements	Mass (g)	Moments of Inertia			Volume (cm ³)	Sfc. Area (cm ²)
				I1	I2	I3		
				(gcm ²)	(gcm ²)	(gcm ²)		
18 (100 elements)	52	100	17.938	76438.3625	71678.69375	18542.85625	6.31897	21.05293
18 (250 elements)	127	250	17.938	78690.0625	73716.75	19150.56875	6.42732	21.37752
18 (500 elements)	252	500	17.938	79291.03125	74229.74375	19381.10469	6.46250	21.41455
18 (1000 elements)	502	1000	17.938	79853.5	74755.425	19491.47188	6.48498	21.42781

Particle Statistics (part 2)							
Particle ID	α	R_g (cm)	ψ	R_v (cm)	L (cm)	I (cm)	S (cm)
18 (100 elements)	3.06609	2.19813	0.78512	1.14688	190.04536	80.59340	61.98303
18 (250 elements)	3.06583	2.21936	0.78201	1.15340	192.72665	82.00146	62.86285
18 (500 elements)	3.06062	2.22096	0.78351	1.15550	193.36444	82.54102	63.17812
18 (1000 elements)	3.06390	2.21116	0.78484	1.15684	194.06790	82.78912	63.34023

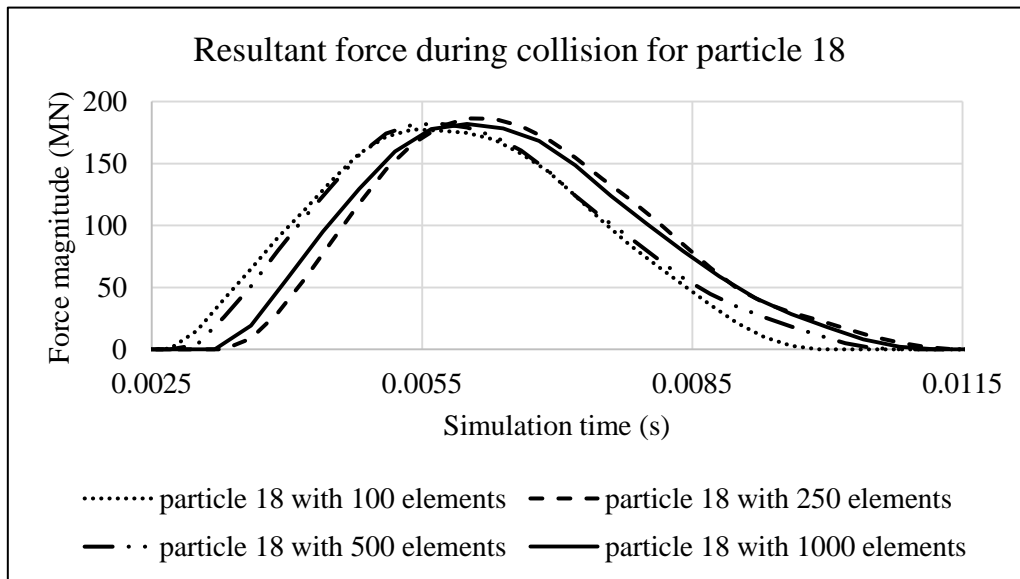


Figure A18.1 Plot of resultant forces during collision event for Particle 18.

Appendix

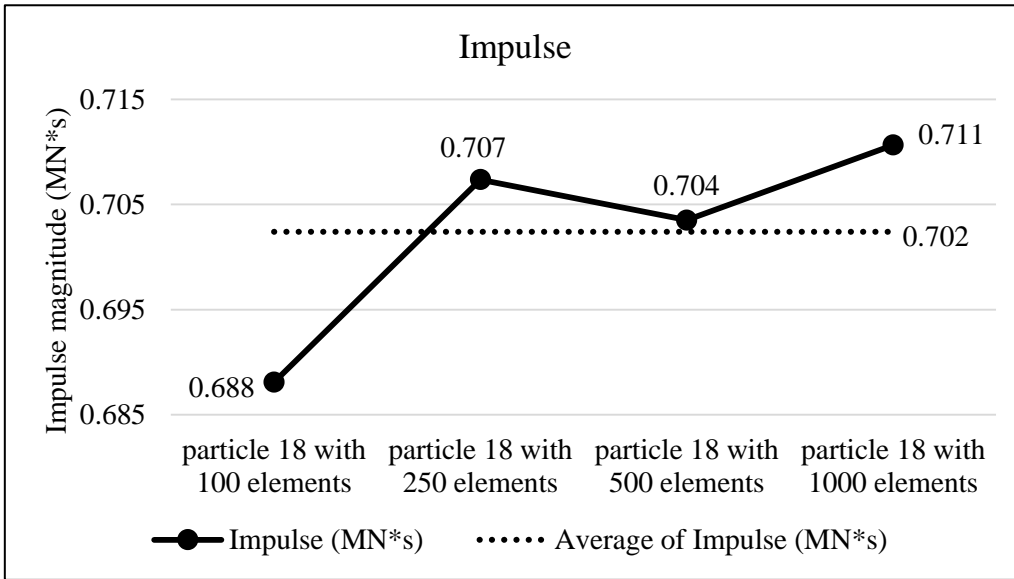


Figure A18.2 Plots of collision impulse for Particle 18.

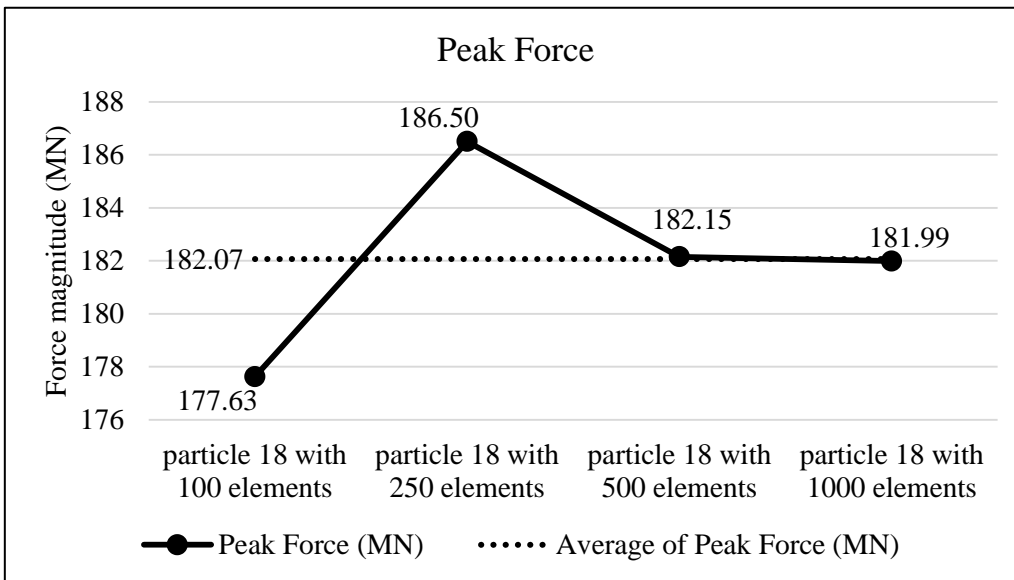


Figure A18.3 Peak collision for the four particle geometry resolutions for Particle 18.

Appendix

Collision results data analysis					
Model	particle 18 with 100 elements	particle 18 with 250 elements	particle 18 with 500 elements	particle 18 with 1000 elements	Average
Impulse (MN*s)	0.688	0.707	0.704	0.711	0.702
Percent difference from Avg. Impulse	-2.04	0.71	0.16	1.17	
Peak Force (MN)	177.63	186.50	182.15	181.99	182.07
Percent difference from Avg. Peak Force	-2.44	2.43	0.05	-0.04	

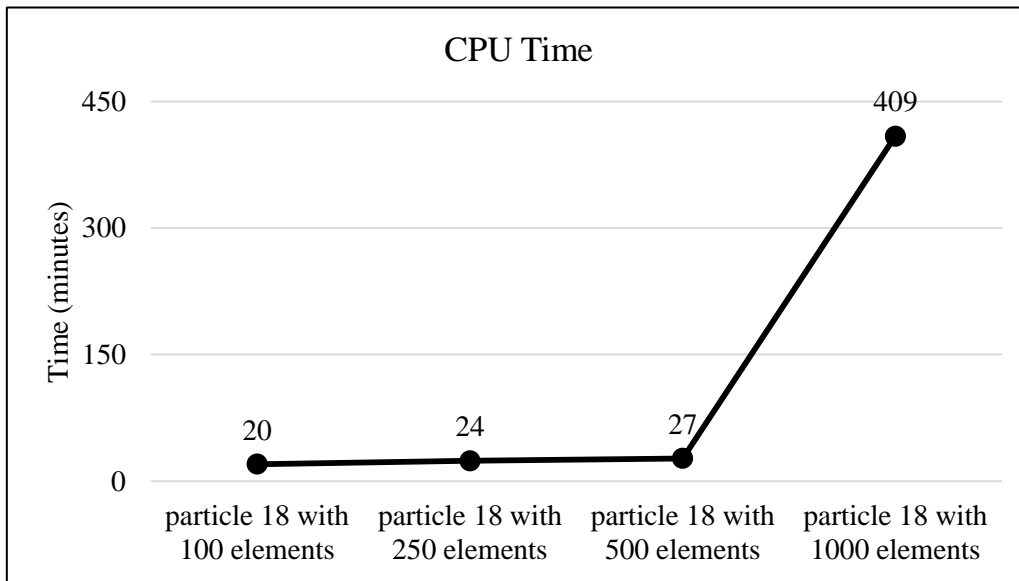
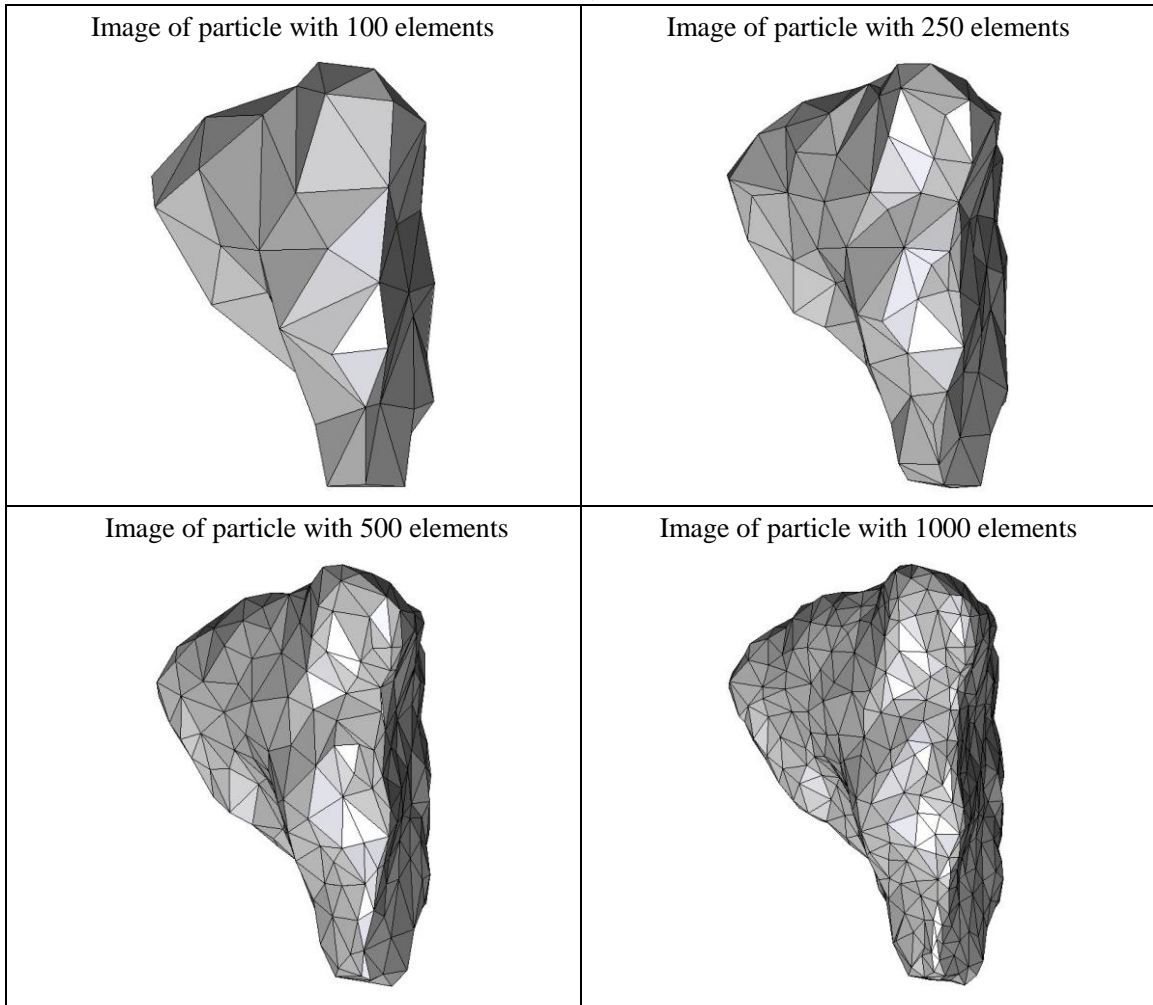


Figure A18.4 CPU computation time vs. model geometry resolution.

Appendix

Percent difference analysis compare to particle 18 with 100 elements for different group of data			
	particle 18 with 250 elements	particle 18 with 500 elements	particle 18 with 1000 elements
Impulse	2.80	2.24	3.28
Peak Force	4.99	2.55	2.46
Start Time	22.22	11.11	33.33
CPU Time	20.00	35.00	1945.00
Simulation Time	12.50	8.33	5.56

Summary of particle characteristics and collision simulation details for Particle 19 (of 50)



Particle statistics (part 1)								
Particle ID	# vertices	# elements	Mass (g)	Moments of Inertia			Volume (cm ³)	Sfc. Area (cm ²)
				I1	I2	I3		
				(gcm ²)	(gcm ²)	(gcm ²)		
19 (100 elements)	52	100	7.622	15511.94844	12196.83047	7845.27188	2.78082	12.82016
19 (250 elements)	127	250	7.622	16076.9375	12629.11094	8138.37734	2.83440	12.89259
19 (500 elements)	252	500	7.622	16241.41094	12716.75156	8251.92266	2.84888	12.85467
19 (1000 elements)	502	1000	7.622	16312.34531	12771.81016	8297.54375	2.85620	12.85457

Appendix

Particle Statistics (part 2)							
Particle ID	α	R_g (cm)	ψ	R_v (cm)	L (cm)	I (cm)	S (cm)
19 (100 elements)	2.09397	1.68914	0.74594	0.87236	114.15068	85.56383	54.51387
19 (250 elements)	2.09402	1.69144	0.75125	0.87793	116.15639	87.18085	55.47055
19 (500 elements)	2.09289	1.70917	0.75603	0.87942	116.54701	87.89419	55.68721
19 (1000 elements)	2.09038	1.70903	0.75733	0.88017	116.77298	88.12338	55.86213

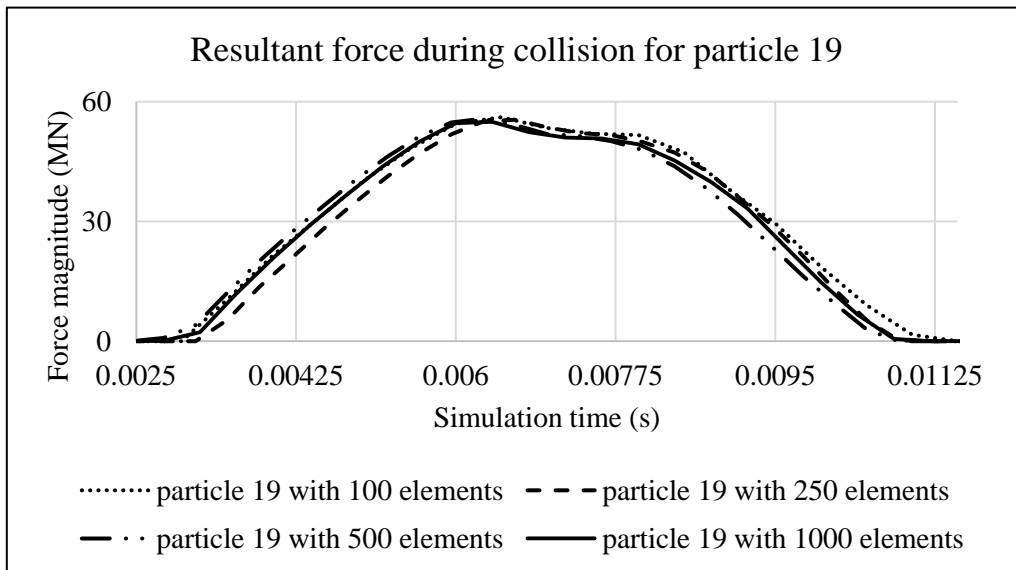


Figure A19.1 Plot of resultant forces during collision event for Particle 19.

Appendix

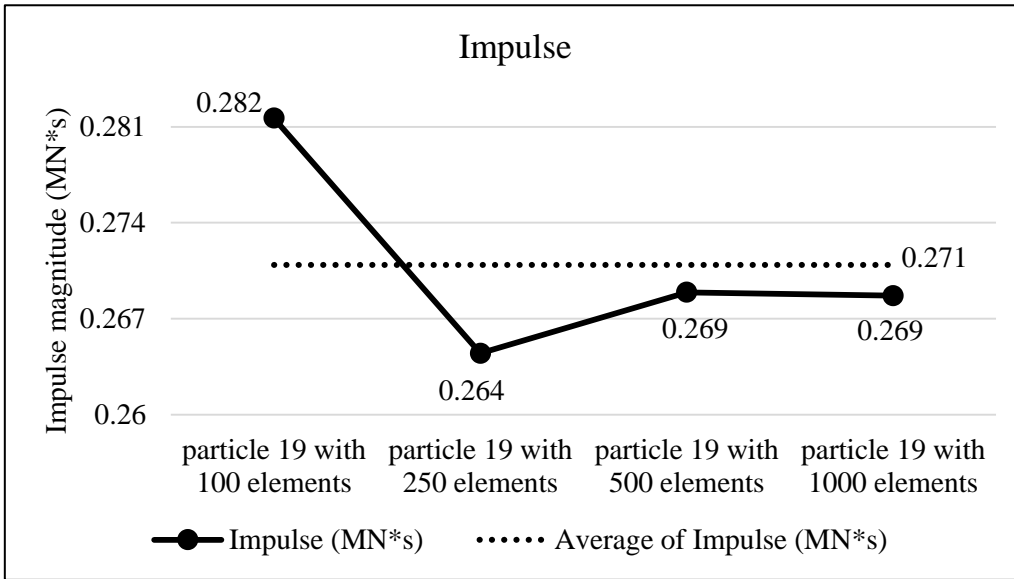


Figure A19.2 Plots of collision impulse for Particle 19.

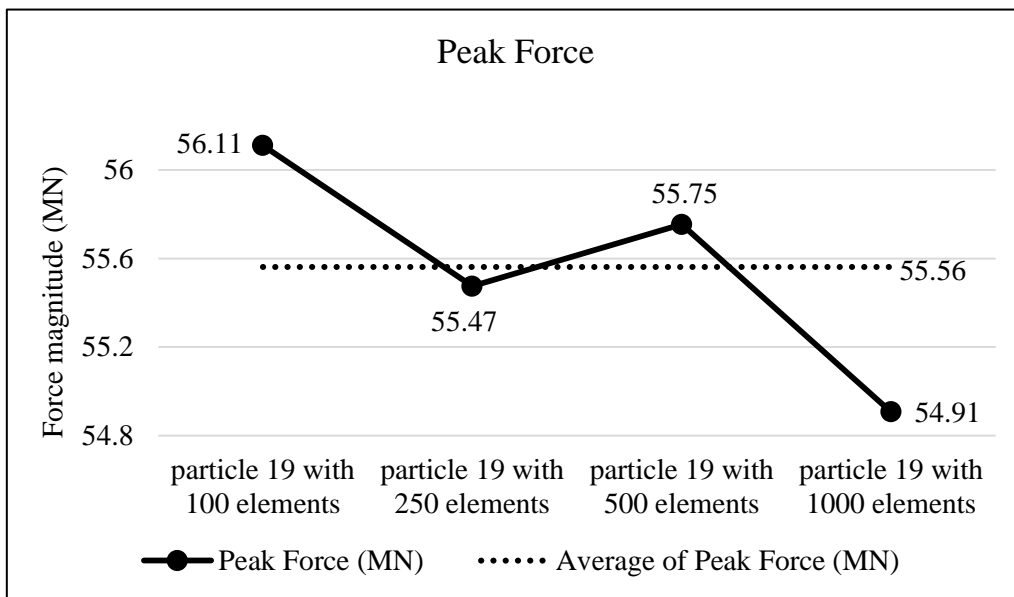


Figure A19.3 Peak collision for the four particle geometry resolutions for Particle 19.

Appendix

Collision results data analysis					
Model	particle 19 with 100 elements	particle 19 with 250 elements	particle 19 with 500 elements	particle 19 with 1000 elements	Average
Impulse (MN*s)	0.282	0.264	0.269	0.269	0.271
Percent difference from Avg. Impulse	3.95	-2.38	-0.74	-0.83	
Peak Force (MN)	56.11	55.47	55.75	54.91	55.56
Percent difference from Avg. Peak Force	0.99	-0.16	0.35	-1.18	

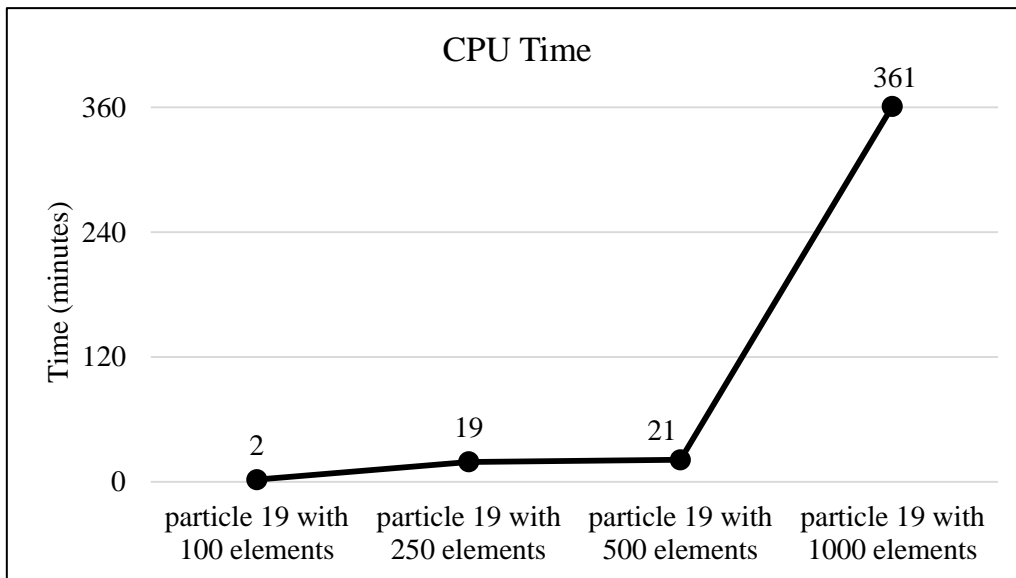
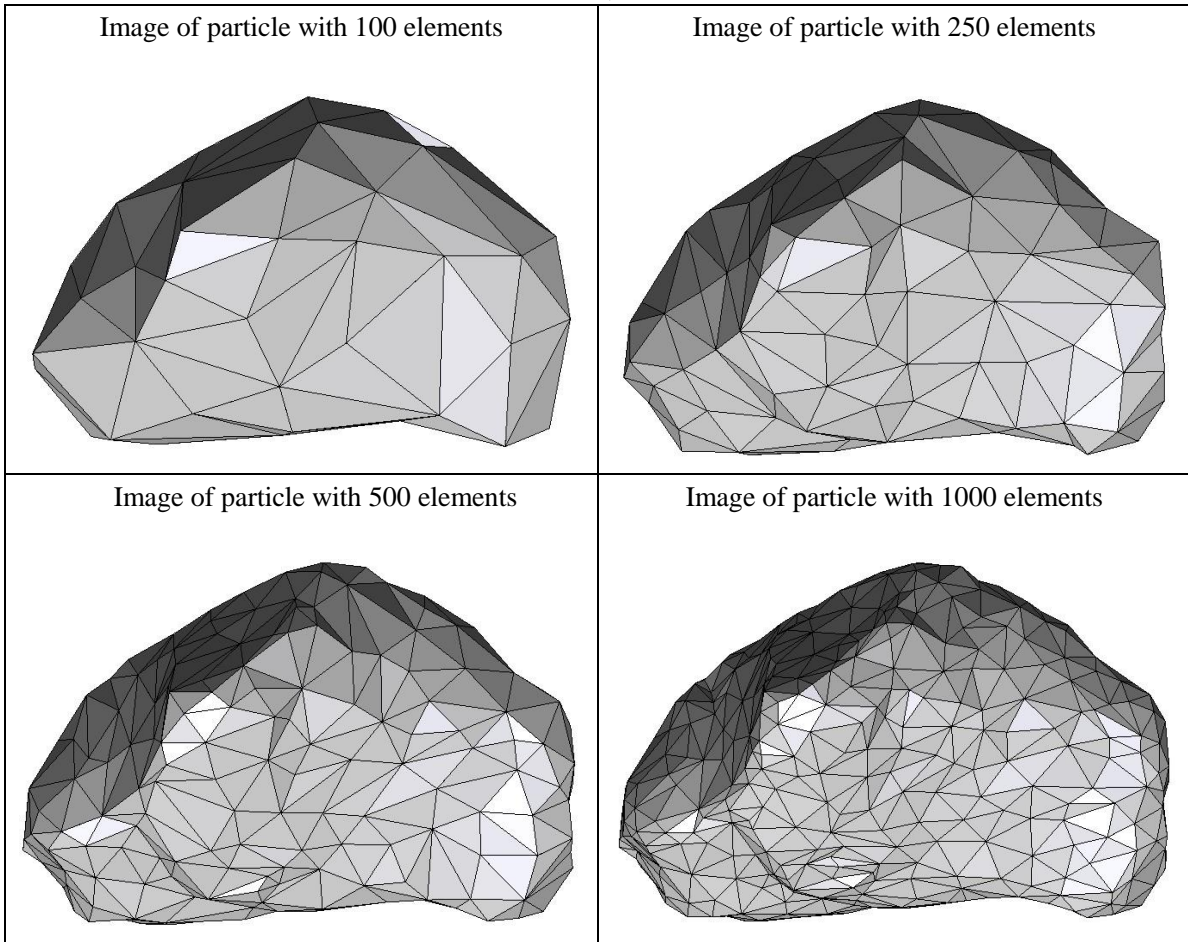


Figure A19.4 CPU computation time vs. model geometry resolution.

Appendix

Percent difference analysis compare to particle 19 with 100 elements for different group of data			
	particle 19 with 250 elements	particle 19 with 500 elements	particle 19 with 1000 elements
Impulse	-6.09	-4.51	-4.60
Peak Force	-1.13	-0.64	-2.15
Start Time	0.00	-20.00	-20.00
CPU Time	850.00	950.00	17950.00
Simulation Time	-2.00	7.33	6.67

Summary of particle characteristics and collision simulation details for Particle 20 (of 50)



Particle statistics (part 1)								
Particle ID	# vertices	# elements	Mass (g)	Moments of Inertia			Volume (cm ³)	Sfc. Area (cm ²)
				I1	I2	I3		
				(gcm ²)	(gcm ²)	(gcm ²)		
20 (100 elements)	52	100	19.278	82130.33125	59097.43125	38445.575	7.32677	23.74987
20 (250 elements)	127	250	19.278	84343.84375	61012.31875	39290.63125	7.43014	24.04223
20 (500 elements)	252	500	19.278	85015.41875	61606.2625	39496.58125	7.46292	24.04582
20 (1000 elements)	502	1000	19.278	85490.55	61969.46875	39709.2375	7.48616	24.02922

Appendix

Particle Statistics (part 2)							
Particle ID	α	R_g (cm)	ψ	R_v (cm)	L (cm)	I (cm)	S (cm)
20 (100 elements)	2.58238	2.23103	0.76812	1.20487	163.27246	126.27447	63.22561
20 (250 elements)	2.57800	2.17941	0.76590	1.21051	165.85980	127.44360	64.33663
20 (500 elements)	2.58049	2.17042	0.76804	1.21229	166.68620	127.73183	64.59476
20 (1000 elements)	2.57995	2.17997	0.77016	1.21355	167.17227	128.06094	64.79667

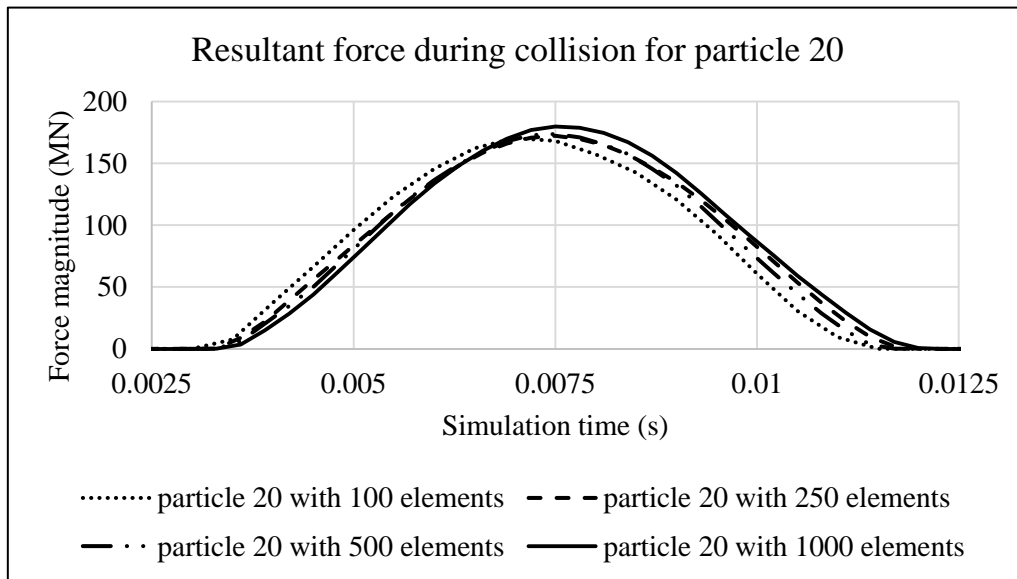


Figure A20.1 Plot of resultant forces during collision event for Particle 20.

Appendix

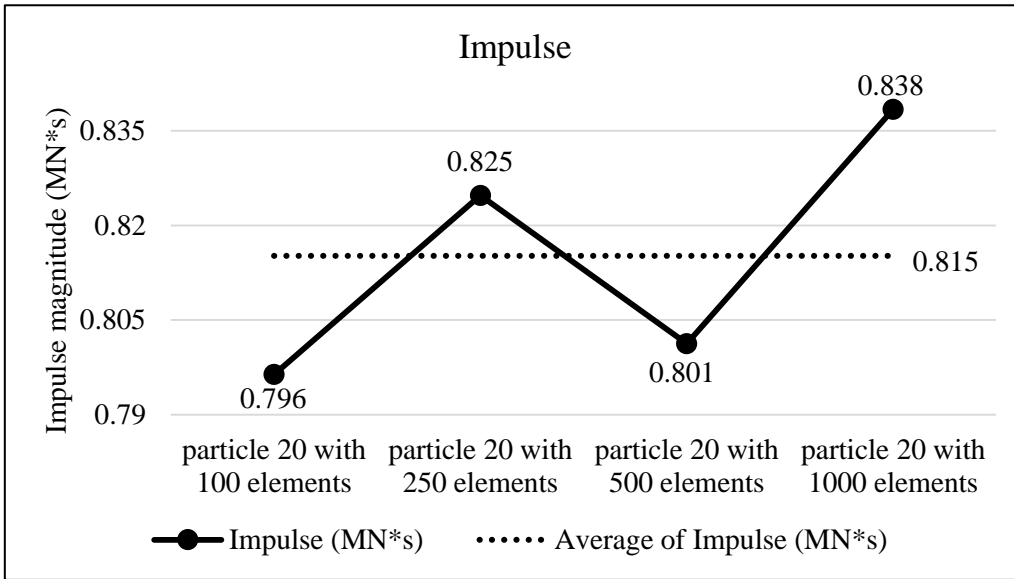


Figure A20.2 Plots of collision impulse for Particle 20.

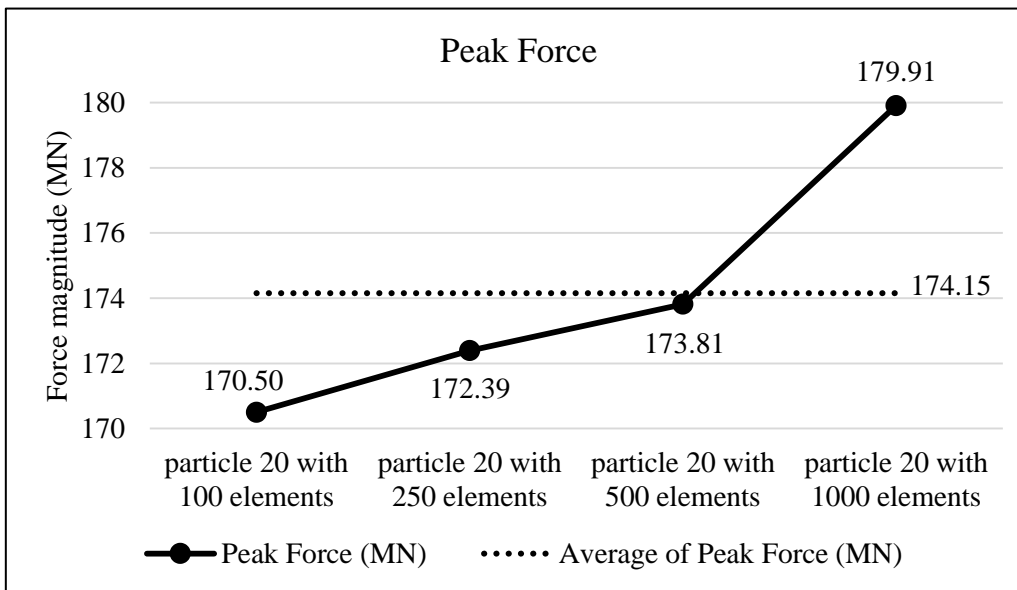


Figure A20.3 Peak collision for the four particle geometry resolutions for Particle 20.

Appendix

Collision results data analysis					
Model	particle 20 with 100 elements	particle 20 with 250 elements	particle 20 with 500 elements	particle 20 with 1000 elements	Average
Impulse (MN*s)	0.796	0.825	0.801	0.838	0.815
Percent difference from Avg. Impulse	-2.31	1.17	-1.71	2.85	
Peak Force (MN)	170.50	172.39	173.81	179.91	174.15
Percent difference from Avg. Peak Force	-2.10	-1.01	-0.19	3.31	

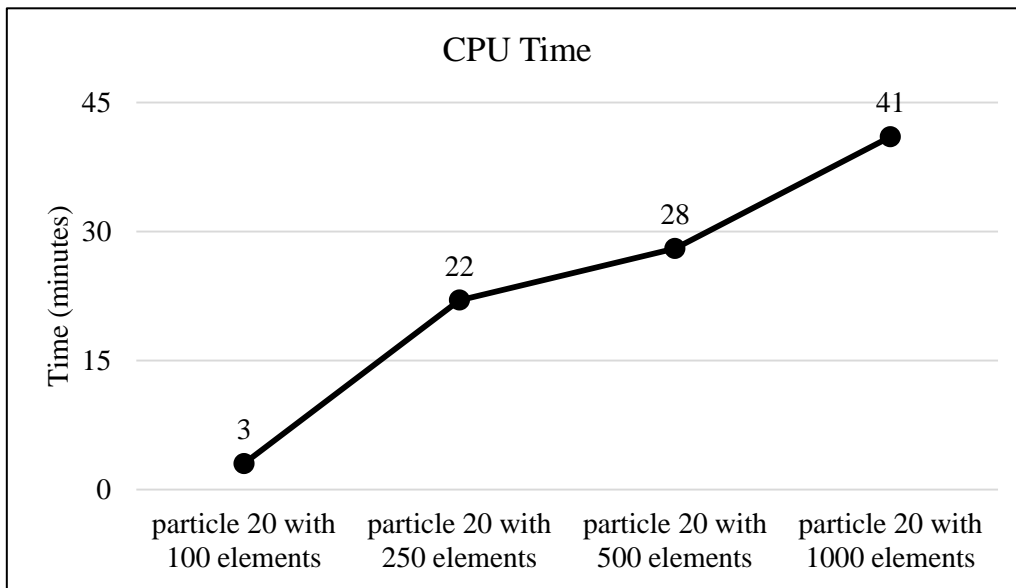


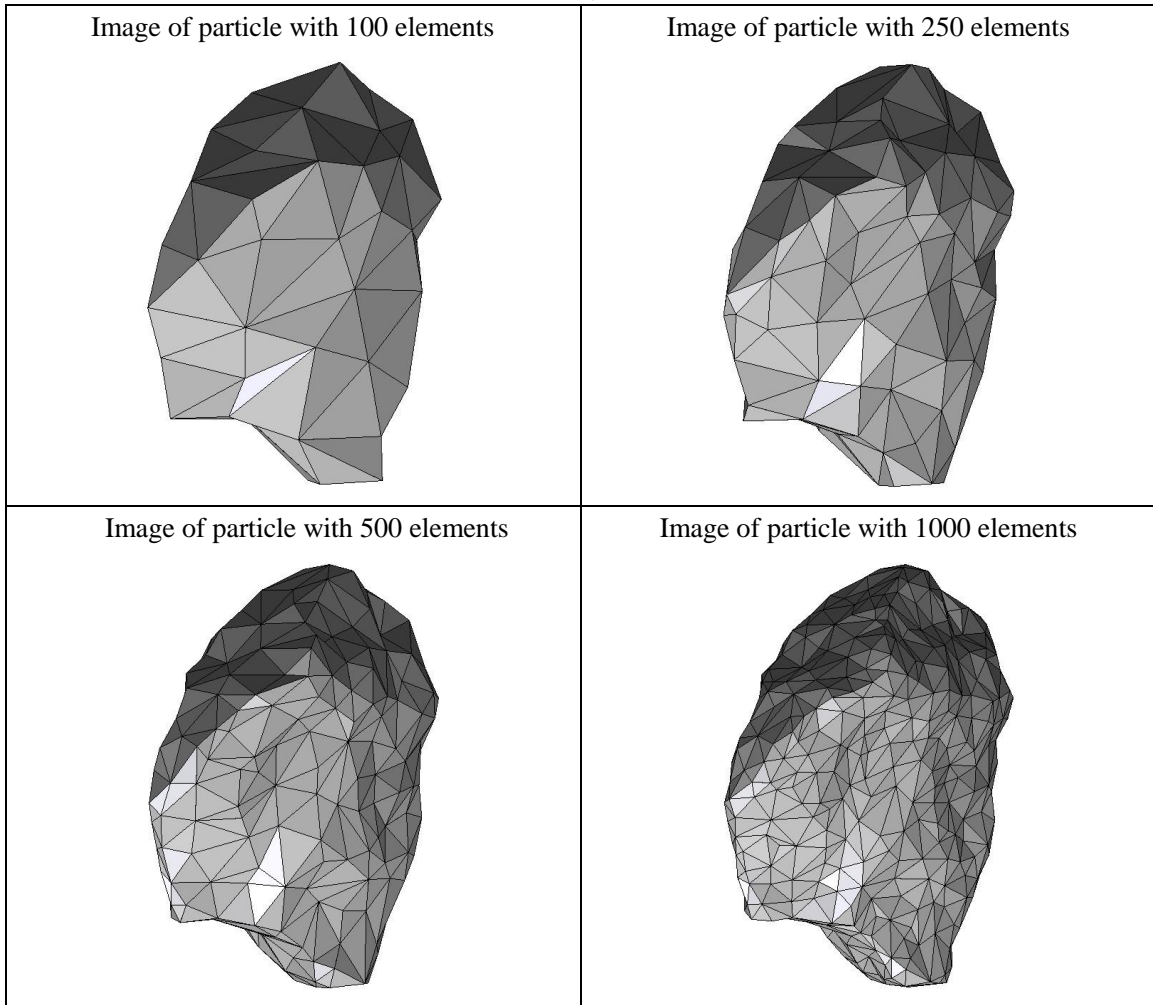
Figure A20.4 CPU computation time vs. model geometry resolution.

Appendix

Percent difference analysis compare to particle 20 with 100 elements for different group of data			
	particle 20 with 250 elements	particle 20 with 500 elements	particle 20 with 1000 elements
Impulse	3.57	0.62	5.28
Peak Force	1.11	1.94	5.52
Start Time	-5.71	-5.71	-5.71
CPU Time	633.33	833.33	1266.67
Simulation Time	12.00	12.00	16.00

Appendix

Summary of particle characteristics and collision simulation details for Particle 21 (of 50)



Particle statistics (part 1)								
Particle ID	# vertices	# elements	Mass (g)	Moments of Inertia			Volume (cm ³)	Sfc. Area (cm ²)
				I1	I2	I3		
				(gcm ²)	(gcm ²)	(gcm ²)		
21 (100 elements)	52	100	22.354	108035.7625	68463.24375	58654.5	8.70083	26.68504
21 (250 elements)	127	250	22.354	109533.575	69333.15	59188.76875	8.72861	26.79313
21 (500 elements)	252	500	22.354	110918.9875	70156.4875	59986.4375	8.78849	26.79078
21 (1000 elements)	502	1000	22.354	111475.2875	70541.975	60234.5625	8.81151	26.76800

Appendix

Particle Statistics (part 2)							
Particle ID	α	R_g (cm)	ψ	R_v (cm)	L (cm)	I (cm)	S (cm)
21 (100 elements)	2.48509	2.18647	0.76664	1.27592	162.35365	148.22548	65.33097
21 (250 elements)	2.51052	2.16952	0.76517	1.27728	163.61174	149.09977	65.17048
21 (500 elements)	2.50975	2.16832	0.76873	1.28019	164.57346	150.11622	65.57353
21 (1000 elements)	2.51189	2.16597	0.77073	1.28131	165.04417	150.42800	65.70525

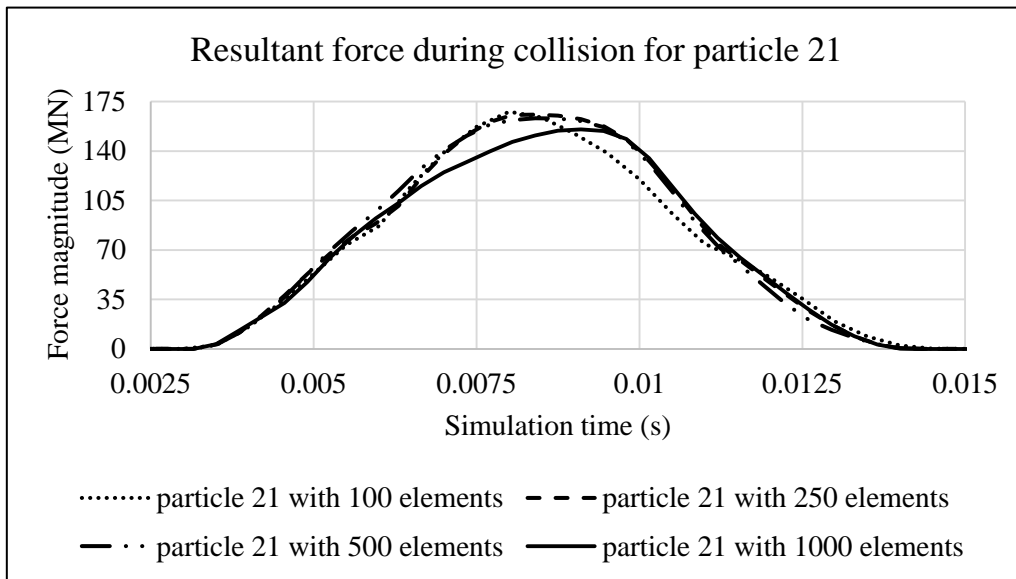


Figure A21.1 Plot of resultant forces during collision event for Particle 21.

Appendix

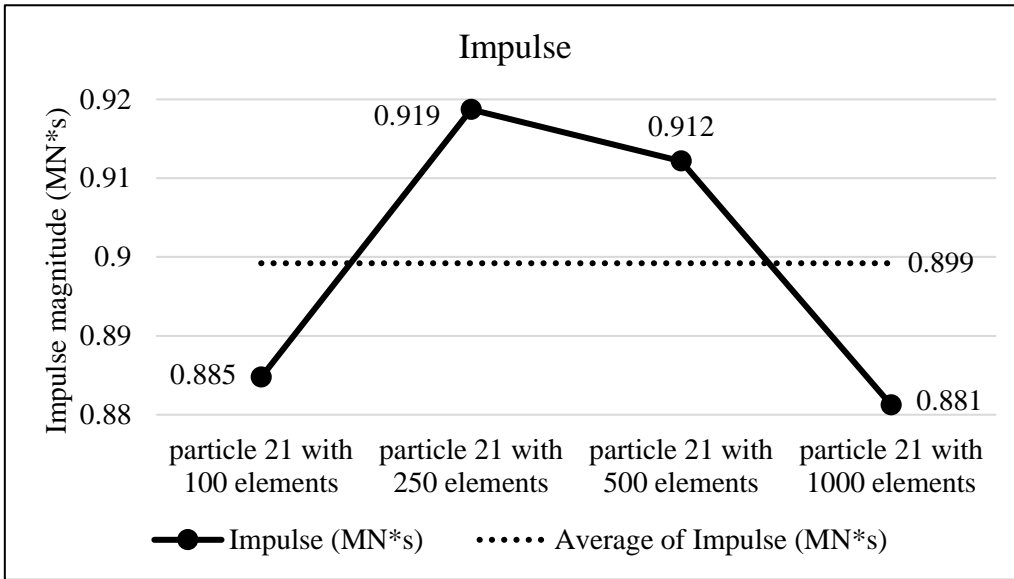


Figure A21.2 Plots of collision impulse for Particle 21.

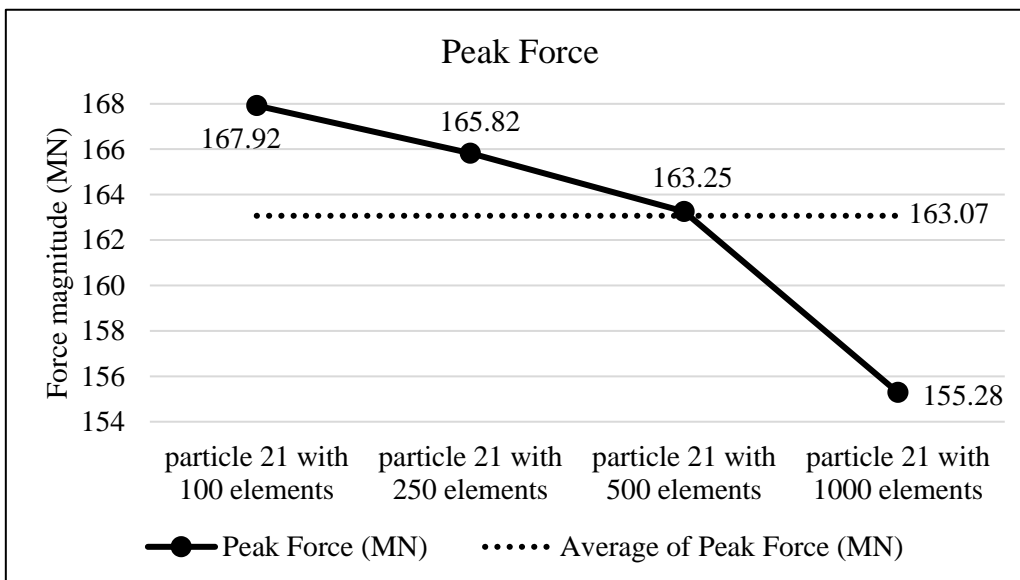


Figure A21.3 Peak collision for the four particle geometry resolutions for Particle 21.

Appendix

Collision results data analysis					
Model	particle 21 with 100 elements	particle 21 with 250 elements	particle 21 with 500 elements	particle 21 with 1000 elements	Average
Impulse (MN*s)	0.885	0.919	0.912	0.881	0.899
Percent difference from Avg. Impulse	-1.61	2.17	1.44	-2.00	
Peak Force (MN)	167.92	165.82	163.25	155.28	163.07
Percent difference from Avg. Peak Force	2.98	1.69	0.11	-4.77	

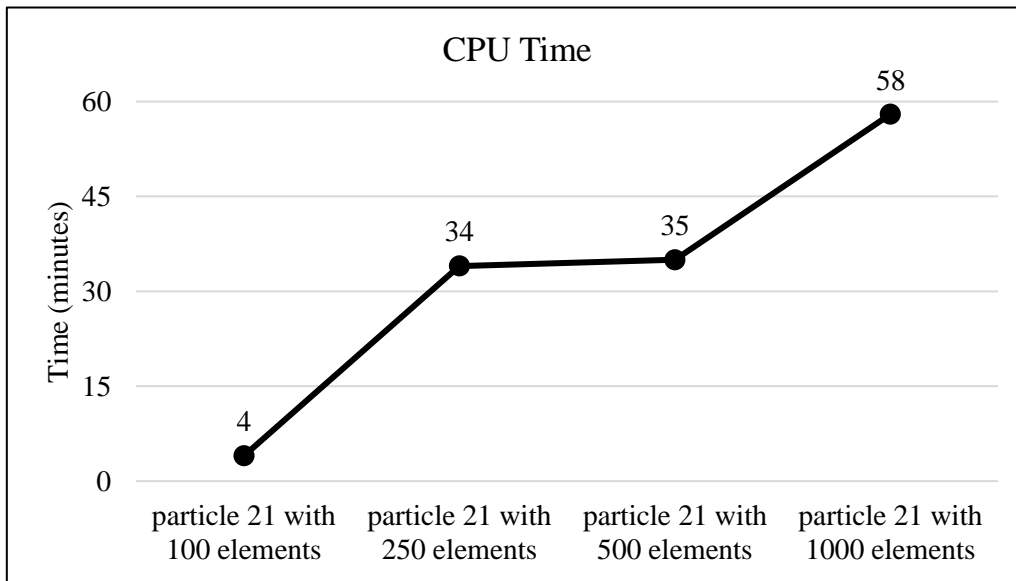


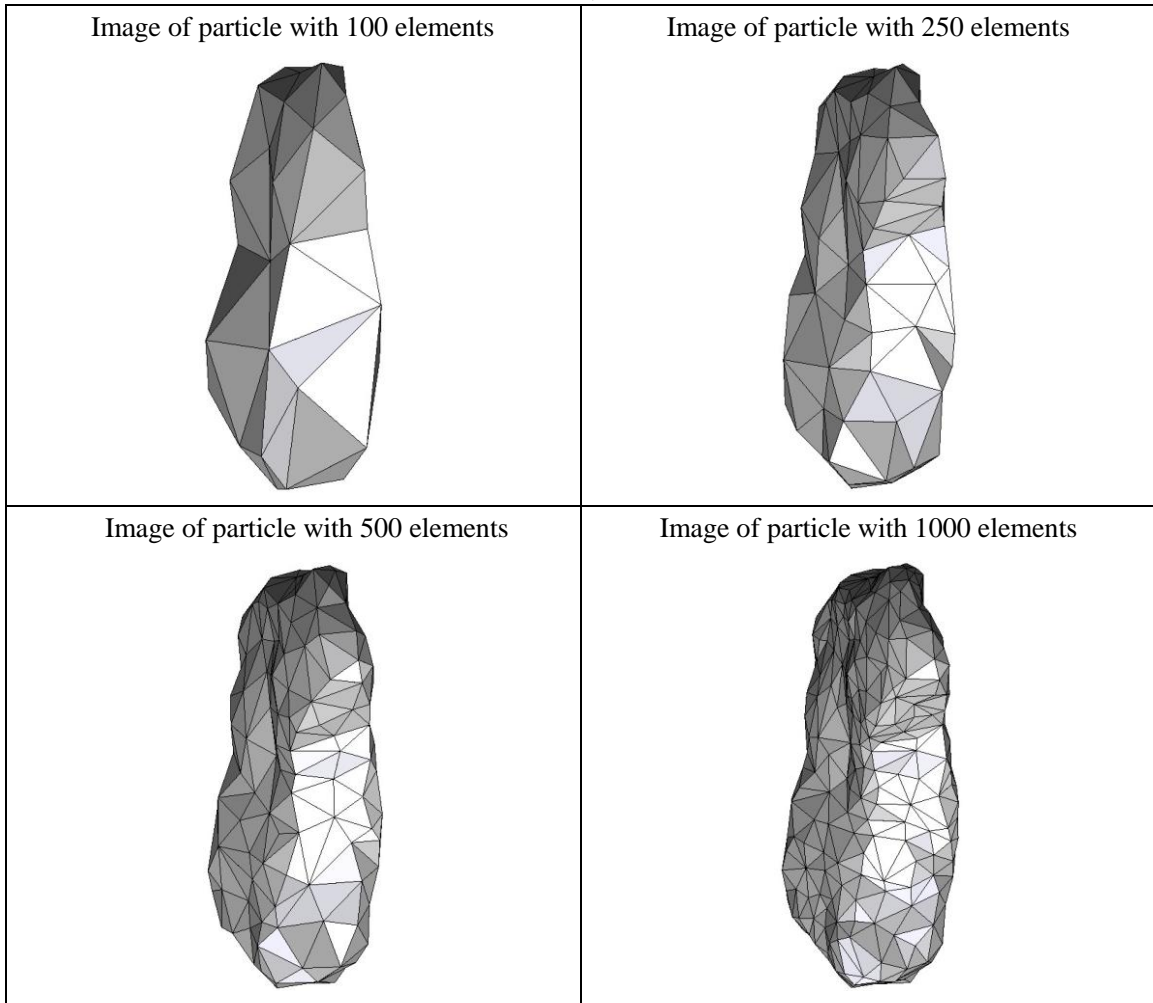
Figure 21.4 CPU computation time vs. model geometry resolution.

Appendix

Percent difference analysis compare to particle 21 with 100 elements for different group of data			
	particle 21 with 250 elements	particle 21 with 500 elements	particle 21 with 1000 elements
Impulse	3.84	3.10	-0.40
Peak Force	-1.25	-2.78	-7.53
Start Time	0.00	0.00	0.00
CPU Time	750.00	775.00	1350.00
Simulation Time	-4.55	-4.55	-4.55

Appendix

Summary of particle characteristics and collision simulation details for Particle 22 (of 50)



Particle statistics (part 1)								
Particle ID	# vertices	# elements	Mass (g)	Moments of Inertia			Volume (cm ³)	Sfc. Area (cm ²)
				I1	I2	I3		
				(gcm ²)	(gcm ²)	(gcm ²)		
22 (100 elements)	52	100	22.811	110603.8	79583.46875	43106.54375	7.53097	26.64782
22 (250 elements)	127	250	22.811	114523.7375	81870.7125	45477.53438	7.72799	27.23114
22 (500 elements)	252	500	22.811	117159.65	83704.80625	46685.32813	7.83393	27.43652
22 (1000 elements)	502	1000	22.811	117699.1625	83953.96875	46989.48125	7.85064	27.39929

Appendix

Particle Statistics (part 2)							
Particle ID	α	R_g (cm)	ψ	R_v (cm)	L (cm)	I (cm)	S (cm)
22 (100 elements)	3.48845	2.37404	0.69725	1.21596	179.55220	127.46786	51.47045
22 (250 elements)	3.43043	2.36285	0.69417	1.22648	181.87868	130.86494	53.01921
22 (500 elements)	3.41370	2.33565	0.69525	1.23206	183.83391	132.53726	53.85186
22 (1000 elements)	3.41727	2.34333	0.69719	1.23293	184.12254	133.02795	53.87994

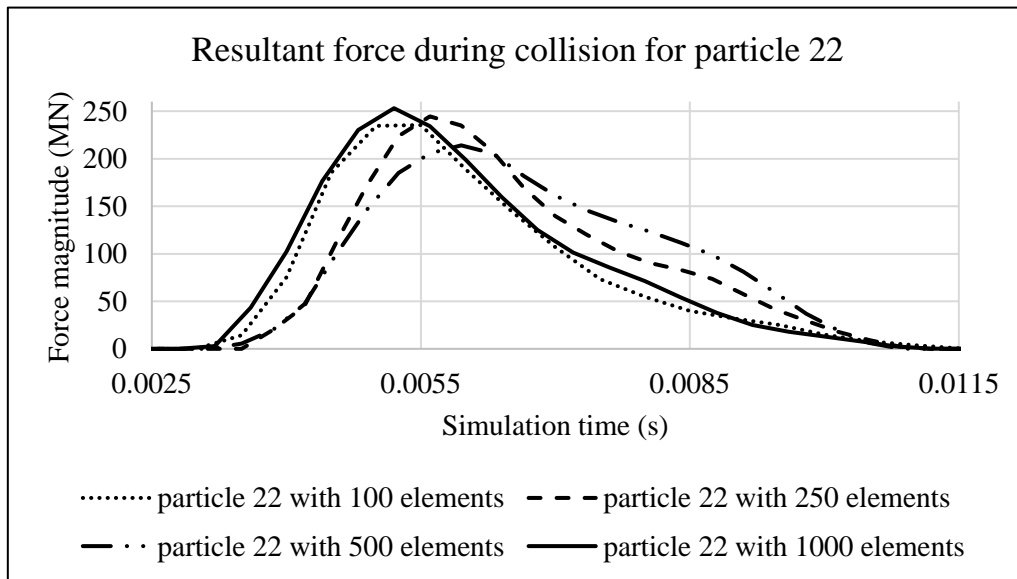


Figure A22.1 Plot of resultant forces during collision event for Particle 22.

Appendix

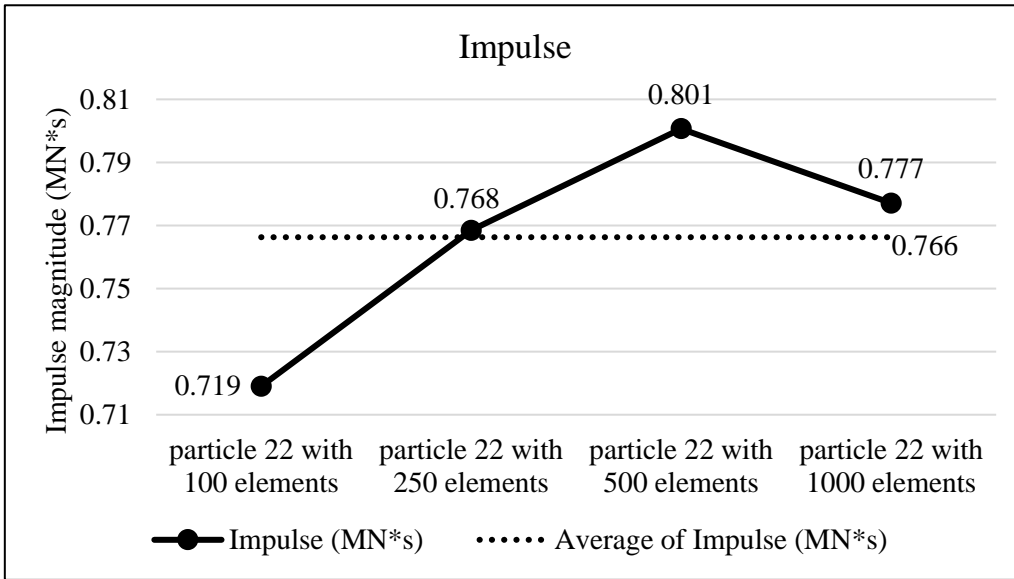


Figure A22.2 Plots of collision impulse for Particle 22.

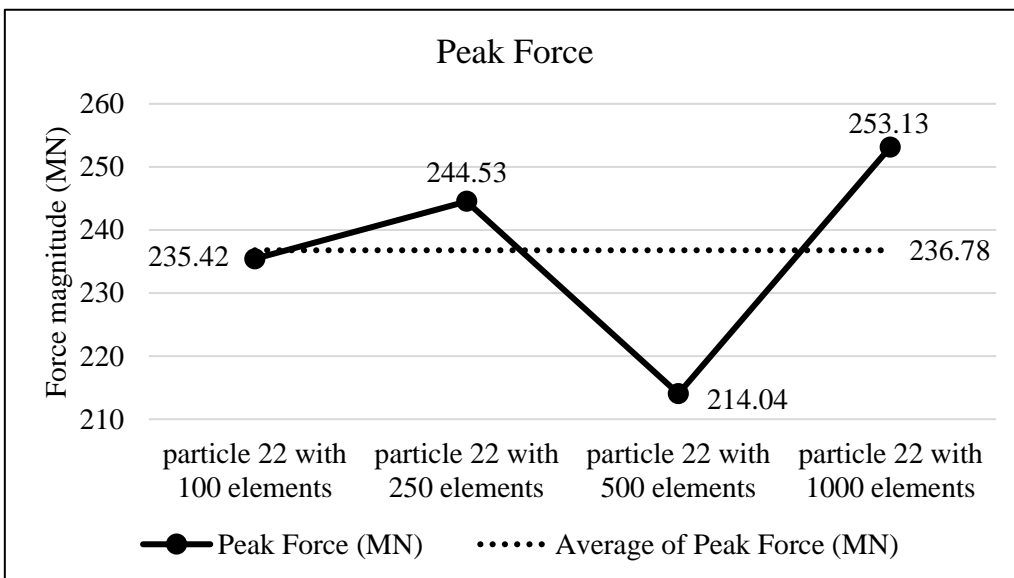


Figure A22.3 Peak collision for the four particle geometry resolutions for Particle 22.

Appendix

Collision results data analysis					
Model	particle 22 with 100 elements	particle 22 with 250 elements	particle 22 with 500 elements	particle 22 with 1000 elements	Average
Impulse (MN*s)	0.719	0.768	0.801	0.777	0.766
Percent difference from Avg. Impulse	-6.17	0.28	4.48	1.40	
Peak Force (MN)	235.42	244.53	214.04	253.13	236.78
Percent difference from Avg. Peak Force	-0.57	3.27	-9.60	6.90	

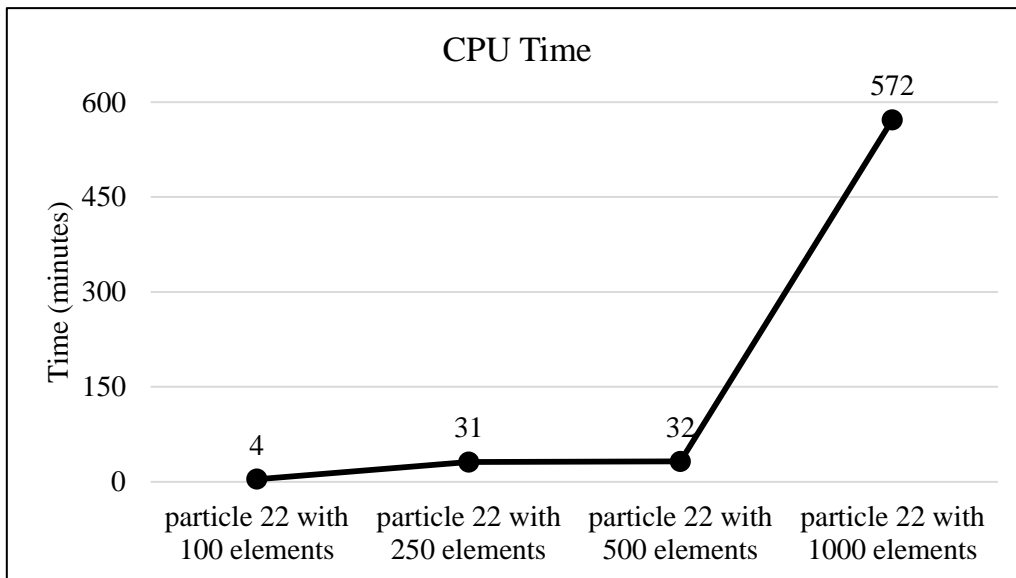
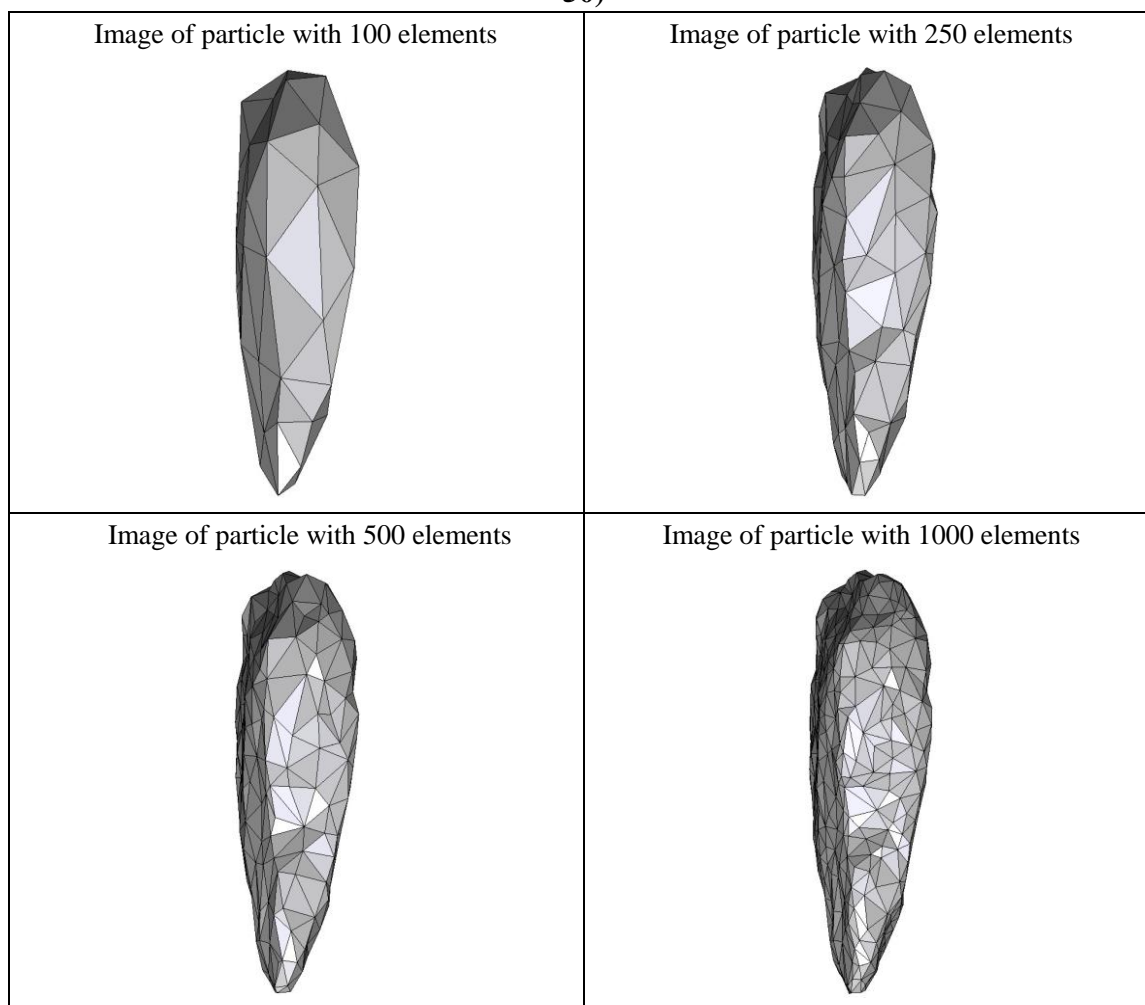


Figure A22.4 CPU computation time vs. model geometry resolution.

Appendix

Percent difference analysis compare to particle 22 with 100 elements for different group of data			
	particle 22 with 250 elements	particle 22 with 500 elements	particle 22 with 1000 elements
Impulse	6.87	11.35	8.07
Peak Force	3.87	-9.08	7.52
Start Time	10.00	0.00	-8.57
CPU Time	675.00	700.00	14200.00
Simulation Time	-8.13	-8.13	0.00

Summary of particle characteristics and collision simulation details for Particle 23 (of 50)



Particle statistics (part 1)								
Particle ID	# vertices	# elements	Mass (g)	Moments of Inertia			Volume (cm ³)	Sfc. Area (cm ²)
				I1	I2	I3		
				(gcm ²)	(gcm ²)	(gcm ²)		
23 (100 elements)	52	100	18.32	101559.575	83063.78125	26036.325	6.62197	24.78276
23 (250 elements)	127	250	18.32	104610.8188	85825.7625	26457.1875	6.69599	25.03955
23 (500 elements)	252	500	18.32	105519.275	86611.3375	26572.275	6.71123	24.97843
23 (1000 elements)	502	1000	18.32	105855.5125	86877.2875	26674.6125	6.72464	24.98183

Appendix

Particle Statistics (part 2)							
Particle ID	α	R_g (cm)	ψ	R_v (cm)	L (cm)	I (cm)	S (cm)
23 (100 elements)	4.58599	2.71457	0.68811	1.16493	208.04443	110.24501	45.36524
23 (250 elements)	4.62314	2.66966	0.68612	1.16925	211.55189	111.12054	45.75940
23 (500 elements)	4.64770	2.66402	0.68884	1.17014	212.56796	111.41239	45.73615
23 (1000 elements)	4.64501	2.66434	0.68967	1.17092	212.88860	111.62363	45.83168

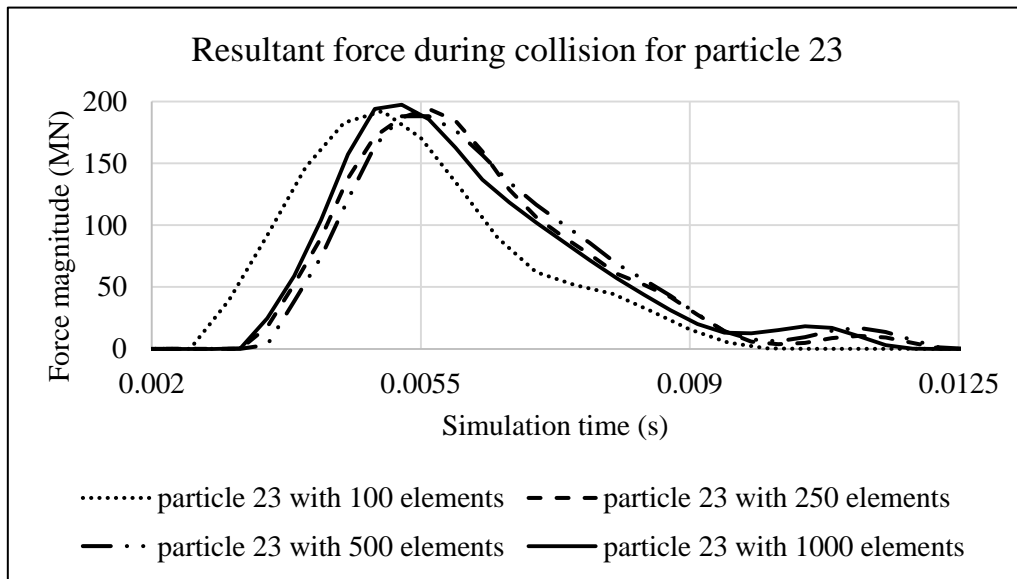


Figure A23.1 Plot of resultant forces during collision event for Particle 23.

Appendix

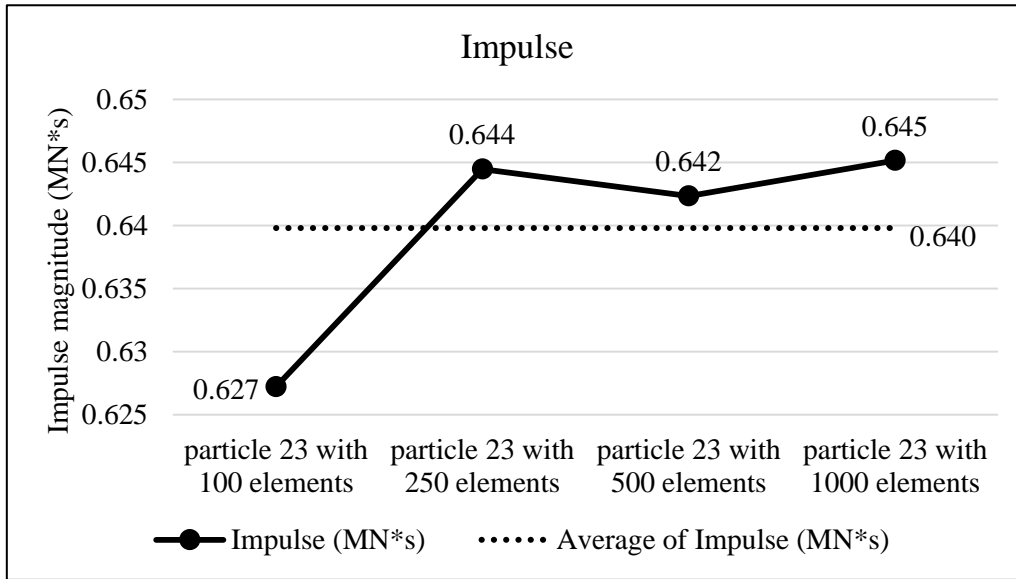


Figure A23.2 Plots of collision impulse for Particle 23.

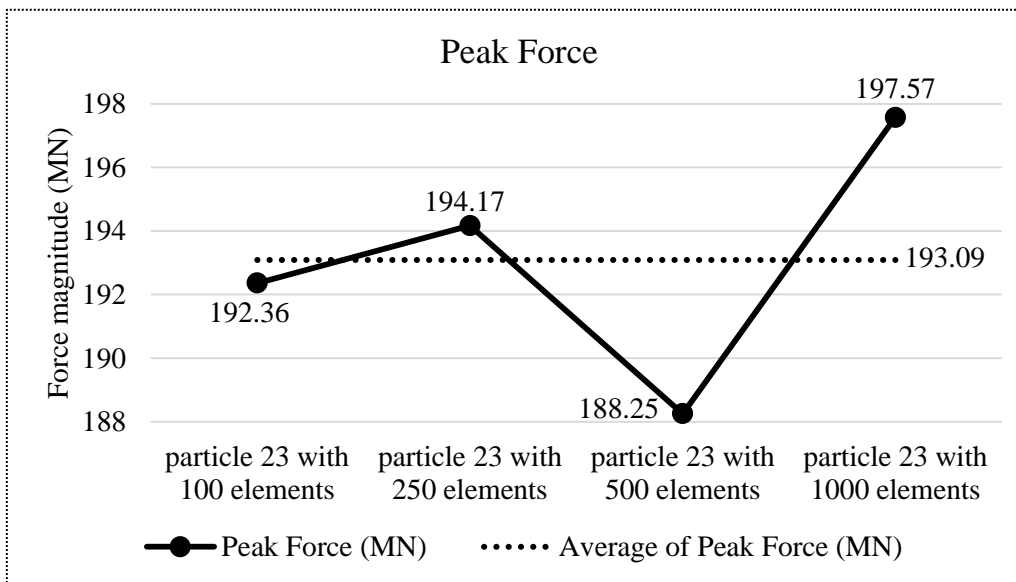


Figure A23.3 Peak collision for the four particle geometry resolutions for Particle 23.

Appendix

Collision results data analysis					
Model	particle 23 with 100 elements	particle 23 with 250 elements	particle 23 with 500 elements	particle 23 with 1000 elements	Average
Impulse (MN*s)	0.627	0.644	0.642	0.645	0.640
Percent difference from Avg. Impulse	-1.97	0.73	0.40	0.84	
Peak Force (MN)	192.36	194.17	188.25	197.57	193.09
Percent difference from Avg. Peak Force	-0.38	0.56	-2.50	2.32	

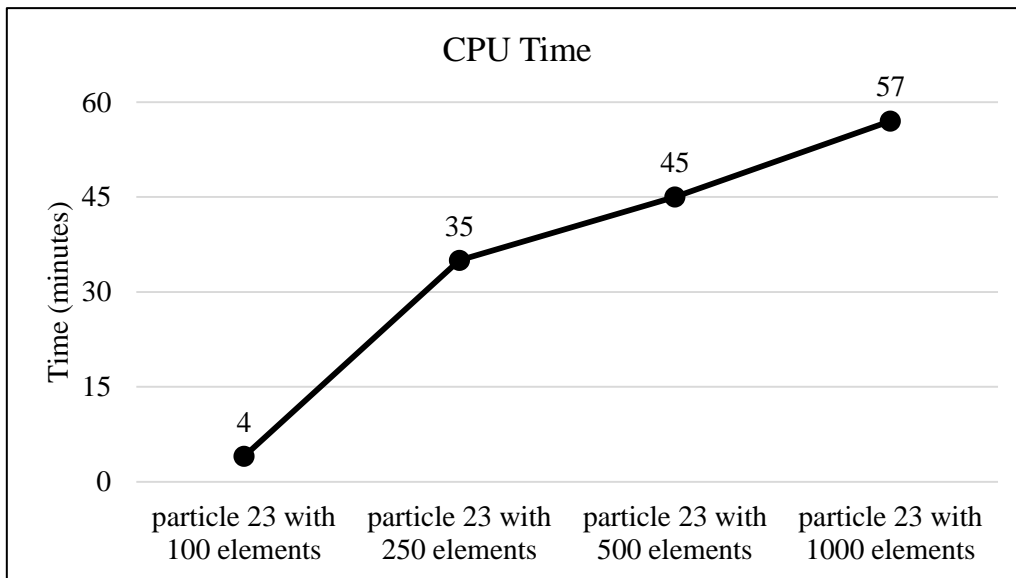
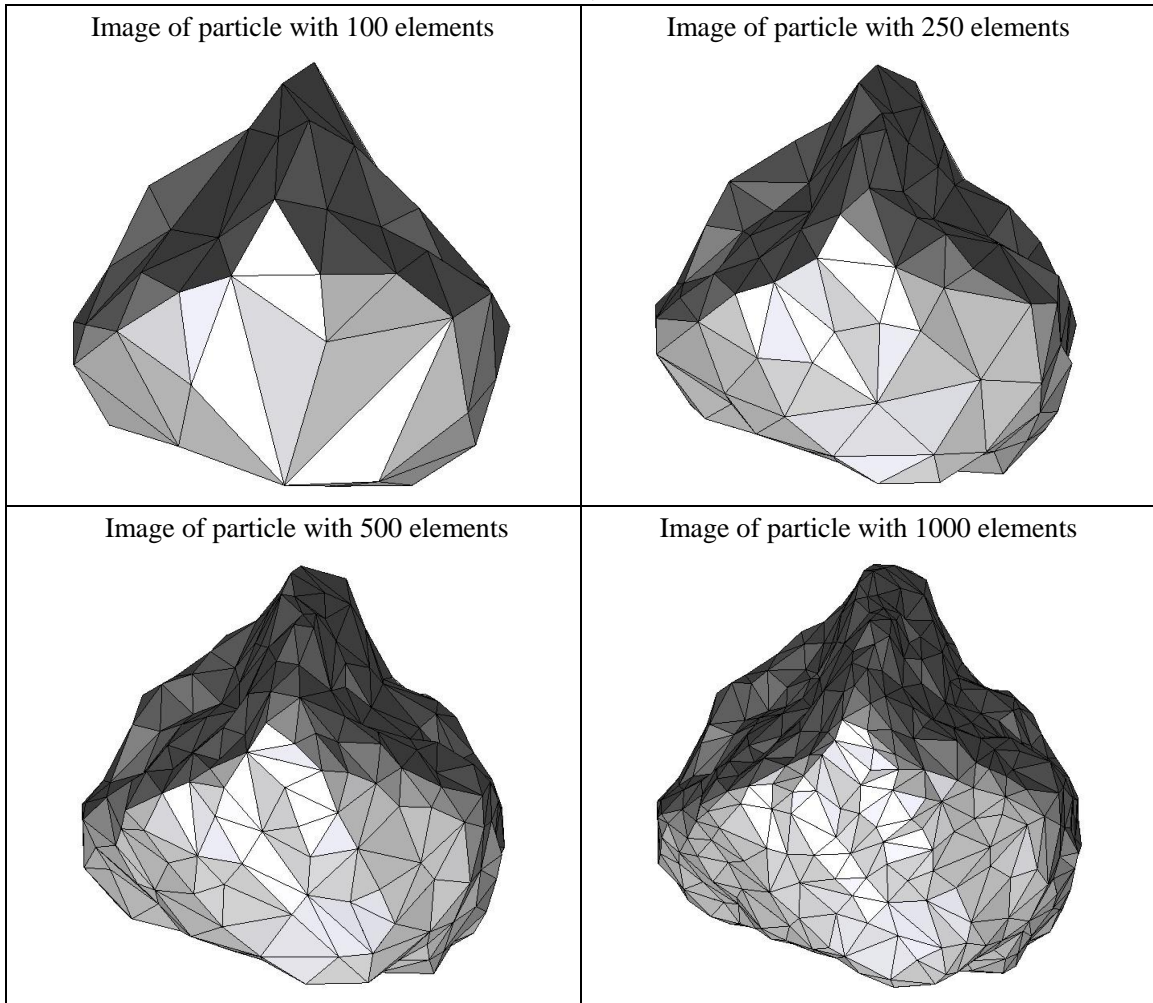


Figure A23.4 CPU computation time vs. model geometry resolution.

Appendix

Percent difference analysis compare to particle 23 with 100 elements for different group of data			
	particle 23 with 250 elements	particle 23 with 500 elements	particle 23 with 1000 elements
Impulse	2.75	2.41	2.86
Peak Force	0.94	-2.14	2.71
Start Time	16.67	16.67	5.00
CPU Time	775.00	1025.00	1325.00
Simulation Time	25.00	25.00	25.00

Summary of particle characteristics and collision simulation details for Particle 24 (of 50)



Particle statistics (part 1)								
Particle ID	# vertices	# elements	Mass (g)	Moments of Inertia			Volume (cm ³)	Sfc. Area (cm ²)
				I1	I2	I3		
				(gcm ²)	(gcm ²)	(gcm ²)		
24 (100 elements)	52	100	29.353	89006.225	83563.90625	71031.23125	10.23462	26.86805
24 (250 elements)	127	250	29.353	92339.83125	87242.375	73865.25	10.47335	27.37359
24 (500 elements)	252	500	29.353	93175.3	88159.6625	74657.46875	10.52620	27.46218
24 (1000 elements)	502	1000	29.353	93614.38125	88523.4375	74959.56875	10.55122	27.42962

Appendix

Particle Statistics (part 2)							
Particle ID	α	R_g (cm)	ψ	R_v (cm)	L (cm)	I (cm)	S (cm)
24 (100 elements)	1.24423	2.00431	0.84846	1.34688	131.51491	114.13383	105.69975
24 (250 elements)	1.23988	1.94161	0.84569	1.35727	134.19338	115.97644	108.23091
24 (500 elements)	1.23766	1.92289	0.84579	1.35955	134.80163	116.49697	108.91654
24 (1000 elements)	1.23855	1.93231	0.84814	1.36062	135.11765	116.77256	109.09375

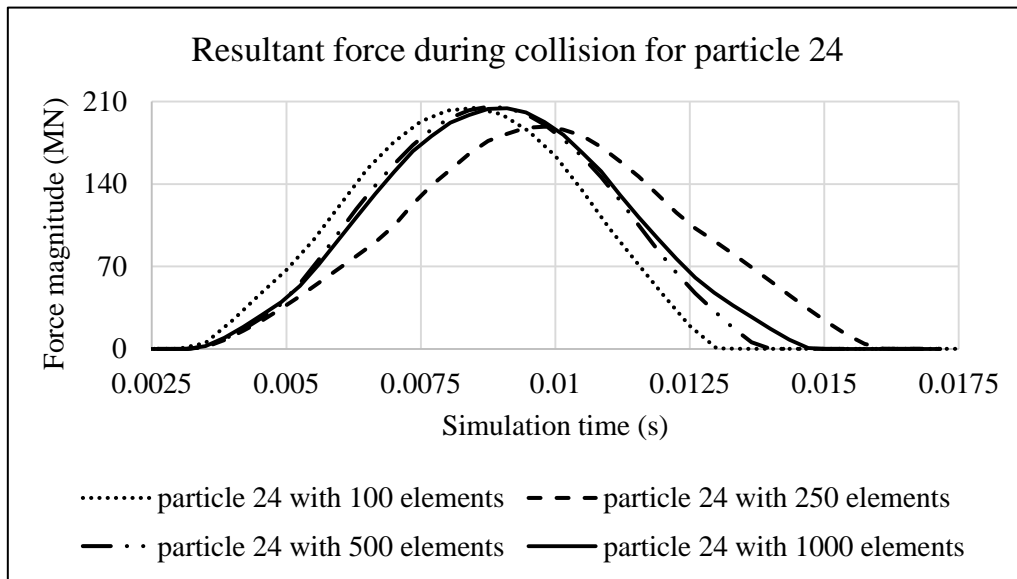


Figure A24.1 Plot of resultant forces during collision event for Particle 24.

Appendix

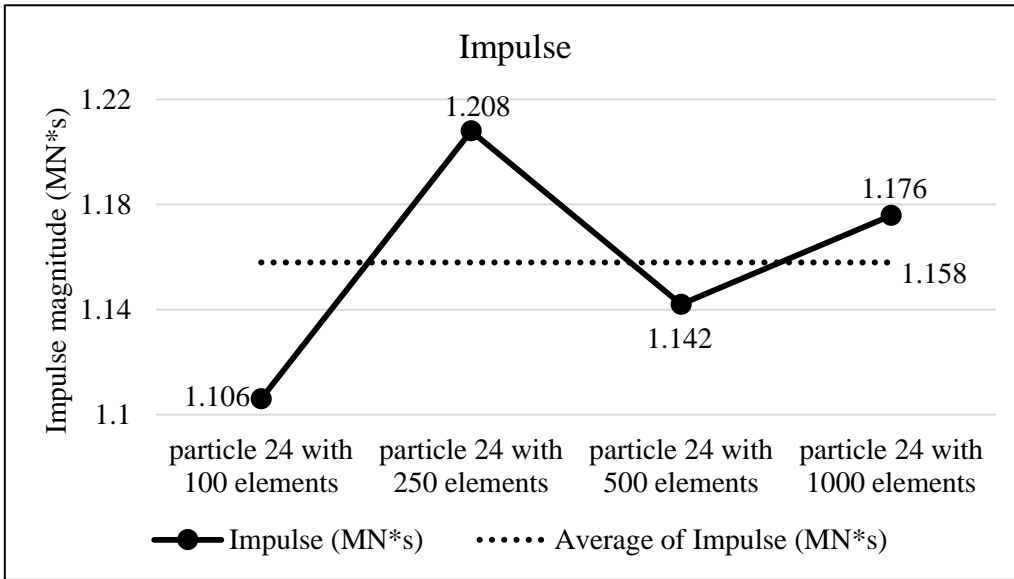


Figure A24.2 Plots of collision impulse for Particle 24.

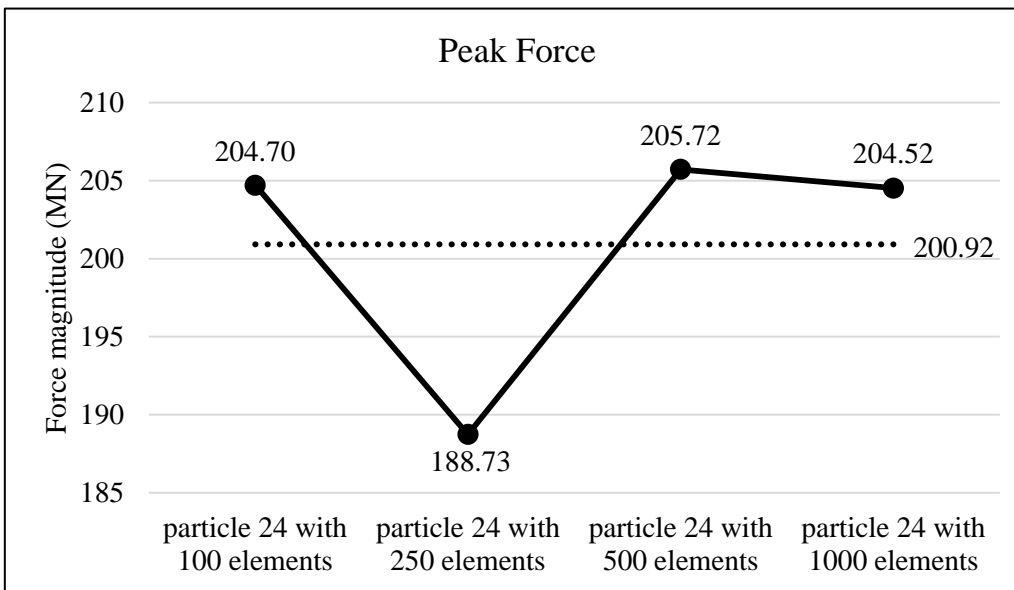


Figure A24.3 Peak collision for the four particle geometry resolutions for Particle 24.

Appendix

Collision results data analysis					
Model	particle 24 with 100 elements	particle 24 with 250 elements	particle 24 with 500 elements	particle 24 with 1000 elements	Average
Impulse (MN*s)	1.106	1.208	1.142	1.176	1.158
Percent difference from Avg. Impulse	-4.48	4.32	-1.38	1.54	
Peak Force (MN)	204.70	188.73	205.72	204.52	200.92
Percent difference from Avg. Peak Force	1.88	-6.07	2.39	1.79	

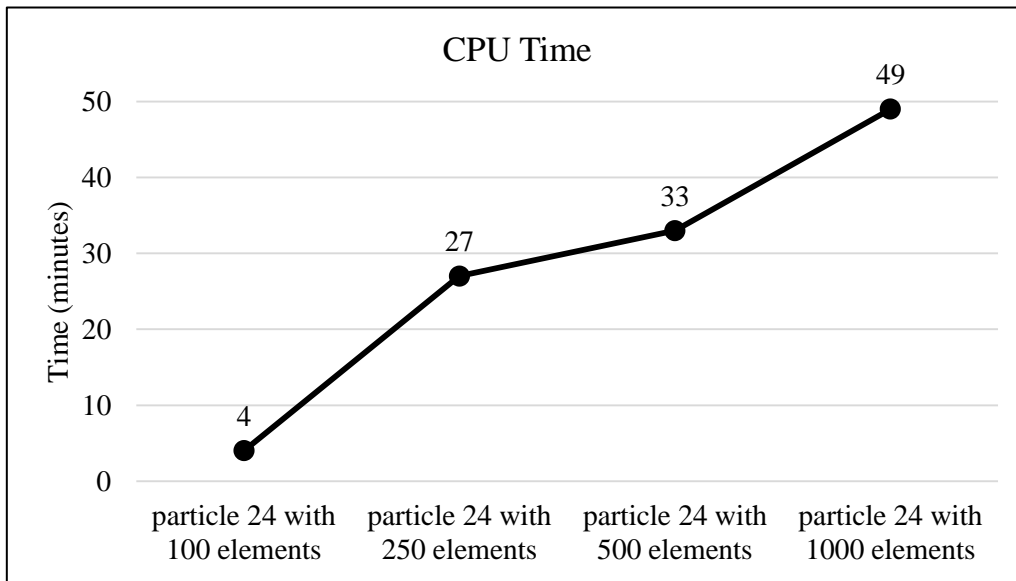
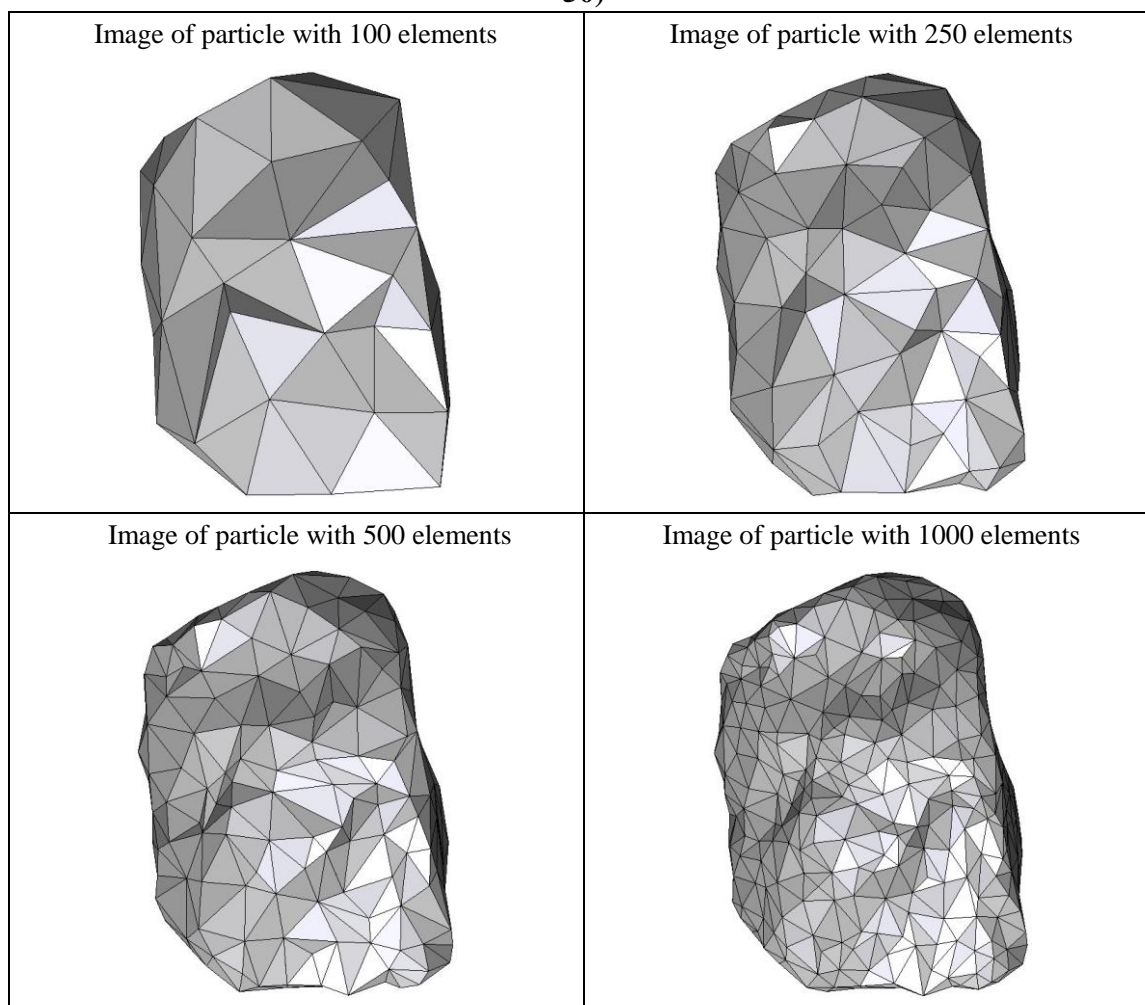


Figure A24.4 CPU computation time vs. model geometry resolution.

Appendix

Percent difference analysis compare to particle 24 with 100 elements for different group of data			
	particle 24 with 250 elements	particle 24 with 500 elements	particle 24 with 1000 elements
Impulse	9.22	3.25	6.31
Peak Force	-7.80	0.50	-0.09
Start Time	0.00	0.00	0.00
CPU Time	575.00	725.00	1125.00
Simulation Time	32.63	45.00	60.00

Summary of particle characteristics and collision simulation details for Particle 25 (of 50)



Particle statistics (part 1)								
Particle ID	# vertices	# elements	Mass (g)	Moments of Inertia			Volume (cm ³)	Sfc. Area (cm ²)
				I1	I2	I3		
				(gcm ²)	(gcm ²)	(gcm ²)		
25 (100 elements)	52	100	15.885	47435.325	36533.24688	23846.89688	5.63401	19.84241
25 (250 elements)	127	250	15.885	48475.67813	37302.35	24335.01094	5.69527	19.84574
25 (500 elements)	252	500	15.885	48820.34688	37591.60625	24548.3125	5.72002	19.90250
25 (1000 elements)	502	1000	15.885	49084.275	37796.43438	24671.04219	5.73600	19.88513

Appendix

Particle Statistics (part 2)							
Particle ID	α	R_g (cm)	ψ	R_v (cm)	L (cm)	I (cm)	S (cm)
25 (100 elements)	2.15510	1.94079	0.77168	1.10385	137.56468	104.58331	63.83214
25 (250 elements)	2.16063	1.88180	0.77713	1.10784	139.06814	105.71986	64.36460
25 (500 elements)	2.15513	1.88800	0.77716	1.10944	139.54335	106.11913	64.74952
25 (1000 elements)	2.15600	1.87108	0.77928	1.11047	139.93306	106.38845	64.90399

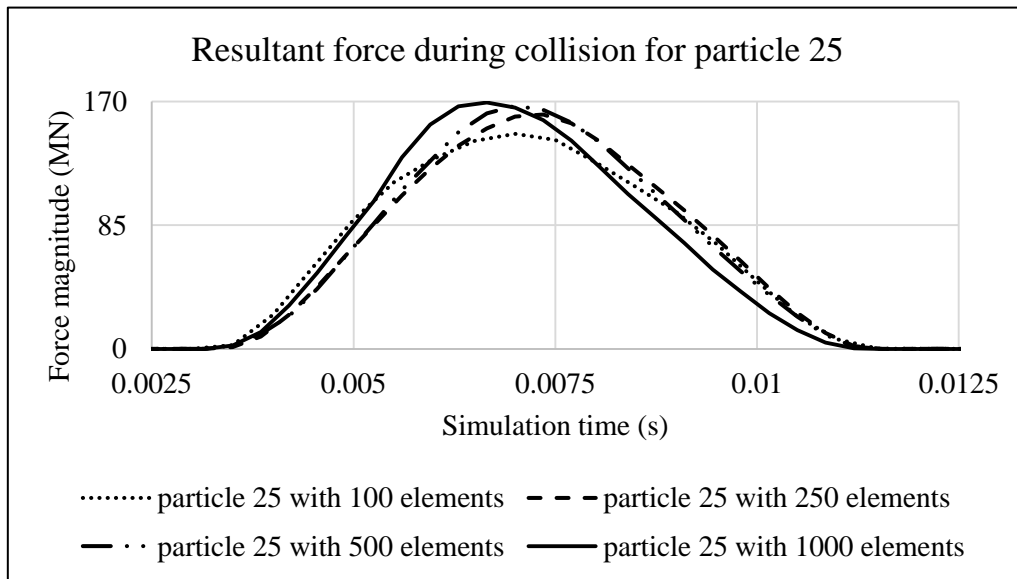


Figure A25.1 Plot of resultant forces during collision event for Particle 25.

Appendix

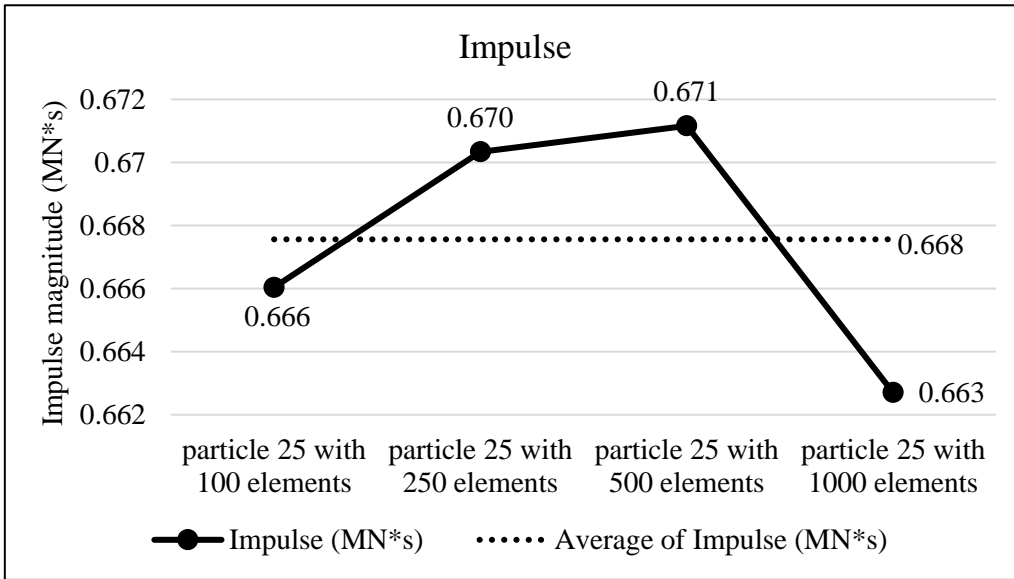


Figure A25.2 Plots of collision impulse for Particle 25.

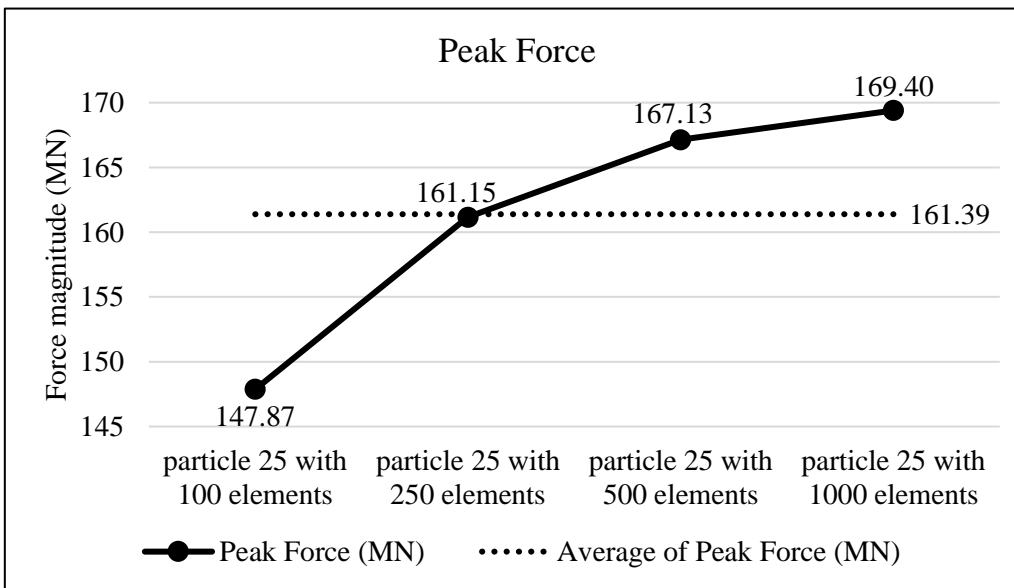


Figure A25.3 Peak collision for the four particle geometry resolutions for Particle 25.

Appendix

Collision results data analysis					
Model	particle 25 with 100 elements	particle 25 with 250 elements	particle 25 with 500 elements	particle 25 with 1000 elements	Average
Impulse (MN*s)	0.666	0.670	0.671	0.663	0.668
Percent difference from Avg. Impulse	-0.23	0.42	0.54	-0.73	
Peak Force (MN)	147.87	161.15	167.13	169.40	161.39
Percent difference from Avg. Peak Force	-8.37	-0.15	3.56	4.96	

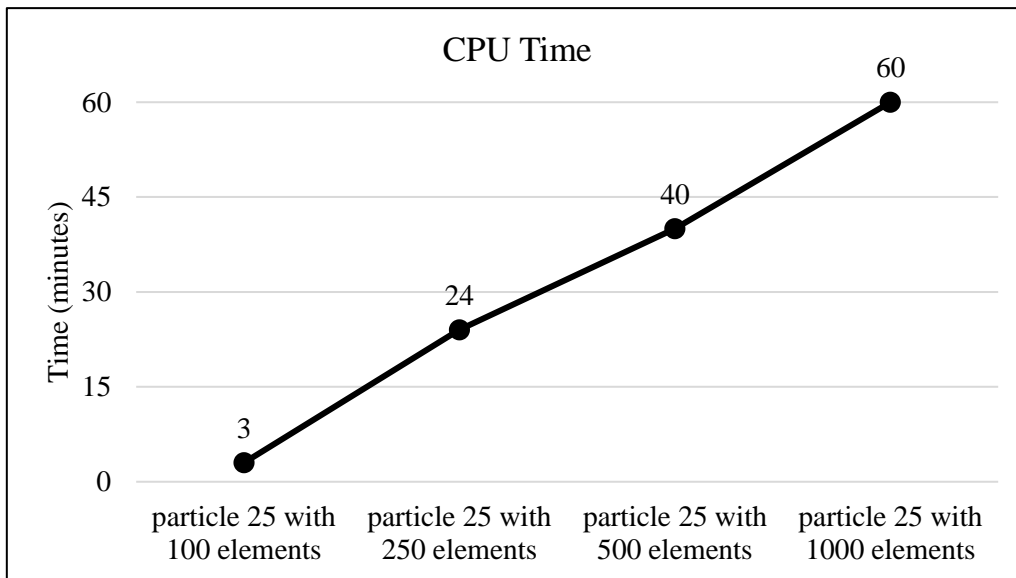
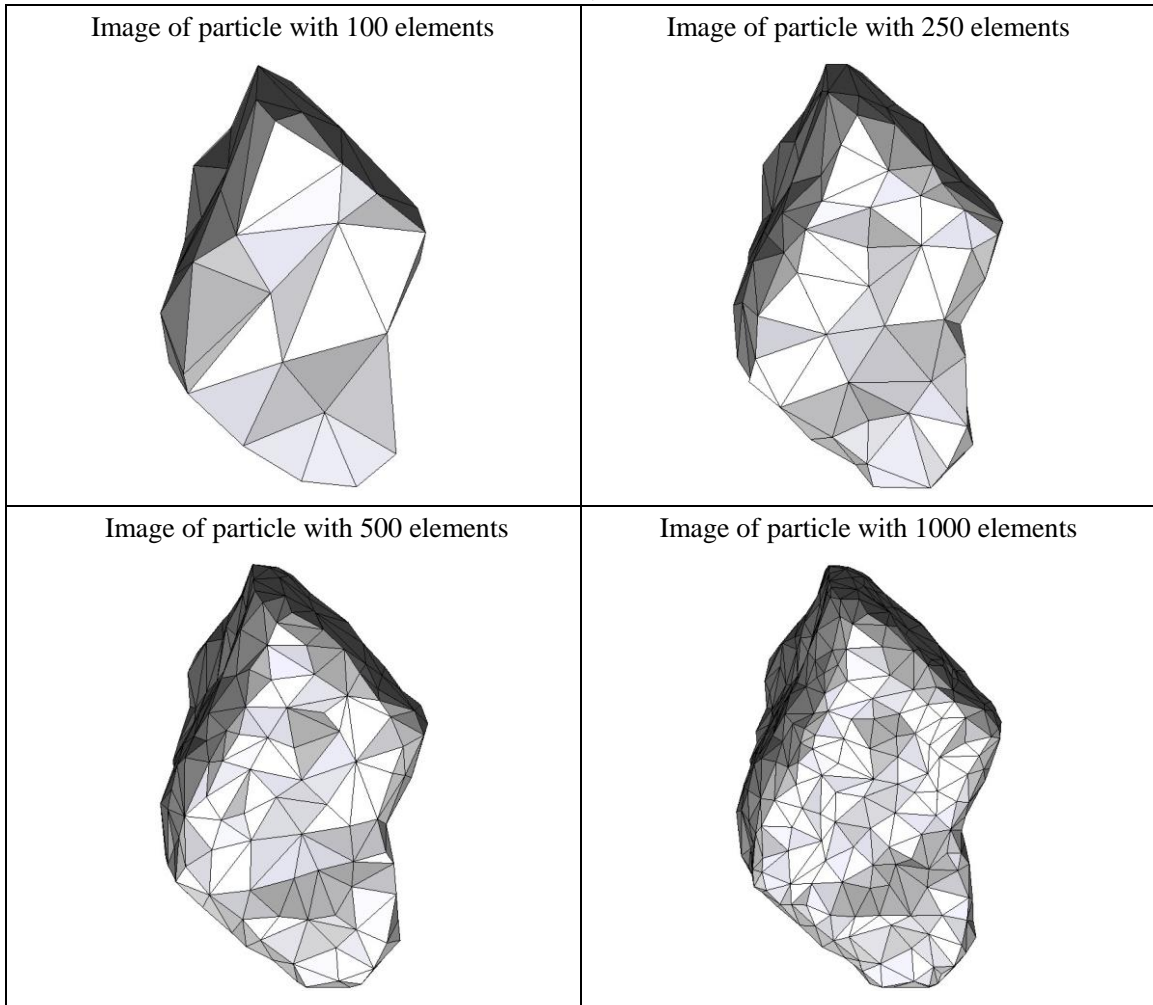


Figure A25.4 CPU computation time vs. model geometry resolution.

Appendix

Percent difference analysis compare to particle 25 with 100 elements for different group of data			
	particle 25 with 250 elements	particle 25 with 500 elements	particle 25 with 1000 elements
Impulse	0.65	0.77	-0.50
Peak Force	8.98	13.02	14.56
Start Time	0.00	0.00	0.00
CPU Time	700.00	1233.33	1900.00
Simulation Time	-9.41	-9.41	-9.41

Summary of particle characteristics and collision simulation details for Particle 26 (of 50)



Particle statistics (part 1)								
Particle ID	# vertices	# elements	Mass (g)	Moments of Inertia			Volume (cm ³)	Sfc. Area (cm ²)
				I1	I2	I3		
				(gcm ²)	(gcm ²)	(gcm ²)		
26 (100 elements)	52	100	10.32	21264.89063	18542.52813	11085.51719	3.68261	14.53637
26 (250 elements)	127	250	10.32	21835.2625	19036.32344	11412.72813	3.74930	14.53810
26 (500 elements)	252	500	10.32	21958.57344	19156.06094	11441.80234	3.75732	14.58920
26 (1000 elements)	502	1000	10.32	22045.07813	19228.95469	11482.16875	3.76409	14.58082

Appendix

Particle Statistics (part 2)							
Particle ID	α	R_g (cm)	ψ	R_v (cm)	L (cm)	I (cm)	S (cm)
26 (100 elements)	1.85320	1.63190	0.79335	0.95798	117.96461	81.79159	63.65466
26 (250 elements)	1.84931	1.62929	0.80280	0.96373	119.46842	82.97890	64.60145
26 (500 elements)	1.85328	1.62441	0.80113	0.96441	119.90151	83.07416	64.69700
26 (1000 elements)	1.85412	1.62607	0.80256	0.96499	120.14176	83.23141	64.79711

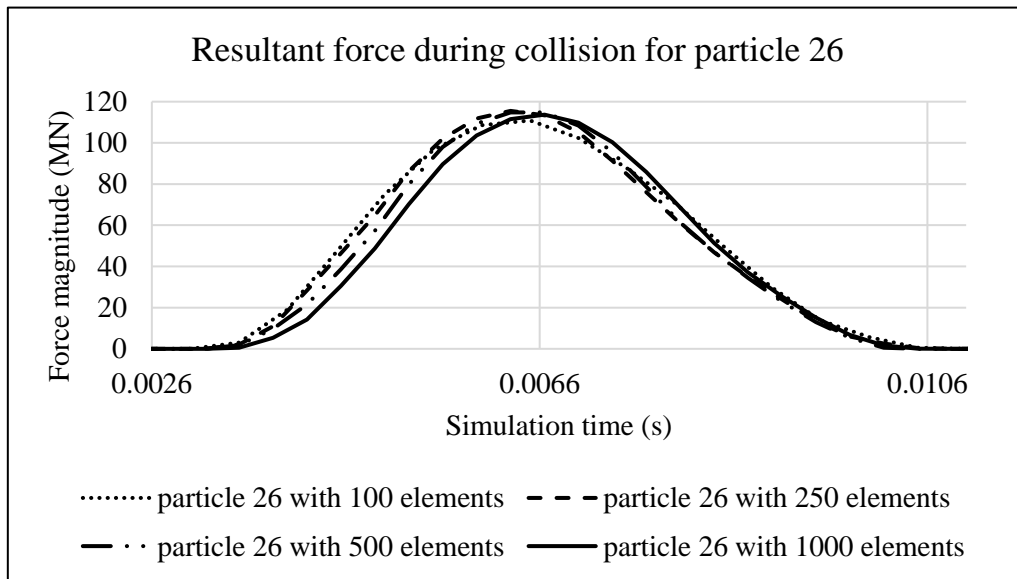


Figure A26.1 Plot of resultant forces during collision event for Particle 26.

Appendix

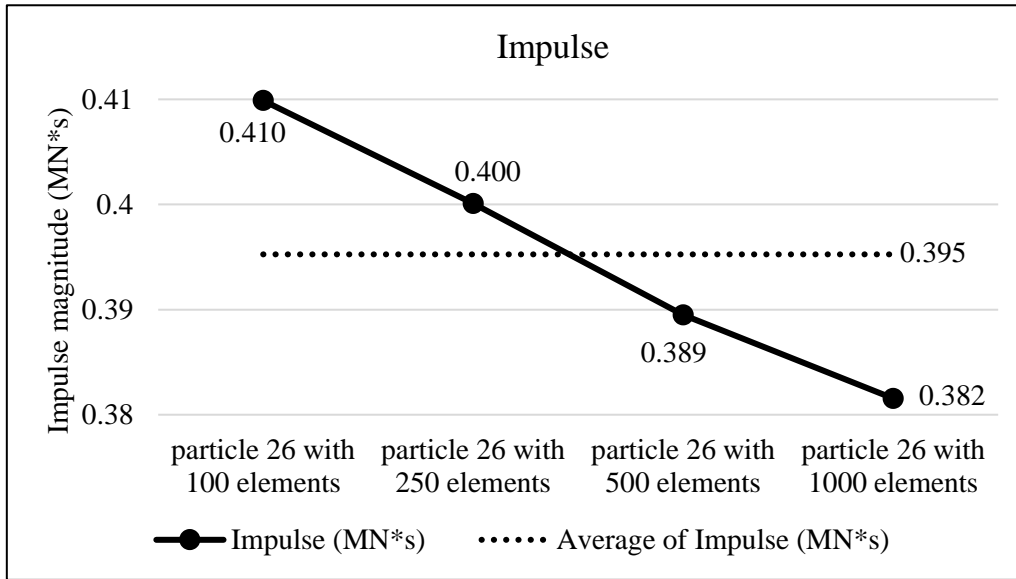


Figure A26.2 Plots of collision impulse for Particle 26.

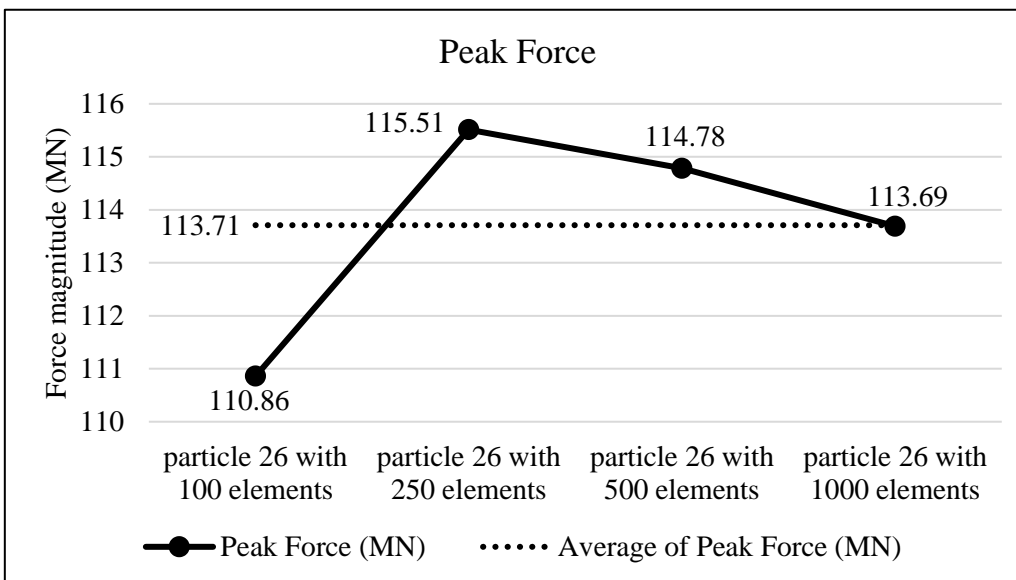


Figure A26.3 Peak collision for the four particle geometry resolutions for Particle 26.

Appendix

Collision results data analysis					
Model	particle 26 with 100 elements	particle 26 with 250 elements	particle 26 with 500 elements	particle 26 with 1000 elements	Average
Impulse (MN*s)	0.410	0.400	0.389	0.382	0.395
Percent difference from Avg. Impulse	-0.23	0.42	0.54	-0.73	
Peak Force (MN)	147.87	161.15	167.13	169.40	161.39
Percent difference from Avg. Peak Force	-8.37	-0.15	3.56	4.96	

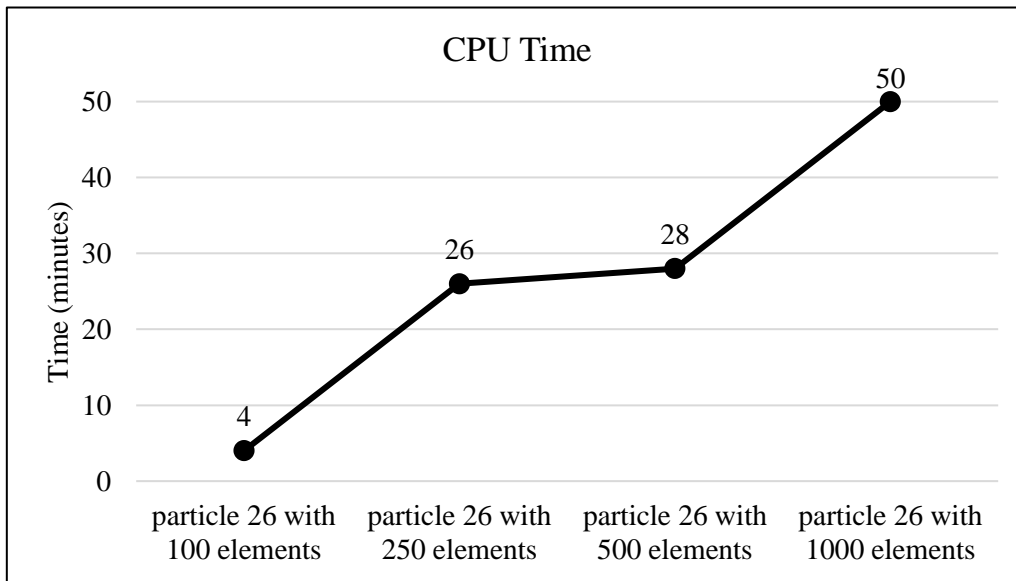
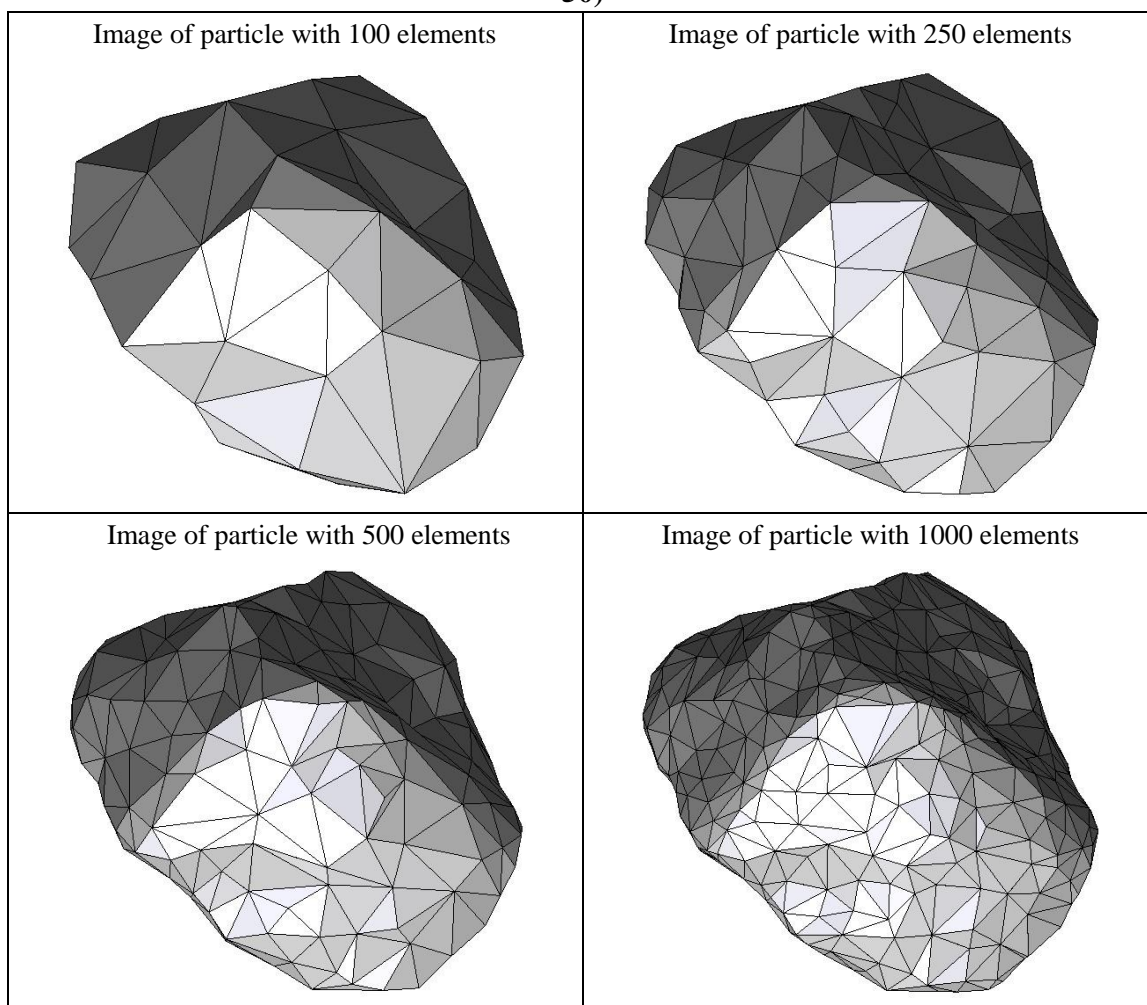


Figure A26.4 CPU computation time vs. model geometry resolution.

Appendix

Percent difference analysis compare to particle 26 with 100 elements for different group of data			
	particle 26 with 250 elements	particle 26 with 500 elements	particle 26 with 1000 elements
Impulse	-2.39	-4.97	-6.91
Peak Force	4.20	3.54	2.55
Start Time	0.00	0.00	0.00
CPU Time	550.00	600.00	1150.00
Simulation Time	0.00	-5.00	0.00

Summary of particle characteristics and collision simulation details for Particle 27 (of 50)



Particle statistics (part 1)								
Particle ID	# vertices	# elements	Mass (g)	Moments of Inertia			Volume (cm ³)	Sfc. Area (cm ²)
				I1	I2	I3		
				(gcm ²)	(gcm ²)	(gcm ²)		
27 (100 elements)	52	100	14.506	30492.83438	25486.64844	20801.81094	5.10058	16.30764
27 (250 elements)	127	250	14.506	31598.175	26353.32188	21794.58281	5.21982	16.55411
27 (500 elements)	252	500	14.506	31884.37188	26608.7	22023.63125	5.24981	16.58275
27 (1000 elements)	502	1000	14.506	31994.92188	26689.47188	22096.23125	5.25866	16.57305

Appendix

Particle Statistics (part 2)							
Particle ID	α	R_g (cm)	ψ	R_v (cm)	L (cm)	I (cm)	S (cm)
27 (100 elements)	1.49233	1.47988	0.87870	1.06785	110.11455	94.31664	73.78695
27 (250 elements)	1.47809	1.46594	0.87905	1.07611	111.63666	96.54060	75.52776
27 (500 elements)	1.47565	1.46578	0.88089	1.07816	112.11810	97.00340	75.97874
27 (1000 elements)	1.47616	1.44959	0.88240	1.07877	112.30044	97.18512	76.07582

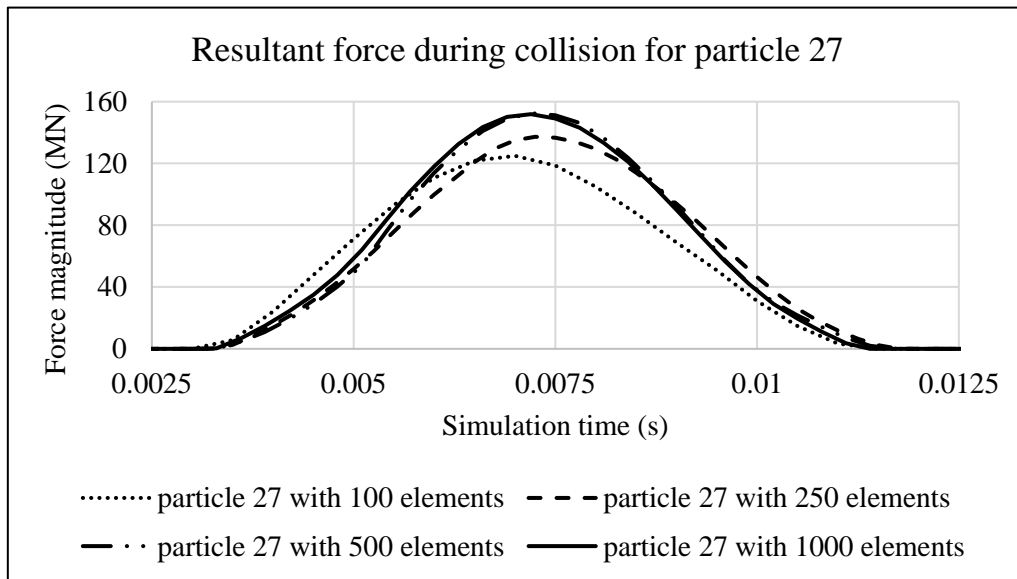


Figure A27.1 Plot of resultant forces during collision event for Particle 27.

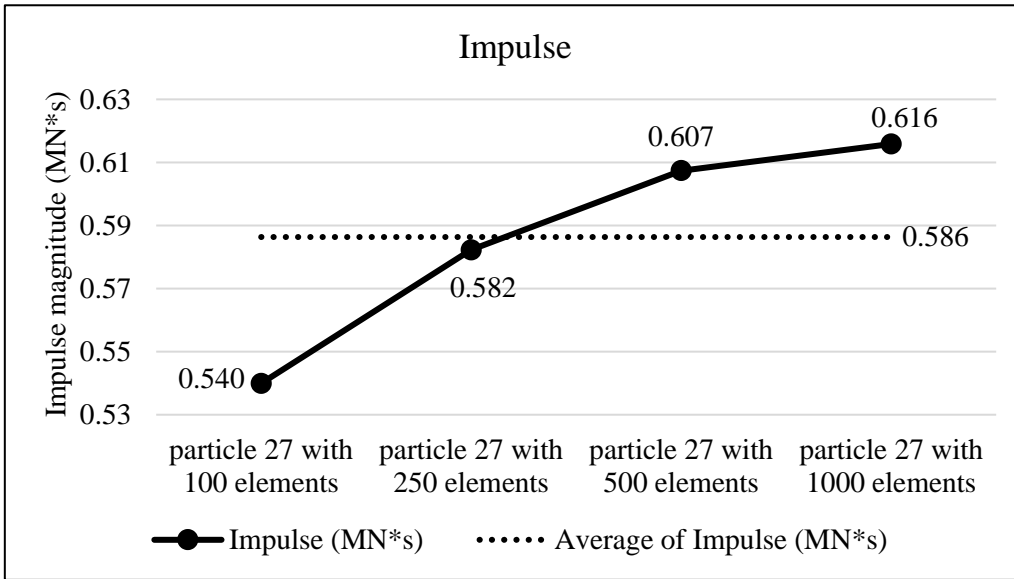


Figure 27.2 Plots of collision impulse for Particle 27.

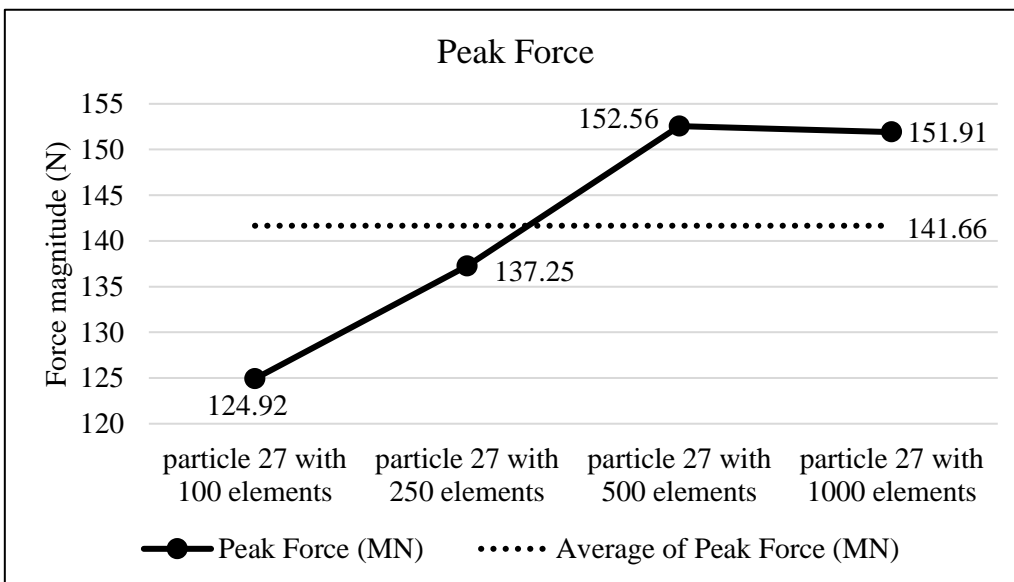


Figure A27.3 Peak collision for the four particle geometry resolutions for Particle 27.

Appendix

Collision results data analysis					
Model	particle 27 with 100 elements	particle 27 with 250 elements	particle 27 with 500 elements	particle 27 with 1000 elements	Average
Impulse (MN*s)	0.540	0.582	0.607	0.616	0.586
Percent difference from Avg. Impulse	-7.91	-0.70	3.59	5.03	
Peak Force (MN)	124.92	137.25	152.56	151.91	141.66
Percent difference from Avg. Peak Force	-11.82	-3.11	7.69	7.24	

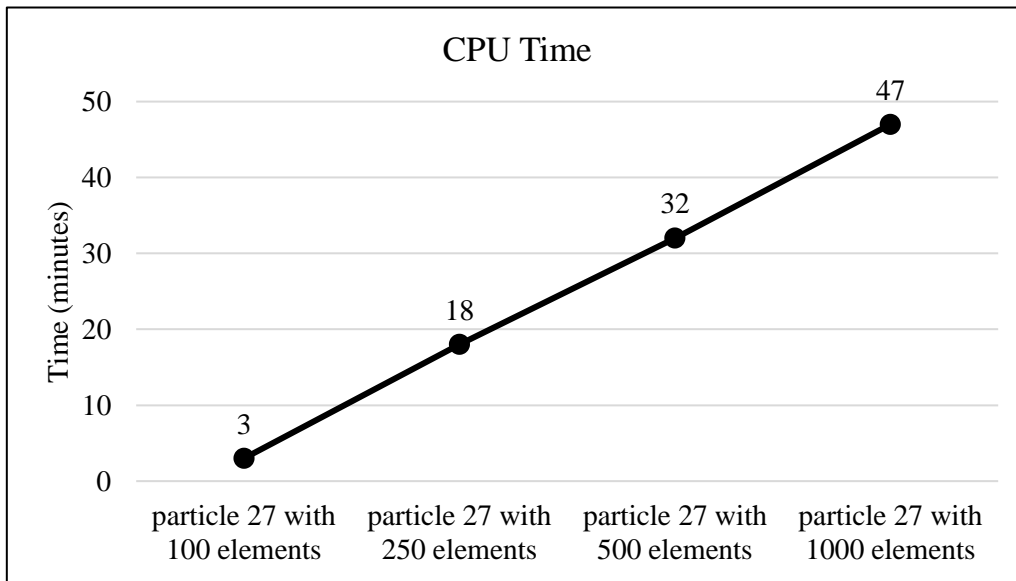


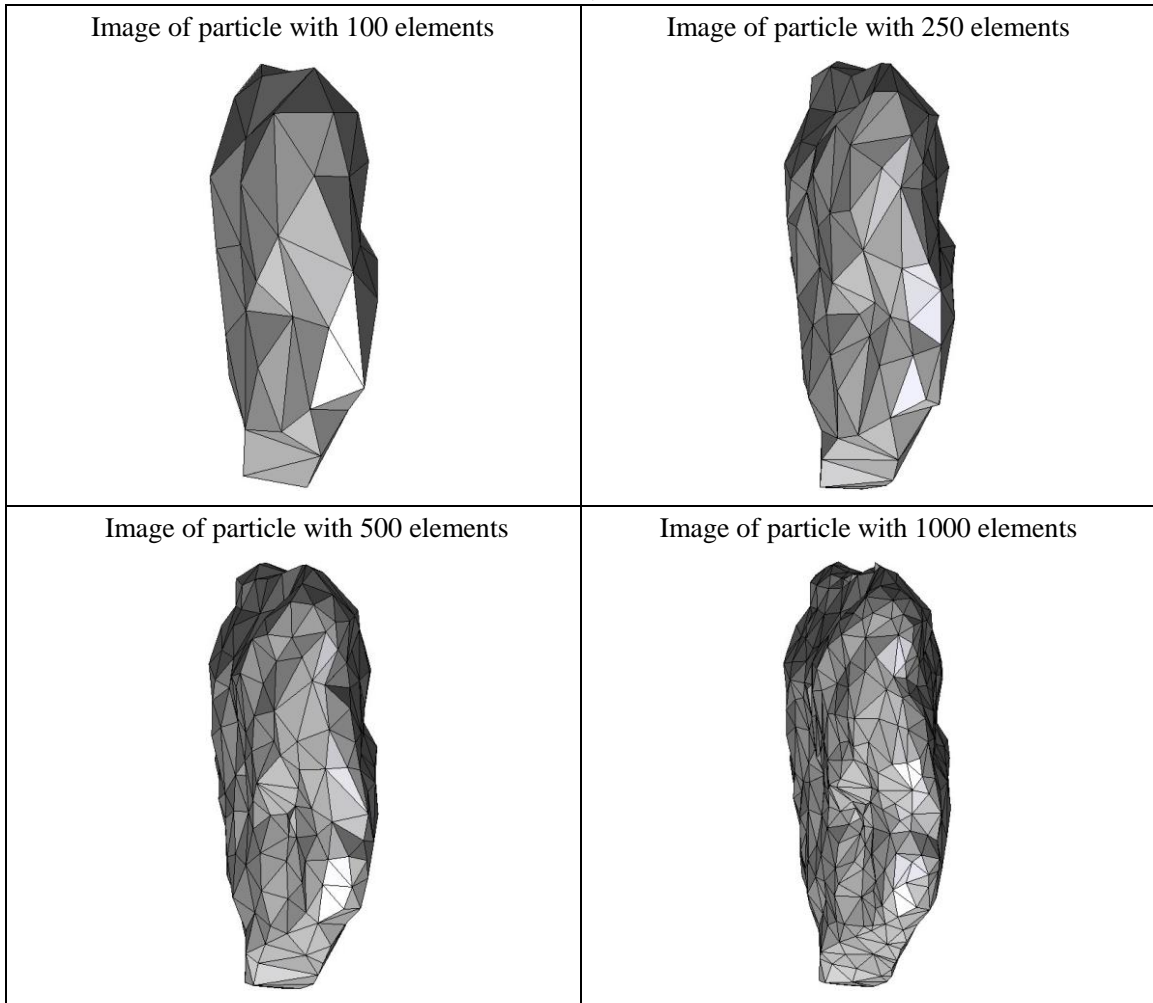
Figure A27.4 CPU computation time vs. model geometry resolution.

Appendix

Percent difference analysis compare to particle 27 with 100 elements for different group of data			
	particle 27 with 250 elements	particle 27 with 500 elements	particle 27 with 1000 elements
Impulse	7.83	12.49	14.06
Peak Force	9.87	22.12	21.60
Start Time	-7.14	-5.71	-5.71
CPU Time	500.00	966.67	1466.67
Simulation Time	13.33	12.00	4.00

Appendix

Summary of particle characteristics and collision simulation details for Particle 28 (of 50)



Particle statistics (part 1)								
Particle ID	# vertices	# elements	Mass (g)	Moments of Inertia			Volume (cm ³)	Sfc. Area (cm ²)
				I1	I2	I3		
				(gcm ²)	(gcm ²)	(gcm ²)		
28 (100 elements)	52	100	11.726	33079.34688	20725.43281	16287.36406	4.02712	16.53288
28 (250 elements)	127	250	11.726	34724.99063	21671.19844	17123.325	4.13448	16.70071
28 (500 elements)	252	500	11.726	35230.14063	21927.19063	17414.77813	4.16695	16.72792
28 (1000 elements)	502	1000	11.726	35349.82188	21982.27031	17508.38281	4.17827	16.73456

Appendix

Particle Statistics (part 2)							
Particle ID	α	R_g (cm)	ψ	R_v (cm)	L (cm)	I (cm)	S (cm)
28 (100 elements)	3.08837	1.67451	0.74040	0.98697	126.48136	110.51119	40.95405
28 (250 elements)	3.10652	1.67457	0.74593	0.99566	129.40658	113.43548	41.65646
28 (500 elements)	3.10893	1.65697	0.74861	0.99826	130.17810	114.44705	41.87237
28 (1000 elements)	3.10118	1.65338	0.74967	0.99916	130.31095	114.74139	42.01978

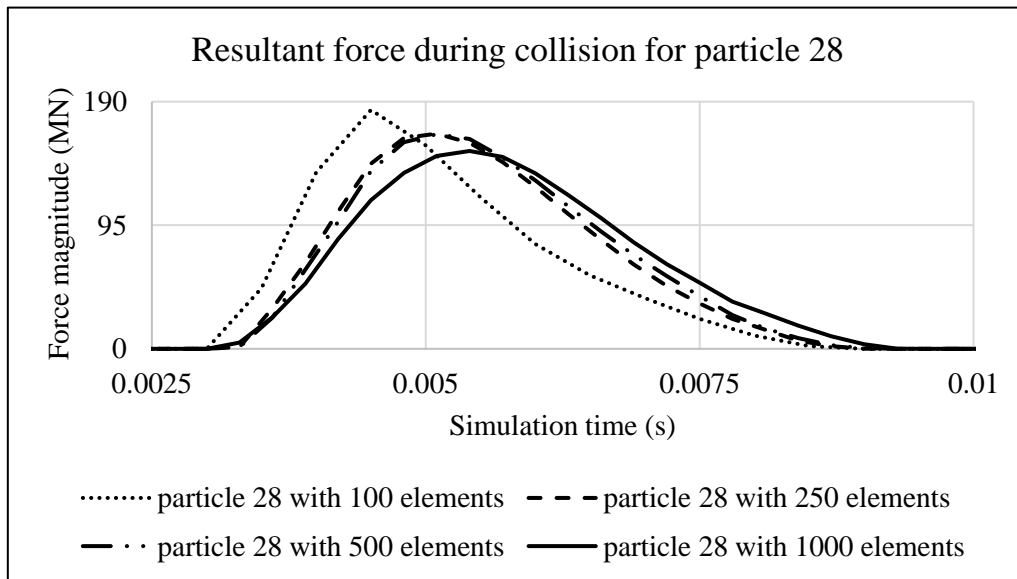


Figure A28.1 Plot of resultant forces during collision event for Particle 28.

Appendix

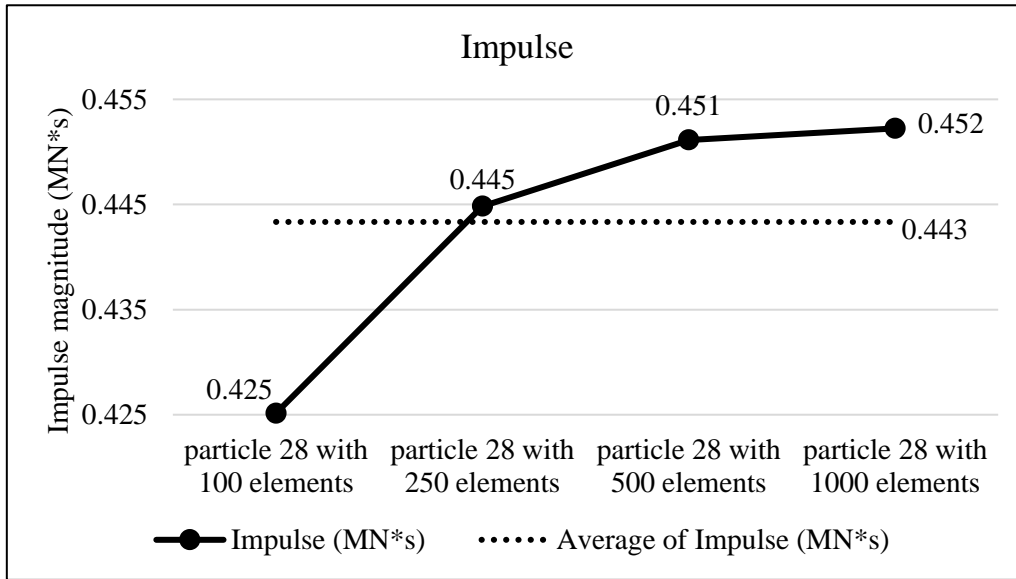


Figure A28.2 Plots of collision impulse for Particle 28.

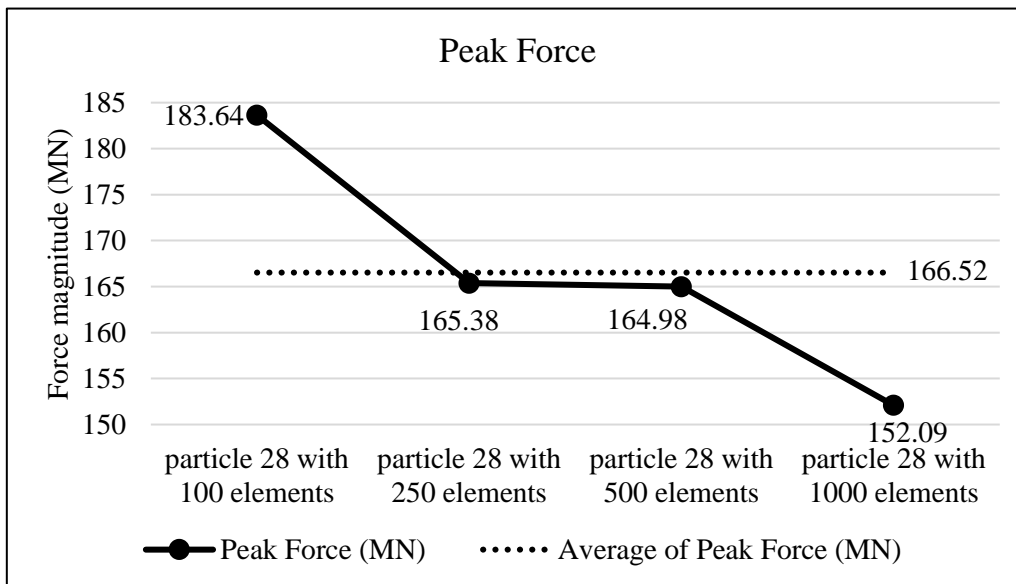


Figure A28.3 Peak collision for the four particle geometry resolutions for Particle 28.

Appendix

Collision results data analysis					
Model	particle 28 with 100 elements	particle 28 with 250 elements	particle 28 with 500 elements	particle 28 with 1000 elements	Average
Impulse (MN*s)	0.425	0.445	0.451	0.452	0.443
Percent difference from Avg. Impulse	-4.10	0.34	1.76	2.01	
Peak Force (MN)	183.64	165.38	164.98	152.09	166.52
Percent difference from Avg. Peak Force	10.28	-0.69	-0.92	-8.67	

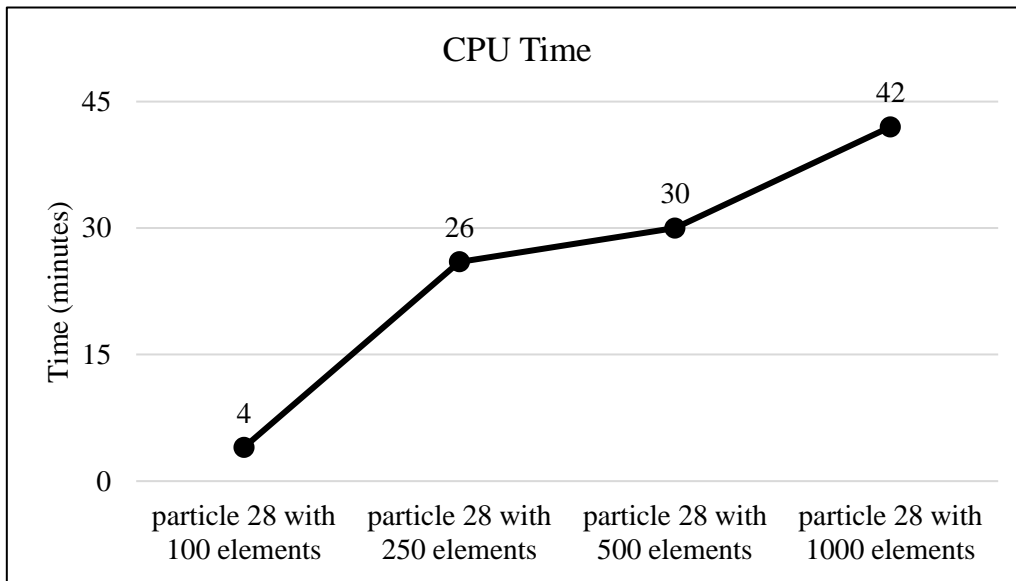


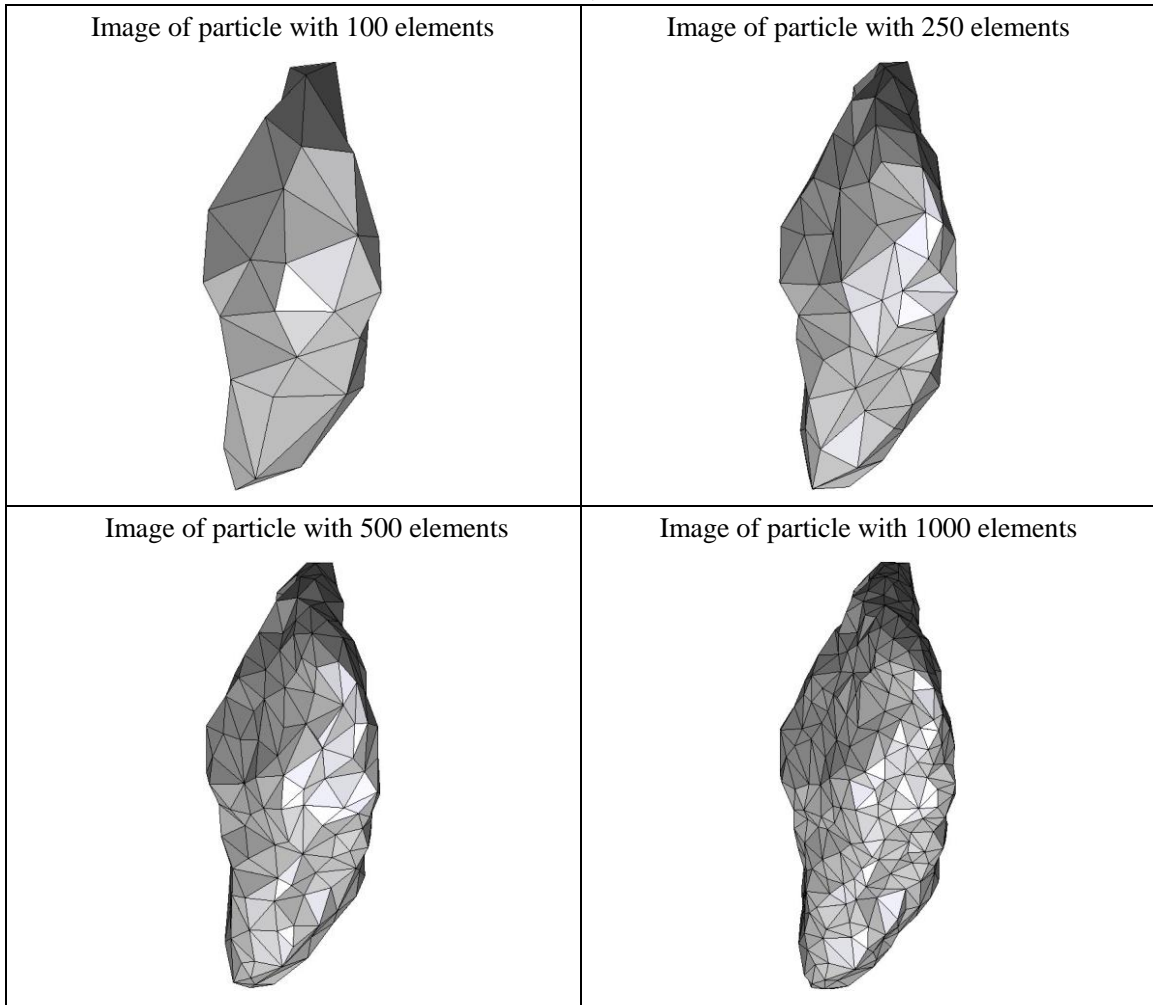
Figure A28.4 CPU computation time vs. model geometry resolution.

Appendix

Percent difference analysis compare to particle 28 with 100 elements for different group of data			
	particle 28 with 250 elements	particle 28 with 500 elements	particle 28 with 1000 elements
Impulse	4.63	6.11	6.37
Peak Force	-9.95	-10.16	-17.18
Start Time	-5.71	-5.71	-5.71
CPU Time	550.00	650.00	950.00
Simulation Time	14.00	14.00	20.00

Appendix

Summary of particle characteristics and collision simulation details for Particle 29 (of 50)



Particle statistics (part 1)								
Particle ID	# vertices	# elements	Mass (g)	Moments of Inertia			Volume (cm ³)	Sfc. Area (cm ²)
				I1	I2	I3		
				(gcm ²)	(gcm ²)	(gcm ²)		
29 (100 elements)	52	100	45.96	327928.425	263245.95	116330.3625	15.95295	40.74309
29 (250 elements)	127	250	45.96	347792.4	279284.3	121868.4875	16.43253	41.31782
29 (500 elements)	252	500	45.96	351749.3	282495.575	122886.7875	16.50176	41.49636
29 (1000 elements)	502	1000	45.96	354654.625	284857.625	123713.7375	16.56900	41.59366

Appendix

Particle Statistics (part 2)							
Particle ID	α	R_g (cm)	ψ	R_v (cm)	L (cm)	I (cm)	S (cm)
29 (100 elements)	3.03214	2.98900	0.75218	1.56165	227.28484	140.32973	74.95857
29 (250 elements)	3.07699	2.97478	0.75651	1.57715	234.43918	143.91357	76.19114
29 (500 elements)	3.08778	2.99626	0.75537	1.57936	235.86177	144.57875	76.38556
29 (1000 elements)	3.09299	20.1621	0.75564	1.58149	236.88362	145.09336	76.58731

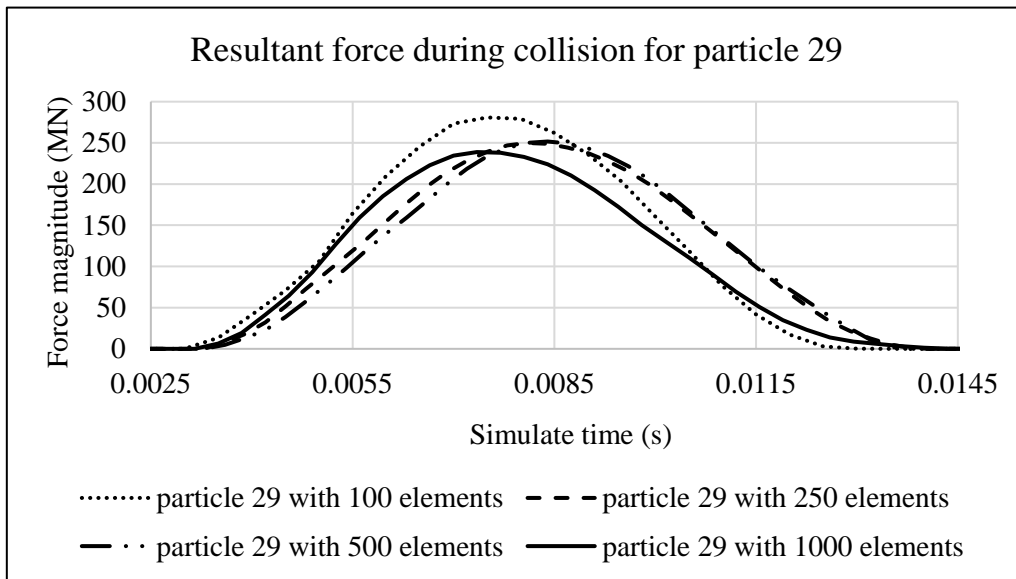


Figure A29.1 Plot of resultant forces during collision event for Particle 29

Appendix

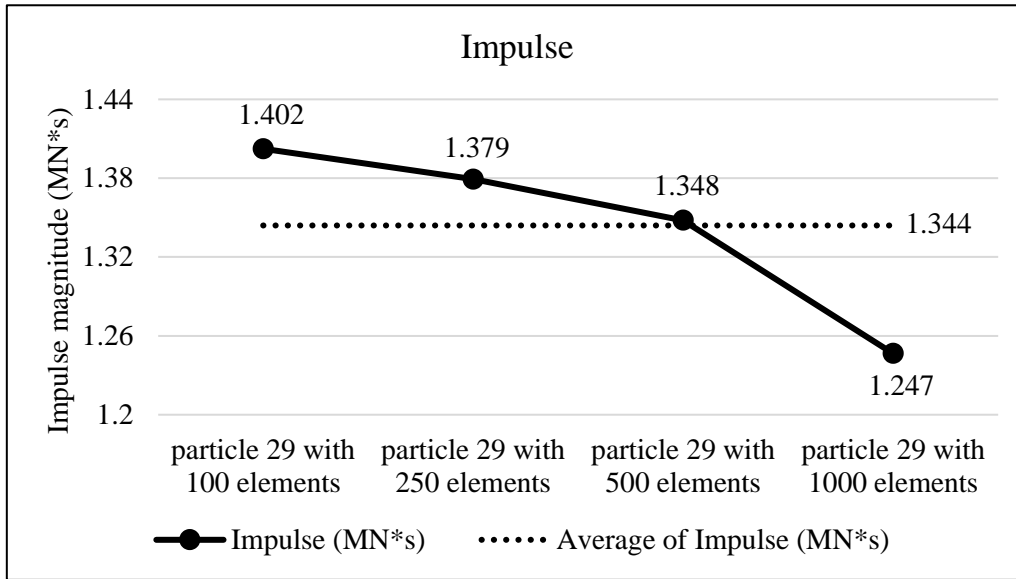


Figure A29.2 Plots of collision impulse for Particle 29

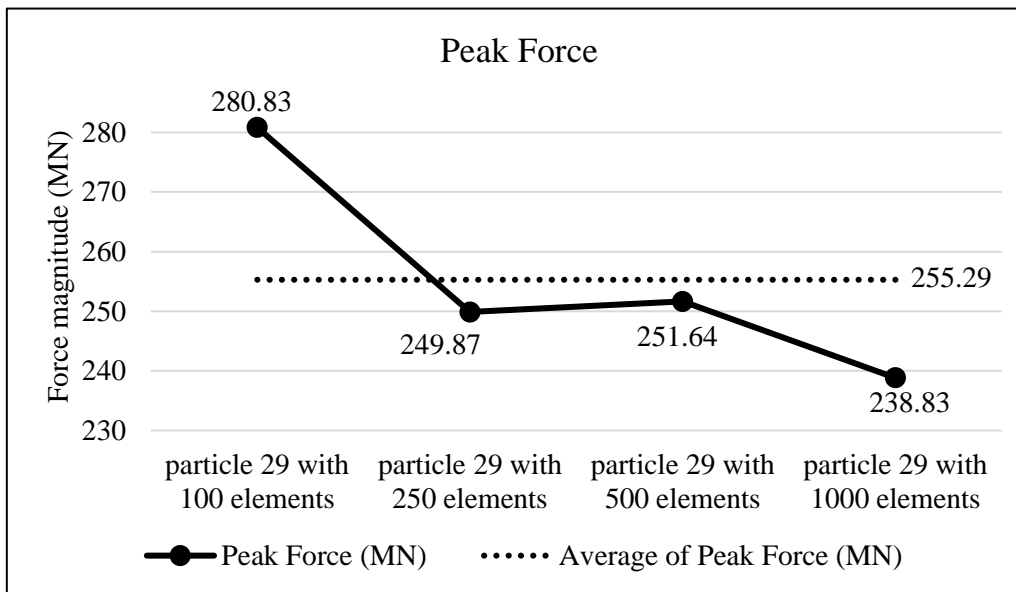


Figure A29.3 Peak collision for the four particle geometry resolutions for Particle 29

Appendix

Collision results data analysis					
Model	particle 29 with 100 elements	particle 29 with 250 elements	particle 29 with 500 elements	particle 29 with 1000 elements	Average
Impulse (MN*s)	1.402	1.379	1.348	1.247	1.344
Percent difference from Avg. Impulse	4.34	2.62	0.29	-7.25	
Peak Force (MN)	280.83	249.87	251.64	238.83	255.29
Percent difference from Avg. Peak Force	10.00	-2.12	-1.43	-6.45	

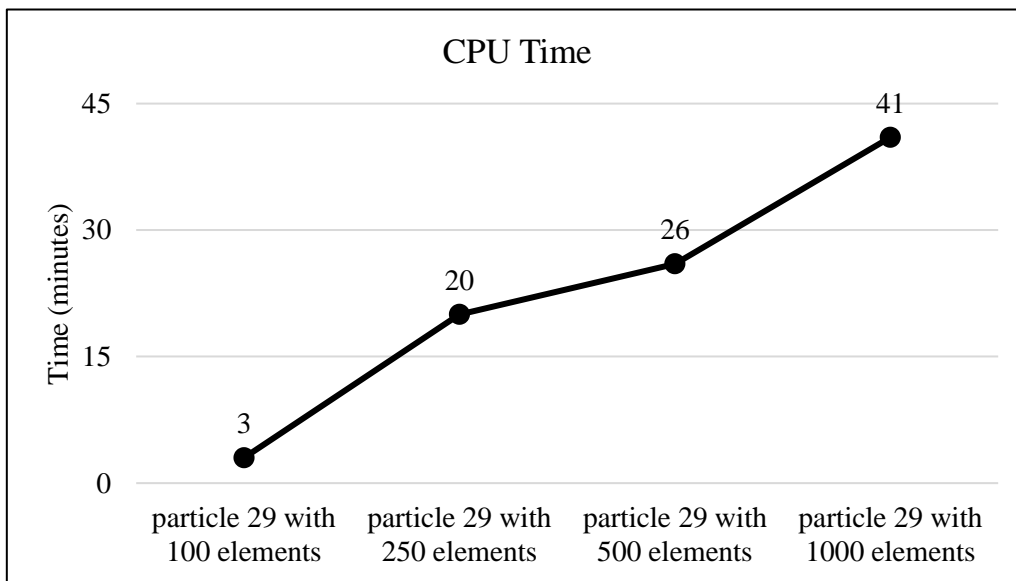


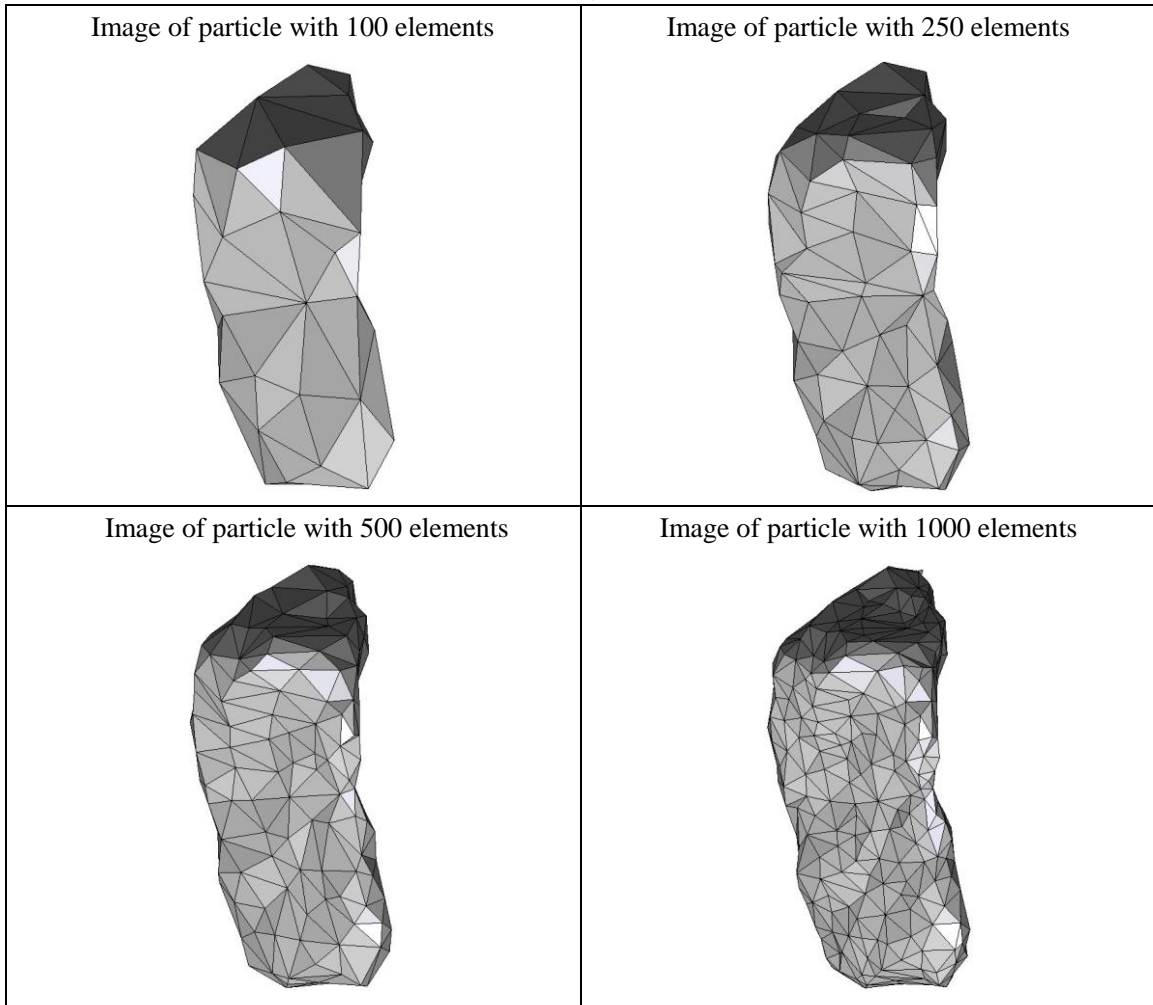
Figure A29.4 CPU computation time vs. model geometry resolution

Appendix

Percent difference analysis compare to particle 29 with 100 elements for different group of data			
	particle 29 with 250 elements	particle 29 with 500 elements	particle 29 with 1000 elements
Impulse	-1.65	-3.88	-11.11
Peak Force	-11.02	-10.39	-14.95
Start Time	-5.71	-5.71	0.00
CPU Time	566.67	766.67	1266.67
Simulation Time	10.53	10.53	14.21

Appendix

Summary of particle characteristics and collision simulation details for Particle 30 (of 50)



Particle statistics (part 1)								
Particle ID	# vertices	# elements	Mass (g)	Moments of Inertia			Volume (cm ³)	Sfc. Area (cm ²)
				I1	I2	I3		
				(gcm ²)	(gcm ²)	(gcm ²)		
30 (100 elements)	52	100	19.176	81146.10625	68499.9	27049.93438	6.64312	23.63416
30 (250 elements)	127	250	19.176	83919.275	70628.775	27985.2375	6.71888	23.94465
30 (500 elements)	252	500	19.176	84991.85	71507.81875	28452.46563	6.76131	24.09203
30 (1000 elements)	502	1000	19.176	85631.49375	72067.3875	28584.00938	6.78159	24.10690

Appendix

Particle Statistics (part 2)							
Particle ID	α	R_g (cm)	ψ	R_v (cm)	L (cm)	I (cm)	S (cm)
30 (100 elements)	2.91743	2.17278	0.72309	1.16617	178.79043	101.73728	61.28348
30 (250 elements)	2.93476	2.16825	0.71913	1.17058	181.65989	103.74171	61.89947
30 (500 elements)	2.92480	2.16429	0.71774	1.17304	182.72208	104.56879	62.47326
30 (1000 elements)	2.93194	2.15846	0.71873	1.17421	183.48228	104.83229	62.58058

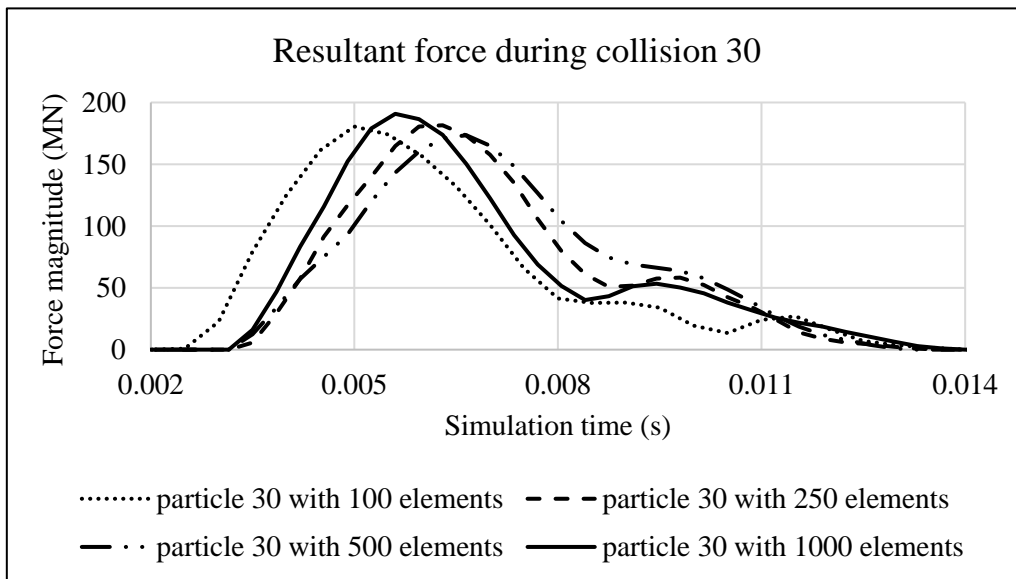


Figure A30.1 Plot of resultant forces during collision event for Particle 30

Appendix

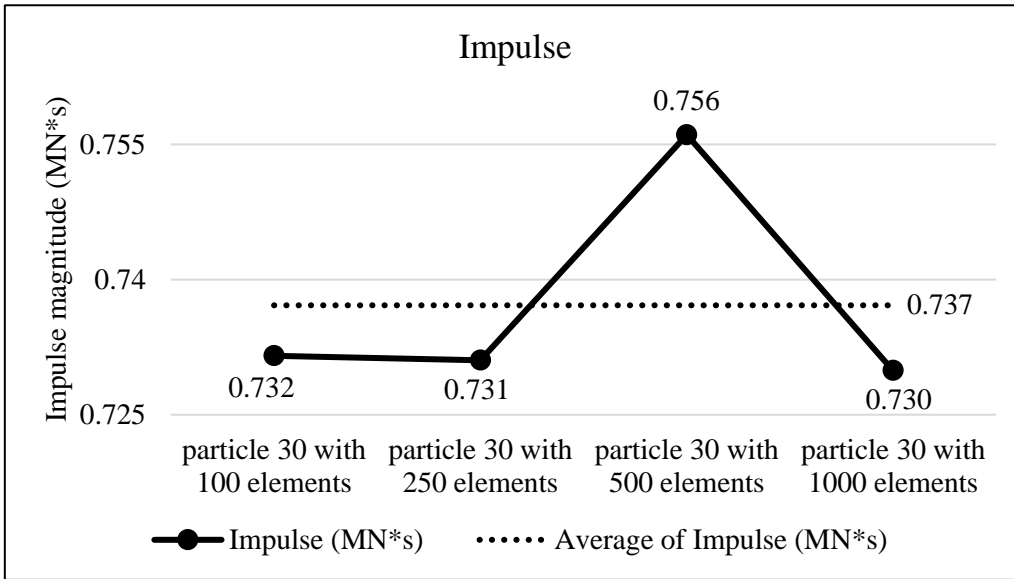


Figure A30.2 Plots of collision impulse for Particle 30

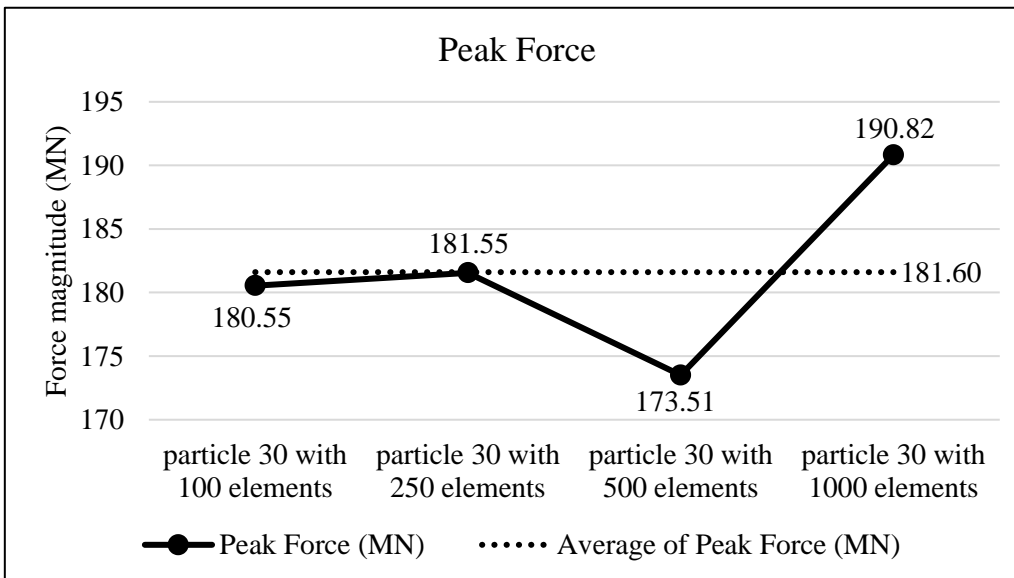


Figure A30.3 Peak collision for the four particle geometry resolutions for Particle 30

Appendix

Collision results data analysis					
Model	particle 30 with 100 elements	particle 30 with 250 elements	particle 30 with 500 elements	particle 30 with 1000 elements	Average
Impulse (MN*s)	0.732	0.731	0.756	0.730	0.737
Percent difference from Avg. Impulse	-0.76	-0.83	2.57	-0.98	
Peak Force (MN)	180.55	181.55	173.51	190.82	181.60
Percent difference from Avg. Peak Force	-0.58	-0.03	-4.46	5.07	

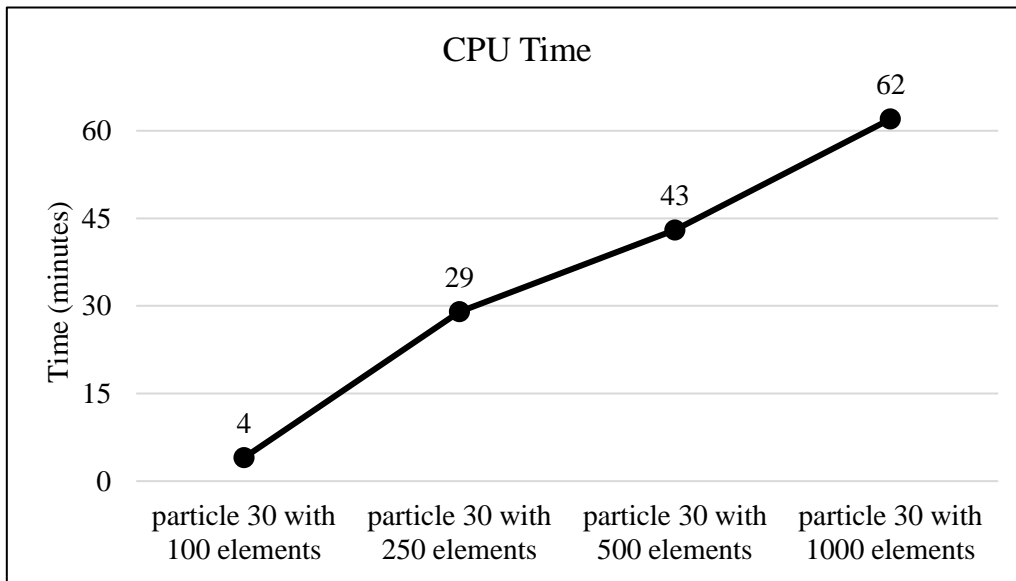


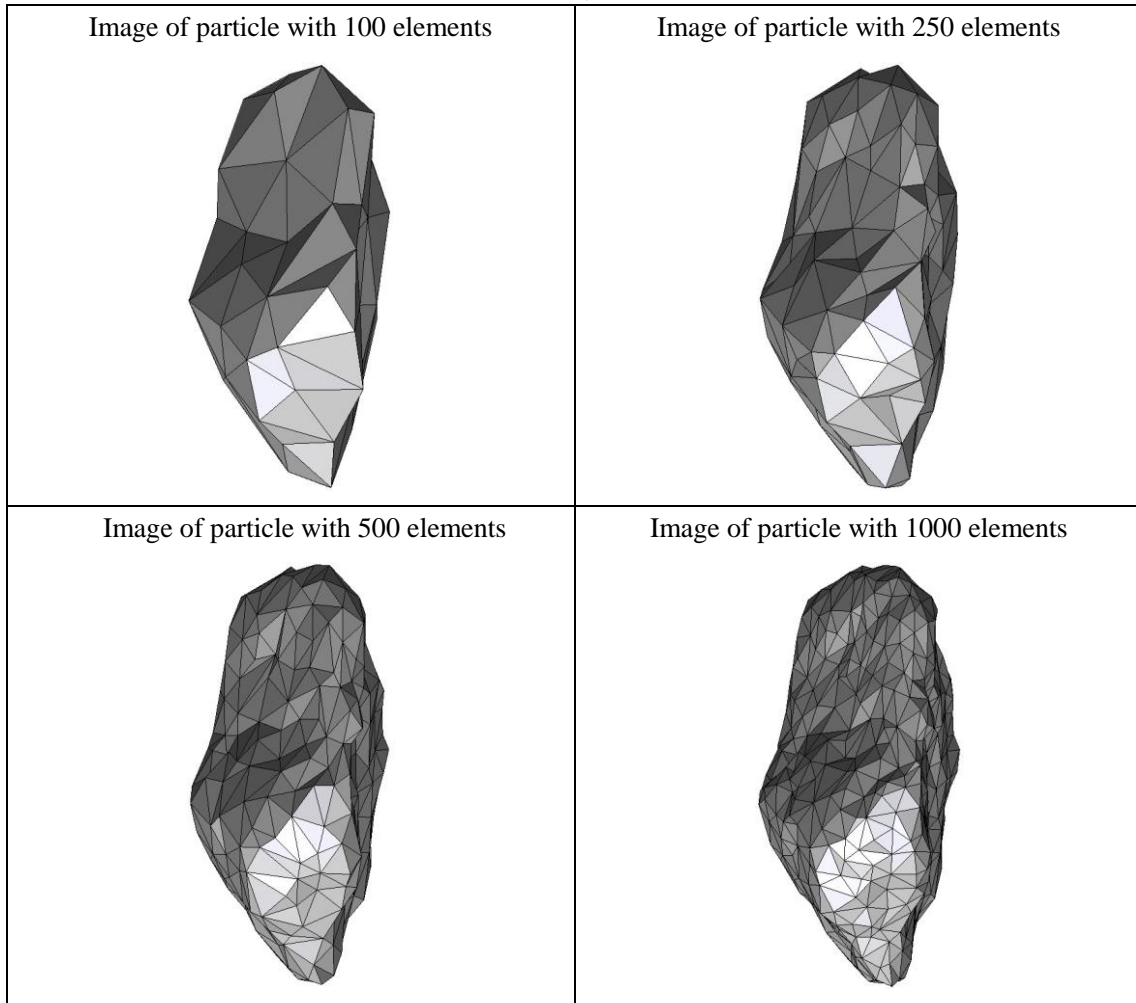
Figure A30.4 CPU computation time vs. model geometry resolution

Appendix

Percent difference analysis compare to particle 30 with 100 elements for different group of data			
	particle 30 with 250 elements	particle 30 with 500 elements	particle 30 with 1000 elements
Impulse	-0.07	3.35	-0.23
Peak Force	0.56	-3.90	5.69
Start Time	40.00	40.00	26.00
CPU Time	625.00	975.00	1450.00
Simulation Time	-11.74	-17.83	-5.65

Appendix

Summary of particle characteristics and collision simulation details for Particle 31 (of 50)



Particle statistics (part 1)								
Particle ID	# vertices	# elements	Mass (g)	Moments of Inertia			Volume (cm ³)	Sfc. Area (cm ²)
				I1	I2	I3		
				(gcm ²)	(gcm ²)	(gcm ²)		
31 (100 elements)	52	100	46.717	314320.875	261278.375	125557.0625	16.36542	41.17912
31 (250 elements)	127	250	46.717	328182.075	274063.45	130394.075	16.74717	41.76545
31 (500 elements)	252	500	46.717	331516.45	276973.525	131605.7625	16.82825	42.04230
31 (1000 elements)	502	1000	46.717	333823.675	279174.35	132398.6625	16.89808	42.07919

Appendix

Particle Statistics (part 2)							
Particle ID	α	R_g (cm)	ψ	R_v (cm)	L (cm)	I (cm)	S (cm)
31 (100 elements)	2.49123	2.90187	0.75699	1.57500	219.46948	138.25719	88.09680
31 (250 elements)	2.48720	2.87931	0.75793	1.58715	224.72437	140.52729	90.35245
31 (500 elements)	2.48762	2.88788	0.75537	1.58971	225.91965	141.14891	90.81760
31 (1000 elements)	2.48624	2.88311	0.75679	1.59190	226.79795	141.48945	91.22122

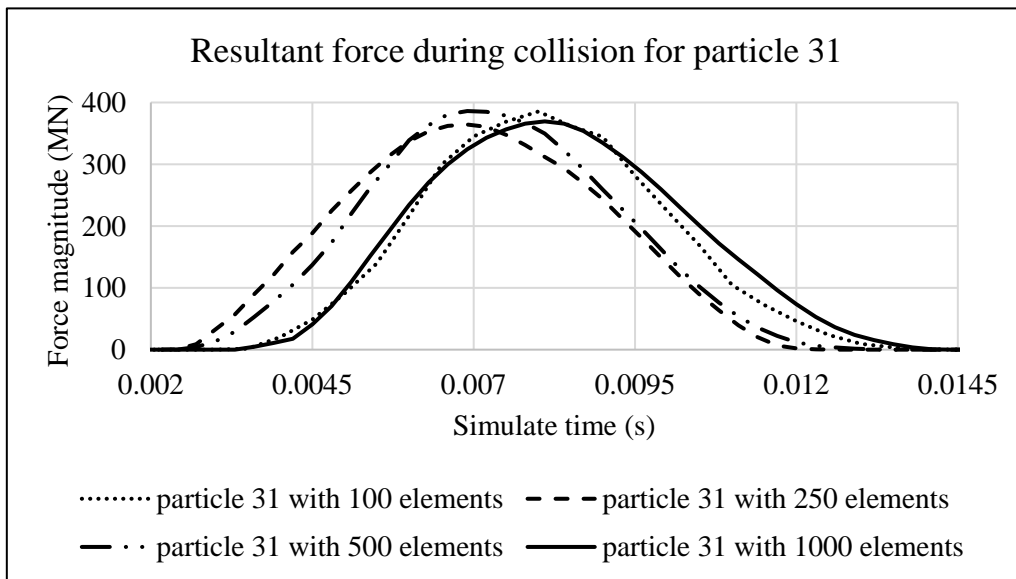


Figure A31.1 Plot of resultant forces during collision event for Particle 31

Appendix

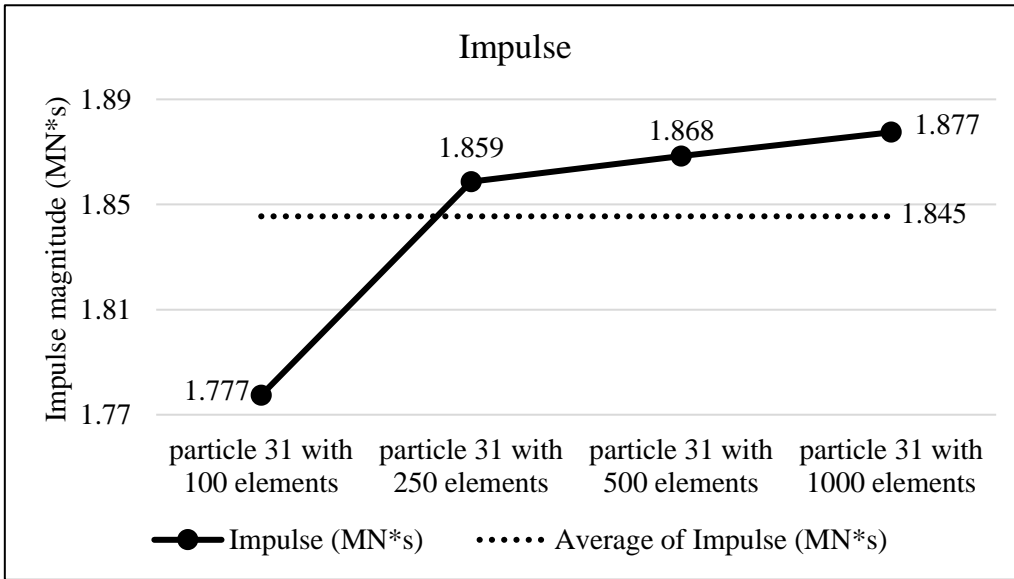


Figure A31.2 Plots of collision impulse for Particle 31

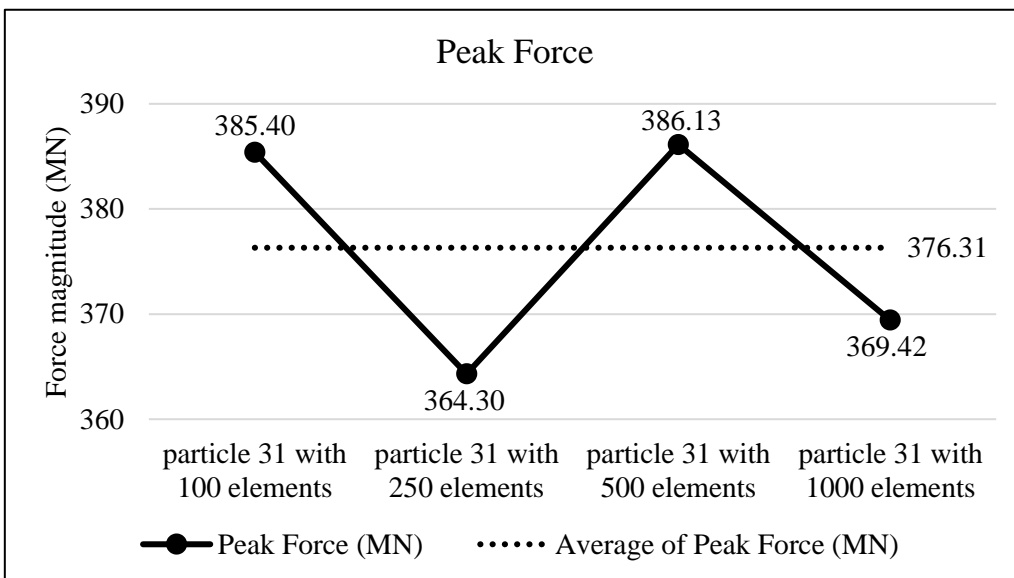


Figure A31.3 Peak collision for the four particle geometry resolutions for Particle 31

Appendix

Collision results data analysis					
Model	particle 31 with 100 elements	particle 31 with 250 elements	particle 31 with 500 elements	particle 31 with 1000 elements	Average
Impulse (MN*s)	1.777	1.859	1.868	1.877	1.845
Percent difference from Avg. Impulse	-3.69	0.71	1.24	1.73	
Peak Force (MN)	385.40	364.30	386.13	369.42	376.31
Percent difference from Avg. Peak Force	2.41	-3.19	2.61	-1.83	

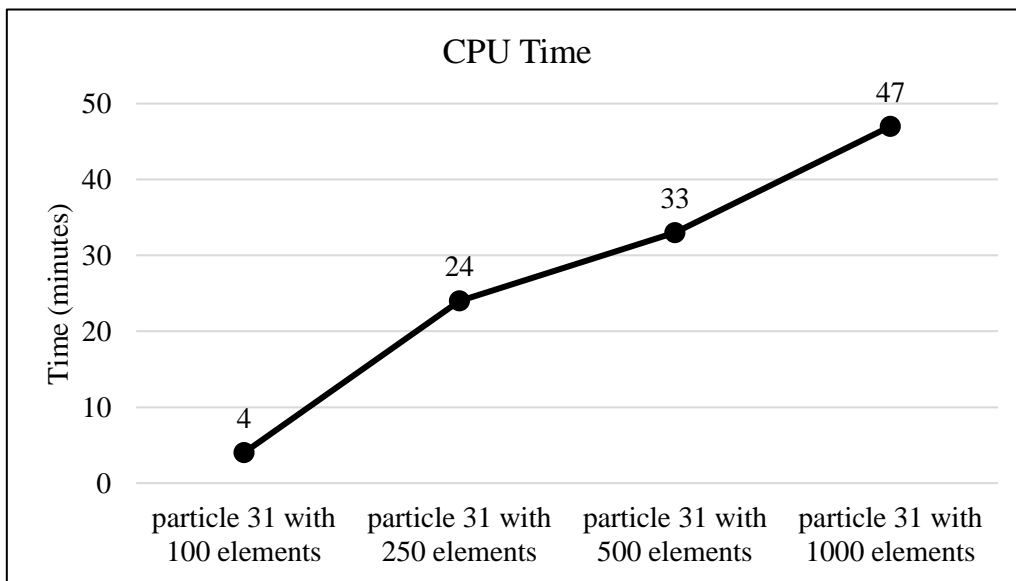


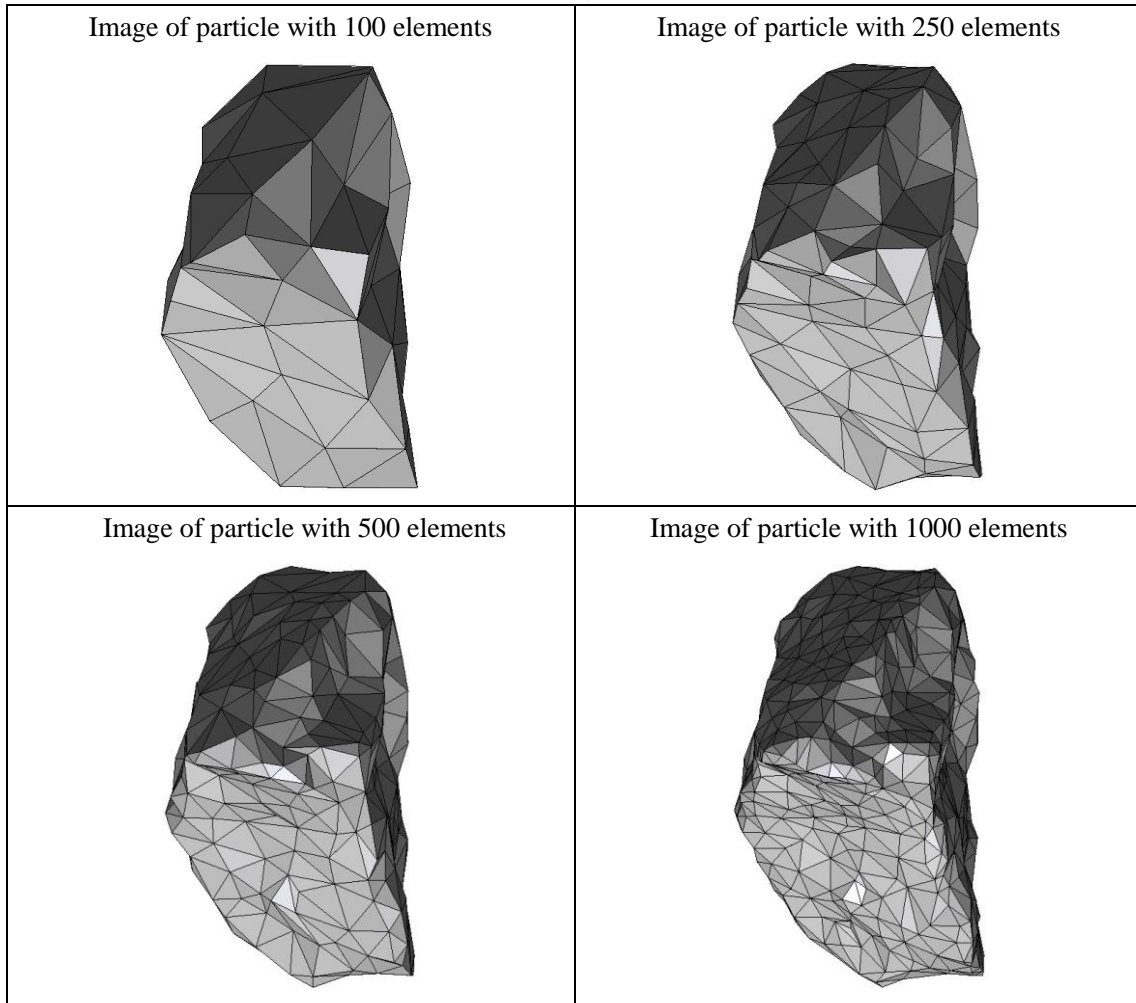
Figure A31.4 CPU computation time vs. model geometry resolution

Appendix

Percent difference analysis compare to particle 31 with 100 elements for different group of data			
	particle 31 with 250 elements	particle 31 with 500 elements	particle 31 with 1000 elements
Impulse	4.57	5.12	5.63
Peak Force	-5.47	0.19	-4.15
Start Time	-31.43	-22.86	-5.71
CPU Time	500.00	725.00	1075.00
Simulation Time	-2.86	0.00	2.86

Appendix

Summary of particle characteristics and collision simulation details for Particle 32 (of 50)



Particle statistics (part 1)								
Particle ID	# vertices	# elements	Mass (g)	Moments of Inertia			Volume (cm ³)	Sfc. Area (cm ²)
				I1	I2	I3		
				(gcm ²)	(gcm ²)	(gcm ²)		
32 (100 elements)	52	100	18.909	62932.83125	52061.425	37187.88125	7.12510	22.97069
32 (250 elements)	127	250	18.909	64749.44375	53631.48125	38313.19063	7.24265	23.11998
32 (500 elements)	252	500	18.909	65283.35	54057.03125	38485.97813	7.26241	23.04311
32 (1000 elements)	502	1000	18.909	65595.83125	54317.49375	38587.21875	7.27624	23.01830

Appendix

Particle Statistics (part 2)							
Particle ID	α	R_g (cm)	ψ	R_v (cm)	L (cm)	I (cm)	S (cm)
32 (100 elements)	1.71947	2.07321	0.77954	1.19372	143.43605	112.72997	83.41892
32 (250 elements)	1.71586	2.02642	0.78300	1.20024	145.50553	114.32760	84.80024
32 (500 elements)	1.72223	2.02629	0.78704	1.20133	146.21858	114.65226	84.90063
32 (1000 elements)	1.72569	2.03509	0.78889	1.20210	146.64448	114.82886	84.97725

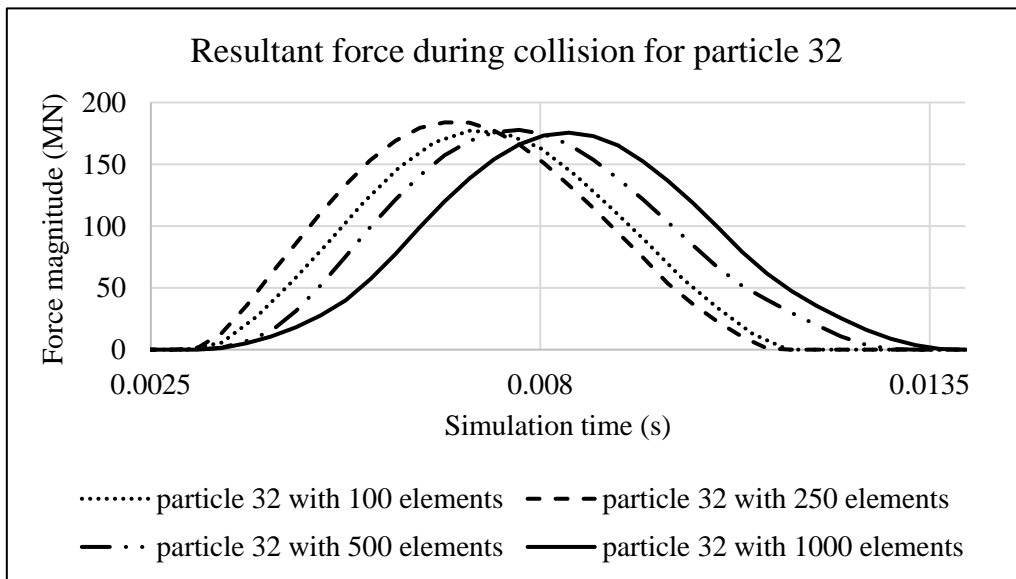


Figure A32.1 Plot of resultant forces during collision event for Particle 32

Appendix

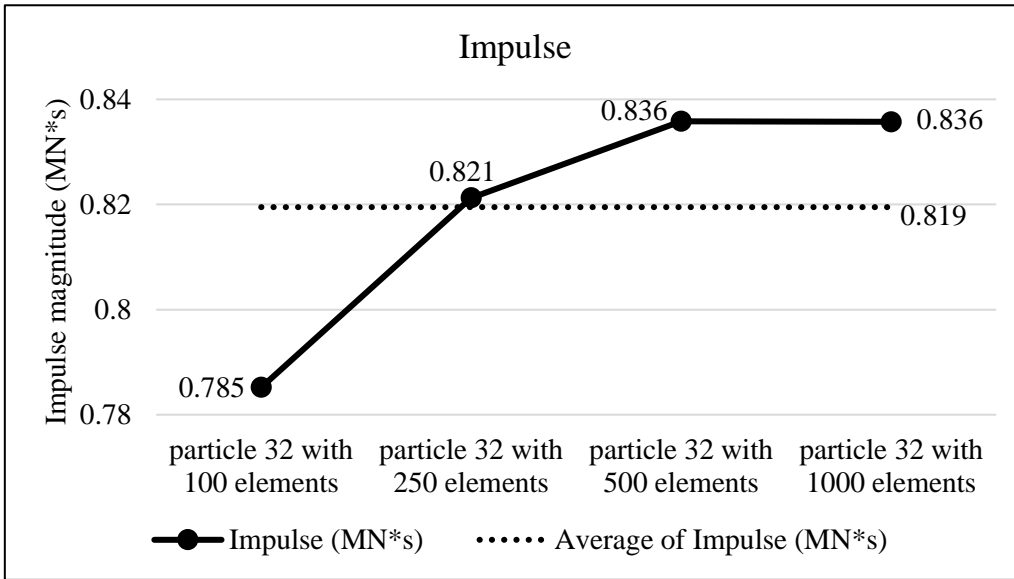


Figure A32.2 Plots of collision impulse for Particle 32

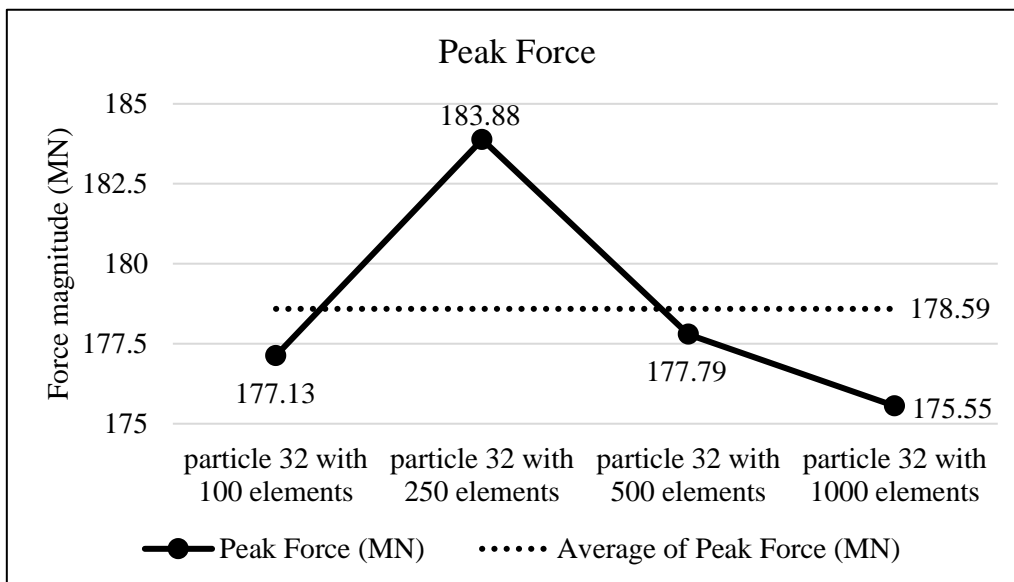


Figure A32.3 Peak collision for the four particle geometry resolutions for Particle 32

Appendix

Collision results data analysis					
Model	particle 32 with 100 elements	particle 32 with 250 elements	particle 32 with 500 elements	particle 32 with 1000 elements	Average
Impulse (MN*s)	0.785	0.821	0.836	0.836	0.819
Percent difference from Avg. Impulse	-4.19	0.21	1.99	1.98	
Peak Force (MN)	177.13	183.88	177.79	175.55	178.59
Percent difference from Avg. Peak Force	-0.82	2.96	-0.45	-1.70	

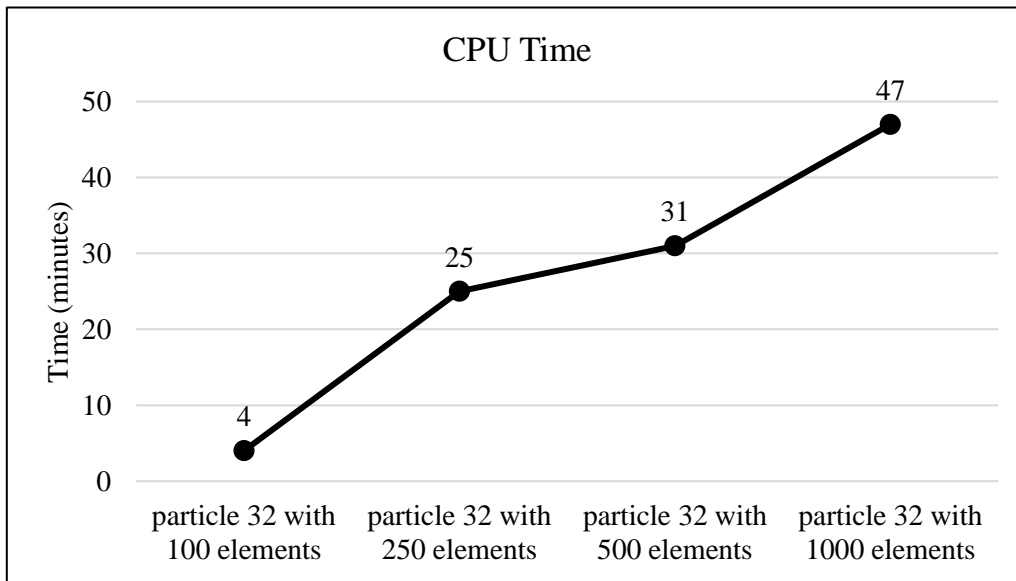
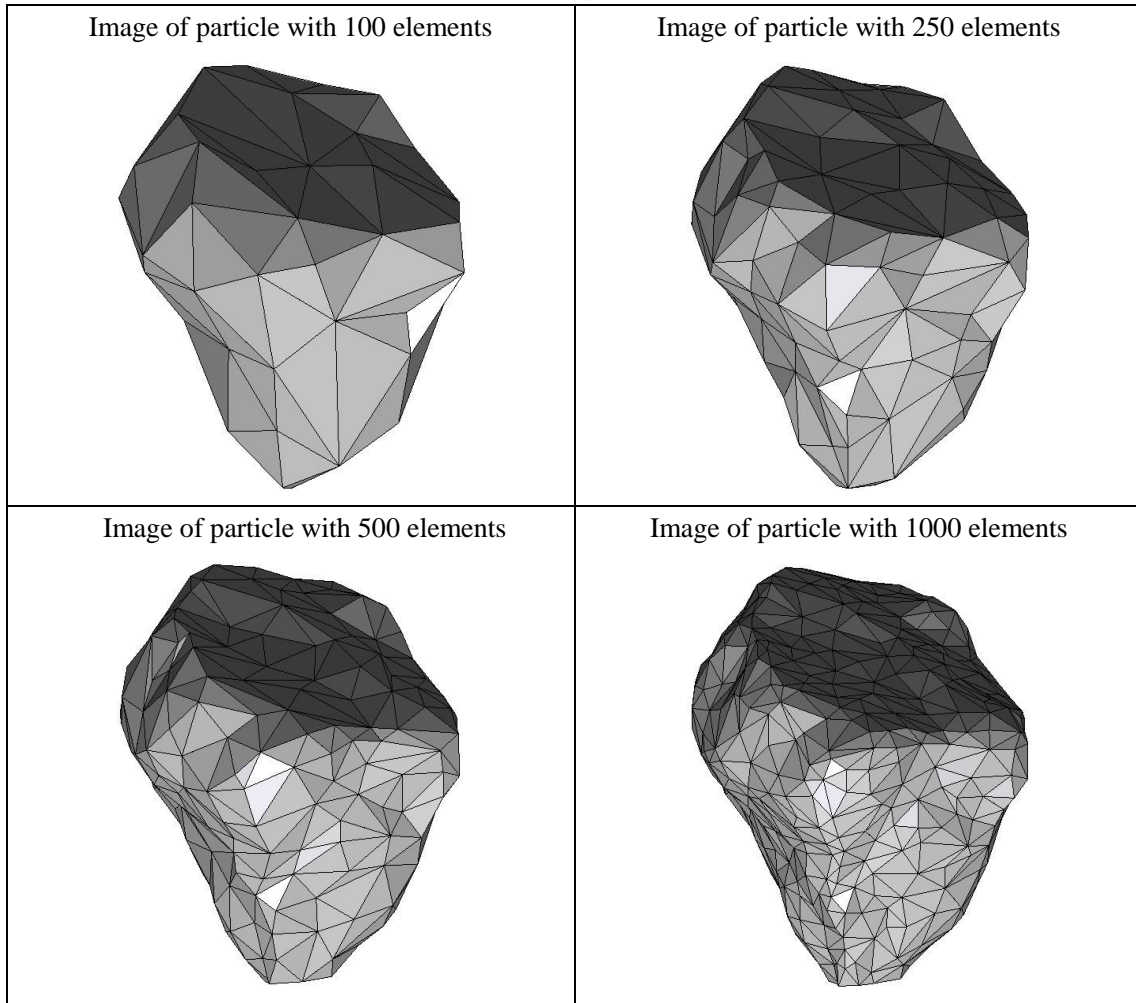


Figure A32.4 CPU computation time vs. model geometry resolution

Appendix

Percent difference analysis compare to particle 32 with 100 elements for different group of data			
	particle 32 with 250 elements	particle 32 with 500 elements	particle 32 with 1000 elements
Impulse	4.59	6.45	6.44
Peak Force	3.81	0.38	-0.89
Start Time	-10.00	0.00	0.00
CPU Time	525.00	675.00	1075.00
Simulation Time	7.33	26.00	35.33

Summary of particle characteristics and collision simulation details for Particle 33 (of 50)



Particle statistics (part 1)								
Particle ID	# vertices	# elements	Mass (g)	Moments of Inertia			Volume (cm ³)	Sfc. Area (cm ²)
				I1	I2	I3		
				(gcm ²)	(gcm ²)	(gcm ²)		
33 (100 elements)	52	100	23.259	66025.13125	58542.75625	47192.67188	8.20484	22.79434
33 (250 elements)	127	250	23.259	68277.19375	60066.9562	48679.19375	8.35635	23.01246
33 (500 elements)	252	500	23.259	68680.59375	60362.81875	48979.475	8.38134	23.04391
33 (1000 elements)	502	1000	23.259	68937.71875	60589.94375	49163.58438	8.39813	23.01307

Appendix

Particle Statistics (part 2)							
Particle ID	α	R_g (cm)	ψ	R_v (cm)	L (cm)	I (cm)	S (cm)
33 (100 elements)	1.39588	1.79998	0.86305	1.25120	128.97051	108.41367	92.39342
33 (250 elements)	1.40305	1.75960	0.77931	1.25886	130.86489	110.58731	93.27183
33 (500 elements)	1.40322	1.75799	0.86591	1.26011	131.19218	110.98298	93.49368
33 (1000 elements)	1.40319	1.75854	0.86822	1.26095	131.43786	111.19015	93.67068

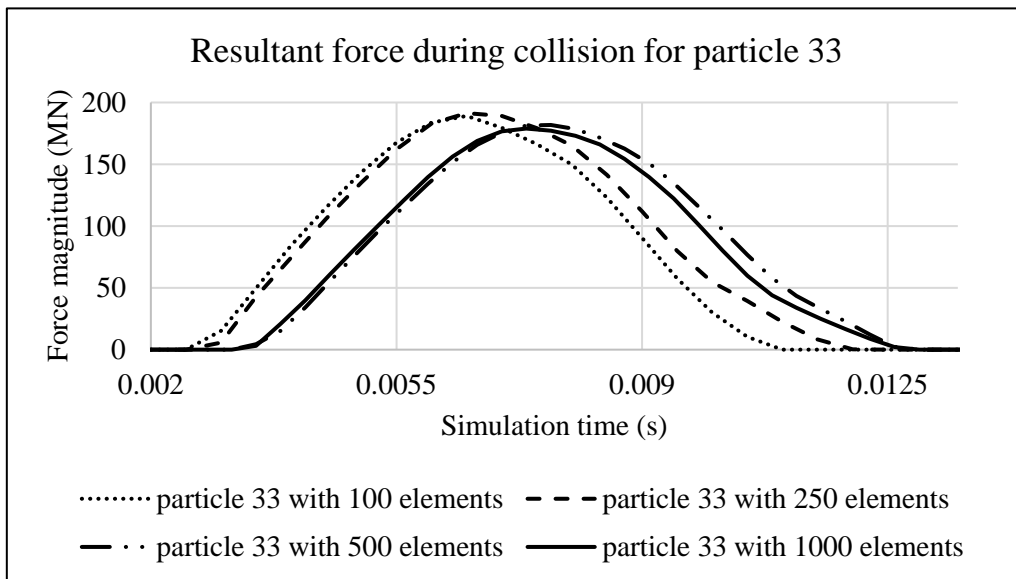


Figure A33.1 Plot of resultant forces during collision event for Particle 33

Appendix

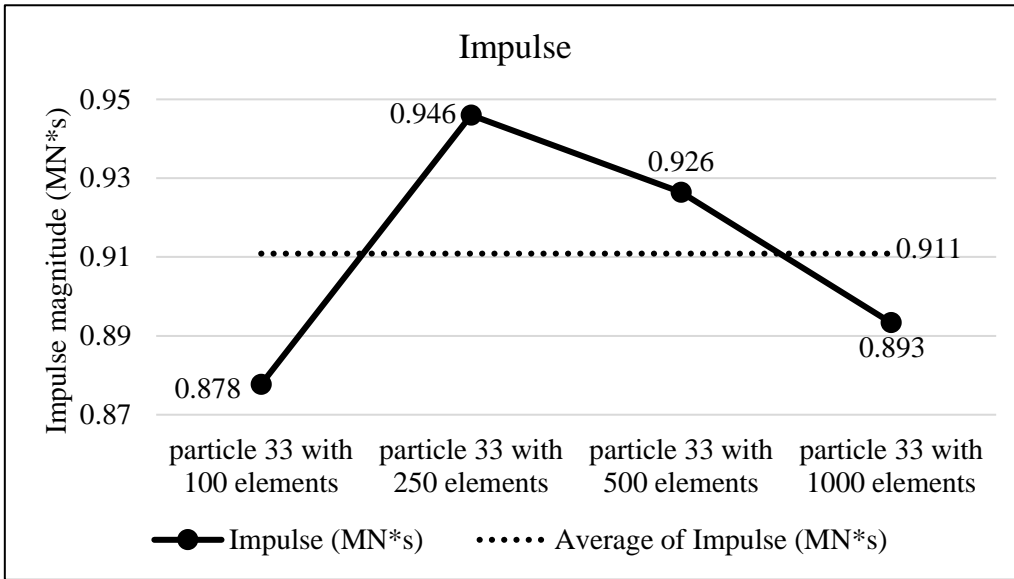


Figure A33.2 Plots of collision impulse for Particle 33

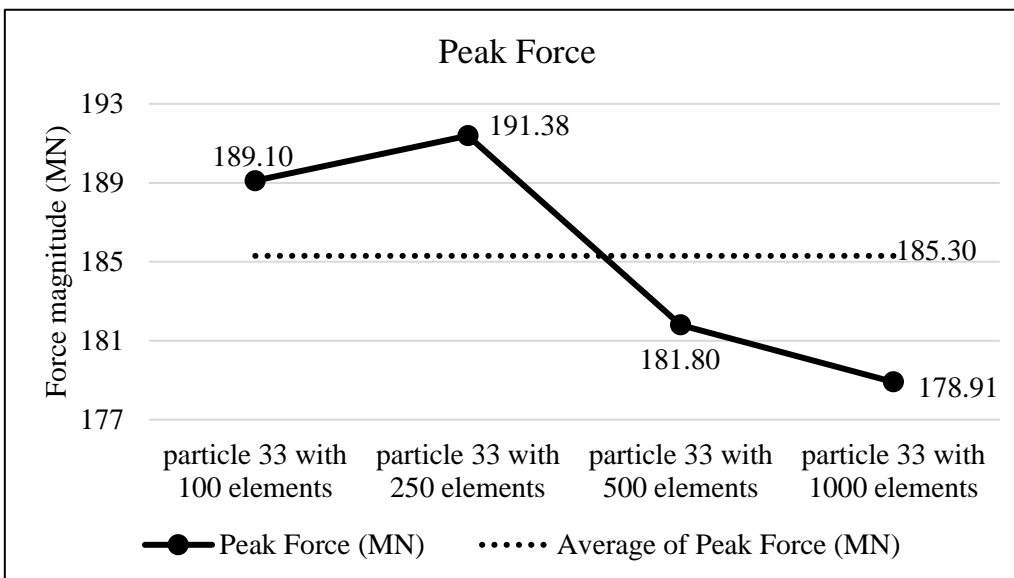


Figure A33.3 Peak collision for the four particle geometry resolutions for Particle 33

Appendix

Collision results data analysis					
Model	particle 33 with 100 elements	particle 33 with 250 elements	particle 33 with 500 elements	particle 33 with 1000 elements	Average
Impulse (MN*s)	0.878	0.946	0.926	0.893	0.911
Percent difference from Avg. Impulse	-3.64	3.86	1.71	-1.92	
Peak Force (MN)	189.10	191.38	181.80	178.91	185.30
Percent difference from Avg. Peak Force	2.05	3.28	-1.89	-3.45	

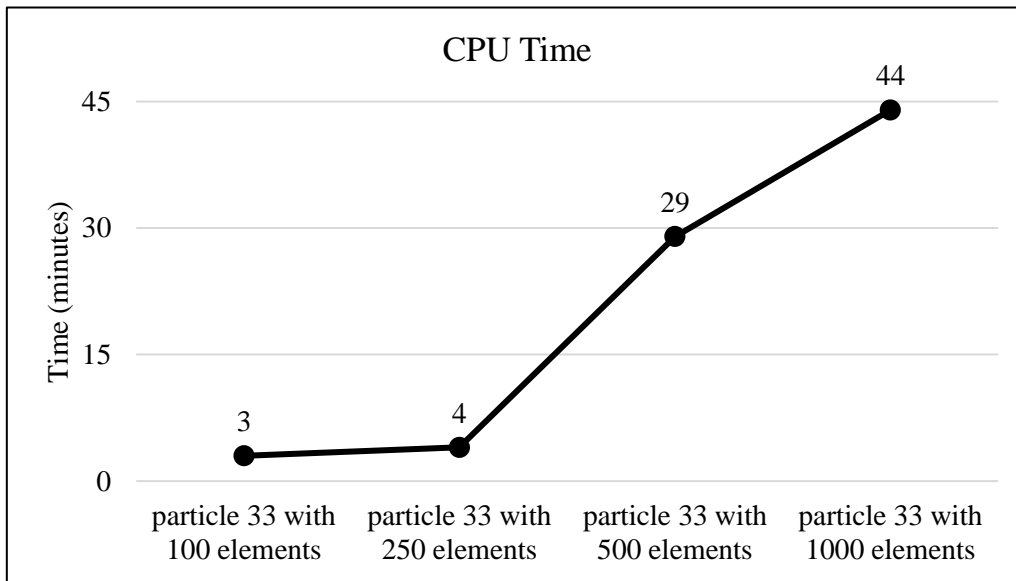
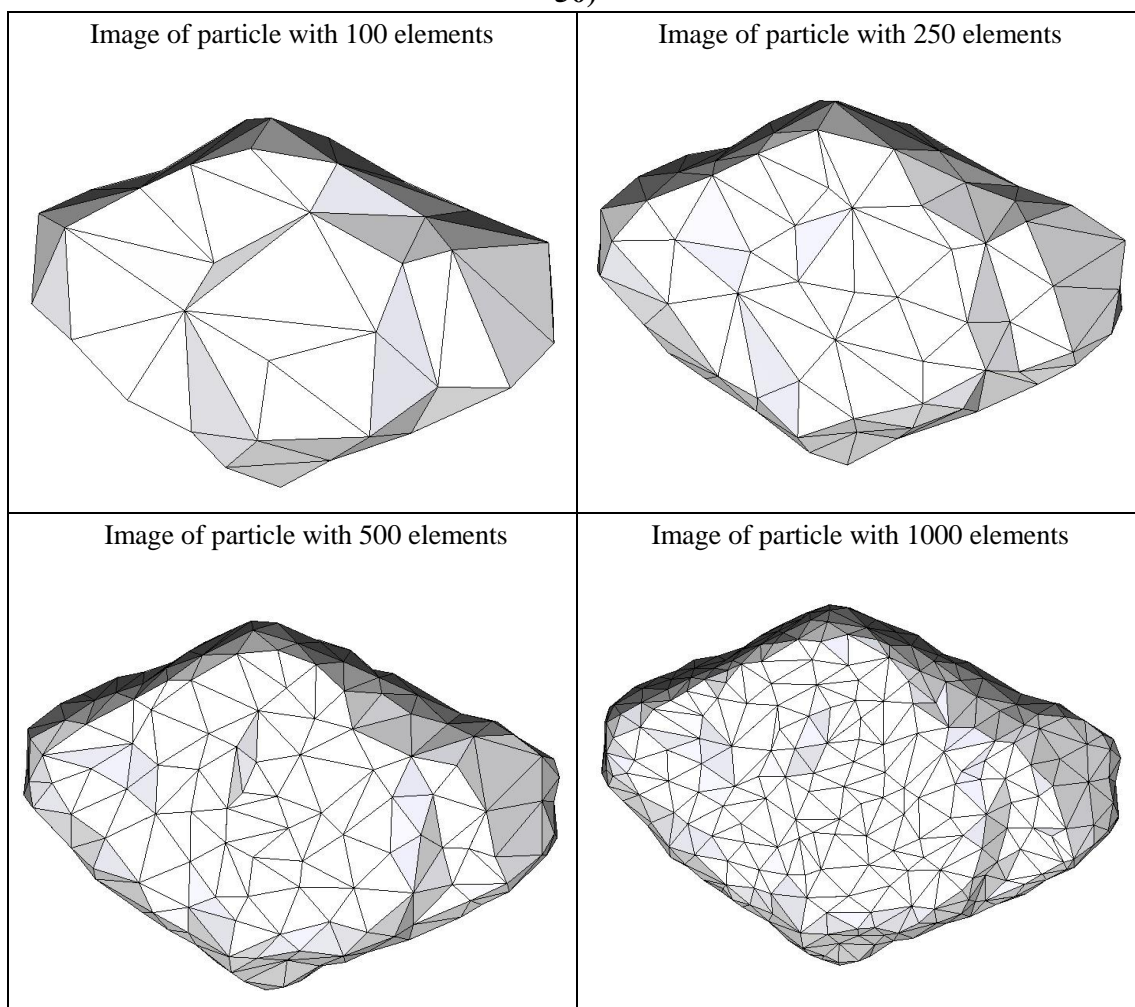


Figure A33.4 CPU computation time vs. model geometry resolution

Appendix

Percent difference analysis compare to particle 33 with 100 elements for different group of data			
	particle 33 with 250 elements	particle 33 with 500 elements	particle 33 with 1000 elements
Impulse	7.78	5.55	1.78
Peak Force	1.21	-3.86	-5.39
Start Time	0.00	16.67	16.67
CPU Time	33.33	866.67	1366.67
Simulation Time	12.50	13.75	13.75

Summary of particle characteristics and collision simulation details for Particle 34 (of 50)



Particle statistics (part 1)								
Particle ID	# vertices	# elements	Mass (g)	Moments of Inertia			Volume (cm ³)	Sfc. Area (cm ²)
				I1	I2	I3		
				(gcm ²)	(gcm ²)	(gcm ²)		
34 (100 elements)	52	100	13.774	54402.31875	38431.52813	19748.56719	4.71834	19.97886
34 (250 elements)	127	250	13.774	56230.55625	39841.30625	20160.74844	4.76785	19.94657
34 (500 elements)	252	500	13.774	56912.5875	40287.27188	20417.3625	4.79586	19.94849
34 (1000 elements)	502	1000	13.774	57319.9625	40575.275	20554.57188	4.81189	19.93647

Particle Statistics (part 2)							
Particle ID	α	R_g (cm)	ψ	R_v (cm)	L (cm)	I (cm)	S (cm)
34 (100 elements)	4.39842	2.08313	0.68094	1.04048	162.88081	113.86933	37.03165
34 (250 elements)	4.48638	2.12009	0.68680	1.04411	165.99983	115.18572	37.00087
34 (500 elements)	4.49981	2.10637	0.68942	1.04615	166.94987	115.95945	37.10153
34 (1000 elements)	4.50555	2.107	0.69137	1.04731	167.55559	116.36036	37.18869

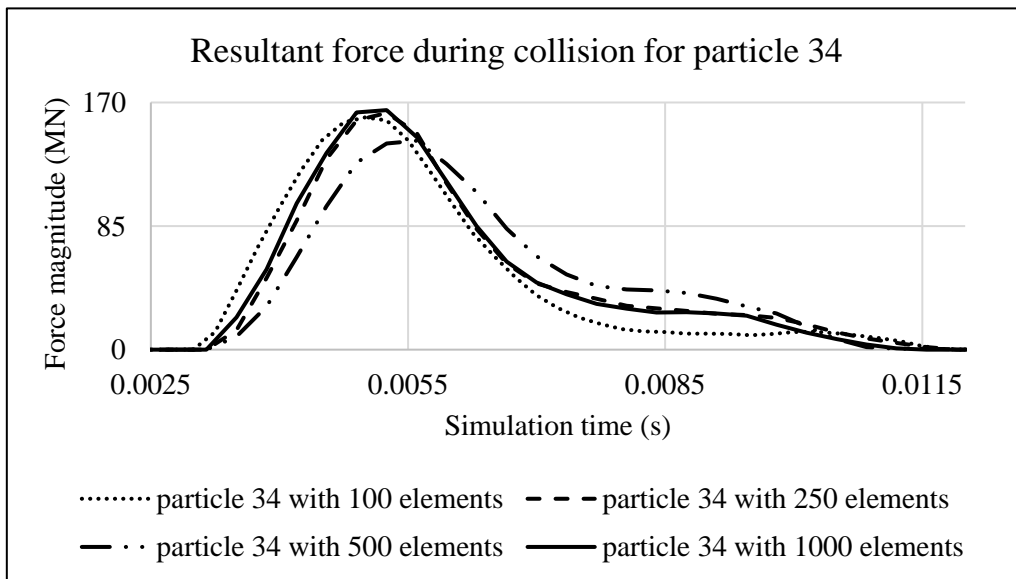


Figure A34.1 Plot of resultant forces during collision event for Particle 34

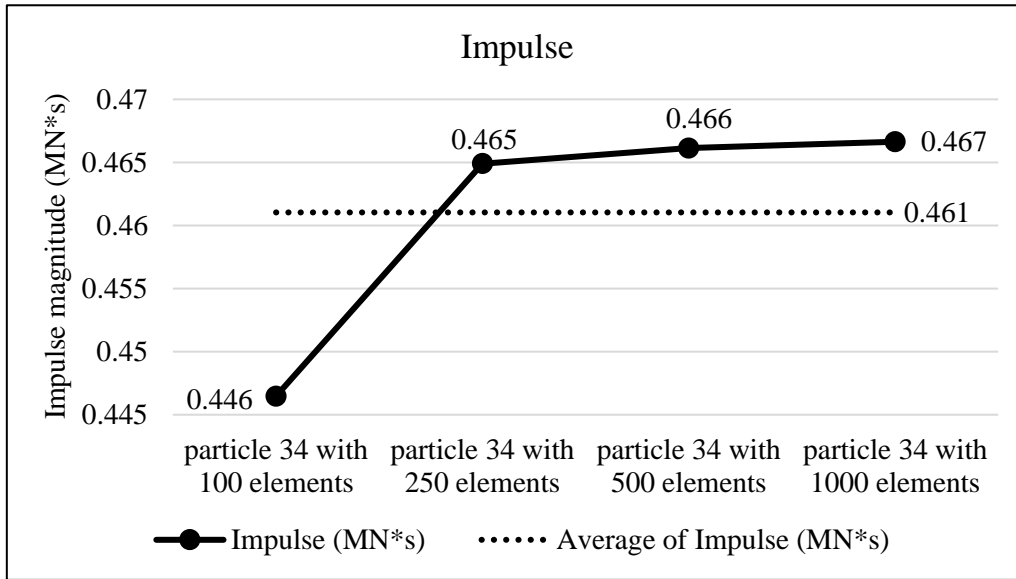


Figure A34.2 Plots of collision impulse for Particle 34

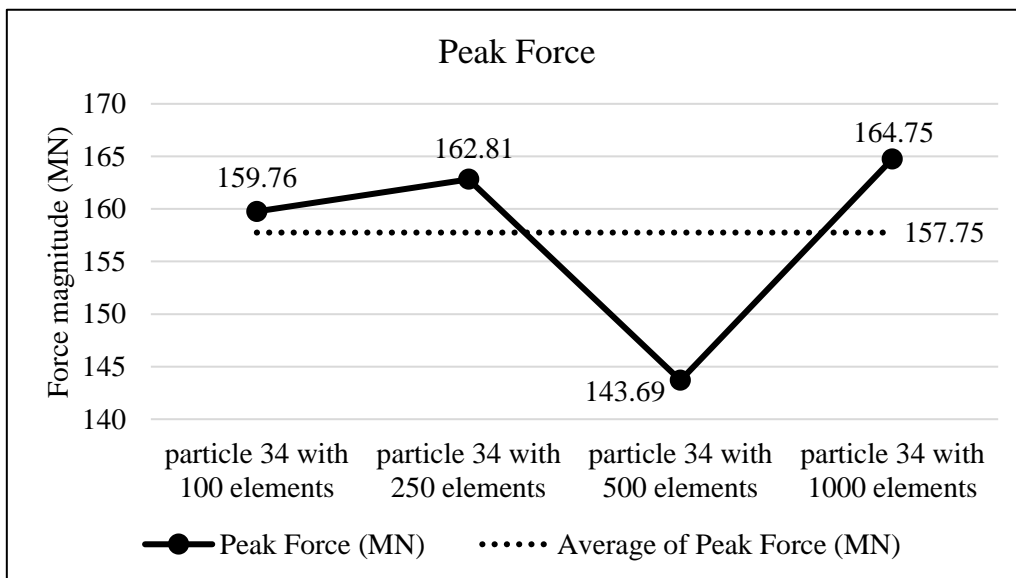


Figure A34.3 Peak collision for the four particle geometry resolutions for Particle 34

Appendix

Collision results data analysis					
Model	particle 34 with 100 elements	particle 34 with 250 elements	particle 34 with 500 elements	particle 34 with 1000 elements	Average
Impulse (MN*s)	0.446	0.465	0.466	0.467	0.461
Percent difference from Avg. Impulse	-3.16	0.84	1.11	1.22	
Peak Force (MN)	159.76	162.81	143.69	164.75	157.75
Percent difference from Avg. Peak Force	1.27	3.21	-8.92	4.44	

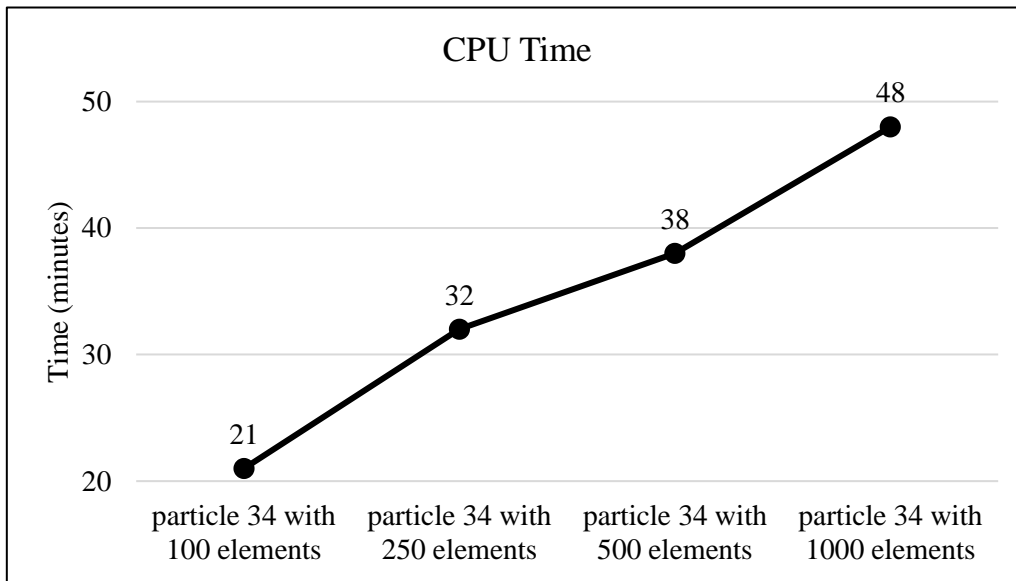


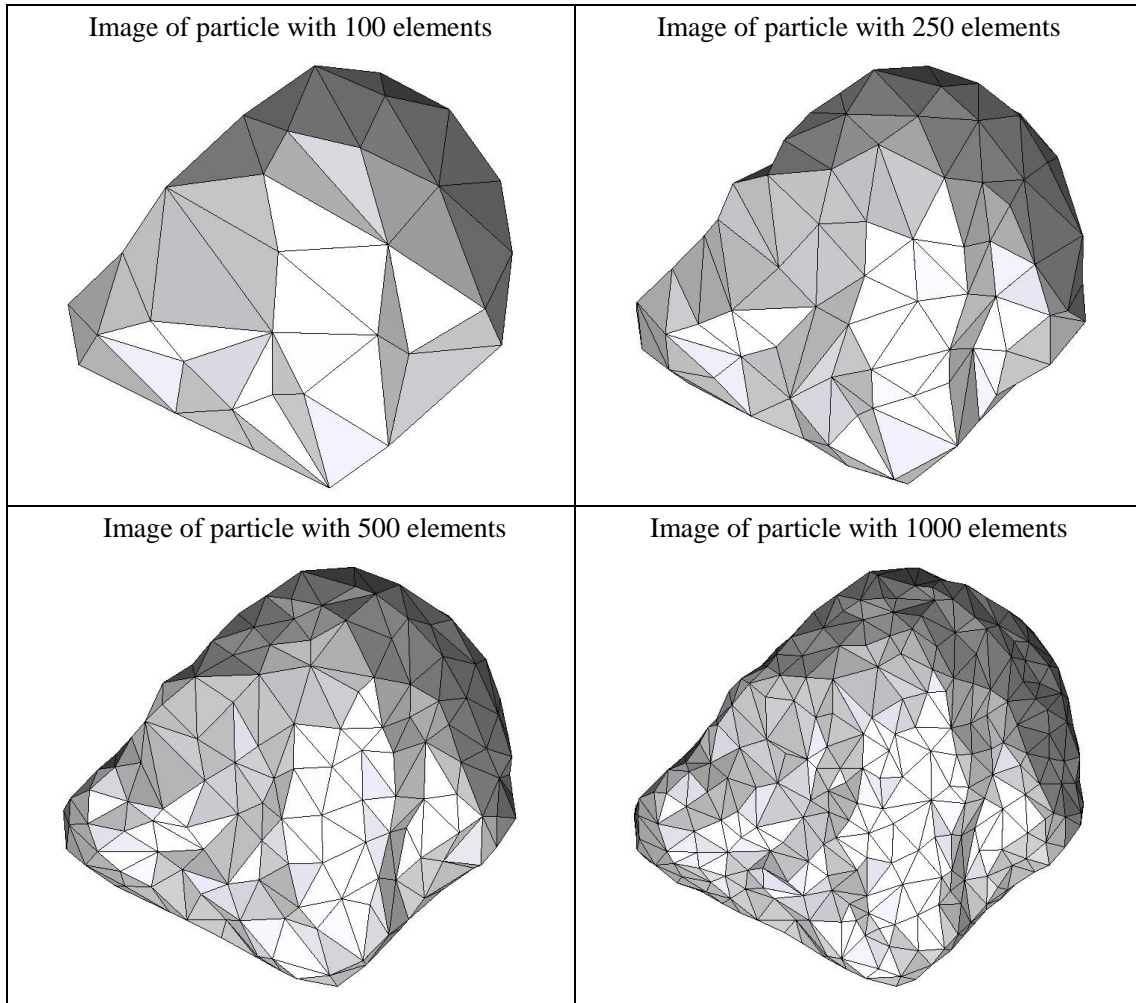
Figure A34.4 CPU computation time vs. model geometry resolution

Appendix

Percent difference analysis compare to particle 34 with 100 elements for different group of data			
	particle 34 with 250 elements	particle 34 with 500 elements	particle 34 with 1000 elements
Impulse	4.13	4.41	4.52
Peak Force	1.91	-10.06	3.12
Start Time	16.67	16.67	16.67
CPU Time	52.38	80.95	128.57
Simulation Time	-4.00	0.00	-12.00

Appendix

Summary of particle characteristics and collision simulation details for Particle 35 (of 50)



Particle statistics (part 1)								
Particle ID	# vertices	# elements	Mass (g)	Moments of Inertia			Volume (cm ³)	Sfc. Area (cm ²)
				I1	I2	I3		
				(gcm ²)	(gcm ²)	(gcm ²)		
35 (100 elements)	52	100	50.43	411837	289434.9	204171.5625	19.69202	45.20042
35 (250 elements)	127	250	50.43	425952.8	301990.025	208925.275	20.03864	45.78094
35 (500 elements)	252	500	50.43	430626.65	305699.25	210365.675	20.12587	45.81890
35 (1000 elements)	502	1000	50.43	432454.4	306923.05	211370.575	20.16891	45.82370

Appendix

Particle Statistics (part 2)							
Particle ID	α	R_g (cm)	ψ	R_v (cm)	L (cm)	I (cm)	S (cm)
35 (100 elements)	2.46562	3.08769	0.78019	1.67520	222.00489	179.94140	90.04013
35 (250 elements)	2.47160	3.07082	0.77931	1.68497	226.84622	181.67268	91.78129
35 (500 elements)	2.48113	3.07370	0.78092	1.68742	228.35839	182.32777	92.03791
35 (1000 elements)	2.48014	3.06294	0.78196	1.68862	228.80226	182.76468	92.25362

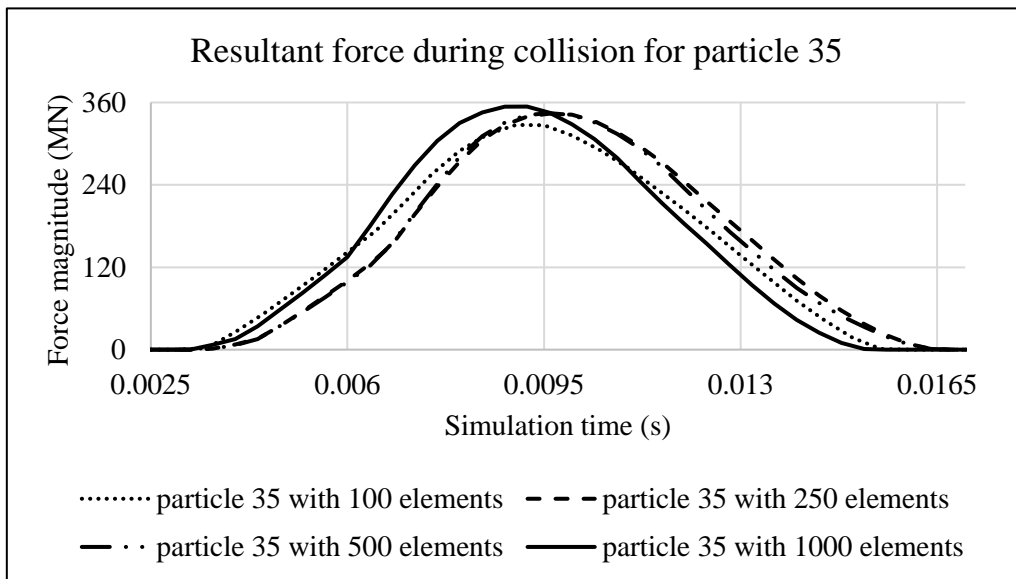


Figure A35.1 Plot of resultant forces during collision event for Particle 35

Appendix

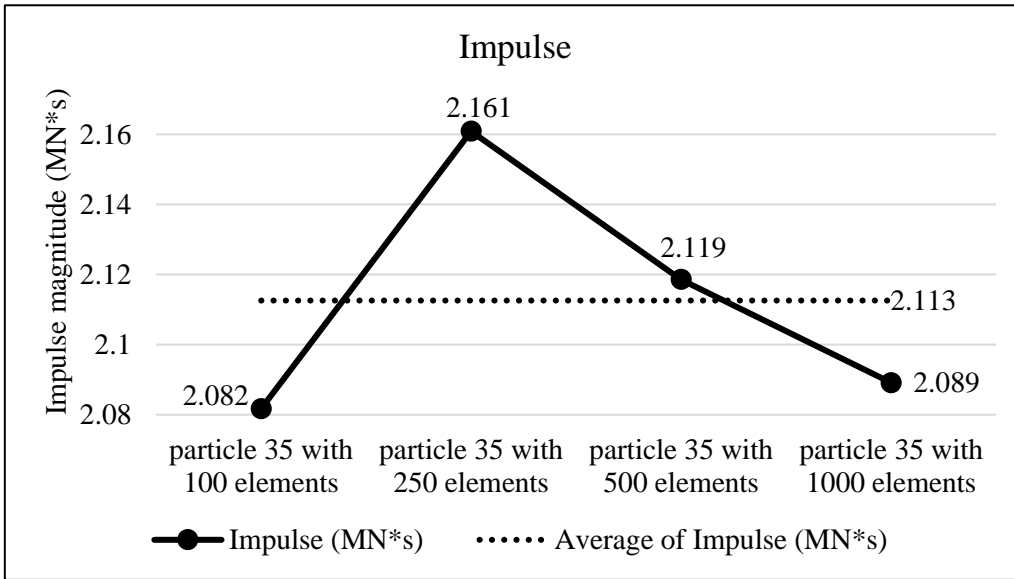


Figure A35.2 Plots of collision impulse for Particle 35

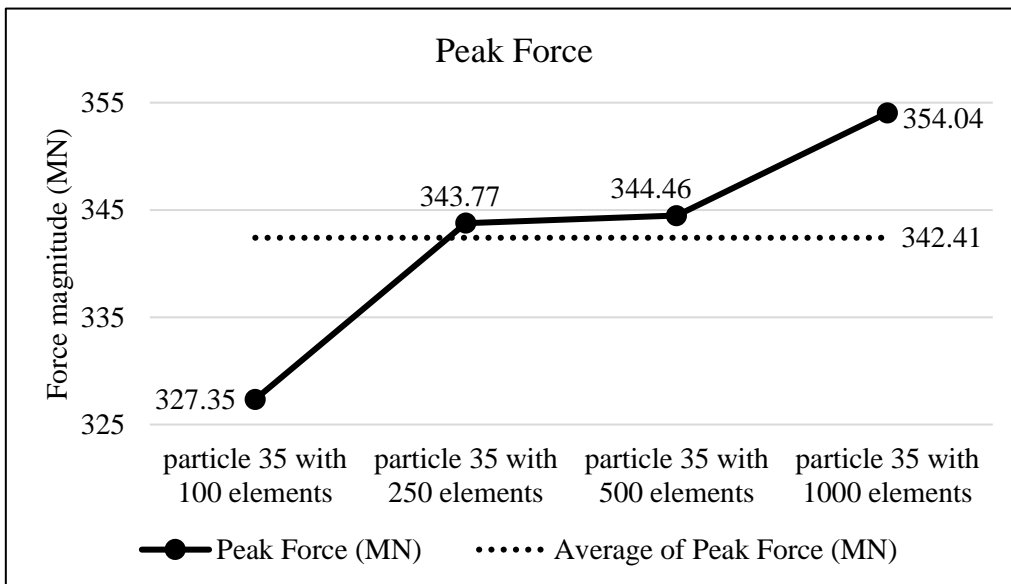


Figure A35.3 Peak collision for the four particle geometry resolutions for Particle 35

Appendix

Collision results data analysis					
Model	particle 35 with 100 elements	particle 35 with 250 elements	particle 35 with 500 elements	particle 35 with 1000 elements	Average
Impulse (MN*s)	2.082	2.161	2.119	2.089	2.113
Percent difference from Avg. Impulse	-1.46	2.29	0.28	-1.11	
Peak Force (MN)	327.35	343.77	344.46	354.04	342.41
Percent difference from Avg. Peak Force	-4.40	0.40	0.60	3.40	

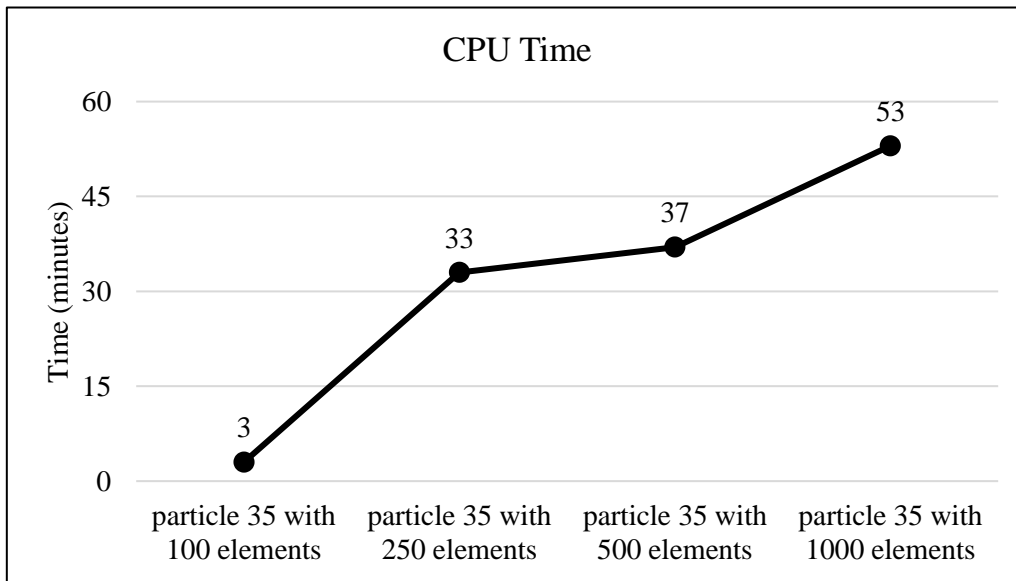


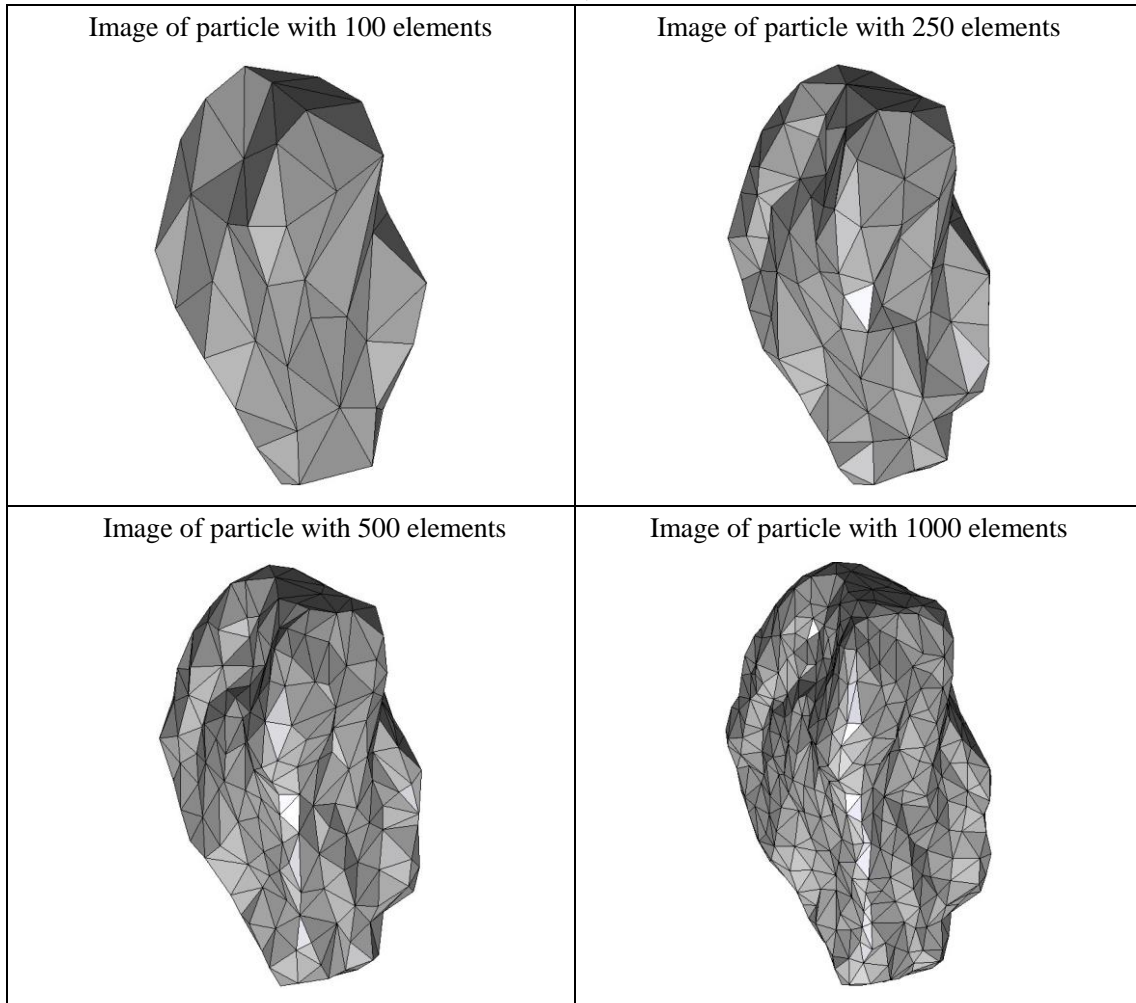
Figure A35.4 CPU computation time vs. model geometry resolution

Appendix

Percent difference analysis compare to particle 35 with 100 elements for different group of data			
	particle 35 with 250 elements	particle 35 with 500 elements	particle 35 with 1000 elements
Impulse	3.80	1.77	0.36
Peak Force	5.02	5.23	8.16
Start Time	2.86	2.86	-8.57
CPU Time	1000.00	1133.33	1666.67
Simulation Time	6.67	6.67	0.00

Appendix

Summary of particle characteristics and collision simulation details for Particle 36 (of 50)



Particle statistics (part 1)								
Particle ID	# vertices	# elements	Mass (g)	Moments of Inertia			Volume (cm ³)	Sfc. Area (cm ²)
				I1	I2	I3		
				(gcm ²)	(gcm ²)	(gcm ²)		
36 (100 elements)	52	100	45.905	300698.2	273650.4	121492.5625	16.62871	40.72583
36 (250 elements)	127	250	45.905	313099.4	283722.525	127073.1125	16.98352	41.50660
36 (500 elements)	252	500	45.905	314788.35	285265.175	127993.95	17.02638	41.71356
36 (1000 elements)	502	1000	45.905	316162.875	286621.05	128725.1875	17.06774	41.72181

Appendix

Particle Statistics (part 2)							
Particle ID	α	R_g (cm)	ψ	R_v (cm)	L (cm)	I (cm)	S (cm)
36 (100 elements)	2.18973	2.84360	0.77361	1.58340	222.09311	127.19711	101.42475
36 (250 elements)	2.19277	2.82281	0.76981	1.59458	226.19753	130.53975	103.15587
36 (500 elements)	2.18950	2.80319	0.76728	1.59592	226.75319	130.98419	103.56397
36 (1000 elements)	2.18623	2.80576	0.76837	1.59721	227.23283	131.29561	103.93802

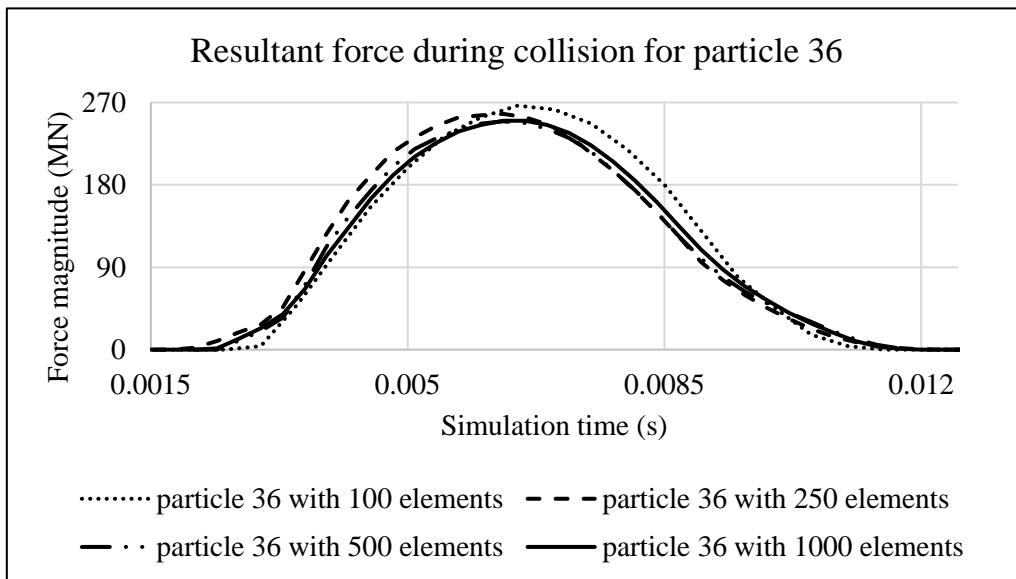


Figure A36.1 Plot of resultant forces during collision event for Particle 36

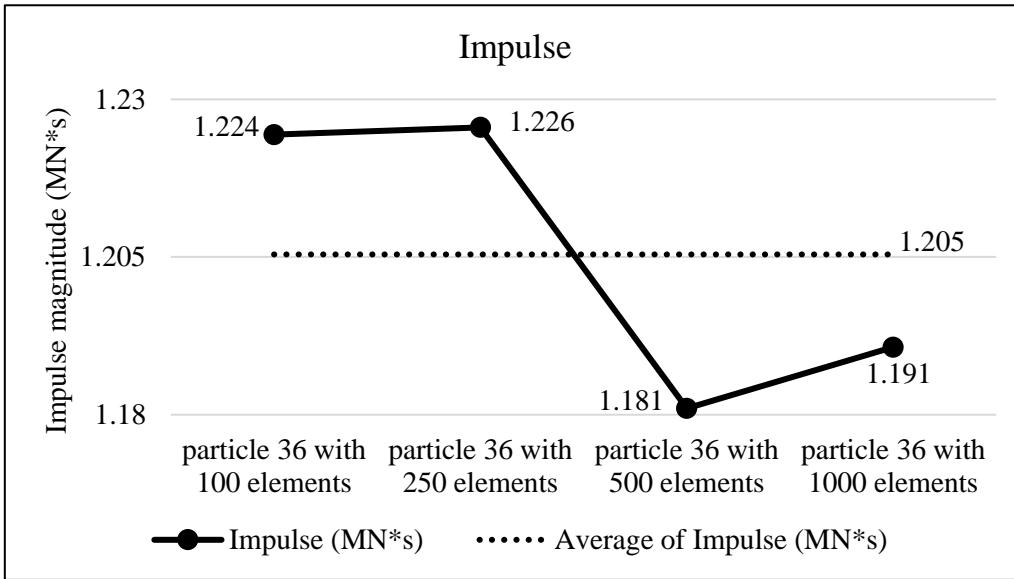


Figure A36.2 Plots of collision impulse for Particle 36

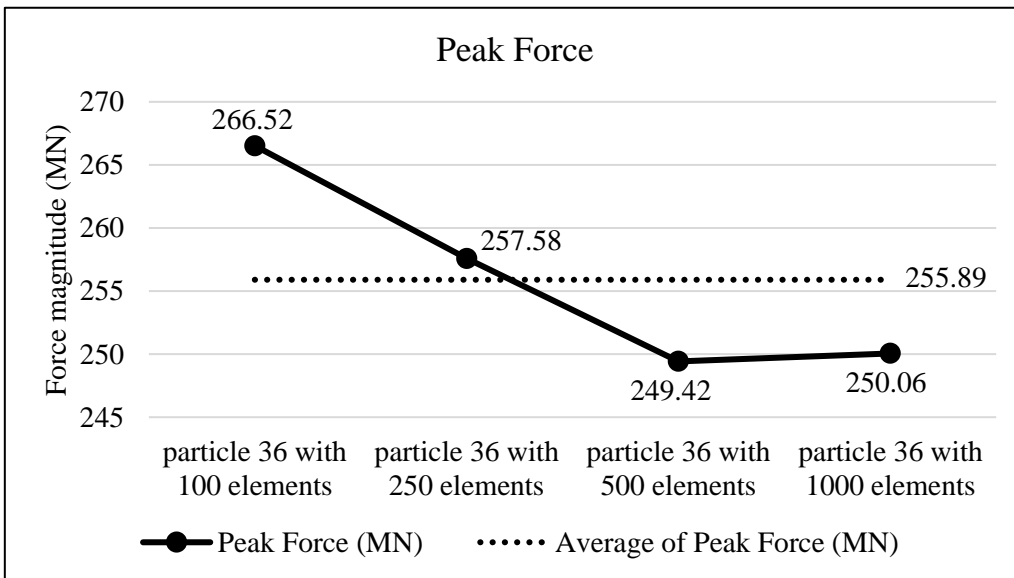


Figure A36.3 Peak collision for the four particle geometry resolutions for Particle 36

Appendix

Collision results data analysis					
Model	particle 36 with 100 elements	particle 36 with 250 elements	particle 36 with 500 elements	particle 36 with 1000 elements	Average
Impulse (MN*s)	1.224	1.226	1.181	1.191	1.205
Percent difference from Avg. Impulse	1.57	1.67	-2.02	-1.22	
Peak Force (MN)	266.52	257.58	249.42	250.06	255.89
Percent difference from Avg. Peak Force	4.15	0.66	-2.53	-2.28	

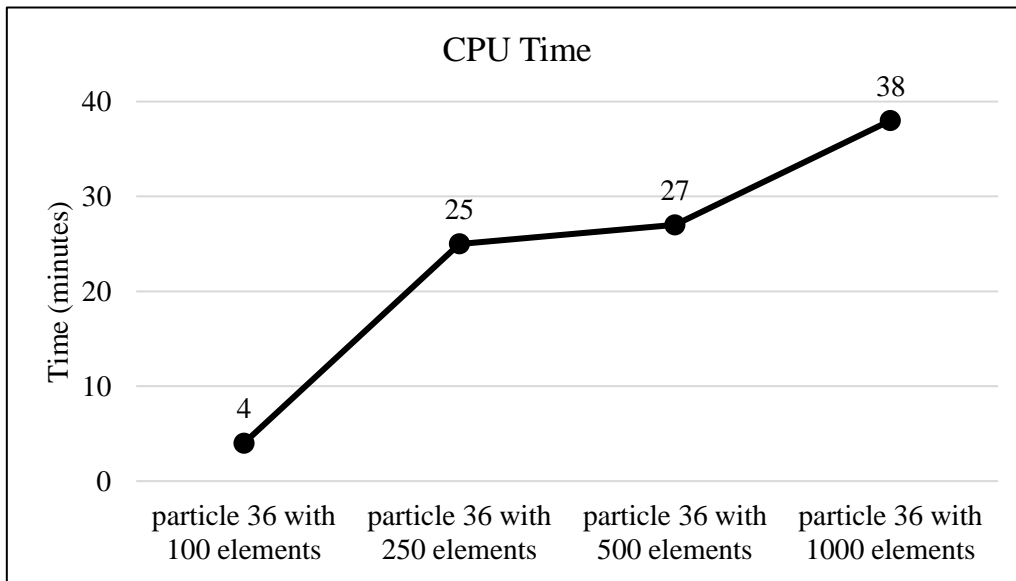
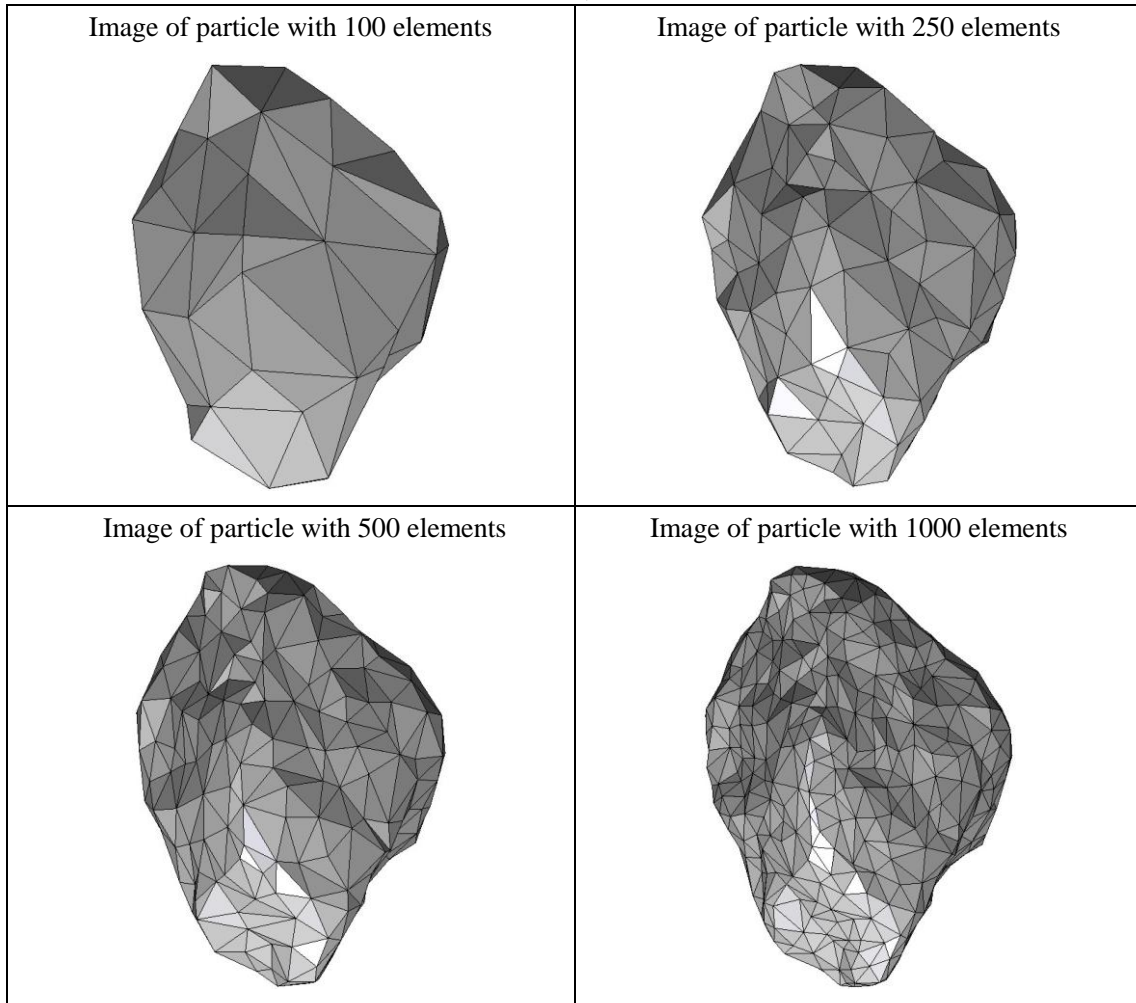


Figure A36.4 CPU computation time vs. model geometry resolution

Appendix

Percent difference analysis compare to particle 36 with 100 elements for different group of data			
	particle 36 with 250 elements	particle 36 with 500 elements	particle 36 with 1000 elements
Impulse	0.09	-3.54	-2.75
Peak Force	-3.36	-6.41	-6.18
Start Time	-30.00	-10.00	-20.00
CPU Time	525.00	575.00	850.00
Simulation Time	16.47	9.41	12.94

Summary of particle characteristics and collision simulation details for Particle 37 (of 50)



Particle statistics (part 1)								
Particle ID	# vertices	# elements	Mass (g)	Moments of Inertia			Volume (cm ³)	Sfc. Area (cm ²)
				I1	I2	I3		
				(gcm ²)	(gcm ²)	(gcm ²)		
37 (100 elements)	52	100	25.445	95674.58125	76277.5625	54188.20625	9.27305	25.71883
37 (250 elements)	127	250	25.445	99465.75625	79635.4	55335.5125	9.42567	25.92479
37 (500 elements)	252	500	25.445	100613.55	80546.425	56015.95	9.48749	26.01520
37 (1000 elements)	502	1000	25.445	101035.2313	80804.48125	56244.7125	9.50472	26.01904

Appendix

Particle Statistics (part 2)							
Particle ID	α	R_g (cm)	ψ	R_v (cm)	L (cm)	I (cm)	S (cm)
37 (100 elements)	1.83980	2.09622	0.82994	1.30330	152.12127	120.24834	82.68341
37 (250 elements)	1.86704	2.07217	0.83236	1.31041	155.94944	121.53297	83.52750
37 (500 elements)	1.86579	2.07309	0.83309	1.31327	156.81544	122.27222	84.04776
37 (1000 elements)	1.86746	2.07498	0.83397	1.31407	157.09774	122.58712	84.12387

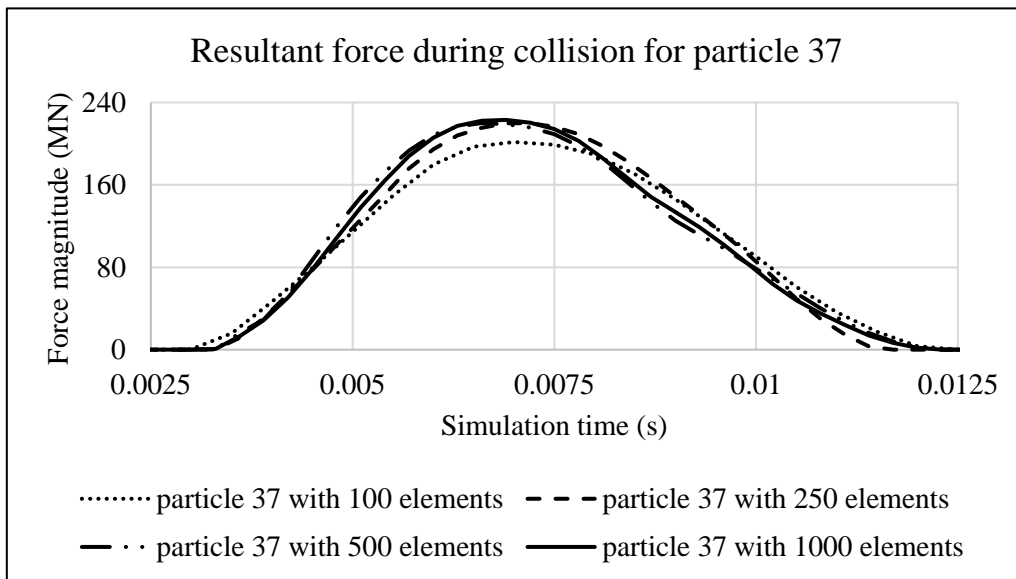


Figure A37.1 Plot of resultant forces during collision event for Particle 37

Appendix

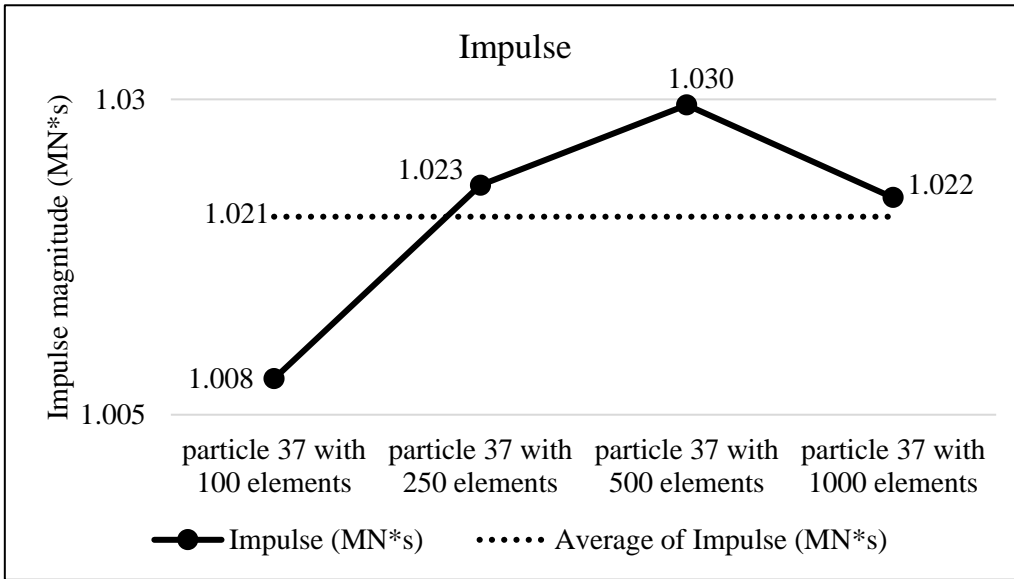


Figure A37.2 Plots of collision impulse for Particle 37

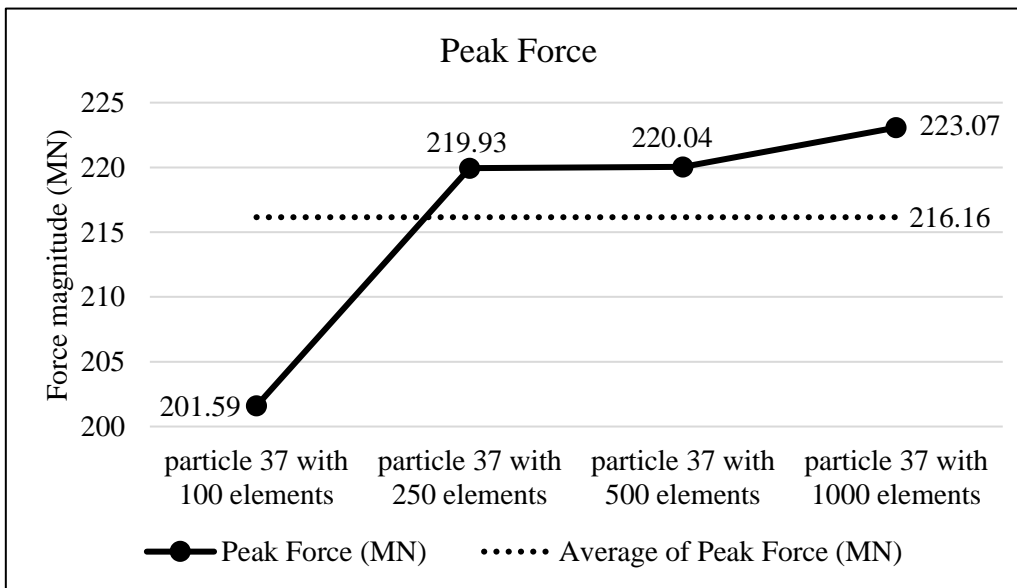


Figure A37.3 Peak collision for the four particle geometry resolutions for Particle 37

Appendix

Collision results data analysis					
Model	particle 37 with 100 elements	particle 37 with 250 elements	particle 37 with 500 elements	particle 37 with 1000 elements	Average
Impulse (MN*s)	1.008	1.023	1.030	1.022	1.021
Percent difference from Avg. Impulse	-1.26	0.24	0.87	0.15	
Peak Force (MN)	201.59	219.93	220.04	223.07	216.16
Percent difference from Avg. Peak Force	-6.74	1.75	1.79	3.20	

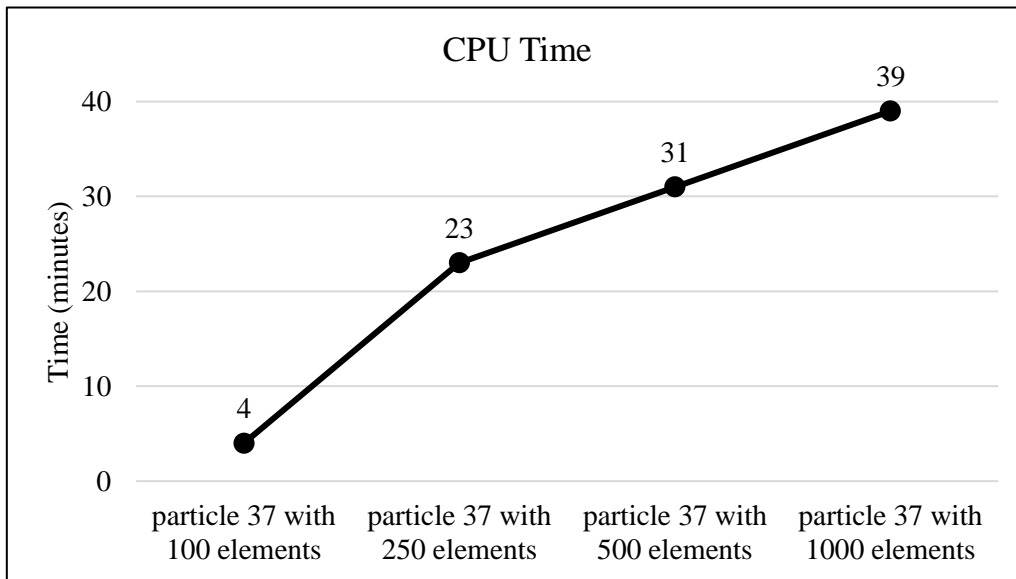
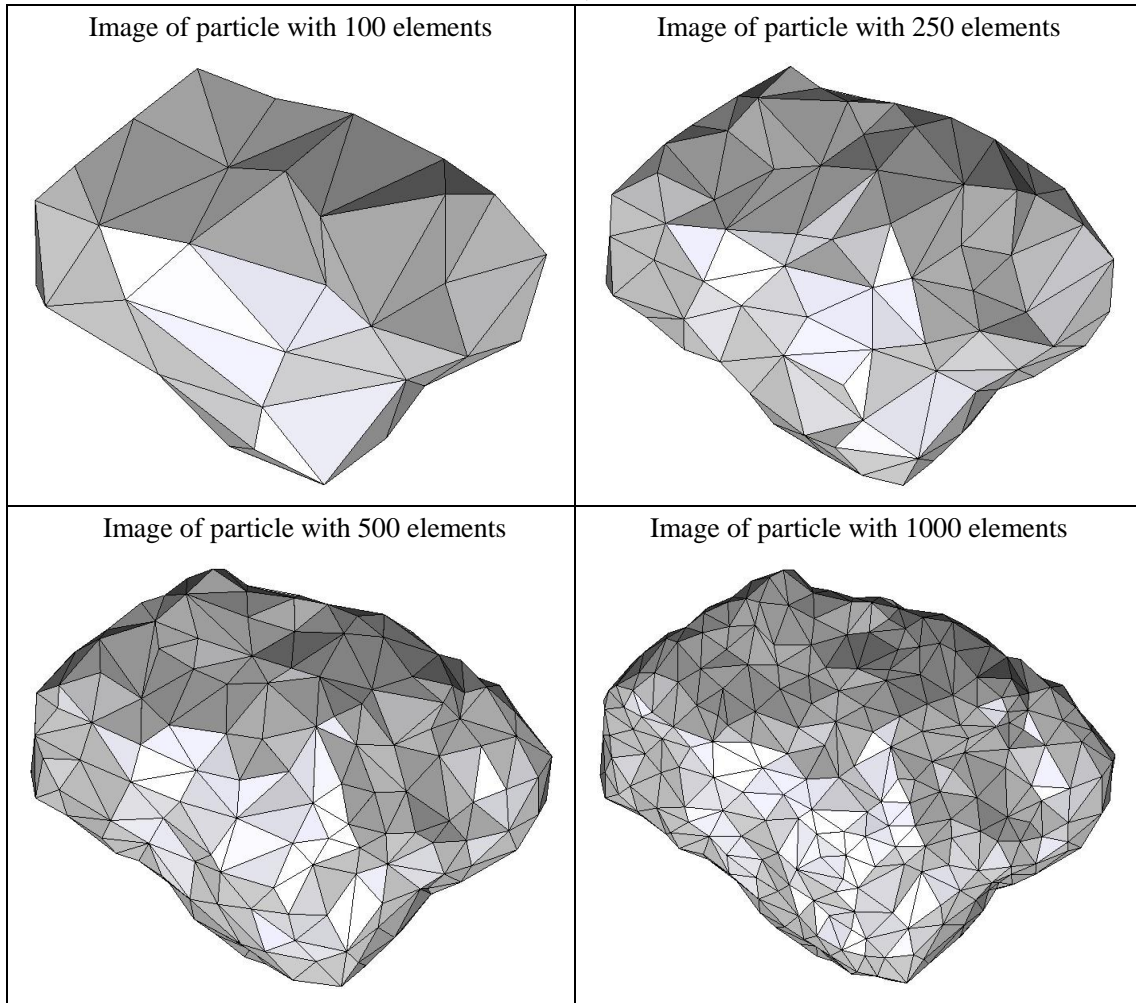


Figure A37.4 CPU computation time vs. model geometry resolution

Appendix

Percent difference analysis compare to particle 37 with 100 elements for different group of data			
	particle 37 with 250 elements	particle 37 with 500 elements	particle 37 with 1000 elements
Impulse	1.52	2.15	1.42
Peak Force	9.10	9.15	10.66
Start Time	10.00	10.00	10.00
CPU Time	475.00	675.00	875.00
Simulation Time	-10.00	0.00	0.00

Summary of particle characteristics and collision simulation details for Particle 38 (of 50)



Particle statistics (part 1)								
Particle ID	# vertices	# elements	Mass (g)	Moments of Inertia			Volume (cm ³)	Sfc. Area (cm ²)
				I1	I2	I3		
				(gcm ²)	(gcm ²)	(gcm ²)		
38 (100 elements)	52	100	17.949	52720.43125	40176.95313	23892.69844	5.85759	20.08556
38 (250 elements)	127	250	17.949	54693.11875	41502.11563	24736.46719	5.96220	20.21235
38 (500 elements)	252	500	17.949	55337.1125	41957.74375	24986.50313	5.99226	20.23832
38 (1000 elements)	502	1000	17.949	55646.225	42199.83125	25087.025	6.00781	20.20223

Appendix

Particle Statistics (part 2)							
Particle ID	α	R_g (cm)	ψ	R_v (cm)	L (cm)	I (cm)	S (cm)
38 (100 elements)	2.46579	2.04762	0.78237	1.11826	138.64499	100.74680	56.22739
38 (250 elements)	2.48784	1.96873	0.78669	1.12488	141.08883	102.78786	56.71143
38 (500 elements)	2.49593	1.97861	0.78832	1.12677	141.92507	103.38021	56.86269
38 (1000 elements)	2.50009	1.97874	0.79110	1.12774	142.36667	103.60570	56.94468

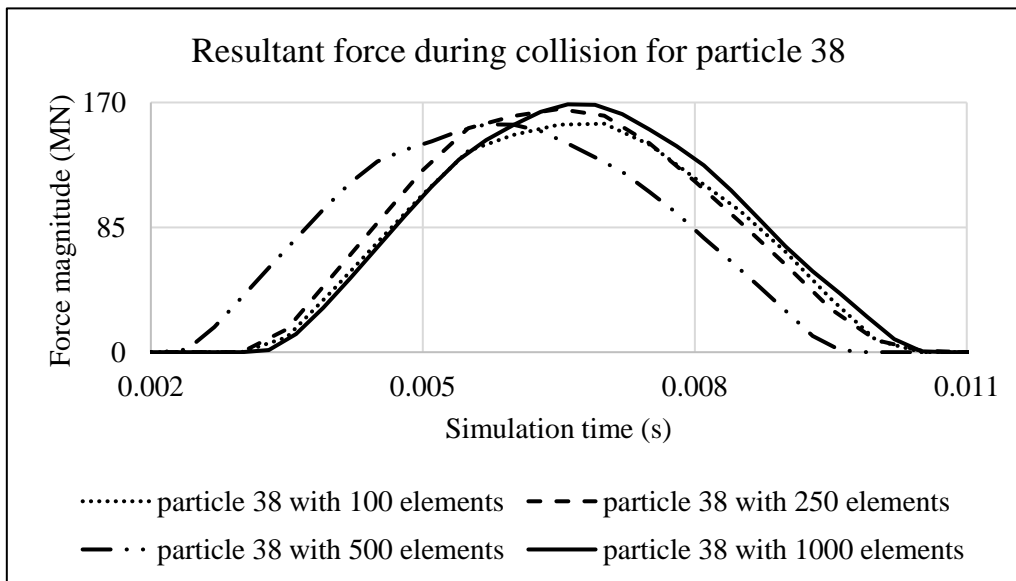


Figure A38.1 Plot of resultant forces during collision event for Particle 38

Appendix

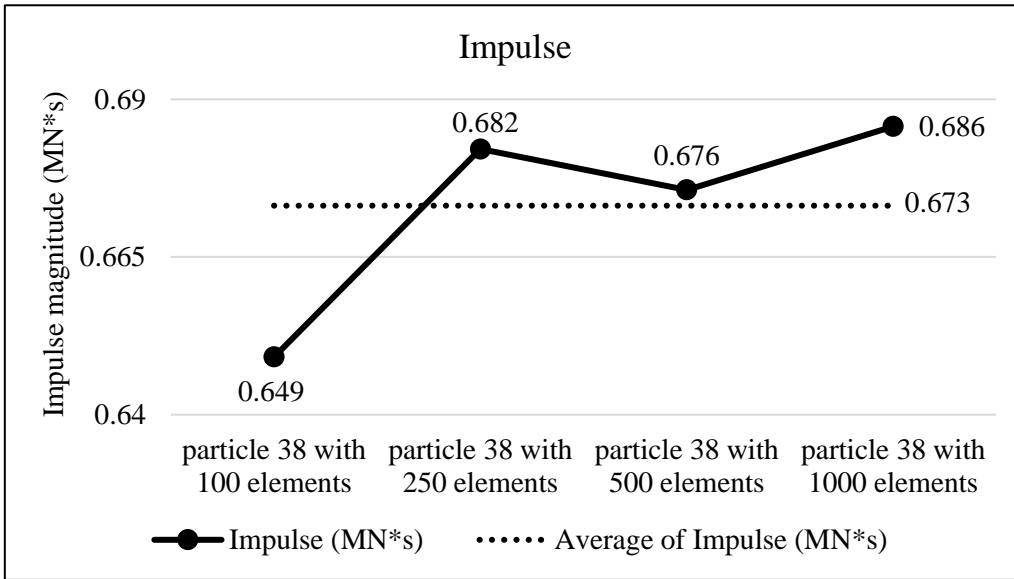


Figure A38.2 Plots of collision impulse for Particle 38

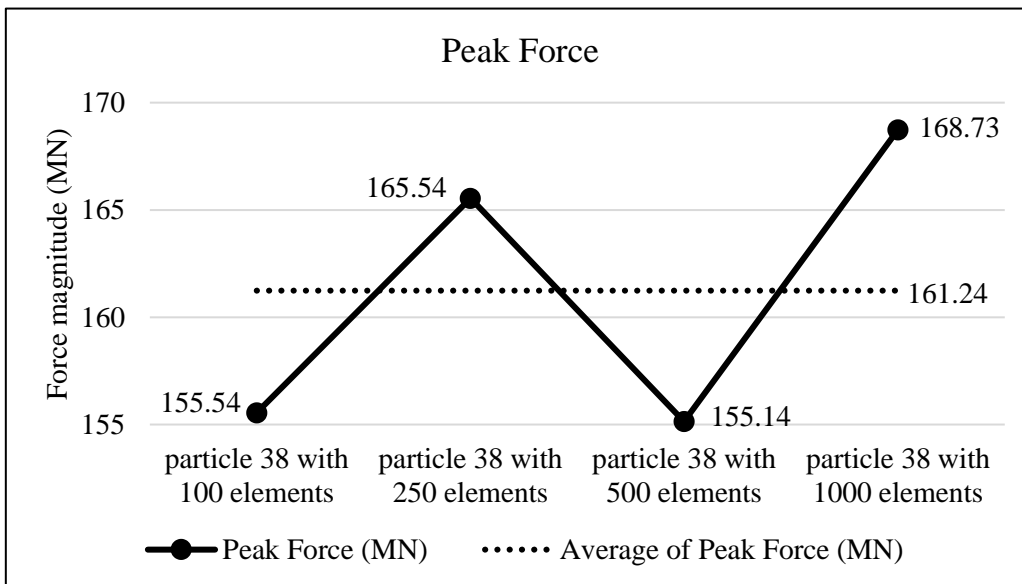


Figure A38.3 Peak collision for the four particle geometry resolutions for Particle 38

Appendix

Collision results data analysis					
Model	particle 38 with 100 elements	particle 38 with 250 elements	particle 38 with 500 elements	particle 38 with 1000 elements	Average
Impulse (MN*s)	0.649	0.682	0.676	0.686	0.673
Percent difference from Avg. Impulse	-3.57	1.33	0.37	1.86	
Peak Force (MN)	155.54	165.54	155.14	168.73	161.24
Percent difference from Avg. Peak Force	-3.53	2.67	-3.78	4.65	

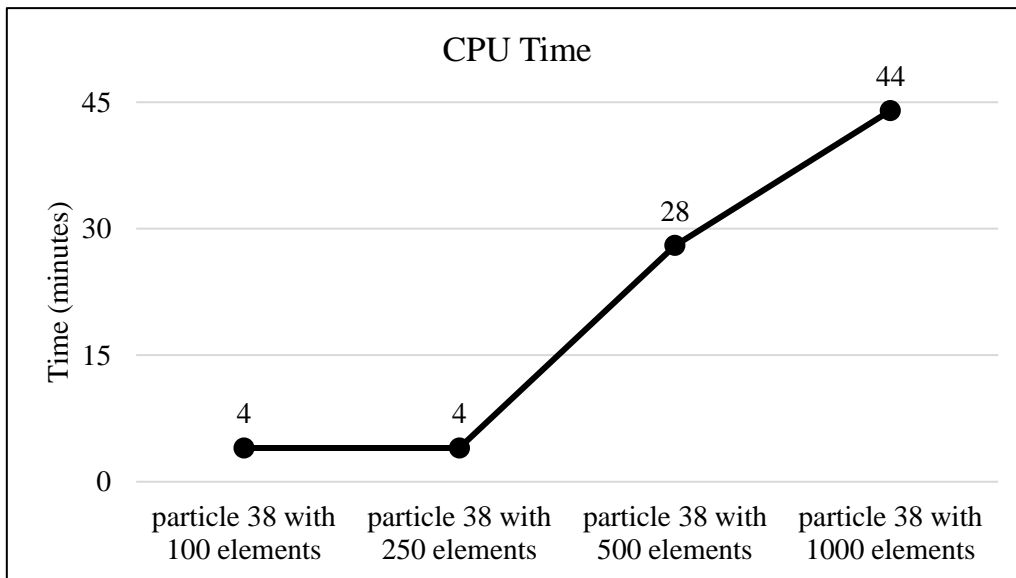
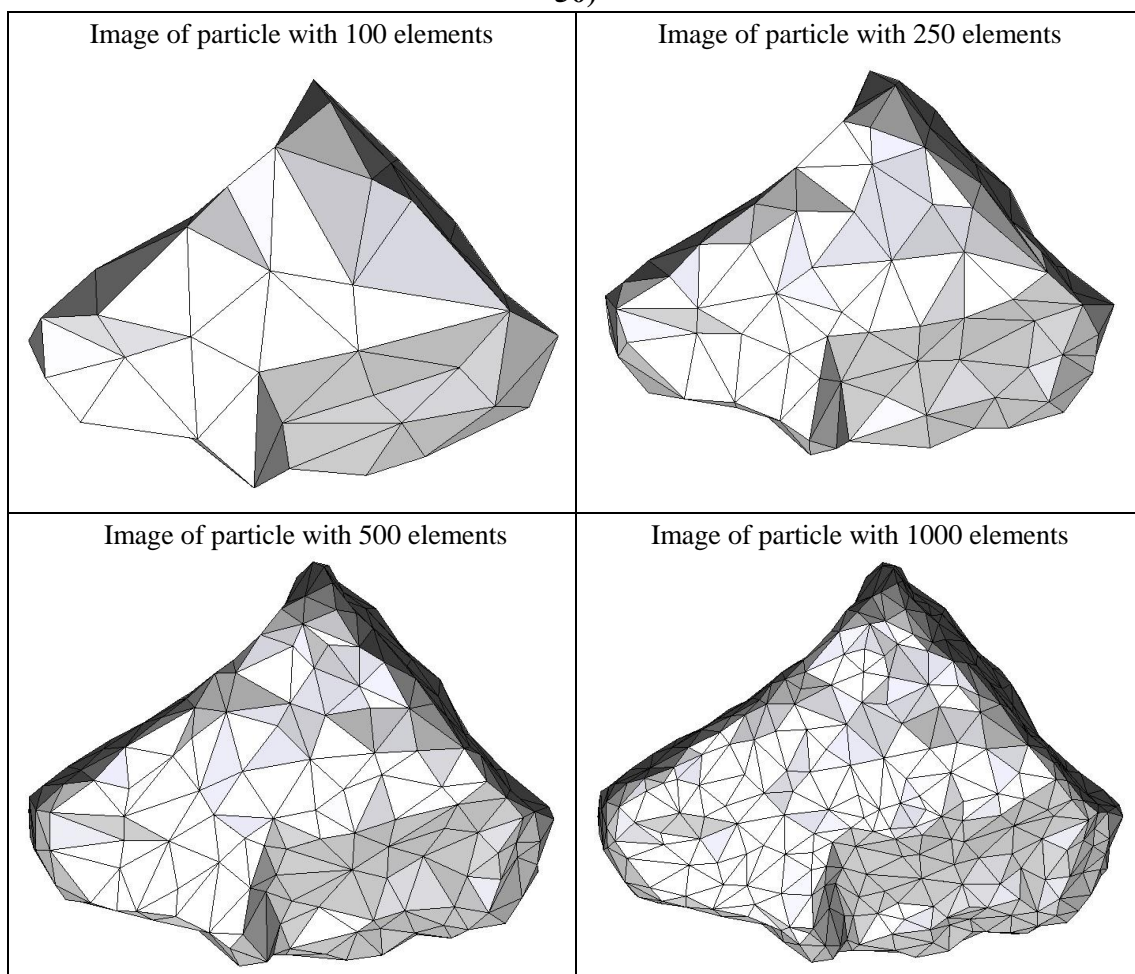


Figure A38.4 CPU computation time vs. model geometry resolution

Appendix

Percent difference analysis compare to particle 38 with 100 elements for different group of data			
	particle 38 with 250 elements	particle 38 with 500 elements	particle 38 with 1000 elements
Impulse	5.08	4.08	5.63
Peak Force	6.43	-0.26	8.48
Start Time	0.00	-31.43	-5.71
CPU Time	0.00	600.00	1000.00
Simulation Time	7.69	10.77	10.77

Summary of particle characteristics and collision simulation details for Particle 39 (of 50)



Particle statistics (part 1)								
Particle ID	# vertices	# elements	Mass (g)	Moments of Inertia			Volume (cm ³)	Sfc. Area (cm ²)
				I1	I2	I3		
				(gcm ²)	(gcm ²)	(gcm ²)		
39 (100 elements)	52	100	28.098	177846.5	130182.9375	69257.675	10.39854	32.82607
39 (250 elements)	127	250	28.098	189218.675	139095.3	72587.48125	10.67670	33.57299
39 (500 elements)	252	500	28.098	192526.075	141493.675	73710.9375	10.75802	33.59034
39 (1000 elements)	502	1000	28.098	193422.9625	142085.2	74146.025	10.78611	33.53167

Appendix

Particle Statistics (part 2)							
Particle ID	α	R_g (cm)	ψ	R_v (cm)	L (cm)	I (cm)	S (cm)
39 (100 elements)	3.32525	2.68020	0.70185	1.35403	206.12885	144.24275	61.98905
39 (250 elements)	3.37399	2.63390	0.69842	1.36600	213.32176	147.77086	63.22544
39 (500 elements)	3.38795	2.64029	0.70160	1.36946	215.22451	148.98961	63.52648
39 (1000 elements)	3.38513	2.63655	0.70405	1.37065	215.65952	149.43114	63.70792

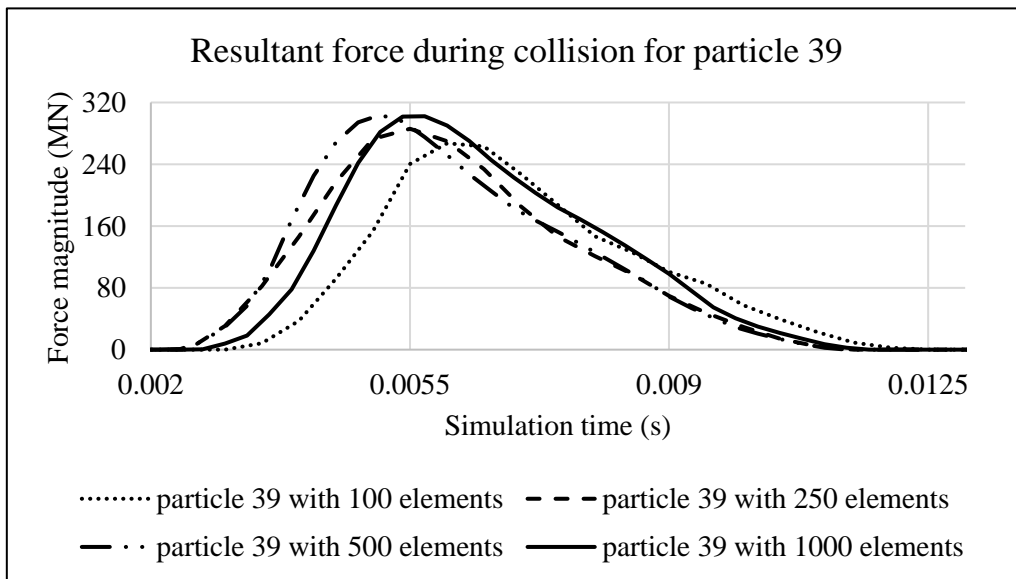


Figure A39.1 Plot of resultant forces during collision event for Particle 39

Appendix

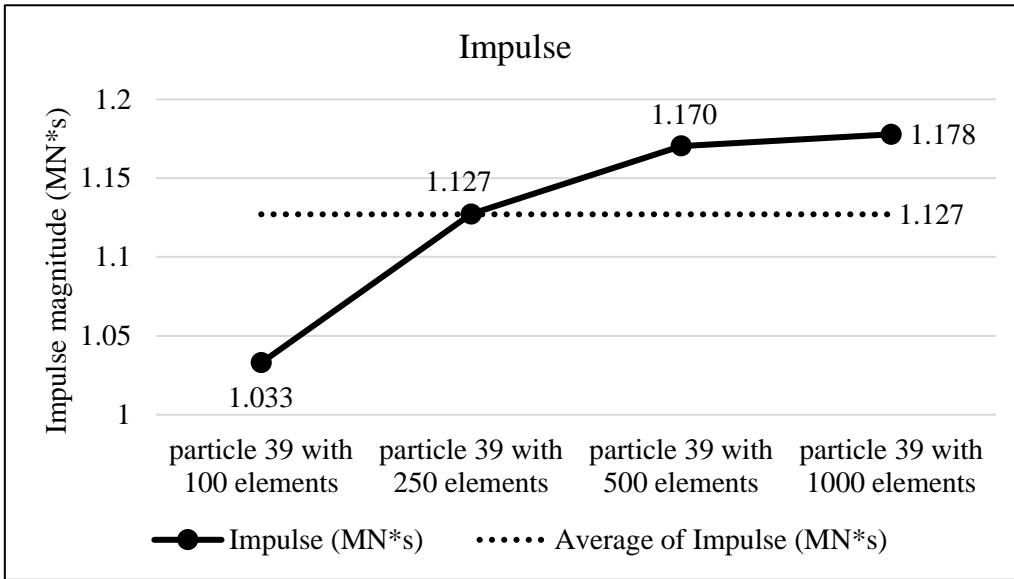


Figure A39.2 Plots of collision impulse for Particle 39

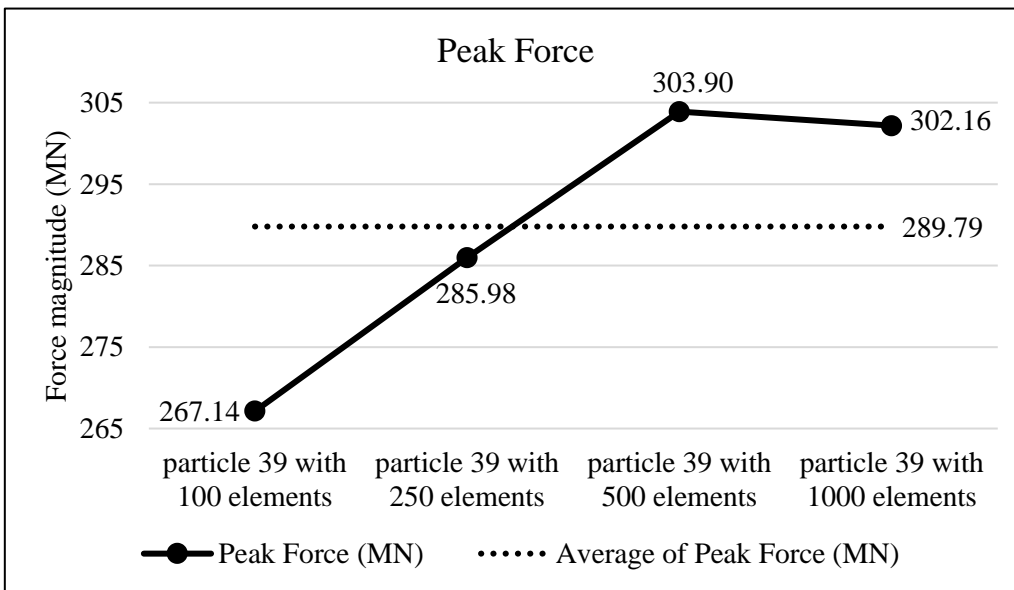


Figure A39.3 Peak collision for the four particle geometry resolutions for Particle 39

Appendix

Collision results data analysis					
Model	particle 39 with 100 elements	particle 39 with 250 elements	particle 39 with 500 elements	particle 39 with 1000 elements	Average
Impulse (MN*s)	1.033	1.127	1.170	1.178	1.127
Percent difference from Avg. Impulse	-8.36	0.02	3.84	4.50	
Peak Force (MN)	267.14	285.98	303.90	302.16	289.79
Percent difference from Avg. Peak Force	-7.82	-1.32	4.87	4.27	

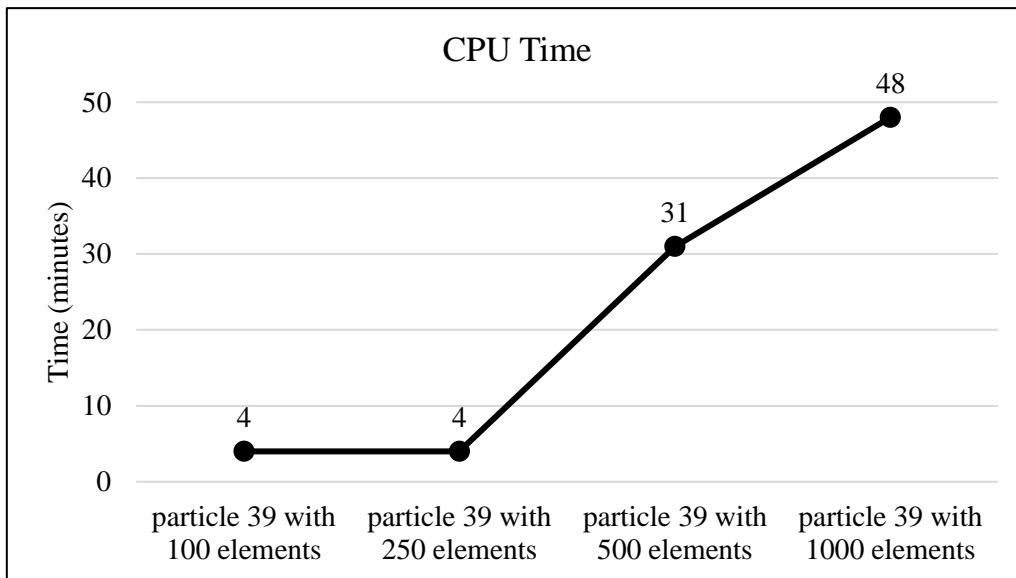
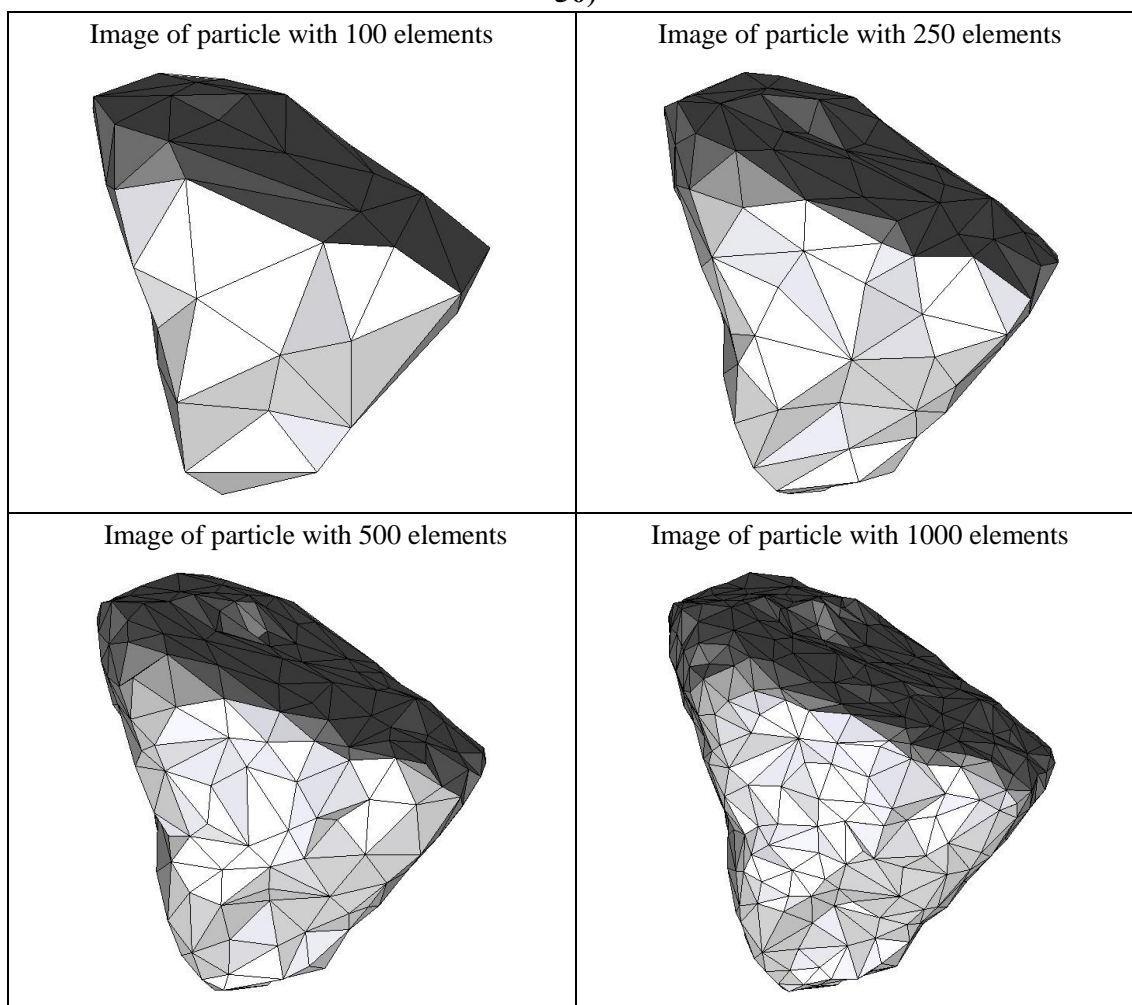


Figure A39.4 CPU computation time vs. model geometry resolution

Appendix

Percent difference analysis compare to particle 39 with 100 elements for different group of data			
	particle 39 with 250 elements	particle 39 with 500 elements	particle 39 with 1000 elements
Impulse	9.14	13.31	14.03
Peak Force	7.05	13.76	13.11
Start Time	-14.29	-31.43	-22.86
CPU Time	0.00	675.00	1100.00
Simulation Time	-5.56	0.00	0.00

Summary of particle characteristics and collision simulation details for Particle 40 (of 50)



Particle statistics (part 1)								
Particle ID	# vertices	# elements	Mass (g)	Moments of Inertia			Volume (cm ³)	Sfc. Area (cm ²)
				I1	I2	I3		
				(gcm ²)	(gcm ²)	(gcm ²)		
40 (100 elements)	52	100	30.774	103520.1	98055.44375	75243.83125	10.79907	28.14724
40 (250 elements)	127	250	30.774	107428.7	100682.6437	77591.6125	10.99747	28.51680
40 (500 elements)	252	500	30.774	108797.7	101765.7688	78511.63125	11.07209	28.55177
40 (1000 elements)	502	1000	30.774	109472.025	102228.0813	79034.19375	11.10990	28.55021

Appendix

Particle Statistics (part 2)							
Particle ID	α	R_g (cm)	ψ	R_v (cm)	L (cm)	I (cm)	S (cm)
40 (100 elements)	1.34553	2.00704	0.83941	1.37119	143.26801	114.51243	106.47703
40 (250 elements)	1.35732	2.04601	0.83865	1.37954	145.62338	117.05873	107.28755
40 (500 elements)	1.35919	2.03560	0.84140	1.38265	146.47559	117.89264	107.76665
40 (1000 elements)	1.35940	2.02088	0.84336	1.38423	146.81577	118.39774	108.00050

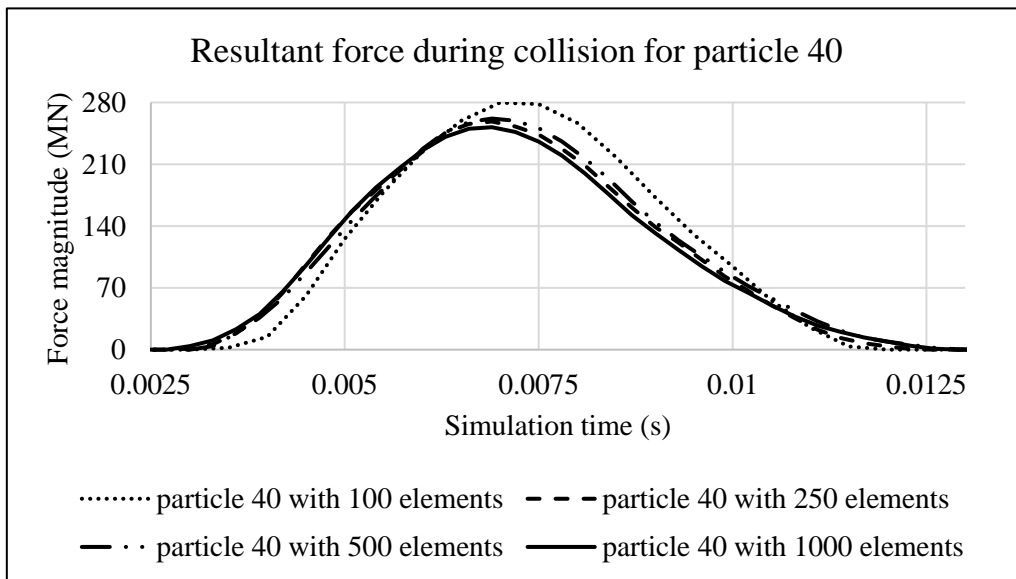


Figure A40.1 Plot of resultant forces during collision event for Particle 40

Appendix

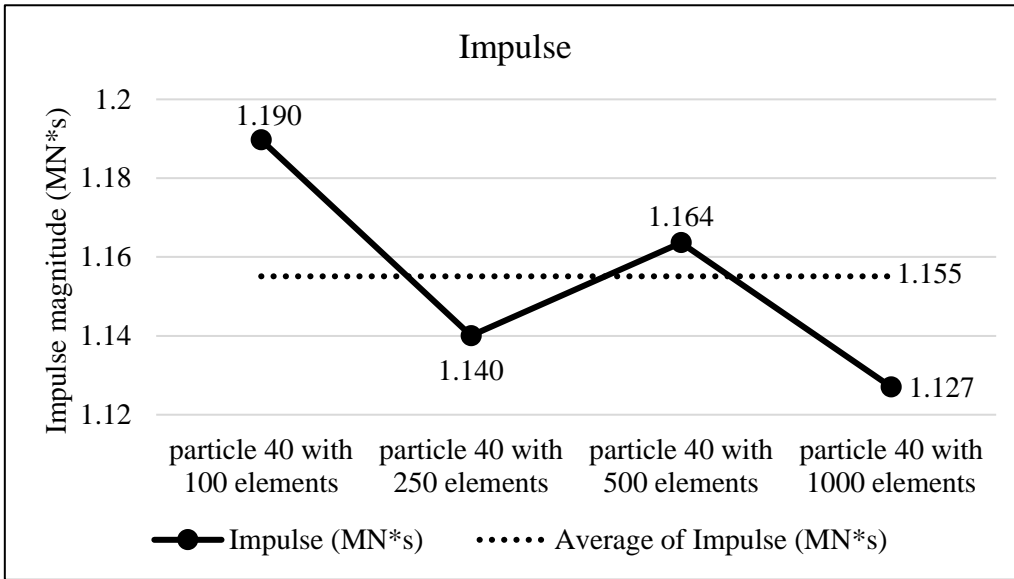


Figure A40.2 Plots of collision impulse for Particle 40

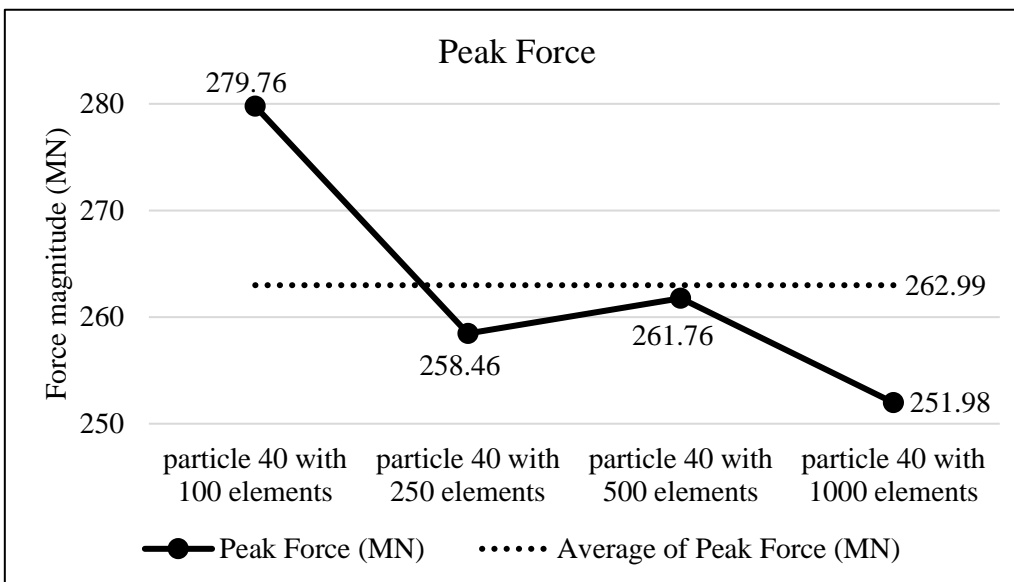


Figure A40.3 Peak collision for the four particle geometry resolutions for Particle 40

Appendix

Collision results data analysis					
Model	particle 40 with 100 elements	particle 40 with 250 elements	particle 40 with 500 elements	particle 40 with 1000 elements	Average
Impulse (MN*s)	1.190	1.140	1.164	1.127	1.155
Percent difference from Avg. Impulse	2.99	-1.30	0.74	-2.43	
Peak Force (MN)	279.76	258.46	261.76	251.98	262.99
Percent difference from Avg. Peak Force	6.38	-1.72	-0.47	-4.19	

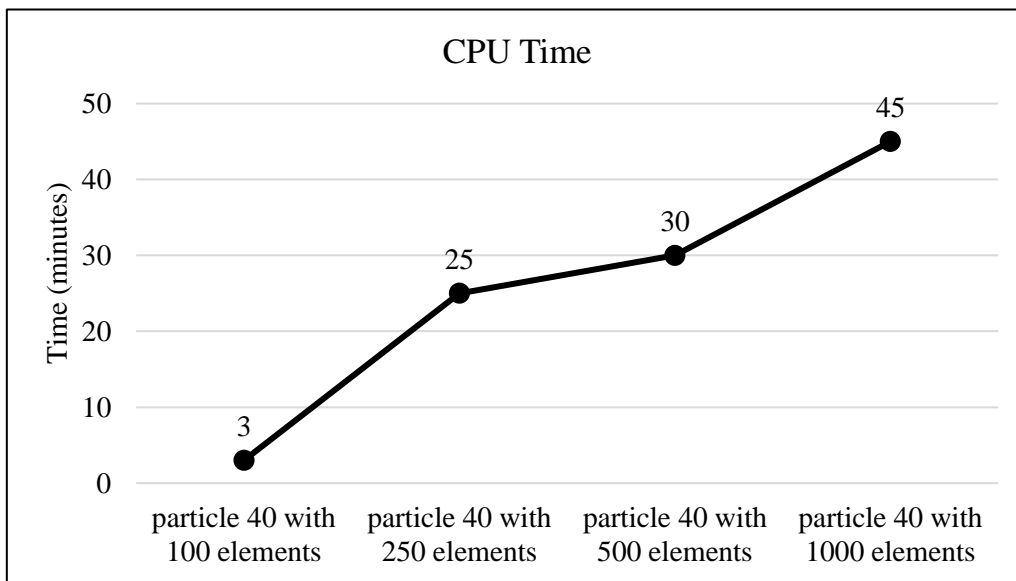
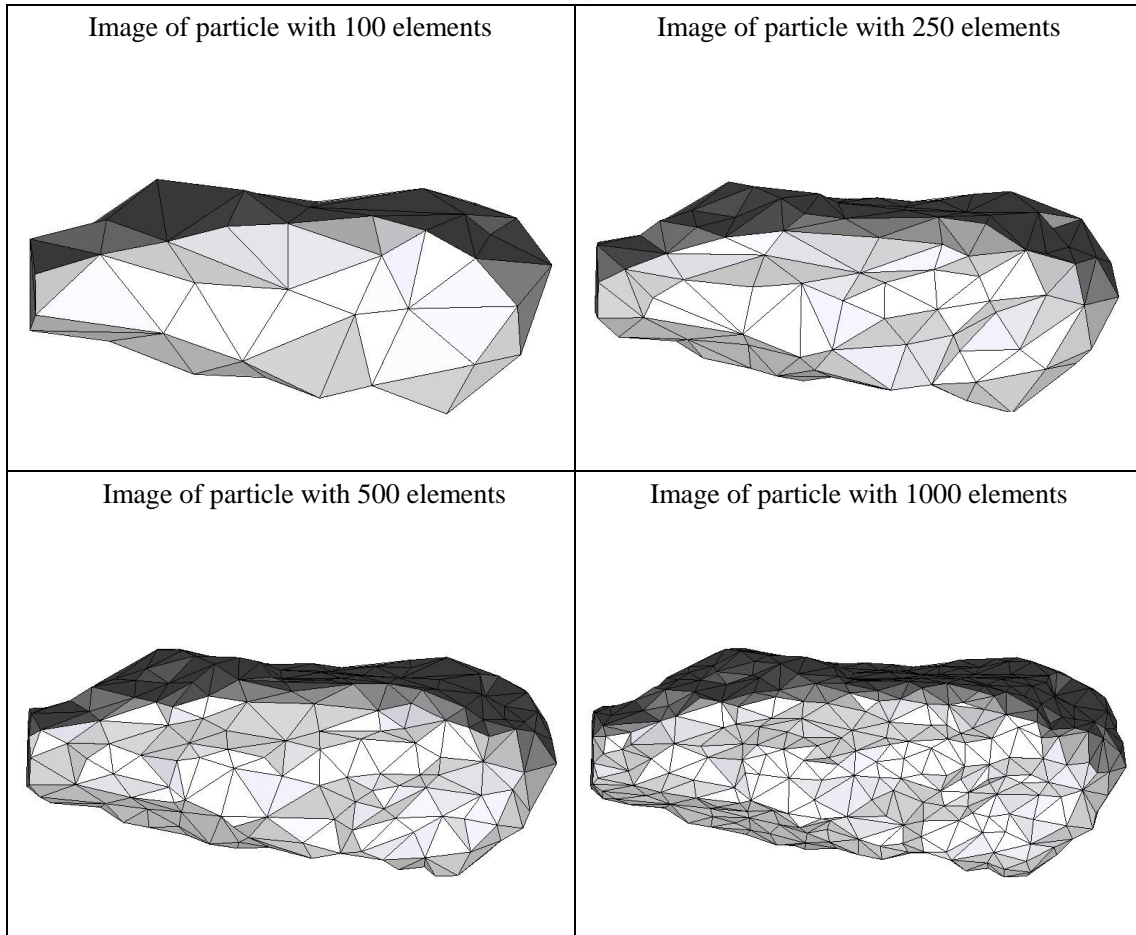


Figure A40.4 CPU computation time vs. model geometry resolution

Appendix

Percent difference analysis compare to particle 40 with 100 elements for different group of data			
	particle 40 with 250 elements	particle 40 with 500 elements	particle 40 with 1000 elements
Impulse	-4.17	-2.19	-5.27
Peak Force	-7.61	-6.44	-9.93
Start Time	-14.29	-5.71	-14.29
CPU Time	733.33	900.00	1400.00
Simulation Time	16.25	20.00	20.00

Summary of particle characteristics and collision simulation details for Particle 41 (of 50)



Particle statistics (part 1)								
Particle ID	# vertices	# elements	Mass (g)	Moments of Inertia			Volume (cm ³)	Sfc. Area (cm ²)
				I1	I2	I3		
				(gcm ²)	(gcm ²)	(gcm ²)		
41 (100 elements)	52	100	24.276	134889.7	128082.3375	30097.14688	8.47678	26.95256
41 (250 elements)	127	250	24.276	139172.1	131985.725	30662.13125	8.57976	27.25720
41 (500 elements)	252	500	24.276	141371.1875	134021.8375	31114.62813	8.65421	27.29598
41 (1000 elements)	502	1000	24.276	142138.1875	134780.975	31283.5	8.68038	27.33043

Appendix

Particle Statistics (part 2)							
Particle ID	α	R_g (cm)	ψ	R_v (cm)	L (cm)	I (cm)	S (cm)
41 (100 elements)	3.16212	2.79833	0.74594	1.26487	219.00689	87.18387	69.25947
41 (250 elements)	3.20069	2.79220	0.74357	1.26998	222.56153	88.29189	69.53544
41 (500 elements)	3.20606	2.79960	0.74680	1.27364	224.30501	89.00687	69.96291
41 (1000 elements)	3.20411	2.79897	0.74736	1.27492	224.92729	89.21112	70.19951

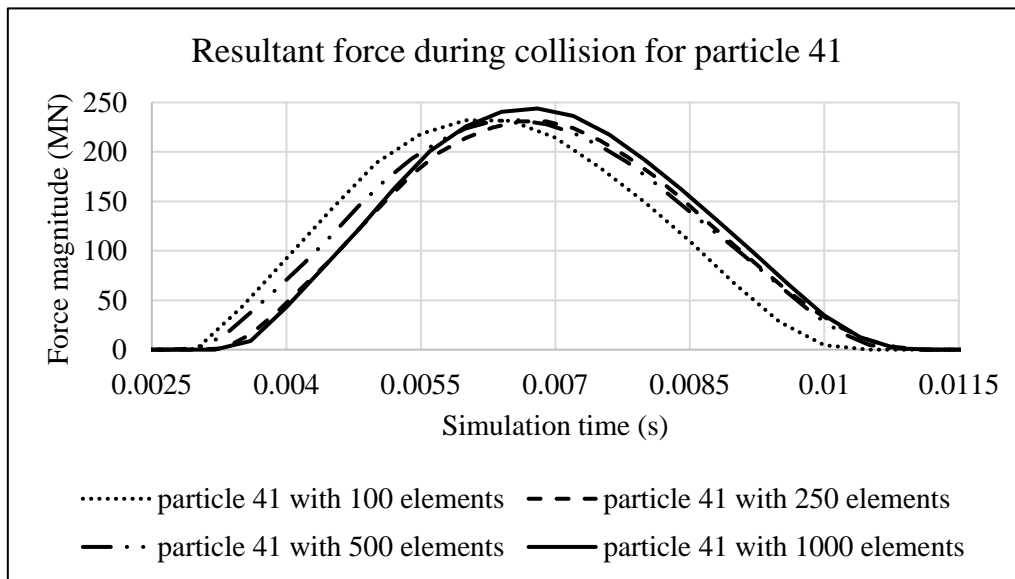


Figure A41.1 Plot of resultant forces during collision event for Particle 41

Appendix

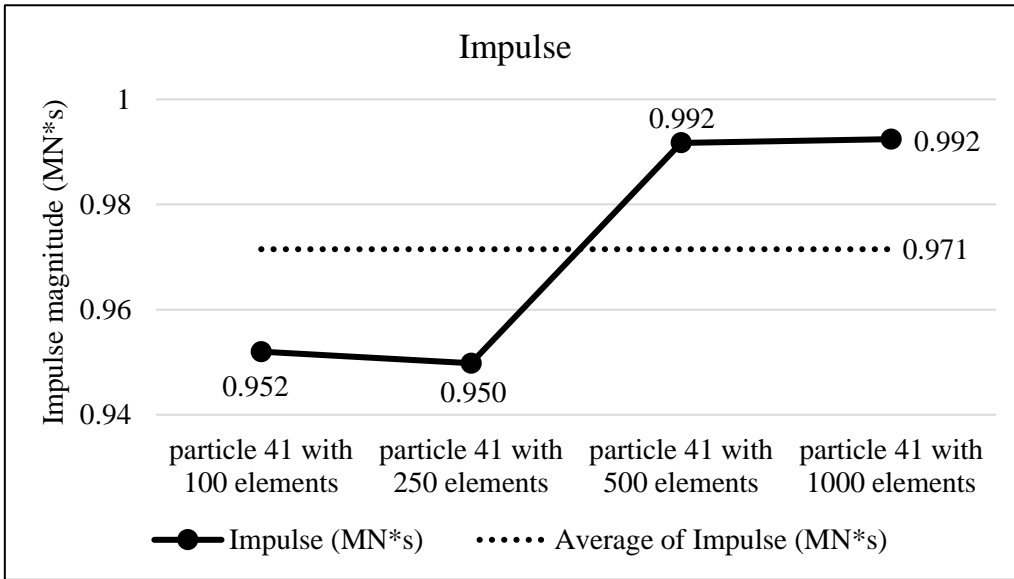


Figure A41.2 Plots of collision impulse for Particle 41

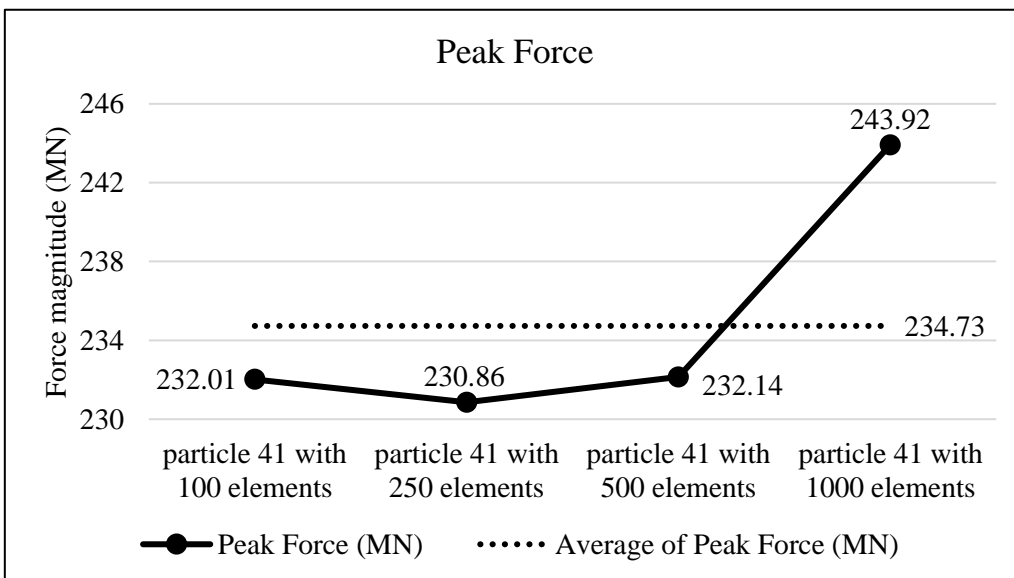


Figure A41.3 Peak collision for the four particle geometry resolutions for Particle 41

Appendix

Collision results data analysis					
Model	particle 41 with 100 elements	particle 41 with 250 elements	particle 41 with 500 elements	particle 41 with 1000 elements	Average
Impulse (MN*s)	0.952	0.950	0.992	0.992	0.971
Percent difference from Avg. Impulse	-2.01	-2.23	2.08	2.16	
Peak Force (MN)	232.01	230.86	232.14	243.92	234.73
Percent difference from Avg. Peak Force	-1.16	-1.65	-1.11	3.91	

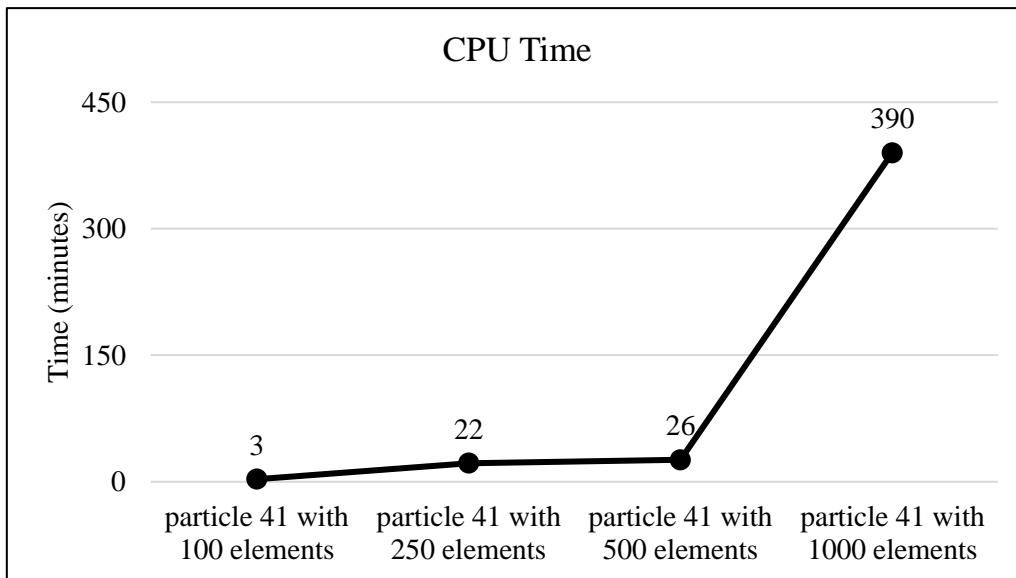
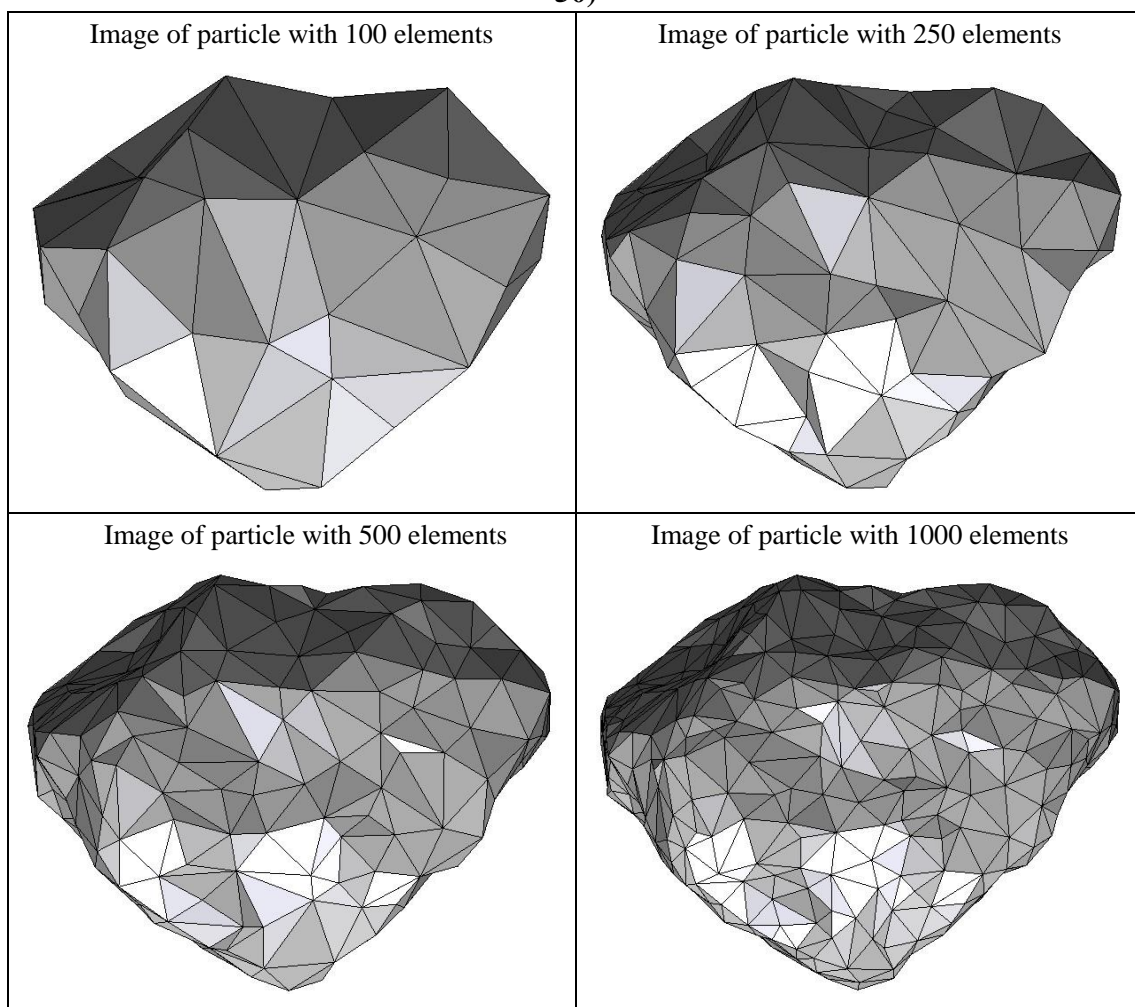


Figure A41.4 CPU computation time vs. model geometry resolution

Appendix

Percent difference analysis compare to particle 41 with 100 elements for different group of data			
	particle 41 with 250 elements	particle 41 with 500 elements	particle 41 with 1000 elements
Impulse	-0.23	4.17	4.25
Peak Force	-0.50	0.05	5.13
Start Time	10.00	0.00	20.00
CPU Time	633.33	766.67	12900.00
Simulation Time	11.43	11.43	2.86

Summary of particle characteristics and collision simulation details for Particle 42 (of 50)



Particle statistics (part 1)								
Particle ID	# vertices	# elements	Mass (g)	Moments of Inertia			Volume (cm ³)	Sfc. Area (cm ²)
				I1	I2	I3		
				(gcm ²)	(gcm ²)	(gcm ²)		
42 (100 elements)	52	100	18.738	49839.07813	44602.71875	31988.04688	6.76737	20.40203
42 (250 elements)	127	250	18.738	50969.8375	45531.18125	32500.4375	6.83818	20.60151
42 (500 elements)	252	500	18.738	51298.14063	45946.11563	32674.67813	6.86085	20.58882
42 (1000 elements)	502	1000	18.738	51597.07813	46209.74375	32887.80313	6.88418	20.58624

Appendix

Particle Statistics (part 2)							
Particle ID	α	R_g (cm)	ψ	R_v (cm)	L (cm)	I (cm)	S (cm)
42 (100 elements)	1.52793	1.76571	0.84806	1.17339	129.09299	99.66376	84.48877
42 (250 elements)	1.53785	1.75850	0.84569	1.17747	130.68187	100.61596	84.97704
42 (500 elements)	1.53728	1.75641	0.84808	1.17877	131.26150	100.73206	85.38564
42 (1000 elements)	1.53644	1.75922	0.85011	1.18011	131.61620	101.06057	85.66303

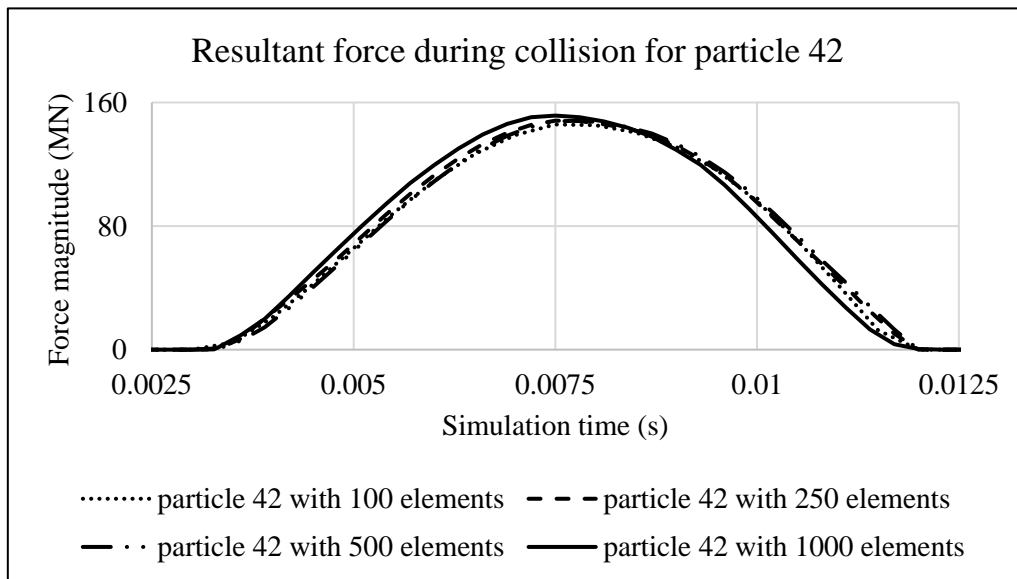


Figure A42.1 Plot of resultant forces during collision event for Particle 42

Appendix

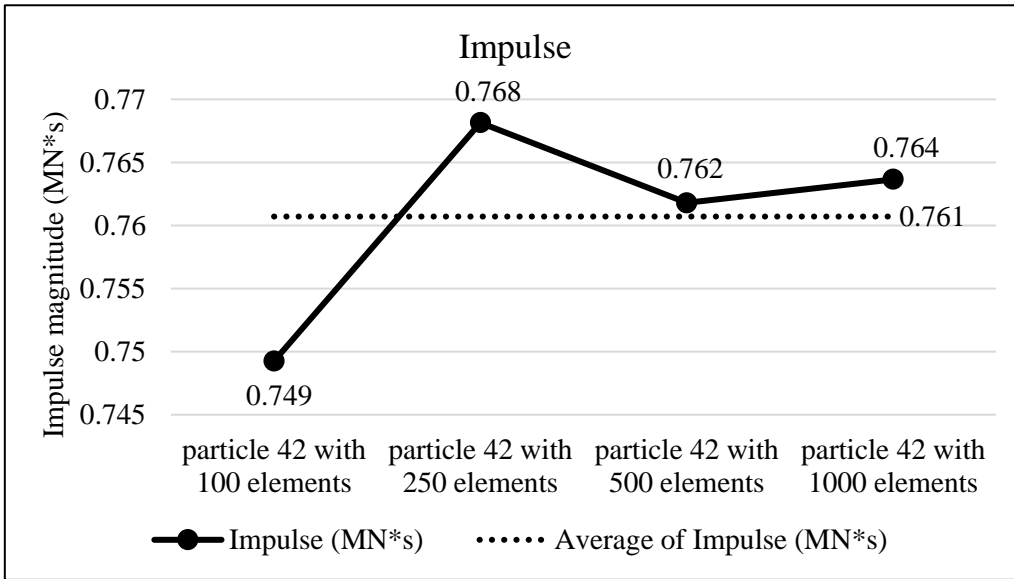


Figure A42.2 Plots of collision impulse for Particle 42

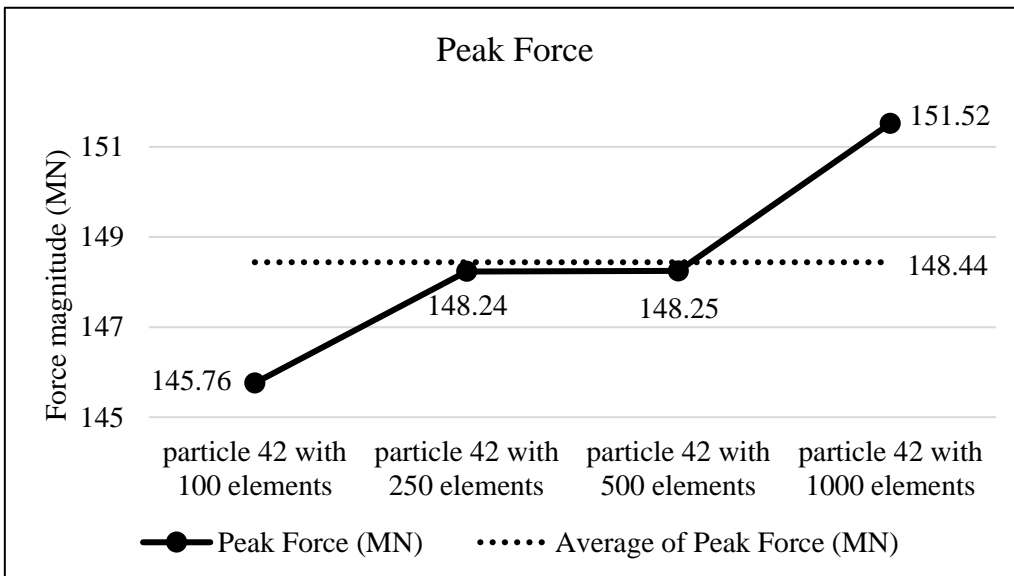


Figure A42.3 Peak collision for the four particle geometry resolutions for Particle 42

Appendix

Collision results data analysis					
Model	particle 42 with 100 elements	particle 42 with 250 elements	particle 42 with 500 elements	particle 42 with 1000 elements	Average
Impulse (MN*s)	0.749	0.768	0.762	0.764	0.761
Percent difference from Avg. Impulse	-1.51	0.98	0.14	0.39	
Peak Force (MN)	145.76	148.24	148.25	151.52	148.44
Percent difference from Avg. Peak Force	-1.81	-0.14	-0.13	2.07	

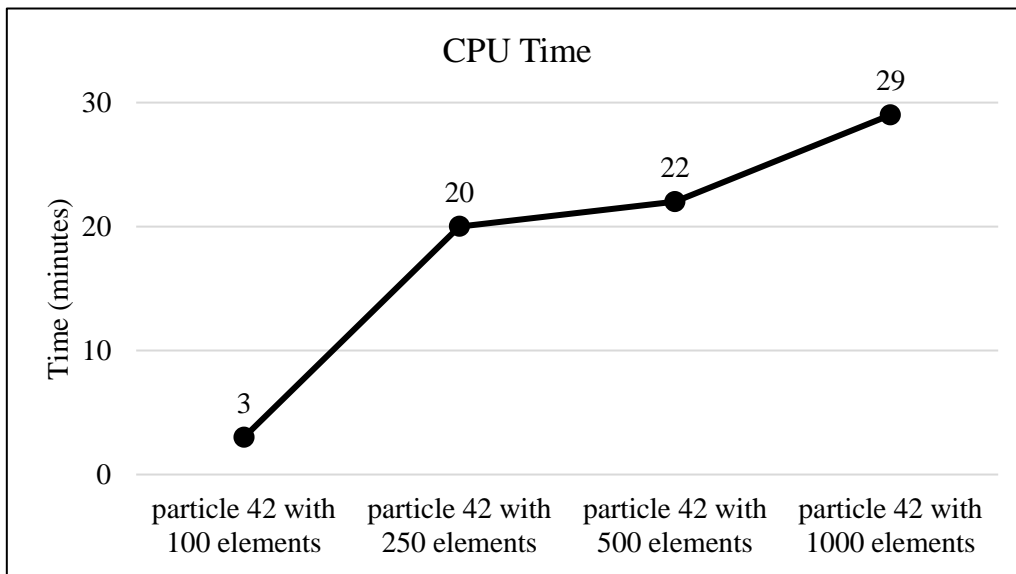
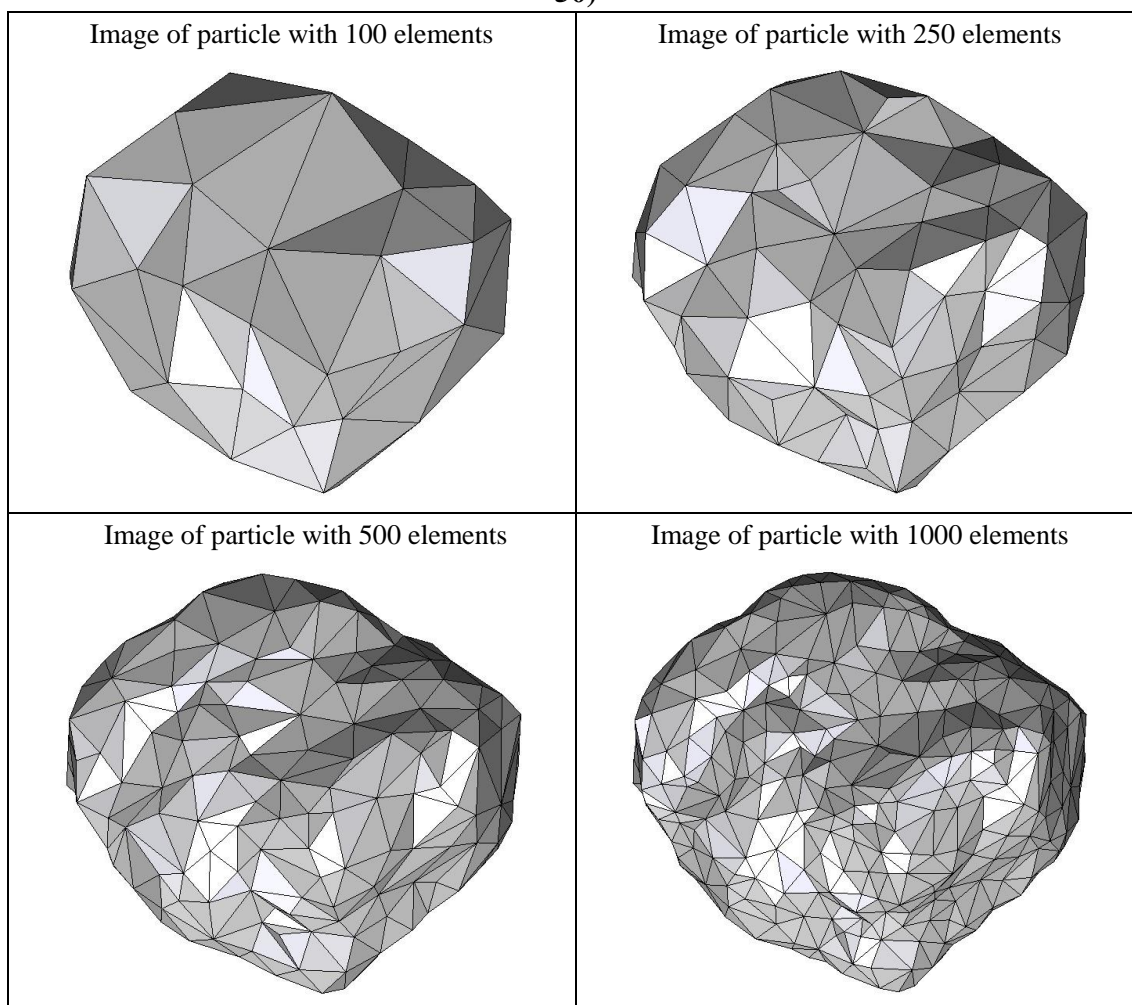


Figure A42.4 CPU computation time vs. model geometry resolution

Appendix

Percent difference analysis compare to particle 42 with 100 elements for different group of data			
	particle 42 with 250 elements	particle 42 with 500 elements	particle 42 with 1000 elements
Impulse	2.52	1.67	1.92
Peak Force	1.70	1.71	3.95
Start Time	-5.71	-5.71	-5.71
CPU Time	566.67	633.33	866.67
Simulation Time	-1.18	-1.18	2.35

Summary of particle characteristics and collision simulation details for Particle 43 (of 50)



Particle statistics (part 1)								
Particle ID	# vertices	# elements	Mass (g)	Moments of Inertia			Volume (cm ³)	Sfc. Area (cm ²)
				I1	I2	I3		
				(gcm ²)	(gcm ²)	(gcm ²)		
43 (100 elements)	52	100	22.346	75549.04375	59206.6875	43112.46563	8.05718	23.34229
43 (250 elements)	127	250	22.346	77043.36875	60947.20625	43355.08125	8.14011	23.59037
43 (500 elements)	252	500	22.346	78197.85	61779.6375	44075.04688	8.20802	23.69009
43 (1000 elements)	502	1000	22.346	78593.50625	62122.775	44298.14063	8.23082	23.69901

Appendix

Particle Statistics (part 2)							
Particle ID	α	R_g (cm)	ψ	R_v (cm)	L (cm)	I (cm)	S (cm)
43 (100 elements)	1.85023	1.78485	0.83265	1.24365	143.19748	115.33965	77.39451
43 (250 elements)	1.86326	1.78029	0.82954	1.24790	145.51646	115.33618	78.09791
43 (500 elements)	1.86215	1.81260	0.83063	1.25136	146.48729	116.34256	78.66587
43 (1000 elements)	1.86141	1.81417	0.83186	1.25252	146.88061	116.60729	78.90808

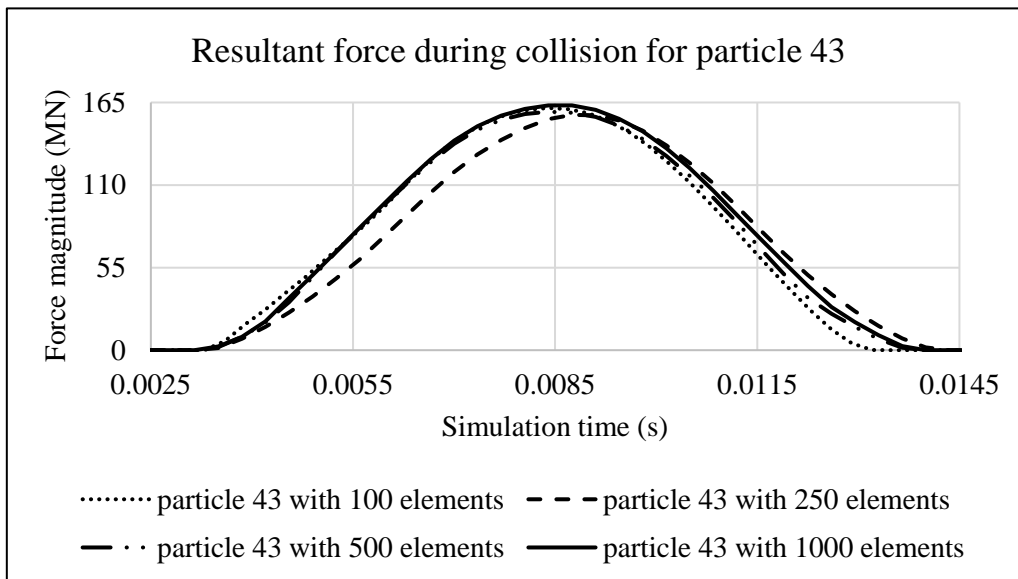


Figure A43.1 Plot of resultant forces during collision event for Particle 43

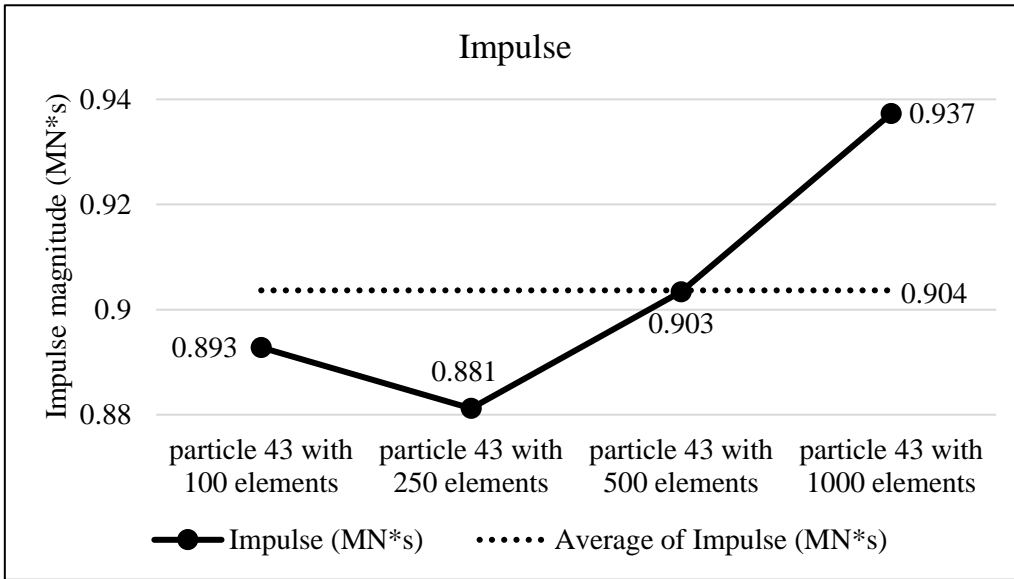


Figure A43.2 Plots of collision impulse for Particle 43

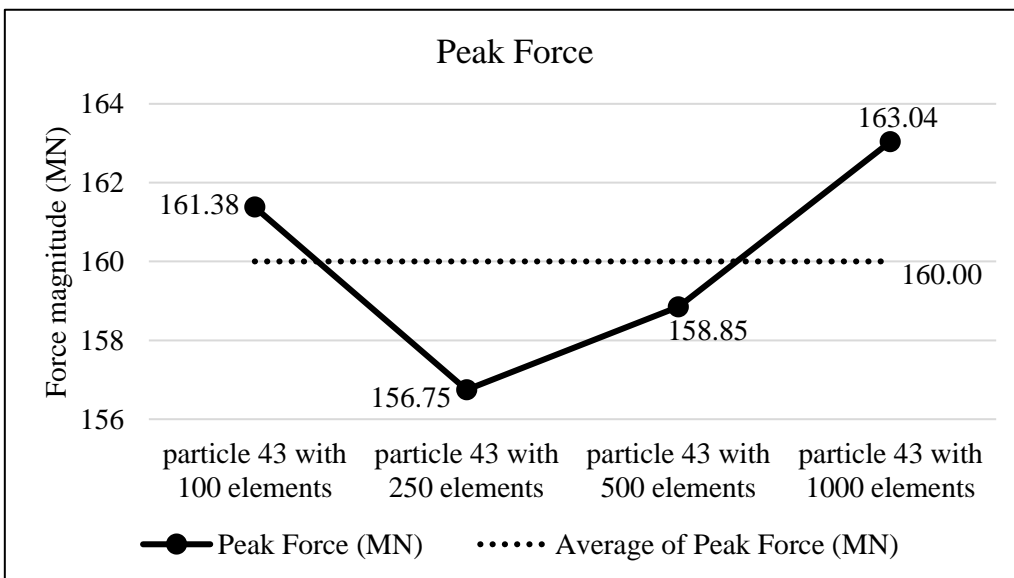


Figure A43.3 Peak collision for the four particle geometry resolutions for Particle 43

Appendix

Collision results data analysis					
Model	particle 43 with 100 elements	particle 43 with 250 elements	particle 43 with 500 elements	particle 43 with 1000 elements	Average
Impulse (MN*s)	0.893	0.881	0.903	0.937	0.904
Percent difference from Avg. Impulse	-1.21	-2.48	-0.03	3.72	
Peak Force (MN)	161.38	156.75	158.85	163.04	160.00
Percent difference from Avg. Peak Force	0.86	-2.04	-0.72	1.90	

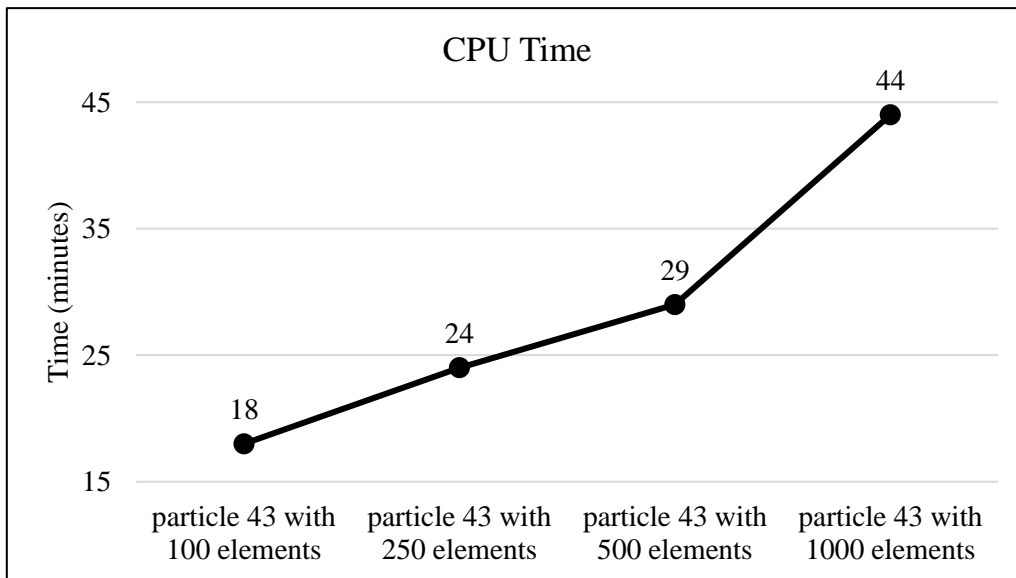
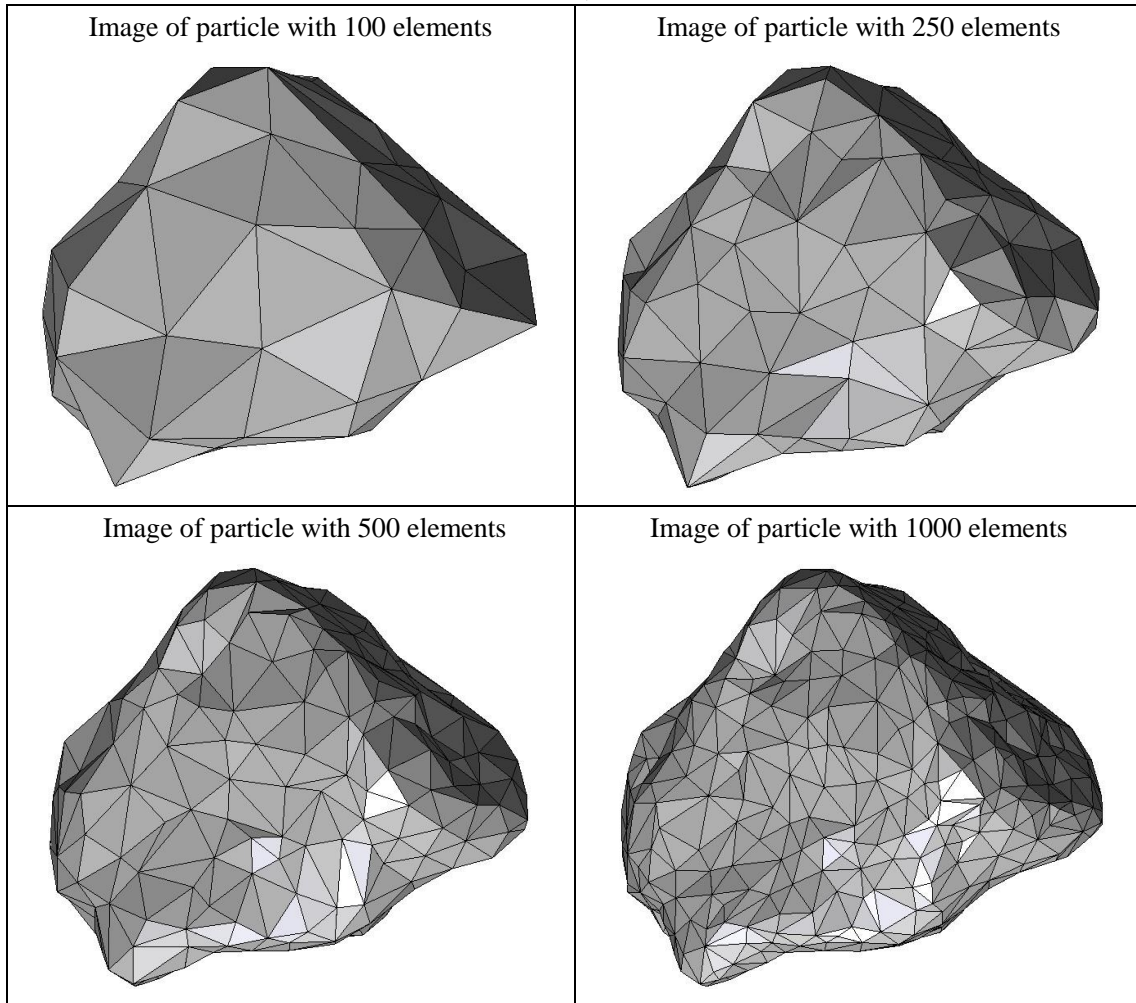


Figure A43.4 CPU computation time vs. model geometry resolution

Appendix

Percent difference analysis compare to particle 43 with 100 elements for different group of data			
	particle 43 with 250 elements	particle 43 with 500 elements	particle 43 with 1000 elements
Impulse	-1.30	1.19	4.99
Peak Force	-2.87	-1.57	1.03
Start Time	6.06	6.06	6.06
CPU Time	33.33	61.11	144.44
Simulation Time	6.06	2.53	2.53

Summary of particle characteristics and collision simulation details for Particle 44 (of 50)



Particle statistics (part 1)								
Particle ID	# vertices	# elements	Mass (g)	Moments of Inertia			Volume (cm ³)	Sfc. Area (cm ²)
				I1	I2	I3		
				(gcm ²)	(gcm ²)	(gcm ²)		
44 (100 elements)	52	100	11.898	25637.44531	21374.55781	14950.66094	4.25754	15.27314
44 (250 elements)	127	250	11.898	26232.45313	21815.66563	15183.52656	4.29320	15.39188
44 (500 elements)	252	500	11.898	26716.325	22216.125	15410.14063	4.33335	15.43330
44 (1000 elements)	502	1000	11.898	26830.26875	22319.46094	15481.92813	4.34484	15.43498

Appendix

Particle Statistics (part 2)							
Particle ID	α	R_g (cm)	ψ	R_v (cm)	L (cm)	I (cm)	S (cm)
44 (100 elements)	1.73200	1.62087	0.83175	1.00544	116.07505	89.85698	67.01803
44 (250 elements)	1.74712	1.57165	0.82994	1.00824	117.52010	90.75688	67.26515
44 (500 elements)	1.75289	1.57642	0.83286	1.01137	118.69023	91.47183	67.71100
44 (1000 elements)	1.75179	1.5797	0.83425	1.01227	118.94752	91.66090	67.90058

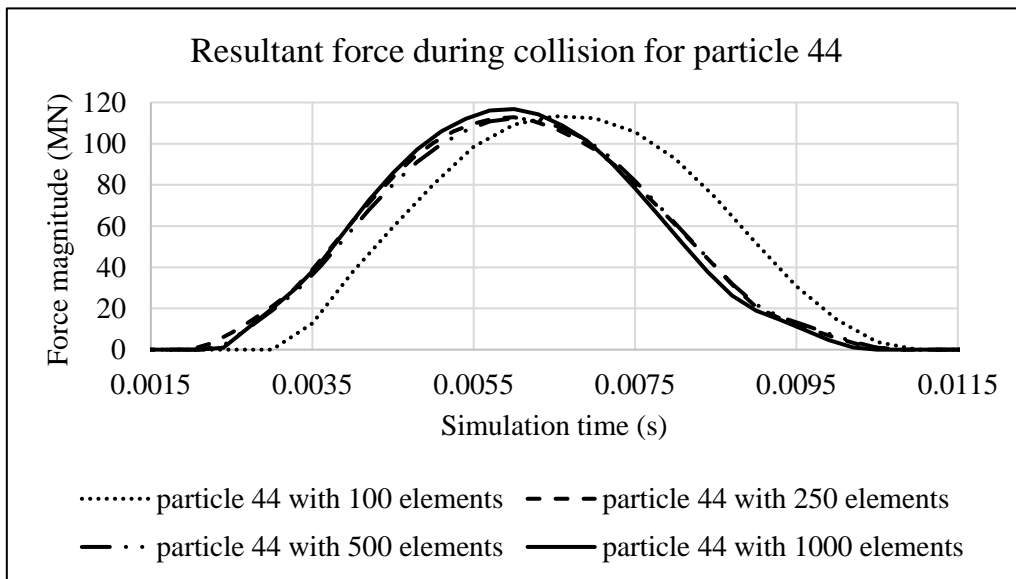


Figure A44.1 Plot of resultant forces during collision event for Particle 44.

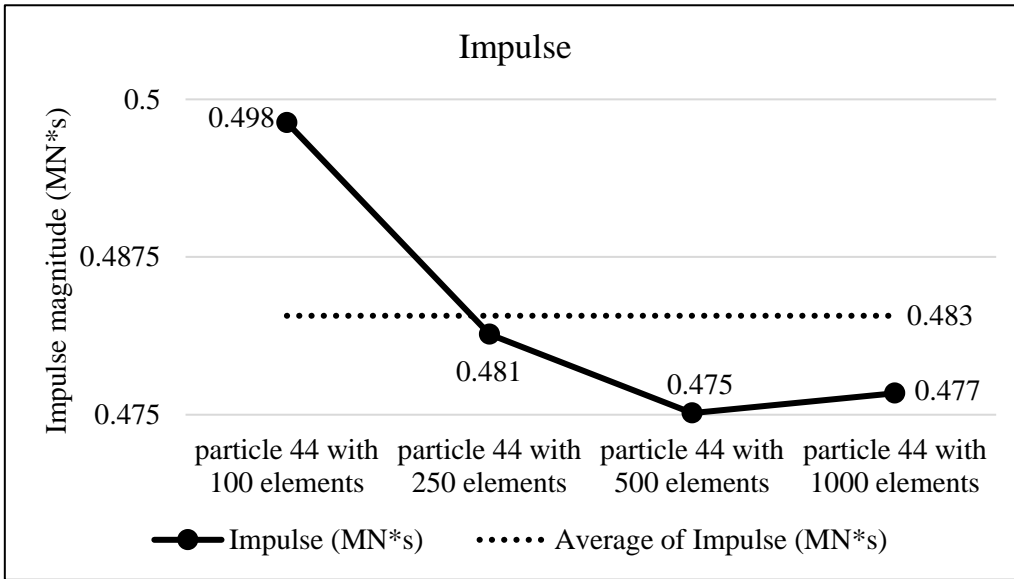


Figure A44.2 Plots of collision impulse for Particle 44

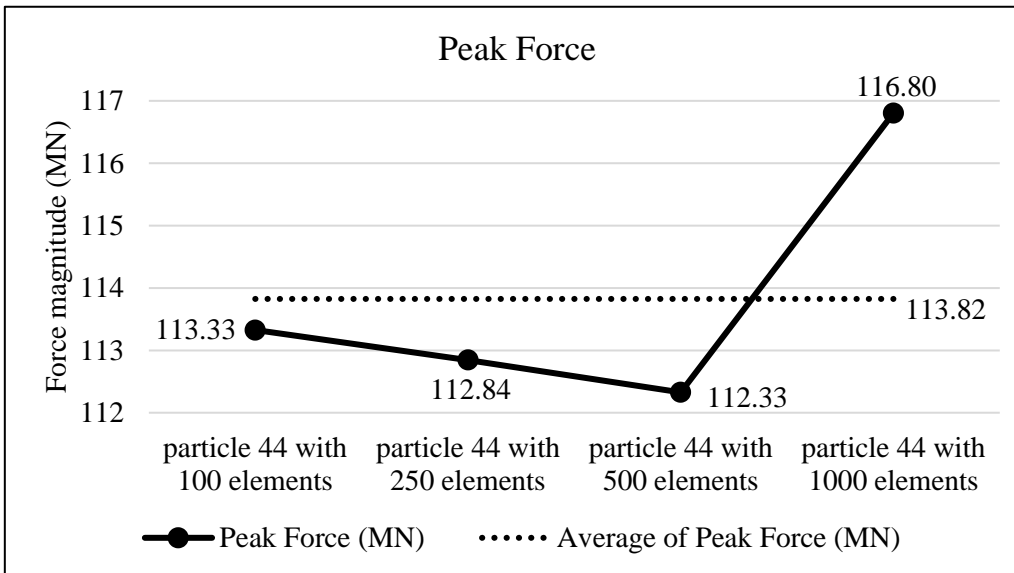


Figure A44.3 Peak collision for the four particle geometry resolutions for Particle 44

Appendix

Collision results data analysis					
Model	particle 44 with 100 elements	particle 44 with 250 elements	particle 44 with 500 elements	particle 44 with 1000 elements	Average
Impulse (MN*s)	0.498	0.481	0.475	0.477	0.483
Percent difference from Avg. Impulse	3.17	-0.30	-1.60	-1.27	
Peak Force (MN)	113.33	112.84	112.33	116.80	113.82
Percent difference from Avg. Peak Force	-0.44	-0.86	-1.32	2.62	

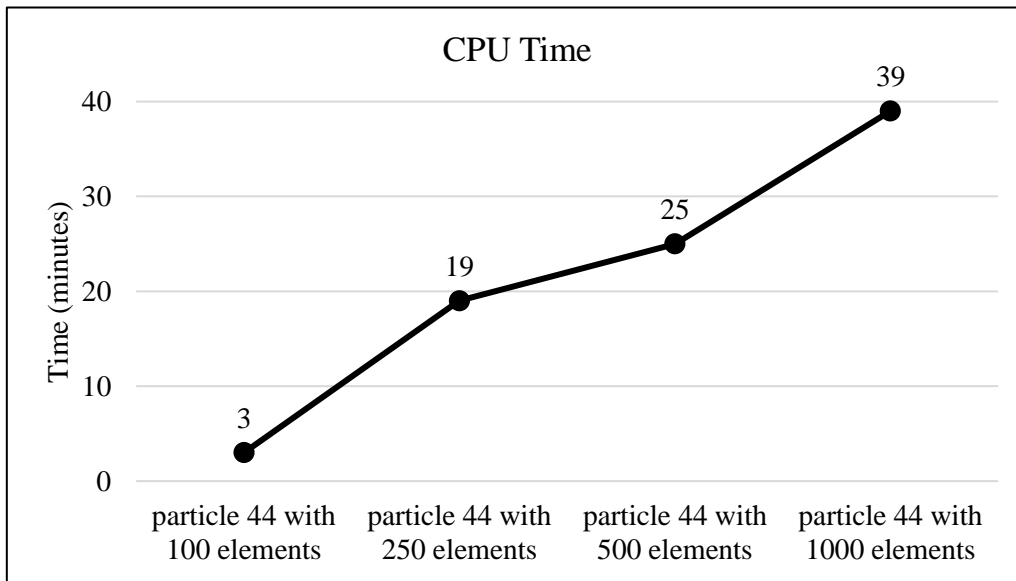


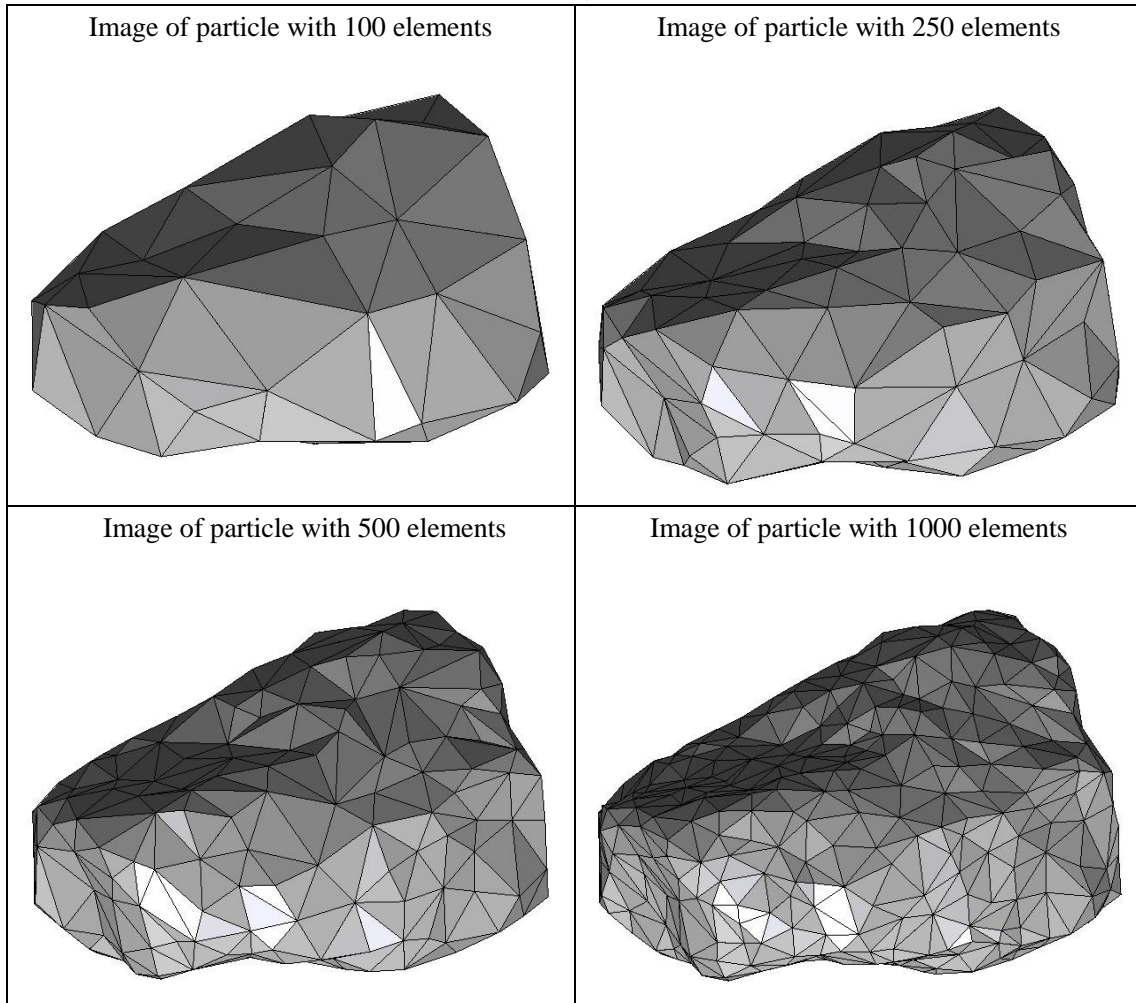
Figure A44.4 CPU computation time vs. model geometry resolution

Appendix

Percent difference analysis compare to particle 44 with 100 elements for different group of data			
	particle 44 with 250 elements	particle 44 with 500 elements	particle 44 with 1000 elements
Impulse	-3.37	-4.62	-4.31
Peak Force	-0.42	-0.88	3.07
Start Time	-42.86	-31.43	-31.43
CPU Time	533.33	733.33	1200.00
Simulation Time	16.67	8.00	4.00

Appendix

Summary of particle characteristics and collision simulation details for Particle 45 (of 50)



Particle statistics (part 1)								
Particle ID	# vertices	# elements	Mass (g)	Moments of Inertia			Volume (cm ³)	Sfc. Area (cm ²)
				I1	I2	I3		
				(gcm ²)	(gcm ²)	(gcm ²)		
45 (100 elements)	52	100	20.84	77043.91875	66730.50625	31557.29063	7.46035	22.44142
45 (250 elements)	127	250	20.84	78544.125	68104.8125	32200.23438	7.52626	22.72981
45 (500 elements)	252	500	20.84	79109.16875	68564.525	32327.26875	7.54389	22.80248
45 (1000 elements)	502	1000	20.84	79367.65	68805.55625	32499.4375	7.56373	22.79708

Appendix

Particle Statistics (part 2)							
Particle ID	α	R_g (cm)	ψ	R_v (cm)	L (cm)	I (cm)	S (cm)
45 (100 elements)	2.29833	1.96017	0.82276	1.21215	164.08381	100.22851	71.39257
45 (250 elements)	2.29333	1.92400	0.81710	1.21571	165.70728	101.14454	72.25615
45 (500 elements)	2.30116	1.93092	0.81577	1.21666	166.35590	101.41976	72.29217
45 (1000 elements)	2.29628	1.92908	0.81739	1.21772	166.59179	101.64380	72.54845

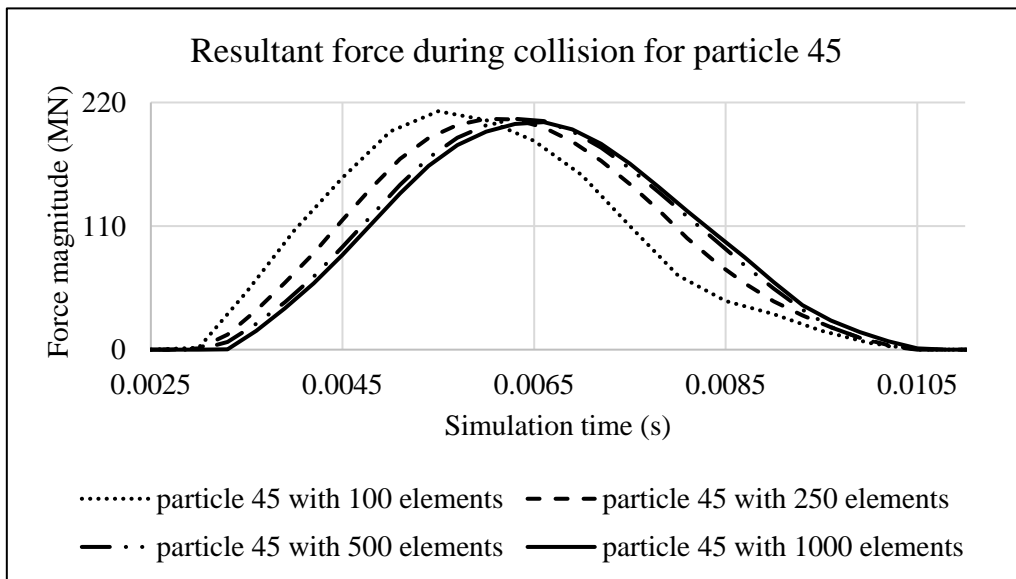


Figure A45.1 Plot of resultant forces during collision event for Particle 45

Appendix

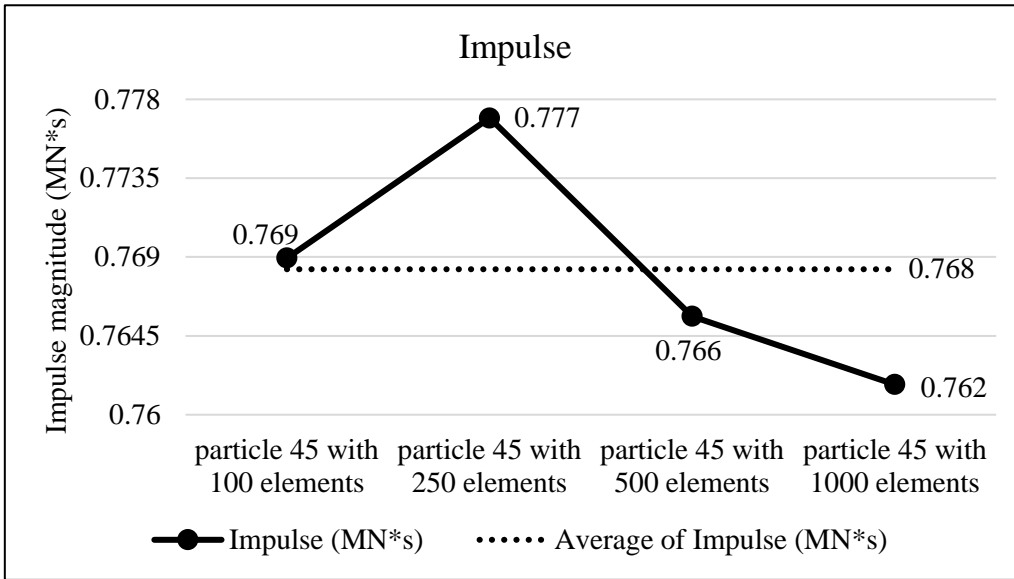


Figure A45.2 Plots of collision impulse for Particle 45

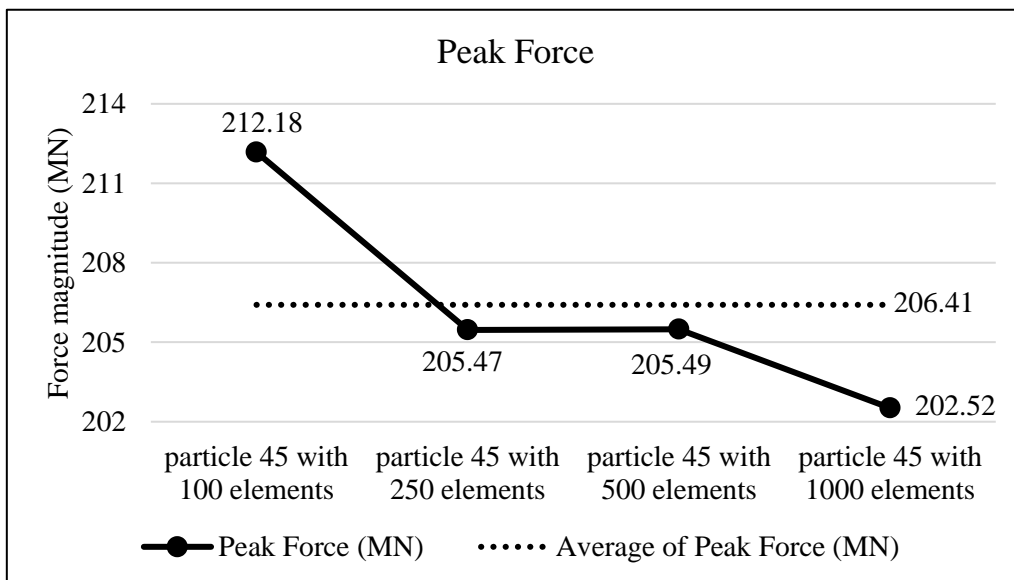


Figure A45.3 Peak collision for the four particle geometry resolutions for Particle 45

Appendix

Collision results data analysis					
Model	particle 45 with 100 elements	particle 45 with 250 elements	particle 45 with 500 elements	particle 45 with 1000 elements	Average
Impulse (MN*s)	0.769	0.777	0.766	0.762	0.768
Percent difference from Avg. Impulse	0.08	1.12	-0.35	-0.86	
Peak Force (MN)	212.18	205.47	205.49	202.52	206.41
Percent difference from Avg. Peak Force	2.79	-0.46	-0.45	-1.89	

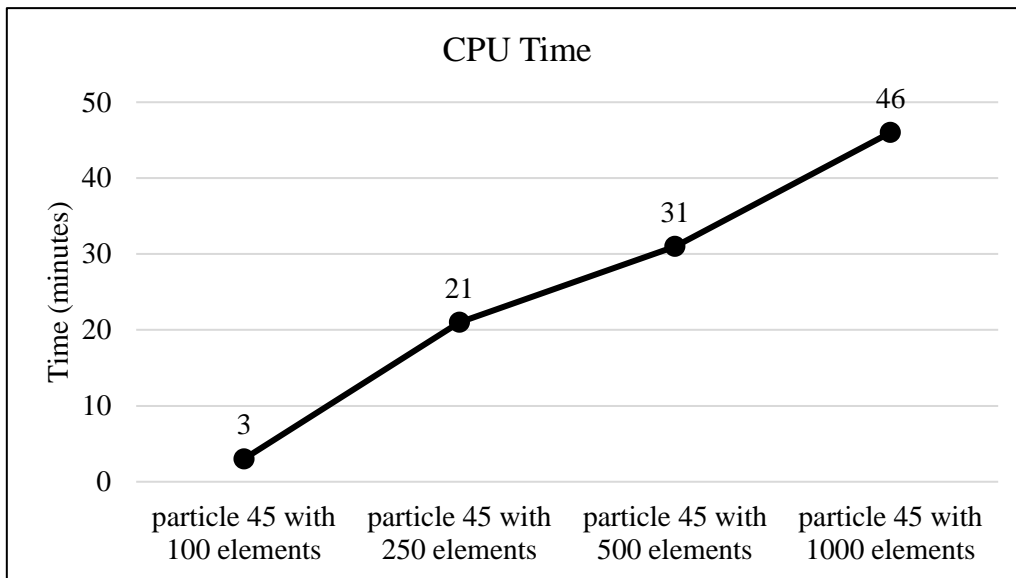
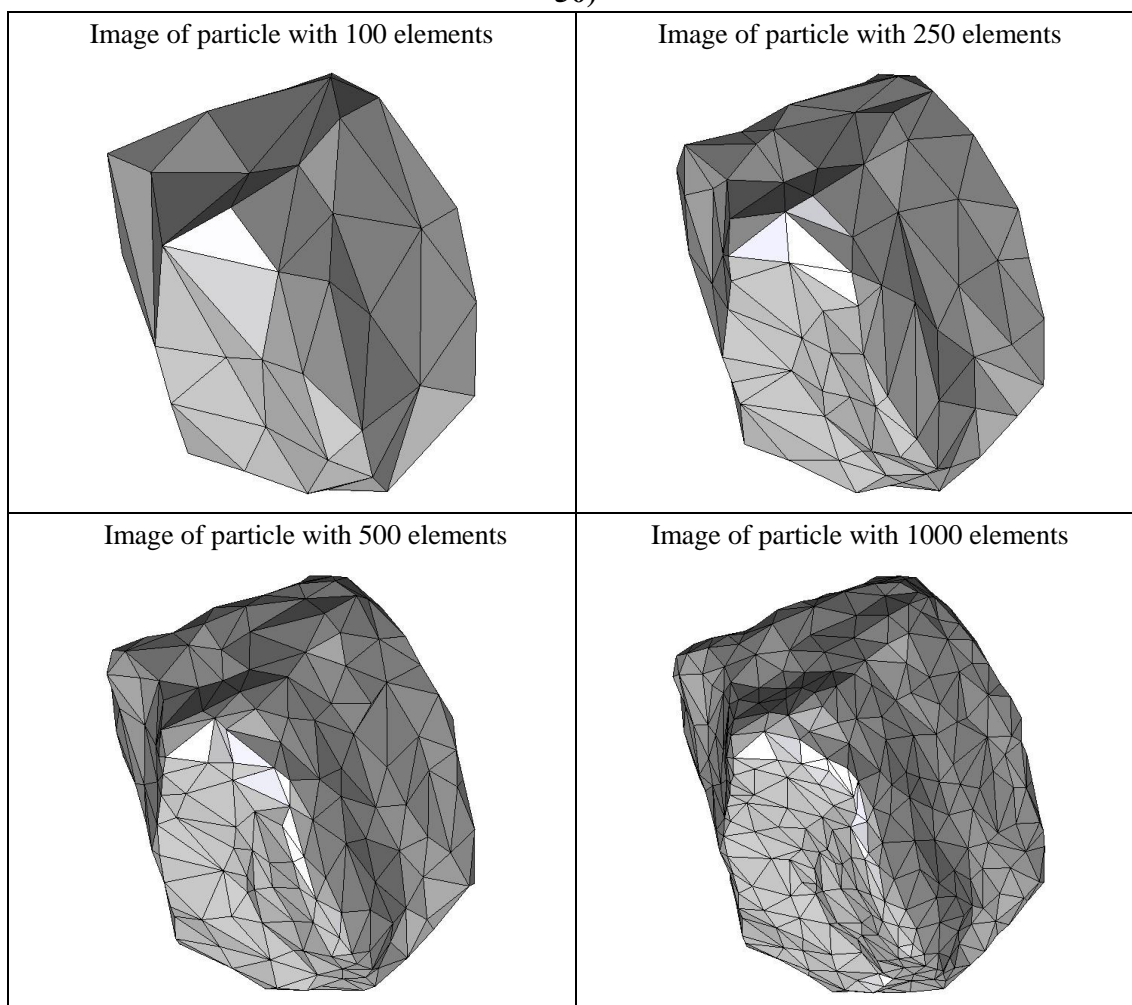


Figure A45.4 CPU computation time vs. model geometry resolution

Appendix

Percent difference analysis compare to particle 45 with 100 elements for different group of data			
	particle 45 with 250 elements	particle 45 with 500 elements	particle 45 with 1000 elements
Impulse	1.04	-0.43	-0.94
Peak Force	-3.16	-3.15	-4.55
Start Time	0.00	0.00	10.00
CPU Time	600.00	933.33	1433.33
Simulation Time	0.00	-4.00	-4.00

Summary of particle characteristics and collision simulation details for Particle 46 (of 50)



Particle statistics (part 1)								
Particle ID	# vertices	# elements	Mass (g)	Moments of Inertia			Volume (cm ³)	Sfc. Area (cm ²)
				I1	I2	I3		
				(gcm ²)	(gcm ²)	(gcm ²)		
46 (100 elements)	52	100	31.947	124773.025	121395.1625	88363.5	12.26823	30.00924
46 (250 elements)	127	250	31.947	125357.8125	122032.6125	89180.01875	12.32041	30.06568
46 (500 elements)	252	500	31.947	126316.45	123190.7375	89788.475	12.36937	30.11559
46 (1000 elements)	502	1000	31.947	126684.2875	123595.9375	90119.49375	12.39072	30.07645

Appendix

Particle Statistics (part 2)							
Particle ID	α	R_g (cm)	ψ	R_v (cm)	L (cm)	I (cm)	S (cm)
46 (100 elements)	1.36266	2.07262	0.82276	1.43075	157.15562	119.82641	115.33012
46 (250 elements)	1.35749	2.06064	0.81710	1.43278	157.35751	120.32423	115.91838
46 (500 elements)	1.35757	2.04524	0.85886	1.43467	158.10582	120.58991	116.46253
46 (1000 elements)	1.35657	2.02699	0.86097	1.43550	158.32445	120.78032	116.70980

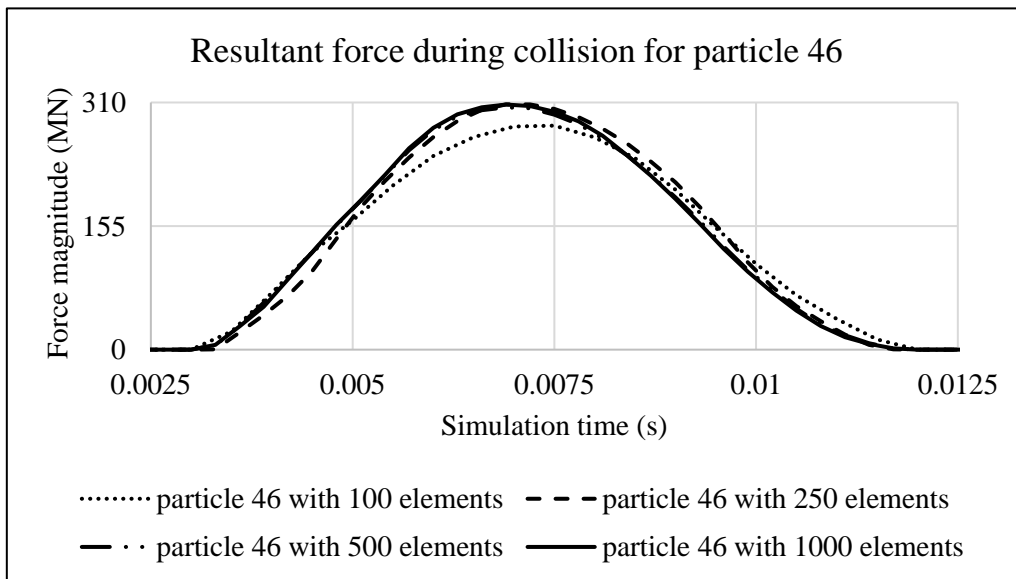


Figure A46.1 Plot of resultant forces during collision event for Particle 46

Appendix

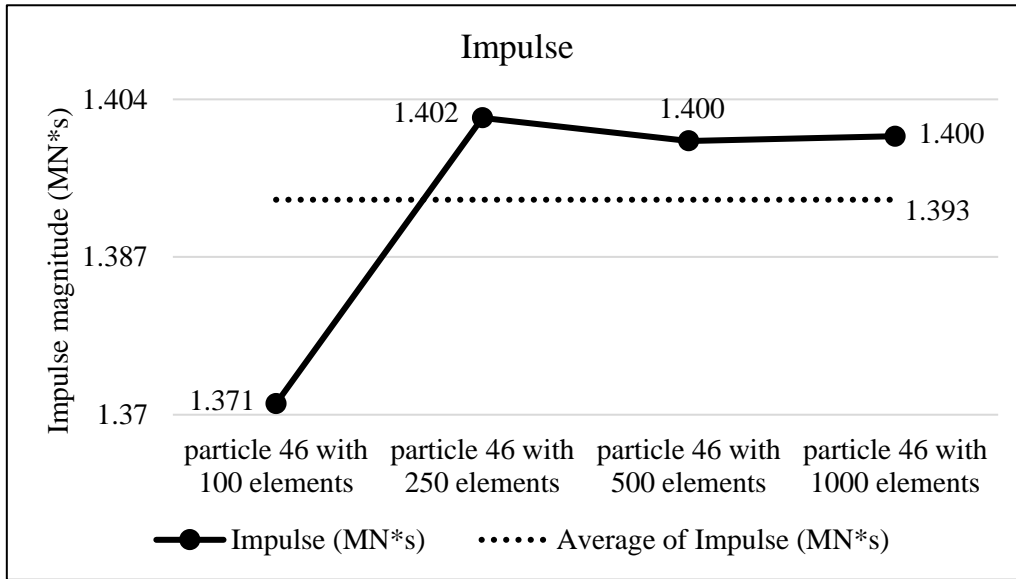


Figure A46.2 Plots of collision impulse for Particle 46

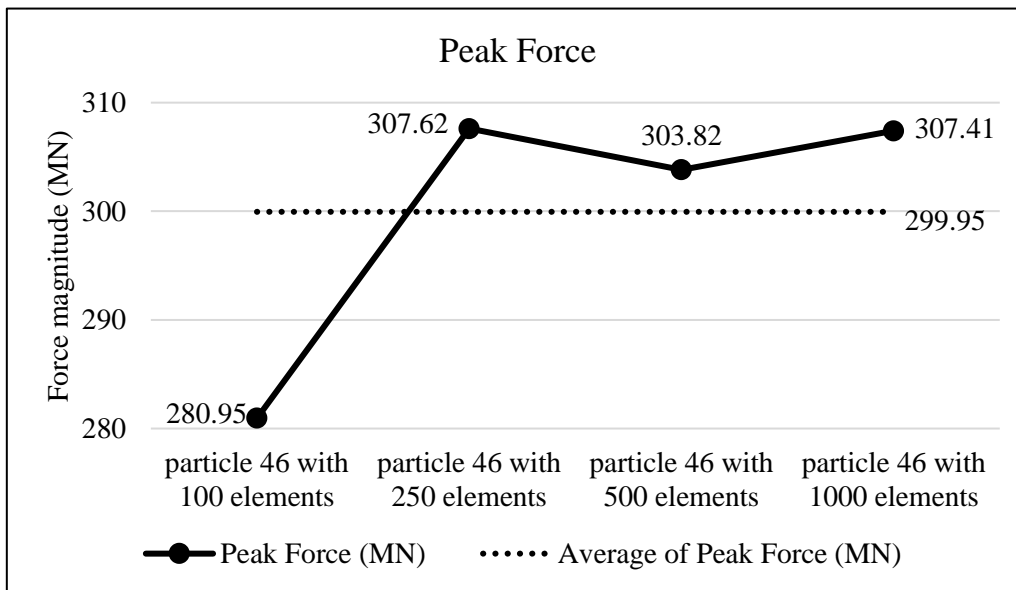


Figure A46.3 Peak collision for the four particle geometry resolutions for Particle 46

Appendix

Collision results data analysis					
Model	particle 46 with 100 elements	particle 46 with 250 elements	particle 46 with 500 elements	particle 46 with 1000 elements	Average
Impulse (MN*s)	1.371	1.402	1.400	1.400	1.393
Percent difference from Avg. Impulse	-1.58	0.63	0.45	0.49	
Peak Force (MN)	280.95	307.62	303.82	307.41	299.95
Percent difference from Avg. Peak Force	-6.33	2.56	1.29	2.49	

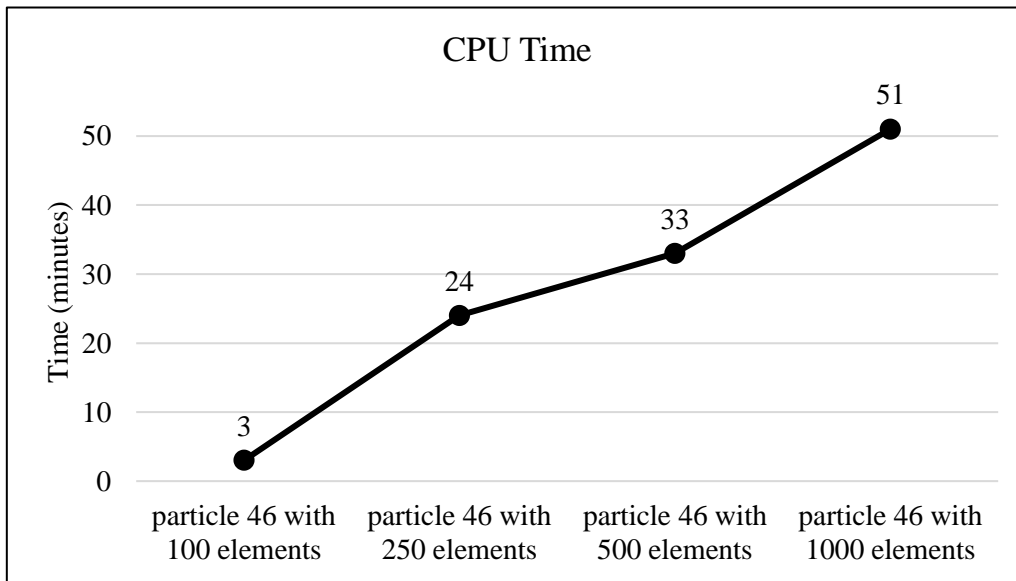
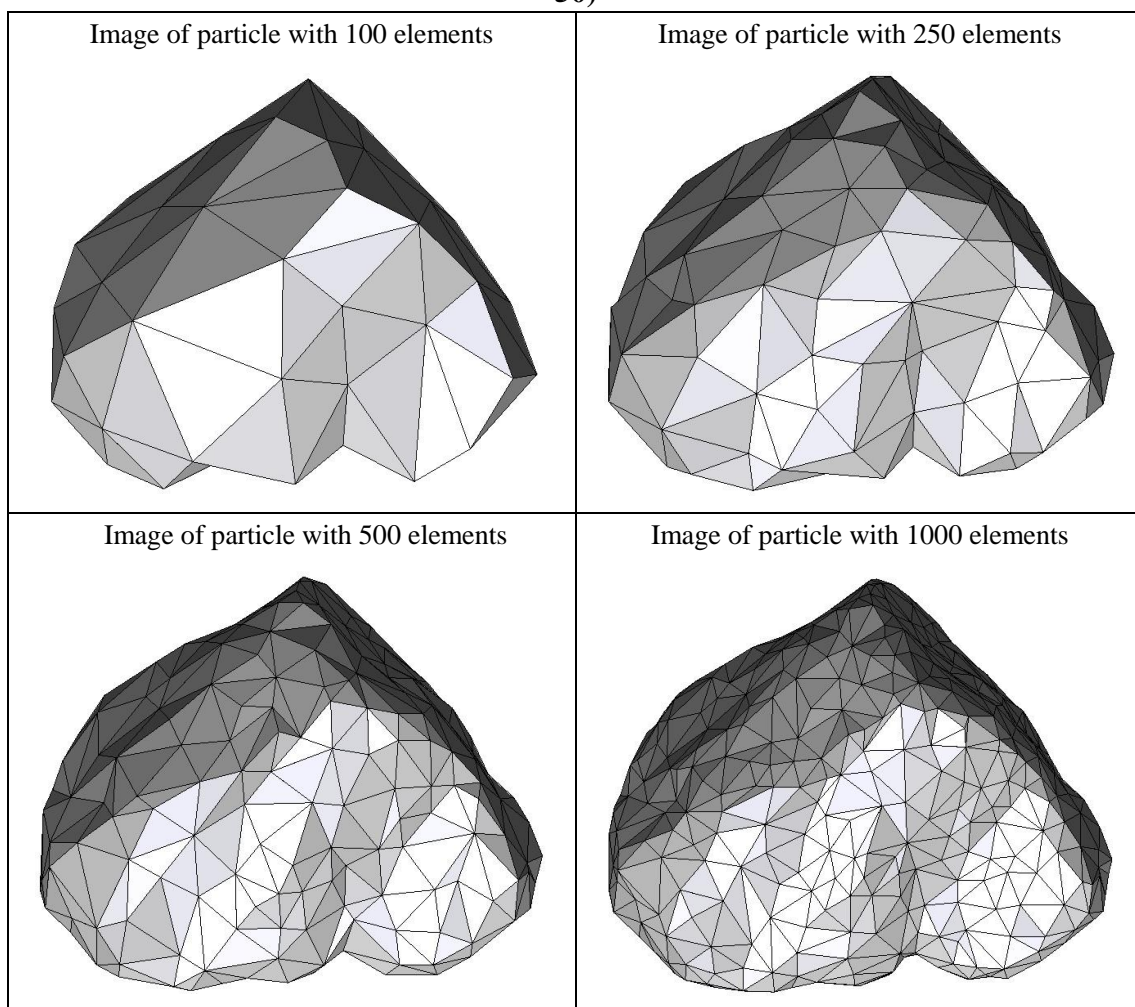


Figure A46.4 CPU computation time vs. model geometry resolution

Appendix

Percent difference analysis compare to particle 46 with 100 elements for different group of data			
	particle 46 with 250 elements	particle 46 with 500 elements	particle 46 with 1000 elements
Impulse	2.25	2.06	2.10
Peak Force	9.49	8.14	9.42
Start Time	-5.71	-5.71	-5.71
CPU Time	700.00	1000.00	1600.00
Simulation Time	-1.18	-1.18	-1.18

Summary of particle characteristics and collision simulation details for Particle 47 (of 50)



Particle statistics (part 1)								
Particle ID	# vertices	# elements	Mass (g)	Moments of Inertia			Volume (cm ³)	Sfc. Area (cm ²)
				I1	I2	I3		
				(gcm ²)	(gcm ²)	(gcm ²)		
47 (100 elements)	52	100	22.534	93792.43125	71448.25625	50491.16875	8.57624	26.30173
47 (250 elements)	127	250	22.534	96310.73125	72497.45625	52756.39375	8.71372	26.35709
47 (500 elements)	252	500	22.534	97290.525	73096.80625	53249.1	8.75696	26.37792
47 (1000 elements)	502	1000	22.534	97693.98125	73447.25	53477.16875	8.78162	26.33476

Appendix

Particle Statistics (part 2)							
Particle ID	α	R_g (cm)	ψ	R_v (cm)	L (cm)	I (cm)	S (cm)
47 (100 elements)	2.01911	2.18744	0.77037	1.26980	159.56634	127.12675	79.02816
47 (250 elements)	2.00241	2.18963	0.77694	1.27655	160.46924	130.34496	80.13800
47 (500 elements)	2.00787	2.17109	0.77890	1.27866	161.21862	131.08604	80.29327
47 (1000 elements)	2.00634	2.17291	0.78164	1.27986	161.58006	131.32371	80.53479

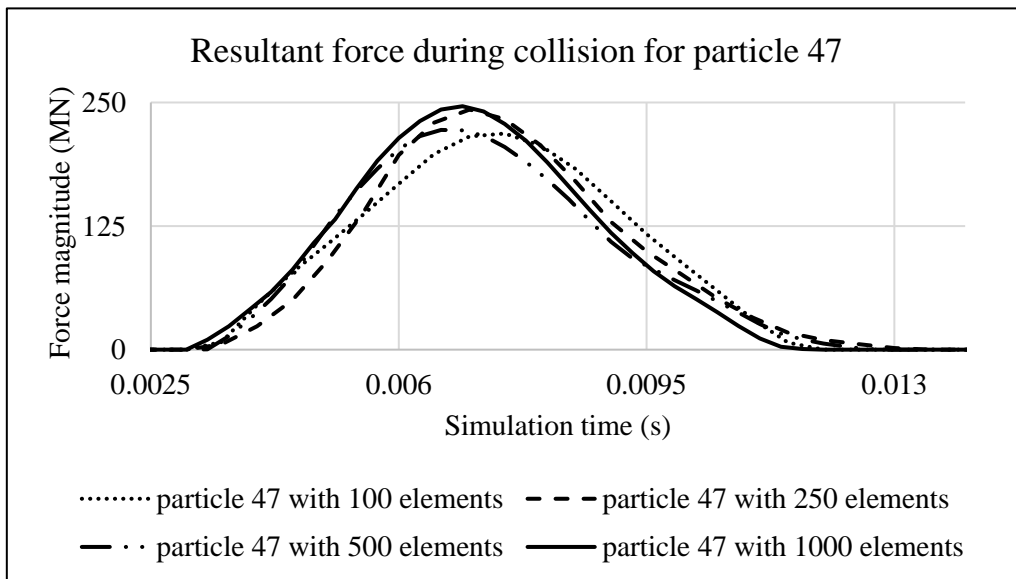


Figure A47.1 Plot of resultant forces during collision event for Particle 47

Appendix

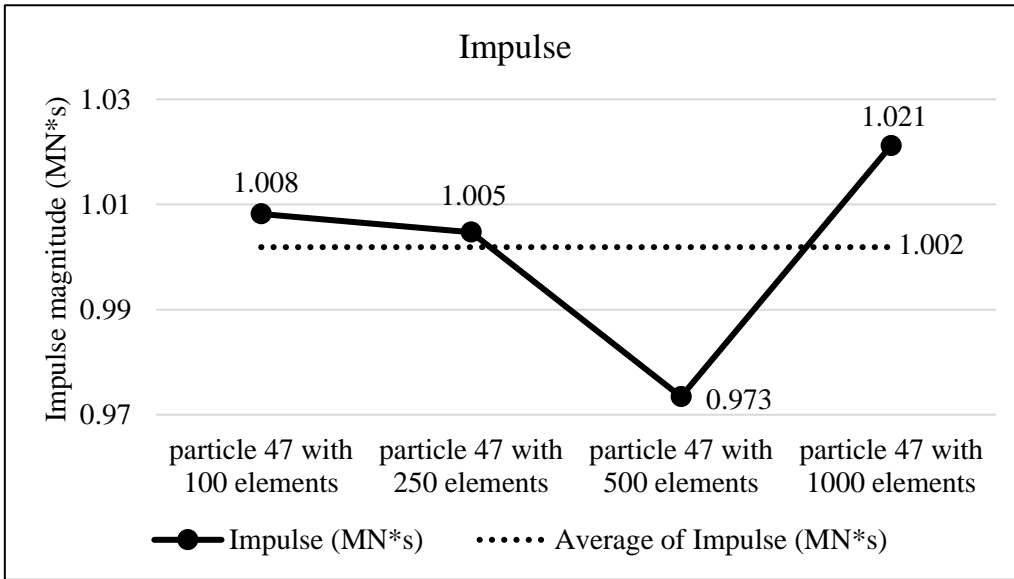


Figure A47.2 Plots of collision impulse for Particle 47

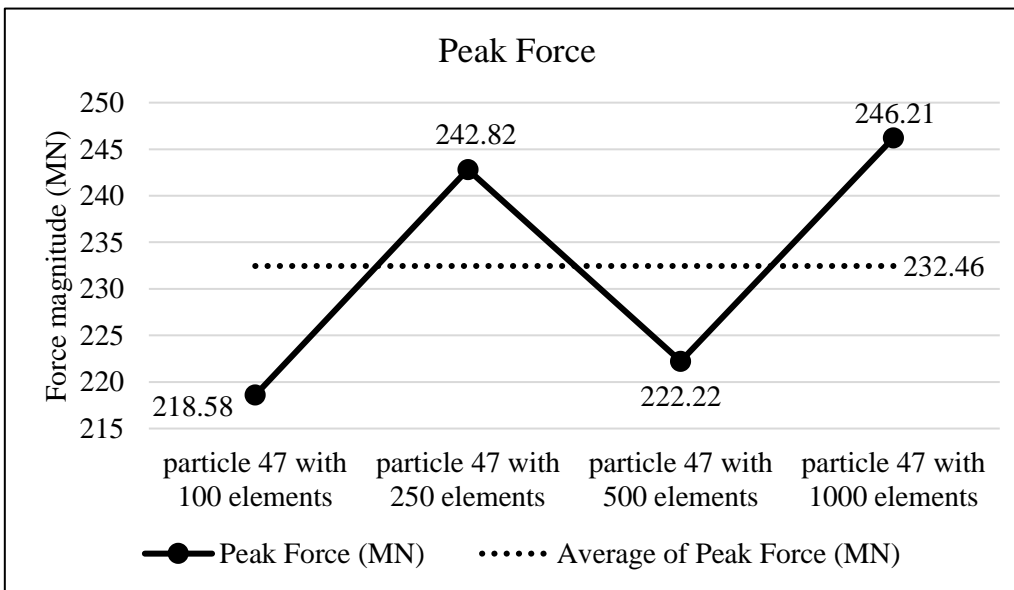


Figure A47.3 Peak collision for the four particle geometry resolutions for Particle 47

Appendix

Collision results data analysis					
Model	particle 47 with 100 elements	particle 47 with 250 elements	particle 47 with 500 elements	particle 47 with 1000 elements	Average
Impulse (MN*s)	1.008	1.005	0.973	1.021	1.002
Percent difference from Avg. Impulse	0.63	0.28	-2.84	1.93	
Peak Force (MN)	218.58	242.82	222.22	246.21	232.46
Percent difference from Avg. Peak Force	-5.97	4.46	-4.41	5.92	

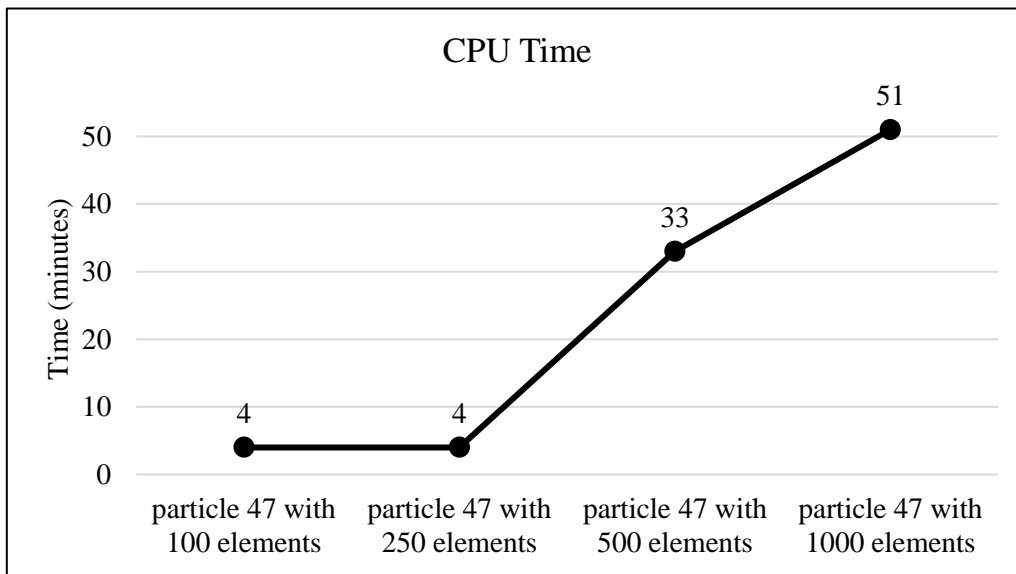


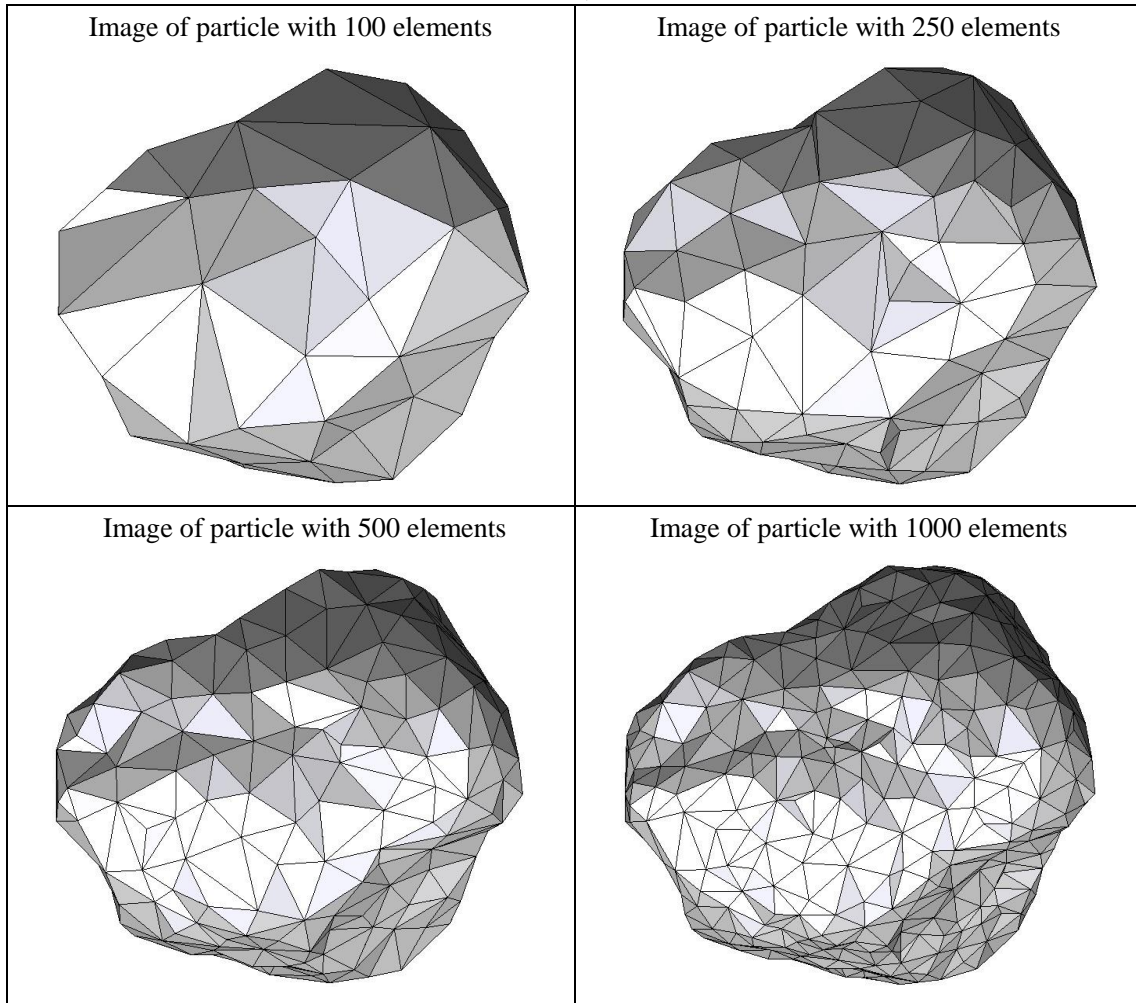
Figure A47.4 CPU computation time vs. model geometry resolution

Appendix

Percent difference analysis compare to particle 47 with 100 elements for different group of data			
	particle 47 with 250 elements	particle 47 with 500 elements	particle 47 with 1000 elements
Impulse	-0.34	-3.45	1.29
Peak Force	11.09	1.66	12.64
Start Time	0.00	-5.71	-5.71
CPU Time	0.00	725.00	1175.00
Simulation Time	17.65	9.41	-1.18

Appendix

Summary of particle characteristics and collision simulation details for Particle 48 (of 50)



Particle statistics (part 1)								
Particle ID	# vertices	# elements	Mass (g)	Moments of Inertia			Volume (cm ³)	Sfc. Area (cm ²)
				I1	I2	I3		
				(gcm ²)	(gcm ²)	(gcm ²)		
48 (100 elements)	52	100	29.482	130630.175	94967.525	69441.55625	10.41703	28.33498
48 (250 elements)	127	250	29.482	135947.7375	98621.6125	72534.09375	10.64583	28.68334
48 (500 elements)	252	500	29.482	137477.5375	99883.15625	73449.65	10.72253	28.81320
48 (1000 elements)	502	1000	29.482	138095.1375	100255.05	73731.03125	10.74077	28.85356

Appendix

Particle Statistics (part 2)							
Particle ID	α	R_g (cm)	ψ	R_v (cm)	L (cm)	I (cm)	S (cm)
48 (100 elements)	2.15009	2.17180	0.81406	1.35483	162.73691	133.51086	75.68840
48 (250 elements)	2.14528	2.12708	0.81591	1.36468	165.77204	136.49815	77.27287
48 (500 elements)	2.13810	2.12813	0.81613	1.36795	166.72881	137.23160	77.97996
48 (1000 elements)	2.14165	2.87899	0.81591	1.36872	167.08856	137.55691	78.01875

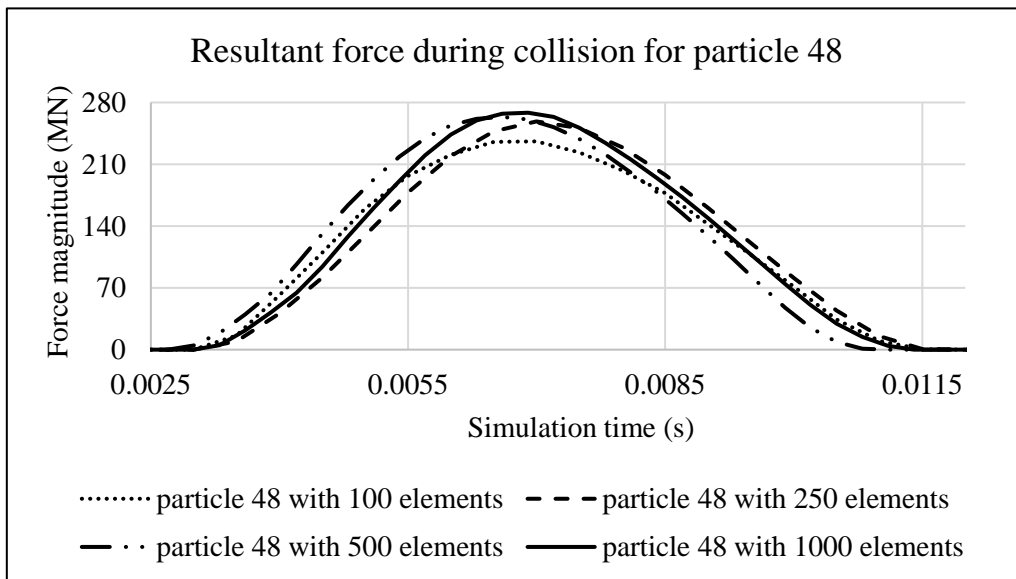


Figure A48.1 Plot of resultant forces during collision event for Particle 48

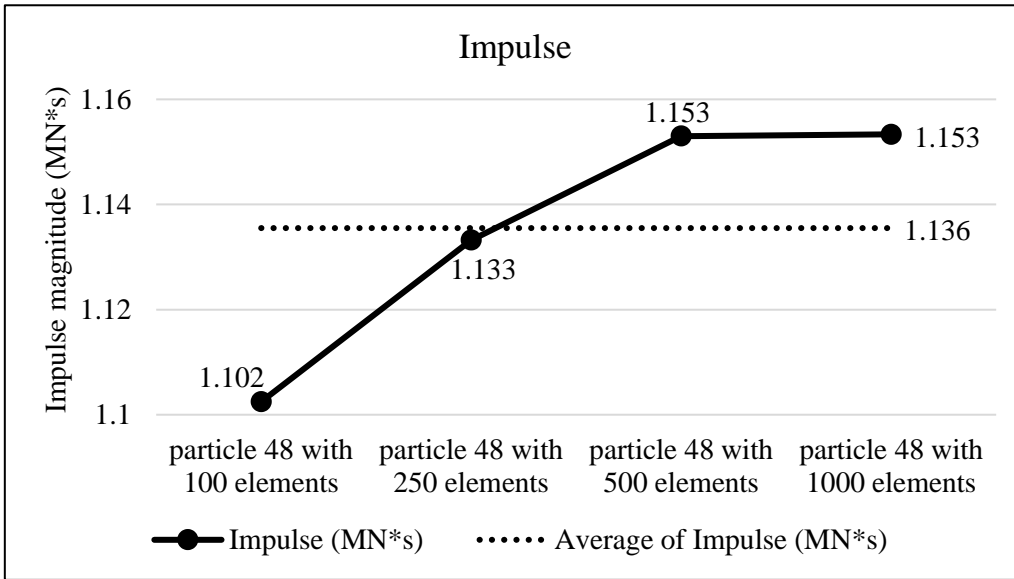


Figure A48.2 Plots of collision impulse for Particle 48

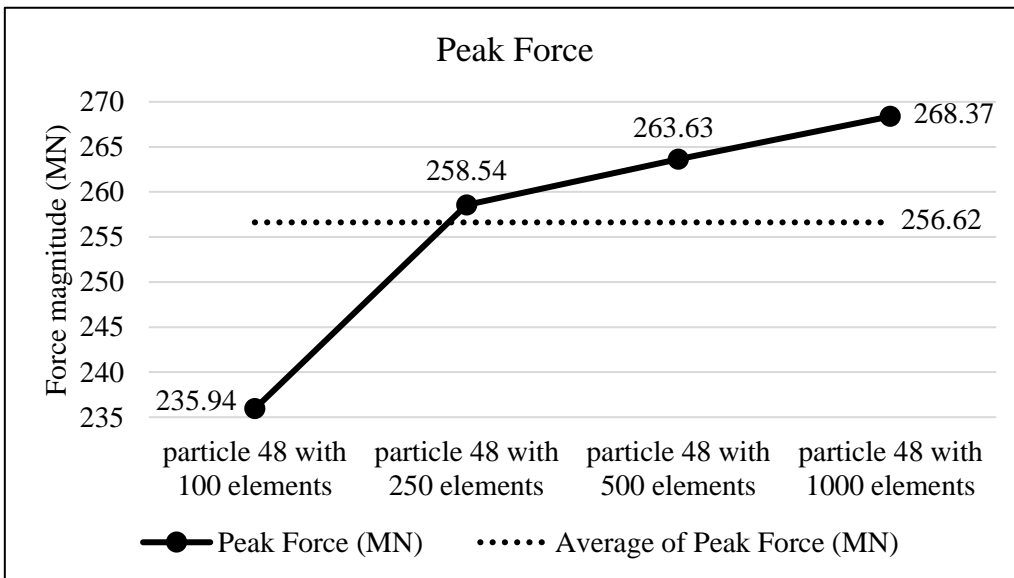


Figure A48.3 Peak collision for the four particle geometry resolutions for Particle 48

Appendix

Collision results data analysis					
Model	particle 48 with 100 elements	particle 48 with 250 elements	particle 48 with 500 elements	particle 48 with 1000 elements	Average
Impulse (MN*s)	1.102	1.133	1.153	1.153	1.136
Percent difference from Avg. Impulse	-2.91	-0.20	1.54	1.57	
Peak Force (MN)	235.94	258.54	263.63	268.37	256.62
Percent difference from Avg. Peak Force	-8.06	0.75	2.73	4.58	

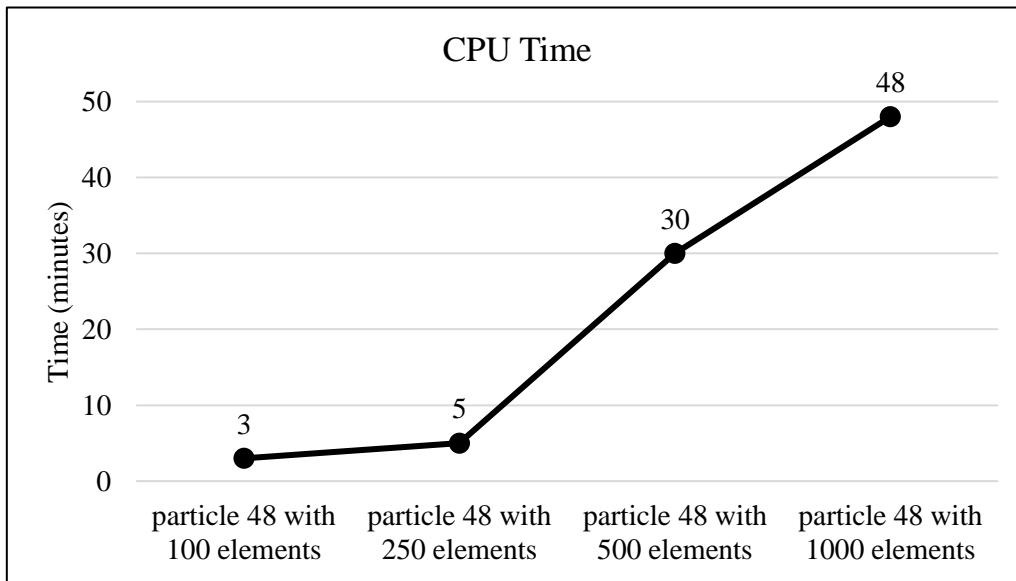


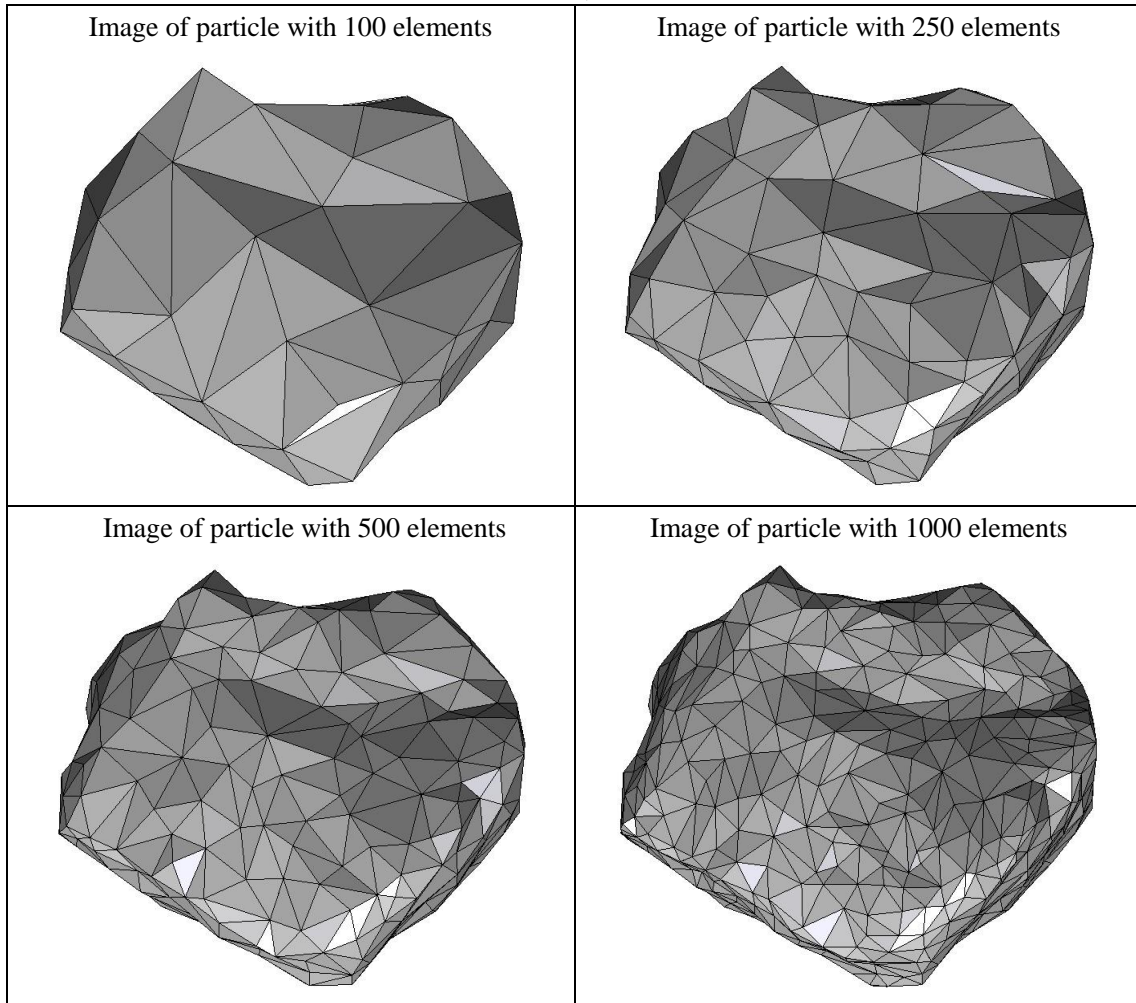
Figure A48.4 CPU computation time vs. model geometry resolution

Appendix

Percent difference analysis compare to particle 48 with 100 elements for different group of data			
	particle 48 with 250 elements	particle 48 with 500 elements	particle 48 with 1000 elements
Impulse	2.79	4.58	4.62
Peak Force	9.58	11.74	13.75
Start Time	-14.29	-22.86	-14.29
CPU Time	66.67	900.00	1500.00
Simulation Time	6.25	1.25	5.00

Appendix

Summary of particle characteristics and collision simulation details for Particle 49 (of 50)



Particle statistics (part 1)								
Particle ID	# vertices	# elements	Mass (g)	Moments of Inertia			Volume (cm ³)	Sfc. Area (cm ²)
				I1	I2	I3		
				(gcm ²)	(gcm ²)	(gcm ²)		
49 (100 elements)	52	100	33.504	193277.0375	139847.8	85655.58125	11.97908	33.24530
49 (250 elements)	127	250	33.504	199196.125	142949.7125	89051.24375	12.17912	33.57618
49 (500 elements)	252	500	33.504	200887.2625	144023.1875	90008.79375	12.24454	33.65584
49 (1000 elements)	502	1000	33.504	201751.025	144800.5625	90268.375	12.27319	33.67124

Appendix

Particle Statistics (part 2)							
Particle ID	α	R_g (cm)	ψ	R_v (cm)	L (cm)	I (cm)	S (cm)
49 (100 elements)	2.77112	2.48048	0.76156	1.41942	192.17518	144.07099	69.34932
49 (250 elements)	2.77762	2.42030	0.76242	1.42728	194.34712	147.25362	69.96899
49 (500 elements)	2.77319	2.41305	0.76334	1.42983	195.03969	148.04968	70.33052
49 (1000 elements)	2.77346	2.41168	0.76418	1.43095	195.56753	148.22394	70.51403

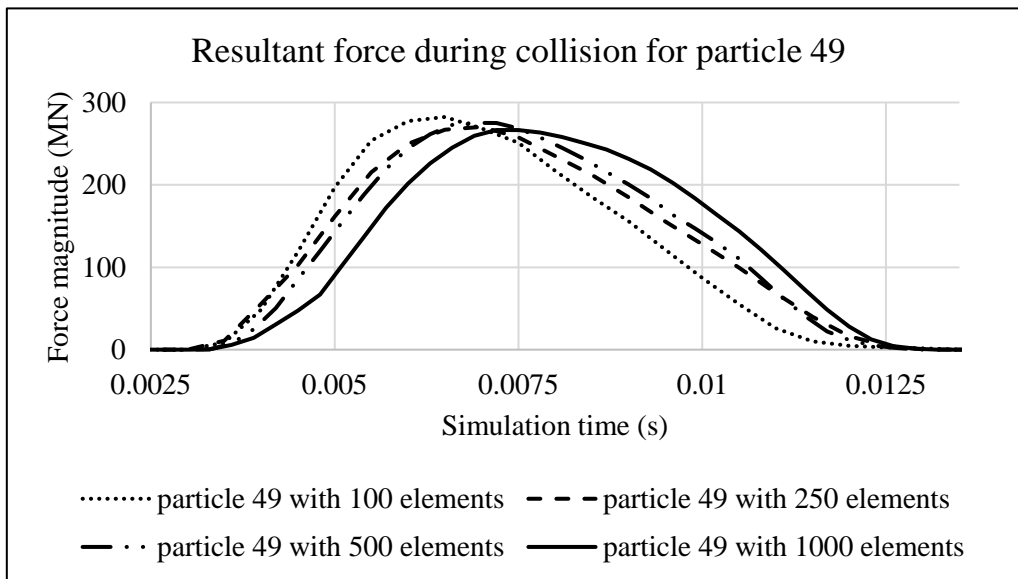


Figure A49.1 Plot of resultant forces during collision event for Particle 49

Appendix

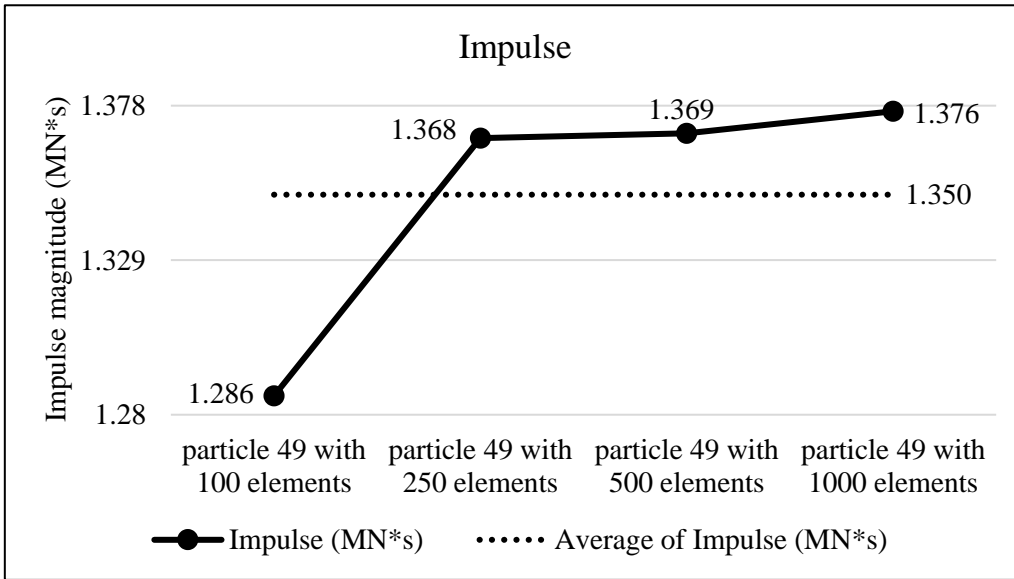


Figure A49.2 Plots of collision impulse for Particle 49

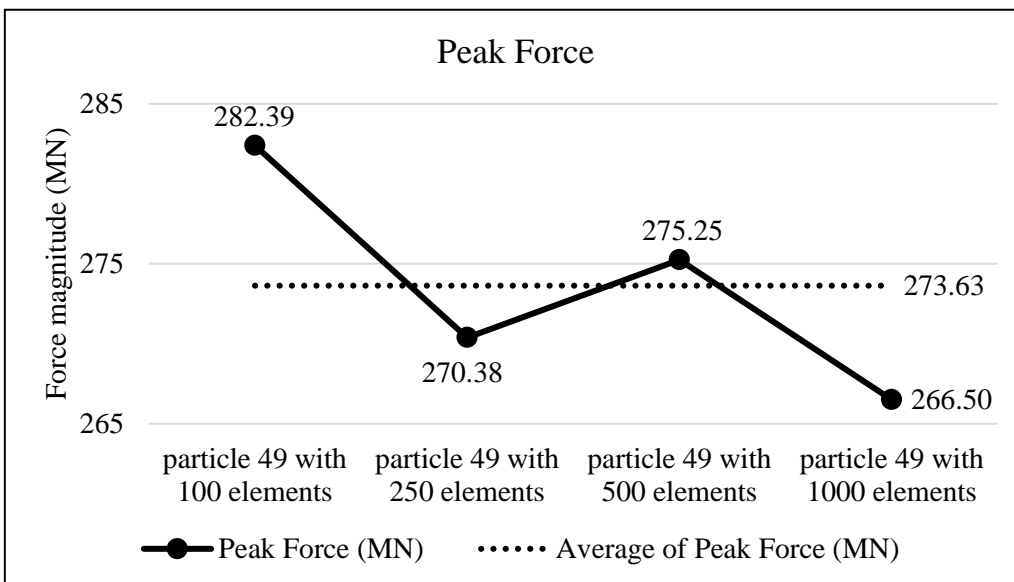


Figure A49.3 Peak collision for the four particle geometry resolutions for Particle 49

Appendix

Collision results data analysis					
Model	particle 49 with 100 elements	particle 49 with 250 elements	particle 49 with 500 elements	particle 49 with 1000 elements	Average
Impulse (MN*s)	1.286	1.368	1.369	1.376	1.350
Percent difference from Avg. Impulse	-4.73	1.33	1.44	1.96	
Peak Force (MN)	282.39	270.38	275.25	266.50	273.63
Percent difference from Avg. Peak Force	3.20	-1.19	0.59	-2.60	

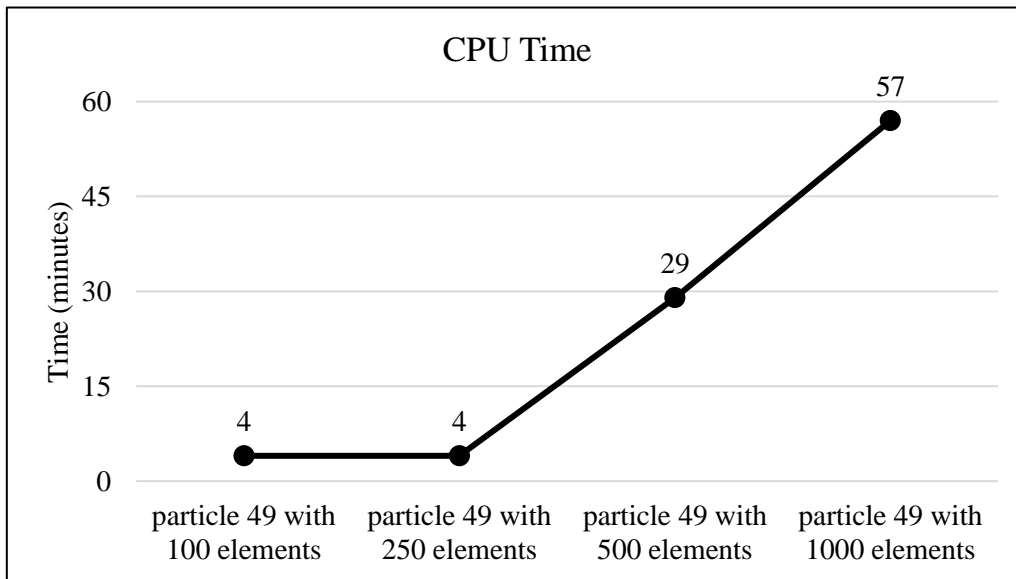
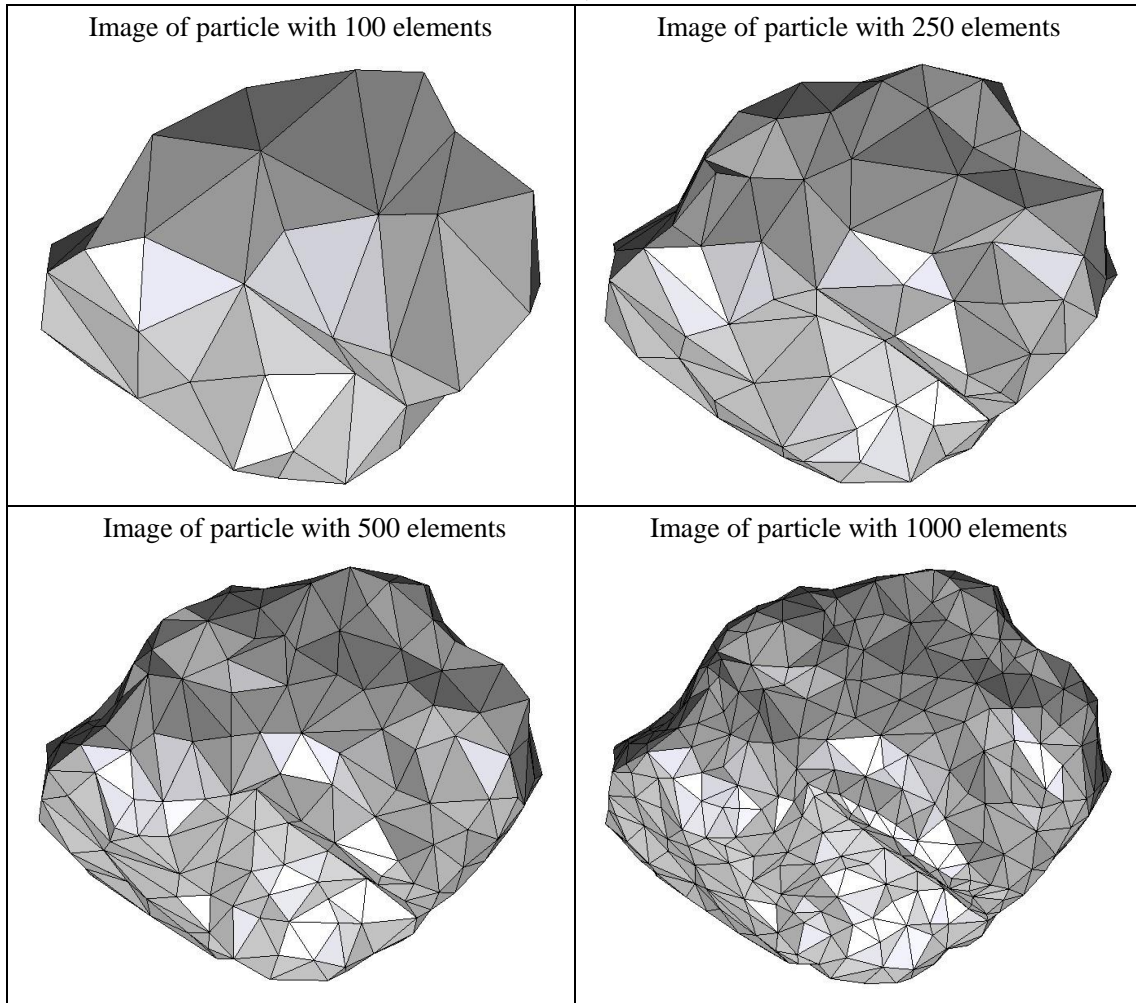


Figure A49.4 CPU computation time vs. model geometry resolution

Appendix

Percent difference analysis compare to particle 49 with 100 elements for different group of data			
	particle 49 with 250 elements	particle 49 with 500 elements	particle 49 with 1000 elements
Impulse	6.35	6.47	7.02
Peak Force	-4.25	-2.53	-5.63
Start Time	0.00	-5.71	-5.71
CPU Time	0.00	625.00	1325.00
Simulation Time	-5.00	-4.00	-1.00

Summary of particle characteristics and collision simulation details for Particle 50 (of 50)



Particle statistics (part 1)								
Particle ID	# vertices	# elements	Mass (g)	Moments of Inertia			Volume (cm ³)	Sfc. Area (cm ²)
				I1	I2	I3		
				(gcm ²)	(gcm ²)	(gcm ²)		
50 (100 elements)	52	100	50.655	327671.725	271968.975	144427.3875	17.94963	41.67344
50 (250 elements)	127	250	50.655	336234.775	276882.05	149935.375	18.22402	42.11500
50 (500 elements)	252	500	50.655	338645.2	278682.325	151448.65	18.31963	42.13357
50 (1000 elements)	502	1000	50.655	340661.05	280205.175	152515.1875	18.38204	42.13452

Appendix

Particle Statistics (part 2)							
Particle ID	α	R_g (cm)	ψ	R_v (cm)	L (cm)	I (cm)	S (cm)
50 (100 elements)	2.26509	2.63885	0.79554	1.62426	211.97338	140.54975	93.58278
50 (250 elements)	2.26127	2.60822	0.79520	1.63250	213.82054	143.72956	94.55758
50 (500 elements)	2.25663	2.59866	0.79763	1.63534	214.44225	144.45686	95.02779
50 (1000 elements)	2.25555	2.60654	0.79942	1.63720	215.01046	144.98870	95.32520

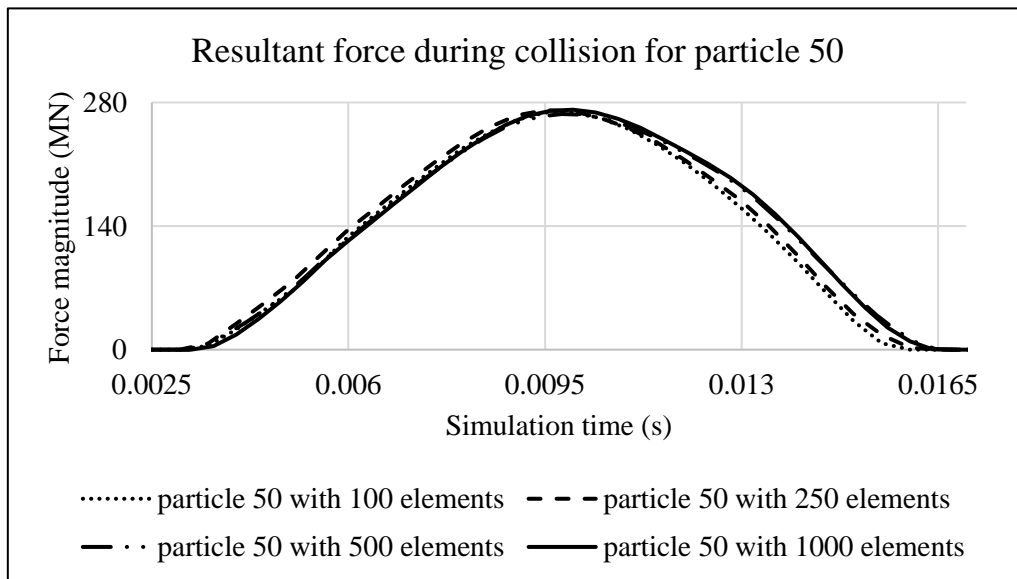


Figure A50.1 Plot of resultant forces during collision event for Particle 50

Appendix

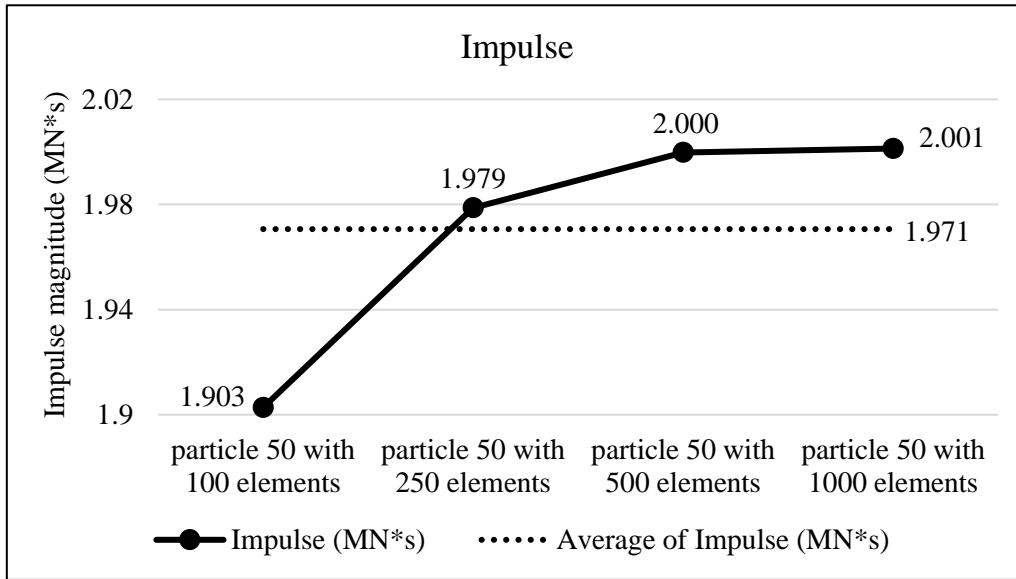


Figure A50.2 Plots of collision impulse for Particle 50

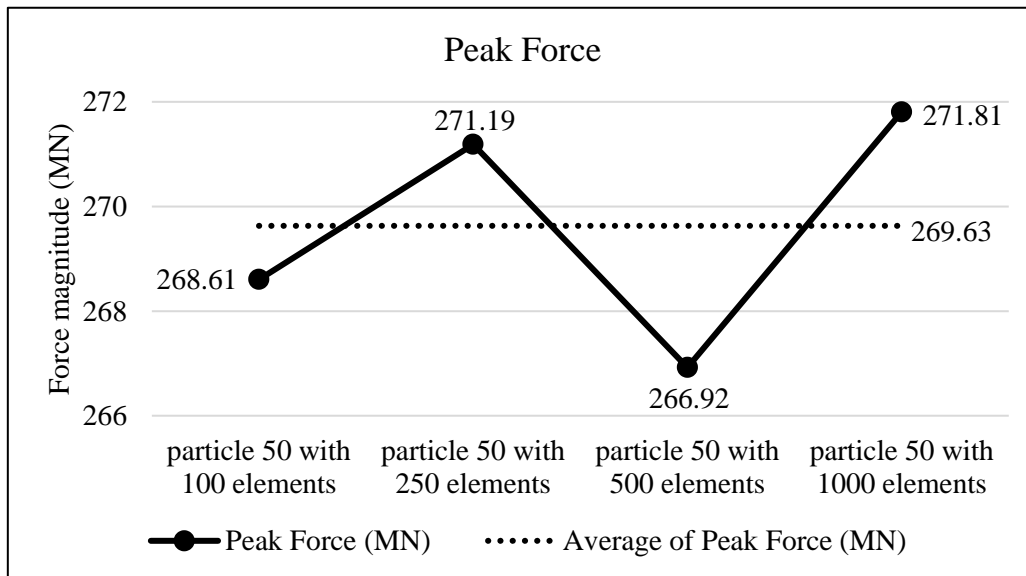


Figure A50.3 Peak collision for the four particle geometry resolutions for Particle 50

Appendix

Collision results data analysis					
Model	particle 50 with 100 elements	particle 50 with 250 elements	particle 50 with 500 elements	particle 50 with 1000 elements	Average
Impulse (MN*s)	1.903	1.979	2.000	2.001	1.971
Percent difference from Avg. Impulse	-3.44	0.41	1.48	1.56	
Peak Force (MN)	268.61	271.19	266.92	271.81	269.63
Percent difference from Avg. Peak Force	-0.38	0.58	-1.00	0.81	

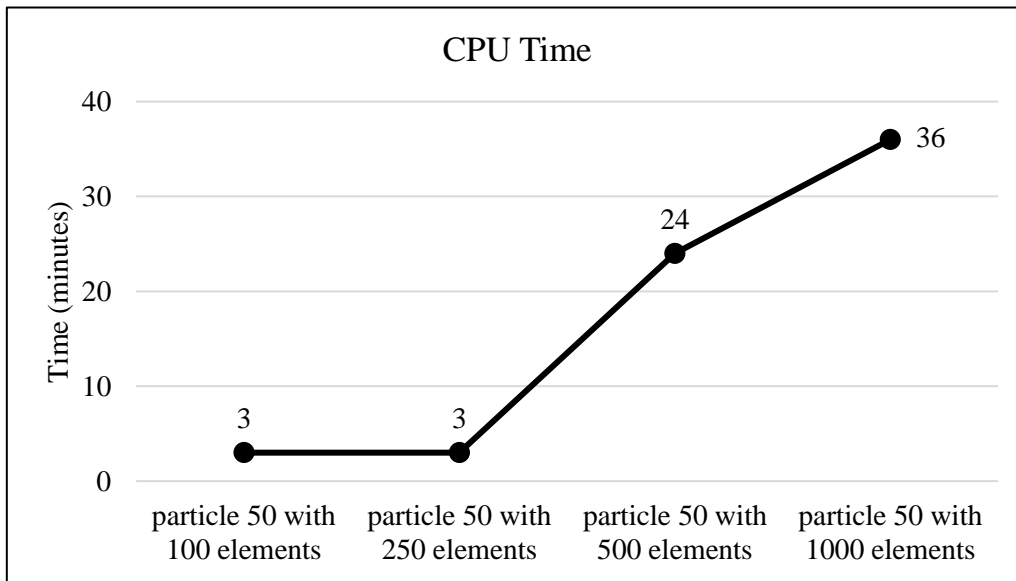


Figure A50.4 CPU computation time vs. model geometry resolution

Appendix

Percent difference analysis compare to particle 50 with 100 elements for different group of data			
	particle 50 with 250 elements	particle 50 with 500 elements	particle 50 with 1000 elements
Impulse	3.99	5.10	5.18
Peak Force	0.96	-0.63	1.19
Start Time	0.00	0.00	2.86
CPU Time	0.00	700.00	1100.00
Simulation Time	4.17	7.92	6.67